frontiers | Research Topics

Women in radiation oncology: 2021

Edited by
Christina Tsien, Radka Stoyanova and Alina Mihaela Mihai

Published in
Frontiers in Oncology

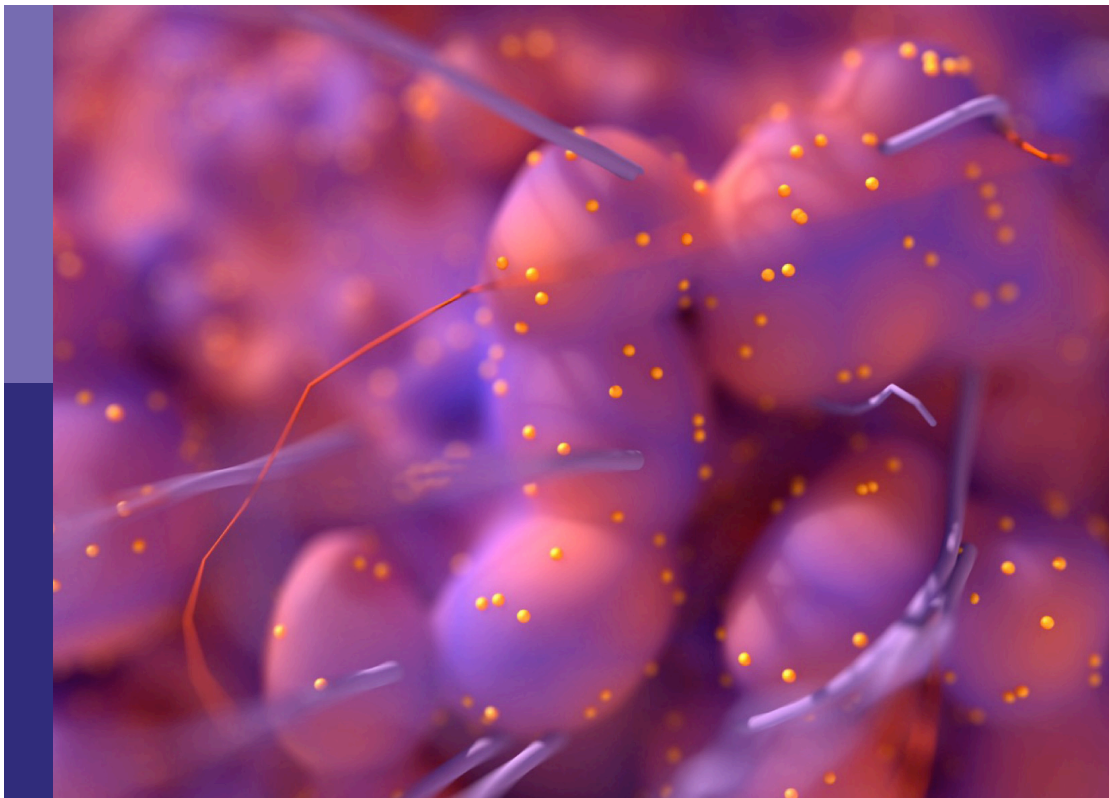

ISSN 1664-8714
ISBN 978-2-83252-052-9
DOI 10.3389/978-2-83252-052-9

About Frontiers

Frontiers is more than just an open access publisher of scholarly articles: it is a pioneering approach to the world of academia, radically improving the way scholarly research is managed. The grand vision of Frontiers is a world where all people have an equal opportunity to seek, share and generate knowledge. Frontiers provides immediate and permanent online open access to all its publications, but this alone is not enough to realize our grand goals.

Frontiers journal series

The Frontiers journal series is a multi-tier and interdisciplinary set of open-access, online journals, promising a paradigm shift from the current review, selection and dissemination processes in academic publishing. All Frontiers journals are driven by researchers for researchers; therefore, they constitute a service to the scholarly community. At the same time, the *Frontiers journal series* operates on a revolutionary invention, the tiered publishing system, initially addressing specific communities of scholars, and gradually climbing up to broader public understanding, thus serving the interests of the lay society, too.

Dedication to quality

Each Frontiers article is a landmark of the highest quality, thanks to genuinely collaborative interactions between authors and review editors, who include some of the world's best academicians. Research must be certified by peers before entering a stream of knowledge that may eventually reach the public - and shape society; therefore, Frontiers only applies the most rigorous and unbiased reviews. Frontiers revolutionizes research publishing by freely delivering the most outstanding research, evaluated with no bias from both the academic and social point of view. By applying the most advanced information technologies, Frontiers is catapulting scholarly publishing into a new generation.

What are Frontiers Research Topics?

Frontiers Research Topics are very popular trademarks of the *Frontiers journals series*: they are collections of at least ten articles, all centered on a particular subject. With their unique mix of varied contributions from Original Research to Review Articles, Frontiers Research Topics unify the most influential researchers, the latest key findings and historical advances in a hot research area.

Find out more on how to host your own Frontiers Research Topic or contribute to one as an author by contacting the Frontiers editorial office: frontiersin.org/about/contact

Women in radiation oncology: 2021

Topic editors

Christina Tsien — Sibley Memorial Hospital, Johns Hopkins Medicine, United States
Radka Stoyanova — University of Miami, United States
Alina Mihaela Mihai — Beacon Hospital, Ireland

Citation

Tsien, C., Stoyanova, R., Mihai, A. M., eds. (2023). *Women in radiation oncology: 2021*. Lausanne: Frontiers Media SA. doi: 10.3389/978-2-83252-052-9

Table of contents

frontiers | Frontiers in Oncology

TYPE Editorial
PUBLISHED 17 March 2023
DOI 10.3389/fonc.2023.1162683

OPEN ACCESS

EDITED AND REVIEWED BY
Timothy James Kinsella,
Brown University, United States

*CORRESPONDENCE
Christina Tsien
christina.tsien@gmail.com

SPECIALTY SECTION
This article was submitted to Radiation Oncology, a section of the journal Frontiers in Oncology

RECEIVED 09 February 2023
ACCEPTED 09 March 2023
PUBLISHED 17 March 2023

CITATION
Martinez C and Tsien C (2023) Editorial: Women in radiation oncology: 2021. *Front. Oncol.* 13:1162683. doi: 10.3389/fonc.2023.1162683

Editorial: Women in radiation oncology: 2021

Constanza Martinez and Christina Tsien*

Department of Radiation Oncology, McGill University Health Centre, Montreal, QC, Canada

KEYWORDS

breast cancer, artificial intelligence (AI), stereotactic ablation body radiation therapy, palliation therapy, partial breast irradiation (PBI)

Editorial on the Research Topic
Women in radiation oncology: 2021

In this special edition of Frontiers in Oncology, we would like to start by thanking all the contributors and congratulating them for their fine efforts. This edition highlights the importance of research mentorship, especially for women in the subspecialty of radiation oncology.

During the recent pandemic, there has been an increased emphasis on innovative ways to improve access to cancer care for women. In this edition, we will highlight papers that aim to shed light on novel advances, including the use of accelerated radiation, stereotactic body radiation therapy (SBRT), and artificial intelligence.

Highly aggressive triple-negative breast cancer (TNBC) is typically treated with neoadjuvant chemotherapy and immunotherapy (1–3). The specific radiobiological characteristics of TNBC tumor cells and their response to different RT fractionation regimens had not been fully elucidated. To address this, Grosche et al. studied the effects of normo-fractionated RT (NormRT) of 50Gy in 2Gy per fraction compared to hypo-fractionated RT (HypoRT) of 40Gy in 2.67Gy per fraction in a normal epithelial breast cancer cell line (MCF10A) and compared these results to those of 2 TNBC BRCA mutant cell lines (HCC1395 and HCC1937). Altogether, these preclinical data support previous studies on the equal effectiveness at the cellular level of NormoRT and HypoRT as tested by this group *in vitro*. The additional use of preclinical models, including patient-derived xenografts, to assess the impact of metabolic and spatial heterogeneity (4) in short- and long-term responses to treatment should also be examined.

The use of accelerated partial breast irradiation (APBI) for younger patients with high-risk features, including the TNBC subtype, continues to be an area of controversy. Goulding et al. reported on a retrospective analysis of 269 patients with high-risk characteristics, including TNBC, ER, tumor size < 3 cm, and age 40-50, who were receiving 38.5 Gy BID in 10 fx. High-risk features, including TNBC and ER histology, were significantly correlated with an increased risk of axillary recurrence. These data highlight the need for further investigation into the use of APBI for younger patients with high-risk features (5).

The benefit of SBRT for breast cancer patients with oligometastatic disease remains an area of continued investigation (6, 7). Lemoine et al. performed a retrospective analysis of the use of SBRT in oligometastatic breast cancer treated with SBRT. In this study, 44 patients were included who had between two and five lesions. The patients had metastatic

disease in the bone (44.4%), liver (40.7%), and lung (11.1%). Overall, the results showed high local control, low toxicities, and, in combination with systemic treatment, a progression-free survival (PFS) of greater than 80%.

Vazquez et al. conducted a retrospective analysis of 708 patients who received palliative radiation therapy (RT) for metastatic disease from primary lung (31%), breast (14.8%), and gastrointestinal (14.8%) cancer. Predominantly, palliative RT was delivered to bone metastases (56%), and a single-fraction treatment was used on 34.4% (243) of the patients. The results identified that the 30-day mortality (30-DM) rate was 14.5% (124/708 patients). Importantly, the predictive factor for the 30-DM rate was performance status (ECOG) 2-3 (p= 0.0001). Increased use of single-fraction RT should be taken into consideration when offering palliative radiotherapy compared to the best supportive care. The main objective of treatment—symptom relief—should be discussed with and emphasized to our patients.

Artificial intelligence (AI) is being incorporated into radiation oncology to predict outcomes, improve patient selection, optimize treatment planning, and generate auto-contouring or auto-segmentation tools. Artificial intelligence or machine learning may ultimately be a useful tool for physicians to improve patient selection and treatment. Volpe et al. performed a systematic review of electronic databases that used machine learning (ML) or radiomics specifically in head and neck radiotherapy. They identified 48 studies, including 21 on auto-segmentation, 12 on oncologic outcome prediction, 10 on toxicity prediction, and 4 on treatment planning. Quantitative image features were used in 9/48 studies (19%), and computed tomography was the most used imaging modality in 40% of cases. The clinical applications of AI in radiation oncology continue to increase. The use of CT/MR imaging, auto-segmentation and auto-contouring tools, and virtual reality tools are essential for improving outcomes in radiation oncology.

We hope that our readers enjoy this special edition with its emphasis on women scientists in the field of radiation oncology and that they are inspired to work together and support the mentorship of young investigators in this field. Embracing novel advances and tools is essential for improving outcomes in radiation oncology. Training our future oncologists is a necessary factor in the continued value and importance of radiation oncology in improving cancer care outcomes for women. We have a strong group of talented investigators, and the future of our field remains bright.

Author contributions

Writing and editing the editorial CM, CT, review editorial. All authors contributed to the article and approved the submitted version.

Acknowledgments

Thank you to Dr. Stoyanova and Mihai for their contributions.

Conflict of interest

The authors declare that the research was conducted in the absence of any commercial or financial relationships that could be construed as a potential conflict of interest.

Publisher's note

References

1. Von Minckwitz G, Untch M, Blohmer JU, Costa SD, Eidtmann H, Fasching PA, et al. Definition and impact of pathologic complete response on prognosis after neoadjuvant chemotherapy in various intrinsic breast cancer subtypes. *J Clin Oncol* (2012) 30:1796–804. doi: 10.1200/JCO.2011.38.8595

2. Liedtke C, Mazouni C, Hess KR, André F, Tordai A, Mejia JA, et al. Response to neoadjuvant therapy and long-term survival in patients with triple-negative breast cancer. *J Clin Oncol* (2008) 26:1275–81. doi: 10.1200/JCO.2007.14.4147

3. Schmid P, Cortes J, Pusztai L, McArthur H, Kummel S, Bergh J, et al. Pembrolizumab for early triple-negative breast cancer. *N Engl J Med* (2020) 382:810–21. doi: 10.1056/NEJMoa1910549

4. Casasent AK, Schalck A, Gao R, Sei E, Long A, Pangbum W, et al. Multiclonal invasion in breast tumors identified by topographic single cell sequencing. *Cell* (2018) 172:205–217.e12. doi: 10.1016/j.cell.2017.12.007

5. Kumar S, Sharife H, Kreisel T, Mogilevsky M, Bar-Lev L, Grunewald M, et al. Intra-Tumoral Metabolic Zonation and Resultant Phenotypic Diversification Are Dictated by Blood Vessel Proximity. *Cell Metab.* 30, 201–211.e6 (2019).

6. Palma DA, Olson R, Harrow S, Gaede S, Louie AV, Haasbeek C, et al. Stereotactic ablative radiotherapy versus standard of care palliative treatment in patients with oligometastatic cancers (SABR-COMET): a randomised, phase 2, open-label trial. *Lancet (London England)* (2019) 393:2051–8. doi: 10.1016/S0140-6736(18)32487-5

7. Chmura SJ, Winter KA, Woodward WA, Borges VF, Salama JK, Al-Hallag HA, et al. *Oral abstract session NRG-BR002 : A phase IIR/III trial of standard of care systemic therapy with or without stereotactic body radiotherapy (SBRT) and/or surgical resection (SR) for newly oligometastatic breast cancer (NCT02364557)* (2022) American Socierty of Clinical Oncology (ASCO) 2022. 04, 2364557.

frontiers in Oncology

ORIGINAL RESEARCH
published: 25 February 2021
doi: 10.3389/fonc.2021.631618

Adjuvant Radiation in Older Patients With Glioblastoma: A Retrospective Single Institution Analysis

Jessica W. Lee[1], John P. Kirkpatrick[1], Frances McSherry[2], James E. Herndon II[2], Eric S. Lipp[3], Annick Desjardins[3], Dina M. Randazzo[3], Henry S. Friedman[3], David M. Ashley[3], Katherine B. Peters[3] and Margaret O. Johnson[3]*

[1] Department of Radiation Oncology, Duke University School of Medicine, Durham, NC, United States, [2] Department of Biostatistics & Bioinformatics, Duke University School of Medicine, Durham, NC, United States, [3] Department of Neurosurgery, The Preston Robert Tisch Brain Tumor Center, Duke University Medical Center, Durham, NC, United States

OPEN ACCESS

Edited by:
Sharad Goyal, George Washington University, United States

Reviewed by:
Sunit Das, St. Michael's Hospital, Canada
Yuan James Rao, George Washington University, United States
Parima Daroui, MemorialCare Health System, United States

***Correspondence:**
Jessica W. Lee
Jessica.Lee@duke.edu

Specialty section:
This article was submitted to Radiation Oncology, a section of the journal Frontiers in Oncology

Received: *20 November 2020*
Accepted: *14 January 2021*
Published: *25 February 2021*

Citation:
Lee JW, Kirkpatrick JP, McSherry F, Herndon JE II, Lipp ES, Desjardins A, Randazzo DM, Friedman HS, Ashley DM, Peters KB and Johnson MO (2021) Adjuvant Radiation in Older Patients With Glioblastoma: A Retrospective Single Institution Analysis. Front. Oncol. 11:631618. doi: 10.3389/fonc.2021.631618

Objectives: Standard 6-week and hypofractionated 3-week courses of adjuvant radiation therapy (RT) are both options for older patients with glioblastoma (GBM), but deciding the optimal regimen can be challenging. This analysis explores clinical factors associated with selection of RT course, completion of RT, and outcomes following RT.

Materials and Methods: This IRB-approved retrospective analysis identified patients ≥70 years old with GBM who initiated adjuvant RT at our institution between 2004 and 2016. We identified factors associated with standard or hypofractionated RT using the Cochran-Armitage trend test, estimated time-to-event endpoints using the Kaplan-Meier method, and found predictors of overall survival (OS) using Cox proportional hazards models.

Results: Sixty-two patients with a median age of 74 (range 70–90) initiated adjuvant RT, with 43 (69%) receiving standard RT and 19 (31%) receiving hypofractionated RT. Selection of short-course RT was associated with older age ($p = 0.04$) and poor KPS ($p = 0.03$). Eight (13%) patients did not complete RT, primarily for hospice care due to worsening symptoms. After a median follow-up of 37 months, median OS was 12.3 months (95% CI 9.0–15.1). Increased age ($p < 0.05$), poor KPS ($p < 0.0001$), lack of MGMT methylation ($p < 0.05$), and lack of RT completion ($p < 0.0001$) were associated with worse OS on multivariate analysis. In this small cohort, GTV size and receipt of standard or hypofractionated RT were not associated with OS.

Conclusions: In this cohort of older patients with GBM, age and KPS was associated with selection of short-course or standard RT. These regimens had similar OS, though a subset of patients experienced worsening symptoms during RT and discontinued treatment. Further investigation into predictors of RT completion and survival may help guide adjuvant therapies and supportive care for older patients.

Keywords: glioblastoma, frail elderly, aged, radiotherapy, radiation dose hypofractionation, radiation oncology

INTRODUCTION

Glioblastoma (GBM) is a malignancy of older adults. The median age at diagnosis is 65 years old, and the incidence increases with age, peaking in the 75–84 years old age group (1). The Stupp trial established the current standard treatment of maximal safe resection followed by adjuvant radiation therapy (RT) for 6 weeks with concurrent and adjuvant temozolomide (2). However, this trial excluded patients >70 years old, and as age is both a negative prognostic factor and predictor of response to RT, other randomized studies have investigated radiation or temozolomide alone for older adults (3–5). The Canadian trial found that in patients ≥60 years old, 40 Gy in 15 fractions was non-inferior to 60 Gy in 30 fractions, with median survival of 5.1 and 5.6 months, respectively (6). The Nordic trial found that in patients >70 years old, 34 Gy in 10 fractions or temozolomide alone both had improved survival compared to 60 Gy in 30 fractions, though the latter group had more patients discontinue treatment (7). NOA-08 found that in patients >65 years old, temozolomide was non-inferior to 60 Gy in 30 fractions (8). In both the Nordic and NOA-08 trials, O^6-methylguanine DNA methyltransferase (MGMT) promoter methylation predicted a survival benefit from temozolomide (7, 8). More recently, a randomized study of patients ≥65 years old found that addition of temozolomide to the 40 Gy regimen did improve survival from 7.6 to 9.3 months (9).

Based on the above studies, temozolomide with standard or hypofractionated RT are both options for patients >70 years old with good performance status (10). The optimal RT regimen is not clear, though individualized treatment decisions may take into account factors such as age, performance status, and MGMT methylation (11). Standardized geriatric assessments have also been proposed to help guide treatment decisions (12). Overall, utilization of hypofractionated RT in the United States remains low. In several National Cancer Database (NCDB) analyses of older patients with GBM receiving adjuvant RT, only 2.5–20% received a hypofractionated regimen (13–17).

Here, we report our institutional experience with older patients initiating adjuvant RT, focusing on factors affecting the selection of standard or hypofractionated regimens and clinical outcomes.

MATERIALS AND METHODS

Following institutional review board approval, we identified patients with GBM who were ≥70 years old at time of pathologic diagnosis and initiated adjuvant RT in our radiation oncology department between 2004 and 2016.

Patient characteristics including age, sex, Karnofsky performance status (KPS), and MGMT methylation status were obtained from the medical record. KPS was documented following maximal resection at the time of radiation oncology consultation. Treatment details including radiation technique, gross tumor volume (GTV), planning target volume (PTV), and receipt of concurrent temozolomide or bevacizumab were also obtained. Standard radiation therapy to primary and boost volumes was delivered per Radiation Therapy Oncology Group (RTOG) guidelines (18, 19). Specifically, the primary PTV consisted of the pre-operative T2-hyperintense GTV plus a 2 cm margin and received 45–50.4 Gy at 1.8–2 Gy/fraction. The boost PTV was the post-operative T1 contrast-enhancing GTV plus a 1.5 cm margin and received a total dose of 59.4–60 Gy at 1.8–2 Gy/fraction. For hypofractionated radiation therapy, the PTV comprised of T1 contrast-enhancing GTV plus a 1.5 cm margin and received 40.05 Gy in 2.67 Gy/fraction. As we used frequent image guidance and stereotactic radiosurgery-capable, custom-molded head immobilization, there was no further expansion for set-up error. PTVs were trimmed where they extended across anatomic boundaries such as the falx, into non-target tissues such as the orbits or outer table of the skull or the scalp. Boost PTVs were also trimmed where they extended into critical organs at risk such as the brainstem and anterior visual pathways. Temozolomide was administered to all patients where possible and dosed per the Stupp trial, and bevacizumab was administered at the discretion of the treating oncologist (2, 20, 21).

Statistics

Association between clinical characteristics and selection of standard or hypofractionated RT was assessed using the Cochran-Armitage test for trend. Overall survival, measured from date of pathologic diagnosis, was estimated by the Kaplan-Meier method and compared *via* log-rank test. Clinical factors associated with overall survival were evaluated using Cox proportional hazards models. Significance was assumed if $p < 0.05$. Statistical analyses were performed using SAS 9.4.

RESULTS

Between 2004 and 2016, 62 older patients initiated adjuvant RT. Baseline patient characteristics are shown in **Table 1**. Overall, patients had a median age of 74 years old, and 34 (55%) were male. Most patients received a resection; 33 (53%) had a gross total resection (GTR) and 10 (16%) had a subtotal resection, while 19 (31%) underwent biopsy only. Forty-four (71%) patients had a Karnofsky performance status (KPS) of ≥70 prior to starting adjuvant RT. MGMT methylation status was known for 46 (74%) patients, and 20 (32%) had MGMT methylation. In patients receiving standard RT, the median initial GTV was 98 cm^3 and the median boost GTV was 31 cm^3. In patients receiving hypofractionated RT, the median GTV was 27 cm^3. Fifty-eight (94%) and 20 (32%) patients received concurrent temozolomide and bevacizumab, respectively.

Forty-three (69%) patients received standard RT while 19 (31%) of patients received hypofractionated RT. As shown in **Figure 1**, increased age ($p = 0.04$, Cochran Armitage test for trend) and decreased KPS ($p = 0.03$, Cochran Armitage test for

Abbreviations: RT, radiation therapy; GBM, glioblastoma; IRB, institutional review board; KPS, Karnofsky performance status; OS, overall survival; MGMT, O^6-methylguanine DNA methyltransferase MGMT.

TABLE 1 | Baseline demographics and treatment details.

Characteristic		Standard (N = 43)	Hypofractionated (N = 19)	All (N = 62)
Age (years)		74 (70–88)	77 (71–91)	74 (70–91)
Sex	Female	17 (40)	11 (58)	28 (45)
	Male	26 (61)	8 (42)	34 (55)
Maximal resection	GTR	26 (61)	7 (37)	33 (53)
	STR	7 (16)	3 (16)	10 (16)
	Biopsy only	10 (23)	9 (47)	19 (31)
KPS	≥70	32 (74)	12 (63)	44 (71)
	<70	6 (14)	4 (22)	10 (16)
	Unknown	5 (12)	3 (16)	8 (13)
MGMT	Methylated	13 (30)	7 (37)	20 (32)
	Unmethylated	18 (42)	8 (42)	26 (42)
	Unknown	12 (28)	4 (21)	16 (26)
Radiation technique	3D	4 (9)	9 (47)	13 (21)
	IMRT	39 (91)	10 (53)	49 (79)
GTV initial (cm^3)		98 (8–283)	27 (6–137)	
GTV boost (cm^3)		31 (7–165)		
PTV initial (cm^3)		459 (121–1,049)	238 (85–505)	
PTV boost (cm^3)		181 (78–410)		
Concurrent TMZ	Yes	43 (100)	15 (79)	58 (94)
	No	0 (0)	4 (21)	4 (6)
Concurrent bevacizumab	Yes	13 (30)	7 (37)	20 (32)
	No	30 (70)	12 (63)	42 (68)
Completed RT	Yes	37 (86)	17 (90)	54 (87)
	No	6 (14)	2 (10)	8 (13)

KPS, Karnofsky Performance Status; MGMT, O^6-methylguanine DNA methyltransferase; GTV, gross target volume; PTV, planning target volume; TMZ, temozolomide; RT, radiation therapy.
Data show number (%) or median (range).

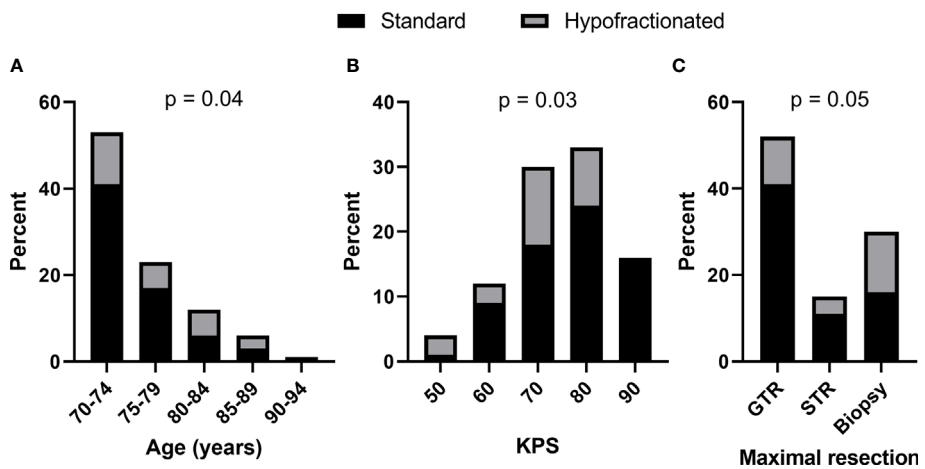

FIGURE 1 | Increased age and decreased KPS were significantly associated with hypofractionated (gray) *vs.* standard (black) adjuvant radiation therapy. Bars show percent of total patients categorized by **(A)** age, **(B)** KPS, and **(C)** extent of maximal resection. Cochran-Armitage test for trend p values shown.

trend) were both significantly associated with receipt of hypofractionated RT rather than standard RT. Patients who underwent biopsy only compared to gross or subtotal resection appeared to receive hypofractionated RT more frequently as well, but the association was not significant. RT regimen was not associated with MGMT methylation status or the volume of enhancing tumor, as approximated by the GTV size.

During RT, 13 patients had unscheduled interruptions, and RT was ultimately discontinued early in six receiving standard RT and two receiving hypofractionated RT. Patients who stopped RT early had a median age of 78 (range 71–85), median pre-RT KPS of 80 (range 50–90), and received a median of 66% (range 3–94%) of the prescribed dose. The most common reason for discontinuation was worsening symptoms prompting transition to hospice. Within this small sample, RT discontinuation was not significantly associated with age, pre-RT KPS, extent of maximal resection, RT dose-fractionation, or size of treatment volumes. Following RT, 41

(66%) patients received adjuvant temozolomide for a median of five cycles (range 1–12), and there was no significant association between receipt of adjuvant temozolomide and RT regimen in this series.

Median follow-up time was 37 months, and two patients were alive at last follow-up. Median overall survival was 12.3 months (95% CI 9.0–15.1 months) across all patients. Median overall survival in patients receiving standard RT and hypofractionated RT was 12.4 months (95% CI 9.0–16.4 months) and 9.9 months (95% CI 3.4–15.1 months), respectively. Kaplan-Meier curves of overall survival categorized by KPS, extent of maximal resection, methylation status, hypofractionated *vs.* standard RT, RT completion, and receipt of concurrent bevacizumab are shown in **Figure 2**. On univariate Cox regression analysis, increased age, KPS <70, biopsy *vs.* GTR, unmethylated MGMT *vs.* methylated MGMT, unknown MGMT status *vs.* methylated MGMT, and early RT discontinuation were significantly associated worse survival, as shown in **Table 2**. STR *vs.* biopsy, use of hypofractionated or standard RT, GTV size, and use of concurrent bevacizumab were not significantly associated with survival. On multivariate analysis with the above covariates, only age (HR 1.09, 95% CI 1.01–1.18), KPS <70 (HR 9.29, 95% CI 3.27–26.38), unmethylated MGMT (HR 2.48, 95% CI 1.09–5.64) or unknown MGMT status (HR 3.58, 95% CI 1.31–9.79), and

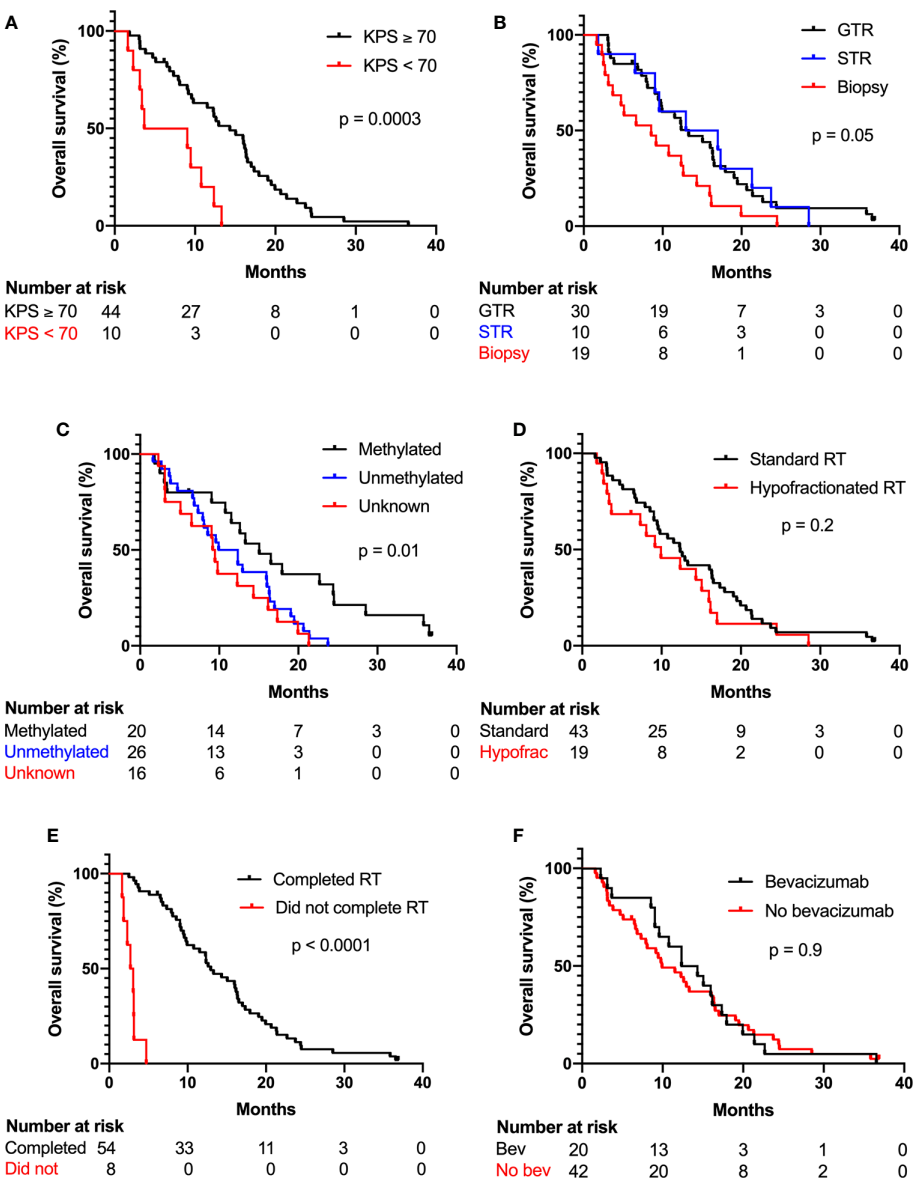

FIGURE 2 | KPS, MGMT methylation status, and RT completion were significantly associated with overall survival. Kaplan-Meier plots show percent overall survival categorized by **(A)** KPS, **(B)** extent of maximal resection, **(C)** methylation status, **(D)** standard or hypofractionated RT, **(E)** completion of RT, and **(F)** receipt of concurrent bevacizumab. Log-rank test p values shown.

TABLE 2 | Univariate and multivariate Cox proportional hazards models of overall survival.

Risk factor	Univariate analysis			Multivariate analysis		
	HR	95% CI	p value	HR	95% CI	p value
Age	1.08	1.02–1.15	0.01	1.09	1.01–1.18	0.02
KPS <70 *vs.* KPS ≥70	3.74	1.74–8.06	<0.001	9.29	3.27–26.38	<0.0001
Maximal resection						
GTR *vs.* biopsy	0.51	0.28–0.91	0.02	1.72	0.67–4.41	0.26
STR *vs.* biopsy	0.51	0.23–1.11	0.09	1.01	0.38–2.67	0.98
MGMT methylation						
Unmethylated *vs.* methylated	2.37	1.19–4.72	0.01	2.48	1.09–5.64	0.03
Unknown *vs.* methylated	2.95	1.37–6.34	0.01	3.58	1.31–9.79	0.01
Hypofractionated *vs.* standard RT	1.39	0.79–2.44	0.25	1.69	0.68–4.18	0.26
Did not complete *vs.* completed RT	32.36	9.85–106.3	<0.0001	71.76	13.32–386.6	<0.0001
GTV size	1.01	1.00–1.01	0.06	1.00	0.99–1.01	0.59
Bevacizumab yes *vs.* no	1.04	0.56–1.64	0.88	0.76	0.38–1.53	0.45

KPS, Karnofsky Performance Status; GTR, gross total resection; STR, subtotal resection; MGMT, O^6-methylguanine DNA methyltransferase; RT, radiation therapy; GTV, gross target volume.

Data show hazard ratios (HR) and 95% confidence intervals (CI).

early RT discontinuation (HR 71.76, 95% CI 13.32–386.6) were significantly associated with decreased survival.

DISCUSSION

Current National Comprehensive Cancer Network (NCCN) guidelines in the United states allow for a range of adjuvant therapies for older GBM patients, including clinical trial, standard RT with temozolomide, hypofractionated RT with temozolomide, temozolomide alone for MGMT methylated patients, or hypofractionated RT alone (10). In the temozolomide era, direct comparisons between standard and hypofractionated RT are limited to retrospective studies, as no randomized data are available. Most retrospective analyses have report similar survival between standard 6-week and hypofractionated 3-week courses of RT (22–27). However, 2 larger series from Italy and California with 129 and 239 patients, respectively, did observe significantly increased survival with standard fractionation (28, 29). A 2019 meta-analysis of 917 patients also detected a significant difference in outcomes, with median OS 13.5 months (95% CI 10.0–16.9) after standard RT and 9.9 months (95% CI 6.5–13.3) after hypofractionated RT both with temozolomide (30).

The present study builds on existing literature and also examines RT details such as GTV size and early RT discontinuation. Similar to prior studies, increased age and poor KPS were significantly associated with selection of hypofractionated rather than standard RT with temozolomide. Median survival following standard and hypofractionated RT was not significantly different at 12.4 and 9.9 months, respectively. Instead, other clinical factors including increased age and poor KPS were associated with decreased survival. Both unmethylated and unknown MGMT status were also associated with poor outcomes, as the latter group likely contained mostly unmethylated patients. Eight (13%) patients discontinued adjuvant RT in the present study due to functional decline, with significantly diminished survival. The majority of these patients had already completed at least half of their RT courses. In this small cohort, no clinical factors were significantly associated with RT discontinuation, and the median pre-RT age was 78 and KPS was 80.

Limitations of the present study as well as other institutional retrospective series include small sample sizes as well as biases in patient and treatment selection. This study includes a highly selected patient population receiving treatment at a tertiary referral center, which may not reflect the patients seen in the community, especially those with limited functional status. This study also included patients ≥70 years old in accordance with NCCN guidelines, however, generally studies of older patients use cutoffs ranging from 65 to 75, making comparison across studies somewhat more challenging (10).

Further investigation into predictors of functional decline may help identify patients where shorter RT courses, palliative care, and other supportive interventions may be more appropriate (31). As noted above, the patients who discontinued RT had similar age and KPS compared to the larger cohort. Thus, in addition to age and KPS, additional measures such as geriatric screening tools and assessments may be helpful to guide selection of adjuvant RT fractionation. For example, the G8 screening tool has been validated in oncology patients >70 years old and more recently in GBM patients ≥65 years old (32, 33). In GBM patients, the G8 score was as stronger predictor of overall survival than age and receipt of radiation or chemotherapy (32). The G8 score also correlated with receipt of standard chemoradiation rather than more radiation alone, chemotherapy alone, or no medical treatment, though all chemoradiation in this study was given per the 6-week Stupp protocol (32). These geriatric screening tools and assessments are also useful for identifying baseline nutrition, mobility, and other functional vulnerabilities that may benefit from early intervention and perhaps even prevent functional decline during RT as well (34).

CONCLUSIONS

In this retrospective single-institution study of 62 GBM patients ≥70 years old who initiated adjuvant RT, median OS was 12.3 months. Age, KPS, MGMT methylation, and RT discontinuation were

significantly associated with OS on multivariate analysis, while extent of maximal resection, use of standard or hypofractionated RT, and GTV size were not. Future investigation into factors associated with RT discontinuation and survival may help guide clinical decision-making on RT dose-fractionation and supportive care.

DATA AVAILABILITY STATEMENT

The raw data supporting the conclusions of this article will be made available by the authors, without undue reservation.

ETHICS STATEMENT

The studies involving human participants were reviewed and approved by Duke University Medical Center Institutional Review Board. Written informed consent for participation was not required for this study in accordance with the national legislation and the institutional requirements.

AUTHOR CONTRIBUTIONS

JL: data collection, data analysis, and writing. JK: supervision. FM: formal data analysis. JH: formal data analysis. EL: data curation. AD: supervision. DR: supervision. HF: supervision. DA: supervision. KP: conceptualization, supervision, and project administration. MJ: data collection, writing, conceptualization, and supervision. All authors contributed to the article and approved the submitted version.

ACKNOWLEDGMENTS

The authors would like to thank Wendy Gentry for assistance with editing and submission of this manuscript.

REFERENCES

1. Ostrom QT, Gittleman H, Truitt G, Boscia A, Kruchko C, Barnholtz-Sloan JS. CBTRUS Statistical Report: Primary Brain and Other Central Nervous System Tumors Diagnosed in the United States in 2011-2015. *Neuro-oncology* (2018) 20(suppl_4):iv1–iv86. doi: 10.1093/neuonc/noy131
2. Stupp R, Mason WP, van den Bent MJ, Weller M, Fisher B, Taphoorn MJ, et al. Radiotherapy plus concomitant and adjuvant temozolomide for glioblastoma. *N Engl J Med* (2005) 352(10):987–96. doi: 10.1056/NEJMoa043330
3. Barker FG,2, Chang SM, Larson DA, Sneed PK, Wara WM, Wilson CB, et al. Age and radiation response in glioblastoma multiforme. *Neurosurgery* (2001) 49(6):1288–97; discussion 97-8. doi: 10.1097/00006123-200112000-00002
4. Kita D, Ciernik IF, Vaccarella S, Franceschi S, Kleihues P, Lutolf UM, et al. Age as a predictive factor in glioblastomas: population-based study. *Neuroepidemiology* (2009) 33(1):17–22. doi: 10.1159/000210017
5. Lutterbach J, Bartelt S, Momm F, Becker G, Frommhold H, Ostertag C. Is older age associated with a worse prognosis due to different patterns of care? A long-term study of 1346 patients with glioblastomas or brain metastases. *Cancer* (2005) 103(6):1234–44. doi: 10.1002/cncr.20895
6. Roa W, Brasher PMA, Bauman G, Anthes M, Bruera E, Chan A, et al. Abbreviated Course of Radiation Therapy in Older Patients With Glioblastoma Multiforme: A Prospective Randomized Clinical Trial. *J Clin Oncol* (2004) 22(9):1583–8. doi: 10.1200/JCO.2004.06.082
7. Malmstrom A, Gronberg BH, Marosi C, Stupp R, Frappaz D, Schultz H, et al. Temozolomide versus standard 6-week radiotherapy versus hypofractionated radiotherapy in patients older than 60 years with glioblastoma: the Nordic randomised, phase 3 trial. *Lancet Oncol* (2012) 13(9):916–26. doi: 10.1016/S1470-2045(12)70265-6
8. Wick W, Platten M, Meisner C, Felsberg J, Tabatabai G, Simon M, et al. Temozolomide chemotherapy alone versus radiotherapy alone for malignant astrocytoma in the elderly: the NOA-08 randomised, phase 3 trial. *Lancet Oncol* (2012) 13(7):707–15. doi: 10.1016/S1470-2045(12)70164-X
9. Perry JR, Laperriere N, O'Callaghan CJ, Brandes AA, Menten J, Phillips C, et al. Short-Course Radiation plus Temozolomide in Elderly Patients with Glioblastoma. *New Engl J Med* (2017) 376(11):1027–37. doi: 10.1056/NEJMoa1611977
10. National Comprehensive Cancer Network Inc. *NCCN Clinical Practice Guidelines in Oncology (NCCN Guidelines®) for Central Nervous System Cancers 2020 [V.1.2020]*. Available at: https://www.nccn.org/professionals/physician_gls/default.aspx.
11. Palmer JD, Bhamidipati D, Mehta M, Williams NL, Dicker AP, Werner-Wasik M, et al. Treatment recommendations for elderly patients with newly diagnosed glioblastoma lack worldwide consensus. *J Neurooncol* (2018) 140(2):421–6. doi: 10.1007/s11060-018-2969-3
12. Lorimer CF, Saran F, Chalmers AJ, Brock J. Glioblastoma in the elderly - How do we choose who to treat? *J Geriatr Oncol* (2016) 7(6):453–6. doi: 10.1016/j.jgo.2016.07.005
13. Glaser SM, Dohopolski MJ, Balasubramani GK, Flickinger JC, Beriwal S. Glioblastoma multiforme (GBM) in the elderly: initial treatment strategy and overall survival. *J Neurooncol* (2017) 134(1):107–18. doi: 10.1007/s11060-017-2493-x
14. Bingham B, Patel CG, Shinohara ET, Attia A. Utilization of hypofractionated radiotherapy in treatment of glioblastoma multiforme in elderly patients not receiving adjuvant chemoradiotherapy: A National Cancer Database Analysis. *J Neurooncol* (2018) 136(2):385–94. doi: 10.1007/s11060-017-2665-8
15. Haque W, Verma V, Butler EB, Teh BS. Patterns of Care and Outcomes of Hypofractionated Chemoradiation Versus Conventionally Fractionated Chemoradiation for Glioblastoma in the Elderly Population. *Am J Clin Oncol* (2018) 41(2):167–72. doi: 10.1097/COC.0000000000000417
16. Nead KT, Swisher-McClure S. Utilization of hypofractionated radiation therapy in older glioblastoma patients. *J Geriatr Oncol* (2019) 10(1):155–8. doi: 10.1016/j.jgo.2018.06.006
17. Mak KS, Agarwal A, Qureshi MM, Truong MT. Hypofractionated short-course radiotherapy in elderly patients with glioblastoma multiforme: an analysis of the National Cancer Database. *Cancer Med* (2017) 6(6):1192–200. doi: 10.1002/cam4.1070
18. Gilbert MR, Wang M, Aldape KD, Stupp R, Hegi ME, Jaeckle KA, et al. Dose-dense temozolomide for newly diagnosed glioblastoma: a randomized phase III clinical trial. *J Clin Oncol* (2013) 31(32):4085–91. doi: 10.1200/JCO.2013.49.6968
19. Cabrera AR, Kirkpatrick JP, Fiveash JB, Shih HA, Koay EJ, Lutz S, et al. Radiation therapy for glioblastoma: Executive summary of an American Society for Radiation Oncology Evidence-Based Clinical Practice Guideline. *Pract Radiat Oncol* (2016) 6(4):217–25. doi: 10.1016/j.prro.2016.03.007
20. Gilbert MR, Dignam JJ, Armstrong TS, Wefel JS, Blumenthal DT, Vogelbaum MA, et al. A randomized trial of bevacizumab for newly diagnosed

glioblastoma. *N Engl J Med* (2014) 370(8):699–708. doi: 10.1056/NEJMoa1308573
21. Chinot OL, Wick W, Mason W, Henriksson R, Saran F, Nishikawa R, et al. Bevacizumab plus radiotherapy-temozolomide for newly diagnosed glioblastoma. *N Engl J Med* (2014) 370(8):709–22. doi: 10.1056/NEJMoa1308345
22. Arvold ND, Tanguturi SK, Aizer AA, Wen PY, Reardon DA, Lee EQ, et al. Hypofractionated versus standard radiation therapy with or without temozolomide for older glioblastoma patients. *Int J Radiat Oncol Biol Phys* (2015) 92(2):384–9. doi: 10.1016/j.ijrobp.2015.01.017
23. Minniti G, Scaringi C, Lanzetta G, Terrenato I, Esposito V, Arcella A, et al. Standard (60 Gy) or short-course (40 Gy) irradiation plus concomitant and adjuvant temozolomide for elderly patients with glioblastoma: a propensity-matched analysis. *Int J Radiat Oncol Biol Phys* (2015) 91(1):109–15. doi: 10.1016/j.ijrobp.2014.09.013
24. Wang TJC, Wu CC, Jani A, Estrada J, Ung T, Chow DS, et al. Hypofractionated radiation therapy versus standard fractionated radiation therapy with concurrent temozolomide in elderly patients with newly diagnosed glioblastoma. *Pract Radiat Oncol* (2016) 6(5):306–14. doi: 10.1016/j.prro.2015.12.001
25. Biau J, Chautard E, De Schlichting E, Dupic G, Pereira B, Fogli A, et al. Radiotherapy plus temozolomide in elderly patients with glioblastoma: a "real-life" report. *Radiat Oncol* (2017) 12(1):197. doi: 10.1186/s13014-017-0929-2
26. Harris G, Jayamanne D, Wheeler H, Gzell C, Kastelan M, Schembri G, et al. Survival Outcomes of Elderly Patients With Glioblastoma Multiforme in Their 75th Year or Older Treated With Adjuvant Therapy. *Int J Radiat Oncol Biol Phys* (2017) 98(4):802–10. doi: 10.1016/j.ijrobp.2017.02.028
27. Lapointe S, Florescu M, Simonyan D, Michaud K. Impact of standard care on elderly glioblastoma patients. *Neurooncol Pract* (2017) 4(1):4–14. doi: 10.1093/nop/npw011
28. Chang-Halpenny CN, Yeh J, Lien WW. Elderly patients with glioblastoma multiforme treated with concurrent temozolomide and standard- versus abbreviated-course radiotherapy. *Perm J* (2015) 19(1):15–20. doi: 10.7812/TPP/14-083
29. Lombardi G, Pace A, Pasqualetti F, Rizzato S, Faedi M, Anghileri E, et al. Predictors of survival and effect of short (40 Gy) or standard-course (60 Gy) irradiation plus concomitant temozolomide in elderly patients with glioblastoma: a multicenter retrospective study of AINO (Italian Association of Neuro-Oncology). *J Neurooncol* (2015) 125(2):359–67. doi: 10.1007/s11060-015-1923-x
30. Lu VM, Kerezoudis P, Brown DA, Burns TC, Quinones-Hinojosa A, Chaichana KL. Hypofractionated versus standard radiation therapy in combination with temozolomide for glioblastoma in the elderly: a meta-analysis. *J Neurooncol* (2019) 143(2):177–85. doi: 10.1007/s11060-019-03155-6
31. Roa W, Kepka L, Kumar N, Sinaika V, Matiello J, Lomidze D, et al. International Atomic Energy Agency Randomized Phase III Study of Radiation Therapy in Elderly and/or Frail Patients With Newly Diagnosed Glioblastoma Multiforme. *J Clin Oncol* (2015) 33(35):4145–50. doi: 10.1200/JCO.2015.62.6606
32. Deluche E, Leobon S, Lamarche F, Tubiana-Mathieu N. First validation of the G-8 geriatric screening tool in older patients with glioblastoma. *J Geriatr Oncol* (2019) 10(1):159–63. doi: 10.1016/j.jgo.2018.07.002
33. Soubeyran P, Bellera C, Goyard J, Heitz D, Cure H, Rousselot H, et al. Screening for vulnerability in older cancer patients: the ONCODAGE Prospective Multicenter Cohort Study. *PloS One* (2014) 9(12):e115060. doi: 10.1371/journal.pone.0115060
34. Szumacher E, Sattar S, Neve M, Do K, Ayala AP, Gray M, et al. Use of Comprehensive Geriatric Assessment and Geriatric Screening for Older Adults in the Radiation Oncology Setting: A Systematic Review. *Clin Oncol (R Coll Radiol)* (2018) 30(9):578–88. doi: 10.1016/j.clon.2018.04.008

Conflict of Interest: JK reports grants from Varian Medical Systems, others from Clearsight RT Products, LLP, outside the submitted work. AD also receives research funding from Triphase Accelerator Corp., Orbus Therapeutics and Symphogen. AD serves as advisor/speaker/consultant for Istari Oncology and Orbus Therapeutics. AD holds stock/ownership interest with Istari Oncology. AD holds a letter of patent for Oncolytic Polio virus for the treatment of human tumors. HF received compensation for serving as Chief Medical Officer with Istari Oncology. HF holds stock/ownership interest with Istarti Oncology, Diverse Biotech, and Cancer Expert. HF serves as advisor/speaker/consultant for Cancer Expert. HF holds a letter of patent for Oncolytic Polio virus for the treatment of human tumors. KP receives research funding from Agios, BioMimetix, and Novocure. KP serves as advisor/speaker/consultant for Agios and Bayer.

The remaining authors declare that the research was conducted in the absence of any commercial or financial relationships that could be construed as a potential conflict of interest.

frontiers in Oncology

CASE REPORT
published: 26 February 2021
doi: 10.3389/fonc.2021.621289

Case Report: Adjuvant Radiotherapy Can Be an Effective Treatment for Intimal Sarcoma of the Heart

Anna Romanowska[1], *Ewa Lewicka*[2], *Grzegorz Sławiński*[2], *Hanna Jankowska*[3] *and Renata Zaucha*[4*]

[1] Department of Oncology and Radiotherapy, University Clinical Centre, Gdańsk, Poland, [2] Department of Cardiology and Electrotherapy, Medical University of Gdańsk, Gdańsk, Poland, [3] Department of Noninvasive Cardiac Diagnostics, Medical University of Gdańsk, Gdańsk, Poland, [4] Department of Oncology and Radiotherapy, Medical University of Gdańsk, Gdańsk, Poland

Intimal sarcoma of the heart is a sporadic disease, which involves symptoms of cardiac insufficiency due to a fast-growing intraluminal mass. Tumor resection is the first-line treatment, although its location precludes excision with wide uninvolved margins. Despite the aggressiveness of this neoplasm and a high risk of recurrence even after removal by microscopically radical surgery, no standard adjuvant therapy has been established. Chemotherapy is used either as an adjuvant treatment or in cases of advanced disease. In contrast, the use of radiotherapy is rare and usually considered in a palliative setting because the risk of radiation-induced heart disease after high-dose radiotherapy to the heart is significant. Herein, we present the cases of two patients, both diagnosed with cardiac intimal sarcoma, who received irradiation after tumor resection. In both cases, radiotherapy was effective, providing long-lasting local disease control. We regularly monitored cardiac function in both patients to assess the impact of radiotherapy on tumor-free heart structures. The excellent local control of the disease with only mild long-term cardiac dysfunction in both patients suggests that radiotherapy can be a useful treatment modality in this indication.

Keywords: cardiac intimal sarcomas, radiotherapy, radiation-induced heart disease, cardiac function analysis, heart radiation dose

OPEN ACCESS

Edited by:
Drexell Hunter Boggs, University of Alabama at Birmingham, United States

Reviewed by:
DeeDee Smart, Radiation Oncology Branch (NCI), United States
Shi Yu, Affiliated Hospital of Nantong University, China

***Correspondence:**
Renata Zaucha
rzaucha@gumed.edu.pl

Specialty section:
This article was submitted to Radiation Oncology, a section of the journal Frontiers in Oncology

Received: *25 October 2020*
Accepted: *22 January 2021*
Published: *26 February 2021*

Citation:
Romanowska A, Lewicka E, Sławiński G, Jankowska H and Zaucha R (2021) Case Report: Adjuvant Radiotherapy Can Be an Effective Treatment for Intimal Sarcoma of the Heart. Front. Oncol. 11:621289. doi: 10.3389/fonc.2021.621289

INTRODUCTION

The incidence of primary cardiac tumors ranges from 0.02% to 0.25% as reported in autopsy studies (1). Approximately 25% of them are malignant tumors, 75% of which are sarcomas. Cardiac intimal sarcoma (CIS), a type of undifferentiated sarcoma, is particularly rare (1). CIS is characterized by rapid aggressive intraluminal growth, symptoms of cardiac insufficiency, and the median survival of 1.5 months in untreated cases. Owing to the rarity of the disease, the standard of care has not been established (2). Given the lack of evidence-based treatment recommendations, any combination of complete tumor resection (including bench resection) with neo- or adjuvant chemotherapy (CTH) and, less commonly, radiotherapy (RTH) is the therapeutic strategy for localized primary cardiac sarcoma (3, 4).

The main concern associated with using RTH for heart sarcoma is the risk of radiation-induced heart disease (RIHD). Therefore, heart tolerance is usually the dose-limiting factor (3). Herein, we present the history of two patients with CIS admitted to the hospital because of the rapid development and progression of cardiac insufficiency symptoms. Initial echocardiography (ECHO) revealed cardiac tumor in each case. Combined treatment consisting of surgical excision and postoperative RTH was carefully followed with regular cardiac assessments. Since both patients achieved long-term survival, we were able to evaluate heart function changes in the context of radiation dose distribution. In both patients, RTH provided local control of the sarcoma with mild cardiac function impairment. Thus, we believe that RTH can be effective and tolerable in this indication.

CASE DESCRIPTION

Patient 1

A 47-year-old man was admitted to the University Clinical Center of the Medical University in Gdansk in December 2017 due to worsening exercise tolerance, leg swelling, dizziness, and fainting during physical activity. In October 2017, he was diagnosed with pulmonary embolism, for which he received oral anticoagulants (dabigatran), with short-term improvement. Otherwise, the patient's medical history was unremarkable. ECHO on admission revealed a tumor filling the right ventricle. The patient underwent an immediate surgical resection of the tumor followed by the reconstruction of the right ventricle (RV) with a BioIntegral patch (BioIntegral Surgical Inc., Mississauga, ON, Canada) and tricuspid annuloplasty using the De Vega technique.

Histopathological examination of the resected specimen confirmed CIS with microscopically positive surgical margins. Postoperatively, the patient presented with symptoms of cardiac insufficiency what excluded him from postoperative CTH. Instead, postoperative RTH was proposed to decrease the risk of recurrence after R1 resection. Computed tomography (CT) scanning for RTH planning performed just 7 weeks after the surgery revealed a recurrence in the RV wall. Therefore the patient received RTH with curative intent at a dose of 66 Gy in 30 fractions. Subsequent heart imaging with magnetic resonance (MR) and CT showed radiation-induced abnormalities with no evidence of local recurrence. At 32 months after the initial surgery, the patient was disease-free. He was diagnosed with a second malignancy during the follow-up period, which was radically resected and confirmed as renal clear cell carcinoma (stage pT1b according to TNM 8th edition) (5).

Patient 2

In September 2016, a 57-year-old man underwent surgical removal of a left atrium (LA) mass that resembled myxoma on ECHO, with pericardial patch reinforcement of the LA. The diagnosis was made after several months of dyspnea, decreasing exercise tolerance, and fainting. Histopathological examination led to the diagnosis of CIS, with microscopically positive resection margins. The patient's medical history was unremarkable, apart from well-controlled hypertension and hypercholesterolemia. His overall clinical status was good; therefore, adjuvant CTH consisting of four cycles of doxorubicin with dacarbazine was administered.

In December 2017, after the diagnosis of a local recurrence 9 months after the last CTH cycle, the patient underwent another surgery, during which tumor resection was incomplete. Due to the high risk of further progression, postoperative RTH at a total dose of 66 Gy in 30 fractions was administered, leading to complete remission of the LA tumor. After a year, the patient was diagnosed with a metastatic lesion in the retroperitoneal space. Radical resection of metastasis (in January 2019) was followed by the second-line CTH (gemcitabine and docetaxel).

TABLE 1 | Dose distribution among cardiac sub-volume and coronal artery categories and target volumes for both patients.

		Heart		
		Patient 1		**Patient 2**
V20		100%		58%
V30		95.7%		47.6%
V60		20%		2.5%
MHD		52.9 Gy		31.7 Gy
		Left atrium		
Dmax		62.4 Gy		67.5 Gy
Dmean		45.3 Gy		57.8 Gy
V30		80%		100%
		Right atrium		
Dmax		62.7 Gy		57.3 Gy
Dmean		50.3 Gy		27.4 Gy
V30		93.5%		34.5%
		Left ventricle		
Dmax		64 Gy		58.4 Gy
Dmean		53 Gy		39.1 Gy
V30		100%		73%
		Right ventricle		
Dmax		63.7 Gy		56.7 Gy
Dmean		59.5 Gy		14.8 Gy
V30		100%		3.5%
		LMCA		
Dmax		62.4 Gy		59.8 Gy
Dmean		60.4 Gy		56.8 Gy
		Cx		
Dmax		61.4 Gy		66.8 Gy
Dmean		60.4 Gy		60.8 Gy
		LADCA		
Dmax		62.4 Gy		59.6 Gy
Dmean		59.5 Gy		22.6 Gy
		RCA		
Dmax		62.5 Gy		37 Gy
Dmean		58.8 Gy		11.4 Gy
		Lung		
V5		80		64
V20		32.5		34
MLD		16.5		16.2
Volume (cm^3)	GTV	CTV	PTVboost	PTV
Patient 1	151.5	606.9	441.6	1246.9
Patient 2	3	210.9	35.3	466

CTV, clinical target volume; Cx, circumflex artery; Dmax and mean, maximal and mean dose adequately; GTV, gross tumor volume; LADCA, left anterior descending coronary artery; LMCA, left main coronary artery; MHD, mean heart dose; MLD, mean lung dose; PTV, planning target volume; RCA, right coronary artery; Vx, the volume of a structure receiving the dose of xGy.

In July 2019, due to further disease progression, the patient was offered oral pazopanib, which he continued for 47 months, achieving reasonable control of the disease.

Radiotherapy Details

RTH planning and treatment were conducted according to the institutional protocol of internal use. The treatment plan for Patient 2 with small residual mass was prepared using a 4-dimensional CT (4D-CT) scan. On the contrary, in Patient 1, 4D-CT did not add any benefit; therefore, we chose a conventional CT scan. Gross tumor volume (GTV) was contoured on the non-contrast-enhanced CT series fused with contrast-enhanced scans and preoperative imaging with the help of an experienced cardio-radiologist. The clinical target volume (CTV) encompassed the GTV with a 20-mm margin adjusted for anatomical structures and areas preoperatively involved by the tumor. Planning target volume (PTV) was created by adding an 8-mm isotropic expansion to CTV, and PTV-boost was created by adding 8-10-mm margin to GTV. The volumes of the target areas are summarized in **Table 1**. Organs at risk were contoured according to institutional and international guidelines (6, 7).

Treatment was planned using intensity-modulated radiation therapy with simultaneous integrated boost technique at a dose of 54 Gy for PTV and 66 Gy for PTV boost. Each RTH plan was evaluated by two medical physicists and two specialists in radiation oncology. The RTH plan for Patient 2 met institutional dose constraints. Patient 1 was informed about the high risk of RIHD due to heart dose violation; he accepted this therapy as his only treatment option. RTH was delivered using a linear accelerator (TrueBeam® SN1403 accelerator, Varian Medical Systems Inc., Palo Alto, California, United States).

We retrospectively contoured the heart sub-volumes, including the coronary arteries and heart chambers, following available atlases. Normal tissue radiation doses are summarized in **Table 1**. An example CT scan with dose distribution is presented in **Figures 1A, B**, respectively.

Cardiac Function

Patient 1

The first ECHO examination revealed a large tumor (82 mm × 63 mm) with irregular borders in the RV, filling the RV outflow tract, and penetrating the pulmonary artery with only the peripheral flow preserved. In addition, significant RV enlargement and impaired RV systolic function, right atrial (RA) enlargement, and severe tricuspid valve regurgitation were found (**Table 2**). The serum concentration of brain

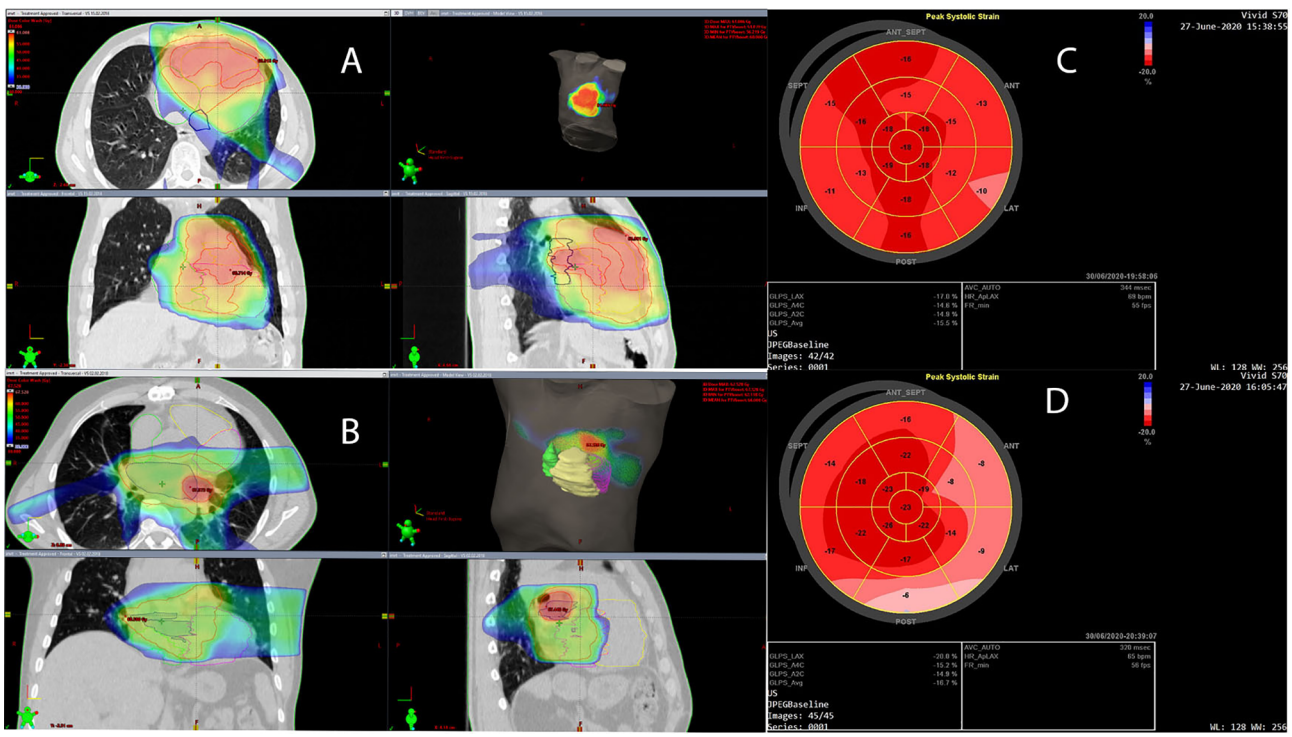

FIGURE 1 | **(A, B)** Dose distribution is presented in dose color wash starting from 30 Gy. Planning target volume (PTV) and PTV boost are indicated with red contours; the left atrium (LA) is indicated with dark blue, the left ventricle (LV) with magenta, the right atrium (RA) with green, and the right ventricle (RV) with yellow. **(C)** Left ventricular global longitudinal strain (GLS) is presented in the bull's-eye diagram obtained with two-dimensional speckle-tracking echocardiography (STE) 26 months after cardiac radiotherapy in a patient with RV intimal sarcoma. The average GLS is -15.5%, and the regional peak longitudinal strain reduction is seen in the basal and partially in the mid-ventricular anterior, lateral, and inferior segments, which may be the result of cardiac irradiation. **(D)** LV GLS in the bull's-eye diagram obtained with two-dimensional STE 27 months after cardiac radiotherapy in a patient with LA intimal sarcoma. The average GLS is -16.7%, however, regional peak longitudinal strain reduction is seen in the basal and partially in the mid-ventricular anterior, lateral, and posterior segments, which may be due to cardiac irradiation.

TABLE 2 | Cardiac dimensions and parameters describing left and right ventricular systolic function in transthoracic echocardiography and cardiac magnetic resonance imaging, and in a patient with right ventricular sarcoma.

Parameter	12.2017 before resection [TTE]	01.2018 after resection before RT [TTE]	01.2018 before RT [CMR]	04.2018 directly after RT [TTE]	06.2019 14 months after RT [TTE]	06.2020 26 months after RT [TTE]
Left atrial area (cm^2)	18	18	19	24	24	25
Right atrial area (cm^2)	41	33	30	27	26	25
LV end-systolic diameter (cm)	3.5	2.8	2.9	3.5	3.4	3.4
LV end-diastolic diameter (cm)	5.0	4.7	4.3	4.4	4.8	4.8
Interventricular septum (cm)	1.0	1.0	0.7	1.1	1.2	1.2
LV posterior wall (cm)	0.6	0.8	0.9	1.0	1.2	1.2
LV ejection fraction (%)	63	63	60	55	45	50
LV GLS (%)	nd	nd	nd	-17.4	-16	-15.5
RVOT (cm)	3.8	4.7	nd	3.8	3.7	3.8
RVID (cm)	5.3	5.0	5.5	5.0	4.9	5.0
TAPSE (mm)	9	7	9	12	10	8
S'RV (cm/s)	6	6	7	8	6	4
TR V_{max} (m/s)	4.0	nd	nd	2.2	1.9	1.9

CMR, cardiac magnetic resonance imaging; GLS, global longitudinal strain; LV, left ventricular; nd, no data; RT, radiotherapy; RV, right ventricular; RVID, RV diastolic diameter at the base in the apical 4-chamber view; RVOT, proximal RV outflow tract diameter in the parasternal long-axis view; S'RV, tricuspid annulus systolic velocity in tissue Doppler; TAPSE, tricuspid annular plane systolic excursion; TR, tricuspid regurgitation jet maximum velocity; TTE, transthoracic echocardiography.

natriuretic peptide (BNP) was 1165 pg/ml. CT angiography excluded pulmonary embolism. Coronary angiography showed no changes in the coronary arteries. After surgical excision within macroscopically healthy borders of the tumor filling the entire RV, the RV defect was closed using a BioIntegral patch. Concurrently, de Vega annuloplasty for tricuspid regurgitation was performed. The patient received bisoprolol 5 mg daily (QD), torasemide 20 mg QD, eplerenone 25 mg QD, and prophylactic dose of enoxaparin QD. After cardiac RTH (March–April 2018), ECHO, CT, and cardiac magnetic resonance (CMR) imaging showed normal left ventricular (LV) size and function, but RV and RA enlargement persisted. RV systolic function was severely impaired after surgery (**Table 2**), with concentric RV hypertrophy (up to 9 mm). The patient was clinically stable and fully ambulatory. Six months thereafter, RTH pharmacotherapy was modified as follows: ramipril 2.5 mg QD, atorvastatin 40 mg QD, bisoprolol dose was increased to 10 mg QD, rivaroxaban was added, and eplerenone and torasemide were discontinued. Electrocardiography (ECG) showed sinus rhythm and right bundle branch block (RBBB) without other abnormalities. Follow-up ECHO (**Table 3**) (26 months after RTH) showed the enlargement of the RV (5.0 cm), LA (25 cm^2), RA (25 cm^2), and mild RV free wall hypertrophy (8 mm). Global LV systolic function was mildly reduced, with LV ejection fraction (LVEF) of 50%, and LV global longitudinal strain (LV GLS) of -15.5% (values <16% considered abnormal). In addition, the hypokinesis of the LV anteroseptal segments was noticed. Analysis of the mitral inflow parameters and pulsed tissue Doppler early diastolic velocities showed preserved LV diastolic function. RV systolic function remained significantly impaired, as indicated by a decrease in the tricuspid annular plane systolic excursion (TAPSE) of 8 mm (norm: >19 mm) and low tricuspid annulus systolic velocity in tissue Doppler (S'RV) of 5 cm/s (norm: >9.5 cm/s). As shown in **Figure 1C**, the bull's eye diagram of LV GLS demonstrates a significantly reduced peak longitudinal strain in the basal and partially in the mid-ventricular segments. Laboratory tests revealed the normal concentration of high-sensitivity cardiac troponin I and BNP elevated to 942 pg/ml. Thus, the administration of torasemide 20 mg and eplerenone 25 mg was resumed.

Patient 2

The first ECHO revealed a 43x28-mm tumor originating in the posterior wall of the LA and infiltrating the posterior part of the mitral annulus. LA and RV were mildly enlarged; otherwise, there were no abnormalities; BNP level was normal and coronary angiography did not show any abnormalities. The patient was discharged with prescribed bisoprolol 2.5 mg QD, amlodipine 5 mg QD, and atorvastatin 40 mg QD, as before surgery. CMR performed 2 months post-surgical excision was clear from local recurrence. After 4 cycles of CTH, with a total doxorubicin dose of 600 mg, ECHO and CMR imaging showed normal LV size and function, and the persistence of RV enlargement, with maintained systolic function (normal RV ejection fraction, TAPSE, and S'RV) (**Table 3**). Ten months after the re-excision of local recurrence (December 2017), sinus rhythm and incomplete RBBB were detected on the ECG. The postoperative courses of RTH and CTH, consisting of five cycles of gemcitabine (800 mg/m^2) and docetaxel (60-75 mg/m^2), administered at distant recurrence, were uneventful. Subsequently (May 2019), the patient developed paroxysmal atrial tachycardia (PAT), requiring electrical cardioversion to restore sinus rhythm. A complete RBBB was recorded on the ECG. Pharmacologic therapy was changed; bisoprolol dose was increased to 5 mg QD, and perindopril 5

TABLE 3 | Cardiac dimensions and parameters describing left and right ventricular systolic function in transthoracic echocardiography and cardiac magnetic resonance imaging and in a patient with left atrial sarcoma.

Parameter	9.2016 before resection TTE	11.2016 after resection before ADIC [CMR]	4.2017 after ADIC [CMR]	1.2018 after recurrent resection CMR	6.2018 3 months after RT [CMR]	1.2019 TTE	5.2019 after 3rd cycle of GDXL [TTE]	6.2020 27 months after RT pazopanib TTE
Left atrial area (cm^2)	25	23	24	24	25	21	22	23
Right atrial area (cm^2)	nd	26.5	28	25	28	nd	27	20
LV end-systolic diameter (cm)	3.0	2.9	2.8	3.1	3.2	3.4	3.5	4.0
LV end-diastolic diameter (cm)	5.4	5.5	5.3	5.4	5.5	5.4	5.7	5.8
Interventricular septum (cm)	1.1	1.0	1.1	1.1	1.2	1.1	1.2	1.1
LV posterior wall (cm)	1.1	0.9	0.9	0.9	0.9	1.1	1.0	0.9
LV ejection fraction (%)	55	61	54	54	55	57	53	50
RVOT (cm)	3.6	3.2	3.4	3.3	3.4	3.5	4.5	4.0
RVID (cm)	nd	5.1	5.3	5.4	5.1	4.4	4.4	4.5
RV ejection fraction (%)	nd	59	52	52	nd	nd	nd	nd
TR V_{max} (m/s)	nd	nd	nd	nd	nd	3.1	3.2	2.3
RVSP (mmHg)	nd	nd	nd	nd	nd	40	45	24
TAPSE (mm)	nd	nd	nd	nd	Nd	21	17	21
S'RV (cm/s)	nd	nd	nd	nd	nd	nd	12	14

ADIC, chemotherapy with doxorubicin and dacarbazine; CMR, cardiac magnetic resonance imaging; GDXL, chemotherapy with gemcitabin and docetaxel; GLS, global longitudinal strain; LV, left ventricular; nd, no data; RT, radiotherapy; RV, right ventricular; RVID, RV diastolic diameter at the base in the apical 4-chamber view; RVOT, proximal RV outflow tract diameter in the parasternal long-axis view; S'RV, tricuspid annulus systolic velocity in tissue Doppler; TAPSE, tricuspid annular plane systolic excursion; TR, tricuspid regurgitation jet maximum velocity; TTE, transthoracic echocardiography.

mg QD was added. During therapy with pazopanib, amiodarone was added due to PAT exacerbation. The patient was free of local sarcoma recurrence and clinically stable, with only the slight worsening of exercise tolerance compared to the pre-disease period. ECHO at 45 months after the diagnosis of sarcoma (27 months after cardiac radiotherapy) showed persistent mild enlargement of the RV (4.5 cm), LA (23 cm^2), and RA (20 cm^2), mildly decreased LV systolic function (LVEF 50%), normal LV diastolic function, and preserved RV systolic function. Of note, LV GLS was -16.7%, and peak longitudinal strain was significantly reduced in the basal anterior, lateral, posterior, and (partially) in the mid-ventricular segments (**Figure 1D**). Laboratory tests were within acceptable limits.

DISCUSSION

In large cohort studies, patients with primary cardiac sarcomas constitute a heterogeneous group that includes a variety of subtypes and primary locations of sarcomas. As primary cardiac sarcomas are rare and treated with a variety of modalities, any retrospective analyses of the impact of either CTH or RTH on outcomes are precluded. In the French Sarcoma Group Study, in which 24 of 124 enrolled patients received radiation, adding RTH was associated with improved progression-free survival (3). Wu et al. reported that among five patients who received postoperative irradiation alone or in combination with chemotherapy, four and one achieved partial and complete remission, respectively (8). There was a trend toward better overall survival in patients receiving any postoperative treatment. In another study, RTH in the dose range of 40–60 Gy was administered to 12 patients with primary cardiac sarcoma. Three of them achieved disease-free survival of 4, 5, and 93 months, respectively (9). However, none of the patients included in these studies was diagnosed with CIS, of which there are only a few case reports involving RTH use (2, 10). While studies on RTH efficacy in CIS are scarce, those on toxicity, especially late effects, remain unavailable.

Herein, we report on two patients with CIS treated with RTH and undergoing regular cardiological control. Based on scarce retrospective reports, the prognosis of patients with primary cardiac sarcoma is dismal, with median overall survival (OS) about 17 months (about 38 months after complete resection, 18 months after incomplete resection, and less than a year in non-resected patients) (3, 4, 8). In our two patients (one with incompletely resected local recurrence and the other with incompletely resected primary tumor), the follow-up period was longer than the expected overall survival—39.5 and 26.5 months since diagnosis and cardiac irradiation, respectively. RTH effectively prevented local recurrence and was well tolerated without acute toxicity symptoms. At the last control visit both patients were in a good general condition, with no early or late RTH-related cardiac complications (e.g. acute pericarditis) despite exceeding the institutional dose constraints for the heart in one of them.

As expected, both patients showed a gradual but slow worsening of LV systolic function (LVEF 50%). STE revealed a significantly reduced LV peak longitudinal strain in the basal and partially mid-ventricular segments, with only mildly reduced global LV strain. The reduction in LV peak longitudinal strain developed within the highest radiation dose (>50 Gy) area. LV diastolic function remained normal. RV enlargement was observed after cardiac surgery, but RV systolic function was normal in the patient with LA sarcoma. In Patient 1, RV systolic function was significantly reduced before surgery, likely due to cancer infiltration and the history of pulmonary embolism. In addition, surgery was more extensive in this patient, and the postsurgical RV defect required the use of a pericardial patch. The regional peak longitudinal strain impairment in the region of the highest RTH dose resembled that seen in Patient 2. However, in this case, the effect of RTH on RV function was unclear. We noted RV hypertrophy in this patient, which could be the result of radiation-related myocardial fibrosis or the sign of compensatory RV remodeling. We did not observe pericardial complications (including pericardial thickening) in either of our patients; however, both patients developed RBBB.

Most previous studies on RIHD involved patients treated with RTH for hematological malignancies or breast cancer; however, no data on the effects of irradiation of the heart sub-volumes have been published to date. It has been shown that radiation causes long-term tissue changes. In the early phase, ionization leads to inflammatory changes with extravasations, edema, and thrombotic state (11–13). This inflammatory phase subsides to a latent fibrotic phase, which is characterized by capillary damage due to endothelial injury, thrombotic lesions and, in the case of the heart, myocardial fibrosis (11–13). The late clinical manifestations of RTH adverse effects include coronary obstruction and premature ischemic heart disease, valvular stenosis and regurgitation, and pericardial and myocardial fibrosis, leading to the constriction and thickening of the LV wall with subsequent diastolic dysfunction as well as conduction abnormalities (14, 15).

Previous studies have shown that the volume of the heart receiving >30 Gy, the mean heart dose of >20 Gy, and the dose per fraction of >2 Gy, is associated with an increased risk of cardiovascular complications (14–17). Meanwhile, it has been shown in breast cancer patients that the risk of major coronary events increases by 7.4% per 1 Gy increase of the mean heart dose, suggesting that the dose-toxicity relationship is continuous without a clearly defined threshold (18). The classic QUANTEC analysis established dose constraints for breast cancer patients with V25 Gy of <10% (dose per fraction = 2 Gy), corresponding to the risk of cardiac mortality of <1%, assessed 15 years post-RTH. The authors also reported the mean pericardium dose of >26 Gy and V30 >46% as risk factors for pericarditis (15). At our institution, we use heart dose constrains of V40 <50% and V60 <25% for chest irradiation other than breast.

LV strain changes after RTH have been previously described; however, their prognostic impact remains unclear (19). Some authors suggest that the decrease in LV GLS persisting 3 years after RTH may indicate permanent LV damage as a result of the fibrotic process (20). The latency period for developing RIHD appears shorter than that reported in previous studies (10–15 years) (21), as 44% of major coronary events attributed to RTH were observed in less than 10 years after irradiation (18).

One of the RIHD manifestations is RV wall thickening, which is considered a late complication (observed at least 5 years after thorax irradiation) (22). Findings on RV systolic function in patients treated with RTH are conflicting (23). It has been shown that the results of TAPSE or S'RV may be falsely underestimated due to geometric rather than structural changes after cardiac surgery (24). Moreover, it has been reported that after RTH, the RV dimension remains unchanged (25, 26). Raina et al. (19) suggested that the larger transverse dimensions of RV (but not RV length) in patients after cardiac surgery may be due to the more spherical shape of RV after surgery. This can explain RV enlargement in one of our patients.

CONCLUSION

RTH might be a feasible treatment for cardiac sarcoma, as it is highly effective and relatively safe even at high doses delivered to the heart. However, it remains associated with the risk of RIHD. Due to high-dose radiation delivered directly to the heart, we anticipate that both our patients develop RIHD earlier than suggested by the literature. Therefore, both patients remain under onco-cardiological supervision. Periodic control and transthoracic examinations with modern ECHO techniques (including STE) and CMR continue in both patients.

DATA AVAILABILITY STATEMENT

The original contributions presented in the study are included in the article/supplementary material. Further inquiries can be directed to the corresponding author.

ETHICS STATEMENT

Ethical review and approval were not required for the retrospective study on human participants in accordance with the local legislation and institutional requirements. The patients/participants provided their written informed consent to participate in this study. Written informed consent was obtained from the individual(s) for the publication of any potentially identifiable images or data included in this article.

AUTHOR CONTRIBUTIONS

Research concept and design—AR and RZ. Data collection—AR, HJ, EL, and GS. Data analysis and interpretation—all authors. Writing the first draft of the manuscript—AR. Writing the section on cardiac function—EL and GS. Critical revision of the article—RZ. Final approval of article—all authors. All authors contributed to the article and approved the submitted version.

REFERENCES

1. Raphael KL, Martinez AP, Clements SD, Isiadinso I. Role of multimodal cardiac imaging in diagnosing a primary intimal sarcoma of the left atrial appendage. *Tex Heart Inst J* (2019) 46:28–31. doi: 10.14503/THIJ-16-5896
2. Barmpas A, Giannakidis D, Fyntanidou V, Koulouris C, Mantalobas S, Pavlidis E, et al. Intimal sarcoma of the pulmonary artery, a diagnostic enigma. *AME Case Rep* (2019) 3:32. doi: 10.21037/acr.2019.07.02
3. Isambert N, Ray-Coquard I, Italiano A, Rios M, Kerbrat P, Gauthier M, et al. Primary cardiac sarcomas: a retrospective study of the French Sarcoma Group. *Eur J Cancer* (2014) 50:128–36. doi: 10.1016/j.ejca.2013.09.012
4. Randhawa JS, Budd GT, Randhawa M, Ahluwalia M, Jia X, Daw H, et al. Primary cardiac sarcoma: 25-year Cleveland Clinic experience. *Am J Clin Oncol* (2016) 39:593–9. doi: 10.1097/COC.0000000000000106
5. Amin MB, Edge S, Greene F, Byrd DR, Brookland RK, Washington MK, et al. *AJCC Cancer Staging Manual. 8th edition*. American Joint Commission on Cancer: Springer International Publishing (2017).
6. Kong FM, Ritter T, Quint DJ, Senan S, Gaspar LE, Komaki R, et al. Consideration of dose limits for organs at risk of thoracic radiotherapy: atlas for lung, proximal bronchial tree, esophagus, spinal cord, ribs, and brachial plexus. *Int J Radiat Oncol Biol Phys* (2011) 81(5):1442–57. doi: 10.1016/j.ijrobp.2010.07.1977
7. Feng M, Moran JM, Koelling T, Chughtai A, Chan JL, Freedman L, et al. Development and validation of a heart atlas to study cardiac exposure to radiation following treatment for breast cancer. *Int J Radiat Oncol Biol Phys* (2011) 79(1):10–8. doi: 10.1016/j.ijrobp.2009.10.058
8. Wu Y, Million L, Moding EJ, Scott G, Berry M, Ganjoo KN. The impact of postoperative therapy on primary cardiac sarcoma. *J Thorac Cardiovasc Surg* (2018) 156:2194–203. doi: 10.1016/j.jtcvs.2018.04.127
9. Thariat J, Clément-Colmou K, Vogin G, Beckendorf V, Ducassou A, Ali A, et al. Radiation therapy of cardiac sarcomas. *Cancer Radiother* (2014) 18:125–31. doi: 10.1016/j.canrad.2014.02.003
10. Drożdż J, Warchoł E, Fijuth J, Filipiak K, Spych M, Maciejewski M, et al. Primary pulmonary artery sarcoma in 36-year-old women: 3-years follow-up after partial resection and radiotherapy. *Kardiol Pol* (2013) 71:858–60. doi: 10.5603/KP.2013.0201
11. Liu LK, Ouyang W, Zhao X, Su S, Yang Y, Ding WJ, et al. Pathogenesis and prevention of radiation-induced myocardial fibrosis. *Asian Pac J Cancer Prev* (2017) 18(3):583–7. doi: 10.22034/APJCP.2017.18.3.583
12. John Yarnold J, Brotons M-C. Pathogenetic mechanisms in radiation fibrosis. *Radiother Oncol* (2010) 97:149–61. doi: 10.1016/j.radonc.2010.09.002
13. Straub JM, New J, Hamilton CD, Lominska C, Shnayder Y, Thomas SM. Radiation-induced fibrosis: mechanisms and implications for therapy. *J Cancer Res Clin Oncol* (2015) 141:1985–94. doi: 10.1007/s00432-015-1974-6
14. Nabiałek-Trojanowska I, Lewicka E, Wrona A, Kaleta AM, Lewicka-Potocka Z, Raczak G, et al. Cardiovascular complications after radiotherapy. *Cardiol J* (2020) 27(6):836–47. doi: 10.5603/CJ.a2018.0120
15. Gagliardi G, Constine LS, Moiseenko V, Correa C, Pierce LJ, Allen AM, et al. Radiation dose-volume effects in the heart. *Int J Radiat Oncol Biol Phys* (2010) 76:S77–85. doi: 10.1016/j.ijrobp.2009.04.093
16. Wang K, Eblan MJ, Deal AM, Lipner M, Zagar TM, Wang Y, et al. Cardiac toxicity after radiotherapy for stage III non–small-cell lung cancer: pooled analysis of dose-escalation trials delivering 70 to 90 Gy. *J Clin Oncol* (2017) 35:1387–94. doi: 10.1200/JCO.2016.70.0229
17. Yegya-Raman N, Wang K, Kim S, Reyhan M, Deek MP, Sayan M, et al. Dosimetric predictors of symptomatic cardiac events after conventional-dose chemoradiation therapy for inoperable NSCLC. *J Thorac Oncol* (2018) 13:1508–18. doi: 10.1016/j.jtho.2018.05.028
18. Darby SC, Ewertz M, McGale P, Bennet AM, Blom-Goldman U, Brønnum D, et al. Risk of ischemic heart disease in women after radiotherapy for breast cancer. *N Engl J Med* (2013) 14368(11):987–98. doi: 10.1056/NEJMoa1209825
19. Raina A, Vaidya A, Gertz ZM, Chambers S, Forfia PR. Marked changes in right ventricular contractile pattern after cardiothoracic surgery: implications for post-surgical assessment of right ventricular function. *J Heart Lung Transplant* (2013) 32:777–83. doi: 10.1016/j.healun.2013.05.004
20. Guerra F, Marchesini M, Contadini D, Menditto A, Morelli M, Piccolo E, et al. Speckle-tracking global longitudinal strain as an early predictor of cardiotoxicity in breast carcinoma. *Support Care Cancer* (2016) 24:3139–45. doi: 10.1007/s00520-016-3137-y
21. Tuohinen SS, Skytta T, Huhtala H, Virtanen V, Kellokumpu-Lehtinen PL, Raatikainen P. Left ventricular speckle tracking echocardiography changes among early-stage breast cancer patients three years after radiotherapy. *Anticancer Res* (2019) 39:4227–36. doi: 10.21873/anticanres.13584
22. Benveniste MF, Gomez D, Carter BW, Betancourt Cuellar SL, Shroff GS, Benveniste APA, et al. Recognizing Radiation Therapy-related Complications in the Chest. *Radiographics* (2019) 39(2):344–66. doi: 10.1148/rg.2019180061
23. Tadic M, Cuspidi C, Hering D, Venneri L, Grozdic-Milojevic I. Radiotherapy-induced right ventricular remodelling: The missing piece of the puzzle. *Arch Cardiovasc Dis* (2017) 110:116–23. doi: 10.1016/j.acvd.2016.10.003
24. Zanobini M, Saccocci M, Tamborini G, Veglia F, Di Minno A, Poggio P, et al. Postoperative Echocardiographic Reduction of Right Ventricular Function: Is Pericardial Opening Modality the Main Culprit? *BioMed Res Int* (2017) 2017:4808757. doi: 10.1155/2017/4808757
25. Tuohinen SS, Skyttä T, Virtanen V, Luukkaala T, Kellokumpu-Lehtinen PL, Raatikainen P. Early effects of adjuvant breast cancer radiotherapy on right ventricular systolic and diastolic function. *Anticancer Res* (2015) 35:2141–7. doi: 10.1093/eurheartj/eht308.P1185
26. Tuohinen SS, Skyttä T, Virtanen V, Virtanen M, Luukkaala T, Kellokumpu-Lehtinen P-L, et al. Detection of radiotherapy-induced myocardial changes by ultrasound tissue characterisation in patients with breast cancer. *Int J Cardiovasc Imaging* (2016) 32:767–6. doi: 10.1007/s10554-016-0837-9

Conflict of Interest: The authors declare that the research was conducted in the absence of any commercial or financial relationships that could be construed as a potential conflict of interest.

frontiers in Oncology

ORIGINAL RESEARCH
published: 11 March 2021
doi: 10.3389/fonc.2021.617439

Outcomes After Accelerated Partial Breast Irradiation in Women With Triple Negative Subtype and Other "High Risk" Variables Categorized as Cautionary in The ASTRO Guidelines

*Anabel Goulding[1], Lina Asmar[2], Yunfei Wang[2], Shannon Tole[1], Lora Barke[3], Jodi Widner[4] and Charles Leonard[1]**

[1] Radiation Oncology, Rocky Mountain Cancer Centers, Denver, CO, United States, [2] Statistics, Linasmar Consulting, Houston, TX, United States, [3] Radiology, Invision Sally Jobe, Greenwood Village, CO, United States, [4] Surgery, SurgOne, Greenwood Village, CO, United States

OPEN ACCESS

Edited by:
Jaroslaw T. Hepel, Rhode Island Hospital, United States

Reviewed by:
Vivek Verma, Allegheny General Hospital, United States
Diane Ling, University of Southern California, United States

***Correspondence:**
Charles Leonard
charles.leonard@usoncology.com

Specialty section:
This article was submitted to Radiation Oncology, a section of the journal Frontiers in Oncology

Received: *14 October 2020*
Accepted: *01 February 2021*
Published: *11 March 2021*

Citation:
Goulding A, Asmar L, Wang Y, Tole S, Barke L, Widner J and Leonard C (2021) Outcomes After Accelerated Partial Breast Irradiation in Women With Triple Negative Subtype and Other "High Risk" Variables Categorized as Cautionary in The ASTRO Guidelines. Front. Oncol. 11:617439. doi: 10.3389/fonc.2021.617439

Purpose: To report a primary objective clinical outcome of ipsilateral breast recurrence following accelerated partial breast irradiation (APBI) in women with triple negative and other high risk breast cancer (as described in 2017 ASTRO guidelines) (i.e., age 40–49, size 2.1–3.0 cm, estrogen receptor negative and invasive lobular breast cancer). Secondary objectives of axillary and regional failure as well as overall survival are also reported.

Methods and Material: Patients from two clinical trials (NCT01185145, NCT01185132) were treated with 38.5 Gy IMRT or 3D-CRT APBI w/3.85 Gy fraction/BID fractionation for 10 fractions. Triple negative and other high risk patients (n=269) were compared to a total of 478 low risk patients which ASTRO defined as "suitable" for APBI. High risk patients, for the purpose of this study, were defined as those who possess one or more high risk criteria: triple negative (n=30), tumor size >2 cm <3 cm (n=50), HER 2+ (n=54), age range 40–50 years (n=120), ER- (n=43), and ILC histology (n=52).

Results: Median follow up was 4.0 years for all patients. No significant difference was found for this high-risk cohort at 5 years for ipsilateral breast, or regional recurrences. Axillary recurrence was significantly adversely impacted by triple negative and ER- statuses (p=0.01, p=0.04). There were significant correlations between triple negative type and axillary recurrence on multivariate analysis (p=0.03). Overall survival for all patients was unaffected by any of the high-risk categories.

Conclusion: The data from this study suggests that women possessing high risk features are at no more meaningful risk for recurrence than other patients considered to be acceptable for APBI treatment. However, the finding of axillary recurrence in patients with triple negative breast cancer does warrant a degree of caution in proceeding with accelerated partial breast irradiation technique in this patient group.

Keywords: young age group, infiltrating lobular breast cancer, HER2 breast cancer +, estrogen receptor negative breast cancer, triple negative breast cancer, partial breast external beam radiotherapy

INTRODUCTION

Accelerated partial breast radiotherapy (APBI) recently has been widely accepted as an alternative breast radiotherapy option for the post-lumpectomy adjuvant management of breast cancer. APBI has the benefit of shortened treatment time and reduced radiation exposure to surrounding tissues when compared to whole breast irradiation (WBI).

Contemporary external beam and brachytherapy APBI reports, including those of the authors, have reported that local control rates in certain early-stage invasive breast cancer patients may be comparable to those treated with standard whole breast (1–4). Optimal treatment outcomes of APBI are contingent upon proper patient selection.

The American Society of Radiation Oncology (ASTRO) has previously issued guidelines for patient categorization into "suitable", "cautionary", and "unsuitable" groups (2). Currently, these guidelines were revised to expand the suitable category to include characteristics previously felt to be cautionary (3). The GEC-ESTRO Brachytherapy Committee have also published recommended APBI clinical guidelines. These guidelines state that APBI could be offered as standard therapy to eligible patients >50 years of age who have T1 invasive ductal carcinoma with a minimum of 2 mm margins (4). The National Comprehensive Cancer Network (NCCN) panel accepts the updated 2016 version of the ASTRO APBI guideline, which now defines patients "suitable" for APBI to be the following: 1) 50 years or older with invasive ductal carcinoma (IDCA) measuring ≤2 cm (T1 disease) with negative margin widths of ≥2 mm, no lymphvascular invasion, estrogen receptor (ER) positive, and BRCA 1/2 negative or 2) screening-detected ductal carcinoma *in situ* (DCIS) with low/intermediate nuclear grade, and tumor size measuring ≤2.5 cm with negative margin widths of ≥3 mm (1).

The cautionary group of patient characteristics now includes: age 40–49, size of 2.1–3 cm, estrogen receptor negative, and invasive lobular histology (according to ASTRO). There have been only a few reports which document the APBI experience with this cautionary subgroup of patients and these pertain nearly exclusively to brachytherapy techniques (5–13).

This is a retrospective analysis of a total of 269 patients with high risk characteristics, including triple negative, who have been enrolled into two separate accelerated partial breast trials, prospective phase II (NCT01185145) and phase III (NCT01185132) clinical trials. Historically, reports have been divided in the outcomes of these patients. There are whole breast radiotherapy reports which state that the local/ipsilateral breast control in patients with triple negative breast cancer are significantly lower than patients without triple negative or basal type tumors (14–19). There were similar conclusions in young patients (20–31) and in patients with infiltrating lobular histologies (32–34) and HER2/neu positive cancers (15–17, 25, 35) which show higher recurrence rates than in older patients with non- lobular or HER2/neu positive tumors. In contrast, other reports utilizing external beam/brachytherapy irradiation have not observed any worse loco-regional recurrence outcomes in patients with triple negative/basal type of breast cancer (36–41), young age (42–44) or infiltrating lobular histologies (45–51) when compared to older patients with non- lobular or HER2/neu positive tumors.

METHODS

A total of 747 patients enrolled in two accelerated partial breast protocols were used in this analysis. Eligibility for both trials were very similar and included patients with clinically unifocal invasive breast cancer which measured up to 3 cm in size. Patient characteristics are in **Table 1** and protocol eligibility requirements including a minimum of ≥2 mm margins and treatment guidelines have been previously reported (52, 53). High risk patients, for the purpose of this study, were defined as those who possess one or more high risk criteria: triple negative (n=30), tumor size ≥2 cm ≤3 cm (n=50), HER2 + (n=54), age range 40-50 years (n=120), ER- (n=43), and ILC histology (n=52). Data collection did not include variables such as limited/focal lymph vascular invasion (LVI) or extensive intraductal component (EIC). **Table 2** also delineates an analysis of shared high risk characteristics. Clinical outcomes of ipsilateral breast, axillary, and combined regional recurrences (ipsilateral or axillary) (RR), and overall survival (OS) were analyzed and compared in each high-risk cohort.

TABLE 1 | Patient characteristics.

Characteristic	All patients
Age at diagnosis (*y*), mean (SD)	62 average (11.0)
Median (range)	62 (37–96)
Menopausal status at study entry, *n (%)*	
Pre/Perimenopausal	148 (19.8%)
Postmenopausal	599 (80.2%)
Primary histology, *n (%)*	
Invasive ductal carcinoma	691 (92.5%)
Invasive lobular carcinoma	52 (7.0%)
Invasive mammary carcinoma	4 (0.5%)
Margin size (cm)	
Median (Range)	0.7 (0–3.0)
Estrogen receptor status (*n*)	
Positive	702 (93.4%)
Negative	43 (5.8%)
Unknown	2 (0.2%)
HER2/neu status (*n*)	
Positive	54 (7.2%)
Negative	683 (91.4%)
Unknown	10 (1.3%)
ER negative and HER2 negative (*n*)	32 (4.3%)
T stage (*n*)	
T1mic	14 (1.9%)
T1a	92 (12.3%)
T1b	332(44.4%)
T1c	279 (37.4)
T2	30 (4%)
N stage (*n*)	
N0	728 (97.5%)
N0(i+)	19 (2.5%)
Bilateral breast MRI prior to enrollment (*n*)	632 (87.1%)

TABLE 2 | Actuarial 5-year overall survival, ipsilateral breast recurrence-free survival (RFS), axillary RFS, and regional (breast and axillary) RFS.

VARIABLE		5-year OS (%)	p	IPSILATERAL BREAST RFS (%)	p	AXILLARY RFS (%)	p	REGIONAL RFS (%)	p
HISTOLOGY	ILCA	88.9	0.14	100	0.45	97.5	0.07	97.5	0.75
	IDCA/IMC	95.8		98		99.7		97.7	
AGE	< 50	96.6	0.1	97	0.28	100	0.45	97	0.55
	>50	95.2		98.3		99.5		97.8	
TRIPLE NEGATIVE	YES	84.3	0.16	100	0.34	96.7	0.01	96.7	0.93
	NO	95.9		97.9		99.7		97.6	
HER2/NEU	NEGATIVE	95.3	0.88	97.9	0.45	99.5	0.64	97.4	0.38
	POSITIVE	95.8		100		100		100	
SIZE	<2 cm	95.9	0.11	98.2	0.56	99.5	0.66	97.7	0.77
	≥2 cm	87.4		95.8		100		95.8	
ER	NEGATIVE	87.5	0.29	100	0.3	97.5	0.04	97.5	0.94
	POSITIVE	96		97.9		99.7		97.6	

Statistical Analyses

Continuous variables were presented as mean with standard deviation and median with ranges. Categorical variables were expressed as counts with percentages. Kaplan-Meier method with log-rank test was used to estimate the overall survival and the recurrence-free survivals. Univariate and multivariable Cox regression models, which including variables of age, histology, tumor size, and hormone receptor status, were performed to evaluate risk factors associated with death and recurrences.

In addition to the main analysis, we performed a sub-analysis matching the recurrent patients with non-recurrent ones. Variables used for matching were age, histology, tumor size and hormone receptor status. For each sub-analysis, we matched variables for patients with and without recurrences and analyzed one risk factor which was not matched. SAS version 9.4 (SAS Institute, Cary, NC, USA) was used for all statistical analyses.

RESULTS

There were 269 patients in the high-risk study group which also includes 30 patients with triple negative subtype breast cancer. High-risk/triple negative patients were compared against a total of 478 patients. Median follow up was 4.0 years for all patients. Of all high- risk patients/triple negative, 70 patients had two or more high-risk characteristics. **Table 3** shows that no significant overall survival, ipsilateral breast or regional relapse-free survival differences were found for this high-risk cohort at 5 years as compared to low risk patients. There were also no significant differences for ipsilateral breast, axillary or regional (ipsilateral breast *or* axillary) recurrences in the infiltrating lobular, age ≤50, HER2/neu positive or tumor size ≥2 cm between cohorts. However, the triple negative subtype was found to significantly adversely impact axillary recurrence. Other "high risk" variables such as the ER negative subtypes were also found to significantly adversely impact axillary recurrence.

On univariate analysis, triple negative status was also associated with decreased axillary recurrence-free survival (p=0.051) (**Table 3**). The multivariate analysis in **Table 4** depicts the only significant correlations which were between triple negative type and decreased axillary recurrence-free survival (p=0.03).

Matched Pair Analysis

The matched pair analysis is shown in **Table 5**. The only significant difference between the high and low risk APBI cohorts was for axillary recurrence free survival and overall survival for ER – patients (p=0.03, p=0.013). There were no significant differences in the remaining high risk cohorts for overall survival, ipsilateral breast recurrence-free, axillary recurrence- free, or regional recurrence-free survival outcomes.

DISCUSSION

The current guidelines from various organizations are not firmly based on APBI data which document that ipsilateral breast tumor recurrences (IBTR) are higher among certain subsets of

TABLE 3 | Univariate analysis.

VARIABLE		HR (95% CI) for 5-year survival	p	HR (95% CI) for IPSILATERAL BREAST recurrence	p	HR (95% CI) for AXILLARY RECURRENCE	p	HR (95% CI) for REGIONAL RECURRENCE	p
HISTOLOGY	ILCA v IDCA/IMC	2.156 (0.756, 6.147)	0.15	N/A*	N/A*	6.88 (0.62,75.84)	0.12	1.39 (0.18,10.78)	0.75
AGE	≤ 50 v >50	0.315 (0.075, 1.319)	0.11	2.07 (0.53, 8.10)	0.3	N/A*	N/A*	1.47 (0.40, 5.40)	0.56
TRIPLE NEGATIVE	YES v NO	2.137 (0.726, 6.286)	0.17	N/A*	N/A*	10.95 (0.99,120.8)	0.05	1.10 (0.13, 9.17)	0.93
HER2/NEU	NEGATIVE v POSITIVE	1.120 (0.267, 4.702)	0.88	N/A*	N/A*	N/A*	N/A*	N/A*	N/A*
SIZE	<2 cm v ≥2 cm	2.300 (0.806, 6.559)	0.12	1.83 (0.23,14.56)	0.6	N/A*	N/A*	1.36 (0.18,10.47)	0.77
ER	NEGATIVE v POSITIVE	0.567 (0.194, 1.653)	0.3	N/A*	N/A*	0.12 (0.01, 1.36)	0.08	1.09 (0.13, 8.84)	0.94

**Due to a lack of any events p-values are not generated.*

TABLE 4 | Multivariate analysis.

VARIABLE		HR (95% CI) for 5-year survival	p	HR (95% CI) for IPSILATERAL BREAST recurrence	p	HR (95% CI) for AXILLARY RECURRENCE	p	HR (95% CI) for REGIONAL RECURRENCE	p
HISTOLOGY	ILCA v IDCA/IMC	2.25 (0.78, 6.47)	0.13	N/A*	N/A*	13.09 (0.82,209.3)	0.07	1.48 (0.19,11.62)	0.71
AGE	< 50 v >50	0.33 (0.08, 1.38)	0.13	2.07 (0.53, 8.10)	0.26	N/A*	N/A*	1.53 (0.41, 5.71)	0.52
TRIPLE NEGATIVE	YES v NO	2.38 (0.78, 7.22)	0.13	N/A*	N/A*	20.35 (1.27,325.4)	0.03	1.07 (0.13, 9.13)	0.95
SIZE	<2 cm v ≥2 cm	1.87 (0.65, 5.43)	0.25	1.83 (0.23,14.56)	0.46	N/A*	N/A*	1.43 (0.18,11.31)	0.74

*Due to a lack of any events p-values are not generated.

TABLE 5 | Matched pair analysis.

VARIABLE	MATCHED PAIR	OS p-value	Ipsilateral Breast RFS p-value	Axillary RFS p-value	REGIONAL RFS p-value
ER -	1:5	0.01	0.37	0.03	0.81
HER2/neu	1:5	0.62	0.41	N/A*	0.41
LOBULAR HISTOLOGY	1:5	0.15	0.37	0.2	0.99
TRIPLE NEGATIVE	1:5	0.57	0.15	0.24	0.54
SIZE	1:5	0.33	0.16	N/A*	0.16
AGE	1:5	0.17	0.21	0.54	0.38

*Due to a lack of any events p-values are not generated.

patients including those with triple negative tumors. Rather, these groupings represent a conservative approach to patient APBI eligibility due to available contradicting data. The authors do recognize that these guidelines are for the use of APBI outside of clinical trial and are updated to reflect new research findings to provide continuing direction for the use of APBI. One can even find a lack of consistency between the ASTRO and GESTRO consensus guideline statements, including tumor size and estrogen receptor status (2, 4).

As well, the publication of other reports would suggest that the standard use of APBI might extend beyond the scope of these recommended patient groups.

Current reports have been relatively inconsistent in identifying particular variables which may impact ipsilateral breast tumor recurrence and have had inconsistent findings in other aspects of regional/distant control. As discussed previously, accelerated partial breast radiotherapy can be administered with brachytherapy as well as external beam radiotherapy (3-dimensional, intensity modulated and proton techniques). Several reports document the APBI brachytherapy experience with patients who are categorized in the "cautionary" and/or "unsuitable" poor prognostic variables (5–13). A combined Mammosite Registry and William Beaumont experience with partial breast brachytherapy reported that there were no significant differences in ipsilateral breast failures in the unsuitable cohort versus the "suitable" or "cautionary" cohorts (4.6% versus 2.5% and 3.3% respectively; p=0.2). However, age (<50 vs ≥50) as well as estrogen receptor status (negative versus positive) were significant factors for ipsilateral breast failures (7).

The University of Wisconsin published findings in patients with "high" risk/cautionary features (17, 18). On univariate analysis, both ER negative receptor status and lobular histology were significantly associated with ipsilateral breast failure (p= 0.002 and 0.0004, respectively). Multivariate analysis, however, failed to identify any cautionary feature associated with breast failure. William Beaumont Hospital did not find any significant differences in local breast failure across "suitable", "cautionary", or "unsuitable" subgroups in 199 APBI patients when compared to a matched cohort of 199 whole breast patients after a median follow-up of 9 and 13 years for the two groups respectively (10). Univariate analysis of APBI patients did not result in any variable which was significantly associated with ipsilateral breast recurrence. However, as noted in our study, regional nodal failure was significantly associated with ER negative receptor status and positive nodal status in the APBI cohort.

Several other accelerated partial breast irradiation reports found that negative estrogen receptor status could result in a higher ipsilateral breast recurrence and/or distant failure (6, 12, 13).

Studies examining the efficacy of WBI on high risk patients have reported similarly inconsistent results as APBI studies in identifying suitable characteristics for treatment (14, 15, 26, 28, 34, 36, 43, 44). Just as in the case of APBI data, these WBI studies have had equivocal conclusions and, as a whole, have not consistently agreed on all exclusion/inclusion criteria for APBI patients.

While continued, supporting data is needed, the comparability in study outcomes of APBI vs WBI treatment suggests that high risk patients are at no more meaningful risk for recurrence when treated with APBI than WBI. The data reported here as well the other studies cited above suggest that APBI might also be used as a standard of care treatment for the cautionary group analyzed in this study.

The larger phase III trials which randomized APBI versus WBI have had varying but similar eligibility criteria (54–59). Generally, these trials have included patients age ≥40 except RTOG 0413 which included patients ≥18 and IMPORT-LOW which only allowed patients ≥50. None of these specifically excluded ER negative patients, HER2/neu positive patients and the Import Low and RAPID trials disallowed invasive lobular. However, infiltrating ductal comprised greater than 85% of the patient populations of these studies with RTOG 0413 stating 4% of their APBI cohort was infiltrating lobular. None of these studies disallowed ER negative patients but this population only was approximately 5%–8% (RTOG 0413 had 19% ER/PR negative patients) of their APBI cohort. Tumor size for the RAPID, IMPORT-LOW, and RTOG 0413 was ≤3 cm and was 2.5 cm and 2 cm for the Florence and Hungarian trials

respectively. Although HER2/neu positivity was not considered to an exclusion criterium in these trials, it has only been reported in the Florence (2.8%) and IMPORT-LOW trials (4%). At this time, however, there have been no data from these phase III studies which have driven any consensus toward definitive data-driven conclusions.

Limitations for this study include the sample size and the length of follow-up. Of all 747 patients that were enrolled in our clinical trials, 269 patients were defined as high risk for the purpose of this study. To our knowledge this is the largest study analyzing the use of APBI in high risk women. Further studies with increased sample sizes are needed for corroboration of the results presented. The median follow-up for this study is 4.0 years. Prior reports have shown that median times to ipsilateral breast relapse in patients with ASTRO defined cautionary characteristics such as triple negative, estrogen receptor negative and HER2/neu positive range from 3–4 years (32, 34, 60). Other studies have also reported median disease-free intervals of 2–3 years in this category (19, 61–63).

CONCLUSION

The data presented in this study shows that there should be continued reconsideration for inclusion of at least several high-risk variables such as estrogen receptor negative, triple negative, HER2/neu positive,/2–3 cm primary tumors, age 40–50 patients, and patients with infiltrating lobular tumors. Age, histology, and tumor size do not appear to affect favorable outcomes. However, although there is evidence to suggest that there should be continued caution for APBI patient selection of triple negative and estrogen receptor negative tumors, these differences may not be of any meaningful clinical differences whether WBI or APBI is utilized. Further studies and/or follow-up must be done to further corroborate whether these patients, especially those with triple negative disease, should be included or not as eligible for APBI.

DATA AVAILABILITY STATEMENT

The raw data supporting the conclusions of this article will be made available by the authors, without undue reservation.

ETHICS STATEMENT

The studies involving human participants were reviewed and approved by Western IRB. The patients/participants provided their written informed consent to participate in this study.

AUTHOR CONTRIBUTIONS

LA and YW provided statistical analysis and manuscript writing. AG, ST, and CL contributed to the data analysis and manuscript preparation. LB and JW contributed to the manuscript preparation. All authors contributed to the article and approved the submitted version.

REFERENCES

1. National Comprehensive Cancer Network. *Breast Cancer (Version 3.2020).* Available at: http://www.nccn.org/professionals/physician_gls/pdf/breast.pdf (Accessed May 7, 2020).
2. Smith BD, Arthur DW, Buchholz TA, Haffty BG, Hahn CA, Hardenbergh PH, et al. Accelerated Partial Breast Irradiation Consensus Statement for the American Society for Radiation Oncology (ASTRO). *Int J Radiat Oncol Biol Phys* (2009) 74:987–1001. doi: 10.1016/j.ijrobp.2009.02.031
3. Correa C, Harris EE, Leonardi MC, Smith BD, Taghian AG, Thompson AM, et al. Accelerated Partial Breast Irradiation: Executive summary for the update of an ASTRO Evidence-Based Consensus Statement. *Pract Radiat Oncol* (2017) 7:73–9. doi: 10.1016/j.prro.2016.09.007
4. Polgár C, Limbergen EV, Pötter R, Kovács G, Polo A, Lyczek J, et al. Patient selection for accelerated partial-breast irradiation (APBI) after breast-conserving surgery: Recommendations of the Groupe Européen de Curiethérapie-European Society for Therapeutic Radiology and Oncology (GEC-ESTRO) breast cancer working group based on clinical evidence (2009). *Radiotherapy and Oncology* (2010) 94(3):264–73. doi: 10.1016/j.ijrobp.2010.07.581
5. Mchaffie DR, Patel RR, Adkison JB, Das RK, Geye HM, Cannon GM. Outcomes after accelerated partial breast irradiation in patients with ASTRO consensus statement cautionary features. *Int J Radiat Oncol Biol Phys* (2011) 81(1):46–51. doi: 10.1016/j.ijrobp.2010.05.011
6. Christoudias MK, Collett AE, Stull TS, Gracely EJ, Frazier TG, Barrio AV. Are the American Society for Radiation Oncology Guidelines accurate predictors of recurrence in early stage breast cancer patients treated with balloon-based brachytherapy? *Int J Surg Oncol* (2013) 8:2013. doi: 10.1155/2013/829050
7. Wilkinson JB, Beitsch PD, Shah C, Arthur D, Haffty BG, Wazer DE, et al. Evaluation of current consensus statement recommendations for accelerated partial breast irradiation: a pooled analysis of William Beaumont Hospital and American Society of Breast SurgeonMammoSite Registry Trial Data. *Int J Radiat Oncol Biol Phys* (2012) 85:1179–85. doi: 10.1016/j.ijrobp.2012.10.010
8. Patel RR, Christensen ME, Hodge CW, Adkison JB, Das RK. Clinical outcomeanalysis in "high-risk" vs. "low-risk" patients eligible for national surgical adjuvant breast and bowel B- 39/radiation therapy oncology group 0413 trial: Five-year results. *Int J Radiat Oncol Biol Phys* (2008) 70:970–3. doi: 10.1016/j.ijrobp.2007.12.005
9. McHaffie DR, Patel RR, Adkison JB, Das RK, Geye HM, Cannon GM. Outcomes after accelerated partial breast irradiation in patients with ASTRO Consensus Statement cautionary features. *Int J Radiat Oncol Biol Phys* (2011) 81:46–51. doi: 10.1016/j.ijrobp.2010.05.011
10. Vicini F, Arthur D, Wazer D, Chen P, Mitchell C, Wallace M, et al. Limitations of the American Society of Therapeutic Radiology and Oncology Consensus Panel guidelines on the use of accelerated partial breast irradiation. *Int J Radiat Oncol Biol Phys* (2011) 79:977–84. doi: 10.1016/j.ijrobp.2009.12.047
11. Zauls AJ, Watkins JM, Wahlquist AE, Brackett C III, Aguero EG, Baker MK, et al. Outcomes in women treated with MammoSite brachytherapy or whole breast irradiation stratified by ASTRO accelerated partial breast irradiation consensus statement groups. *Int J Radiat Oncol Biol Phys* (2012) 82:21–9. doi: 10.1016/j.ijrobp.2010.08.034
12. Shaitelman S, Vicini F, Beitsch P, Haffty B, Keisch M, Lyden M. Five-year Outcome of Patients Classified Using the American Society for Radiation Oncology Consensus Statement Guidelines for the Application of Accelerated Partial Breast Irradiation. *Cancer* (2010) 116:4677–85. doi: 10.1002/cncr.25383

13. Stull TS, Goodwin MC, Gracely EJ, Chernick MR, Carella RJ, Frazier TG, et al. A single-institution review of accelerated partial breast irradiation in patients considered "cautionary" by the American Society for Radiation Oncology. *Ann Surg Oncol* (2012) 19:553–9. doi: 10.1245/s10434-011-1941-7
14. Solin LJ, Hwang WT, Vapiwala N. Outcome after breast conservation treatment with radiation for women with triple negative early stage invasive breast carcinoma. *Clin Breast Cancer* (2009) 9:96–100. doi: 10.3816/CBC.2009.n.018
15. Hattangadi-Gluth JA, Wo JY, Nguyen PL, Raad RF, Sreedhara M, Niemierko A, et al. Basal subtype of invasive breast canceris associated with a higher risk of true recurrence after conventional breast-conserving therapy. *Int J Radiat Oncol Biol Phys* (2012) 82(3):1185–91. doi: 10.1016/j.ijrobp.2011.02.061
16. Nguyen PL, Taghian AG, Katz MS, Niemierko A, Abi Raad RF, Boon WL, et al. Breast cancer subtype approximated by estrogen receptor, progesterone receptor, and HER-2 is associated with local and distant recurrence after breast-conserving therapy. *J Clin Oncol* (2008) 26(14):2373–8. doi: 10.1200/JCO.2007.14.4287
17. Chen J, Jiang P, Wang HJ, Zhang JY, Xu Y, Guo MH, et al. The efficacy of molecular subtyping in predicting postoperative recurrence in breast-conserving therapy: a 15-study meta-analysis. *World J Surg Oncol* (2014) 12 (1):212. doi: 10.1186/1477-7819-12-212
18. Zaky SS, Lund M, May KA, Godette KD, Beitler JJ, Holmes LR, et al. The negative effect of triple-negative breast cancer on outcome after breast-conserving therapy. *Ann Surg Oncol* (2011) 18(10):2858–65. doi: 10.1245/s10434-011-1669-4
19. Lowery AJ, Kell MR, Glynn RW, Kerin MJ, Sweeney KJ. Locoregional recurrence after breast cancer surgery: a systematic review by receptor phenotype. *Breast Cancer Res Treat* (2012) 133(3):831–41. doi: 10.1007/s10549-011-1891-6
20. Cèfaro GA, Genovesi D, Marchese R, Ursini LA, Cianchetti E, Ballone E, et al. Predictors of local recurrence after conservative surgery and whole-breast irradiation. *Breast Cancer Res Treat* (2006) 98(3):329–35. doi: 10.1007/s10549-006-9169-0
21. Voogd AC, Nielsen M, Peterse JL, Blichert-Toft M, Bartelink H, Overgaard M, et al. Danish Breast Cancer Cooperative Group and the Breast Cancer Cooperative Group of the European Organization for Research and Treatment of Cancer. Differences in risk factors for local and distant recurrence after breast-conserving therapy or mastectomy for stage I and II breast cancer: pooled results of two large European randomized trials. *J Clin Oncol* (2001) 19(6):1688–97. doi: 10.1200/JCO.2001.19.6.1688
22. Fourquet A, Campana F, Zafrani B, Mosseri V, Vielh P, Durand JC, et al. Prognostic factors of breast recurrence in the conservative management of early breast cancer: a 25-year follow-up. *Int J Radiat Oncol Biol Phys* (1989) 17 (4):719–25. doi: 10.1016/0360-3016(89)90057-6
23. Oh JL, Bonnen M, Outlaw ED, Schechter NR, Perkins GH, Strom EA, et al. The impact of young age on locoregional recurrence after doxorubicin-based breast conservation therapy in patients 40 years old or younger: How young is "young"? *Int J Radiat Oncol Biol Phys* (2006) 65(5):1345–52. doi: 10.1016/j.ijrobp.2006.03.028
24. Komoike Y, Akiyama F, Iino Y, Ikeda T, Akashi-Tanaka S, Ohsumi S, et al. Ipsilateral breast tumor recurrence (IBTR) after breast- conserving treatment for early breast cancer: risk factors and impact on distant metastases. *Cancer* (2006) 106(1):35–41. doi: 10.1002/cncr.21551
25. Livi L, Meattini I, Saieva C, Borghesi S, Scotti V, Petrucci A, et al. The impact of young age on breast cancer outcome. *Eur J Surg Oncol (EJSO)* (2010) 36 (7):639–45. doi: 10.1016/j.ejso.2010.05.016
26. Jobsen JJ, Van der Palen J, Meerwaldt JH. The impact of age on local control in women with pT1 breast cancer treated with conservative surgery and radiation therapy. *Eur J Cancer* (2001) 37(15):1820–7. doi: 10.1016/S0959-8049(01)00173-3
27. Recht A, Connolly JL, Schnitt SJ, Silver B, Rose MA, Love S, et al. The effect of young age on tumor recurrence in the treated breast after conservative surgery and radiotherapy. *Int J Radiat Oncol Biol Phys* (1988) 14(1):3–10. doi: 10.1016/0360-3016(88)90043-0
28. Vrieling C, Collette L, Fourquet A, Hoogenraad WJ, Horiot JC, Jager JJ, et al. Can patient-, treatment-and pathology-related characteristics explain the high local recurrence rate following breast-conserving therapy in young patients? *Eur J Cancer* (2003) 39(7):932–44. doi: 10.1016/S0959-8049(03)00123-0
29. Boyages J, Recht A, Connolly JL, Schnitt SJ, Gelman R, Kooy H, et al. Early breast cancer: predictors of breast recurrence for patients treated with conservative surgery and radiation therapy. *Radiother Oncol* (1990) 19 (1):29–41. doi: 10.1016/0167-8140(90)90163-Q
30. Harrold EV, Turner BC, Matloff ET, Pathare P, Beinfield M, McKhann C, et al. Local recurrence in the conservatively treated breast cancer patient: a correlation with age and family history. *Cancer J Sci Am* (1998) 4(5):302–7.
31. Dewar JA, Arriagada R, Benhamou S, Benhamou E, Bretel JJ, Pellae-Cosset B, et al. Local relapse and contralateral tumor rates in patients with breast cancer treated with conservative surgery and radiotherapy (Institut Gustave Roussy 1970–1982). *Cancer* (1995) 76(11):2260–5. doi: 10.1002/1097-0142(19951201)76:11<2260::AID-CNCR2820761113>3.0.CO;2-D
32. Mate TP, Carter D, Fischer DB, Hartman PV, McKhann C, Merino M, et al. A clinical and histopathologic analysis of the results of conservation surgery and radiation therapy in stage I and II breast carcinoma. *Cancer* (1986) 58 (9):1995–2002. doi: 10.1002/1097-0142(19861101)58:9<1995::AID-CNCR2820580907>3.0.CO;2-1
33. Du Toit RS, Locker AP, Elis IO, Elston CW, Blarney RW. Evaluation of the prognostic value of triple node biopsy in early breast cancer. *Br J Surg* (1990) 77(2):163–7. doi: 10.1002/bjs.1800770216
34. Livi L, Paiar F, Saieva C, Scoccianti S, Dicosmo D , Borghesi S, et al. Survival and breast relapse breast cancer after conserving in 3834 patients with T1-T2 surgery and adjuvant treatment. *Radiother Oncol* (2007) 82:287–93. doi: 10.1016/j.radonc.2006.11.009
35. Braunstein LZ, Taghian AG, Niemierko A, Salama L, Capuco A, Bellon JR, et al. Breast-cancer subtype, age, and lymph node status as predictors of local recurrence following breast-conserving therapy. *Breast Cancer Res Treat* (2017) Jan 1161(1):173–9. doi: 10.1007/s10549-016-4031-5
36. Freedman GM, Anderson PR, Li T, Nicolaou N. Locoregional recurrence of triple-negative breast cancer after breast-conserving surgery and radiation. *Cancer* (2009) 115(5):946–51. doi: 10.1002/cncr.24094
37. Zumsteg ZS, Morrow M, Arnold B, Zheng J, Zhang Z, Robson M, et al. Breast-conserving therapy achieves locoregional outcomes comparable to mastectomy in women with T1-2N0 triple-negative breast cancer. *Ann Surg Oncol* (2013) 20(11):3469–76. doi: 10.1245/s10434-013-3011-9
38. Adkins FC, Gonzalez-Angulo AM, Lei Xrnandez-Aya LF, Mittendorf EA, Litton JK, Wagner J, et al. Triple-negative breast cancer is not a contraindication for breast conservation. *Ann Surg Oncol* (2011) 18 (11):3164. doi: 10.1245/s10434-011-1920-z
39. Gangi A, Chung A, Mirocha J, Liou DZ, Leong T, Giuliano AE. Breast-conserving therapy for triple-negative breast cancer. *JAMA Surg* (2014) 149 (3):252–8. doi: 10.1001/jamasurg.2013.3037
40. Barbieri V, Sanpaolo P, Genovesi D. Prognostic impact of triple negative phenotype in conservatively treated breast cancer. *Breast J* (2011) 17(4):377–82. doi: 10.1111/j.1524-4741.2011.01100.x
41. Voduc KD, Cheang MC, Tyldesley S, Gelmon K, Nielsen TO, Kennecke H. Breast cancer subtypes and the risk of local and regional relapse. *J Clin Oncol* (2010) 28(10):1684–91. doi: 10.1200/JCO.2009.24.9284
42. Solin LJ, Fowble B, Schultz DJ, Goodman RL. Age as a prognostic factor for patients treated with definitive irradiation for early stage breast cancer. *Int J Radiat Oncol Biol Phys* (1989) 16(2):373–81. doi: 10.1016/0360-3016(89)90333-7
43. Fowble BL, Schultz DJ, Overmoyer B, Solin LJ, Fox K, Jardines L, et al. The influence of young age on outcome in early stage breast cancer. *Int J Radiat Oncol Biol Phys* (1994) 30(1):23–33. doi: 10.1016/0360-3016(94)90515-0
44. Elkhuizen PH, van de Vijver MJ, Hermans JO, Zonderland HM, van de Velde CJ, Leer JW. Local recurrence after breast-conserving therapy for invasive breast cancer: high incidence in young patients and association with poor survival. *Int J Radiat Oncol Biol Phys* (1998) 40(4):859–67. doi: 10.1016/S0360-3016(97)00917-6
45. Peiro G, Bornstein BA, Connolly JL, Gelman R, Hetelekidis S, Nixon AJ, et al. The influence of infiltrating lobular carcinoma on the outcome of patients treated with breast-conserving surgery and radiation therapy. *Breast Cancer Res Treat* (2000) 59(1):49–54. doi: 10.1023/A:1006384407690
46. Kurtz JM, Jacquemier J, Torhorst J, Spitalier JM, Amalric R, Hünig R, et al. Conservation therapy for breast cancers other than infiltrating ductal carcinoma. *Cancer* (1989) 63(8):1630–5. doi: 10.1002/1097-0142(19890415)63:8<1630::AID-CNCR2820630833>3.0.CO;2-U

47. Poen JC, Tran L, Juillard G, Selch MT, Giuliano A, Silverstein M, et al. Conservation therapy for invasive lobular carcinoma of the breast. *Cancer* (1992) 69(11):2789–95. doi: 10.1002/1097-0142(19920601)69:11<2789::AID-CNCR2820691126>3.0.CO;2-J
48. White JR, Gustafson GS, Wimbish K, Ingold JA, Lucas RJ, Levine AJ, et al. Conservative surgery and radiation therapy for infiltrating lobular carcinoma of the breast: The role of preoperative mammograms in guiding treatment. *Cancer* (1994) 74(2):640–7. doi: 10.1002/1097-0142(19940715)74:2<640::AID-CNCR2820740216>3.0.CO;2-V
49. Santiago RJ, Harris EE, Qin L, Hwang WT, Solin LJ. Similar long-term results of breast- conservation treatment for Stage I and II invasive lobular carcinoma compared with invasive ductal carcinoma of the breast: The University of Pennsylvania experience. *Cancer* (2005) 103(12):2447–54. doi: 10.1002/cncr.21071
50. Molland JG, Donnellan M, Janu NC, Carmalt HL, Kennedy CW, Gillett DJ. Infiltrating lobular carcinoma—a comparison of diagnosis, management and outcome with infiltrating duct carcinoma. *Breast* (2004) 13(5):389–96. doi: 10.1016/j.breast.2004.03.004
51. Salvadori B, Biganzoli E, Veronesi P, Saccozzi R, Rilkes F. Conservative surgery for infiltrating lobular breast carcinoma. *Br J Surg* (1997) 84 (1):106–9. doi: 10.1046/j.1365-2168.1997.02540.x
52. Lei RY, Leonard CE, Howell KT, Henkenberns PL, Johnson TK, Hobart TL, et al. Four-year clinical update from a prospective trial of accelerated partial breast intensity-modulated radiotherapy (APBIMRT). *Breast Cancer Res Treat* (2013) 140(1):119–33. doi: 10.1007/s10549-013-2623-x
53. Leonard C, Carter D, Kercher J, Howell K, Henkenberns P, Tallhamer M, et al. Prospective trial of accelerated partial breast intensity-modulated radiotherapy. *Int J Radiat Oncol Biol Phys* (2007) 67(5):1291–8. doi: 10.1016/j.ijrobp.2006.11.016
54. Polgár C, Fodor J, Major T, Sulyok Z, Kásler M. Breast-conserving therapy with partial or whole breast irradiation: ten-year results of the Budapest randomized trial. *Radiother Oncol* (2013) 108(2):197–202. doi: 10.1016/j.radonc.2013.05.008
55. Vicini FA, Cecchini RS, White JR, Arthur DW, Julian TB, Rabinovitch RA, et al. Long-term primary results of accelerated partial breast irradiation after breast-conserving surgery for early-stage breast cancer: a randomised, phase 3, equivalence trial. *Lancet* (2019) 394(10215):2155–64. doi: 10.1016/S0140-6736(19)32514-0
56. Whelan TJ, Julian JA, Berrang TS, Kim DH, Germain I, Nichol AM, et al. External beam accelerated partial breast irradiation versus whole breast irradiation after breast conserving surgery in women with ductal carcinoma in situ and node-negative breast cancer (RAPID): a randomised controlled trial. *Lancet* (2019) 394(10215):2165–72. doi; 10.1016/S0140-6736(19)32515-2
57. Meattini I, Marrazzo L, Saieva C, Desideri I, Scotti V, Simontacchi G, et al. Accelerated partial-breast irradiation compared with whole-breast irradiation for early breast cancer: Long-term results of the randomized phase III APBI-IMRT-Florence trial. *J Clin Oncol* (2020) 38(35):4175–83. doi: 10.1200/JCO.20.00650
58. Coles CE, Griffin CL, Kirby AM, Titley J, Agrawal RK, Alhasso A, et al. Partial-breast radiotherapy after breast conservation surgery for patients with early breast cancer (UK IMPORT LOW trial): 5-year results from a multicentre, randomised, controlled, phase 3, non-inferiority trial. *Lancet* (2017) 390(10099):1048–60. doi: 10.1016/S0140-6736(17)31145-5
59. Strnad V, Ott OJ, Hildebrandt G, Kauer-Dorner D, Knauerhase H, Major T, et al. 5-year results of accelerated partial breast irradiation using sole interstitial multicatheter brachytherapy versus whole-breast irradiation with boost after breast-conserving surgery for low-risk invasive and in-situ carcinoma of the female breast: a randomised, phase 3, non-inferiority trial. *Lancet* (2016) 387(10015):229–38. doi: 10.1016/S0140-6736(15)00471-7
60. Parikh RR, Housman D, Yang Q, Toppmeyer D, Wilson LD, Haffty BG. Prognostic value of triple-negative phenotype at the time of locally recurrent, conservatively treated breast 19 cancer. *Int J Radiat Oncol Biol Phys* (2008) 72 (4):1056–63. doi: 10.1016/j.ijrobp.2008.02.066
61. Gosset M, Hamy AS, Mallon P, Delomenie M, Mouttet D, Pierga JY, et al. Prognostic impact of time to ipsilateral breast tumor recurrence after breast conserving surgery. *PloS One* (2016) 11(8). doi: 10.1371/journal.pone.0159888
62. Wangchinda P, Ithimakin S. Factors that predict recurrence later than 5 years after initial treatment in operable breast cancer. *World J Surg Oncol* (2016) 14 (1):223. doi: 10.1186/s12957-016-0988-0
63. Chumsri S, Li Z, Serie DJ, Mashadi-Hossein A, Colon-Otero G, Song N, et al. Incidence of Late Relapses in Patients with HER2-Positive Breast Cancer Receiving Adjuvant Trastuzumab: Combined Analysis of NCCTG N9831 (Alliance) and NRG Oncology/NSABP B-31. *J Clin Oncol* (2019) 37(35):3425–35. doi: 10.1200/JCO.19.00443

Conflict of Interest: LA and ST were employed by Linasmar Consulting.

The remaining authors declare that the research was conducted in the absence of any commercial or financial relationships that could be construed as a potential conflict of interest.

frontiers in Oncology

ORIGINAL RESEARCH
published: 15 April 2021
doi: 10.3389/fonc.2021.619929

On the Importance of Individualized, Non-Coplanar Beam Configurations in Mediastinal Lymphoma Radiotherapy, Optimized With Automated Planning

Linda Rossi[*‡], *Patricia Cambraia Lopes*[†‡], *Joana Marques Leitão, Cecile Janus, Marjan van de Pol, Sebastiaan Breedveld, Joan Penninkhof and Ben JM Heijmen*

Department of Radiotherapy, Erasmus MC Cancer Institute, Rotterdam, Netherlands

OPEN ACCESS

Edited by:
John Varlotto, Marshall University, United States

Reviewed by:
Taoran Cui, Rutgers Cancer Institute of New Jersey, United States
Yang Sheng, Duke University Medical Center, United States

***Correspondence:**
Linda Rossi
l.rossi@erasmusmc.nl

[†]Present address:
Patricia Cambraia Lopes, HollandPTC, Delft, Netherlands

[‡]These authors have contributed equally to this work

Specialty section:
This article was submitted to Radiation Oncology, a section of the journal Frontiers in Oncology

Received: *21 October 2020*
Accepted: *09 March 2021*
Published: *15 April 2021*

Citation:
Rossi L, Cambraia Lopes P, Marques Leitão J, Janus C, van de Pol M, Breedveld S, Penninkhof J and Heijmen BJM (2021) On the Importance of Individualized, Non-Coplanar Beam Configurations in Mediastinal Lymphoma Radiotherapy, Optimized With Automated Planning. Front. Oncol. 11:619929. doi: 10.3389/fonc.2021.619929

Background and Purpose: Literature is non-conclusive regarding selection of beam configurations in radiotherapy for mediastinal lymphoma (ML) radiotherapy, and published studies are based on manual planning with its inherent limitations. In this study, coplanar and non-coplanar beam configurations were systematically compared, using a large number of automatically generated plans.

Material and Methods: An autoplanning workflow, including beam configuration optimization, was configured for young female ML patients. For each of 25 patients, 24 plans with different beam configurations were generated with autoplanning: 11 coplanar CP_x plans and 11 non-coplanar NCP_x plans with x = 5 to 15 IMRT beams with computer-optimized, patient-specific configurations, and the coplanar VMAT and non-coplanar Butterfly VMAT (B-VMAT) beam angle class solutions (600 plans in total).

Results: Autoplans compared favorably with manually generated, clinically delivered plans, ensuring that beam configuration comparisons were performed with high quality plans. There was no beam configuration approach that was best for all patients and all plan parameters. Overall there was a clear tendency towards higher plan quality with non-coplanar configurations (NCP_x≥12 and B-VMAT). NCP_x≥12 produced highly conformal plans with on average reduced high doses in lungs and patient and also a reduced heart Dmean, while B-VMAT resulted in reduced low-dose spread in lungs and left breast.

Conclusions: Non-coplanar beam configurations were favorable for young female mediastinal lymphoma patients, with patient-specific and plan-parameter-dependent dosimetric advantages of NCP_x≥12 and B-VMAT. Individualization of beam configuration approach, considering also the faster delivery of B-VMAT vs. NCP_x≥12, can importantly improve the treatments.

Keywords: automated multi-criterial planning (MCO), comparison, non-coplanar angle, VMAT versus IMRT, number of beams, mediastinal lymphoma, individualized beam angle optimization, personalized radiotherapy

INTRODUCTION

Patients treated with a combination of multi-agent chemotherapy and radiation for Hodgkin or non-Hodgkin lymphoma are mostly young at diagnosis. About 80% of these patients achieve long-term remission. Given the age at diagnosis and the favorable long-term prognosis, therapy-related late effects including secondary malignancies (1–7) and cardiovascular disease (8–12) have become increasingly important. In recent years, radiotherapy (RT) for lymphoma has evolved by considerably decreasing target volumes (from extended field to involved field to involved site or involved node) and radiation doses (from 40 to 30 Gy or even 20 Gy in selected cases). These factors contribute to a decrease in the risk of late toxicity (1, 6, 13–16).

Applied radiotherapy techniques have also evolved, with intensity modulated radiation therapy (IMRT) and volumetric modulated arc therapy (VMAT) emerging as alternatives to 3D conformal RT (3D-CRT). In this context, the typical low-dose bath of VMAT plans has been pointed at as a cause of concern, as it could increase the risk of secondary cancers relative to 3D-CRT (17). The low-dose bath in the lungs has also been associated with increased risk of radiation pneumonitis (18). Choice of beam arrangement may impact plan quality. This has been investigated in detail for 'butterfly' beam arrangements that can contain non-coplanar beams. In particular, the (non-coplanar) B-VMAT approach described by Fiandra et al. (19) has shown to reduce breast Dmean and V4Gy compared to VMAT, leading to similar calculated lower risks of secondary breast cancer as 3D-CRT (but risk of lung cancer relatively higher), as well as a lower risk of cardiac toxicity, in a group of patients with largely non-bulky disease, without axillary involvement (20). Voong et al. (21) observed a reduction in heart dose (but not in breast dose) by using five to seven IMRT beams (butterfly) with eventually one non-coplanar beam, relative to 3D-CRT in patients without bilateral axillary involvement. Proton therapy has also been proposed for further reductions of late toxicity in selected lymphoma patients (17, 22–25).

Current literature is non-conclusive regarding the optimal choice of RT treatment technique. The International Lymphoma Radiation Oncology Group (26) has benchmarked the best practice of 10 centers in 2013, showing that (i) the applied (photon) RT technique varied largely between institutions leading to large differences in the low-dose volumes, and (ii) in practice, difficult cases were often not planned according to the standard. The authors could not provide universal/consensus recommendations. Moreover, different authors pointed at the necessity for individualized selection of planning technique (19, 21, 27). This was in part attributed to the high heterogeneity in tumor location, shape, and size, as well as patient characteristics.

It is well known that manually generated treatment plans may suffer from inter-and intra-planner quality variations (28, 29). Moreover, finding optimal beam configurations with trial-and-error planning is extremely complex and time-consuming. On the other hand, the large anatomical variability in lymphoma patients (target size/shape and position) is a real challenge for development of a system for automated planning, where the aim is to generate a unique workflow that works well for all patients without further interactive fine-tuning of plans by a user. The issues with manual beam angle selection put heavy constraints on the number of beam configurations that were compared in published ML planning studies, and on the total number of included plans. To the best of our knowledge, in all published studies comparing beam configurations for treatment of lymphoma patients, beam angle class solutions (e.g., B-VMAT) were investigated, or beam angles were selected by planners, i.e. there was no patient-specific computer optimization of angles. So far, only the study by Clemente et al. (30) reported on autoplanning for lymphoma patients, but this did not include optimization of beam directions. Moreover, their workflow worked for OAR sparing, while there were limitations for PTV doses.

In this work, we used a large number of automatically generated plans for comparison of radiotherapy beam configurations for young females with ML. To this purpose, an automatic workflow for IMRT/VMAT plan generation, including integrated coplanar or non-coplanar beam angle and beam profile optimization for IMRT, was implemented and validated. The system was used to systematically compare plan quality differences between 24 coplanar and non-coplanar beam configuration approaches for 25 study patients.

MATERIALS AND METHODS

Patients and Clinical Protocol

The study was based on a database with contoured planning CT-scans and manually generated, clinically delivered plans (CLIN) of 26 previously treated female ML patients (21 Hodgkin lymphoma and 4 B cell non-Hodgkin lymphoma). As explained in detail below, one patient (patient 0) was excluded from population-based analyses, leaving 25 evaluable patients for such analyses (patients 1–25).

Visual inspection of planning CT-scans ensured a heterogeneous selection of anatomical presentations in the patient cohort (superior/inferior mediastinum, with/without involvement of supraclavicular or axillar nodes, bulky disease, complex anatomy; see **Figure B1 in Electronic Supplement B**). The median patient age was 27 (range, 19–50). The PTV volumes varied from 97 to 1654 cc (median 605 cc). The prescription dose was 30 Gy in 15 fractions, excluding the sequential boost applied for some patients (3 × 2 Gy), which was not considered in this study.

In clinical practice, dosimetric aims were largely based on published recommendations (11, 12, 18, 31, 32). At least 95% of the target (ideally 100%) had to be covered by 95% of the prescribed dose (V95% >95%), while respecting the PTV over- and under-dose criteria; V110% <1% and V<90% <5 cc (preferably <2 cc), respectively. OAR requirements were the following, where a preferred value is indicated in parentheses: breast Dmean <5 Gy (<2 Gy), heart Dmean <26 Gy (<10 Gy), lungs Dmean <15 Gy (<13.5 Gy), lungs V5Gy <55% (<50%), and lungs V20Gy <30%. None of the planning requirements was truly a hard constraint (except for PTV V95%), i.e., depending on patient anatomy, violations were sometimes accepted. The 60% isodose was clinically evaluated (visually, not

quantitatively), especially related to dose in the back/neck muscles. Five patients were treated with a coplanar partial-arc VMAT plan, and 20 patients were treated with a coplanar IMRT plan with, on average, 6.0 manually selected mediastinal beams (range, 4–8), mainly from (or close to) anterior and posterior directions (butterfly). For patients with neck involvement, one to four beams from (close to) lateral directions were added for neck irradiation only.

Automated Plan Generation

An automated planning workflow for young ML patients was developed following the clinical planning aims described above. The core of the system was Erasmus-iCycle, an in-house developed multi-criteria optimizer featuring integrated beam angle and profile optimization (33), coupled to a Monte Carlo dose calculation engine (34). Pareto-optimal plans with clinically favorable trade-offs between all treatment requirements were realized with the optimization protocol ['wish-list' (33),] reported and explained in **Electronic Supplement B**. All plans for all patients were automatically generated with the same wish-list without any manual fine-tuning.

For coplanar beam angle optimization (BAO), the candidate beam set consisted of 36 equiangular beams (0°, 10°, …, 350°). For non-coplanar BAO, beam candidates, defined by all combinations of beams with 10 degree separation from each other in all directions, were verified at the linac to exclude beams with (potential) collisions between the patient/couch and the gantry, ending up with a set of 194 candidate beam directions (including the 36 coplanar beams). The applied beam energy was 6 MV.

Compared Beam Configurations

For all 25 study patients, the following 24 autoplans were generated to systematically investigate the impact of beam angle configuration on plan quality (see also **Figure 1**):

a. CP_x: coplanar plans with x = 5–15 beams with computer-optimized, patient-specific directions.
b. NCP_x: non-coplanar plans with x = 5–15 beams with computer-optimized, patient-specific directions.
c. VMAT: IMRT plan with 21 coplanar equiangular beams, reproducing full-arc VMAT dose distribution (35).
d. B-VMAT: non-coplanar class solution, consisting of 20 IMRT beams equally spread in three 60° arcs, two centered at gantry angle = 0° and 180°, with couch 0° (with seven beams each arc, with 10° separation space) and one centered at gantry angle = 0° with couch = 90° (with six beams, with 10° separation space, excluding angle gantry 0° and couch 90°, already present in the anterior arc), mimicking the butterfly geometry described by Fiandra et al. (19).

Plan Evaluations and Comparisons

Plans were mainly evaluated and compared using PTV and OAR planning goals applied in clinical planning (above). On top of that we also reported on breast(s) V4Gy (19), PTV V107%, conformity index (CI, defined as patient V95%/PTV volume),

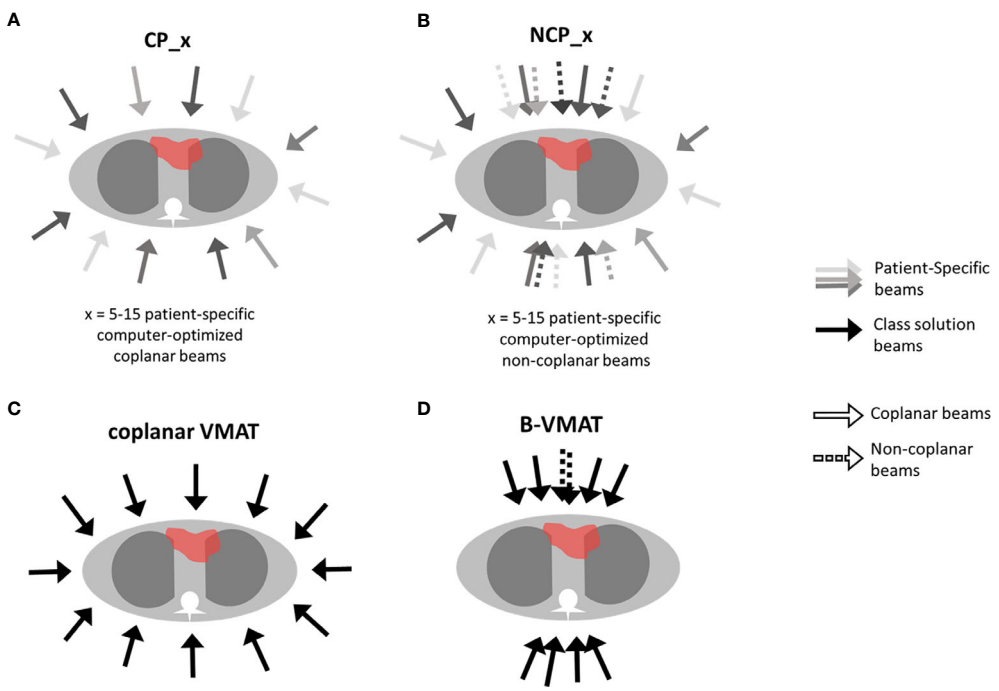

FIGURE 1 | Schematic representation of the investigated beam configurations: CP, coplanar **(A)**, NCP, non-coplanar **(B)**, coplanar VMAT **(C),** and B-VMAT, Butterfly-VMAT **(D)**.

and patient V5Gy (cc) and V20Gy (cc), where the patient is defined by the external skin structure. PTV V110%, mentioned in the clinical planning protocol, was always far below the requested 1%, and was therefore not reported. Two-sided Wilcoxon signed-rank tests were used for statistical analyses, with p-values lower than 0.05 indicating statistical significance in plan parameter differences.

RESULTS

Quality of Autoplans

Prior to the comparisons of beam angle configurations, several analyses were performed to ensure that the autoplans used for these comparisons were clinically acceptable and of high quality. Data is partly presented below, and partly in **Electronic Supplement A**.

From the 624 autoplans defined in the M&M section (24 plans for all 26 patients), 617 (98.9%) satisfied the clinical PTV coverage requirement, i.e. V95% ≥ 95%. The seven autoplans with insufficient PTV coverage were from the same patient (patient 0 in **Figure B1 in Electronic Supplement B**), all with relatively low numbers of coplanar beams (CP_5-11). In the IMRT plan used for treatment of this patient, sufficient PTV coverage was obtained at the cost of exceptionally high breast and heart doses: breast Dmean = 11.9/6.3 Gy left/right, and heart Dmean = 23.2 Gy (by far the highest in the group), all strongly exceeding clinical thresholds. The wish-list for autoplanning (**Table B1 in Electronic Supplement B**) was developed to balance OAR vs. PTV dose, which could result in too low PTV coverage to protect OARs. For 25/26 patients, all autoplans had sufficient coverage while also avoiding constraint violations. As indicated above, for patient 0, 17/24 plans had adequate coverage, the remaining seven had not. To avoid patient group analyses with unacceptable plans, patient 0 was not in such analyses in the remainder of the paper and the Electronic supplements, leaving 600 evaluable plans. The relevance of the proposed autoplanning workflow for patient 0 is further discussed in the Discussion section.

Automatically generated plans had overall favorable plan parameters compared to clinically delivered plans, generated with manual planning (**Table 1**, further analyses in **Electronic Supplement A, section A1**). **Table 1** compares mean autoplan parameters with the corresponding mean parameters for the CLIN plans. All averaged PTV dose parameters of the autoplans were favorable compared to those of the CLIN plans. The values for mean/minimum PTV coverage went up from 98.1%/95.0% to 99.5%/97.1%. A remarkable reduction in PTV V<90% was observed, with mean/maximum values decreasing from 2.9 cc/19.0 cc to 0.5 cc/6.6 cc. Autoplans were also superior to CLIN in all mean OAR plan parameters. For lungs and patient, observed maximum values in the autoplans were slightly higher than those in the CLIN plans. This could be related to the improved PTV dose, but statistics might also contribute here: the more plans generated, the higher the chance on outliers (25 CLIN plans vs. 600 autoplans).

As discussed in Electronic appendix A, section A2, involved clinicians rated positively the automatically generated plans.

Comparisons of Beam Configurations

All analyzed 600 autoplans for patients 1 to 25 showed highly comparable PTV doses (standard deviations for V95%, V<90%, and V107% were 0.2%, 0.4 cc, and 0.3%). Therefore, only OAR doses are reported in this section.

Figure 2 shows population average plan parameters for VMAT, B-VMAT and CP_x and NCP_x (x = 5–15) (p-values for all mutual comparisons are reported in **Figure B2 in Electronic Supplement B**). Below, the main observations are summarized:

- *Beam number x in NCP_x and CP_x*: Both for CP_x and NCP_x plan quality increased with increasing x. For some parameters there was some leveling off for x≥11 beams, but

TABLE 1 | Comparisons of mean (and ranges) autoplan parameters (units are given in parameter column) with corresponding mean (and ranges) clinically delivered plan (CLIN) parameters for patients 1–25, and absolute differences (mean and ranges).

Structure	Parameter	25 CLIN plans		600 Autoplans		Abs. differences (CLIN-auto)	
		Mean	Range	Mean	Range	Mean	Range
PTV	V95% (%)	**98.1**	95.0–99.7	**99.5**	97.1–99.9	**–1.3**	–4.8 to 0.5
	V<90% (cc)	**2.9**	0.0–19.0	**0.5**	0.0–6.6	**2.4**	–2.1 to 18.8
	V107% (%)	**0.9**	0.0–2.6	**0.2**	0.0–5.4	**0.7**	–4.5 to 2.6
	CI	**1.2**	1.1–1.6	**1.2**	1.1–1.5	**0.0**	–0.2 to 0.2
$Breast_R$	Dmean (Gy)	**1.9**	0.1–6.2	**1.6**	0.2–5.2	**0.3**	–1.6 to 3.4
	V4Gy (%)	**10.7**	0.0–35.5	**7.4**	0.0–33.6	**3.2**	–15.6 to 24.8
$Breast_L$	Dmean (Gy)	**1.9**	0.0–5.4	**1.6**	0.1–5.1	**0.2**	–1.9 to 3.6
	V4Gy (%)	**10.0**	0.0–37.7	**8.4**	0.0–38.2	**1.6**	–12.3 to 31.4
Heart	Dmean (Gy)	**6.5**	0.2–20.0	**5.6**	0.2–20.4	**0.9**	–3.3 to 5.9
Lungs	Dmean (Gy)	**8.3**	2.1–14.3	**7.4**	1.8–16.8	**0.9**	–2.4 to 3.3
	V5Gy (%)	**44.2**	10.6–79.5	**38.9**	7.4–88.2	**5.3**	–15.6 to 25.1
	V20Gy (%)	**15.7**	3.0–30.4	**14.4**	2.6–39.2	**1.3**	–11.5 to 8.9
Patient	V5Gy (cc)	**5135.6**	1191.8–	**4861.3**	960.5–10816.9	**273.6**	–978.0 to 2238.7
	V20Gy (cc)	**1869.8**	271.1–10186.8	**1809.6**	259.5–5056.6	**59.6**	–1128.9 to 1145.6

For calculation of the mean autoplan parameters, all 24 plans per patient, used for the beam configuration studies, were considered. Mean autoplan parameters compared favorably with mean CLIN parameters.

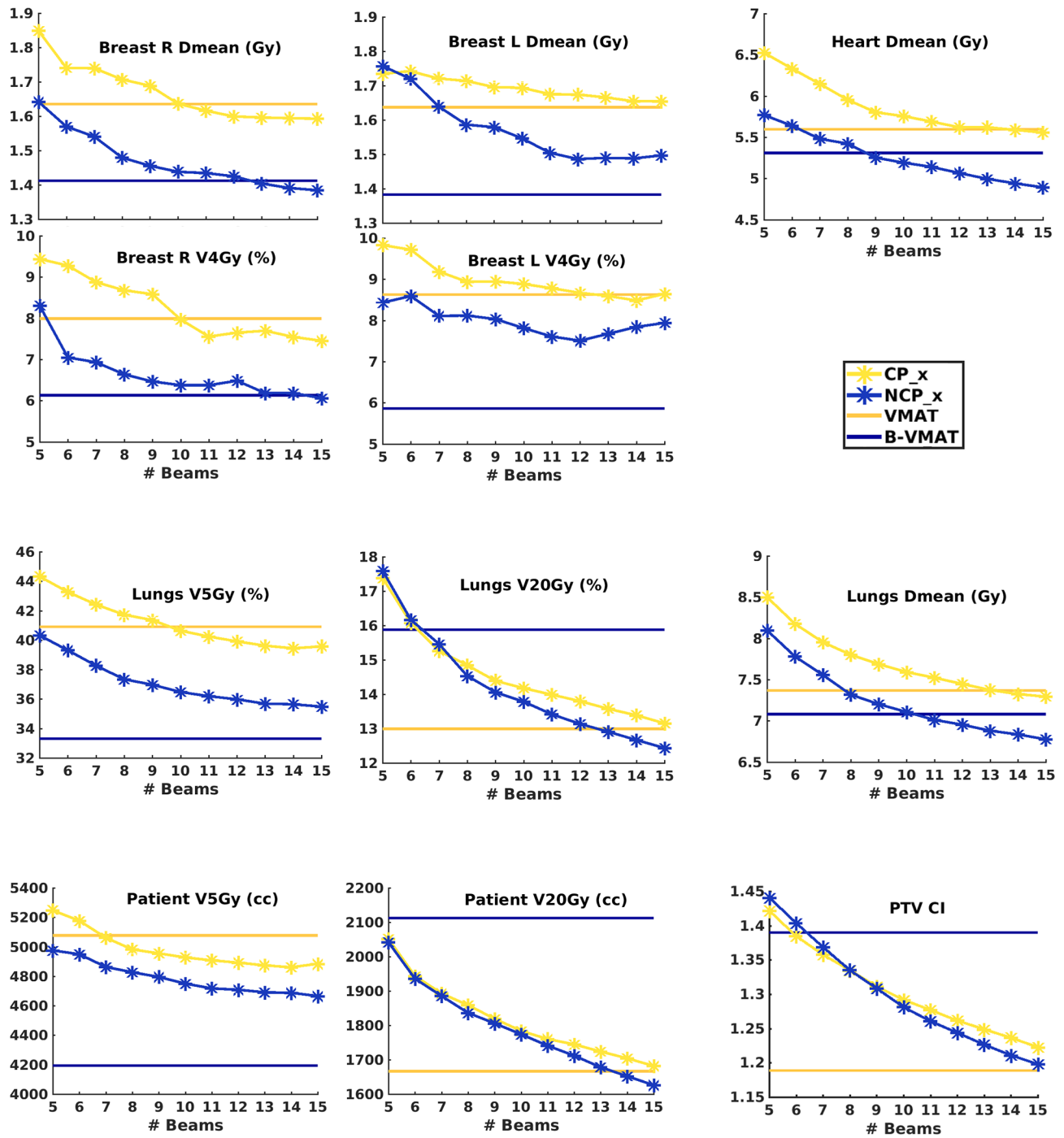

FIGURE 2 | Population mean dosimetric plan parameters for CP_x and NCP_x as a function of the number of beams per plan (x). The dashed horizontal lines indicate the population mean values for VMAT and B-VMAT. p-Values for beam configuration comparisons are presented in **Figure B2 in Electronic Supplement B**.

not for all. Improvements obtained by adding a beam were highly statistically significant for high-dose plan parameters, i.e. lungs and patient V20Gy, heart Dmean and lungs Dmean. For medium dose parameters (lung V5Gy and breast Dmean) differences were almost always statistically significant. Improvements in left breast V4Gy were not statistically significant.

- *NCP_x vs. CP_x*: For equal beam numbers, x, NCP was always better than CP. **Figures 4A**, **B** show that plan improvements with NCP_15 compared to CP_15 were observed for all

patients, although the gain was clearly patient and plan parameter dependent. Differences in mean values were often considered clinically significant.

- *NCP_x vs. VMAT*: NCP_x≥10 was better than or equal to VMAT for all OAR plan parameters. For many parameters, equality was achieved for much less beams.
- *NCP_x vs. B-VMAT*: NCP_x was overall superior for lungs and patient V20Gy and for conformality (CI) (higher doses), and, for larger x, also for heart Dmean and lungs Dmean. **Figures 4C**, **D** show that differences are strongly patient- and parameter dependent. Possibly patients that may benefit most from NCP over B-VMAT in terms of heart or lungs doses are those with targets extending to the lower mediastinum (e.g., pt. 4, **Figure B1**) and/or the supraclavicular region bilaterally (pts. 3,5,11), or with asymmetrical target relative to the midline (e.g., unilateral axilla, pt. 16). Overall, B-VMAT had lower left breast Dmean and V4Gy, lungs V5Gy and patient V5Gy (lower dose parameters). However, some patients did benefit from the individualized beam choice in terms of breast dose, such as patients with axillar involvement (e.g., pts. 8 and 24) and with asymmetrical targets relative to the midline (e.g., pt. 12).
- *VMAT vs. B-VMAT*: Lungs V20Gy, patient V20Gy and CI (higher dose parameters) were on average lowest with VMAT. B-VMAT was on average superior for all other plan parameters. This is consistent with the findings by Fiandra et al. (19). **Figures 4E**, **F** show strong patient- and plan parameter dependences of differences between VMAT and B-VMAT.
- *VMAT vs. CP_x*: For small x, VMAT was clearly superior. For larger x, differences were dependent on plan parameter.
- *Breast*: Non-coplanar approaches scored best. B-VMAT was overall the clear winner, followed by NCP with 12 beams or more (NCP_x≥12). Superiority of B-VMAT could be related to geometrical constraints as defined by the butterfly geometry, limiting the dose delivered to the breasts.
- *Heart*: Non-coplanar approaches were best. NCP_x≥10 plans had on average a lower heart Dmean than B-VMAT. The superior heart sparing with NCP_15 and B-VMAT is illustrated for patient 3 in **Figure 3**.
- *Lung*: NCP_x≥13 was overall best for Dmean and V20Gy. B-VMAT was overall best for V5Gy but resulted in high V20Gy.
- *Low vs high dose in lungs and patient (V5Gy vs V20Gy)*: Compared to B-VMAT, NCP improved lung and patient V20Gy (mostly $p < 0.001$), at the cost of lungs and patient V5Gy (mostly $p < 0.001$) and breast V4Gy (only significant for right breast). This can also be observed in the dose distributions in **Figure 5**, where B-VMAT was less conformal around the tumor (red and yellow isodose lines), but showed less spread of low doses (light green and azure isodose lines in sagittal view), compared to CP_15 and NCP_15.
- *Dose conformality*: On average (**Figure 2**), conformality was best for VMAT (lowest CI), closely followed by NCP_15 and CP_15. B-VMAT was clearly the worst.
- *Overall observations:* In **Figure 4**, patients are sorted according to decreasing heart Dmean in NCP_15 plans. A clear reduction in differences among techniques is visible for patients with decreasing heart Dmean, showing a dependence on patient anatomy (**Figure B1 in Electronic Supplement B**) when selecting the optimal technique. E.g. patient 25 showed smaller differences between techniques, making the less complex CP or VMAT the favorable choice.

Patient-Specific Beam Orientations

For NCP_15 and CP_15, patient group analyses were performed on selected beam directions. The population distributions of selected beam directions are shown in **Figure 5**. The rectangles in the left panel of **Figure 5** show the coplanar and non-coplanar beam directions used for B-VMAT. Non-coplanar beams resulting from a couch angle of 90° and gantry angles between

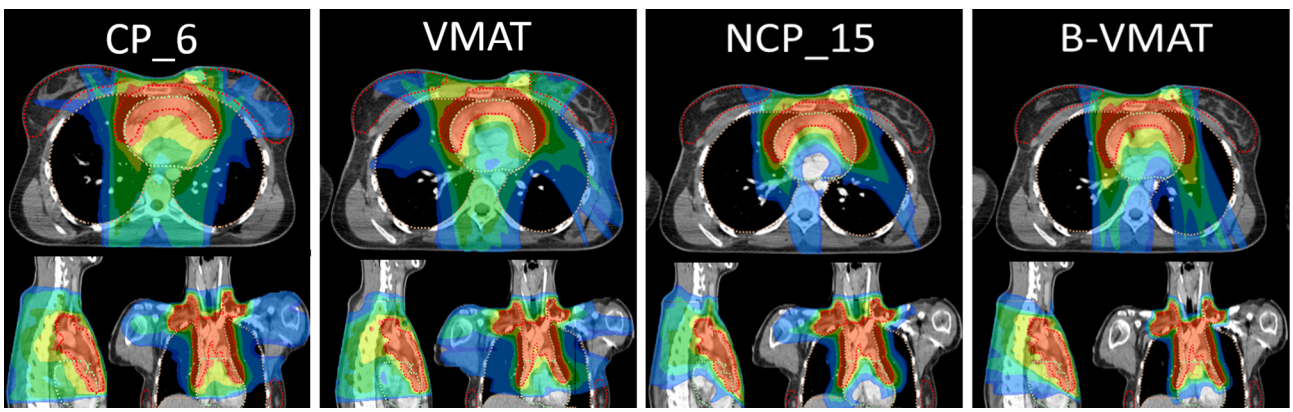

FIGURE 3 | Dose distributions for patient 3. CP_6 was added as, on average, six beams were used clinically. CP_15 was similar to VMAT and was therefore not added. The isodose lines are percentages relative to the prescribe dose, i.e., 100% = 30 Gy, with color legend as light blue, 16.7% (5 Gy as OAR constraints); azure, 20%; light green, 40%; dark green, 60%; yellow, 80%; red, 95%.

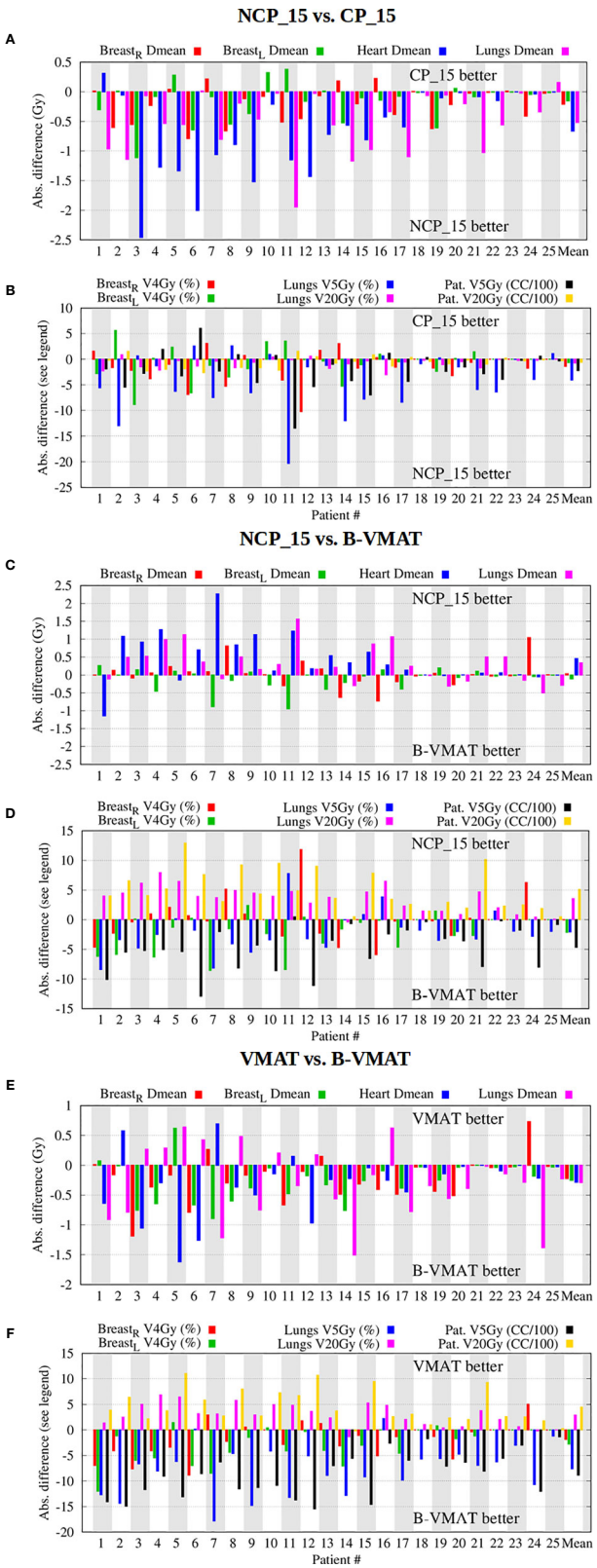

FIGURE 4 | Beam configuration comparisons - NCP_15 vs. CP_15 **(A, B)**, NCP_15 vs. B-VMAT **(C, D)**, and VMAT vs. B-VMAT **(E, F)** - showing large inter-patient and inter-parameter variations in differences in plan parameter values. Patients were ordered according to descending heart Dmean in the NCP_15 plans.

10° and 30°, entering the patient from anterior-inferior directions, were frequently present in NCP_15 plans. These entrance angles have a heart sparing/avoidance effect (see also sagittal views in **Figure 3**). The (couch, gantry) directions around (−70°, −30°) and around (−45°, −15°) were also often present in the NCP_15 plans. A clear prevalence of anterior beams was found in both NCP_15 and CP_15 with gantry angles between ±90°. For all patients, at least one anterior beam was present in the range −10° to 10° for CP_15 plans. Many beams in NCP_15 coincide with the anterior beam directions of B-VMAT. On the other hand, the posterior angles of B-VMAT were hardly selected in NCP_15. Apart from the clustered areas, **Figure 5** shows broad distributions of selected beam directions for NCP_15 and CP_15. This is in agreement with the large inter-patient variations in selected directions, shown in electronic appendix C.

DISCUSSION

To the best of our knowledge, in all published studies comparing beam configurations for treatment of mediastinal lymphoma patients, treatment plans were generated with manual trial-and-error planning, including selection of beam angles. It is well-known that manually generated plans may suffer from inter-and intra-planner quality variations, aggravated by the complex selection of optimal beam configurations. In this paper we present the first study using autoplanning with integrated beam angle optimization to systematically explore advantages and disadvantages of various coplanar and non-coplanar beam configuration approaches for young female mediastinal lymphoma patients. Due to this automation, plan generation became fully independent of planners, and the analyses could be based on a large number of high-quality plans.

From the 624 generated autoplans (26 patients with 24 autoplans), 617 (98.9%) satisfied the clinical PTV coverage requirement. The seven autoplans with insufficient PTV coverage were from the same patient (patient 0). Because of these plans with too low coverage, patient 0 was not included in patient population analyses comparing beam configuration approaches (see also *Results* section). Of the remaining 600 autoplans (25 patients with 24 autoplans), the dosimetric parameters compared favorably with those of corresponding clinically delivered plans, generated with manual plan generation. This observation was in agreement with the evaluations of 100 autoplans by the two physicians involved in this study who considered these plans of high quality (**Electronic Supplement A**).

There was not an overall superior beam configuration approach for the patient population, i.e. being on average best for all plan parameters. Performances of the various approaches were dependent on the considered OAR and the endpoint. There were also large inter-patient variations in the gain of one technique compared to another. However, overall there was a clear tendency towards improved plans with non-coplanar configurations (B-VMAT and NCP_x≥12). NCP_x≥12 was on average better in producing highly conformal plans with reduced high doses in the lungs and patient and also a reduced heart Dmean, while B-VMAT had reduced low-dose spread, related to the confinement of beam angles to the butterfly geometry. Levis et al. (36) have recently reported on a new-generation butterfly

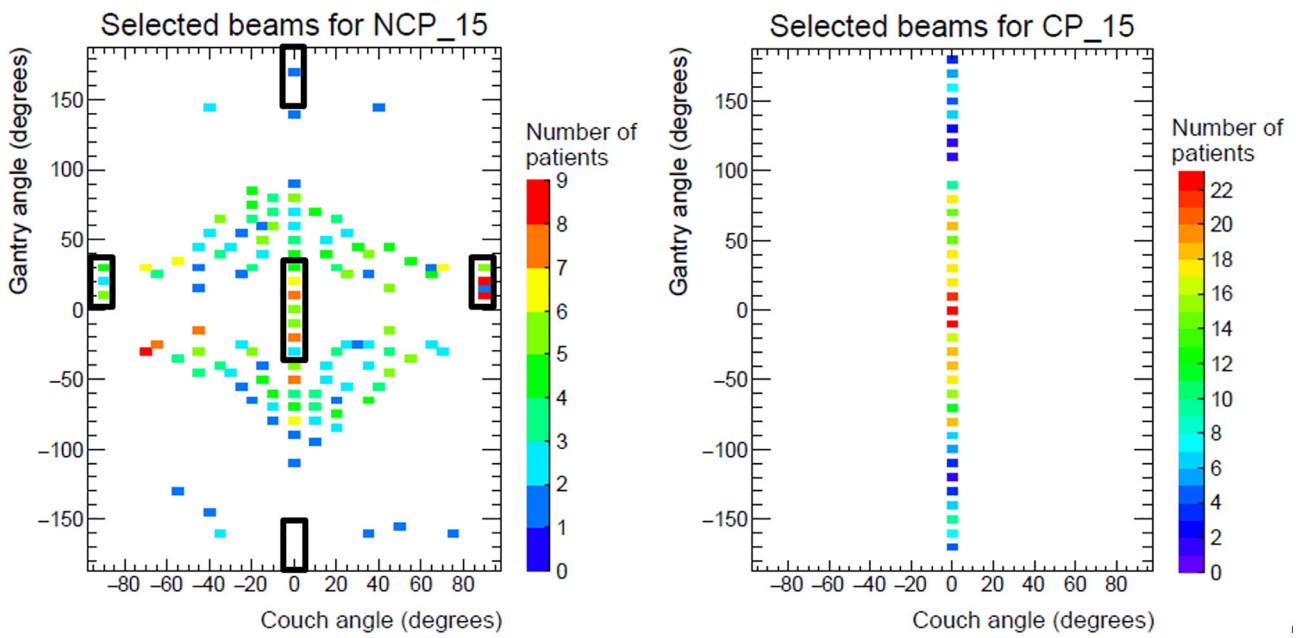

FIGURE 5 | Population distributions of beams selected for NCP_15 (left) and CP_15 (right) for patients 1 to 25 (375 beams per panel). The black rectangles in the left panel indicate the beams present in B-VMAT. Note: B-VMAT beams in the rectangular at couch -90 degrees are in reality delivered with couch angle +90 degrees, while flipping the respective gantry angles to negative values.

VMAT, where the coplanar part consists of a standard full-arc VMAT (FaB-VMAT). While this approach may solve some of the issues pointed out here for the B-VMAT approach (lack of conformity in the high doses), it might not be superior to NCP_15 for selected patients. In fact, the authors report a loss in breast dosimetry with FaB-VMAT for bulky tumors, compared to B-VMAT.

A distinct disadvantage of non-coplanar treatments can be an increase in delivery time. There is also enhanced risk of collisions due to human errors in delivery. Whether the dosimetrical benefit justifies increases in delivery time and complexity remains a clinical choice that may be highly dependent on the patient at hand with her specific plan quality improvements and required number of non-coplanar beams. In most radiotherapy departments, the number of ML patients is limited, which may render non-coplanar treatment (for a selected group) more feasible. Risks of collisions can be mitigated with adequate delivery protocols, and instruction and training of RTTs.

The observed large inter-patient variations in dosimetric differences between various beam set-ups are an incentive for prospective clinical use of automated planning to generate multiple plans for each new patient, and then select the best plan, considering quality and delivery time. This could further personalize radiotherapy for ML patients. We believe that for a clinical application, not all 24 autoplans discussed in this study need to be generated for each new patient. Coplanar plan generation could be limited to VMAT and for non-coplanar treatment, B-VMAT and, e.g., NCP_9 and NCP_15 could be generated. Based on a comparison of these plans, a final plan could be selected, or NCP_x plans with other beam numbers could be generated to refine the choice.

The seven autoplans of patient 0 with insufficient PTV coverage to avoid excessive OAR dose delivery were all coplanar with relatively low numbers of beams (5-11). For the remaining five coplanar plans with 12 to 15 beams and for all 12 non-coplanar plans, adequate coverage was obtained. Many of these plans also had superior OAR dose delivery compared to the clinical plan. The automated workflow presented above, based on automated generation of a small set of treatment plans for each patient, would naturally have avoided generation of the low beam number coplanar plans with unacceptably low PTV coverage.

This study and the proposed clinical workflow, based on generation of a small set of plans for each patient, are incentives for manufactures of treatment planning systems to extend their systems with advanced options for patient-specific beam angle optimization.

The automated planning applied in this study was developed to generate plans that balance all treatment aims in line with the clinical protocol. However, effectively, the various investigated beam angle approaches did in the end result in different overall balances between the objectives, resulting from the respective opportunities and limitations in beam angle choice (above). This could be extremely useful in case of co-morbidities or specific toxicity risks. E.g. for most patients with a heart comorbidity, NCP_x≥12 plans would be favorable, while B-VMAT would often be the modality of choice if low dose in the contralateral breast is of high relevance. Variations in plan quality could be further enhanced by also generating plans with wish-lists that focus on sparing of particular OARs. In a future work we will investigate pre-defined deviations from the clinical planning protocol, each focusing maximally on a specific endpoint/OAR.

In clinical planning, beam energies of 6, 10, and 18 MV were used, often also in combinations. For autoplanning in this study only 6 MV was used to avoid prolonged optimization times due to inclusion of beam energy optimization. Nevertheless, the obtained plan quality was high.

As mentioned in the M&M section, Erasmus-iCycle was used to optimize intensity profiles, i.e. time-consuming segmentation of the 600 plans was avoided. This does not impact the main conclusions of the paper; in many previous studies, we have demonstrated the ability to segment these plans for VMAT (35, 37, 38). Moreover, for the technique comparisons, only differences in plans were evaluated, and interesting differences were generally large.

We used heart Dmean for restricting the risk on radiation-induced cardiac toxicity. This is in line with the study by Darby et al. on radiation-induced cardiac toxicity in breast cancer patients (39). On the other hand, there are indications that selective sparing of heart substructures could be important (31, 40). To the best of our knowledge, there are no systematic studies for ML comparing planning with and without the use of heart substructures, including an evaluation of the impact on target dose and doses in the other OARs. Unfortunately, in our study these substructures were not delineated for clinical treatments, and were therefore not available for detailed analyses.

In research environments, different solutions for beam angle optimization have been proposed (33, 41–43). In our study, the solution developed by Breedveld et al. (33) has been used as shown to produce high quality results (37, 44). Comparisons of different algorithms are lacking.

In conclusion, using autoplanning including computerized coplanar and non-coplanar beam configuration optimization, 24 beam configuration approaches were compared for 25 young female mediastinal lymphoma patients. The quality of the applied autoplans was superior to that of manually generated, clinically delivered plans. Non-coplanar beam configurations were overall favorable, but significant patient-specific and plan-parameter-dependent dosimetric advantages and disadvantages of different beam configurations were observed, suggesting a need for prospective generation of multiple plans per patient to optimally personalize radiotherapy treatment. A workflow was proposed for automated generation of a small set of plans for each patient, followed by a selection.

DATA AVAILABILITY STATEMENT

All relevant data are within the paper and its supplementary files. Access to raw-data underlying the findings in this paper will be made possible on request to corresponding author.

ETHICS STATEMENT

Ethical review and approval was not required for the study on human participants in accordance with the local legislation and institutional requirements. Written informed consent for participation was not required for this study in accordance with the national legislation and the institutional requirements.

AUTHOR CONTRIBUTIONS

LR and PC: conducting main research, brainstorming, and writing manuscript. JL: data, collection, brainstorming about research, and partial data analysis. JP and BH: supervision of research, brainstorming, and writing manuscript. SB: developing code and writing manuscript. MV and CJ: data collection, data revision, and writing manuscript. All authors contributed to the article and approved the submitted version.

FUNDING

This work was in part funded by Elekta AB (Stockholm, Sweden). Erasmus MC Cancer Institute also has research collaborations with Accuray, Inc (Sunnyvale, USA) and Varian Medical Systems, Inc (Palo Alto, USA). The funder bodies were not involved in the study design, collection, analysis, interpretation of data, the writing of this article or the decision to submit it for publication.

ACKNOWLEDGMENTS

The authors thank Rik Bijman for helping with the statistical analysis; Abdul Wahab Sharfo and Steven Habraken for the fruitful discussions and advice on automated planning; Chrysi Papalazarou for helping with patient selection; Erik-Jan Tromp for implementing the Monte Carlo dose calculation; András Zolnay for technical support with data analysis and programming; and Danielle van Nispen, Nicole Bahnerth-Cornelissen, and Nienke Hoffmans-Holtzer for helping with defining the candidate beams feasible at the Linac. Danielle van Nispen also gave useful input for enhancement of the quality of autoplans.

SUPPLEMENTARY MATERIAL

The Supplementary Material for this article can be found online at: https://www.frontiersin.org/articles/10.3389/fonc.2021.619929/full#supplementary-material

REFERENCES

1. Ng A, Patricia Bernardo M, Weller E, Backstrand K, Silver B, Marcus KC, et al. Second malignancy after Hodgkin disease treated with radiation therapy with or without chemotherapy: long-term risks and risk factors. *Blood* (2002) 6:1989–96. doi: 10.1182/blood-2002-02-0634
2. Travis LB, Gospodarowicz M, Curtis RE, et al. Lung cancer following chemotherapy and radiotherapy for Hodgkin's disease. *J Natl Cancer Inst* (2002) 94:182–92. doi: 10.1093/jnci/94.3.182
3. Travis LB, Hill DA, Dores GM, et al. Breast cancer following radiotherapy and chemotherapy among young women with Hodgkin disease. *JAMA* (2003) 290:465–75. doi: 10.1001/jama.290.4.465
4. De Bruin ML, Sparidans J, van't Veer MB, et al. Breast cancer risk in female survivors of Hodgkin's lymphoma: lower risk after smaller radiation volumes. *J Clin Oncol* (2009) 27:4239–46. doi: 10.1200/JCO.2008.19.9174
5. Swerdlow AJ, Higgins CD, Smith P, et al. Second cancer risk after chemotherapy for Hodgkin's lymphoma: a collaborative British cohort study. *J Clin Oncol* (2011) 29:4096–104. doi: 10.1200/JCO.2011.34.8268
6. Schaapveld M, Aleman BM, van Eggermond AM, et al. Second Cancer Risk Up to 40 Years after Treatment for Hodgkin's Lymphoma. *N Engl J Med* (2015) 373:2499–511. doi: 10.1056/NEJMoa1505949
7. Eichenauer DA, Becker I, Monsef I, Chadwick N, de Sanctis V, Federico M, et al. Secondary malignant neoplasms, progression-free survival and overall survival in patients treated for Hodgkin lymphoma: a systematic review and meta-analysis of randomized clinical trials. *Haematologica* (2017) 102:1748–57. doi: 10.3324/haematol.2017.167478
8. Aleman B, van den Belt-Dusebout A, De Bruin M. Late cardiotoxicity after treatment for Hodgkin lymphoma. *Blood* (2008) 5:1878–86. doi: 10.1182/blood-2006-07-034405
9. Maraldo MV, Giusti F, Vogelius IR, Lundemann M, van der Kaaij MAE, Ramadan S, et al. Cardiovascular disease after treatment for Hodgkin's lymphoma: an analysis of nine collaborative EORTC-LYSA trials. *Lancet Haematol* (2015) 2:492–502. doi: 10.1016/S2352-3026(15)00153-2
10. Van Nimwegen FA, Schaapveld M, Janus CP, et al. Cardiovascular disease after Hodgkin lymphoma treatment: 40-year disease risk. *JAMA Intern Med* (2015) 175:1007–17. doi: 10.1001/jamainternmed.2015.1180
11. Van Nimwegen FA, Schaapveld M, Cutter DJ, et al. Radiation Dose-Response Relationship for Risk of Coronary Heart Disease in Survivors of Hodgkin Lymphoma. *J Clin Oncol* (2016) 34:235–43. doi: 10.1200/JCO.2015.63.4444
12. Van Nimwegen FA, Ntentas G, Darby SC, et al. Risk of heart failure in survivors of Hodgkin lymphoma: effects of cardiac exposure to radiation and anthracyclines. *Blood* (2017) 29:2257–65. doi: 10.1182/blood-2016-09-740332
13. Koh ES, Tran TH, Heydarian M, et al. A comparison of mantle versus involved-field radiotherapy for Hodgkin's lymphoma: reduction in normal tissue dose and second cancer risk. *Radiat Oncol* (2007) 2:13. doi: 10.1186/1748-717X-2-13
14. Maraldo MV, Brodin NP, Vogelius IR, et al. Risk of developing cardiovascular disease after involved node radiotherapy versus mantle field for Hodgkin lymphoma. *Int J Radiat Oncol Biol Phys* (2012) 83:1232–7. doi: 10.1016/j.ijrobp.2011.09.020
15. Campbell BA, Hornby C, Cunninghame J, et al. Minimising critical organ irradiation in limited stage Hodgkin lymphoma: a dosimetric study of the benefit of involved node radiotherapy. *Ann Oncol* (2012) 23:1259–66. doi: 10.1093/annonc/mdr439
16. Zhou R, Ng A, Constine LS, et al. A Comparative Evaluation of Normal Tissue Doses for Patients Receiving Radiation Therapy for Hodgkin Lymphoma on the Childhood Cancer Survivor Study and Recent Children's Oncology Group Trials. *Int J Radiat Oncol Biol Phys* (2016) 95:707–11. doi: 10.1016/j.ijrobp.2016.01.053
17. Maraldo MV, Brodin NP, Aznar MC, et al. Estimated risk of cardiovascular disease and secondary cancers with modern highly conformal radiotherapy for early-stage mediastinal Hodgkin lymphoma. *Ann Oncol* (2013) 24:2113–8. doi: 10.1093/annonc/mdt156
18. Pinnix CC, Smith GL, Milgrom S, Osborne EM, Reddy JP, Akhtari M, et al. Predictors of radiation pneumonitis in patients receiving intensity modulated radiation therapy for Hodgkin and non-Hodgkin lymphoma. *Int J Radiat Oncol Biol Phys* (2015) 92:175–82. doi: 10.1016/j.ijrobp.2015.02.010
19. Fiandra C, Filippi AR, Catuzzo P, Botticella A, Ciammella P, Franco P, et al. Dierent IMRT solutions vs. 3D-conformal radiotherapy in early stage Hodgkin's Lymphoma: dosimetric comparison and clinical considerations. *Radiat Oncol* (2012) 186. doi: 10.1186/1748-717X-7-186

20. Filippi AR, Ragona R, Piva C, Scafa D, Fiandra C, Fusella M, et al. Optimized volumetric modulated arc therapy versus 3D-CRT for early stage mediastinal Hodgkin lymphoma without axillary involvement: a comparison of second cancers and heart disease risk. *Int J Radiat Oncol Biol Phys* (2015) 92:161–8. doi: 10.1016/j.ijrobp.2015.02.030
21. Voong KR, McSpadden K, Pinnix CC, et al. Dosimetric advantages of a "butterfly" technique for intensity-modulated radiation therapy for young female patients with mediastinal Hodgkin's lymphoma. *Radiat Oncol* (2014) 9:94. doi: 10.1186/1748-717X-9-94
22. Toltz A, Shin N, Mitrou E, et al. Late radiation toxicity in Hodgkin lymphoma patients: proton therapy's potential. *J Appl Clin Med Phys* (2015) 16:167. doi: 10.1120/jacmp.v16i5.5386
23. Tseng YD, Cutter DJ, Plastaras JP, et al. Evidence-based Review on the Use of Proton Therapy in Lymphoma From the Particle Therapy Cooperative Group (PTCOG) Lymphoma Subcommittee. *Int J Radiat Oncol Biol Phys* (2017) 99:825–42. doi: 10.1016/j.ijrobp.2017.05.004
24. Dabaja BS, Hoppe BS, Plastaras JP, Newhauser W, Rosolova K, Flampouri S, et al. Proton therapy for adults with mediastinal lymphomas: the International Lymphoma Radiation Oncology Group guidelines. *Blood* (2018) 132:1635–46. doi: 10.1182/blood-2018-03-837633
25. Ricardi U, Maraldo MV, Levis M, Parikh RR. Proton Therapy For Lymphomas: Current State Of The Art. *Onco Targets Ther* (2019) 12:8033–46. doi: 10.2147/OTT.S220730
26. Maraldo MV, Dabaja BS, Filippi AR, Illidge T, Tsang R, Ricardi U, et al. Radiation therapy planning for early stage Hodgkin lymphoma: experience of the International Lymphoma Radiation Oncology Group. *Int J Radiat Oncol Biol Phys* (2015) 92:144–52. doi: 10.1016/j.ijrobp.2014.12.009
27. Maraldo MV, Specht L. A decade of comparative dose planning studies for early-stage Hodgkin lymphoma: what can we learn? *Int J Radiat Oncol Biol Phys* (2014) 90:1126–35. doi: 10.1016/j.ijrobp.2014.06.069
28. Nelms BE, Robinson G, Markham J, Velasco K, Boyd S, Narayan S, et al. Variation in external beam treatment plan quality: an inter-institutional study of planners and planning systems. *Pract Radiat Oncol* (2012) 2:296–305. doi: 10.1016/j.prro.2011.11.012
29. Berry SL, Boczkowski A, Hunt M. Interobserver Variability in Radiotherapy Plan Output: Results of a Single-Institution Study. *Pract Radiat Oncol* (2016) 6 (6):442–9. doi: 10.1016/j.prro.2016.04.005
30. Clemente S, Oliviero C, Palma G, D'Avino V, Liuzzi R, Conson M, et al. Auto-versus human-driven plan in mediastinal Hodgkin lymphoma radiation treatment. *Radiat Oncol* (2018) 13:202. doi: 10.1186/s13014-018-1146-3
31. Cutter DJ, Schaapveld M, Darby SC, Hauptmann M, van Nimwegen FA, Krol ADG, et al. Risk of valvular heart disease after treatment for Hodgkin lymphoma. *J Natl Cancer Inst* (2015) 107(4):1–9. doi: 10.1093/jnci/djv008
32. Hoskin PJ, Diez P, Williams M, Lucraft H, Bayne M. Recommendations for the use of radiotherapy in nodal lymphoma. *Clin Oncol (R Coll Radiol)* (2013) 25:49–58. doi: 10.1016/j.clon.2012.07.011
33. Breedveld S, Storchi P, Voet P, Heijmen B. iCycle: Integrated, multicriterial beam angle, and profile optimization for generation of coplanar and noncoplanar IMRT plans. *Med Phys* (2012) 39:951–63. doi: 10.1118/1.3676689
34. Hissoiny S, Ozell B, Després P. GPUMCD, a new GPU-oriented Monte Carlo dose calculation platform. *Med Phys* (2011) 38:754–64. doi: 10.1118/1.3539725
35. Voet P, Dirkx M, Breedveld S, Fransen D, Levendag P, Heijmen B. Towards fully automated multi-criterial plan generation: a prospective clinical study. *Int J Radiat Oncol Biol Phys* (2013) 85:866–72. doi: 10.1016/j.ijrobp.2012.04.015
36. Levis M, Filippi AR, Fiandra C, De Luca V, Bartoncini S, Vella D, et al. Inclusion of heart substructures in the optimization process of volumetric modulated arc therapy techniques may reduce the risk of heart disease in Hodgkin's lymphoma patients. *Radiother Oncol* (2019) 138:52–8. doi: 10.1016/j.radonc.2019.05.009
37. Rossi L, Sharfo AW, Aluwini S, Dirkx M, Breedveld S, Heijmen B. First fully automated planning solution for robotic radiosurgery - comparison with automatically planned volumetric arc therapy for prostate cancer. *Acta Oncol* (2018) 57:1490–8. doi: 10.1080/0284186X.2018.1479068
38. Sharfo A, Voet P, Breedveld S, Mens JWM, Hoogeman MS, Heijmen BJM. Comparison of VMAT and IMRT strategies for cervical cancer patients using automated planning. *Radiother Oncol* (2015) 114:395–401. doi: 10.1016/j.radonc.2015.02.006
39. Darby SC, Ewertz M, McGale P, Bennet AM, Blom-Goldman U, Brønnum D, et al. Risk of Ischemic Heart Disease in Women after Radiotherapy for Breast Cancer. *N Engl J Med* (2013) 368(11):987–98. doi: 10.1056/NEJMoa1209825
40. Moignier A, Broggio D, Derreumaux S, Beaudré A, Girinsky T, Paul JF, et al. Coronary stenosis risk analysis following Hodgkin lymphoma radiotherapy: a study based on patient specific artery segments dose calculation. *Radiother Oncol* (2015) 117:467–72. doi: 10.1016/j.radonc.2015.07.043
41. Yuan L, Wu QJ, Yin L, Li Y, Sheng Y, Kelsey CR, et al. Standardized beam bouquets for lung IMRT planning. *Phys Med Biol* (2015) 60:1831. doi: 10.1088/0031-9155/60/5/1831
42. Yuan L, Zhu W, Ge Y, Jiang Y, Sheng Y, Yin F, et al. Lung IMRT planning with automatic determination of beam angle configurations. *Phys Med Biol* (2018) 63:135024. doi: 10.1088/1361-6560/aac8b4
43. Dong P, Lee P, Ruan D, Long T, Romejin E, Low D, et al. 4π noncoplanar stereotactic body radiation therapy for centrally located or larger lung tumors. *Int J Radiat Oncol Biol Phys* (2013) 86:407–13. doi: 10.1016/j.ijrobp.2013.02.002
44. Sharfo AW, Dirkx ML, Breedveld S, Romero AM, Heijmen BJM. VMATplus a few computer-optimized non-coplanar IMRT beams (VMAT+) tested for liver SBRT. *Radiother Oncol* (2017) 123:49–56. doi: 10.1016/j.radonc.2017.02.018

Conflict of Interest: The authors declare that the research was conducted in the absence of any commercial or financial relationships that could be construed as a potential conflict of interest.

frontiers in Oncology

ORIGINAL RESEARCH
published: 23 April 2021
doi: 10.3389/fonc.2021.668481

30-Day Mortality Following Palliative Radiotherapy

Miriam Vázquez[1], Manuel Altabas[1], Diana C. Moreno[1], Abraham A. Geng[1], Santiago Pérez-Hoyos[2] and Jordi Giralt[1]*

[1] Department of Radiation Oncology, Vall d'Hebron University Hospital, Vall d'Hebron Institute of Oncology, Barcelona, Spain, [2] Unit of Statistics and Bioinformatics, Vall d'Hebron University Hospital, Barcelona, Spain

Purpose: 30-day mortality (30-DM) is a parameter with widespread use as an indicator of avoidance of harm used in medicine. Our objective is to determine the 30-DM followed by palliative radiation therapy (RT) in our department and to identify potential prognosis factors.

Material/Methods: We conducted a retrospective cohort study including patients treated with palliative RT in our center during 2018 and 2019. Data related to clinical and treatment characteristics were collected.

Results: We treated 708 patients to whom 992 palliative irradiations were delivered. The most frequent primary tumor sites were lung (31%), breast (14.8%), and gastrointestinal (14.8%). Bone was the predominant location of the treatment (56%), and the use of single doses was the preferred treatment schedule (34.4%). The 30-DM was 17.5%. For those who died in the first month the median survival was 17 days. Factors with a significant impact on 30-DM were: male gender ($p < 0.0001$); Eastern Cooperative Oncology Group (ECOG) Performance Status (PS) of 2–3 ($p = 0.0001$); visceral metastases ($p = 0.0353$); lung, gastrointestinal or urinary tract primary tumors ($p = 0.016$); and single dose RT ($p = <0.0001$). In the multivariate analysis, male gender, ECOG PS 2–3, gastrointestinal and lung cancer were found to be independent factors related to 30-DM.

Conclusion: Our 30-DM is similar to previous studies. We have found four clinical factors related to 30-DM of which ECOG was the most strongly associated. This data may help to identify terminally ill patients with poor prognosis in order to avoid unnecessary treatments.

Keywords: 30-day mortality, palliative radiation, end-of-life, prognosis, clinical indicator

OPEN ACCESS

Edited by:
Minesh P. Mehta, Baptist Health South Florida, United States

Reviewed by:
Alexandros Papachristofilou, University Hospital of Basel, Switzerland
Adam C. Olson, University of Pittsburgh Medical Center, United States

****Correspondence:***
Miriam Vázquez
miriam.vazquez@vhebron.net

Specialty section:
This article was submitted to Radiation Oncology, a section of the journal Frontiers in Oncology

Received: *16 February 2021*
Accepted: *19 March 2021*
Published: *23 April 2021*

Citation:
Vázquez M, Altabas M, Moreno DC, Geng AA, Pérez–Hoyos S and Giralt J (2021) 30-Day Mortality Following Palliative Radiotherapy. Front. Oncol. 11:668481. doi: 10.3389/fonc.2021.668481

INTRODUCTION

Radiation therapy (RT) has a well-established role in the palliative approach of patients with cancer. When using palliative RT, symptom relief is usually obtained in a wide range of time which varies depending on the primary tumor, the location of the treatment or the patient's health. However, when survival is too short, these patients may die before they benefit from RT.

The use of chemotherapy in dying patients has been previously reported as an aggressive and poor tailored end-of-life care indicator (1). In the last years the use of RT at the end of life has also

been a matter of concern (2–4). When proposing a palliative treatment with radiation, the presumed survival is an essential factor taken into account and may condition fractionation regimen. Therefore, the use of a larger number of fractions in terminally ill patients is likely to require spending a significant amount of their final days visiting a radiation therapy suite (2, 3). This has been suggested to be a consequence of an overoptimistism at survival prediction of dying patients (5).

The National Health Service of the United Kingdom proposed the 30-day mortality (30-DM) parameter as an indicator of aggressive management at the end of the life. Thus, when the estimated survival is less than one month, palliative RT is unlikely to be beneficial. The Royal College of Radiologist agreed that less than 20% of patients receiving palliative RT should die within 30 days of treatment (6). Therefore, it's important to identify these patients with shortened survival and to carefully consider if the treatment should be avoided or not.

The use of palliative RT in the last 30 days of life varies substantially between centers and ranges between 0.7 and 33% (7). The purpose of this study was to determine 30-DM in patients who have received palliative RT in our center and to identify potential prognostic factors for 30-DM.

MATERIAL AND METHODS

We performed a retrospective study including adult patients treated with palliative RT in our center from January 2018 to December 2019. Exclusion criteria were: patients under the age of 18, hematologic tumors, non-melanomatous skin cancer, treatment with stereotactic body radiation therapy or radiosurgery, and when survival status at 30 days was unavailable. All RT treatments were identified using Aria® (Varian Medical Systems) which is a specific electronic record for patients referred for RT. Clinical data was recorded from the hospital electronic medical record. The study was approved by the institutional ethics committee of our center.

Demographic data, radiation treatment parameters, and disease characteristics were collected for each patient. The type of primary tumor was classified into eight groups according to the most frequent tumors: lung, breast, prostate, gastrointestinal, urinary tract, gynecological, head and neck, and others. Episodes were identified when the treatment intent was registered as palliative by a radiation oncologist, and radiotherapy was delivered in less than 15 fractions. Site of the treatment was allocated by primary tumor, bone, brain, lymph nodes, and soft tissue. For patients who were treated more than once, we took into account the last treatment to avoid data duplication. All patients were followed for at least one month and until 6 months.

The primary endpoint of our study was to determine 30-DM. The secondary endpoint was to identify potential prognostic factors in our cohort. 30-DM was assessed from the start of treatment to the moment of death. Patients were grouped according to their vital status within 30 days from the start of treatment: group "better survival" (BS) for survivors and group "lower survival" (LS) for non-survivors at 30 days. All patients were followed up during that period and none was lost. A descriptive analysis was carried using Chi-squared or Exact Fisher as adequate. Potential clinical and dosimetric variables related to mortality were checked fitting a univariate and multivariate logistic regression. Variables that improve the likelihood ($p < 0.1$) were included in the final mode. Covariates considered were the following: age, sex, ECOG PS, primary tumor, presence of visceral disease, treatment location, number of fractions, and reirradiation. A multivariable analysis was performed to identify independent prognostic factors. A Kaplan–Meier survival curve with six months of follow-up has been also estimated. All analyses were carried out with Stata 15.1.

RESULTS

A total of 708 patients were analyzed. **Figure 1** shows the consort flow diagram. The median age of the entire population at

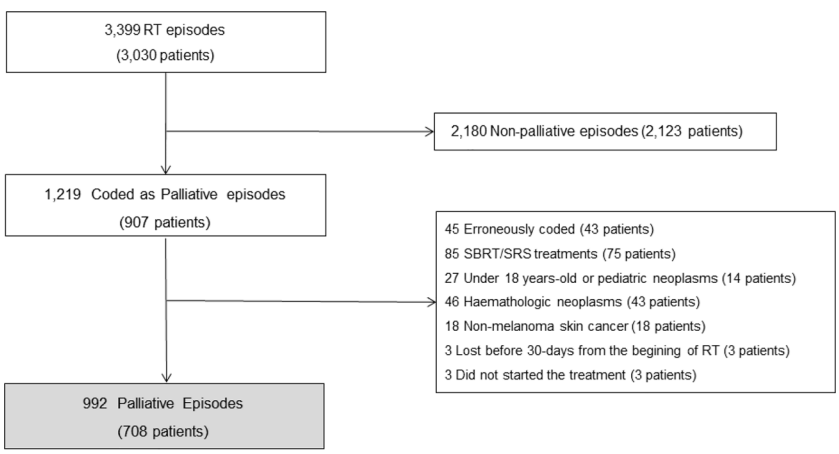

FIGURE 1 | Consort diagram demonstrating exclusions from the study population.

treatment was 66 years, male gender was predominant (58.2%), and the majority had a good performance status with an ECOG PS of 0–1 (59%). The most prevalent tumors were lung, breast, and gastrointestinal (31, 14.8, and 14.8% respectively). Bone was the most frequent site of radiation (56%), and the preferred schedule was single doses (34.4%) followed closely by 10–15 fractions (34%). The completion rate of the treatment was 94.8%. No differences were found according to age, location of the treatment, and reirradiation between groups. Of the 37 patients who did not end the treatment, 28 belonged to the LS group. Patient's characteristics are shown in **Table 1**.

Overall, 124 out of 708 patients died at 30 days (17.5%). The median survival was 17 days for the LS group. For the entire cohort, the median survival was 120 days (**Figure 2A**). Descriptive analysis according to the state at 30-days showed a higher prevalence in the LS group of ECOG 2–3 ($p = 0.0001$), male gender ($p < 0.0001$), visceral metastasis ($p = 0.0353$), and use of single doses ($p < 0.0001$). Primary tumor distribution between groups was different ($p = 0.016$) with a higher prevalence of lung, gastrointestinal, urinary tract, and other tumors in the LS group. Survival according to primary tumor is shown in **Figure 2B**.

The multifactorial analysis shows that male patients were 58% more likely to die within the first month after RT in comparison to female patients (OR 2.37, 95% CI: 1.5; 3.66). ECOG PS was the parameter with the highest impact in 30-DM with an increased risk of 77% of dying for those with an ECOG PS 2–3 (OR 4.22, 95% CI: 2.78; 6.40). According to primary tumor, lung and gastrointestinal neoplasms were also related to 30-DM (OR 1.66, 95% CI: 1.11; 2.48 and OR 1.7, 95% CI: 1.04; 2.78). In patients in whom visceral metastases were present, an increased risk of dying in the first month of 36% was assessed (OR 1.55, 95% CI: 1.03; 2.33). Age, treatment site, and reirradiation did not show any impact in 30-DM (**Table 2**). After adjusting for other characteristics, the multivariate analysis found that male sex, ECOG PS 2–3, gastrointestinal and lung tumors were found to be independent related factors to 30-DM. Although visceral metastases confidence interval includes 1, a trend toward a

TABLE 1 | Sample characteristics and descriptive analysis according to the state at 30-days.

	All patients(n = 708)	BS Group(n = 584)	LS Group(n = 124)	*p* value
Age				0.9865
18–64 years	327 (46.2%)	267 (45.7%)	60 (48.4%)	
≥ 65 years	381 (53.8%)	317 (54.3%)	64 (51.6%)	
Sex				**0.0001**
Male	412 (58.2%)	320 (54.8%)	92 (74.2%)	
Female	296 (41.8%)	264 (45.2%)	32 (25.8%)	
ECOG PS				**<0.0001**
ECOG PS 0-1	418 (59%)	380 (65.1%)	38 (30.6%)	
ECOG PS 2-3	290 (41%)	204 (34.9%)	86 (69.4%)	
Primary tumor				**0.0016**
Breast	105 (14.8%)	100 (17.1%)	5 (4%)	
Gastrointestinal	105 (14.8%)	79 (13.5%)	26 (21%)	
Lung	219 (31%)	169 (28.9%)	50 (40.3%)	
Prostate	82 (11.6%)	70 (12%)	12 (9.7%)	
Urinary tract	72 (10.2%)	59 (10.1%)	13 (10.5%)	
Gynecological	40 (5.6%)	37 (6.3%)	3 (2.4%)	
Head and neck	34 (4.8%)	28 (4.8%)	6 (4.8%)	
Other	51 (7.2%)	42 (7.2%)	9 (7.3%)	
Visceral metastases				**0.0353**
Present	414 (58.5%)	331 (56.7%)	83 (66.9%)	
Absent	294 (41.5%)	253 (43.3%)	41 (33.1%)	
Location of the treatment				0.6162
Bone	397 (56%)	324 (55.5%)	73 (58.9%)	
Brain	181 (25.6%)	153 (26.2%)	28 (22.6%)	
Pimary tumour	70 (9.9%)	56 (9.6%)	14 (11.3%)	
Soft tissue	43 (6.1%)	35 (6%)	8 (6.5%)	
Lymph nodes	17 (2.4%)	16 (2.7%)	1 (0.8%)	
Number of fractions				**<0.0001**
Single dose	243 (34.4%)	187 (32%)	56 (45.2%)	
2-9 fractions	224 (31.6%)	171 (29.3%)	53 (42.7%)	
10-15 fractions	241 (34%)	226 (38.7%)	15 (12.1%)	
Reirradiation				0.6242
Yes	66 (9.3%)	53 (9.1%)	13 (10.5%)	
No	642 (90.7%)	531 (90.9%)	111 (89.5%)	
End of the treatment				0.6242
Yes	671 (94.8%)	575 (98.5%)	96 (77.4%)	
No	37 (5.2%)	9 (1.5%)	28 (22.6%)	

Bold values: statistically significant.

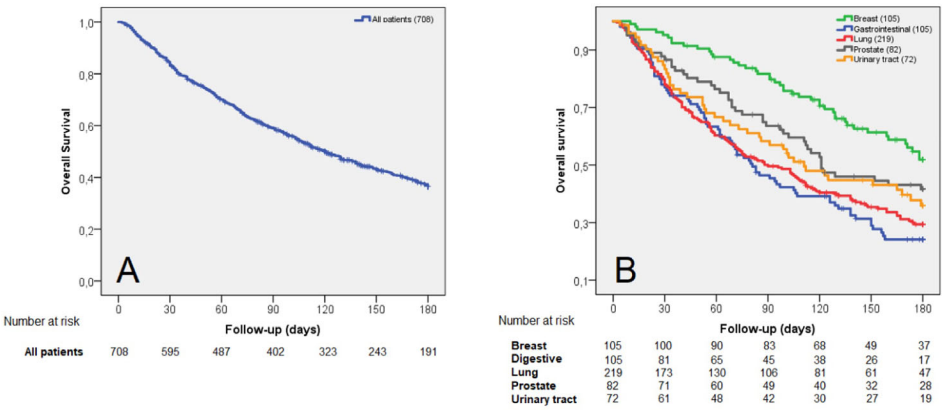

FIGURE 2 | Survival curves including: all patients **(A)** and the five more prevalent primary tumors **(B)**.

TABLE 2 | Univariate analysis investigating potential risk factors of 30-DM.

	OR	CI 95%	*p value*
Age			0.8460
18–64 years	1	1	
≥ 65 years	1.001	(0.987; 1.016)	
Sex			**0.0001**
Female	1		
Male	2.37	(1.5.; 3.66)	
ECOG PS			**<0.0001**
ECOG PS 0–1	1		
ECOG PS 2–3	4.22	(2.78; 6.40)	
Primary tumor			
Breast	1		
Lung	1.66	(1.11; 2.48)	**0.0133**
Prostate	0.79	(0.41; 1.50)	0.4665
Gastrointestinal	1.7	(1.04; 2.78)	**0.0358**
Urinary tract	1.04	(0.55; 1.97)	0.8985
Gynecologic	0,367	(0,111; 1,208)	0,0990
Head and neck	1.01	(0.41; 2.49)	0.9833
Other	1.01	(0.48; 2.13)	0.9793
Visceral Metastases			
Absent	1		
Present	1.55	(1.03; 2.33)	**0.0362**
Location of the treatment			0.6517
Primary tumor	1		
Bone	0.90	(0.44; 1.71)	
Brain	0.73	(0.36; 1.49)	
Lymph nodes	0.25	(0.003; 2.05)	
Soft tissue	0.91	(0.35; 2.40)	

Bold values: statistically significant.

TABLE 3 | Multivariate analysis investigating potential risk factors of 30-DM.

	OR	CI 95%	*p* value
Sex			
Female	1		
Male	2.38	(1.538; 3.703)	**0.0001**
ECOG PS			
ECOG PS 0-1	1		
ECOG PS 2-3	4.38	(2.84; 6.74)	**<0.0001**
Primary tumor			
Lung	1.66	(1.11; 2.48)	**0.0133**
Gastrointestinal	2.38	(1.32; 4.27)	**0.0038**
Visceral metastases			
Absent	1		
Present	1.53	(0.98; 2.40)	0.0606

Bold values: statistically significant.

higher mortality was observed (OR 1.53, 95% CI: 0.98; 2.40) (**Table 3**).

DISCUSSION

30-DM after palliative RT observed in our center was 17.5% of the palliative treatments. For those who died in the first month, the median survival was 17 days. A recent systematic review, showed an overall use of palliative RT rates in the last 30 days of life of 9–15.3% (7). Our results are slightly higher than previous studies (2–4, 7–12), but they are still adjusted to The Royal College of Radiologist recommendation of 30-DM to be inferior to 20%. Therefore, we consider that the selection of our patients for palliative treatment is adequate.

Park and et al. (7) conducted a systematic review and found that major predictors for 30-DM among single institution studies were ECOG PS, lung cancer primary, bladder cancer primary, multiple metastases, and evidence of progressive disease. In our analysis, we have also found the presence of a gastrointestinal tumor to be associated with 30-DM. Our center receives many patients with multi-treated digestive tumors for phase I trials. We believe this fact may partly explain this data. We have not found the presence of visceral metastases to have a statistically significant impact on survival in the multivariate analysis, but there is a clear trend we cannot ignore.

Studies analyzing patients with bone metastases treated with RT show a rather wide range of 30-DM. Ellsworth et al. (13), reported a 30-DM of 26%. The most frequent scheme consisted of 6–10 fractions (56%), while the use of single doses was 8%. On the other hand, a large Canadian population cohort study including

8,301 patients with bone metastases, showed a 30-DM of 14.5%, and a single dose was used in 64.2% of the patients in the last month of life (14). This imbalance is thought to be multifactorial and partially related to historical practice patterns and financing of the treatments. When considering patients treated for bone metastases in our series, 30-DM was 18.3%. The use of single doses was by far the most used (91%). These results are adjusted to international recommendations of a use of single fractions in patients with advanced cancer who have uncomplicated bone metastases (15, 16). Although single fractions schemes seem to be advantageous in terminally ill patients, published data show that the use multiple fractions are preferred among institutions (7). This overuse of fractionated regimens may be related to unrealistic concerns about late radiation damage and can expose dying patients to who are not expected to require a re-treatment. On the contrary, the choice of prescribing single doses has the potential to reduce cost and unnecessary visits to the hospital of terminally ill patients. Our high use of single doses for bone metastases in those with shortened survival, indirectly suggests that the fractionation approach was adapted to the end-of-life.

Since the life expectancy of these patients is sometimes too short, when palliative RT is indicated, its impact on quality of life might doubtful. Symptom relief is usually obtained in a wide range of time. When treating painful bone metastases mostly it is achieved at 3–4 weeks (17), while this benefit can be delayed up to months in brain metastases related symptoms (18). Gripp found that half of the patients treated with palliative RT spend most of their remaining time on therapy, of which a large part did not complete the treatment. Out of the patients who died in one month from the first visit, only 16% of survival estimations were correct (2). Despite the fact that the vast majority of our patients completed the treatment, 37 patients did not, of whom 28 died within the first month from the start of the treatment. This means that this small group of patients probably did not benefit from treatment and their life expectancy was expected to be longer.

Predicting survival in terminally patients evaluated for palliative RT is a difficult task since several factors are involved. The clinical predictors' factor does not seem to be accurate enough to estimate the patient's real-life expectancy (5, 19). Hemoglobin levels or life-threatening related symptoms, such as dyspnea or cachexia, are also relevant in advanced disease. Hence, it is important to develop survival prediction tools to achieve tailored-end-of-life strategies. In our study, we were able to construct a calculator of 30-DM using the variables with impact on 30-DM in the multivariate analysis. Of them, the ECOG PS is the one with the greatest impact on 30-DM. So that, when a male patient referred for palliative RT presents with an ECOG PS 0–1 and lung cancer, the probability of dying within the first month would be 12.3%, but if the same patient presents with an ECOG PS 2–3, this percentage would increase to 21.4%. Nonetheless, this data is not yet validated. Nowadays, there are several prognostic scores for patients with advanced cancer (9, 19–21), although most of them have not been validated in a prospective cohort of patients treated with palliative RT. Angelo et al. developed a six-parameter decision tree that was able to predict the use of palliative RT in the last 30 days of life. However, it was only applicable to patients with primary lung or bladder cancer (9). A recent study performed by Kain et al. applied the TEACHH model retrospectively to 1,744 consecutive patients. This score consists of six easy-collectable variables specifically addressed to patients referred for palliative RT. They were able to separate patients into three different and clinically relevant survival groups (12). There are few prospective studies using prognostic scores in the palliative RT set. PROGRAD stands out as a prospective study which applies two validated prognostic systems in the initial assessment of patients referred for palliative RT. Using the Palliative Prognostic Index (PPI) and the Number of Risk Factors (NRF) score, they were able to stratify the patients into three groups with different prognoses. PPI score seemed to be the one that best discriminated those patients with the worst prognosis (22).

The relevance of this data is that it can discriminate clinically relevant groups based on scales that are simple to apply and include variables easily collectable in the patient's first visit. From our part, we have found the presence of factors related to 30-DM that may help develop a more tailored to life expectancy strategy. However, our study is inherently biased by its retrospective design and reflects the clinical practice of a single center, so its interpretation and generalization must be made cautiously. In the current study we only included patients who started the treatment, but a few patients who were planned for palliative RT and died before initiation are not taken into account. For a better understanding of the decision-making, it would be valuable to include for the analysis the patients who were considered unfit for palliative RT. Other variables with demonstrated impact on 30-DM, such as white blood count, dyspnea, or cachexia, could not be collected in a retrospective setting.

RT can provide the necessary relief of symptoms in patients with advanced cancer. However, the use of palliative RT in the last days of life may not be useful. It is therefore important to select appropriately which patients can benefit from palliative RT. While clinical prediction alone seems to be an inaccurate method for decision-making in these patients, 30-DM is objective and can set a clinically relevant time endpoint for symptom relief in patients with short survival. The reliability of survival prediction might be improved with the implementation of objective prognostic systems including variables related to early mortality. Our study provides useful and comparable results with previous, which may be useful to decide whether palliative RT should be indicated or not. In addition, it also may contribute to a better understanding of the patterns of usual clinical practice. There is now a growing body of evidence supporting the implementation of predicting tools in the palliative RT approach. The challenge is to identify those patients who will not benefit from palliative RT in order to provide a better care near the end of life.

NOMENCLATURE

30-DM, 30-Day Mortality; ECOG, Cooperative Oncology; PS, Performance Status; RT, Radiation Therapy; BS, Better Survival; LS, Lower Survival; PPI, Palliative Prognostic Index; NRF, Number of Risk Factors.

DATA AVAILABILITY STATEMENT

The raw data supporting the conclusions of this article will be made available by the authors, without undue reservation.

ETHICS STATEMENT

The studies involving human participants were reviewed and approved by the Comitè Ètic d'Investigació Clínica (CEIC) of Vall d'Hebron University Hospital. Written informed consent for participation was not required for this study in accordance with the national legislation and the institutional requirements.

AUTHOR CONTRIBUTIONS

Concept and design: MV, MA, and JG. Collection and assembly of data: MV, DM, and AG. Data analysis and interpretation: SP-H and MV. Manuscript writing: MV and JG. Final approval of the manuscript: All authors. All authors contributed to the article and approved the submitted version.

ACKNOWLEDGMENTS

The statistical analysis has been carried out in the Statistics and Bioinformatics Unit (UEB) of the Research Institute of the Vall d'Hebron Hospital (VHIR).

REFERENCES

1. Earle CC, Neville BA, Landrum MB, Ayanian JZ, Block SD, Weeks JC. Trends in the aggressiveness of cancer care near the end of life. *J Clin Oncol* (2004) 22(2):315–21.
2. Gripp S, Mjartan S, Boelke E, Willers R. Palliative radiotherapy tailored to life expectancy in end-stage cancer patients: Reality or myth? *Cancer* (2010) 116 (13):3251–6.
3. Guadagnolo BA, Liao KP, Elting L, Giordano S, Buchholz TA. Use of radiation therapy in the last 30 days of life among a large population-based cohort of elderly patients in the United States. *J Clin Oncol* (2013) 31(1):80.
4. Murphy JD, Nelson LM, Chang DT, Mell LK, Quynh-Thu L. Patterns of care in palliative radiotherapy: A populationbased study. *J Oncol Pract* (2013) 9(5).
5. Hartsell WF, Desilvio M, Bruner DW, Scarantino C, Ivker R, Roach M 3rd, et al. Can physicians accurately predict survival time in patients with metastatic cancer? Analysis of RTOG 97-14. *J Palliat Med* (2008) 11 (5):723–8.
6. Department of Health. *Improving Outcomes : A Strategy for Cancer - 4th Annual Report*. United Kingdom: Department of Health and Public Health (2014). pp. 1–101. Available at: www.dh.gov.uk/publications.
7. Park KR, Lee CG, Tseng YD, liao JJ, Reddy S, Bruera E, et al. Palliative radiation therapy in the last 30 days of life: A systematic review. *Radiother Oncol* (2017) 125(2):193–9.
8. Spencer K, Morris E, Dugdale E, Newsham A, Sebag-Montefiore D, Turner R, et al. 30 Day mortality in adult palliative radiotherapy - A retrospective population based study of 14,972 treatment episodes. *Radiother Oncol* (2015) 115(2):264–71.
9. Angelo K, Norum J, Dalhaug A, Pawinski A, Aadahl G, Haukland E, et al. Development and validation of a model predicting short survival (death within 30 days) after palliative radiotherapy. *Anticancer Res* (2014) 34(2):877–86.
10. Lopez AN, Bingham B, Strickler S, Dvorak T, Morris CG, Yeung AR. 30- and 90-Day Mortality Rates in Patients Treated with Curative or Palliative Radiation Therapy. *Int J Radiat Oncol Abstract* (2017) 99(2):E558.
11. Wu SY, Singer L, Boreta L, Garcia MA, Fogh SE, Braunstein SE. Palliative radiotherapy near the end of life. *BMC Palliat Care* (2019) 18(1):4–11.
12. Kain M, Bennett H, Yi M, Robinson B, James M. 30-Day Mortality Following Palliative Radiotherapy. *J Med Imaging Radiat Oncol* (2020) 64(4):570–9.
13. Ellsworth S, Alcorn S, Hales R, McNutt TR, DeWeese TL, Smith TJ. Patterns of Care Among Patients Receiving Radiation Therapy for Bone Metastases at a Large Academic Institution. *Int J Radiat Oncol* (2014) 89(5):1100–5.
14. Tiwana MS, Barnes M, Kiraly A, Olson RA. Utilization of palliative radiotherapy for bone metastases near end of life in a population-based cohort Cancer palliative care. *BMC Palliat Care* (2016) 15(1):1–5.
15. Chow E, van der Linden Y, Roos D, Hartsell WF, Hoskin P, Wu JSY, et al. Single versus multiple fractions of repeat radiation for painful bone metastases: a randomised, controlled, non-inferiority trial. *Lancet Oncoly* (2014) 15(2):164–71.
16. Lutz S, Balboni T, Jones J, Lo S, Petit J, Rich SE, et al. Palliative radiation therapy for bone metastases: Update of an ASTRO Evidence-Based Guideline. *Pract Radiat Oncol* (2017) 7(1):4–12.
17. McDonald R, Ding K, Brundage M, Meyer RM, Nabid A, Chabot P, et al. Effect of radiotherapy on painful bone metastases: A secondary analysis of the NCIC Clinical Trials Group Symptom Control Trial SC.23. *JAMA Oncol* (2017) 3(7):953–9.
18. Lin NU, Lee EQ, Aoyama H, Barani IJ, Baumert BG, Brown PD, et al. Challenges relating to solid tumour brain metastases in clinical trials, part 1: patient population, response, and progression. A report from the RANO group. *Lancet Oncol* (2013) 14(10):e396–406.
19. Krishnan MS, Epstein-Peterson Z, Chen YH, Tseng YD, Wright AA, Temel JS, et al. Predicting life expectancy in patients with metastatic cancer receiving palliative radiotherapy: The TEACHH model. *Cancer* (2014) 120(1):134–41.
20. Baba M, Maeda I, Morita T, Inoue S, Ikenaga M, Matsumoto Y, et al. Survival prediction for advanced cancer patients in the real world: A comparison of the Palliative Prognostic Score, Delirium-Palliative Prognostic Score, Palliative Prognostic Index and modified Prognosis in Palliative Care Study predictor model. *Eur J Cancer* (2015) 51(12):1618–29.
21. Zhang WY, Li HF, Su M, Lin RF, Chen XX, Zhang P, et al. A simple scoring system predicting the survival time of patients with bone metastases after RT. *PloS One* (2016) 11(7):1–9.
22. Chen ATC, Mauro GP, Gabrielli F, Gonçalves C, Castro I, Moutinho K, et al. PROGRAD – An observational study of the prognosis of inpatients evaluated for palliative radiotherapy. *Radiother Oncol* (2018) 127(2):299–303.

Conflict of Interest: The authors declare that the research was conducted in the absence of any commercial or financial relationships that could be construed as a potential conflict of interest.

frontiers in Oncology

ORIGINAL RESEARCH
published: 15 June 2021
doi: 10.3389/fonc.2021.673886

Prospective Assessment of Early Proton Therapy-Induced Optic Neuropathy in Patients With Intracranial, Orbital or Sinonasal Tumors: Impact of A Standardized Ophthalmological Follow Up

Marie Lecornu[1], Paul Lesueur[1,2,3], Julia Salleron[4], Jacques Balosso[1], Dinu Stefan[5], William Kao[1], Tiphaine Plouhinec[1], Anthony Vela[1], Pauline Dutheil[1], Jordan Bouter[1], Pierre-Alban Marty[6], Juliette Thariat[1†] and Jean-Claude Quintyn[6†]*

[1] Radiation Oncology Department, Centre François Baclesse, Caen, France, [2] Radiation Oncology Department, Centre Guillaume le Conquérant, Caen, France, [3] ISTCT UMR6030-CNRS, CEA, Université de Caen-Normandie, Equipe CERVOxy, Caen, France, [4] Cellule Data Biostatistique, Institut de Cancerologie de Lorraine, Nancy, France, [5] Radiation Oncology Department, Institut Universitaire du Cancer de Toulouse, Toulouse, France, [6] Ophthalmology Department, University Hospital of Caen, Caen, France

OPEN ACCESS

Edited by:
Susan Lynne McGovern, University of Texas MD Anderson Cancer Center, United States

Reviewed by:
William F. Hartsell, Northwestern University, United States
Ima Paydar, Hospital of the University of Pennsylvania, United States

***Correspondence:**
Marie Lecornu
lecornumarie01@gmail.com

†These authors have contributed equally to this work

Specialty section:
This article was submitted to Radiation Oncology, a section of the journal Frontiers in Oncology

Received: 28 February 2021
Accepted: 27 May 2021
Published: 15 June 2021

Citation:
Lecornu M, Lesueur P, Salleron J, Balosso J, Stefan D, Kao W, Plouhinec T, Vela A, Dutheil P, Bouter J, Marty P-A, Thariat J and Quintyn J-C (2021) Prospective Assessment of Early Proton Therapy-Induced Optic Neuropathy in Patients With Intracranial, Orbital or Sinonasal Tumors: Impact of A Standardized Ophthalmological Follow Up. Front. Oncol. 11:673886. doi: 10.3389/fonc.2021.673886

Purpose: Proton therapy (PT) can be a good option to achieve tumor control while reducing the probability of radiation induced toxicities compared to X-ray-based radiotherapy. However, there are still uncertainties about the effects of PT on the organs in direct contact with the irradiated volume. The aim of this prospective series was to report 6-month follow-up of clinical and functional optic neuropathy rates of patients treated by proton therapy using a standardized comprehensive optic examination.

Methods and Materials: Standardized ophthalmological examinations were performed to analyze subclinical anomalies in a systematic way before treatment and 6 months after the end of proton therapy with: Automatic visual field, Visual evoked potential (VEP) and optic coherence of tomography (OCT).

Results: From October 2018 to July 2020 we analyzed 81 eyes. No significant differences were found in the analysis of the clinical examination of visual functions by the radiation oncologist. However, considering VEP, the impairment was statistically significant for both fibers explored at 30'angle (p:0.007) and 60'angle ($p < 0.001$). In patients with toxicity, the distance of the target volume from the optical pathways was more important with a p-value for 30'VEP at 0.035 and for 60'VEP at 0.039.

Conclusions: These results confirm uncertainties concerning relative biological effectiveness of proton therapy, linear energy transfer appears to be more inhomogeneous especially in areas close to the target volumes. The follow-up of patients after proton therapy is not an easy process to set up but it is necessary to improve our knowledges about the biological effects of proton therapy in real life. Our

study which will continue during the coming years, suggests that follow-up with in-depth examinations such as VEP as a biomarker could improve the detection of early abnormalities.

Keywords: proton therapy, radiation-induced optic neuropathy, optic toxicity, optic pathway tolerance, radiation neuropathy

INTRODUCTION

The treatment of skull base tumors often relies on surgery and radiotherapy (1, 2). The delivery of a high dose to the tumor nearby organs at risk (OAR) such as optic nerves and chiasma can be challenging. Consequences of radiation induced optic toxicities are various and may induce a loss of visual acuity, visual field disorder or retinopathy. These anomalies can appear from 3 months to 10 years after radiotherapy (3). Radiation-induced optic neuropathy (RION) is defined by a painless defect of visual acuity, in one or both eyes after a latency of months to years after radiotherapy (4). Due to damages to the optic nerve, the visual field is reduced to a variable extend. According to the literature, optical toxicities appear from a cumulative dose between 55 to 60Gy (EQD2) or for single fraction greater than 10Gy (5–7). Most treatments are still carried out by X-ray. Although new photonic techniques allow excellent coverage of target volume and a better respect of OAR's dose constraints (8–10) than conventional technics. In complex or large tumors involving areas in direct proximity of the anterior optic pathways, damage to the optic structures may be frequent and somehow unavoidable. The advantageous dose distribution of proton may be used to spare OARs located close to the tumor (11–13) and to spare healthy brain. In such cases, the aim of proton therapy (PT) is to achieve tumor control while reducing the probability of radiation induced toxicities compared to modern X-ray-based radiotherapy (RT), such as intensity modulated radiation therapy (IMRT) or stereotactic radiation therapy (SRT). However, there are still uncertainties about the effects of PT on the organs in direct contact with the irradiated volume, in particular regarding relative biological effectiveness (RBE). Indeed RBE could be underestimated at the beam end due to high linear energy transfer (LET) (14). Proton therapy series report a 7% risk to develop severe optic neuropathy (15). These rates may be underestimated because data are generally based on patient's spontaneous reporting instead of systematic and standardized collection. Moreover, these optic toxicities do not appear to follow the previously established dose volume effects for optic neuropathy, based on photons irradiation (X-rays). Consequently, proton induced optic toxicities may differ from those of photons. Only few data are published, mainly retrospective (15–18). As an attempt to fill this gap we designed, in the context of our rising proton therapy activity, a prospective and comprehensive assessment of optic outcomes using a standardized optic workup at baseline and during patients' follow up. The aim of this study was to find predictive early subclinical alterations because when radiation induced optic disorder are clinically significant, they are unfortunately irreversible. An additional aim, at the populational scale could be to contribute to improve biomathematical modelling for outcome predictions, and therefore treatment planning optimization, for safer treatments.

Accordingly, this prospective series is an initial and preliminary report of 6-month follow-up of clinical and functional optic neuropathy rates of patients treated by proton therapy using a standardized comprehensive optic examination.

METHODS AND MATERIALS

Population Analysis

The first comprehensive optic examination (optic Work-up) was performed in October 2018. Patients ≥ 18 years old, with tumors (benign or malignant) within 1cm of the optic tract were included in this Institutional Review Board approved study, after multidisciplinary staff meeting and technical expert committee meeting. An information letter is sent to each patient informing them that data from patients treated with proton therapy in Caen were related to clinical research. Patients were referred from multiple institutions but all were treated at the Normandy proton therapy center (Caen, France) and underwent optic examinations at the University hospital of Caen. Exclusion criteria were pediatrics, secondary or intraocular tumors and refusal to undergo optic examinations. To properly assess dose volume effects and the impact of previous damage from tumor, surgery, or any other treatment on the optic nerves, chiasm, and other optic structures, we adjusted outcomes on status before PT. Past medical history, treatments and comorbidities were reported, some have been recognized as risk factors for RT induced toxicities: diabetes, hypertension, glaucoma, smoking for example.

Tumors and Location

Tumor diagnoses were distributed into different groups: meningiomas, pituitary adenoma, craniopharyngioma and other rarer diagnoses. The minimal distance to optical structures was assessed and tumors were separated in three groups: those invading or abutting the optic pathways, tumors located between 0 and 3mm from the optic pathway and tumors between >3 and 10mm.

Treatment

Tumor and OAR delineation was based on millimetric CT scan and multimodal imaging including systematically a contrast enhanced fusion MRI in treatment position. Proton therapy was performed using pencil beam scanning (PBS) with a ProteusOne®

machine (IBA, Louvain la Neuve, Belgium). PBS corresponds to a three dimensions scanning obtained by successive plan scanning done by individually modulated mono-energy beams of adapted energy (19). First treatments were delivered in IMPT (Intensity Modulated Proton therapy) with Single field optimization (SFO) and after one year, IMPT multiple field optimization (MFO) was applied when necessary, depending on OAR (Organ at risk) constraints (20). During the planning process we checked that the end of the beam range was never in front of the optical structures. The intensity of the spots and their location were analyzed. In case of positioning of spots too intense in the heart of a volume at risk this was modified. The LET mapping was not routinely performed before treatment because the software did not allow it. The treatment plan was calculated using robust optimization (assuming 3mm positioning uncertainty and 3% proton range uncertainty unless filling cavity uncertainties) (21) using the Treatment planning system (TPS) Raystation (Raysearch®). We performed also a robust evaluation. Calculations includes a 1.1 relative biological effectiveness. Treatment was delivered in 1.8-2Gy (RBE) fractions, five days a week. Some patients benefited from a combination of photon and proton treatment. In some cases, a boost dose of 12 to 21.6Gy in 2.4Gy per fraction was delivered by SRT by a Cyberknife® machine (Accuray, Madison, WI, USA). These were applied because they represented a dosimetric advantage. In the event of beam downtime and so as to hold the tumor control probability, some patients underwent photon-based replanning until PT resumed.

Practical Ophthalmological Examinations

A standard clinical examination was carried out by radiation oncologist including: subjective deficit of visual acuity, oculomotor nerve disorders and visual field disorder. Then, he prescribed the complementary follow-up examinations. Each patient was addressed to the ophthalmologist who performed in first, clinical exam with: photo-motor reflex, a measure of visual acuity, a dilated fundus and a measure of lens opacity.

More specific examinations were systematically performed: a visual field exam, papillary optical coherence tomography (OCT), and visual evoked potentials.

The visual field corresponds to the entire area that a person can see when looking at a point. The average corrected deficit was collected allowing to make a discrimination between normal and pathological examinations and specially to obtain a follow-up for each patient. If the average corrected deficit was more than 3 points different from the general population, the result was considered pathological. Visual field tests results can help to determine the location of the radiation-induced damage. In order to specify the available data concerning the visual field, the perimetry has been detailed in 6 sectors to allow locating the anomalies: nasal, upper nasal, lower nasal, temporal, lower temporal and upper temporal.

Patients also benefit from a measurement of visual evoked potentials (VEP). VEP is the physiological response of the occipital cortex to a sensory stimulus of vision. Latency and amplitude are evaluated. VEP provide information about optic neuritis (22). We collected P100 data for each eye and for the 60' and 30' visual angles to obtain data from different macular fibers. The latency of the P100 (**Figure 1**) wave was considered pathological if it was greater than 120ms. The amplitude was considered pathological if it was less than 6 microvolts. If the disorders were symmetrical on the right and left occipital lobe, it was an impairment of the anterior optic pathways.

The Optical coherence tomography (OCT) was performed to obtain high resolution images of the retina. Measurement of retinal nerve fiber layers (RNFL) is used to assess optic nerve fiber damage. A fiber thickness of less than 60μm was considered pathological.

At the end of this paraclinical assessment, the patient was seen in consultation with an ophthalmologist.

Follow-Up

Prospective assessment was performed at baseline, i.e. before PT, 6 and 12 months after the end of treatment, and every year. Clinical exam and MRI or CT were performed every 3 months after PT.

Statistical Analysis

Qualitative parameters were described as frequency and percentage, quantitative parameters as median and interquartile range. Normality of the distribution was investigated with Shapiro-Wilks test. The comparisons of qualitative parameters from T0 to T6 were performed with Mac-Nemar test (paired Chi-squared test). Eyes with and without toxicity were compared by Chi-squared test or Fisher Exact test for qualitative parameters and with Wilcoxon U test for quantitative ones.

Significance level was set at 0.05. Statistical analyses were performed with SAS software, version 9.4 (SAS Institute Inc., Cary, NC, USA.).

RESULTS

From October 2018 to July 2020 we recruited 41 patients for this study. Sixty patients were initially eligible, but 2 patients were deceased, 2 were too impaired to perform the follow-up. One patient was no longer living in France, 7 ophthalmological examinations has been cancelled because of the global pandemic COVID-19 and 7 exams are missing because the patients did not show up. The median follow-up time was 8 months, interquartile range from 7 to 9 months. In **Table 1** are summarized the patients' baseline characteristics. Most patients were treated for meningiomas (53.7%). Clinical deficits were initially in 13 (31.7%) patients. The median age was 57 years old {19-92}. Most of patients (73.2%) had already undergone at least one local treatment: 27 patients (65.9%) were treated with at least one surgery and 3 (7.3%) with previous radiotherapy. We included these 3 patients because the doses received at the previous optical structures were not significant. Two patients had a rather distant irradiation (maxillary and cervical). The third patient had already received 66Gy on the same volum but had no toxicity from his previous irradiation 5 years earlier. The eleven remaining patients received radiotherapy as first line treatment. The tumor abutted or invaded the optic tract (in

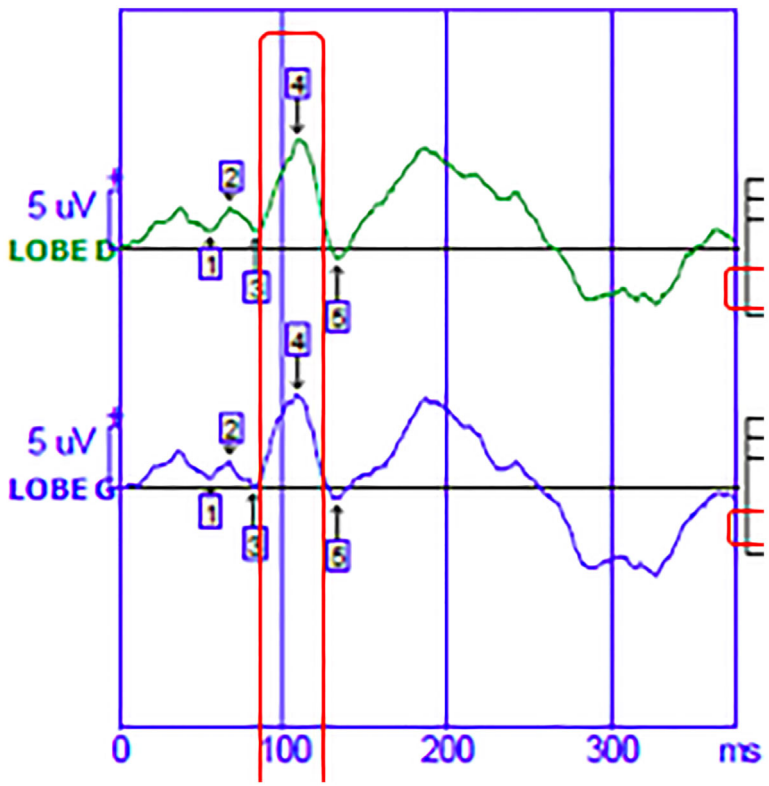

FIGURE 1 | Visual evoked potential.The green curve corresponds to the nerve signal born in the visual cortex of the right occipital lobe. The blue curve corresponds to the nerve signal born in the visual cortex of the left occipital lobe.The abscissa shows the time in milliseconds. On the ordinate is the amplitude of the wave in microvolt.

the case of malignant tumors) in 23 patients (56%), i.e., the distance to the optic tract was 0mm on MRI. Considering PT, the majority of patients received single field SFO (single field optimization) type PT (92.7%). Some patients received treatment with photon. On 41 patients, 18 patients received a combined photon-proton therapy. For 15 patients it was due to machine failure. Three patients had benefited from an additional dose of 12 and 21.6Gy in stereotactic condition with 2.4Gy per fraction. Boost were applied because it was represented a dosimetric advantageous. The **Table 2** summarized the treatment characteristics of the patients.

Radiation Oncologist Examination

We analyzed specifically the evolution of results of the clinical examination by the radiation oncologist. No significant difference was found. Results clinical examination by radiation oncologist at baseline and after 6 months were summarized in **Table 3**.

Ophthalmological Examinations

Results of ophthalmological examinations are summarized in **Table 4**. They were analyzed by eye, so we had 81 eyes for 41 patients because 1 patient undergone an enucleation. Concerning baseline's results, 11% of patients had a loss of visual acuity. At 6 months, there was no significant difference since visual deficit was found in 12.4% of eyes. Concerning the visual field, the impairment severity decreased over time. In fact, the number of eyes with more than 3 sectors affected was 8.6% at 6 months compared to 23.5% at baseline. However, the analysis of the mean corrected deficit did not show a significant difference with p-value: 0.317.

The initial deficit of VEP for 30' fibers represented 33 eyes (41.8%) and at 6 months VEP deficit affected 47 eyes (59.5%). Twenty-seven (33.3%) 60' VEPs were abnormal at baseline and 44 (55.7%) at 6 months. This impairment was statistically significant for both fibers explored at 30' and 60' angles with a p-value of 0.007 and <0.001 respectively.

Analysis of the results for optical coherence tomography (OCT) did not reveal any significant difference.

On Fifty-three 60' VEP normal at baseline 21 became pathological after 6 months of follow-up. For the 30' VEP, 45 eyes were normal prior to treatment, and 18 of them developed toxicity. We compared for the 30' VEP and 60' VEP those that remained normal compared to those that became pathological after proton therapy.

Distance from optical structures was a significant factor influencing the evolution of VEP in both groups, with a p-value for 30'VEP at 0.035 and for 60'VEP at 0.039. In fact,

TABLE 1 | Population baseline characteristics.

	n (%)
WHO performance status	
0	30 (73.2)
1	9 (21.9)
2	2 (4.9)
Age (years), Median [interquartile range]	57 [43; 63]
Sex	
Male	15 (36.6)
Female	26 (63.4)
Months since diagnosis: Median [interquartile range]	12[4-50]
Comorbidities	22 (53.7)
Diabetes	3 (7.4)
Hypertension	10 (24.4)
Smoking	10 (24.4)
Vascular disease	6 (14.6)
Histology	
Meningioma	22 (53.7)
Adenoma/craniopharyngioma	7 (17.1)
Other	12 (29.3)
Initial deficits	13 (31.7)
Previous treatment history	28 (68.3)
Radiotherapy	3 (7.3)
Surgery	27 (65.9)
Enucleation	1 (2.4)
Medical treatments	4 (9.8)
Chemotherapy	3 (7.5)
Immunosuppressor	1 (2.4)
Distance of optical structures	
0mm	23 (56)
0-3mm	8 (19.5)
>3mm	10 (24.4)
Glaucoma	2 (4.9)
Clinical exam	
Neurological deficit	17 (41.5)
Oculomotor deficit	12 (29.3)
VA deficit	10 (24.4)
VF deficit	9 (22)

WHO, world health organization performance status; n, number of patients; VA, visual acuity; VF, visual field.

patients whose tumors were in direct contact with the optical pathways, 30' VEP and 60' VEP were less affected.

Treatment history i.e. radiotherapy or surgery were more frequent for patients with toxicity on 30' VEP (p= 0.017). The results are summarized in **Table 5**.

For 60' VEP, the dose received by 50% of the volume of the chiasma (D50%) was significantly higher in patients with toxicity (p=0.04), the D2% for optic nerve was also more important, 51.2Gy for eyes with toxicity and 41.9Gy for eyes free of injury, p: 0.042. Age appeared to be an influenced factor with p= 0.057. The results are summarized in **Table 6**.

DISCUSSION

Optical toxicities may limit the treatment of tumors of the skull-base. Proton therapy is a good option to reduce the irradiated volume of healthy brain. However, there are still some debate about the effects of proton therapy on the organs in direct contact with the irradiated volume, particularly because of uncertainties of RBE and linear energic transfer. In the treatment of para optic tumors, RION is the main limiting toxicity and its detection needs a careful follow-up so as to ensure an early detection and ophthalmological care. Unfortunately, data for monitoring visual function after these treatments are rare and incomplete (23). The difficulty of follow-up is mainly related to the limited number of proton therapy centers, so the treated population comes from different remote regions and patients lost to follow-up are frequent. We tried to obtain a large amount of data by doing the follow-up in a systematic way but in nearly 30% of cases data of 6 months examinations were lacking. It can be explained by the asymptomatic nature of impairment, patients are less motivated for follow up. Eight ophthalmological examinations have been cancelled because of the global pandemic COVID-19. Specific ophthalmological examinations were performed to analyze subclinical anomalies. The results presented are exploratory.

As shown by our results, the clinical examination of the radiation oncologist is not a sensitive examination for the detection of abnormalities or improvements in visual functions.

Overall, with 6 months of delay we did not observe any significant increase in optical damage after proton therapy, this suggests that proton therapy might be a safe and well-tolerated treatment, at least at short term. This is in agreement with the results of previous studies that have demonstrated the safety of proton therapy on visual function at early follow-up.

TABLE 2 | Characteristics of treatment for 41 patients.

	n (%)	Median (range)
Proton only	23 (56)	
Proton + photon	18 (44)	
SFUD	36 (87.8)	
IMPT	5 (12.2)	
Number of beams		
1	1 (2.4)	
2	38 (92.7)	
3	2 (4.9)	
Volume CTV (cm3)		26.7 (6.8 to 237.4)
Prescription dose (Gy (RBE))		54 (24 to 73.8)

n, number of patients; SFUD, single field uniform dose; IMPT, intensity modulated proton therapy; CTV, clinical target volume; RBE, relative biological efficiency (considered as 1.1 for protons).

TABLE 3 | Clinical examination at 0 and 6 months.

	Baseline	At 6 months	p-value
Oculomotor deficit	12	11	0.66
VA deficit	10	4	0.083
VF deficit	9	6	0.37

VA, visual acuity; VF, visual field.

To our knowledge, few studies have been conducted to analyze the subclinical effects and long-term consequences of proton therapy on visual functions. Moreover, these studies were based on retrospective data and the ophthalmological examinations were performed only in case of clinical abnormality in a non-standardized way. In 2018, Li *and al* published a study evaluating visual functions after PT for chordoma and chondrosarcoma, the results involved a large number of patients with a long-term follow-up of 4.8 years. Considering retrospective and not standardized data, the low level of optical toxicity reported was probably underestimated: only 1% among patients receiving <59Gy (RBE) and 5.8% among patients receiving ≥ 60Gy (RBE) to the optic pathway developed optic toxicities. In this study, RION was defined as the loss of visual acuity. However in optic neuropathy, the decrease of visual acuity is a late sign that is not necessary for early diagnosis (24).

El Shafie et al. (25), in a prospective study, suggested that proton therapy was an effective and safe treatment, but only acute toxicities were assessed. In Kountouri's data published in 2019, optic toxicity was rare with 7% of patients developing optic troubles (15), but most of them were severe (8 patients of 14 with grade IV RION). Given that, in this study, patients did not benefit from a full standardized ophthalmologic follow up, it suggests that much more patients could present infra clinical or low-grade optic impairment.

In our study, the assessment of visual fields showed an improvement between baseline and the 6-month examination. These results could be biased by the patient's learning curve and requires more follow-up to characterize the objective evolution over time. The validity of information obtained from a visual field test depends on the ability of the patient to perform the test correctly with caution (26). According to studies carried out by ophthalmologists as part of glaucoma follow-up, assessments of the first visual fields were often impaired due to a lack of reliability. Katz et al. (27) found that 19% of normal, 28% of ocular hypertensives, and 37% of glaucoma patients were unreliable on their first visual field. Sherafat et al. (26), in a randomized and controlled trial found that the use of brief video information about the visual field test improved the reliability of the results for those being tested for the first time. In our study this may explain the trend for improvement in visual field abnormalities at 6 months.

Considering visual evoked potentials, the impairment was statistically significant for both fibers explored at 30' and 60' angles with a p-value of 0.007 and <0.001 respectively.

Visual evoked potential is an important visual electrophysiological diagnostic exam, which can be used as an objective measure of optic nerve function. Correlations between the magnitude of VEP latency parameters and automated visual parameters have suggested that cortex responses in glaucoma patients could be tested by electrophysiological methods (28). Electrophysiology in glaucoma brings valued information, which detects macular ganglion cell dysfunction and VEP can be of aid in the evaluation of "glaucoma suspects" even before a detectable loss appears by visual field examination (29). Visual evoked potential seems to be the more sensitive exam for detection of visual toxicity. It can be also an interesting exam to describe partial radiation's effects because it explores different optic fibers.

In our study, D50% was a significant factor in the alteration of 60'VEP. In most of the studies, the dose constraints mainly

TABLE 4 | Summary of abnormal result of each ophthalmological exam for 81 eyes.

DEFICIT	T0	T6	p-value
VA	9 (11.1%)	10 (12.35%)	0.564
VF	23 (30.3%)	16 (21.9%)	0.317
Number of sectors impaired:			
0	37 (45.68%)	50 (61.73%)	0.027
1-2	15 (18.52%)	15 (18.52%)	
3	10 (12.35%)	9 (11.11%)	
>3	19 (23.46%)	7 (8.64%)	
Cataract	27 (33.33%)	31 (38.3%)	0.165
30' VEP	33 (41.8%)	47 (59.5%)	0.007
60' VEP	27 (33.3%)	44 (55.7%)	<0.001
OCT	12 (15.6%)	11 (14.9)	1

T0, number of deficits at baseline; T6, number of deficits at 6 months; VA, visual acuity (abnormal if ETDRS <55); VF, visual field (pathological if average corrected deficit different by 3 points from general population); OCT, optical coherence tomography (abnormal if thickness < 60 micrometers); VEP, visual evoked potentials (abnormal if amplitude < 6 μV or latency > 120ms).

TABLE 5 | Comparison of patients who experienced VEP toxicity to those who remained normal, analyses for VEP 30'.

	Eyes with toxicity n=18	Eyes without toxicity n=27	p-value
Age (years): Median [interquartile range]	47.4 [41.7;60.5]	58.4 [50.4;60.8]	0.224
Time from diagnostic	46[11;61]	14 [2;51]	0.168
Time from baseline	8.8 [7;9.4]	7.8 [5.8;8.9]	0.242
Sex			
1	8 (44.4%)	6 (22.2%)	0.115
2	10 (55.6%)	21 (77.8%)	
Comorbidities	9 (50.0%)	17 (63.0%)	0.388
Histology			0.140
Meningioma	9 (50.0%)	21 (77.8%)	
Adenoma/craniopharyngioma	4 (22.2%)	2 (7.4%)	
Other	5 (27.8%)	4 (14.8%)	
Initial deficits	8 (44.4%)	10 (37.0%)	0.620
Treatments history	15 (83.3%)	13 (48.1%)	0.017
Distance of optical structures			0.035
0mm	5 (27.8%)	18 (66.7%)	
0-3mm	5 (27.8%)	4 (14.8%)	
>3mm	8 (44.4%)	5 (18.5%)	
Clinical exam			
Neurological deficit	6 (33.3%)	13 (48.1%)	0.324
Oculomotor deficit	5 (27.8%)	12 (44.4%)	0.259
VA deficit	2 (11.1%)	5 (18.5%)	0.502
VF	3 (16.7%)	3 (11.1%)	0.670
Other	2 (11.1%)	1 (3.7%)	–
CTV (cm3)	35.7 [10.9;73.2]	24.3 [12.6;53.1]	0.108
Prescription dose	54 [54;59.4]	54 [54;54]	0.447
D1% chiasma	51.3 [47.7;52.1]	51.7 [39.2;52.4]	0.651
D2% chiasma	51.1 [47.2;52]	51.6 [38.9;52.2]	0.577
D50% chiasma	48.2 [40.6;50.7]	44.3 [29.7;50.9]	0.685
Dose per fraction chiasma	1.7 [1.5;1.7]	1.7 [1.2;1.8]	0.468
D1% ON	51.1 [33.5;52.1]	51.6 [11.9;52.2]	0.790
D2% ON	51 [31.5;52]	51.1 [9.6;52.1]	0.790
D50% ON	18.4 [1.4;39]	13.5 [0.4;38.8]	0.635
Dose per fraction ON	1.6 [1.1;1.7]	1.7 [0.4;1.7]	0.785

D1%, D2%, D50% are respectively the doses received by 1%, 2% or 50% of an irradiated volume. ON, Optic nerve.

concerned Dmax or D2% for the optical pathways, considering as a whole these organs as so-called "serial" organs. In term of Dmax delivered on optic pathways we were below the dose constraints usually described since in our study the median prescription dose to the optic pathways was 54Gy (RBE). Usually the dose constraint for Dmax is between 54 et 60Gy (EQD2). But in the study published by Ozkaya et al[4], visual field and contrast sensitivity were affected significantly with a volume receiving more than 55Gy (V55) >50% of the OAR volume, and a Dmean > 50Gy. Visual evoked potential latency was affected significantly with Dmean > 50Gy, D5% > 55Gy, and Dmax > 60Gy. These results are consistent with the VEP toxicities data obtained in our study.

In our study, we noted no significant change in OCT results after 6 months of treatment. As report in literature the damage to the optic nerve observed by the reduction of the ganglion cell layer and the thickness of retinal fiber revealed by OCT correlates with the VEP latency parameters (28). However, these anomalies are later and appear after the impairment of the visual field. Optical coherence tomography would be more useful for the characterization of the RIONs found in our patients but does not seem to be an appropriate screening test for early toxicities.

The most surprising result observed is the one concerning the link between optical structures distance and toxicities on VEPs. Indeed, in patients with toxicity, the distance of the target volume from the optical pathways was increased. These results confirm uncertainties concerning RBE of proton therapy, LET appears to be more inhomogeneous, especially in areas close to the target volumes.

CONCLUSION

Because of the low demography of proton therapy center, the follow-up of patients after proton therapy is not an easy process to set up but it is necessary to improve our knowledges about the biological effects of proton therapy in real life. Our study which will continue and expand during the coming years, suggests that follow-up with in-depth examinations such as VEP could improve the detection of early abnormalities as a biomarker. This could allow us to consider, in the future, early treatments before irreversible consequences appear. Long-term follow-up is thus necessary to clarify these toxicities. Collaboration between ophthalmologist and radiation oncologist is essential to better understand the characteristics

TABLE 6 | Comparison of patients who experienced VEP toxicity to those who remained normal, analyses for VEP 60'.

	Eyes with toxicity n=21	Eyes without toxicity n=32	p-value
Age (years): Median [interquartile range]	60.5 [42.8;75]	52.8 [37;60.2]	0.057
Time from diagnostic	14.2 [4.2;49.3]	14 [2.3;54.7]	0.723
Time from baseline	8.9 [7.6;9.2]	8.5 [6.8;9.5]	0.461
Sex			
1	9 (42.9%)	12 (37.5%)	0.696
2	12 (57.1%)	20 (62.5%)	
Comorbidities	10 (47.6%)	16 (50.0%)	0.865
Histology			0.757
Meningioma	10 (47.6%)	18 (56.2%)	
Adenoma/craniopharyngioma	4 (19.1%)	4 (12.5%)	
Other	7 (33.3%)	10 (31.3%)	
Initial deficits	8 (38.1%)	11 (34.4%)	0.782
Treatments history	15 (71.4%)	22 (68.7%)	0.835
Distance of optical structures			
0mm	6 (28.6%)	16 (50.0%)	0.039
0-3mm	9 (42.9%)	4 (12.5%)	
>3mm	6 (28.6%)	12 (37.5%)	
Clinical exam			
Neurological deficit	8 (38.1%)	12 (37.5%)	1
Oculomotor deficit	8 (38.1%)	10 (31.2%)	0.607
VA deficit	3 (14.3%)	4 (12.5%)	1
VF deficit	3 (14.3%)	3 (9.4%)	–
Other	1 (4.8%)	2 (6.2%)	–
CTV (cm3)	34 [12.6;42.4]	25.5 [11.8;107.6]	0.518
Prescription dose	54 [54;54]	54 [54;56.7]	0.992
D1% chiasma	51.1 [49.3;52.3]	50.6 [14;52.3]	0.164
D2% chiasma	50.9 [49.3;52.2]	50.1 [12.3;52.1]	0.148
D50% chiasma	48.2 [40.6;50.9]	42 [1.8;49.2]	0.040
Dose per fraction chiasma	1.6 [1.5;1.7]	1.6 [0.4;1.7]	0.494
D1% ON	52 [43.4;52.3]	43.3 [15.4;52]	0.028
D2% ON	51.2 [43;52.2]	41.9 [13.6;51.8]	0.042
D50% ON	22.9 [10.8;36.5]	8 [0.4;33.1]	0.120
Dose per fraction ON	1.6 [1.4;1.7]	1.5 [0.4;1.7]	0.098

D1%, D2%, D50% are respectively the doses received by 1%, 2% or 50% of an irradiated volume. ON, Optic nerve.

of optic neuropathies and to pursue research with more specific and standardized examinations.

DATA AVAILABILITY STATEMENT

The raw data supporting the conclusions of this article will be made available by the authors, without undue reservation.

ETHICS STATEMENT

The studies involving human participants were reviewed and approved by CNIL. The patients/participants provided their written informed consent to participate in this study.

AUTHOR CONTRIBUTIONS

ML: first author, bibliography, data collection, interpretation of ophthalmological examinations, writing of the manuscript. PL: physician, participation of follow-up, help for redaction and submission. JS: statistics and methodology. JBa: physician, methodology, help for redaction and submission. DS: physician, participation of follow-up. WK: physician, participation of follow-up. TP: data collection. AV: contribution in physic and technic interpretation and collection data. PD: collection dosimetric data. JBo: data collection. PM: performed ophthalmologic examination and follow-up. JT: original idea of the project, coordination, methodologist. JQ: performed ophthalmologic examination and follow-up, interpretation of ophthalmological results, coordination, methodologist. All authors contributed to the article and approved the submitted version.

REFERENCES

1. Apra C, Peyre M, Kalamarides M. Current Treatment Options for Meningioma. *Expert Rev Neurother* (2018) 18:241–9. doi: 10.1080/14737175.2018.1429920
2. Noel G, Gondi V. Proton Therapy for Tumors of the Base of the Skull. *Chin Clin Oncol* (2016) 5:51. doi: 10.21037/cco.2016.07.05
3. Mihalcea O, Arnold AC. Side Effect of Head and Neck Radiotherapy: Optic Neuropathy. *Oftalmologia* (2008) 52:36–40.
4. Ozkaya Akagunduz O, Guven Yilmaz S, Yalman D, Yuce B, Demirkilinc Biler E, Afrashi F, et al. Evaluation of the Radiation Dose–Volume Effects of Optic Nerves and Chiasm by Psychophysical, Electrophysiologic Tests, and Optical Coherence Tomography in Nasopharyngeal Carcinoma. *Technol Cancer Res Treat* (2017) 16:969–77. doi: 10.1177/1533034617711613

5. Marks LB, Yorke ED, Jackson A, Ten Haken RK, Constine LS, Eisbruch A, et al. The Use of Normal Tissue Complication Probability (Ntcp) Models in the Clinic. *Int J Radiat Oncol Biol Phys* (2010) 76:S10–9. doi: 10.1016/j.ijrobp.2009.07.1754
6. Jiang GL, Tucker SL, Guttenberger R, Peters LJ, Morrison WH, Garden AS, et al. Radiation-Induced Injury to the Visual Pathway. *Radiother Oncol* (1994) 30:17–25. doi: 10.1016/0167-8140(94)90005-1
7. Danesh-Meyer HV. Radiation-Induced Optic Neuropathy. *J Clin Neurosci* (2008) 15:95–100. doi: 10.1016/j.jocn.2007.09.004
8. Brecht S, Boda-Heggemann J, Budjan J, Siebenlist K, Stieler F, Steil V, et al. Radiation-Induced Optic Neuropathy After Stereotactic and Image Guided Intensity-Modulated Radiation Therapy (IMRT). *Radiother Oncol* (2019) 134:166–77. doi: 10.1016/j.radonc.2019.02.003
9. Wilson HP, Price PM, Ashkan K, Edwards A, Green MM, Cross T, et al. Cyberknife Radiosurgery of Skull-base Tumors: A Uk Center Experience. *Cureus* (2018) 10:e2380. doi: 10.7759/cureus.2380
10. Kaul D, Budach V, Misch M, Wiener E, Exner S, Badakhshi H. Meningioma of the Skull Base: Long-Term Outcome After Image-Guided Stereotactic Radiotherapy. *Cancer Radiother* (2014) 18:730–5. doi: 10.1016/j.canrad.2014.07.159
11. Schulz-Ertner D, Tsujii H. Particle Radiation Therapy Using Proton and Heavier Ion Beams. *JCO* (2007) 25:953–64. doi: 10.1200/JCO.2006.09.7816
12. Lesueur P, Calugaru V, Nauraye C, Stefan D, Cao K, Emery E, et al. Proton Therapy for Treatment of Intracranial Benign Tumors in Adults: A Systematic Review. *Cancer Treat Rev* (2019) 72:56–64. doi: 10.1016/j.ctrv.2018.11.004
13. Visual Outcomes of Parapapillary Uveal Melanomas Following Proton Beam Therapy. - Abstract - Europe Pmc. Available at: https://europepmc.org/article/med/27084650 (Accessed November 23, 2020).
14. Paganetti H. Proton Relative Biological Effectiveness – Uncertainties and Opportunities. *Int J Part Ther* (2018) 5:2–14. doi: 10.14338/IJPT-18-00011.1
15. Kountouri M, Pica A, Walser M, Albertini F, Bolsi A, Kliebsch U, et al. Radiation-Induced Optic Neuropathy After Pencil Beam Scanning Proton Therapy for Skull-Base and Head and Neck Tumours. *Br J Radiol* (2020) 93:20190028. doi: 10.1259/bjr.20190028
16. Seibel I, Cordini D, Hager A, Tillner J, Riechardt AI, Heufelder J, et al. Predictive Risk Factors for Radiation Retinopathy and Optic Neuropathy After Proton Beam Therapy for Uveal Melanoma. *Graefes Arch Clin Exp Ophthalmol* (2016) 254:1787–92. doi: 10.1007/s00417-016-3429-4
17. Busch C, Löwen J, Pilger D, Seibel I, Heufelder J, Joussen AM. Quantification of Radiation Retinopathy After Beam Proton Irradiation in Centrally Located Choroidal Melanoma. *Graefes Arch Clin Exp Ophthalmol* (2018) 256:1599–604. doi: 10.1007/s00417-018-4036-3
18. Espensen CA, Kiilgaard JF, Appelt AL, Fog LS, Herault J, Maschi C, et al. Dose-Response and Normal Tissue Complication Probabilities After Proton Therapy for Choroidal Melanoma. *Ophthalmology* (2020) 128(1):152–61. doi: 10.1016/j.ophtha.2020.06.030
19. Chuong M, Badiyan SN, Yam M, Li Z, Langen K, Regine W, et al. Pencil Beam Scanning Versus Passively Scattered Proton Therapy for Unresectable Pancreatic Cancer. *J Gastrointest Oncol* (2018) 9:687–93. doi: 10.21037/jgo.2018.03.14
20. Beddok A, Vela A, Calugaru V, Tessonnier T, Kubes J, Dutheil P, et al. Proton Therapy for Head and Neck Squamous Cell Carcinomas: A Review of the Physical and Clinical Challenges. *Radiother Oncol* (2020) 147:30–9. doi: 10.1016/j.radonc.2020.03.006
21. Liu W, Mohan R, Park P, Liu Z, Li H, Li X, et al. Dosimetric Benefits of Robust Treatment Planning for Intensity Modulated Proton Therapy for Base-of-Skull Cancers. *Pract Radiat Oncol* (2014) 4:384–91. doi: 10.1016/j.prro.2013.12.001
22. Sand T, Kvaløy MB, Wader T, Hovdal H. Evoked Potential Tests in Clinical Diagnosis. *Tidsskrift Den norske legeforening* (2013) 133(9):960–5. doi: 10.4045/tidsskr.12.1176
23. Ahmed SK, Brown PD, Foote RL. Protons vs Photons for Brain and Skull Base Tumors. *Semin Radiat Oncol* (2018) 28:97–107. doi: 10.1016/j.semradonc.2017.11.001
24. Recommendations | Glaucoma: Diagnosis and Management | Guidance | Nice. Available at: https://www.nice.org.uk/guidance/ng81/chapter/Recommendations#diagnosis (Accessed February 1, 2021).
25. El Shafie RA, Czech M, Kessel KA, Habermehl D, Weber D, Rieken S, et al. Clinical Outcome After Particle Therapy for Meningiomas of the Skull Base: Toxicity and Local Control in Patients Treated With Active Rasterscanning. *Radiat Oncol* (2018) 13(1):54. doi: 10.1186/s13014-018-1002-5
26. Sherafat H, Spry PGD, Waldock A, Sparrow JM, Diamond JP. Effect of a Patient Training Video on Visual Field Test Reliability. *Br J Ophthalmol* (2003) 87:153–6. doi: 10.1136/bjo.87.2.153
27. Katz J, Sommer A, Witt K. Reliability of Visual Field Results Over Repeated Testing. *Ophthalmology* (1991) 98:70–5. doi: 10.1016/s0161-6420(91)32339-x
28. Firan AM, Istrate S, Iancu R, Tudosescu R, Ciuluvică R, Voinea L. Visual Evoked Potential in the Early Diagnosis of Glaucoma. Literature Review. *Rom J Ophthalmol* (2020) 64(1):15–20.
29. Robson AG, Nilsson J, Li S, Jalali S, Fulton AB, Tormene AP, et al. ISCEV Guide to Visual Electrodiagnostic Procedures. *Doc Ophthalmol* (2018) 136:1–26. doi: 10.1007/s10633-017-9621-y

Conflict of Interest: The authors declare that the research was conducted in the absence of any commercial or financial relationships that could be construed as a potential conflict of interest.

frontiers in Oncology

REVIEW
published: 03 August 2021
doi: 10.3389/fonc.2021.704664

The Influence of miRNAs on Radiotherapy Treatment in Prostate Cancer – A Systematic Review

Sílvia Soares[1,2,3,4,5,6], *Susana G. Guerreiro*[3,7,8*], *Natália Cruz-Martins*[3,8,9], *Isabel Faria*[10], *Pilar Baylina*[2,3,10], *Maria Goreti Sales*[1,5,11†], *Miguel A. Correa-Duarte*[4,12,13] *and Rúben Fernandes*[2,3,10*]

[1] BioMark@ISEP, School of Engineering, Polytechnic Institute of Porto, Porto, Portugal, [2] LaBMI – Laboratory of Medical & Industrial Biotechnology, Porto Research, Technology & Innovation Center (PORTIC), P.PORTO – Polytechnic Institute of Porto, Porto, Portugal, [3] Institute for Research and Innovation in Health (i3S), Porto, Portugal, [4] Faculty of Chemistry, University of Vigo, Vigo, Spain, [5] CEB, Centre of Biological Engineering of Minho University, Braga, Portugal, [6] Institute of Biomedical Sciences Abel Salazar, University of Porto, Porto, Portugal, [7] Institute of Molecular Pathology and Immunology of the University of Porto-IPATIMUP, Porto, Portugal, [8] Department of Biomedicine, Biochemistry Unit, Faculty of Medicine, University of Porto, Porto, Portugal, [9] Institute of Research and Advanced Training in Health Sciences and Technologies (CESPU), Gandra, Portugal, [10] School of Health, Polytechnic of Porto, Porto, Portugal, [11] Biomark@UC, Department of Chemical Engineering, Faculty of Sciences and Technology, University of Coimbra, Coimbra, Portugal, [12] CINBIO, University of Vigo, Vigo, Spain, [13] Southern Galicia Institute of Health Research (IISGS), and Biomedical Research Networking Center for Mental Health (CIBERSAM), Vigo, Spain

OPEN ACCESS

Edited by:
Alan Jay Katz,
St. Francis Hospital, United States

Reviewed by:
Laure Marignol,
Trinity College Dublin, Ireland
Simeng Suy,
Georgetown University, United States

***Correspondence:**
Rúben Fernandes
rfernandes@ess.ipp.pt
Susana G. Guerreiro
guerreiro.su@gmail.com

†ORCID:
Maria Goreti Sales
orcid.org/0000-0001-9936-7336

Specialty section:
This article was submitted to Radiation Oncology, a section of the journal Frontiers in Oncology

Received: *03 May 2021*
Accepted: *06 July 2021*
Published: *03 August 2021*

Citation:
Soares S, Guerreiro SG, Cruz-Martins N, Faria I, Baylina P, Sales MG, Correa-Duarte MA and Fernandes R (2021) The Influence of miRNAs on Radiotherapy Treatment in Prostate Cancer – A Systematic Review. Front. Oncol. 11:704664. doi: 10.3389/fonc.2021.704664

In the last years, extensive investigation on miRNomics have shown to have great advantages in cancer personalized medicine regarding diagnosis, treatment and even clinical outcomes. Prostate cancer (PCa) is the second most common male cancer and about 50% of all PCa patients received radiotherapy (RT), despite some of them develop radioresistance. Here, we aim to provide an overview on the mechanisms of miRNA biogenesis and to discuss the functional impact of miRNAs on PCa under radiation response. As main findings, 23 miRNAs were already identified as being involved in genetic regulation of PCa cell response to RT. The mechanisms of radioresistance are still poorly understood, despite it has been suggested that miRNAs play an important role in cell signaling pathways. Identification of miRNAs panel can be thus considered an upcoming and potentially useful strategy in PCa diagnosis, given that radioresistance biomarkers, in both prognosis and therapy still remains a challenge.

Keywords: prostate cancer, radiotherapy, RNA therapy, microRNA, oncomiR, oncosupressor miR

INTRODUCTION

Small non-protein-coding RNA molecules, composed of around 22 nucleotides, are commonly named as miRNAs (1–3). Briefly, miRNAs are expected to account for 1-5% of the human genome and to interfere with at least 30% of the protein-coding genes (4, 5). The first miRNA was discovered in 1993 by Lee, Freinbaum and Ambros (6, 7), and since then an increasing load of literature data have pointed that they can act as both tumor suppressors and oncogenes (1–3). Indeed, it has been shown that miRNAs play an important role in gene expression, mainly when associated with the monitoring of several cell and metabolic pathways, being also an essential component of the gene silencing machinery in most eukaryotic organisms (4, 8).

In recent years, many studies have confirmed the involvement of miRNAs in biological processes of several types of cancer (4, 9, 10). The relationship between miRNAs and cancer was demonstrated for the first time in 2002, with miRNAs being stated as a potential mechanism that may contribute to improve some cancer therapeutic approaches through restoring or blocking the miRNAs function (11). Among the various types of cancer with increasing prevalence nowadays, prostate cancer (PCa) is the second most common in male and the fifth leading cause of death in men. Based on Global Cancer Observatory (GLOBOCAN) 2020, more than 1.4 million new cases of PCa and 375,304 associated deaths were recorded (12). One of the treatments applied in cancer is radiotherapy (RT), a therapeutic modality that uses ionizing radiation to induce damage in unwanted cells. The main goal of RT consists in delivering a precise dose of radiation in a target volume, such as tumor, promoting the tumor cells eradication with as minimal damage as possible in surrounding normal tissues (13). Currently, RT is one of the most often used therapeutic approaches in PCa patients, featured by several levels of complexity (13, 14), with around 50% of all PCa patients receiving RT at some stage of treatment, while 10–45% of PCa cases are resistant to irradiation (15, 16). Besides the RT dose is standardized among patients, local recurrences are common and can occur even when modern techniques are used (17). Patient's local recurrences appear mostly as a result of uncontrolled cell reproduction and unregulated cancer cells growth that invades and interferes with the normal function of surrounding tissues and organs (1). Various regulatory factors and genes have shown to be able to directly modulate cell cycle, differentiation and even death. For instance, tumor-suppressor genes or oncogenes or both are regulatory factors able to modulate the environmental conditions contributing to cancer development (2, 4, 18). In this way, miRNAs may be viewed as promising biomarkers capable of predicting radiation response and to develop a customized treatment for each patient, ultimately opening a new therapeutic window for personalized intervention in PCa patients.

Therefore, in the present work, we aimed to explore the mechanisms of miRNA biogenesis, the role of miRNAs in cancer, and the functional impact of miRNAs on PCa radiation response, towards to provide a detailed review of the miRNA expression signatures in PCa tumor and cell lines with therapeutic impact in RT.

METHODS

For data selection 'PICOS Worksheet and Search Strategy' was followed. A detailed and careful literature search was done using PubMED and Web of Science databases. For the Boolean search combinations, the terms used were "miRNA AND prostate cancer OR prostate neoplasia OR prostate carcinoma AND radiotherapy OR radiation therapy", resulting in 71 papers from PubMED and 46 from "Web of Science". Inclusion criteria include articles written in English, published between January 2000 and June 2021, and works referred to clinical studies and pre-clinical studies with cell lines and animal models. Exclusion criteria include not repeat articles on different databases, articles not available and papers that employ non-conventional RT, that with focus on radiotoxicity, and papers on radio sensitization-related biomarkers applied for either diagnostic or prognostic purposes. Then, these 117 articles were analyzed by independent researchers, and 54 articles were selected for further analysis, with 63 articles being eliminated because did not fulfil with the inclusion criteria. Papers related to other malignancies in addition to PCa and those in whom was unable to obtain the whole data were also excluded (**Figure 1**).

RESULTS AND DISCUSSION

miRNA Biogenesis

miRNA biogenesis is controlled at multiple steps, and transcriptional regulation has been proposed to be the major mechanism controlling tissue and cell type-specific expression of miRNAs (4, 19). Briefly, the miRNAs biogenesis includes their transcription at cell nucleus, export to the cytoplasm and subsequent processing and maturation (20), with two processes being involved in achieving the mature miRNA: canonical or non-canonical biogenesis of miRNA (**Figure 2**).

In the canonical pathway, the miRNA gene is typically transcribed by RNA polymerase II to generate long primary transcripts (pre-miRNA) in the nucleus. Subsequently, the pre-miRNA is processed by RNA polymerase III (Drosha protein) and DiGeorge syndrome critical region gene 8 (DGCR8) protein, thus producing the pre-miRNA, a double-stranded miRNA of variable length with approximately 18-25 nucleotides (4, 5, 19, 21, 22). The resulting structure is exported to the cytoplasm *via* Exportin-5 and RanGTP (5, 19, 21, 23). In the cytoplasm, pre-miRNA is cleaved by the Dicer protein to create a duplex miRNA, which contains the mature miRNA. When the duplex unwinds, both RNA strands are separated by helicases and the resulting mature miRNA is incorporated into a functional ribonucleoprotein complex, called RNA-Induced Silencing Complex (RISC), while the other strand is degraded (4, 9, 19). RISC is a ribonucleoprotein complex composed by a set of proteins linked to a small molecule of RNA and it is responsible to perform cell surveillance, inhibiting the translation of the gene into a protein through enzymatic destruction, which effectively silences the gene (5). Both miRNA and RISC complex (miRISC) regulate gene expression through two mechanisms: messenger RNA (mRNA) degradation and mRNA translation repression (22, 23).

Non-canonical pathway is an alternative biogenesis pathway, where miRNA is associated with spliceosome-dependent mechanisms (19). In this pathway, the miRNAs located within the introns of coding or non-coding genes of proteins ("mirtrons") enter in the miRNA processing pathway without Drosha-mediated cleavage (23).

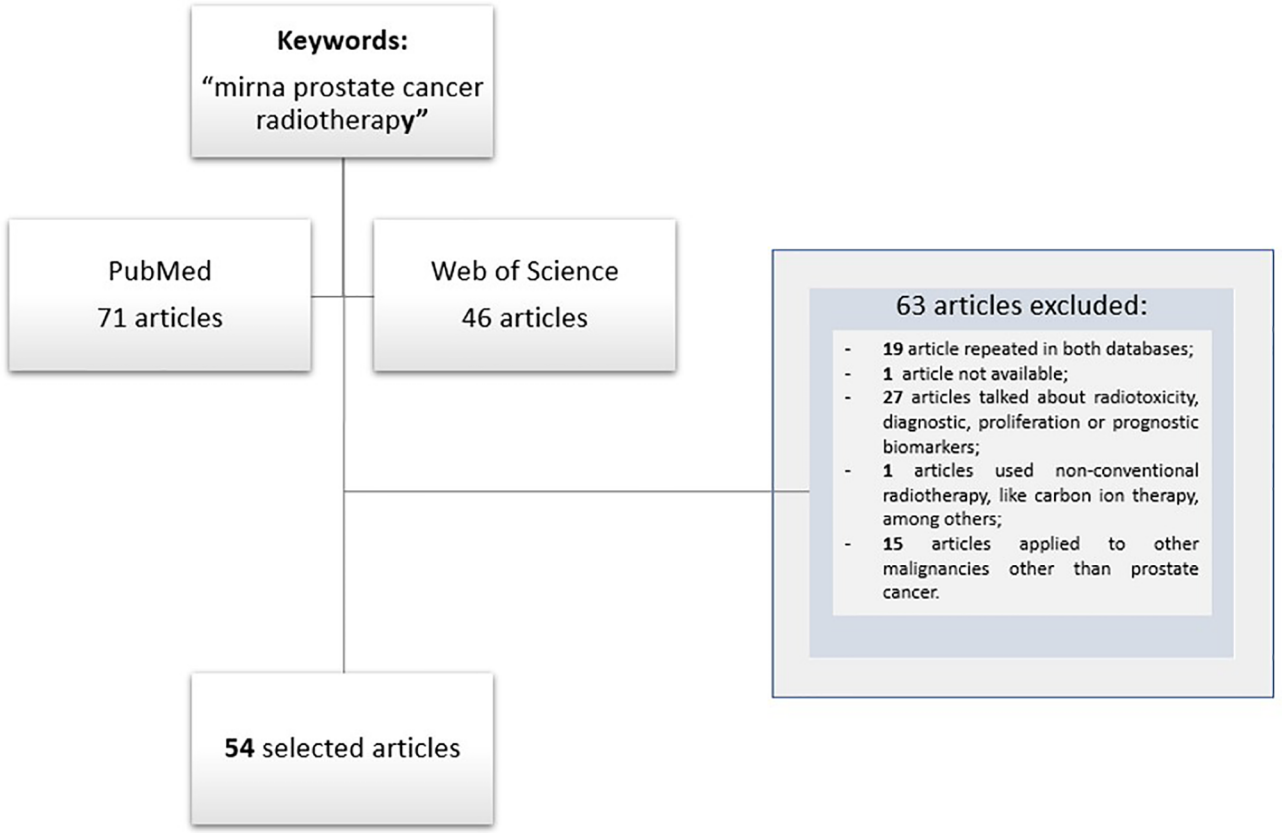

FIGURE 1 | Flow diagram of studies selection.

miRNAs in Cancer Hallmarks

miRNAs can be used in cancer diagnosis to improve the treatment planning and therapeutic sensitivity, to prevent the occurrence of several medications-associated side effects and toxicity, and even to monitor treatment (**Figure 3**). Accumulating evidence underline that miRNAs have an extensive impact due to their involvement in cancer hallmarks, and thus has been considered an important therapeutic target in cancer management (24).

In PCa, there is a dysregulation in miRNAs expression, which can modulate the expression of oncogenes and tumor suppressor genes (20, 22, 23, 25). Moreover, treatment resistance is still a huge problem, so that miRNAs modulation therapy could be a new therapeutic target in cancer patients and used to monitor the therapeutic responses, besides could be useful to predict response to therapies, such chemotherapy and RT (20, 22, 23, 26). The miRNAs therapeutic board approaches include oligonucleotides, small artificial molecules and miRNA-mediated virus or non-virus transfection. In the case of oligonucleotides and small artificial molecules they could be used to inhibit miRNAs or to interfere indirectly with other transcription factors or target genes associated with miRNA-specific modulation. Consequently, several methods have been examined using anti-sense oligonucleotides and it is expected that someday they will be safely implemented (27, 28). Other promissory strategy includes the downregulation of miRNAs using a miRNA-mediated virus or non-virus transfection methods that increases the targeted miRNA. Several studies are being carried out on such matter, taking into account the introduction of artificial double-stranded miRNA – mimic of targeted downregulated miRNA (18).

At that time, biological samples, such as blood, serum and urine, allow to classify the cancer risk at same time that provide prognostic data, allowing to address the cancer aggressiveness, predisposition to metastization or development of radio/chemoresistance. Moreover, depending on the cancer risk, an active surveillance or some specific treatments should be recommended. In the last case, miRNAs can help to predict the response to radiation and the likelihood of side effects' occurrence. So, miRNA expression provides new insights if treatment is being the most appropriate, and if not, treatment must be changed or adjusted (**Figure 4**). Regarding side effects, changes in miRNAs expression can be used to overcome these toxicities or to understand their signs before the need to interrupt the therapy with a possible impairment in therapeutics results (29–31).

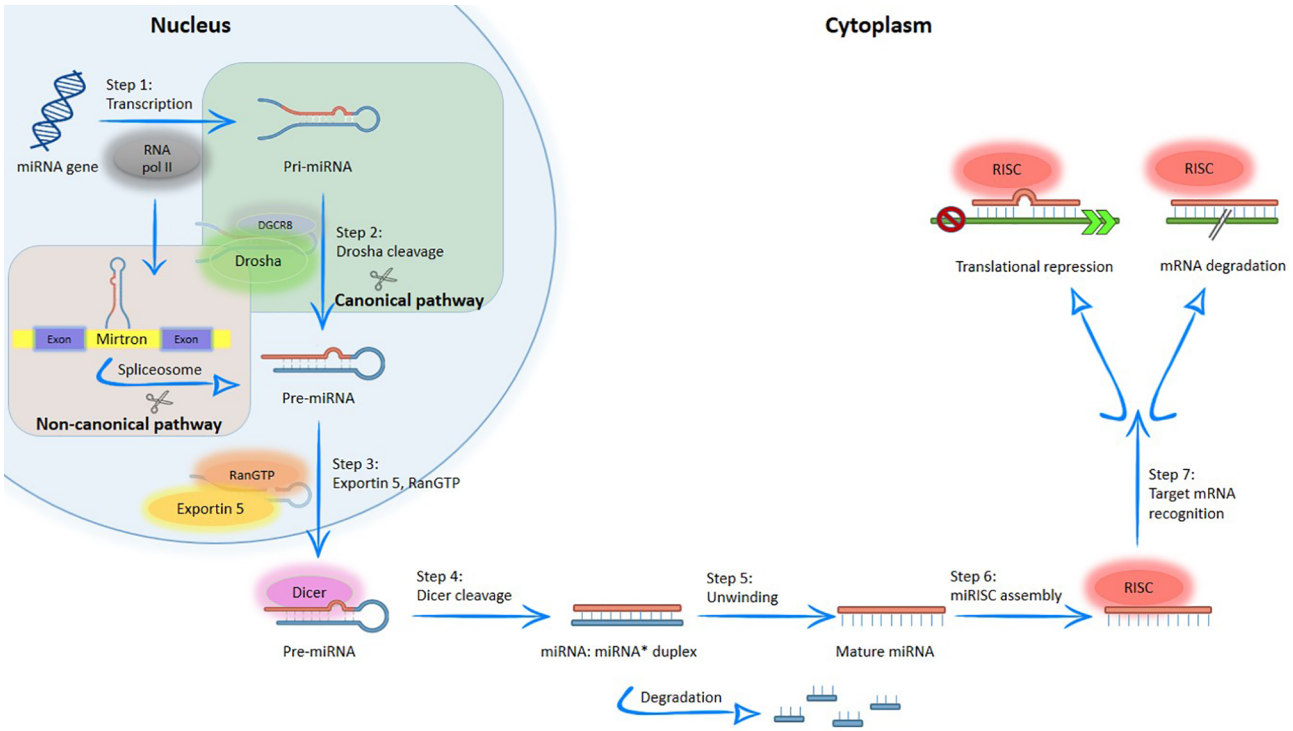

FIGURE 2 | Simplified overview of the canonical and non-canonical miRNA biogenesis pathways. MiRNA generated by canonical pathway is transcribed by RNA polymerase II to a primary transcript called pre-miRNA. Subsequently, this structure is processed into the nucleus by DGCR8/Drosha complex; producing the pre-miRNA, which is exported to the cytoplasm by exportin-5. In the cytoplasm, pre-miRNA is cleaved by RNase III endonuclease (Dicer protein), resulting in a double stranded miRNA, which contains the mature miRNA. After, double strand is separated by helicases and create the mature miRNA; on the contrary, in non-canonical pathways, miRNA located within of mirtrons and are associated with spliceosome-dependent mechanisms. After, the mature miRNA produced by different pathways enters into the RISC complex and regulated genes through messenger RNA (mRNA) degradation and mRNA translation repression.

miRNAs as Therapeutic Agents in Radiation Therapy

Currently, the adoption and promotion of personalized therapy has been increasingly notorious, and it is even considered essential in multiple clinical conditions. Specifically, there is increasing evidence underlining those miRNAs can influence the way that cells respond to ionizing radiation, making them more radiosensitive or radioresistant through several specific pathways. These include modifying DNA repair pathways which interfere with cell cycle checkpoints activation, tumor microenvironment and apoptosis. Some miRNAs are involved in controlling cell cycle progression, tumor microenvironment, apoptosis, and radio-related signals pathway (32–34).

In the context of tumor microenvironment, miRNAs have aroused a high interest. MiRNAs play an important role in regulating tumor radiation response, which involve DNA repair, epithelial-to-mesenchymal transition (EMT), and stemness (35–39). However, radio resistance is a complex phenomenon, and thus more studies are needed to better understand such processes. The response rates to radiation differ according to the modality used, namely the way through which radiation is delivered, the dose of radiation used, tumor stage/grade, confounding medical co-morbidities, and intrinsic tumor microenvironment (40, 41).

As mentioned above, miRNAs can be employed in therapeutic approaches to mimic or inhibit gene expression at translation level - **Figure 4** (42, 43). In the first approach, if the miRNA is under expressed, it can be restored by adding miRNA. In the second approach, if the miRNA is overexpressed, artificial anti-miRNAs can be added to block miRNA (29, 33, 42). Preclinical studies have shown that the use of miRNAs is well-tolerated without triggering significant adverse effects. However, it is necessary to improve both the efficiency and targeted delivery to the tumor before treating patients (15).

To the best of authors' knowledge, only few clinical trials have investigated the miRNA expression profile induced by RT in PCa patients (**Figure 5**). For example, Zedan et al. measured miRNA-21, miRNA-93, miRNA-125b, and miRNA-221 levels in plasma from PCa patients. Among other aspects the authors verified that miRNA-221 and miRNA-93 transcription decreased in patients' plasma following RT, being thus radiosensitive (44, 45). Also, Linuma et al., in a study where low-dose rate prostate brachytherapy (BT) was applied to PCa patients, they stated that miRNA-93 was significantly downregulated in extracellular vesicles from patients' serum after BT (34). In addition, miRNA-145 expression was analyzed in tumor tissue of 30 PCa patients and it was suggested that miRNA-145 can improve response to RT reducing the efficiency of the repair of radiation-induced DNA

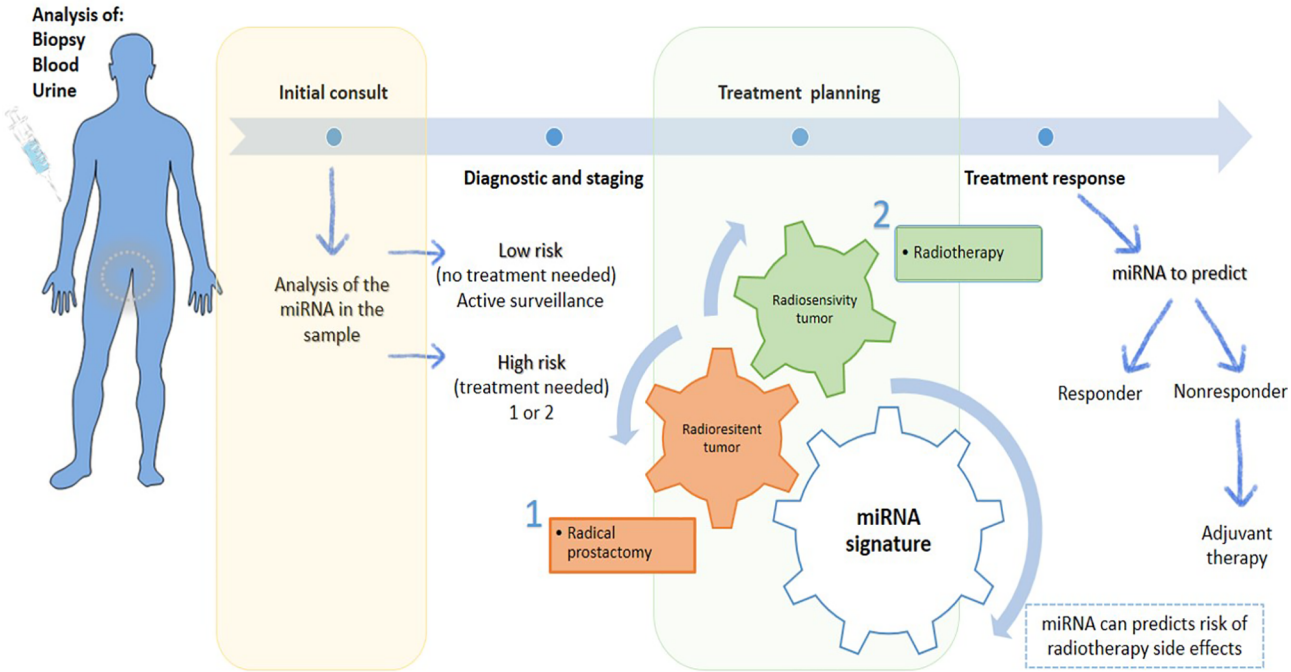

FIGURE 3 | Scheme of the potential of miRNAs in personalized prostate cancer. MiRNAs are present in biological samples, which could be a useful tool for diagnosis and staging in the first consult, allowing an accurate risk stratification. Based on information collected, the treatment can be planned. Treatments can be personalized according to radioresistance or radiosensitive of cancer. If cancer is radioresistance, radical prostatectomy is the therapeutic approach more indicated. Otherwise, RT is ideal treatment to apply to radiosensitive tumors. Also, miRNA signature can give information about the risk of develop side effects or if the patient is responding or not to treatment, leading to a better tumor control with reduced side effects, which contribute to a better patient quality life.

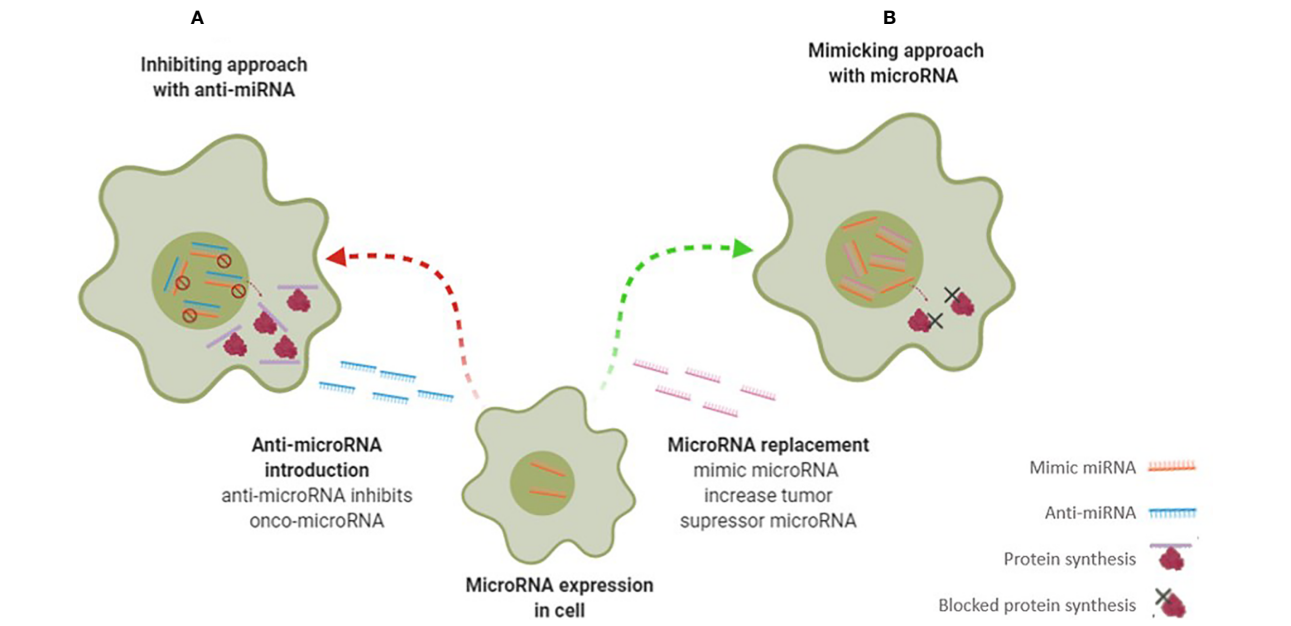

FIGURE 4 | Scheme illustrates different microRNA therapy approaches – anti-microRNA therapy **(A)** and mimicking microRNA therapy **(B)** to change miRNA-regulated gene expression. In therapy **(A)** the microRNA inhibitors are transfected to cells and suppressing onco-microRNA functions and consequently increased protein production. In contrast, in therapy **(B)** are introduced microRNA mimetics to target cells where interact with tumor suppressor microRNA target, suppressing of protein production.

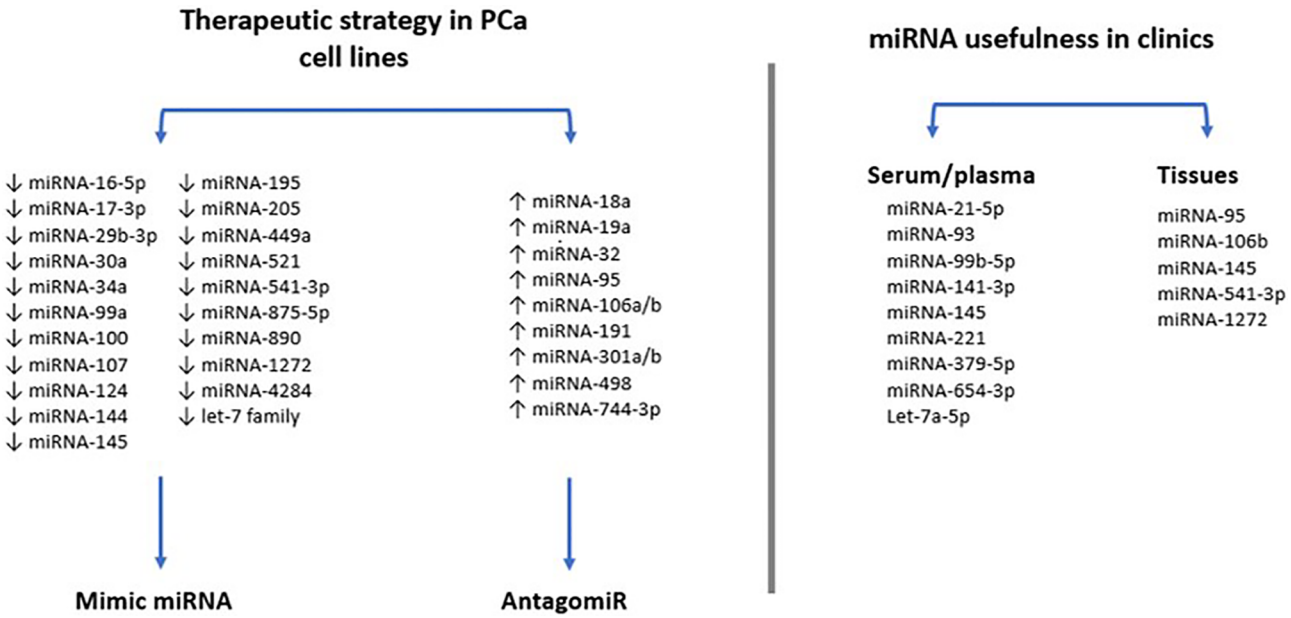

FIGURE 5 | Scheme illustration on the use of miRNAs as a therapeutic strategy in prostate cancer (PCa) cell lines. MiRNAs can be divided into mimic or antagomiR and some have also revealed to be useful in clinics.

double-strand breaks (DSB). Thus, when miRNA-145 is overexpressed, PCa cells are sensitized to ionizing radiation (46).

Other study verified an upregulation of miRNA-95 in 9 tissue specimens of PCa patients, related to radiation resistance by targeting sphingosine-1-phosphatase 1 (SGPP1) (47). Ambs and colleagues analyzed the miRNA-106b-25 cluster expression in 60 primary PCa and 16 non-tumor PCa tissues and concluded that this miRNA has high levels of expression in primary PCa tissues compared to non-tumor prostate tissues (48). In contrast, miRNA-1272 was found downregulated in PCa tissues (49).

Two other studies investigated miRNAs in extracellular vesicles as markers of therapeutic efficacy. Li et al. found a panel of 9 serum-derived extracellular vesicles-miRNAs (miRNA-200c-3p, miRNA-323-3p, miRNA-379-5p, miRNA-409-3p, miRNA-411-5p, miRNA-493-5p, miRNA-494-3p, miRNA-543, and miRNA-654-3p) with potential to predict the therapeutic benefit of carbon ion RT. Additionally, miRNA-654-3p in serum exosomes was considered a potential non-invasive biomarker to predict the efficacy of carbon ion RT in PCa (50). Likewise, Malla et al. collected 25 serum-derived extracellular vesicles-miRNAs from patients treated with RT. Five miRNAs were identified (let-7a-5p, miRNA-141-3p, miRNA-145-5p, miRNA-21-5p, and miRNA-99b-5p), but only let-7a-5p and miRNA-21-5p were overexpressed in high-risk PCa patients after RT.

More recently, miRNA-541-3p was studied in 33 PCa tissues and normal adjacent tissues before and after RT treatments. Interestingly, He et al. found that miRNA-541-3p enhances the radiosensitivity of PCa by inhibiting HSP27 expression and downregulating β-catenin (51).

However, further studies need to be carried out to confirm the miRNAs potential as new outcome biomarkers for PCa patients, as well as to validate the results already obtained, namely through larger patients'cohorts, due to the small sample size of studies-derived data available to date.

Effect of miRNA Expression on Radiation Response in PCa

The Radiation Therapy Oncology Group (RTOG) has performed several potential trials in the field of RT, exploring tissue-based molecular biomarkers with predictive or prognostic value.

More recently, Croce et al. revealed data on the miRNAs potential in cancer, and then other studies demonstrated that the ectopic modulation of specific miRNAs can influence the cancer hallmarks by deregulating its mechanisms (52, 53). In comparison with invasive methods, miRNAs, whose origin seems to be specific from tissue, are very stable and directly detectable in circulating biofluids (54). Also, miRNAs can be isolated and purified from serum, plasma, urine, saliva, peripheral blood cells, among other biological samples (55). Also, miRNAs can circulate in the interstitial fluids and bloodstream through membrane-bound vesicles, such as exosomes (50–90 nm) and microvesicles (1 μm), and even in non-vesicles, such as the ribonucleoprotein complex, which corresponds to the main mechanism. Indeed, accumulating evidence identified circulating miRNAs in apoptotic bodies, exosomes, high-density lipoprotein, and RNA binding proteins as a form of a cell-to-cell communication channel (56).

Circulating miRNA are evolutionarily conserved across species and can be measured easily and efficiently using real

time quantitative protein chain reaction (RT-qPCR), microarray platforms, nanostring techniques, next-generation sequencing (NGS) and biosensors (56). Furthermore, evidence reveals that tumor-associated signature of miRNAs allows to discriminate different cancer subtypes and pathologies by using high-quality measurement techniques. Such finding can significantly contribute to the selection of a more efficient therapeutic approach (57, 58). Indeed, since miRNAs are involved in different cancer mechanisms, they can also be used in targeted therapy, however it continuous to be a challenge regarding stability of miRNAs and its tissue specificity and permeability (55). With the technological advance, such as in the field of nanotechnology, and with the raise in miRNA research, it is expected that, in the future, one of the therapeutic approaches for cancer may be the administration of synthetic anti-sense or mimics oligonucleotides (59, 60).

Several studies have shown the clinical usefulness of some miRNAs and their potential in therapeutic efficacy of RT (54, 61–63). Some miRNAs exhibit predictive value regarding the treatment response through sample analysis extracted from non-invasive liquid biopsies. Thus, miRNAs can give relevant data to achieve a proper patient therapeutic monitoring, as they promote an early detection of PCa relapse/progression, ultimately providing a better control of cancer (44). To underlined that this ability to predict whether a patient is responsive or nonresponsive to a particular treatment modality will allow the expansion of personalized medicine, with individual and personalized treatments being selected for a particular patient, avoiding the risks of toxicity, side effects and relapses. Moreover, "real-time" monitoring of miRNAs may provide an early identification of patients who are failing to radiation therapy response, offering the opportunity to try a more efficient alternative treatment (64). In 2008, it was published the first evidence of a miRNA signature that changed the response to RT (65). Subsequently, increasing evidence has been generated with the intent of discovering an "universal" miRNA molecular profile.

Function and Targets of miRNAs Involved in Radiation Response in PCa

The interaction of ionizing radiation with cells induces some biological responses, including direct DNA damage from ionization or indirectly by ROS generation. Then, different pathways are activated in an intent to repair the damaged DNA, induce cell cycle arrest or even cell death (66). As stated above, RT induce damages, including single-strand breaks (SSB) and DSB. These breaks can be restored by DNA repair pathways, such as base excision repair (BER), nucleotide excision repair (NER), mismatch Repair (MMR), nonhomologous end-joining (NHEJ) or homologous recombination (HR) (67). But radiation can also change the miRNA expression and consequently alters the levels of associated proteins. Most of these studies have been done *in vitro* using PCa cell lines, such as, PC3, DU145, LNCaP and 22Rv1.

MiRNA are involved in the management of such different cell processes (**Figure 6**). For example, MiRNA-99a, a member of miRNA-99 family, and miRNA-100 have a role in DNA repair. The inhibition of this miRNAs will prevent p53 dependent apoptosis, increasing the recruitment of DNA repair proteins (BRCA1, RAD51), consequently influencing SWI/SNF-related matrix-associated actin-dependent regulator of chromatin subfamily A member 5 (SMARCA5) and spinal muscular atrophy with respiratory distress type 1 (SMARD1) in LNCaP, PC3 and DU145 cells after irradiation exposure (68, 69).

Josson et al. reported that miRNA-521 modulates the radio sensitivity of LNCaP cells by specifically restoring DNA repair protein, Cockayne syndrome protein A (CSA) and manganese superoxide dismutase (MnSOD), an anti-apoptotic enzyme. If miRNA-521 is overexpressed it will further sensitize cells to RT contributing to a raise in RT efficacy (65).

Furthermore, miRNA-890 is downregulated in LNCaP, PC3 and DU145 cells and targets mitotic pathways composed of several regulators, including mitotic arrested deficient 2 like 2 (MAD2L2), WEE1 kinase, xeroderma pigmentosum complementation group C (XPC), and KU80 proteins. Also, Hatano et al. revealed that miRNA-744-3p can directly influence RAD23 Homolog B, Nucleotide Excision Repair Protein (RAD23B) in LNCaP, PC3 and DU145 cells. Both miRNAs are involved in DDR systems induced by irradiation, such as DNA DSB repair and NER pathways (70, 71). El Bezawy et al. mentioned that miRNA-875-3p inhibits HR pathway in PC3 and DU145 cells by controlling checkpoint kinase 1 (CHK1) expression and zinc finger E-box-binding homeobox (ZEB), which have impact on EMT (72).

Similarly, there are some miRNAs involved in cell cycle arrest. MicroRNA–16–5p is located at chromosome 13q14 and it is downregulated in LNCaP cells. Wang et al. showed that this miRNA is a tumor suppressor and is involved in PCa onset. The overexpression of miRNA-16-5p is linked to cell proliferation suppression and modulates the Cyclin D1/E1-pRb-E2F1 pathway, inducing G0/G1 phase arrest after irradiation, which consequently increase the radio sensitivity in LNCaP cells (34).

In G2/M phase, elevated levels of miRNA-95 promote radio resistance in PC3 cells. The target of this miRNA is associated with SGPP1, an antagonist of sphingosine-1-phosphate signaling (S1P) that is responsible to protect against ionizing radiation-induced cell death. Briefly, SGPP1 suppresses the G2/M checkpoint, while increases proliferation, invasiveness, and the migratory capabilities of cancer cells (47, 73).

Also, miRNA-106 has been implicated in several pathways involved in raising the PCa cells radioresistance. Hoey et al. analyzed miRNA-106a and concluded that it is overexpressed in PC3 and DU145 cells and is significantly increased in high-grade than low-to-intermediate-grade cancer. The miRNA-106a targets lipopolysaccharide-induced TNF-α factor (LITAF), which is responsible to confer a radioresistant phenotype that increases cell survival and proliferation after irradiation (74). Li et al. showed that miRNA-106b have a novel role in RT due to its involvement in p21-activated cell cycle arrest regulation. Therefore, an inhibitory approach with addition of anti-miRNA-106b may reduce the miRNA-106b levels and will then change the p21 levels. After irradiation, a marked

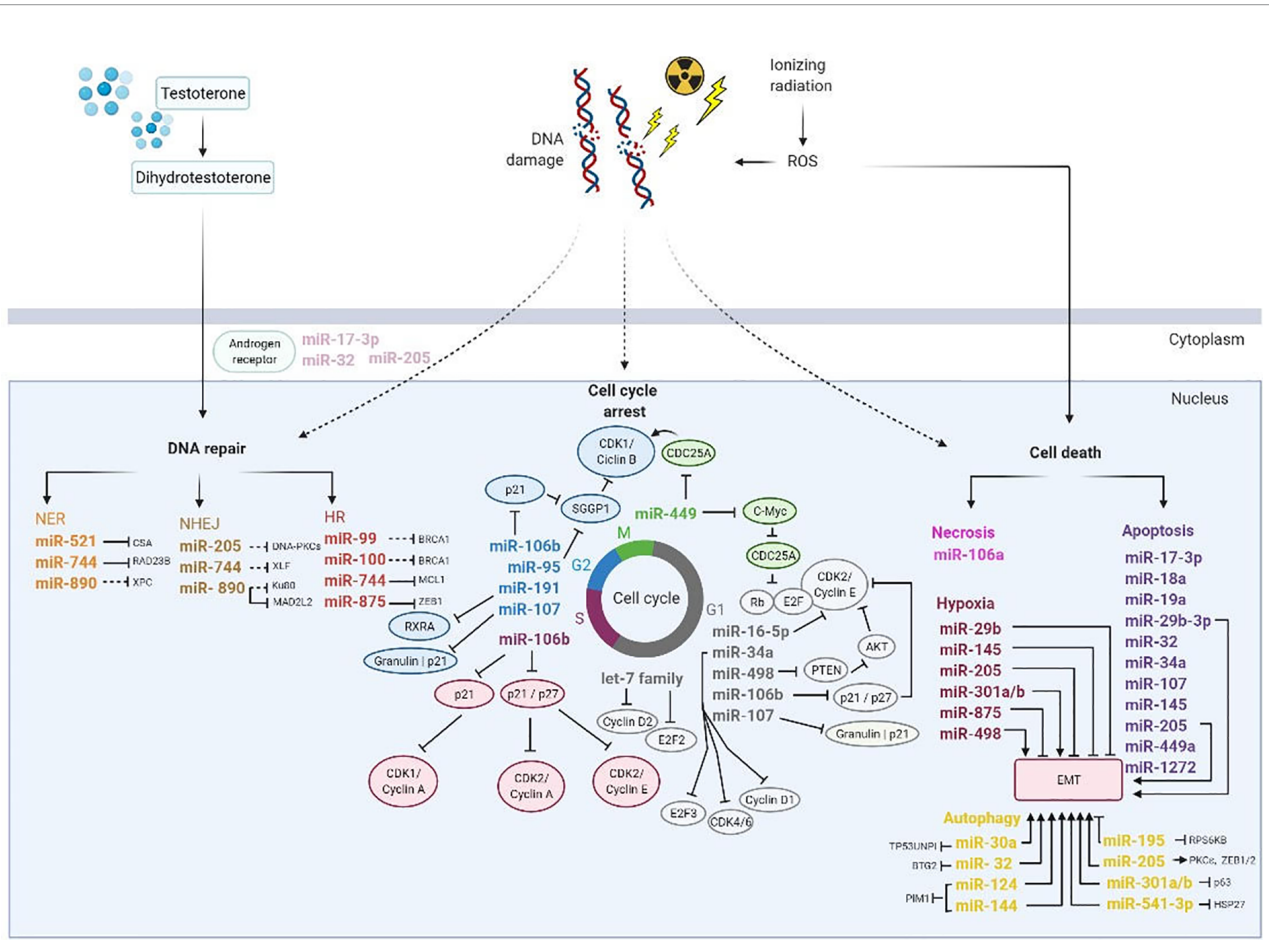

FIGURE 6 | Overview of miRNAs involved on DNA damage repair, cell cycle arrest, and cell death induced by ionizing radiation. Thus, photon beams cause DNA damage directly or indirectly by reactive oxygen species (ROS). In order to repair DNA damage, the cell activate DNA damage response pathways including nucleotide excision repair (NER), non-homologous end joining (NHEJ) and homologous recombination (HR). Additionally, miRNAs regulated cell cycle progression to allow DNA damage repair and depends on cyclin dependent kinases (CDKs), cyclins and transcription factors family EF2. Also, miRNAs are influenced by several factors in the tumor microenvironment such as hypoxia and epithelial mesenchymal transition (EMT) and play an important role in biological processes as apoptosis and autophagy. Consequently, hypoxia promotes DNA repair by transcription of the androgen receptor expression. AKT, Protein kinase B; CDC25A, Cell division cycle 25 A; G1 and G2, transition phases of the cell cycle; HSP27, Heat shock protein 27; M, Mitosis; PTEN, Phosphatase and TENsin homolog; Rb, Retinoblastoma protein; RXRA, Retinoid X receptor alpha; S, phase S; SGGP1, Sphingosine-1-phosphate phosphatase 1. Black inhibition line displays direct targeting; black dashed-inhibition line displays indirect targeting; arrow display an induction of tumor microenvironment.

decreased in miRNA-106b expression was also stated in LNCaP cells (48, 73, 75), along with a correlation between miRNA-106b and Caspase-7 (76, 77).

Mao et al. showed that miRNA-449a targets c-Myc in LNCaP, PC3 and DU145 cells, which controls cdc2/Cyclin B1 cell cycle signal. This miRNA also enhances radiation-induced growth inhibition, radiation-induced G2/M arrest, and apoptosis by modulating the Cdc25A/Rb/E2F1 pathway. Likewise, c-Myc, which controls Cdc25A expression, is a miRNA449a target and is involved in PCa progression and its expression decreases after cells are submitted to radiation. So, when miRNA-449a is overexpressed, it promotes radio sensitivity *in vitro* by triggering destabilization and decreasing the expression of c-Myc and increasing both G2/M arrest and apoptosis (78, 79).

Moreover, miRNA-191 was correlated with radiation response *in vitro* and *in vivo*. Normally, this miRNA is overexpressed in PCa and it was related with radiation resistance through interaction with a novel target, retinoid X receptor alpha (RXRA) in PCa cell lines (PC3 and DU45). Low levels of RXRA expression was linked with a higher risk of distant relapse following RT. Mechanistically, miR-191 also effects cell cycle distribution and proliferation, reducing G2-M phase arrest post-radiation (80).

More recently, miRNA-107 has been related with radiation response of PCa. Lo et al. found that miRNA-107 regulated granulin and is downregulated in response to ionizing radiation in PC3 cells. MiRNA-107 was downregulated in PCa cells and tissues in comparison with normal prostate cells, but when is overexpressed, blocked granulin and promoted the

radiosensitivity in PC3 cells. Mechanistically, miR-107 induced G1/S phase arrest and G2/M phase transit. Besides, also enhancing delayed apoptosis through suppression of p21 and CHK2-phosphorylation (81).

According to Duan et al., miR-498 is linked to PCa cells proliferation, radio sensitivity, invasion, and migration. After exposure to ionizing radiation, this miRNA is under expressed and induces radiation resistance in LNCaP and DU145 cells by reducing radiation-induced apoptosis through BAX and Bcl-2 expression regulation (82). Additionally, miR-498 is related to an important cell cycle regulator, phosphatase and TENsin homolog (PTEN), that suppresses the protein kinase B (AKT) signaling pathway, inhibits cell cycle progression, and affects ionizing radiation-induced apoptosis triggered by caspase 3/7 activity. In addition, with PTEN and AKT inhibition, EMT changes through influence of a raised expression of vimentin and a decreased of E-cadherin (82). Also, delays in response to DNA damage trigger cell death through several mechanisms, such as apoptosis, senescence and autophagy (83). Hsu et al. suggested that miR-18a acts as an oncomiRNA in cancer progression and it is upregulated in 22Rv1, PC3, LNCaP and DU145 cells. MiR-18a is related to STK4, a pro-apoptotic kinase that mediated AKT apoptosis cascade by phosphorylate Caspase 9 and Bad (84). In addition, Yang et al. showed that miR-18a were modulated by growth arrest-specific 5 (GAS5), which protects from radiation and promotes apoptosis when low expressed (85).

Recently, miR-541-3p has been investigated in radiation response in PCa tissue samples and cell lines. MiR-541-3p has low expression in PCa tissues, however, when submitted to RT is overexpressed in PCa cells (LNCaP, DU-145, PC3, and PrEC). Thus, using the mimic approach, miRNA-541-3p interacted directly with HSP27 and increased the radiosensitivity by enhanced apoptosis (51).

In a loss-of-function setting, miR-541-3p knockdown increased the proliferative potential and decreased the apoptotic rate of irradiated cells, ultimately reducing cell radiosensitivity. Conversely, miR-541-3p overexpression by miRNA mimic increased cell sensitivity as a result of a reduction in cell viability and colony formation, paralleled by increased apoptosis. Mechanistically, HSP27, validated as a direct target of the miRNA, was proposed as the potential mediator of miR-541-3p-induced radiosensitization, as suggested by rescue experiments showing a partial reversion of miRNA biological effects upon HSP27 ectopic overexpression.

Also, miR-29b expression or deletion was observed in tumor tissues and cell lines. Mao et al. demonstrated that miR-29b-3p improves radiation-induced cell apoptosis and sensitizes LNCaP cells to radiation by targeting Wnt1-inducible-signaling protein 1 (WISP1). Also, this miRNA was found to be a regulator of EMT and inhibits the PCa cells proliferation and invasion by controlling different targets, among them MCL-1, MMP-2, DNMT3B, and AKT3 (86).

MiRNA-19a was also analyzed in LNCaP, PC3 and DU145 cell lines and it was found downregulated in p53 positive radiosensitive LNCaP cells. Thus, it was suggested that miRNA-19a inhibition can provide a new therapeutic strategy for radioresistant PCa with mutated p53. This miRNA is related with prostate transmembrane protein, androgen-induced l (*PMEPA1*), and tumor protein p53 inducible nuclear protein 1 (*TP53INP1*) (87). Another miRNA, miRNA-17-3p was found at reduced amounts in PC3 cells and there have been some suggestions that this miRNA promotes carcinogenesis, by inhibition of mitochondrial antioxidant enzymes, such as manganese superoxide dismutase (MnSOD), glutathione, peroxidase 2 (Gpx2), and thioredoxin reductase 2 (Trx2) (88). In this context, Xu et al. provided a proof-of-concept evidence that miR-17-3p upregulation influences the radiotherapeutic efficiency through suppressing ionizing irradiation-mediated antioxidant responses, and in turn contributing to a raise in ROS level (89).

MiRNA-32 regulates DAB2 interacting protein (DAB2IP) and may contribute to the radioresistant PCa cells due to reduced ionizing radiation-induced cell apoptosis. Moreover, when this miRNA is overexpressed in LNCaP, PC3 and DU145 cells, it inhibits the expression of Bim protein, a pro-apoptotic member of the BCL-2 family and induces autophagy by targeting DAB2IP (48, 90). MiRNA-32 is also regulated by androgen and it has been implicated to another target gene, B-cell translocation gene 2 (BTG2), which is associated with PCa aggressiveness (91). Another functional study in DU145 and PC3 cell lines showed that miRNA-124 or miRNA-144 overexpression inhibit hypoxia-induced autophagy and enhance radiosensitivity by regulating PIM1 (92).

A recent study on miR-1272 has revealed a relation with radio sensitivity of DU145 cells due to a consistent reduction of clonogenic cell survival mediated by miR-1272 upon irradiation. Authors transformed cells in a manner of gain-of-function using miR-1272 mimics. They found that besides reduced tumor growth and enhanced response to RT, miR-1272 affected the GFR/AKT/ERK1 pathways, ultimately affecting migration, invasiveness, and preventing EMT, all essential steps of the metastatic cascade (49).

Several studies have also shown that miRNA-145 overexpression sensitizes LNCaP and PC3 cells to ionizing radiation. This miRNA suppresses DNA (cytosine-5-)-methyltransferase 3 beta (DNMT3b), which have a crucial role in carcinogenesis, influencing PCa cells cycle, apoptosis, growth, and migration. Some data suggest that the overexpression of miRNA-145 can improve radio sensitivity through DNA DSB downregulation and directly targeting oncogenes (46, 65, 93). More recently, El Bezawy et al. described that miRNA-145 mimics can silence and deregulate the Speckle-type pox virus and zinc finger protein (POZ) protein (SPOP), causing an increase in PCa cells radio sensitivity by decreasing RAD51 and CHK1 expression and targeting ZEB1, that increases E-cadherin expression (94).

Another important feature linked to cancer cells is hypoxia, responsible for promoting tumor progression and the aggressive phenotype (95). In this sense, miRNA-301a and 301b, members of miRNA-301 family, also present clinical interest. It is known that miRNA-301a is an oncomir and it has been proposed that miRNA-301b can act as a tumor suppressor in LNCaP, PC3 and DU145 cells. However, in study of Wang et al. both these

miRNAs were related to hypoxia and led to a decrease in autophagy in LNCaP, PC3 and DU145 cells by targeting N-myc downstream-regulated gene 2 (NDRG2). If these miRNAs are overexpressed, they may induce radio resistance in PCa cells by decreasing NDRG2 that suppresses EMT (96–98). Also, cancer change EMT. Several pathways have been clarified as involved in EMT deregulation, namely those linked to a control in transcription factors and epithelial specific markers, such as a decrease in cytokeratins and E-cadherin, and an increase in mesenchymal markers, such as fibronectin, N-cadherin, and vimentin (99). Indeed, El Bezawy et al. demonstrated that miRNA-875-5p is under expressed in PC3 and DU145 cells. MiRNA-875-5p is directly related to E-cadherin, with neutralization of EMT and improvement of radiation response through targeting epidermal growth factor receptor (EGFR), being these some of the major roles of E-cadherin. Also, it is involved in HR to repair DNA by regulating checkpoint kinase 1 (CHK1) expression and ZEB 1 (72, 100).

Also, MiR-34a and let-7 family (let-7a, let-7b, let-7c, let-7d, let-7e, let-7f, let-7g and let-7i) appeared upregulated following fractionated irradiation in LNCaP and PC3 cells, but not in DU145 cells. All these miRNAs are related to p53 gene, but only miRNA-34a has been proposed to be used as a radio sensitivity predictor, as it targets cyclin E2, besides to also interact with EMT (87, 101). Other studies suggest that miRNA-34 can be used to potentiate the therapeutic effect, as it is overexpressed in LNCaP and underexpressed in PC3 cell line (65, 102, 103). Also, other study should that let-7 family expression was downregulated in LNCaP, PC3 and DU145 cells and revealed to be able to regulate the expression of RAS oncogene, such KRAS and c-Myc (104). Furthermore, Dong et al. demonstrated that let-7a induced cell cycle arrest at the G1/S phase modulating the expression of E2F Transcription Factor 2 (E2F2) and G1/S-specific cyclin-D2 (CCND2) (105).

MiRNA-205 is under expressed and mediates autophagy, which is an important mechanism that can influence the

TABLE 1 | MiRNA expression in radiation response in prostate cancer cell lines.

miRNA	Cell line used	Function	miRNA expression before irradiation	Functional role	Therapeutic strategy	D	P	References
hsa-miRNA-16-5p	LNCaP	TS	↓	RR	Mimicking	✓	✓	(34)
hsa-miRNA-17-3p	PC3	–	↓	RR	Mimicking	✓	–	(89)
hsa-miRNA-18a	22Rv1, PC3, LNCaP, DU145	OM	↑	RR	Antagomirs	–	✓	(84, 85)
hsa-miRNA-19a	LNCaP, PC3, DU145	OM	↑	RR	Antagomirs	✓	✓	(87)
has-miRNA-29b-3p	LNCaP	TS	↓	RR	Mimicking	✓	✓	(86)
Has-miRNA-30a	LNCaP, DU145	TS	↓	RR	Mimicking	✓	✓	(107)
hsa-miRNA-32	LNCaP, PC3, DU145	OM	↑	RR	Antagomirs	✓	–	(48, 90)
hsa-miRNA-34a	LNCaP, PC3, DU145	TS	↓	RR	Mimicking	✓	✓	(87)
hsa-miRNA-95	PC3	–	↑	RR	Antagomirs	✓	✓	(47, 73)
hsa-miRNA-99a	LNCaP, PC3, DU145	TS	↓	RR	Mimicking	✓	✓	(68)
hsa-miRNA-100	LNCaP, PC3, DU145	TS	↓	RR	Mimicking	✓	✓	(68)
hsa-miRNA-106a	PC3, DU145	OM	↑	RR	Antagomirs	✓	✓	(74, 110)
hsa-miRNA-106b	LNCaP	OM	↑	RR	Antagomirs	✓	–	(48, 75)
hsa-miRNA-107	PC3	–	↓	RR	Mimicking	✓	✓	(81)
has-miRNA-124	PC3, DU145	TS	↓	RR	Mimicking	✓	✓	(92)
Has-miRNA-144	PC3, DU145	TS	↓	RR	Mimicking	✓	✓	(92)
hsa-miRNA-145	LNCaP, PC3	TS	↓	RR	Mimicking	✓	✓	(46, 65, 70, 93, 94)
Has-miRNA-191	PC3, DU145	OM	↑	RR	Antagomirs	–	✓	(80)
hsa-miRNA-195	PC3, DU145	TS	↓	RS	Mimicking	✓	✓	(108)
hsa-miRNA-205	LNCaP, PC3, DU145	TS	↓	RR	Mimicking	✓	✓	(40, 106, 107, 110)
hsa-miRNA-301a	LNCaP, PC3, DU145	–	↑	RR	Antagomirs	–	✓	(97, 110)
hsa-miRNA-301b	LNCaP, PC3, DU145	–	↑	RR	Antagomirs	–	–	(97)
hsa-miRNA-449a	LNCaP, PC3, DU145	TS	↓	RR	Mimicking	✓	–	(78)
hsa-miRNA-498	LNCaP, DU145	–	↑	RR	Antagomirs	–	✓	(82)
hsa-miRNA-521	LNCaP	–	↓	RR	Mimicking	–	–	(65)
hsa-miRNA-541-3p	LNCaP, DU-145, PC3, and PrEC	TS	↓	RR	Mimicking	✓	✓	(51)
hsa-miRNA-744-3p	LNCaP, PC3, DU145	OM	↑	RR	Antagomirs	–	–	(70, 71)
hsa-miRNA-875-5p	PC3, DU145	TS	↓	RR	Mimicking	–	–	(72)
hsa-miRNA-890	LNCaP, PC3, DU145	–	↓	RR	Mimicking	–	–	(70)
hsa-miRNA-1272	DU145	TS	↓	RR	Mimicking	–	✓	(49)
hsa-miRNA-4284	22Rv1	–	↓	RR	Mimicking	–	–	(109)
Let-7 family	LNCaP, PC3, DU145	TS	↓	RR	Mimicking	–	✓	(87, 104)

D, Diagnostics; P, Prognostics; TS, Tumour suppressor miRNA; OM, Oncogenic miRNAs; RR, Radioresistant; RS, Radiosensitive; ✓, present; –, absent of information; ↑, increased expression; ↓, decreased expression.

LNCaP, PC3, DU145 cells radio sensitivity (106). Autophagy acts like a protective mechanism of PCa cells to stressful conditions, including radiation-induced cell apoptosis (107). Also, a potential direct functional target of miRNA-205 is tumor protein p53-inducible nuclear protein 1 (TP53INP1), which can interact with other protein families, such as Light chain 3 (LC3) and autophagy-related protein 8 (ATG8), thereby promoting autophagy and apoptosis targeting several cells signaling components, namely mitogen-activated protein kinase (MAPK) and androgen receptor (106, 107). Furthermore, miRNA-205 is also important to support the basal membrane in prostate epithelium, protein kinase C epsilon (PKCε) and ZEB1 expression, proteins involved in EMT (40). In the same context, miRNA-30a has been able to suppress autophagy and enhance radiosensitivity of PCa cells by targeting TP53INP1 (107).

Still related to autophagy, miRNA-195 is linked to PC3 and DU145 progression by targeting ribosomal protein S6 kinase B1 (RPS6KB1), with its overexpression being responsible to enhance the RT efficacy through T cell by blocking the PD-L1 immune checkpoint, which is related to regulation of cytokines secretions in the tumor (108).

McDermott et al. showed that miR-4284 negatively regulates ring finger protein, LIM domain interacting (RLIM) and RasGEF domain family member 1A (RASGEF1A) genes. These genes are associated with RT resistance and oncogenesis. Authors also underlined that miR-4284 is down-regulated in RR-22Rv1 and AMC-22Rv1 cells, and stated a non-significant trend towards the acquisition of age-related radio resistance. Besides, another five miRNAs (miR-210, miR-23a, miR23b, miR-24, and miR-29) were identified in both hypoxic and isogenic radioresistant 22Rv1 models, when compared to the more radiosensitive WT-22Rv1 cell line (109).

Thus, a set of evidence in PCa treatment show that RT can significantly change the miRNA expression levels, but only a few studies investigate the impact of miRNA expression on radiation response in PCa (**Table 1**).

Anyway, and despite the accumulating evidence on this subject, it is important to mention that miRNA expression levels can be modified following PCa irradiation (29, 87, 111, 112). But, despite such alterations in miRNA expression patterns are inconsistent, even within the same cell line, because it largely depends on radiation dose and recovery time post-irradiation of cells (15), it is also a matter of high focus nowadays.

CONCLUSION AND FUTURE PERSPECTIVES

Despite the relative few numbers of studies exploiting the miRNAs relation with radiation response of PCa cells, this subject has been progressively explored and it continuous to be a challenge regarding the role of miRNAs as predictive markers for therapeutic targets.

One limitation of the miRNAs signature is linked to the inconsistency found among studies, mostly attributed to the methodologies applied: clinical trials/experimental studies, therapeutic conditions, pathology type, cell type, among others. Thus, to overcome this drawback, further studies must be designed to get high-quality, reproducible, and valid representative miRNAs to achieve results capable of promoting a patient-tailored treatment. Also worth of note is that most studies analyzed the potential role of miRNAs *in vitro*, so that new experiments should be done *in vivo* or in human tissue samples to support such findings. Thus, the selection of the most appropriate miRNAs remains a challenge.

In short, it has been shown that several miRNAs that modulated the cell response to ionizing radiation. Thus, miRNAs can be applied in therapy to reduce the radio resistance of cells through modulation of cell pathways and biological processes. However, larger and prospective studies are essential to define the value of miRNAs as therapeutic adjuvant to RT. Also, in this context, and since the number of studies is increasing, it is important to ensure a proper organization of data by creating databases of miRNA expressions for cancer research. In the future, we hope to find miRNA target relevant in daily clinical practice, with those capable of predicting the RT efficacy response being highly valuable in RT treatment management.

AUTHOR CONTRIBUTIONS

All authors have contributed equally to this work. All authors contributed to the article and approved the submitted version.

ACKNOWLEDGMENTS

The authors would like to acknowledge Fundação para a Ciência e Tecnologia by the PhD fellowship (SFRH/BD/138271/2018) for SS.

REFERENCES

1. Esquela-Kerscher A, Slack FJ. Oncomirs - microRNAs With a Role in Cancer. *Nat Rev Cancer* (2006) 6(4):259–69. doi: 10.1038/nrc1840
2. Wang D, Qiu C, Zhang H, Wang J, Cui Q, Yin Y. Human microRNA Oncogenes and Tumor Suppressors Show Significantly Different Biological Patterns: From Functions to Targets. *PLoS One* (2010) 5(9):e13067. doi: 10.1371/journal.pone.0013067
3. Zhou K, Liu M, Cao Y. New Insight Into microRNA Functions in Cancer: Oncogene–microRNA–Tumor Suppressor Gene Network. *Front Mol Biosci* (2017) 4:46. doi: 10.3389/fmolb.2017.00046
4. MacFarlane LA, Murphy PR. MicroRNA: Biogenesis, Function and Role in Cancer. *Curr Genomics* (2010) 11(7):537–61. doi: 10.2174/138920210793175895
5. Wilson RC, Doudna JA. Molecular Mechanisms of RNA Interference. *Annu Rev Biophys* (2013) 42:217–39. doi: 10.1146/annurev-biophys-083012-130404
6. Sedwick C. Victor Ambros: The Broad Scope of microRNAs. *J Cell Biol* (2013) 201:492–3. doi: 10.1083/jcb.2014pi
7. Lee RC, Feinbaum RL, Ambros V. The C. Elegans Heterochronic Gene Lin-4 Encodes Small RNAs With Antisense Complementarity to Lin-14. *Cell* (1993) 75(5):843–54. doi: 10.1016/0092-8674(93)90529-Y
8. Achkar NP, Cambiagno DA, Manavella PA. miRNA Biogenesis: A Dynamic Pathway. *Trends Plant Sci* (2016) 21(12):1034–44. doi: 10.1016/j.tplants.2016.09.003

9. Lu M, Zhang Q, Deng M, Miao J, Guo Y, Gao W, et al. An Analysis of Human microRNA and Disease Associations. *PLoS One* (2008) 3(10):e3420. doi: 10.1371/journal.pone.0003420
10. Ling H, Fabbri M, Calin GA. MicroRNAs and Other Non-Coding RNAs as Targets for Anticancer Drug Development. *Nat Rev Drug Discov* (2013) 12 (11):847–65. doi: 10.1038/nrd4140
11. Slaby O, Laga R, Sedlacek O. Therapeutic Targeting of Non-Coding RNAs in Cancer. *Biochem J* (2017) 474(24):4219–51. doi: 10.1042/BCJ20170079
12. Ferlay J, Ervik M, Lam F, Colombet M, Mery L, Piñeros M, et al. *Global Cancer Observatory: Cancer Today*. Lyon, France: International Agency for Research on Cancer (2020). Available at: http://gco.iarc.fr/today/home.
13. Perez C, Halperin E, Brady L. *Principles and Practice of Radiation Oncology 5ª edition*. Philadelphia: Wolters Kluwer Health/Lippincott Williams & Wilkins (2008).
14. Brausi M, Hoskin P, Andritsch E, Banks I, Beishon M, Boyle H, et al. ECCO Essential Requirements for Quality Cancer Care: Prostate Cancer. *Crit Rev Oncology/Hematol* (2020) 148:102861. doi: 10.1016/j.critrevonc.2019.102861
15. Gandellini P, Rancati T, Valdagni R, Zaffaroni N. miRNAs in Tumor Radiation Response: Bystanders or Participants? *Trends Mol Med* (2014) 20(9):529–39. doi: 10.1016/j.molmed.2014.07.004
16. Xu M, Gong S, Li Y, Zhou J, Du J, Yang C, et al. Identifying Long Non-Coding RNA of Prostate Cancer Associated With Radioresponse by Comprehensive Bioinformatics Analysis. *Front Oncol* (2020) 10:498. doi: 10.3389/fonc.2020.00498
17. Fabris L, Ceder Y, Chinnaiyan AM, Jenster GW, Sorensen KD, Tomlins S, et al. The Potential of MicroRNAs as Prostate Cancer Biomarkers. *Eur Urol* (2016) 70(2):312–22. doi: 10.1016/j.eururo.2015.12.054
18. Christopher AF, Kaur RP, Kaur G, Kaur A, Gupta V, Bansal P. MicroRNA Therapeutics: Discovering Novel Targets and Developing Specific Therapy. *Perspect Clin Res* (2016) 7(2):68–74. doi: 10.4103/2229-3485.179431
19. Li Z, Rana TM. Therapeutic Targeting of microRNAs: Current Status and Future Challenges. *Nat Rev Drug Discov* (2014) 13(8):622–38. doi: 10.1038/nrd4359
20. Staedel C, Tran TPA, Giraud J, Darfeuille F, Di Giorgio A, Tourasse NJ, et al. Modulation of Oncogenic miRNA Biogenesis Using Functionalized Polyamines. *Sci Rep* (2018) 8(1):1667. doi: 10.1038/s41598-018-20053-5
21. Velagapudi SP, Vummidi BR, Disney MD. Small Molecule Chemical Probes of microRNA Function. *Curr Opin Chem Biol* (2015) 24:97–103. doi: 10.1016/j.cbpa.2014.10.024
22. Di Giorgio A, Tran TP, Duca M. Small-Molecule Approaches Toward the Targeting of Oncogenic miRNAs: Roadmap for the Discovery of RNA Modulators. *Future Med Chem* (2016) 8(7):803–16. doi: 10.4155/fmc-2016-0018
23. Iorio MV, Croce CM. microRNA Involvement in Human Cancer. *Carcinogenesis* (2012) 33(6):1126–33. doi: 10.1093/carcin/bgs140
24. Van Roosbroeck K, Calin GA. Cancer Hallmarks and MicroRNAs: The Therapeutic Connection. *Adv Cancer Res* (2017) 135:119–49. doi: 10.1016/bs.acr.2017.06.002
25. Gu LQ, Wanunu M, Wang MX, McReynolds L, Wang Y. Detection of miRNAs With a Nanopore Single-Molecule Counter. *Expert Rev Mol Diagn* (2012) 12(6):573–84. doi: 10.1586/erm.12.58
26. Rothschild SI. microRNA Therapies in Cancer. *Mol Cell Ther* (2014) 2:7. doi: 10.1186/2052-8426-2-7
27. Wen D, Danquah M, Chaudhary AK, Mahato RI. Small Molecules Targeting microRNA for Cancer Therapy: Promises and Obstacles. *J Control Release* (2015) 219:237–47. doi: 10.1016/j.jconrel.2015.08.011
28. Ishida M, Selaru FM. miRNA-Based Therapeutic Strategies. *Curr Anesthesiol Rep* (2013) 1(1):63–70. doi: 10.1007/s40139-012-0004-5
29. Cellini F, Morganti AG, Genovesi D, Silvestris N, Valentini V. Role of microRNA in Response to Ionizing Radiations: Evidences and Potential Impact on Clinical Practice for Radiotherapy. *Molecules* (2014) 19(4):5379–401. doi: 10.3390/molecules19045379
30. Kopcalic K, Petrovic N, Stanojkovic TP, Stankovic V, Bukumiric Z, Roganovic J, et al. Association Between miR-21/146a/155 Level Changes and Acute Genitourinary Radiotoxicity in Prostate Cancer Patients: A Pilot Study. *Pathol Res Pract* (2019) 215(4):626–31. doi: 10.1016/j.prp.2018.12.007
31. Balázs K, Antal L, Sáfrány G, Lumniczky K. Blood-Derived Biomarkers of Diagnosis, Prognosis and Therapy Response in Prostate Cancer Patients. *J Pers Med* (2021) 11(4):296. doi: 10.3390/jpm11040296
32. Zhao L, Lu X, Cao Y. MicroRNA and Signal Transduction Pathways in Tumor Radiation Response. *Cell Signal* (2013) 25(7):1625–34. doi: 10.1016/j.cellsig.2013.04.004
33. Korpela E, Vesprini D, Liu SK. MicroRNA in Radiotherapy: Mirage or Mirador? *Br J Cancer* (2015) 112(5):777–82. doi: 10.1038/bjc.2015.6
34. Wang F, Mao A, Tang J, Zhang Q, Yan J, Wang Y, et al. microRNA-16-5p Enhances Radiosensitivity Through Modulating Cyclin D1/E1-pRb-E2F1 Pathway in Prostate Cancer Cells. *J Cell Physiol* (2019) 234(8):13182–90. doi: 10.1002/jcp.27989
35. Xing F, Wu K, Watabe K. MicroRNAs in Cancer Stem Cells: New Regulators of Stemness. *Curr Pharm Des* (2014) 20(33):5319–27. doi: 10.2174/1381612820666140128210912
36. Muhammad N, Bhattacharya S, Steele R, Ray RB. Anti-miR-203 Suppresses ER-Positive Breast Cancer Growth and Stemness by Targeting SOCS3. *Oncotarget* (2016) 7(36):58595–605. doi: 10.18632/oncotarget.11193
37. Zhang P, Wang L, Rodriguez-Aguayo C, Yuan Y, Debeb BG, Chen D, et al. miR-205 Acts as a Tumour Radiosensitizer by Targeting ZEB1 and Ubc13. *Nat Commun* (2014) 5:5671. doi: 10.1038/ncomms6671
38. Yadav S, Kowolik CM, Lin M, Zuro D, Hui SK, Riggs AD, et al. SMC1A is Associated With Radioresistance in Prostate Cancer and Acts by Regulating Epithelial-Mesenchymal Transition and Cancer Stem-Like Properties. *Mol Carcinog* (2019) 58(1):113–25. doi: 10.1002/mc.22913
39. Mao A, Liu Y, Zhang H, Di C, Sun C. microRNA Expression and Biogenesis in Cellular Response to Ionizing Radiation. *DNA Cell Biol* (2014) 33 (10):667–79. doi: 10.1089/dna.2014.2401
40. El Bezawy R, Tinelli S, Tortoreto M, Doldi V, Zuco V, Folini M, et al. miR-205 Enhances Radiation Sensitivity of Prostate Cancer Cells by Impairing DNA Damage Repair Through PKCepsilon and ZEB1 Inhibition. *J Exp Clin Cancer Res* (2019) 38(1):51. doi: 10.1186/s13046-019-1060-z
41. Palacios DA, Miyake M, Rosser CJ. Radiosensitization in Prostate Cancer: Mechanisms and Targets. *BMC Urol* (2013) 13:4. doi: 10.1186/1471-2490-13-4
42. Bai Z, Wei J, Yu C, Han X, Qin X, Zhang C, et al. Non-Viral Nanocarriers for Intracellular Delivery of microRNA Therapeutics. *J Mater Chem B* (2019) 7:1209–25. doi: 10.1039/C8TB02946F
43. Matin F, Jeet V, Clements JA, Yousef GM, Batra J. MicroRNA Theranostics in Prostate Cancer Precision Medicine. *Clin Chem* (2016) 62(10):1318–33. doi: 10.1373/clinchem.2015.242800
44. Zedan AH, Hansen TF, Assenholt J, Madsen JS, Osther PJS. Circulating miRNAs in Localized/Locally Advanced Prostate Cancer Patients After Radical Prostatectomy and Radiotherapy. *Prostate* (2019) 79(4):425–32. doi: 10.1002/pros.23748
45. Labbé M, Hoey C, Ray J, Potiron V, Supiot S, Liu SK, et al. microRNAs Identified in Prostate Cancer: Correlative Studies on Response to Ionizing Radiation. *Mol Cancer* (2020) 19(1):63. doi: 10.1186/s12943-020-01186-6
46. Gong P, Zhang T, He D, Hsieh JT. MicroRNA-145 Modulates Tumor Sensitivity to Radiation in Prostate Cancer. *Radiat Res* (2015) 184(6):630–8. doi: 10.1667/RR14185.1
47. Huang X, Taeb S, Jahangiri S, Emmenegger U, Tran E, Bruce J, et al. miRNA-95 Mediates Radioresistance in Tumors by Targeting the Sphingolipid Phosphatase SGPP1. *Cancer Res* (2013) 73(23):6972–86. doi: 10.1158/0008-5472.CAN-13-1657
48. Ambs S, Prueitt RL, Yi M, Hudson RS, Howe TM, Petrocca F, et al. Genomic Profiling of microRNA and Messenger RNA Reveals Deregulated microRNA Expression in Prostate Cancer. *Cancer Res* (2008) 68(15):6162–70. doi: 10.1158/0008-5472.CAN-08-0144
49. Rotundo F, Cominetti D, El Bezawy R, Percio S, Doldi V, Tortoreto M, et al. miR-1272 Exerts Tumor-Suppressive Functions in Prostate Cancer *via* HIP1 Suppression. *Cells* (2020) 9(2):435. doi: 10.3390/cells9020435
50. Yu Q, Li P, Weng M, Wu S, Zhang Y, Chen X, et al. Nano-Vesicles Are a Potential Tool to Monitor Therapeutic Efficacy of Carbon Ion Radiotherapy in Prostate Cancer. *J BioMed Nanotechnol* (2018) 14(1):168–78. doi: 10.1166/jbn.2018.2503
51. He Z, Shen F, Qi P, Zhai Z, Wang Z. miR-541-3p Enhances the Radiosensitivity of Prostate Cancer Cells by Inhibiting HSP27 Expression and Downregulating β-Catenin. *Cell Death Discov* (2021) 7(1):18. doi: 10.1038/s41420-020-00387-8
52. Peng Y, Croce CM. The Role of MicroRNAs in Human Cancer. *Signal Transduct Targeted Ther* (2016) 1(1):15004. doi: 10.1038/sigtrans.2015.4

53. Zaheer U, Faheem M, Qadri I, Begum N, Yassine HM, Al Thani AA, et al. Expression Profile of MicroRNA: An Emerging Hallmark of Cancer. *Curr Pharm Des* (2019) 25(6):642–53. doi: 10.2174/1386207322666190325122821
54. Małachowska B, Tomasik B, Stawiski K, Kulkarni S, Guha C, Chowdhury D, et al. Circulating microRNAs as Biomarkers of Radiation Exposure: A Systematic Review and Meta-Analysis. *Int J Radiat OncologyBiologyPhys* (2020) 106(2):390–402. doi: 10.1016/j.ijrobp.2019.10.028
55. Cui M, Wang H, Yao X, Zhang D, Xie Y, Cui R, et al. Circulating MicroRNAs in Cancer: Potential and Challenge. *Front Genet* (2019) 10:626–. doi: 10.3389/fgene.2019.00626
56. Singh VK, Pollard HB. Ionizing Radiation-Induced Altered microRNA Expression as Biomarkers for Assessing Acute Radiation Injury. *Expert Rev Mol Diag* (2017) 17(10):871–4. doi: 10.1080/14737159.2017.1366316
57. He Y, Lin J, Kong D, Huang M, Xu C, Kim T-K, et al. Current State of Circulating MicroRNAs as Cancer Biomarkers. *Clin Chem* (2015) 61 (9):1138–55. doi: 10.1373/clinchem.2015.241190
58. Wang H, Peng R, Wang J, Qin Z, Xue L. Circulating microRNAs as Potential Cancer Biomarkers: The Advantage and Disadvantage. *Clin Epigenet* (2018) 10(1):1–10. doi: 10.1186/s13148-018-0492-1
59. Ganju A, Khan S, Hafeez BB, Behrman SW, Yallapu MM, Chauhan SC, et al. miRNA Nanotherapeutics for Cancer. *Drug Discov Today* (2017) 22(2):424–32. doi: 10.1016/j.drudis.2016.10.014
60. Goyal R, Kapadia CH, Melamed JR, Riley RS, Day ES. Layer-By-Layer Assembled Gold Nanoshells for the Intracellular Delivery of miR-34a. *Cell Mol Bioeng* (2018) 11(5):383–96. doi: 10.1007/s12195-018-0535-x
61. Filella X, Foj L. miRNAs as Novel Biomarkers in the Management of Prostate Cancer. *Clin Chem Lab Med* (2017) 55(5):715–36. doi: 10.1515/cclm-2015-1073
62. Doldi V, El Bezawy R, Zaffaroni N. MicroRNAs as Epigenetic Determinants of Treatment Response and Potential Therapeutic Targets in Prostate Cancer. *Cancers* (2021) 13(10):2380. doi: 10.3390/cancers13102380
63. Leung CM, Li SC, Chen TW, Ho MR, Hu LY, Liu WS, et al. Comprehensive microRNA Profiling of Prostate Cancer Cells After Ionizing Radiation Treatment. *Oncol Rep* (2014) 31(3):1067–78. doi: 10.3892/or.2014.2988
64. Mueller A-K, Lindner K, Hummel R, Haier J, Watson DI, Hussey DJ. MicroRNAs and Their Impact on Radiotherapy for Cancer. *Radiat Res* (2016) 185(6):668–77. doi: 10.1667/RR14370.1
65. Josson S, Sung SY, Lao K, Chung LW, Johnstone PA. Radiation Modulation of microRNA in Prostate Cancer Cell Lines. *Prostate* (2008) 68(15):1599–606. doi: 10.1002/pros.20827
66. Srinivas US, Tan BWQ, Vellayappan BA, Jeyasekharan AD. ROS and the DNA Damage Response in Cancer. *Redox Biol* (2019) 25:101084. doi: 10.1016/j.redox.2018.101084
67. Ford JM, Kastan MB. 11 - DNA Damage Response Pathways and Cancer. In: Niederhuber JE, Armitage JO, Kastan MB, Doroshow JH, Tepper JE, editors. *Abeloff's Clinical Oncology, Sixth Edition*. Philadelphia: Elsevier (2020). p. 154–64.e4.
68. Rane JK, Erb HH, Nappo G, Mann VM, Simms MS, Collins AT, et al. Inhibition of the Glucocorticoid Receptor Results in an Enhanced miR-99a/100-Mediated Radiation Response in Stem-Like Cells From Human Prostate Cancers. *Oncotarget* (2016) 7(32):51965–80. doi: 10.18632/oncotarget.10207
69. Sun D, Lee YS, Malhotra A, Kim HK, Matecic M, Evans C, et al. miR-99 Family of microRNAs Suppresses the Expression of Prostate Specific Antigen and Prostate Cancer Cell Proliferation. *Cancer Res* (2011) 71 (4):1313–24. doi: 10.1158/0008-5472.CAN-10-1031
70. Hatano K, Kumar B, Zhang Y, Coulter JB, Hedayati M, Mears B, et al. A Functional Screen Identifies miRNAs That Inhibit DNA Repair and Sensitize Prostate Cancer Cells to Ionizing Radiation. *Nucleic Acids Res* (2015) 43 (8):4075–86. doi: 10.1093/nar/gkv273
71. Zhang M, Li H, Zhang Y. Oncogenic miR-744 Promotes Prostate Cancer Growth Through Direct Targeting of LKB1. *Oncol Lett* (2019) 17(2):2257–65. doi: 10.3892/ol.2018.9822
72. El Bezawy R, Cominetti D, Fenderico N, Zuco V, Beretta GL, Dugo M, et al. miR-875-5p Counteracts Epithelial-to-Mesenchymal Transition and Enhances Radiation Response in Prostate Cancer Through Repression of the EGFR-ZEB1 Axis. *Cancer Lett* (2017) 395:53–62. doi: 10.1016/j.canlet.2017.02.033
73. Razdan A, de Souza P, Roberts TL. Role of MicroRNAs in Treatment Response in Prostate Cancer. *Curr Cancer Drug Targets* (2018) 18(10):929–44. doi: 10.2174/1568009618666180315160125
74. Hoey C, Ray J, Jeon J, Huang X, Taeb S, Ylanko J, et al. miRNA-106a and Prostate Cancer Radioresistance: A Novel Role for LITAF in ATM Regulation. *Mol Oncol* (2018) 12(8):1324–41. doi: 10.1002/1878-0261.12328
75. Li B, Shi XB, Nori D, Chao CK, Chen AM, Valicenti R, et al. Down-Regulation of microRNA 106b is Involved in P21-Mediated Cell Cycle Arrest in Response to Radiation in Prostate Cancer Cells. *Prostate* (2011) 71 (6):567–74. doi: 10.1002/pros.21272
76. Hudson RS, Yi M, Esposito D, Glynn SA, Starks AM, Yang Y, et al. MicroRNA-106b-25 Cluster Expression is Associated With Early Disease Recurrence and Targets Caspase-7 and Focal Adhesion in Human Prostate Cancer. *Oncogene* (2013) 32(35):4139–47. doi: 10.1038/onc.2012.424
77. Eron SJ, Raghupathi K, Hardy JA. Dual Site Phosphorylation of Caspase-7 by PAK2 Blocks Apoptotic Activity by Two Distinct Mechanisms. *Structure* (2017) 25(1):27–39. doi: 10.1016/j.str.2016.11.001
78. Mao A, Zhao Q, Zhou X, Sun C, Si J, Zhou R, et al. MicroRNA-449a Enhances Radiosensitivity by Downregulation of C-Myc in Prostate Cancer Cells. *Sci Rep* (2016) 6:27346. doi: 10.1038/srep27346
79. Mao A, Liu Y, Wang Y, Zhao Q, Zhou X, Sun C, et al. miR-449a Enhances Radiosensitivity Through Modulating pRb/E2F1 in Prostate Cancer Cells. *Tumour Biol* (2016) 37(4):4831–40. doi: 10.1007/s13277-015-4336-8
80. Ray J, Haughey C, Hoey C, Jeon J, Murphy R, Dura-Perez L, et al. miR-191 Promotes Radiation Resistance of Prostate Cancer Through Interaction With RXRA. *Cancer Lett* (2020) 473:107–17. doi: 10.1016/j.canlet.2019.12.025
81. Lo H-C, Hsu J-H, Lai L-C, Tsai M-H, Chuang EY. MicroRNA-107 Enhances Radiosensitivity by Suppressing Granulin in PC-3 Prostate Cancer Cells. *Sci Rep* (2020) 10(1):14584–. doi: 10.1038/s41598-020-71128-1
82. Duan XM, Liu XN, Li YX, Cao YQ, Silayiding A, Zhang RK, et al. MicroRNA-498 Promotes Proliferation, Migration, and Invasion of Prostate Cancer Cells and Decreases Radiation Sensitivity by Targeting PTEN. *Kaohsiung J Med Sci* (2019) 35(11):659–71. doi: 10.1002/kjm2.12108
83. Borges HL, Linden R, Wang JYJ. DNA Damage-Induced Cell Death: Lessons From the Central Nervous System. *Cell Res* (2008) 18(1):17–26. doi: 10.1038/cr.2007.110
84. Hsu TI, Hsu CH, Lee KH, Lin JT, Chen CS, Chang KC, et al. MicroRNA-18a is Elevated in Prostate Cancer and Promotes Tumorigenesis Through Suppressing STK4 *In Vitro* and In Vivo. *Oncogenesis* (2014) 3:e99. doi: 10.1038/oncsis.2014.12
85. Yang J, Hao T, Sun J, Wei P, Zhang H. Long Noncoding RNA GAS5 Modulates α-Solanine-Induced Radiosensitivity by Negatively Regulating miR-18a in Human Prostate Cancer Cells. *Biomed Pharmacother* (2019) 112:108656. doi: 10.1016/j.biopha.2019.108656
86. Mao A, Tang J, Tang D, Wang F, Liao S, Yuan H, et al. MicroRNA-29b-3p Enhances Radiosensitivity Through Modulating WISP1-Mediated Mitochondrial Apoptosis in Prostate Cancer Cells. *J Cancer* (2020) 11 (21):6356–64. doi: 10.7150/jca.48216
87. John-Aryankalayil M, Palayoor ST, Makinde AY, Cerna D, Simone CB2nd, Falduto MT, et al. Fractionated Radiation Alters Oncomir and Tumor Suppressor miRNAs in Human Prostate Cancer Cells. *Radiat Res* (2012) 178(3):105–17. doi: 10.1667/RR2703.1
88. Dai H, Wang C, Yu Z, He D, Yu K, Liu Y, et al. MiR-17 Regulates Prostate Cancer Cell Proliferation and Apoptosis Through Inhibiting JAK-STAT3 Signaling Pathway. *Cancer Biother Radiopharm* (2018) 33(3):103–9. doi: 10.1089/cbr.2017.2386
89. Xu Z, Zhang Y, Ding J, Hu W, Tan C, Wang M, et al. miR-17-3p Downregulates Mitochondrial Antioxidant Enzymes and Enhances the Radiosensitivity of Prostate Cancer Cells. *Mol Ther Nucleic Acids* (2018) 13:64–77. doi: 10.1016/j.omtn.2018.08.009
90. Liao H, Xiao Y, Hu Y, Yin Z, Liu L. microRNA-32 Induces Radioresistance by Targeting DAB2IP and Regulating Autophagy in Prostate Cancer Cells. *Oncol Lett* (2015) 10(4):2055–62. doi: 10.3892/ol.2015.3551
91. Jalava SE, Urbanucci A, Latonen L, Waltering KK, Sahu B, Janne OA, et al. Androgen-Regulated miR-32 Targets BTG2 and Is Overexpressed in Castration-Resistant Prostate Cancer. *Oncogene* (2012) 31(41):4460–71. doi: 10.1038/onc.2011.624
92. Gu H, Liu M, Ding C, Wang X, Wang R, Wu X, et al. Hypoxia-Responsive miR-124 and miR-144 Reduce Hypoxia-Induced Autophagy and Enhance Radiosensitivity Of Prostate Cancer Cells *via* Suppressing PIM1. *Cancer Med* (2016) 5(6):1174–82. doi: 10.1002/cam4.664

93. Xue G, Ren Z, Chen Y, Zhu J, Du Y, Pan D, et al. A Feedback Regulation Between miR-145 and DNA Methyltransferase 3b in Prostate Cancer Cell and Their Responses to Irradiation. *Cancer Lett* (2015) 361(1):121–7. doi: 10.1016/j.canlet.2015.02.046
94. El Bezawy R, Tripari M, Percio S, Cicchetti A, Tortoreto M, Stucchi C, et al. SPOP Deregulation Improves the Radiation Response of Prostate Cancer Models by Impairing DNA Damage Repair. *Cancers (Basel)* (2020) 12 (6):1462. doi: 10.3390/cancers12061462
95. Petrova V, Annicchiarico-Petruzzelli M, Melino G, Amelio I. The Hypoxic Tumour Microenvironment. *Oncogenesis* (2018) 7(1):10. doi: 10.1038/s41389-017-0011-9
96. Fort RS, Matho C, Oliveira-Rizzo C, Garat B, Sotelo-Silveira JR, Duhagon MA. An Integrated View of the Role of miR-130b/301b miRNA Cluster in Prostate Cancer. *Exp Hematol Oncol* (2018) 7:10. doi: 10.1186/s40164-018-0102-0
97. Wang W, Liu M, Guan Y, Wu Q. Hypoxia-Responsive Mir-301a and Mir-301b Promote Radioresistance of Prostate Cancer Cells *via* Downregulating Ndrg2. *Med Sci Monit* (2016) 22:2126–32. doi: 10.12659/MSM.896832
98. Kolluru V, Chandrasekaran B, Tyagi A, Dervishi A, Ankem M, Yan X, et al. miR-301a Expression: Diagnostic and Prognostic Marker for Prostate Cancer. *Urol Oncol* (2018) 36(11):503.e9–.e15. doi: 10.1016/j.urolonc.2018.07.014
99. Ribatti D, Tamma R, Annese T. Epithelial-Mesenchymal Transition in Cancer: A Historical Overview. *Trans Oncol* (2020) 13(6):100773. doi: 10.1016/j.tranon.2020.100773
100. Fenderico N, Cominetti D, El Bezawy R, Tortoreto M, Dugo M, Valdagni R, et al. MiR-875-5p Impairs Prostate Cancer Metastasis by Remodeling Tumor Secretome and Enhances Tumor Radiation Response *via* EGFR Suppression (Abstract). *Mol Cancer Ther* (2015) 14(12):A134–A134. doi: 10.1158/1535-7163.TARG-15-A134
101. Zhang L, Liao Y, Tang L. MicroRNA-34 Family: A Potential Tumor Suppressor and Therapeutic Candidate in Cancer. *J Exp Clin Cancer Res* (2019) 38(1):53. doi: 10.1186/s13046-019-1059-5
102. Kojima K, Fujita Y, Nozawa Y, Deguchi T, Ito M. MiR-34a Attenuates Paclitaxel-Resistance of Hormone-Refractory Prostate Cancer PC3 Cells Through Direct and Indirect Mechanisms. *Prostate* (2010) 70(14):1501–12. doi: 10.1002/pros.21185
103. Bertoli G, Cava C, Castiglioni I. MicroRNAs as Biomarkers for Diagnosis, Prognosis and Theranostics in Prostate Cancer. *Int J Mol Sci* (2016) 17 (3):421. doi: 10.3390/ijms17030421
104. Weidhaas JB, Babar I, Nallur SM, Trang P, Roush S, Boehm M, et al. MicroRNAs as Potential Agents to Alter Resistance to Cytotoxic Anticancer Therapy. *Cancer Res* (2007) 67(23):11111–6. doi: 10.1158/0008-5472.CAN-07-2858
105. Dong Q, Meng P, Wang T, Qin W, Qin W, Wang F, et al. MicroRNA Let-7a Inhibits Proliferation of Human Prostate Cancer Cells *In Vitro* and *In Vivo* by Targeting E2F2 and CCND2. *PLoS One* (2010) 5(4):e10147. doi: 10.1371/journal.pone.0010147
106. Wang W, Liu J, Wu Q. MiR-205 Suppresses Autophagy and Enhances Radiosensitivity of Prostate Cancer Cells by Targeting TP53INP1. *Eur Rev Med Pharmacol Sci* (2016) 20(1):92–100.
107. Xu CG, Yang MF, Fan JX, Wang W. MiR-30a and miR-205 are Downregulated in Hypoxia and Modulate Radiosensitivity of Prostate Cancer Cells by Inhibiting Autophagy *via* TP53INP1. *Eur Rev Med Pharmacol Sci* (2016) 20(8):1501–8.
108. Tao Z, Xu S, Ruan H, Wang T, Song W, Qian L, et al. MiR-195/-16 Family Enhances Radiotherapy *via* T Cell Activation in the Tumor Microenvironment by Blocking the PD-L1 Immune Checkpoint. *Cell Physiol Biochem* (2018) 48(2):801–14. doi: 10.1159/000491909
109. McDermott N, Meunier A, Wong S, Buchete V, Marignol L. Profiling of a Panel of Radioresistant Prostate Cancer Cells Identifies Deregulation of Key miRNAs. *Clin Transl Radiat Oncol* (2017) 2:63–8. doi: 10.1016/j.ctro.2017.01.005
110. Kanwal R, Plaga AR, Liu X, Shukla GC, Gupta S. MicroRNAs in Prostate Cancer: Functional Role as Biomarkers. *Cancer Lett* (2017) 407:9–20. doi: 10.1016/j.canlet.2017.08.011
111. Templin T, Paul S, Amundson SA, Young EF, Barker CA, Wolden SL, et al. Radiation-Induced Micro-RNA Expression Changes in Peripheral Blood Cells of Radiotherapy Patients. *Int J Radiat Oncol Biol Phys* (2011) 80 (2):549–57. doi: 10.1016/j.ijrobp.2010.12.061
112. Morii A, Ogawa R, Watanabe A, Cui ZG, Takasaki I, Doi N, et al. Utilization of microRNAs With Decreased Expression Levels in Response to X-Ray Irradiation for Fine-Tuning Radiation-Controlled Gene Regulation. *Int J Mol Med* (2013) 32(1):9–16. doi: 10.3892/ijmm.2013.1360

Conflict of Interest: The authors declare that the research was conducted in the absence of any commercial or financial relationships that could be construed as a potential conflict of interest.

frontiers in Oncology

ORIGINAL RESEARCH
published: 19 August 2021
doi: 10.3389/fonc.2021.714709

Hippocampus-Avoidance Whole-Brain Radiation Therapy Is Efficient in the Long-Term Preservation of Hippocampal Volume

Ilinca Popp[1], Alexander Rau[2], Elias Kellner[3], Marco Reisert[3], Jamina Tara Fennell[1], Thomas Rothe[1], Carsten Nieder[4,5], Horst Urbach[2], Karl Egger[2], Anca Ligia Grosu[1,6] and Christoph P. Kaller[2]*

[1] Department of Radiation Oncology, Medical Center, Faculty of Medicine, University of Freiburg, Freiburg, Germany, [2] Department of Neuroradiology, Medical Center, Faculty of Medicine, University of Freiburg, Freiburg, Germany, [3] Medical Physics, Department of Radiology, Medical Center, Faculty of Medicine, University of Freiburg, Freiburg, Germany, [4] Department of Oncology and Palliative Medicine, Nordland Hospital, Bodø, Norway, [5] Department of Clinical Medicine, Faculty of Health Sciences, University of Tromsø, Tromsø, Norway, [6] German Cancer Consortium (DKTK), Partner Site Freiburg, German Cancer Research Center (DKFZ), Heidelberg, Germany

OPEN ACCESS

Edited by:
Christina Tsien, Johns Hopkins Medicine, United States

Reviewed by:
Simon S. Lo, University of Washington, United States
Raphael Pfeffer, Assuta Medical Center, Israel
Wenyin Shi, Thomas Jefferson University, United States

***Correspondence:**
Ilinca Popp
ilinca.popp@uniklinik-freiburg.de

Specialty section:
This article was submitted to Radiation Oncology, a section of the journal Frontiers in Oncology

Received: *25 May 2021*
Accepted: *26 July 2021*
Published: *19 August 2021*

Citation:
Popp I, Rau A, Kellner E, Reisert M, Fennell JT, Rothe T, Nieder C, Urbach H, Egger K, Grosu AL and Kaller CP (2021) Hippocampus-Avoidance Whole-Brain Radiation Therapy Is Efficient in the Long-Term Preservation of Hippocampal Volume. Front. Oncol. 11:714709. doi: 10.3389/fonc.2021.714709

Background and Purpose: With improved life expectancy, preventing neurocognitive decline after cerebral radiotherapy is gaining more importance. Hippocampal damage has been considered the main culprit for cognitive deficits following conventional whole-brain radiation therapy (WBRT). Here, we aimed to determine to which extent hippocampus-avoidance WBRT (HA-WBRT) can prevent hippocampal atrophy compared to conventional WBRT.

Methods and Materials: Thirty-five HA-WBRT and 48 WBRT patients were retrospectively selected, comprising a total of 544 contrast-enhanced T1-weighted magnetic resonance imaging studies, longitudinally acquired within 24 months before and 48 months after radiotherapy. HA-WBRT patients were treated analogously to the ongoing HIPPORAD-trial (DRKS00004598) protocol with 30 Gy in 12 fractions and dose to 98% of the hippocampus ≤ 9 Gy and to 2% ≤ 17 Gy. WBRT was mainly performed with 35 Gy in 14 fractions or 30 Gy in 10 fractions. Anatomical images were segmented and the hippocampal volume was quantified using the Computational Anatomy Toolbox (CAT), including neuroradiological expert review of the segmentations.

Results: After statistically controlling for confounding variables such as age, gender, and total intracranial volume, hippocampal atrophy was found after both WBRT and HA-WBRT ($p < 10^{-6}$). However, hippocampal decline across time following HA-WBRT was approximately three times lower than following conventional WBRT ($p < 10^{-6}$), with an average atrophy of 3.1% *versus* 8.5% in the first 2 years after radiation therapy, respectively.

Conclusion: HA-WBRT is a therapeutic option for patients with multiple brain metastases, which can effectively and durably minimize hippocampal atrophy compared to conventional WBRT.

Keywords: hippocampus, atrophy, WBRT (whole-brain radiation therapy), cognitive function, MRI

INTRODUCTION

Cerebral radiation therapy (RT) is a central pillar in the treatment of brain metastases (1). For patients with multiple metastases, whole-brain RT (WBRT) is a common treatment option, as it was shown to significantly improve distant intracerebral tumor control and reduce the neurological death rate compared to local therapies alone (2). However, with increased survival due to improved systemic and supportive therapies, reported neurocognitive deficits following cerebral irradiation and in particular WBRT have gained substantial importance (3, 4). More specifically, WBRT is associated with an increased risk of cognitive dysfunction and decline in quality of life (3–6), with numerous prior studies having deemed RT-induced hippocampal damage the most important culprit (7–11). Cognitive decline can be observed as early as 6 weeks after WBRT (3, 5) and appears to predominantly involve verbal memory (3, 12, 13).

Hippocampus-avoidance WBRT (HA-WBRT) selectively restricts the radiation dose in the hippocampal region with the intention of preserving cognitive functions. It is generally considered a safe method, with a low risk of hippocampal and peri-hippocampal relapse (10, 14–16). The protective effect of HA-WBRT on the hippocampi has been and is currently still being investigated in prospective clinical trials, but mainly indirectly by means of neurocognitive testing. In the single arm RTOG 0933 trial (9) and in the randomized phase III NRG Oncology CC001 trial (10), a reduction in neurocognitive decline was observed following HA-WBRT compared to conventional WBRT. The evaluation of neurocognitive functions in these trials could only be reliably performed for a maximum of 6 months following RT, although more than 50% of patients were still alive after this point (10). High death rates and noncompliance with neurocognitive testing may thus hinder a comprehensive long-term evaluation using neurocognitive testing as a proxy of hippocampal damage. Furthermore, distinguishing tumor fatigue and declining physical health from a specific RT-related hippocampal neurocognitive failure remains challenging.

A more direct measurement of hippocampal cellular loss after irradiation can be the assessment of changes in hippocampal volume as a function of dose and time. Hippocampal neuronal and volume loss have been systematically linked to cognitive decline, independently of concomitant neuropathological diseases (17–19). However, at present, it is unknown to which extent and over which period of time HA-WBRT can prevent hippocampal cellular loss compared to conventional WBRT. To close this gap, we retrospectively identified WBRT and HA-WBRT patients longitudinally monitored with magnetic resonance (MR) imaging and extracted hippocampal volume as a morphological parameter to elucidate both immediate and long-term effects of WBRT and HA-WBRT and to determine the extent to which HA-WBRT can prevent hippocampal atrophy compared to conventional WBRT over time.

MATERIALS AND METHODS

Patient Sample

The current study was approved by the local ethics committee. We used a retrospective longitudinal study design and identified 756 patients having received WBRT or HA-WBRT between December 2003 and December 2016 in the Department of Radiation Oncology of the Medical Center—University of Freiburg. Patients were evaluated with respect to inclusion/exclusion criteria on the patient level and image level, as is specified in the flowchart in **Figure 1**.

Patients were included if they had cerebral metastases of solid tumors, no meningeal spread at the time of WBRT/HA-WBRT, no known central nervous system pathologies accompanied by cognitive deficits or radiological changes (e.g., dementia, stroke, and meningitis), and at least one gross artifact-free three-dimensional (3D) contrast-enhanced sagittal T1-weighted MR (CE-T1-MR) imaging study before and after irradiation. Patients with hippocampal metastases or hippocampal interventions prior to study treatment were not considered suitable for analysis. Hippocampal interventions were defined as hippocampal resections or RT to the head with a total mean hippocampal dose (D_{mean}, summed across all RT series) ≥ 3 Gy (equivalent dose delivered in 2 Gy fractions [EQD2, $\alpha/\beta = 2$]) and a total maximal hippocampal dose (D_{max}, summed across all RT series) ≥ 14.4 Gy (EQD2, $\alpha/\beta = 2$). The thresholds were set taking into consideration the strictest hippocampal constraints imposed in clinical trials (10, 20, 21).

After this first selection on the patient level, patients were evaluated on the image level. In patients with any further hippocampal interventions (see definition above) after RT, all imaging studies acquired after these interventions were excluded to avoid any bias on the target analyses. Studies lacking the appropriate quality for processing were also excluded. To this end, image quality was assessed by means of the Image Quality Rating (IQR) derived from the brain tissue segmentation using the Computational Anatomy Toolbox (CAT). The IQR metric is a continuous index that scales between 0% and 100% and is graded from A+ to F, which corresponds to an image quality from 100% to 50% (and below), respectively. Images with grades A, B, and C are considered to be of excellent, good, to satisfactory quality, whereas grades D, E, and F denote a sufficient, critical,

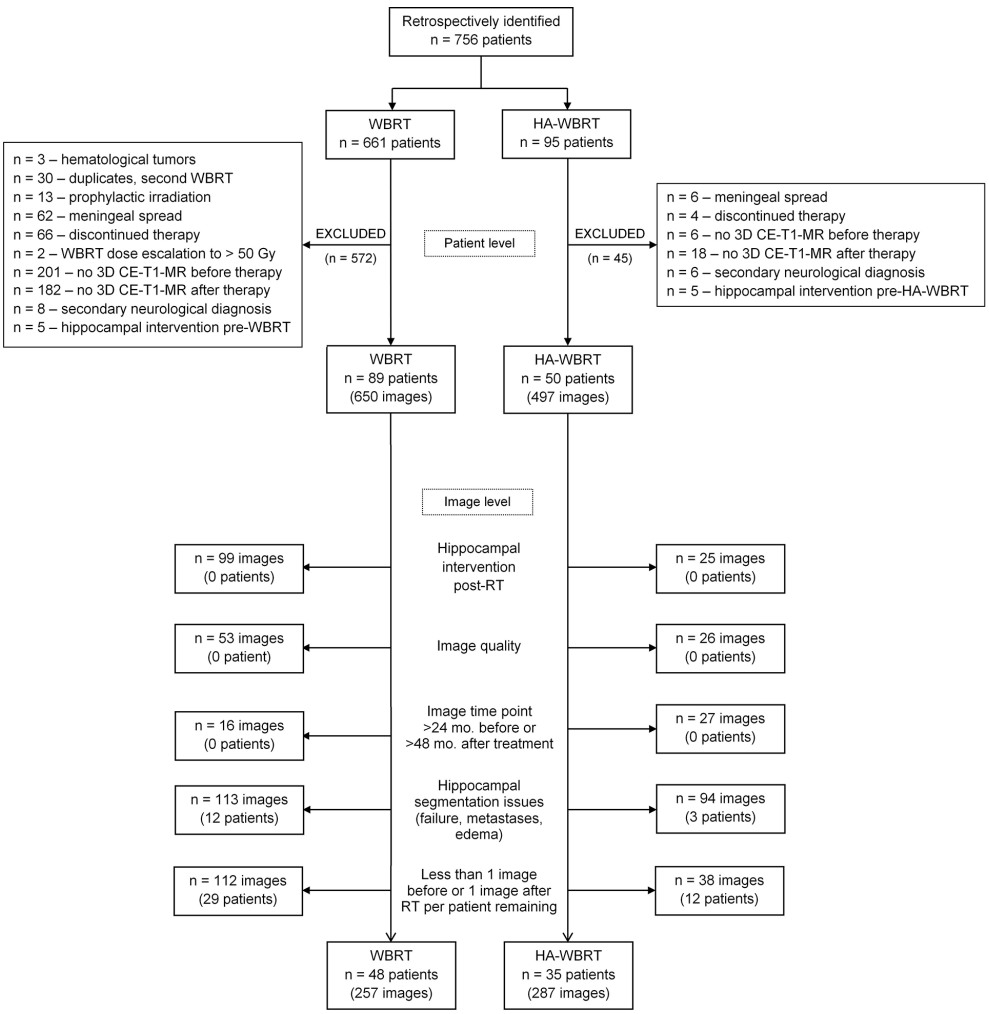

FIGURE 1 | Flowchart of patient selection. CE-T1-MR, contrast-enhanced T1-weighted magnetic resonance; HA-WBRT, hippocampus-avoidance whole-brain radiation therapy; RT, radiation therapy; WBRT, whole-brain radiation therapy.

and unacceptable image quality, respectively. For the present analyses, the threshold for inclusion of individual image studies was set to ≥70%, which corresponds to an image quality of at least C- (satisfactory).

MR imaging at follow-up examinations had been performed every 3 months or as required according to clinical routine. The interval for inclusion of image time points into the present analysis was set to 24 months before and 48 months after RT, in order to account for a maximal general life expectancy of cerebrally metastasized patients (22).

Insufficient quality of the automatic segmentation of the hippocampi with the CAT (see below) and the presence of edema or metastases in the hippocampi as further exclusion criteria were visually checked by an experienced neuroradiologist (AR). Finally, after exclusion of individual imaging studies, only those patients having at least two imaging studies (minimum one study before and minimum one after RT) remained in the analysis.

Radiation Treatment Planning

Patients underwent RT-planning computer tomography (CT) in thermoplastic mask immobilization (BrainLab, Feldkirchen, Germany). CE-T1-MR and CT images were rigidly co-registered based on mutual information (iPlan RT Image 4.1.1, BrainLab, Feldkirchen, Germany) and served for target volume and organ at risk delineation.

For HA-WBRT, a hippocampus-avoidance region (HAR) was defined as a 7-mm 3D margin around the hippocampus, as described previously (23, 24). The planning tumor volume (PTV) for brain was defined as the whole brain (clinical target volume, CTV) plus 3 mm, excluding PTVs of metastases and the HAR. The prescribed dose for the brain PTV was 30 Gy in 12 fractions, with or without simultaneous integrated boost of 51 Gy or 42 Gy in 12 fractions to the metastases. The hippocampal avoidance was performed according to the constraints of the currently ongoing prospective randomized trial HIPPORAD (NOA-14, ARO 2015-3, DRKS00004598): dose to 98% of the

hippocampal volume ($D_{98\%}$) ≤ 9 Gy, dose to 2% of the hippocampal volume ($D_{2\%}$) ≤ 17 Gy, and D_{mean} ≤ 10 Gy (17). Patients were treated by volumetric modulated arc therapy (VMAT) based on 2–4 arcs.

The WBRT was performed in the majority of cases by conventional two-dimensional planning (98.1%). A minority received CT-based three-dimensional planning (1.9%). The prescribed dose was 35 Gy in 14 fractions in 43.9%, 30 Gy in 10 fractions in 30.8%, 40 Gy in 20 fractions in 11.2%, and other fractionations in 14% of cases.

Dosimetry and Interfering Events

The D_{max} and D_{mean} applied to the hippocampi and to the whole brain during WBRT and HA-WBRT were extracted from the dose-volume histograms and converted into equivalent doses delivered in 2 Gy fractions (EQD2), considering an $\alpha/\beta = 2$, in order to account for the different prescription doses and fractionations. Previous and subsequent RT to the brain, head or neck structures and their corresponding doses to the hippocampi, as well as hippocampal resections and edema were also documented.

Image Processing

CE-T1-MR images were segmented using the CAT (version 12.5, release 1364; http://dbm.neuro.uni-jena.de/cat/) with default parameter settings running in the Statistical Parametric Mapping (SPM, version 12.5; https://www.fil.ion.ucl.ac.uk/spm/software/) software package in Matlab (version 7.14; The Mathworks Inc., Natick, MA). Deformation field parameters for nonlinear normalization into the stereotactic Montreal Neurological Institute (MNI) standard space were computed using the DARTEL (Diffeomorphic Anatomical Registration Through Exponentiated Lie algebra) approach (25) implemented in CAT. Atlas-based segmentation of the hippocampus and resulting hippocampal volumes were computed based on the *in vivo* high-resolution Computational Brain Anatomy (CoBrA) atlas of the hippocampus (26) implemented in CAT. An example of a hippocampus segmentation using CAT is shown in **Figure 2**.

CAT segmentation was found to be reliable and robust compared to the ground truth (27). However, for quality assurance, the automatized segmentation was verified by an experienced neuroradiologist (AR). CE-T1-MR images were evaluated in a 3D reformation with regard to the accuracy of the segmentation of the hippocampi, the total intracranial volume (TIV), and the brain volume. In addition, occurrence of hippocampal or parahippocampal metastases with hippocampal edema was assessed. Imaging studies featuring insufficient hippocampal segmentation accuracy or the presence of metastases and/or edema were excluded from the analysis (see above).

Statistical Analysis

We hypothesized that treatment with WBRT compared to HA-WBRT leads to a stronger decrease in hippocampal volume across time following RT. Given presumably non-linear patterns of volume change across time, we took advantage of the statistical software R (version 3.4.4 (28)) and the package *mgcv* [version 1.8-31 (29, 30)] for generalized additive mixed modelling (GAMM). Additive modeling fits a smoothing curve on subsegments of the data using regression splines (29–31) and can cope with non-linear patterns without the need of prior knowledge on the exact shape of the function underlying the relationship of interest. Effective degrees of freedom (edf) for the individual model terms are estimated from the data but were in the present analyses restricted by default to $k = 10$ (30). Univariate smooths with thin plate regression splines were used as smoothing functions. Reported model estimates were based on a restricted maximum likelihood (REML) approach.

Hippocampal volume as derived from the CAT segmentation (see above) constituted the dependent variable. Given that the raw hippocampal volume data were substantially correlated between hemispheres ($r = 0.823$) and that no hypotheses were specified for differential effects of RT on left versus right hippocampus, we decided to use the average of the raw hippocampal volumes across hemispheres as dependent variable to reduce the dimensionality of the data.

Therapy group (WBRT vs. HA-WBRT) and time (as continuous measure in months centered at the time point of RT) comprised the independent variables of interest to be modeled as fixed effects. The effects of time and the interaction of time by group were thereby modeled using non-linear smoothing functions.

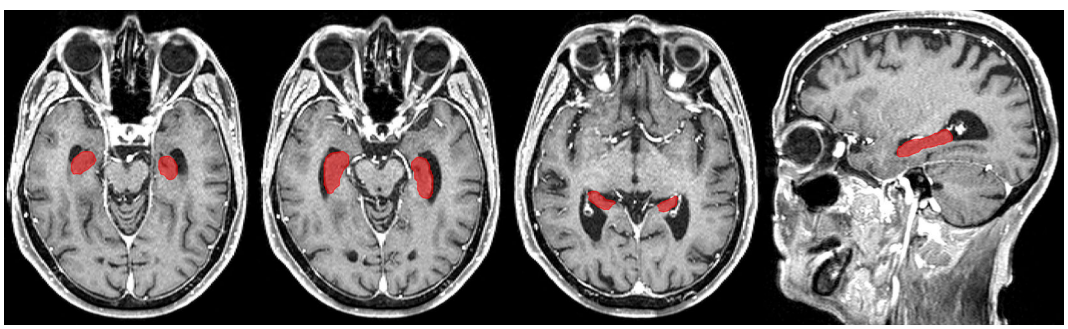

FIGURE 2 | Example of a hippocampus segmentation on CE-T1-MR imaging using the CAT and the *in vivo* high-resolution CoBrA atlas of the hippocampus (26).

Age at RT, gender, and TIV constituted nuisance variables that were expected to have a systematic impact on interindividual variation in hippocampal volume but were of no interest and modeled as fixed effects. As an exploratory analysis indicated an expectably strong confound between TIV and gender [$r = 0.602$; see also (32)], we decided to orthogonalize the two variables by regressing TIV on gender and to further use the residuals as gender-adjusted index of interindividual variation in TIV.

The longitudinal design with different number of observations for individual patients irregularly spaced in time and measured on different MR scanners was taken into account by modeling variations between patients and MR scanners as random intercepts.

Taken together, our target analysis on the differential time course of changes in hippocampal volume following WBRT vs. HA-WBRT thus comprised a GAMM model with the dependent variable volume, the three fixed effects of interest (time, group, and the interaction between group and time), three fixed effects for nuisance variables (age at RT, gender, and gender-adjusted TIV), and two random effects (patient and MR scanner). By restricting the maximum possible number of smoothing functions to $k-1 = 9$ for the effects of age and the interaction between age and group (see above), the possible total number of individual fixed-effects parameters including the intercept ranged between 7 and 23 (for potentially resulting $k-1$ numbers of smoothing functions between 1 and 9, respectively). Furthermore, given a total of 544 valid data points (see below), this corresponded to a ratio of at minimum ≥ 23 to at maximum ≤ 77 observations per fixed-effect parameter, which was hence sufficient for a valid model estimation and not prone to overfitting (30).

RESULTS

Final Patient Sample

On the patient level, 617 out of the initially identified 756 suitable patients were considered unsuitable and excluded from further analysis (see **Figure 1** for details). Starting in 2012, all patients in our department with multiple metastases of solid tumors, without (peri)hippocampal metastases and eligible for CT-based RT-planning, underwent HA-WBRT with or without simultaneous integrated boost. The remaining patients (with hematological malignancies, prophylactic or repeated WBRT, meningeal spread, or extremely poor prognosis without possibility of follow-up) were treated with conventional WBRT, but were removed from further analysis as per set exclusion criteria. In contrast, all patients before 2012 consistently received WBRT. Thus, the two resulting cohorts were chronologically shifted, but with a low risk of biased selection.

After this first selection on the patient level, 139 patients remained, cumulating in 1,147 CE-T1-MR imaging studies that were further evaluated on the image level. This resulted in the exclusion of another 603 studies and 56 patients (see **Figure 1** for details).

The final data set comprised 544 CE-T1-MR imaging studies (WBRT, $n = 257$; HA-WBRT, $n = 287$) of 83 patients (WBRT, $n = 48$; HA-WBRT, $n = 35$) acquired on 16 different MR scanners (**Figure 1**). The utilized MR scanners were sufficiently overlapping between groups to allow for including MR scanners into the model as a random effect. The individual number of included imaging studies before and after RT ranged between 1 and 10 and between 1 and 20 per patient, respectively.

An overview on the selected patients' demographic and clinical characteristics is provided in **Table 1**. Patients in the two groups showed imbalances regarding age ($p = 0.049$) and gender ($p = 0.061$), which were statistically accounted for in the target analyses on hippocampal volume (see below). Groups did not significantly differ in the patients' TIV ($p = 0.894$) and individual maximum follow-up time covered post RT ($p = 0.974$). Primary tumors comprised 12 different etiologies (breast cancer, gastrointestinal tumors, germinal tumors, gynecologic tumors, malignant melanoma, small and non-small cell lung cancer [NSCLC], pancreas tumors, renal cell carcinoma, salivary gland carcinoma, sarcoma, and carcinoma of unknown primary). Considering recent improvements in systemic therapies for NSCLC and melanoma through the introduction of immune checkpoint inhibitors and third-generation tyrosine kinase inhibitors, we decided to evaluate the frequency of these primary tumors versus the remaining etiologies. The analysis indicated a percentage of approximately

TABLE 1 | Clinical details of selected patients.

Patient Characteristics	WBRT	HA-WBRT	Differences between groups (test, *p*-value)
Age (years), median, range	59, 34–80	54, 33–84	Mann–Whitney $U = 1{,}053.5$, $p = 0.049$
Gender (no.), male/female	25/23	11/24	$\chi^2 = 3.52$, $p = 0.061$
Total intracranial volume before RT (ml), median, range	1,438, 1,240–1,715	1,435, 1,209–1,934	Mann–Whitney $U = 855$, $p = 0.894$
Hippocampal volume before RT (ml), median, range	3.37, 2.36–4.03	3.24, 2.45–4.25	Mann–Whitney $U = 908$, $p = 0.536$
Follow-up time (months), median, range	6.9, 2.5–39.1	7.8, 1.8–47.0	Mann–Whitney $U = 836$, $p = 0.974$
Additional low-dose RT hippocampal exposure (before and/or after WBRT/HA-WBRT) with total $D_{mean} < 3$ Gy and $D_{max} < 14.4$ Gy (no.): yes/no	10/38	18/17	$\chi^2 = 8.48$, $p = 0.004$
Primary tumor (no.): melanoma+NSCLC/other	23/25	20/15	$\chi^2 = 0.69$, $p = 0.406$

50% NSCLC/melanoma, similar in both RT groups ($p = 0.406$). A detailed listing of all applied systemic therapy agents can be found in **Supplementary Table S1**. Finally, there was a significantly higher proportion of HA-WBRT patients (51.1%) than WBRT patients (20.8%) with a history of additional radiotherapy (radiosurgery and stereotactic fractionated radiotherapy) with very low-dose hippocampal exposure ($p = 0.004$; **Table 1**).

RT was performed according to the prescribed doses, achieving a median D_{mean} (EQD2 $\alpha/\beta = 2$) for the whole brain of 39.4 Gy (range 37.5–40.0 Gy) in the WBRT group and 34.9 Gy (range 33.4–39.7 Gy) in the HA-WBRT group. WBRT in the selected patients was performed exclusively by conventional two-dimensional planning. Thus, D_{mean} and D_{max} (EQD2 $\alpha/\beta = 2$) for both hippocampi were identical to the whole-brain doses and ranged between 37.5 and 40.0 Gy, with a median of 39.4 Gy. In the HA-WBRT group, D_{mean} for the left hippocampus ranged between 5.8 and 8.4 Gy, with a median of 6.8 Gy, while D_{max} ranged between 12.5 and 24.1 Gy, with a median of 15.7 Gy (EQD2 $\alpha/\beta = 2$). For the right hippocampus, D_{mean} was in median 6.7 Gy (range 5.5–9.2 Gy), while D_{max} was 14.8 Gy (range 11.3–21.8 Gy).

Finally, controlling for selection bias, we compared characteristics of patients included in the present analyses to those of the excluded patients (cf. flowchart in **Figure 1**), revealing a significant difference for age (median of 54 vs. 63 years, respectively; $p = 4.34 \times 10^{-5}$) but neither for gender (male vs. female, $n = 36/47$ vs. $n = 316/327$; $p = .322$) nor for type of primary tumor (NSCLC/melanoma vs. other, $n = 43/40$ vs. $n = 293/350$, $p = .283$). The significantly higher median age in the group of excluded patients was concomitant with a significantly shorter median survival time (3.8 vs. 12.7 months; $p = 4.17 \times 10^{-13}$).

Target Analysis on RT-Induced Hippocampal Atrophy

A generalized additive mixed model (GAMM) of the differential time course of changes in hippocampal volume between groups revealed a significant main effect of time ($F = 10.19$, $edf = 2.63$, $p = 7.48 \times 10^{-7}$) and a significant interaction of time by group ($F = 8.44$, $edf = 4.04$, $p = 1.14 \times 10^{-7}$), whereas the simple effect of group was not significant ($t = -0.05$, $p = 0.957$). Fixed effects of nuisance variables age ($t = -3.77$, $p = 1.19 \times 10^{-4}$), gender ($t = 4.61$, $p = 5.19 \times 10^{-6}$), and gender-adjusted TIV ($t = 11.78$, $p < 10^{-16}$), as well as random effects of patient ($F = 19.57$, $edf = 74.13$, $p < 10^{-16}$) and MR scanner ($F = 11.96$, $edf = 7.46$, $p = 1.25 \times 10^{-4}$), also reached significance. Model validation indicated no relevant deviations from the underlying assumptions (**Supplementary Figure S1**).

As can be seen in **Figure 3**, treatment with WBRT was associated with a significantly steeper atrophy of hippocampal volume compared to treatment with HA-WBRT. In the WBRT patients, the estimated average hippocampal volume loss after 6, 12, 24, and 48 months (with time of RT as reference) comprised −0.113 ml (95% prediction interval [−0.288, +0.063]), −0.190 ml [−0.369, −0.012], −0.320 ml [−0.505, −0.136], and −0.519 ml [−0.873, −0.165]. This was equivalent to a volume loss at 6, 12, 24, and 48 months of −3.0% [−7.8%, +1.82%], −5.1% [−10.0%, −0.1%], −8.5% [−13.9%, −3.1%], and −13.8% [−24.7%, −2.9%]. In the HA-WBRT patients, the estimated average hippocampal volume loss after 6, 12, 24, and 48 months (with time of RT as reference) was −0.027 ml [−0.158, +0.104], −0.055 ml [−0.187, +0.077], −0.116 ml [−0.252; +0.019], and −0.196 ml [−0.358, −0.033]. This was equivalent to a volume loss at 6, 12, 24, and 48 months of −0.7% [−4.2%, +2.8%], −1.5% [−5.0%, +2.1%], −3.1% [−6.8%, +0.6%], and −5.2% [−9.75%, −0.7%].

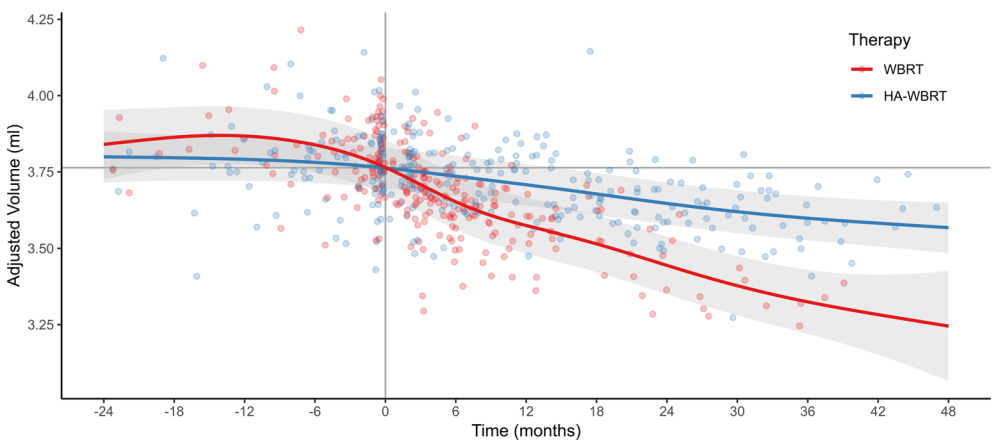

FIGURE 3 | Evolution of hippocampal atrophy 24 months before and 48 months after WBRT versus HA-WBRT (averaged for left and right hippocampus) across time (with the gray vertical line denoting the time of RT and the gray horizontal line depicting the average hippocampal volume at the time of RT as reference). The two treatment groups, WBRT and HA-WBRT, show significantly distinct time courses. Dots represent individual data points, and bands represent standard errors. Adjusted volume refers to the estimated marginal means after accounting for variation of nuisance variables (effects of age, gender, TIV, patient, and MR scanner). The number of patients with adequate imaging studies still in follow-up was $n = 49$ at 6 months, $n = 29$ at 12 months, $n = 14$ at 24 months, and $n = 5$ at 36 months. HA-WBRT, hippocampus-avoidance whole-brain radiation therapy; WBRT, whole-brain radiation therapy.

The predicted hippocampal volume decline following WBRT was therefore approximately three times higher in the first 2 years posttreatment than following HA-WBRT.

In contrast, volume changes 24, 12, and 6 months before the time of RT as reference comprised +0.076 ml ([−0.148, +0.299]; +2.0% [−3.8%, +7.8%]), +0.103 ml ([−0.082, +0.288]; +2.7% [−2.0%, +7.5%]), and +0.074 ml ([−0.105, +0.253]; +2.0% [−2.7%, +6.6%) in the WBRT patients and +0.037 ml ([−0.128, +0.201]; +1.0% [−3.3%, +5.3%]), +0.028 ml ([−0.109, +0.166]; +0.8% [−2.9%, +4.4%]), and +0.018 ml ([−0.144, +0.151]; +0.5% [−3.0%, +4.0%]) in the HA-WBRT patients, respectively. That is, predicted hippocampal volume changes before RT were substantially lower, not significantly different from zero, and comparable between groups.

Supplementary Analyses

We computed several control analyses, which are in brief reported below. (i) To answer the question whether hippocampal atrophy over time was significant on the level of the individual treatments, we computed two GAMMs on the effect of time separately for the two groups (each including only the effect of time, but neither group nor the interaction between time and group; plus fixed nuisance effects of age, gender, gender-adjusted TIV, and random intercepts for patient and scanner). Results confirmed significant changes in hippocampal volume across time for both WBRT (F = 28.52, edf = 4.47, $p < 10^{-16}$) and HA-WBRT (F = 13.51, edf = 2.18, $p = 1.91 \times 10^{-7}$). (ii) Furthermore, to more directly consider the time of RT as the actual onset of the observed hippocampal atrophy, we extended the original GAMM of our target analysis by the factor pre/post and accordingly centered the continuous variable time pre RT to −24 months and restricted the post RT data to the first 24 months. The model hence comprised the fixed effects of time (continuous), group, time point (pre vs. post RT), and their two-way and three-way interactions, as well as the fixed nuisance effects of age, gender, gender-adjusted TIV, and random intercepts for patient and scanner. Results revealed the critical three-way interaction of time by group by pre/post (F = 9.94, edf = 2.00, $p = 6.13 \times 10^{-5}$), thus statistically confirming that the differential effects in hippocampal volume decline between groups and across time were indeed manifest post RT (see also **Figure 3**). (iii) Finally, given the chronological shift between the data acquisitions in the two treatment groups and potentially confounding changes in secondary systemic therapies for melanoma and NSCLC tumors, we conducted a control analysis explicitly testing whether the interaction effect of time by RT group on the evolution of hippocampal atrophy was differentially driven by primary tumor (melanoma and NSCLC *vs.* other). That is, we extended our target analysis by the factor primary tumor type, thus resulting in model with fixed effects for time, group, primary tumor, and their two-way and three-way interactions, as well as the fixed nuisance effects of age, gender, gender-adjusted TIV, and random intercepts for patient and scanner. However, neither the critical three-way interaction of time by RT group by primary tumor nor any lower-order effects of primary tumor were significant (all $p > 0.266$).

DISCUSSION

The current study used retrospective longitudinal analysis of hippocampal volume as a direct morphological marker to determine the impact of moderate RT doses on the hippocampus in the context of whole-brain irradiation. In a sample of patients with multiple (>3) brain metastases closely followed-up with serial MR imaging, we found significant hippocampal atrophy over time after both WBRT and HA-WBRT, with considerably lower atrophy rates following the latter. To our knowledge, this is the first study to show the differential time course of the effects of WBRT with and without hippocampal avoidance on hippocampal volume.

Hippocampal Atrophy Following Radiotherapy

For the fractionated, partial brain RT of primary brain tumors, Seibert et al. (33) similarly measured the hippocampal volume in 52 patients before and 1 year after treatment. The authors found a significant reduction in volume after high-dose RT (D_{mean} > 40 Gy), but not after low-dose RT (D_{mean} < 10 Gy). Our results substantially extend these findings by longitudinally demonstrating the impact of moderate-dose RT (median D_{mean} < 40 Gy) and low-dose RT (median D_{mean} < 7 Gy) on the hippocampus as applied in the WBRT and HA-WBRT group, respectively. Moreover, the here observed annual atrophy rate of approximately 5% in the first 2 years after WBRT clearly exceeds the reported mean annualized rates of 3.5%–4% for patients with Alzheimer's disease (17). Furthermore, these values also surpass those observed in elderly patients experiencing worsening cognitive decline (17).

In normal aging, hippocampal atrophy relative to the rest of gray matter is reported to begin after the ages of 63 in men and 67 in women (34) and increase to an estimated annual decline rate of 1.7% after the age of 80 (17). In the HA-WBRT cohort, the median age was 54, with only 14% of patients over the age of 63. Thus, the significant hippocampal atrophy of 1.6% per year in the first 2 years after RT seems higher than what would be expected for this age group (34) and contrasts notably the lack of volume change in the 2 years prior to HA-WBRT in the same patients. Since hippocampal D_{mean} for HA-WBRT was generally below 7 Gy EQD2 $\alpha/\beta = 2$ and a significant atrophy was noticed only after this intervention, our data suggest a possibly high hippocampal radiosensitivity to lower doses, similar to the observations of Mizumatsu et al. in animal studies (7). These results are in line with the data of Nagtegaal et al., who found a dose-dependent increase in hippocampal age of 2–20 years and a hippocampal volume loss rate of 0.16%/Gy in 33 patients having undergone RT for grade II–IV glioma (35). Compared to this, the atrophy rate obtained for our HA-WBRT cohort was slightly higher (1.6% versus 0.16 × 6.8 Gy = 1.1%). Whether and to which extent additional low-dose hippocampal exposure (with a total D_{mean} < 3 Gy, EQD2 $\alpha/\beta = 2$) from previous and subsequent radiotherapies may have contributed to the hippocampal atrophy in the HA-WBRT group is unclear and has to be explored in future trials.

Although hippocampal volume assessment may not be sensitive to all forms of neurodegeneration, hippocampal volume loss has been systematically associated with cognitive decline in dementia, with significantly higher atrophy rates in patients showing clinical worsening (17, 18). Following RT, hippocampal atrophy in general (36, 37) and the inhibition of neurogenesis in the neural stem cell niche found in the subgranular zone of the dentate gyrus in particular are considered to be responsible for memory impairment (7, 38). Although data on the persistence of human hippocampal neurogenesis in adults is controversial (39, 40), sparing of the hippocampi in RT planning appears to be clinically relevant and effective in preventing cognitive deterioration (9, 10, 41).

In this respect, various hippocampal constraints have been considered safe for irradiation. In the NRG Oncology CC001 trial (10) and the preceding single-arm RTOG 0933 trial (9), 100% of the hippocampus did not exceed a dose of 9 Gy (6.5 Gy EQD2 $\alpha/\beta = 2$), and the hippocampal D_{max} did not exceed 16 Gy in 10 fractions (14.4 Gy EQD2 $\alpha/\beta = 2$). Dosimetric analyses performed after stereotactic fractionated RT for benign or low-grade adult brain tumors revealed an equivalent dose of 7.3 Gy in 40% of the bilateral hippocampi (D40%, EQD2 $\alpha/\beta = 2$) as cutoff for the occurrence of long-term cognitive impairment (11). Another clinical trial exploring hippocampal sparing prophylactic cranial irradiation in patients with small-cell lung cancer limited hippocampal D_{mean} to 8 Gy in 10 fractions (5.6 Gy EQD2 $\alpha/\beta = 2$) (21). In the ongoing prospective randomized HIPPORAD trial (NOA-14, ARO 2015-3, DRKS00004598), the hippocampal constraints include $D_{98\%} \leq 9$ Gy (6.2 Gy EQD2 $\alpha/\beta = 2$), $D_{2\%} \leq 17$ Gy (14.5 Gy EQD2 $\alpha/\beta = 2$), and an aimed $D_{mean} \leq 10$ Gy (7.1 Gy EQD2 $\alpha/\beta = 2$) (20). The equivalent dose applied in our HA-WBRT-cohort was therefore in alignment with these data and could be considered sufficient for neurocognitive protection. Consistent with clinical observations, our results showed that HA-WBRT prevents considerable hippocampal volume loss compared to conventional WBRT. Evaluating the time course of hippocampal decline in both groups, the atrophy rate was highest within the first six months following RT and decreased thereafter. Despite this deceleration across time, the differential three-times lower atrophy rate for HA-WBRT persisted over a time frame of 4 years after RT and remained significant after accounting for patient age, gender, and TIV.

Limitations

Because of the retrospective study design, a major limitation of the study is that clinically relevant neurocognitive functional parameters have not been systematically assessed so that a direct link between clinical neurocognitive outcome and hippocampal atrophy after RT could not be established. Furthermore, the final data set was also considerably smaller compared to the initially identified patient list. While the stringent patient selection may impact the generalizability of results, this was necessary to ensure homogeneity and a correct data interpretation. The analysis of excluded patients showed no major discrepancies in gender and tumor type, but revealed lower survival rates corresponding to older age and poorer prognosis. The selected cohort could thus be not representative for all cerebrally metastasized patients, but for the population most eligible for HA-WBRT.

In spite of this selection, there are still several medical conditions that may also influence the size of the hippocampus with increasing age (e.g., cardiovascular disease, obesity, diabetes, hypertension, anxiety, or clinical depression) (42). However, considering the chronological shift of the two groups, the risk of biased selection based on potentially relevant comorbidities was minimized.

Another possible confounder is represented by the cancer and treatment-related neurocognitive dysfunction, reported in the majority of cancer patients and colloquially known as "chemobrain" (43, 44). Although differences in applied systemic therapies did not seem to influence the degree of hippocampal atrophy in our cohort, differences in type and duration of systemic therapies due to the chronological shift may still have had disparate effects on hippocampal volume, as preclinical data suggest a negative impact on neurological pathways and cognition. In particular, hippocampal neurogenesis seems to be inhibited by a wide range of chemotherapeutic agents, including the commonly used cisplatin, oxaliplatin, and paclitaxel (45–47). Morphological alterations and synaptic dysfunction were also noticed in the treatment with certain immune, targeted, and hormone therapies (48–51). However, clinical data on these effects are extremely scarce. While some MRI studies suggest reductions of hippocampal volume in patients receiving systemic treatment (52), others do not (53). Moreover, to our knowledge, the influence of dose and duration of the applied therapies was not investigated as of now. These particularities may thus constitute unknown confounders, which were not systematically documented and could not be included in the present analysis. Given its detailed documentation and prospective design, these interfering aspects will be further explored in the ongoing randomized HIPPORAD trial (20).

Finally, the allowed small RT doses to the hippocampus (in total $D_{mean} < 3$ Gy and $D_{max} < 14.4$ Gy, EQD2 $\alpha/\beta = 2$) during additional interventions (radiosurgery and stereotactic fractionated radiotherapy) before and after study treatment (WBRT vs. HA-WBRT) may have also had an effect on hippocampal volume. However, this affected the HA-WBRT group substantially more than the WBRT group, so that the results of our target analysis showing a preservation of hippocampal volume after HA-WBRT remain valid. Similarly, the prescribed RT regimens were not uniform, but heterogeneous in both the WBRT and the HA-WBRT group, with higher doses applied to the whole brain in the WBRT group. While the effect of the whole brain dose on hippocampal volume independently of hippocampal dose is not known, this difference may have also had an impact on the dynamics of hippocampal atrophy. However, the variation in hippocampal dose between groups (difference in median hippocampal D_{mean} of 32.6 Gy) was higher by one order of magnitude compared to the hippocampal

dose variation within the individual groups (D_{mean} range of 2.5 Gy and 3.7 Gy for WBRT and HA-WBRT, respectively) and to the whole-brain dose variation between groups (difference in median D_{mean} of 4.5 Gy). Therefore, we do not expect a significant impact on the results of our target analysis.

CONCLUSION

The current study shows that HA-WBRT may effectively and durably minimize hippocampal damage compared to conventional WBRT, achieving a threefold reduction in atrophy over a time frame of 4 years following irradiation. To which extent low or cumulative radiation doses over time or applied systemic therapies may also have a significantly negative impact on hippocampal volume and hippocampal-related cognition is still unclear and warrants further investigation in clinical trials.

DATA AVAILABILITY STATEMENT

The metadata supporting the conclusions of this article will be made available by the authors, without undue reservation. Requests to access the datasets should be directed to Ilinca Popp (ilinca.popp@uniklinik-freiburg.de).

ETHICS STATEMENT

The studies involving human participants were reviewed and approved by Ethics Committee of the Albert-Ludwigs-University Freiburg. Written informed consent for participation was not required for this study in accordance with the national legislation and the institutional requirements.

AUTHOR CONTRIBUTIONS

Study design: AG, CK, IP, KE, and CN. Patient treatment according to protocol: IP, AG, TR, KE, and HU. Data collection: IP. Quality assurance: AR and KE. Analysis and interpretation of data: CK and IP. Provision of data analysis tools: EK and MR. Writing of the manuscript: IP and CK. Revision of the manuscript and input: AR, JF, TR, CN, HU, KE, and AG. All authors contributed to the article and approved the submitted version.

FUNDING

IP was partially funded by the Else Kröner-Fresenius-Stiftung, Germany, within the EXCEL (Excellent Clinician Scientists in Freiburg—Education for Leadership) Program "Immunological Causes and Therapies of Cancer" and by the IMM-PACT-Programme for Clinician Scientists, Department of Medicine II, Medical Center—University of Freiburg and Faculty of Medicine, University of Freiburg, funded by the Deutsche Forschungsgemeinschaft (DFG, German Research Foundation) —413517907. CPK was supported by the BrainLinks–BrainTools Cluster of Excellence funded by the German Research Foundation (EXC 1086). The funding sources had no involvement in the writing of the manuscript or in the decision to submit the article for publication.

SUPPLEMENTARY MATERIAL

The Supplementary Material for this article can be found online at: https://www.frontiersin.org/articles/10.3389/fonc.2021.714709/full#supplementary-material

REFERENCES

1. Tsao MN, Xu W, Wong RK, Lloyd N, Laperriere N, Sahgal A, et al. Whole Brain Radiotherapy for the Treatment of Newly Diagnosed Multiple Brain Metastases. *Cochrane Database Syst Rev* (2018) 25(1):CD003869. doi: 10.1002/14651858.CD003869.pub4
2. NCCN Clinical Practice Guidelines in Oncology (NCCN Guidelines®). *Central Nervous System Cancers (Version 3.2019 - October 18, 2019)*. Available at: https://www.nccn.org/professionals/physician_gls/pdf/cns.pdf (Accessed May 4, 2021).
3. Chang EL, Wefel JS, Hess KR, Allen PK, Lang FF, Kornguth DG, et al. Neurocognition in Patients With Brain Metastases Treated With Radiosurgery or Radiosurgery Plus Whole-Brain Irradiation: A Randomised Controlled Trial. *Lancet Oncol* (2009) 10(11):1037–44. doi: 10.1016/S1470-2045(09)70263-3
4. Brown PD, Jaeckle K, Ballman KV, Farace E, Cerhan JH, Anderson SK, et al. Effect of Radiosurgery Alone vs Radiosurgery With Whole Brain Radiation Therapy on Cognitive Function in Patients With 1 to 3 Brain Metastases: A Randomized Clinical Trial. *JAMA* (2016) 316(4):401–9. doi: 10.1001/jama.2016.9839
5. Welzel G, Fleckenstein K, Schaefer J, Hermann B, Kraus-Tiefenbacher U, Mai SK, et al. Memory Function Before and After Whole Brain Radiotherapy in Patients With and Without Brain Metastases. *Int J Radiat Oncol Biol Phys* (2008) 72:1311–8. doi: 10.1016/j.ijrobp.2008.03.009
6. Soffietti R, Kocher M, Abacioglu UM, Villa S, Fauchon F, Baumert BG, et al. A European Organisation for Research and Treatment of Cancer Phase III Trial of Adjuvant Whole-Brain Radiotherapy Versus Observation in Patients With One to Three Brain Metastases From Solid Tumors After Surgical Resection or Radiosurgery: Quality-of-Life Results. *J Clin Oncol* (2013) 31(1):65–72. doi: 10.1200/JCO.2011.41.0639
7. Mizumatsu S, Monje ML, Morhardt DR, Rola R, Palmer TD, Fike JR. Extreme Sensitivity of Adult Neurogenesis to Low Doses of X-Irradiation. *Cancer Res* (2003) 63:4021–7.
8. Monje ML, Mizumatsu S, Fike JR, Palmer TD. Irradiation Induces Neural Precursor-Cell Dysfunction. *Nat Med* (2002) 8:955–62. doi: 10.1038/nm749
9. Gondi V, Pugh SL, Tome WA, Caine C, Corn B, Kanner A, et al. Preservation of Memory With Conformal Avoidance of the Hippocampal Neural Stem-Cell Compartment During Whole-Brain Radiotherapy for Brain Metastases (RTOG 0933): A Phase II Multi-Institutional Trial. *J Clin Oncol* (2014) 32 (34):3810–6. doi: 10.1200/JCO.2014.57.2909
10. Brown PD, Gondi V, Pugh S, Tome WA, Wefel JS, Armstrong TS, et al. Hippocampal Avoidance During Whole-Brain Radiotherapy Plus Memantine for Patients With Brain Metastases: Phase III Trial NRG Oncology Cc001. *J Clin Oncol* (2020) 38(10):1019–29. doi: 10.1200/JCO.19.02767
11. Gondi V, Hermann BP, Mehta MP, Tomé WA. Hippocampal Dosimetry Predicts Neurocognitive Function Impairment After Fractionated Stereotactic Radiotherapy for Benign or Low-Grade Adult Brain Tumors. *Int J Radiat Oncol Biol Phys* (2012) 83(4):e487–93. doi: 10.1016/j.ijrobp.2011.10.021

12. Regine WF, Schmitt FA, Scott CB, Dearth C, Patchell RA, Nichols RC Jr, et al. Feasibility of Neurocognitive Outcome Evaluations in Patients With Brain Metastases in a Multi-Institutional Cooperative Group Setting: Results of Radiation Therapy Oncology Group Trial BR-0018. *Int J Radiat Oncol Biol Phys* (2004) 58(5):1346–52. doi: 10.1016/j.ijrobp.2003.09.023
13. Meyers CA, Smith JA, Bezjak A, Mehta MP, Liebmann J, Illidge T, et al. Neurocognitive Function and Progression in Patients With Brain Metastases Treated With Whole-Brain Radiation and Motexafin Gadolinium: Results of a Randomized Phase III Trial. *J Clin Oncol* (2004) 22:157–65. doi: 10.1200/JCO.2004.05.128
14. Sun Q, Li M, Wang G, Xu H, He Z, Zhou Y, et al. Distribution of Metastasis in the Brain in Relation to the Hippocampus: A Retrospective Single-Center Analysis of 565 Metastases in 116 Patients. *Cancer Imaging* (2019) 19(1):2. doi: 10.1186/s40644-019-0188-6
15. Popp I, Rau S, Hintz M, Schneider J, Bilger A, Fennell JT, et al. Hippocampus-Avoidance Whole-Brain Radiation Therapy With a Simultaneous Integrated Boost for Multiple Brain Metastases. *Cancer* (2020) 126(11):2694–703. doi: 10.1002/cncr.32787
16. Kundapur V, Ellchuk T, Ahmed S, Gondi V. Risk of Hippocampal Metastases in Small Cell Lung Cancer Patients at Presentation and After Cranial Irradiation: A Safety Profile Study for Hippocampal Sparing During Prophylactic or Therapeutic Cranial Irradiation. *Int J Radiat Oncol Biol Phys* (2015) 91(4):781–6. doi: 10.1016/j.ijrobp.2014.12.026
17. Jack CR Jr, Petersen RC, Xu Y, O'Brien PC, Smith GE, Ivnik RJ, et al. Rates of Hippocampal Atrophy Correlate With Change in Clinical Status in Aging and AD. *Neurology* (2000) 55(4):484–9. doi: 10.1212/wnl.55.4.484
18. den Heijer T, van der Lijn F, Koudstaal PJ, Hofman A, van der Lugt A, Krestin GP, et al. A 10-Year Follow-Up of Hippocampal Volume on Magnetic Resonance Imaging in Early Dementia and Cognitive Decline. *Brain* (2010) 133(Pt 4):1163–72. doi: 10.1093/brain/awq048
19. Dawe RJ, Yu L, Arfanakis K, Schneider JA, Bennett DA, Boyle PA. Late-Life Cognitive Decline Is Associated With Hippocampal Volume, Above and Beyond Its Associations With Traditional Neuropathologic Indices. *Alzheimers Dement* (2020) 16(1):209–18. doi: 10.1002/alz.12009
20. Grosu AL, Frings L, Bentsalo I, Oehlke O, Brenner F, Bilger A, et al. Whole-Brain Irradiation With Hippocampal Sparing and Dose Escalation on Metastases: Neurocognitive Testing and Biological Imaging (HIPPORAD) - a Phase II Prospective Randomized Multicenter Trial (NOA-14, ARO 2015-3, DKTK-ROG). *BMC Cancer* (2020) 20(1):532. doi: 10.1186/s12885-020-07011-z
21. Redmond KJ, Hales RK, Anderson-Keightly H, Zhou XC, Kummerlowe M, Sair HI, et al. Prospective Study of Hippocampal-Sparing Prophylactic Cranial Irradiation in Limited-Stage Small Cell Lung Cancer. *Int J Radiat Oncol Biol Phys* (2017) 98(3):603–11. doi: 10.1016/j.ijrobp.2017.03.009
22. Hall WA, Djalilian HR, Nussbaum ES, Cho KH. Long-Term Survival With Metastatic Cancer to the Brain. *Med Oncol* (2000) 17(4):279–86. doi: 10.1007/BF02782192
23. Prokic V, Wiedenmann N, Fels F, Schmucker M, Nieder C, Grosu A-L. Whole Brain Irradiation With Hippocampal Sparing and Dose Escalation on Multiple Brain Metastases: A Planning Study on Treatment Concepts. *Int J Radiat Oncol Biol Phys* (2013) 85(1):264–70. doi: 10.1016/j.ijrobp.2012.02.036
24. Oehlke O, Wucherpfennig D, Fels F, Frings L, Egger K, Weyerbrock A, et al. Whole Brain Irradiation With Hippocampal Sparing and Dose Escalation on Multiple Brain Metastases: Local Tumour Control and Survival. *Strahlenther Onkol* (2015) 191(6):461–9. doi: 10.1007/s00066-014-0808-9
25. Ashburner J. A Fast Diffeomorphic Image Registration Algorithm. *Neuroimage* (2007) 38(1):95–113. doi: 10.1016/j.neuroimage.2007.07.007
26. Winterburn JL, Pruessner JC, Chavez S, Schira MM, Lobaugh NJ, Voineskos AN, et al. A Novel *In Vivo* Atlas of Human Hippocampal Subfields Using High-Resolution 3 T Magnetic Resonance Imaging. *Neuroimage* (2013) 74:254–65. doi: 10.1016/j.neuroimage.2013.02.003
27. Fillmer A, Kuehne A, Goeschel L, Köbe T, Flöel A, Ittermann B. Brain Tissue Segmentation and Subcortical Parcellation: How Reliable Are Different Tools? In: . *Proceedings of the Joint Annual Meeting ISMRM-ESMRMB*. Paris, France. Berkeley, CA: International Society for Magnetic Resonance in Medicine (2018). p. p.0698.
28. R Core Team. *R: A Language and Environment for Statistical Computing* (2018). Vienna, Austria: R Foundation for Statistical Computing. Available at: https://www.R-project.org/ (Accessed May 4, 2021).
29. Wood SN. Stable and Efficient Multiple Smoothing Parameter Estimation for Generalized Additive Models. *J Am Stat Assoc* (2004) 99:673–86. doi: 10.1198/016214504000000980
30. Wood SN. *Generalized Additive Models: An Introduction With R. 2nd edition*. Boca Raton, USA: Chapman and Hall/CRC (2017).
31. Zuur AF, Ieno EN, Walker NJ, Saveliev AA, Smith GM. *Mixed Effects Models and Extensions in Ecology With R*. New York, USA: Springer Science+Business Media (2009).
32. Ruigrok AN, Salimi-Khorshidi G, Lai MC, Baron-Cohen S, Lombardo MV, Tait RJ, et al. A Meta-Analysis of Sex Differences in Human Brain Structure. *Neurosci Biobehav Rev* (2014) 39(100):34–50. doi: 10.1016/j.neubiorev.2013.12.004
33. Seibert TM, Karunamuni R, Bartsch H, Kaifi S, Krishnan AP, Dalia Y, et al. Radiation Dose-Dependent Hippocampal Atrophy Detected With Longitudinal Volumetric Magnetic Resonance Imaging. *Int J Radiat Oncol Biol Phys* (2017) 97(2):263–9. doi: 10.1016/j.ijrobp.2016.10.035
34. Nobis L, Manohar SG, Smith SM, Alfaro-Almagro F, Jenkinson M, Mackay CE, et al. Hippocampal Volume Across Age: Nomograms Derived From Over 19,700 People in UK Biobank. *NeuroImage Clin* (2019) 23:101904. doi: 10.1016/j.nicl.2019.101904
35. Nagtegaal SHJ, David S, Philippens MEP, Snijders TJ, Leemans A, Verhoeff JJC. Dose-Dependent Volume Loss in Subcortical Deep Grey Matter Structures After Cranial Radiotherapy. *Clin Transl Radiat Oncol* (2020) 26:35–41. doi: 10.1016/j.ctro.2020.11.005
36. Tringale KR, Nguyen TT, Karunamuni R, Seibert T, Huynh-Le M-P, Connor M, et al. Quantitative Imaging Biomarkers of Damage to Critical Memory Regions Are Associated With Post–Radiation Therapy Memory Performance in Brain Tumor Patients. *Int J Radiat Oncol Biol Phys* (2019) 105(4):773–83. doi: 10.1016/j.ijrobp.2019.08.003
37. Lv X, He H, Yang Y, Han L, Guo Z, Chen H, et al. Radiation-Induced Hippocampal Atrophy in Patients With Nasopharyngeal Carcinoma Early After Radiotherapy: A Longitudinal MR-Based Hippocampal Subfield Analysis. *Brain Imaging Behav* (2019) 13(4):1160–71. doi: 10.1007/s11682-018-9931-z
38. Madsen TM, Kristjansen PE, Bolwig TG, Wörtwein G. Arrested Neuronal Proliferation and Impaired Hippocampal Function Following Fractionated Brain Irradiation in the Adult Rat. *Neuroscience* (2003) 119:635–42. doi: 10.1016/s0306-4522(03)00199-4
39. Sorrells SF, Paredes MF, Cebrian-Silla A, Sandoval K, Qi D, Kelley KW, et al. Human Hippocampal Neurogenesis Drops Sharply in Children to Undetectable Levels in Adults. *Nature* (2018) 555(7696):377–81. doi: 10.1038/nature25975
40. Moreno-Jiménez EP, Flor-García M, Terreros-Roncal J, Rábano A, Cafini F, Pallas-Bazarra N, et al. Adult Hippocampal Neurogenesis is Abundant in Neurologically Healthy Subjects and Drops Sharply in Patients With Alzheimer's Disease. *Nat Med* (2019) 25(4):554–60. doi: 10.1038/s41591-019-0375-9
41. Ma TM, Grimm J, McIntyre R, Anderson-Keightly H, Kleinberg LR, Hales RK, et al. A Prospective Evaluation of Hippocampal Radiation Dose Volume Effects and Memory Deficits Following Cranial Irradiation. *Radiother Oncol* (2017) 125(2):234–40. doi: 10.1016/j.radonc.2017.09.035
42. Fotuhi M, Do D, Jack C. Modifiable Factors That Alter the Size of the Hippocampus With Ageing. *Nat Rev Neurol* (2012) 8(4):189–202. doi: 10.1038/nrneurol.2012.27
43. Wefel JS, Lenzi R, Theriault RL, Davis RN, Meyers CA. The Cognitive Sequelae of Standard-Dose Adjuvant Chemotherapy in Women With Breast Carcinoma: Results of a Prospective, Randomized, Longitudinal Trial. *Cancer* (2004) 100(11):2292–9. doi: 10.1002/cncr.20272
44. Tannock IF, Ahles TA, Ganz PA, Van Dam FS. Cognitive Impairment Associated With Chemotherapy for Cancer: Report of a Workshop. *J Clin Oncol* (2004) 22(11):2233–9. doi: 10.1200/JCO.2004.08.094
45. Manohar S, Jamesdaniel S, Salvi R. Cisplatin Inhibits Hippocampal Cell Proliferation and Alters the Expression of Apoptotic Genes. *Neurotox Res* (2014) 25(4):369–80. doi: 10.1007/s12640-013-9443-y

46. Sadeghinezhad J, Amrein I. Stereological Analysis of Hippocampus in Rat Treated With Chemotherapeutic Agent Oxaliplatin. *Folia Morphol (Warsz)* (2021) 80(1):26–32. doi: 10.5603/FM.a2020.0031
47. Lee BE, Choi BY, Hong DK, Kim JH, Lee SH, Kho AR, et al. The Cancer Chemotherapeutic Agent Paclitaxel (Taxol) Reduces Hippocampal Neurogenesis *via* Down-Regulation of Vesicular Zinc. *Sci Rep* (2017) 7 (1):11667. doi: 10.1038/s41598-017-12054-7
48. Latzer P, Schlegel U, Theiss C. Morphological Changes of Cortical and Hippocampal Neurons After Treatment With VEGF and Bevacizumab. *CNS Neurosci Ther* (2016) 22(6):440–50. doi: 10.1111/cns.12516
49. Borsini A, Cattaneo A, Malpighi C, Thuret S, Harrison NAMRC ImmunoPsychiatry Consortium, et al. Interferon-Alpha Reduces Human Hippocampal Neurogenesis and Increases Apoptosis *via* Activation of Distinct STAT1-Dependent Mechanisms. *Int J Neuropsychopharmacol* (2018) 21(2):187–200. doi: 10.1093/ijnp/pyx083
50. Gervais NJ, Remage-Healey L, Starrett JR, Pollak DJ, Mong JA, Lacreuse A. Adverse Effects of Aromatase Inhibition on the Brain and Behavior in a Nonhuman Primate. *J Neurosci* (2019) 39(5):918–28. doi: 10.1523/JNEUROSCI.0353-18.2018
51. Lee S, Lee HJ, Kang H, Kim EH, Lim YC, Park H, et al. Trastuzumab Induced Chemobrain, Atorvastatin Rescued Chemobrain With Enhanced Anticancer Effect and Without Hair Loss-Side Effect. *J Clin Med* (2019) 8(2):234. doi: 10.3390/jcm8020234
52. Lepage C, Smith AM, Moreau J, Barlow-Krelina E, Wallis N, Collins B, et al. A Prospective Study of Grey Matter and Cognitive Function Alterations in Chemotherapy-Treated Breast Cancer Patients. *Springerplus* (2014) 19(3):444. doi: 10.1186/2193-1801-3-444
53. Koppelmans V, de Ruiter MB, van der Lijn F, Boogerd W, Seynaeve C, van der Lugt A, et al. Global and Focal Brain Volume in Long-Term Breast Cancer Survivors Exposed to Adjuvant Chemotherapy. *Breast Cancer Res Treat* (2012) 132(3):1099–106. doi: 10.1007/s10549-011-1888-1

Conflict of Interest: The authors declare that the research was conducted in the absence of any commercial or financial relationships that could be construed as a potential conflict of interest.

Publisher's Note: All claims expressed in this article are solely those of the authors and do not necessarily represent those of their affiliated organizations, or those of the publisher, the editors and the reviewers. Any product that may be evaluated in this article, or claim that may be made by its manufacturer, is not guaranteed or endorsed by the publisher.

frontiers in Oncology

ORIGINAL RESEARCH
published: 16 September 2021
doi: 10.3389/fonc.2021.720052

Recurrence Patterns After IMRT/VMAT in Head and Neck Cancer

Heleen Bollen[1,2*†], *Julie van der Veen*[1,2†], *Annouschka Laenen*[3] *and Sandra Nuyts*[1,2]

[1] Laboratory of Experimental Radiotherapy, Department of Oncology, KU Leuven, Leuven, Belgium, [2] Department of Radiation Oncology, Leuven Cancer Institute, University Hospitals Leuven, Leuven, Belgium, [3] Leuven Biostatistics and Statistical Bioinformatics Center, KU Leuven, Leuven, Belgium

Purpose: Intensity-modulated radiotherapy (IMRT) and volumetric modulated arc therapy (VMAT), two advanced modes of high-precision radiotherapy (RT), have become standard of care in the treatment of head and neck cancer. The development in RT techniques has markedly increased the complexity of target volume definition and accurate treatment delivery. The aim of this study was to indirectly investigate the quality of current TV delineation and RT delivery by analyzing the patterns of treatment failure for head and neck cancer patients in our high-volume RT center.

Methods: Between 2004 and 2014, 385 patients with pharyngeal, laryngeal, and oral cavity tumors were curatively treated with primary RT (IMRT/VMAT). We retrospectively investigated locoregional recurrences (LRR), distant metastases (DM), and overall survival (OS).

Results: Median follow-up was 6.4 years (IQR 4.7–8.3 years) during which time 122 patients (31.7%) developed LRR (22.1%) and DM (17.7%). The estimated 2- and 5-year locoregional control was 78.2% (95% CI 73.3, 82.3) and 74.2% (95% CI 69.0, 78.8). One patient developed a local recurrence outside the high-dose volume and five patients developed a regional recurrence outside the high-dose volume. Four patients (1.0%) suffered a recurrence in the electively irradiated neck and two patients had a recurrence outside the electively irradiated neck. No marginal failures were observed. The estimated 2- and 5-year DM-free survival rates were 83.3% (95% CI 78.9, 86.9) and 80.0% (95% CI 75.2, 84.0). The estimated 2- and 5-year OS rates were 73.6% (95% CI 68.9, 77.8) and 52. 6% (95% CI 47.3, 57.6). Median OS was 5.5 years (95% CI 4.5, 6.7).

Conclusion: Target volume definition and treatment delivery were performed accurately, as only few recurrences occurred outside the high-dose regions and no marginal failures were observed. Research on dose intensification and identification of high-risk subvolumes might decrease the risk of locoregional relapses. The results of this study may serve as reference data for comparison with future studies, such as dose escalation or proton therapy trials.

Keywords: radiotherapy, intensity-modulated radiotherapy, volumetric modulated arc therapy, recurrence, head and neck cancer, proton therapy, tumor resistance, delineation

OPEN ACCESS

Edited by:
John Varlotto,
Marshall University, United States

Reviewed by:
Nam Phong Nguyen,
International Geriatric Radiotherapy Group, United States
Michael McKay,
University of Tasmania, Australia

***Correspondence:**
Heleen Bollen
heleen.bollen@uzleuven.be

†These authors have contributed equally to this work and share first authorship

Specialty section:
This article was submitted to Radiation Oncology, a section of the journal Frontiers in Oncology

Received: *03 June 2021*
Accepted: *30 August 2021*
Published: *16 September 2021*

Citation:
Bollen H, van der Veen J, Laenen A and Nuyts S (2021) Recurrence Patterns After IMRT/VMAT in Head and Neck Cancer. Front. Oncol. 11:720052. doi: 10.3389/fonc.2021.720052

INTRODUCTION

Head and neck cancer (HNC) is the seventh most common cancer worldwide and is usually diagnosed in a locally advanced but curable stage (1). As surgical resection can be mutilating, radiation therapy (RT), with or without concurrent chemotherapy, has emerged as the treatment of choice in the management of local and locoregionally advanced HNC (2–4). Intensity-modulated radiotherapy (IMRT) and volumetric modulated arc therapy (VMAT) are two radiation techniques that enable steeper dose gradients, allowing better sparing of the surrounding structures compared with the older 3D techniques, thereby reducing toxicity (5) and improving quality of life (6, 7). The trade-off for these more conformal RT techniques is an increased reliance on precise TV definition and accurate treatment delivery. Tumor tissue that is not defined as target volume (TV) by the radiation oncologist will not receive the prescribed dose, and geographical misses, leading to locoregional recurrences, are a potential risk (8, 9). In addition, several studies have proven experience with more conformal RT techniques to be essential for optimal outcomes in HNC (10–12). IMRT was routinely implemented in University Hospitals Leuven for the definitive treatment of HNC in 2004. Since 2010, VMAT has become the standard of care. In preparation for the implementation of proton therapy in our RT center, we investigated the quality of our current TV delineation and RT delivery by retrospectively analyzing the incidence and location of local recurrence (LR) and regional recurrence (RR) compared with the TVs. Knowledge about treatment failure patterns is especially relevant when implementing more conformal RT techniques, such as proton therapy. In the treatment of HNC, efforts are continuously being made to optimize the therapeutic ratio to improve disease outcome while keeping toxicity to a minimum. By analyzing the patterns of failure in the HNC population, we hope to refine future strategies in TV delineation and dose escalation. Moreover, the results of this study may serve as reference data for comparison with future studies, such as dose escalation or proton therapy trials.

MATERIALS AND METHODS

Patient Selection

In this retrospective analysis, patients treated with curative intent for a HNC with R(C)T between June 2004 and December 2014 were included, to allow a follow-up of at least 3 years. We included patients with primary pharyngeal, oral cavity, and laryngeal squamous cell carcinoma. We excluded patients previously treated with RT in the head and neck region, patients with metastatic disease, postoperative patients or patients who received induction chemotherapy, primary sinonasal or nasopharyngeal tumor patients, and patients who did not finish RT as planned. The medical files were reviewed for each patient. The study was approved by the ethical committee of University Hospitals Leuven/KU Leuven (S59803). All methods were performed in accordance with the relevant guidelines and regulations.

Target Volume Delineation and Treatment Planning

The gross tumor volume (GTV) was defined as the macroscopic tumor volume seen on planning CT and using information from clinical investigation and diagnostic and functional imaging. Patients with locally advanced disease underwent FDG-PET scan as staging exam, and PET scans were used "side-by-side" during the process of contouring with the diagnostic CT and/or MR scan. The clinical target volume of the primary tumor (CTVp) and adenopathies (CTVn) were created with a 3D 10-mm expansion around the GTV and cropped for anatomical boundaries, e.g., uninvolved bone and air. Neck regions at risk of harboring microscopic tumor cells were delineated using international guidelines (13–15) to create the elective CTV (CTVe) which received a lower dose than CTVp and CTVn. To ensure an adequate coverage of CTV, a planning target volume (PTV) was created by expanding CTV by 5 mm. The clinical target volumes of the macroscopically affected tumor sites (CTVp and CTVn) were treated up to a normalized iso-effective dose in 2 Gy fractions (NID2 Gy) of 70 Gy. CTVe was treated up to a NID2 Gy of 50 Gy, except for 19 patients that were included in a dose de-escalation trial and received a lower dose to CTVe up to a NID2 Gy of 40 Gy (16). Concurrent chemotherapy (cisplatin 100 mg/m^2, q3w) was offered to fit patients with advanced stage disease, according to hospital guidelines. Neck dissection post-RT was not routinely performed. Treatment plans were planned using IMRT/VMAT and tumors were classified according the American Joint Committee on Cancer seventh TNM edition (17).

Recurrence Identification and Patient Evaluation

Recurrence and OS rates were measured starting at the start of RT until recurrence or death from any cause. CT or MRI images of the first recurrence (local/regional) were visually inspected and compared with the planning CT. Recurrences were defined as either local (LR), regional (RR), or distant metastases (DM) and further as 1) in CTVp or n, 2) marginal to CTVp or CTVn (overlap but also more than 50% of tumor load outside the original tumor site), 3) outside CTVp or CTVn, 4) outside CTVn but inside CTVe, and (5) outside CTVe. If the primary tumor or adenopathy was still visible on imaging 6 months after the start of treatment, this was classified as persistent disease (PD). Second primary (SP) HNCs were classified as such if the new tumor was more than 2 cm from the index tumor, or if it was less than 2 cm from the index tumor, but developed more than 3 years after RT.

Patients were seen 2 months after the end of therapy for a clinical evaluation which was repeated every 2 months for the first year. A CT or MRI scan was performed 4 months after the end of therapy to evaluate treatment response and once more during the first year of follow-up. Thereafter, imaging was only done in case of clinical suspicion of a recurrence. During the second, third, and fourth year, clinical follow-up was planned every 3, 4, and 6 months, respectively. Thereafter, a yearly review was planned.

Statistical Analysis

The patients were followed up from the date of start of RT to either date of death or the cutoff date April 2018. Locoregional

recurrence rates (LRR) and overall survival (OS) were estimated using the Kaplan–Meier method. The Cox proportional hazards model was used for analyzing the prognostic effect of patient or disease characteristics on oncological outcomes. Results are reported as hazard ratios with 95% confidence intervals. Univariate analysis was performed for several potential prognostic factors: age, sex, smoking status, stage, site, and tumor grade. Follow-up summary statistics were obtained using the Kaplan–Meier estimate of potential follow-up (18). Analyses were performed using SAS software (version 9.4 of the SAS System for Windows).

RESULTS

Patient Characteristics

Patient characteristics of the 385 patients are shown in **Table 1**. Median age was 61 years old (range 34–89 years) and the majority were men (326 *vs.* 59 women). Seventeen patients had a multifocal tumor and two patients had an unknown primary. The primary tumor sites were the oropharynx (46.2%), hypopharynx (23.9%), supraglottis (20.8%), larynx (10.6%), and oral cavity (3.9%). Of the 178 oropharynx tumors, 39 were p16 positive, 42 were p16 negative, and 97 were of unknown

TABLE 1 | Patient characteristics.

Patient characteristics		*n* = 385	%
Gender	Male	326	84.7%
	Female	59	15.3%
Age (years), median (range)		61	(34–89)
	<60	160	41.6%
	60–70	158	41.0%
	>70	67	17.4%
Subsite	Oropharynx	178	46.2%
	Oral cavity	15	3.9%
	Hypopharynx	92	23.9%
	Larynx	41	10.6%
	Supraglottis	80	20.8%
	CUP	2	0.5%
	Multifocal	17	4.4%
	Unifocal	368	95.6%
Grade	1	19	4.9%
	2	106	27.5%
	3	69	17.9%
	Unknown	191	49.6%
T stage	1	31	8.1%
	2	120	31.2%
	3	107	27.8%
	4	125	32.5%
	Unknown	2	0.5%
N stage	0	116	30.1%
	1	34	8.8%
	2	222	57.7%
	3	13	3.4%
Stage	1	13	3.4%
	2	51	13.2%
	3	65	16.9%
	4	256	66.5%
P16 status in oropharyngeal tumors (*n* = 178)	Negative	42	23.6%
	Positive	39	21.9%
	Unknown	97	54.5%
Smoking	Never	38	9.9%
	Former	92	23.9%
	Current	255	66.2%
Ethyl	Never	154	40.0%
	Former	85	22.1%
	Current	146	37.9%
Concomitant systemic therapy	None	132	34.3%
	Chemotherapy	217	56.4%
	EGFR inhibitor	36	9.4%
RT dose, median (range)		72 Gy	(66–75 Gy)
	66 Gy	16	4.2%
	66.1–69.99 Gy	7	1.8%

CUP, cancer of unknown primary; EGFR, epidermal growth factor.

status. Stage IV tumors were most common (66.5%), followed by stage III (16.9%), stage II (13.2%), and stage I (3.4%). More than half of patients were treated with concurrent chemotherapy (56.4%) and 36 were treated with an EGFR inhibitor (9.4%). Three hundred twenty-six patients were treated with accelerated RT (72 Gy in 6 weeks). Twenty-one patients were treated with adaptive RT as part of a trial and 19 patients received a lower dose to CTVe (40 Gy) in a dose de-escalation trial (16).

Survival

The median follow-up period was 6.4 years (IQR 4.7–8.3 years). The estimated 2- and 5-year OS rates were 73.6% (95% CI 68.9, 77.8) and 52.56% (95% CI 47.3, 57.6). Median OS was 5.5 years (95% CI 4.5, 6.7). The type of recurrence had a significant impact on OS; 96 of 237 patients (40.5%) with no recurrence died during follow-up *vs.* 44 of 60 patients (73.3%, RR 1.7, 95% CI 1.4, 2.1) with LRR as first recurrence and 58 of 62 patients (93.5%, RR 2.3, 95% CI 2.0, 2.7) with distant metastases. Regarding the development of a second primary in the head and neck, this had no significant impact on OS (10 of 26 patients died, 38.5%, RR 0.9, 95% CI 0.6–1.6).

Recurrence Patterns

One hundred twenty-two patients suffered a recurrence, of which the LR, RR, and DM distribution is shown in **Figure 1** for first recurrence only. Among the patients with recurrence, the median time to failure was 9.6 months (range 3.3 months to 5.5 years). Fifty-four patients (14.0%) had LR, 49 patients (12.7%) had RR, and 62 patients (16.1%) developed DM as first site of recurrence. The estimated 2- and 5-year locoregional control was 78.2% (95% CI 73.3, 82.3) and 74.2% (95% CI 69.0, 78.8). On univariate analysis, a history of ethyl abuse, a higher tumor stage, and a higher tumor grade were significantly associated with more LRR (**Table 2**). The estimated 2- and 5-year DM-free survival rates were 83.3% (95% CI 78.9, 86.9) and 80.0% (95% CI 75.2, 84.0).

T-Site Failure

There were 53 LRs in the high-dose volume (CTVp), no marginal recurrences, and one isolated LR outside CTVp. The latter concerned a 46-year-old female patient with two synchronous tumors: a T2 retromolar trigone tumor and a T4 tumor in the vallecula (**Figure 2A**) with multiple lymph nodes (N2b). She was treated with accelerated RT to 72 Gy concurrently with cisplatin. Ten months after the start of RT, there was a recurrence in the prelaryngeal space (**Figure 2B**) approximately 1 cm caudal of the primary tumor in the vallecula, for which she underwent a total laryngectomy. Six months later, she developed a new recurrence next to the tracheostoma for which she had re-irradiation (16 × 3.125 Gy). Half a year later, there was again local progression in combination with distant metastases. Palliative chemotherapy was started, but the patient died 6 months later.

N-Site Failure

Of the 49 patients with RRs, 44 had recurrences inside the high-dose volume (CTVn). Four patients developed recurrences in CTVe

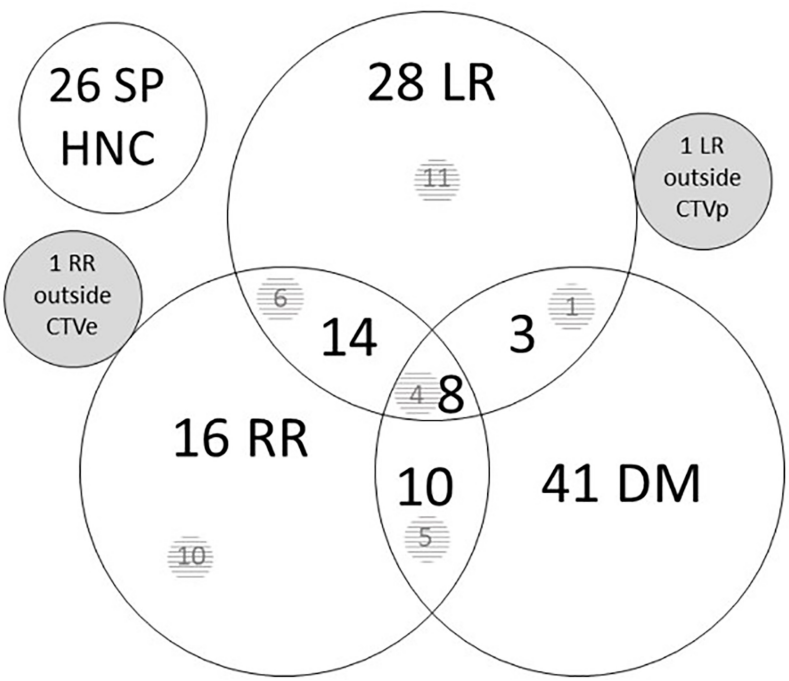

FIGURE 1 | Site of first recurrence. Number of patients with a recurrence in the different sites. Overlapping circles show combination possibilities. There were one isolated local recurrence outside CTVp and one isolated regional recurrence outside CTVe. The numbers in the shaded area represent persistent tumors after the end of treatment, included in the total number of recurrences, e.g., 10 of 16 RR were persistent after treatment. CTVe, elective clinical target volume; DM, distant metastases; HNC, head and neck cancer; LR, local recurrence; RR, regional recurrence; SP, second primary.

TABLE 2 | Univariate analysis for locoregional recurrence.

Variable	Test	Hazard ratio (95% CI)	*P*-value
Sex	Female *vs.* male	0.928 (0.514, 1.675)	0.8039
Age	+1 year	1.010 (0.987, 1.033)	0.3938
Smoking	Global test		0.3281
	Current smoker *vs.* stopped >6 m	1.462 (0.843, 2.536)	0.1764
	Current smoker *vs.* never	1.370 (0.655, 2.863)	0.4029
	Stopped >6 m *vs.* never	0.937 (0.401, 2.189)	0.8805
Ethyl	Global test		0.0064
	Stopped *vs.* yes	2.215 (1.290, 3.801)	0.0039
	Stopped *vs.* none	1.997 (1.195, 3.340)	0.0083
	Yes *vs.* none	0.902 (0.537, 1.513)	0.6956
Grade	+1 level	0.574 (0.369, 0.892)	0.0136
Highest TNM stage[a]	+1 level	1.935 (1.343, 2.788)	0.0004
Oral	Yes *vs.* no	1.888 (0.764, 4.664)	0.1683
Oropharynx	Yes *vs.* no	0.734 (0.475, 1.133)	0.1621
Glottis	Yes *vs.* no	0.939 (0.485, 1.817)	0.8513
Hypopharynx	Yes *vs.* no	1.435 (0.889, 2.316)	0.1396
Supraglottis	Yes *vs.* no	1.428 (0.885, 2.305)	0.1442

Continuous variables: HR > (<) 1 means higher (lower) risk for increasing level. Categorical variables: pairwise tests only presented if significant global P-value. Binary variables/pairwise tests: R > (<) 1 means higher (lower) risk for first category.

CI, confidence interval; m, months; TNM, tumor, node, metastasis stage.

[a]*In case patients had multiple tumors, the tumor with the highest TNM stage was used.*

(1.0%), of which one also had a recurrence outside CTVe in ipsilateral level V 5 years after RT. Recurrence in level II and the retropharyngeal neck level (VIIa) were the most common (level II: one ipsilateral, three contralateral; level VIIa: two ipsilateral, one contralateral). There were two RRs in level Ib (one ipsilateral and one contralateral). One patient had an isolated RR outside the irradiated volume, in the ipsilateral retropharyngeal neck 4 months after RT (**Table 3**). There were no marginal recurrences.

Second Primary HNC

Twenty-six patients developed SP in the head and neck region. In 8 patients, the SP developed less than 2 cm from the index tumor more than 3 years after treatment. In 3 patients, the SP was diagnosed less than 3 years after treatment of the index tumor but was more than 2 cm from the index tumor, and in 15 patients, the SP occurred more than 3 years later and more than 2 cm from the index tumor.

DISCUSSION

Thirty percent of HNC patients will develop a locoregional relapse, while therapy failure due to metastases is less common (19, 20). The prognosis for HNC patients after failure of first-line therapy is poor, with a median overall survival of less than 1 year (21).

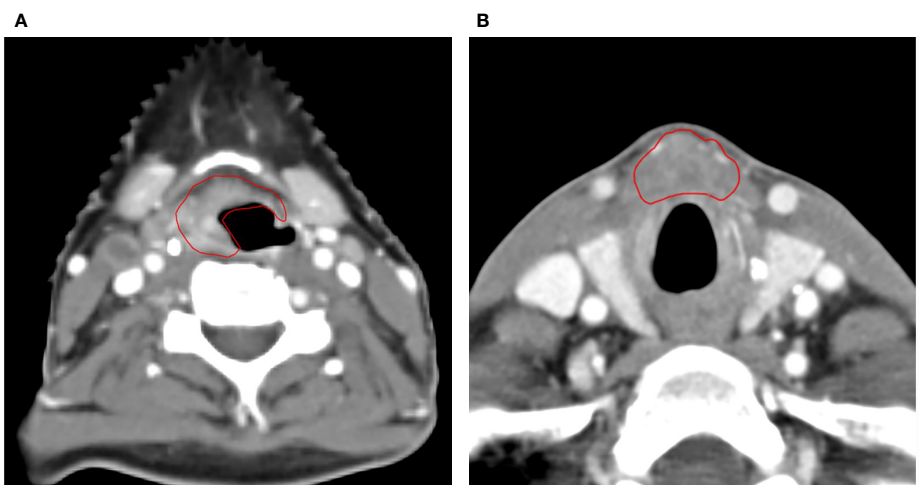

FIGURE 2 | Axial CT scan images of the only patient with a local recurrence outside of the high-dose volume. **(A)** The primary tumor originating in the vallecula and **(B)** CT scan of the local recurrence in the prelaryngeal space, approximately 1 cm caudal of the index tumor.

TABLE 3 | Demographics of patients with regional recurrence outside CTVn.

No.	Sex, age, smoking	Subsite	Stage	Treatment	Failure type	Time to recurrence	Elective levels irradiated	Regional recurrence
1	Male, 46 y, former, multifocal	Piriform sinus (R) Supraglottis (L) Esophagus (mid) Oropharynx (R)	Tis T3N0 T2 Tis	70 Gy (50 Gy) + cisplatin	N+M	5 years and 2 months	Ipsi (R): Ib, II–IVa+b, Vc, VI, VIIa+b; Contra (L): II–IVa+b, Vc, VI, VIIa+b	Ipsi (R): Ib, II, V, VIIa Contra (L): Ib, II, VIIa
2	Male, 63 y, current, multifocal	1. Floor of mouth (L) 2. Tongue (R) 3. Supraglottis 4. Glottis	T2 T2N2b (R) T1 T1	72 Gy (46.4 Gy) + cisplatin	T+N+M	1 year and 6 months	Ipsi (R): Ib, II–IVa, V, VIIb Contra (L): Ib, II–IVa	Contra (L): II–III
3	Male, 67 y, former	Piriform sinus	T3N2b	72 Gy (40 Gy) + cisplatin	N+M	4 months	Ipsi: Ib, II–IVa, V, VIa+b, VIIa+b Contra: II–IVa, VIa+b, VIIa	Contra: II
4	Male, 68 y, current	Piriform sinus	T4aN2b	72 Gy (40 Gy) + cisplatin	T+N	7 months	Ipsi: II–IVa, V, VIIa+b Contra: II–III	Ipsi: VIIa-b
5	Female, 75 y, former	Piriform sinus	T2N2b	72 Gy (40 Gy)	N	4 months	Ipsi: II–IVa, V Contra: II–III	Ipsi: VIIa

Four patients had a recurrence in CTVe, of which one (patient 1) also had a recurrence outside the irradiated volume (ipsilateral level V). One patient had an isolated regional recurrence outside the elective target volume (patient 5, ipsilateral retropharyngeal adenopathy). Dose in brackets shows dose to CTVe. TNM classification according to TNM7.
Contra, contralateral; CTVe, elective clinical target volume; Ipsi, ipsilateral; L, left; N, nodal classification; R, right; T, tumor classification; y, years; M, metastasis.

In order to guide future attempts to improve the therapeutic ratio and outcomes for HNC patients, understanding of the patterns of treatment failure is essential. Particularly with the introduction of IMRT and VMAT, more conformal RT techniques allowing the prescribed radiation dose to be delivered precisely to the TV, concerns about an increased risk for marginal misses were raised. Indeed, the trade-off for these more conformal RT techniques is an increased reliance on precise TV definition and accurate treatment delivery.

The present study reports the patterns of recurrence after RT in 385 HNC patients treated between 2004 and 2014 with IMRT/VMAT at the University Hospitals Leuven. Thirty-one percent of patients suffered a LRR, which corresponds with previously reported recurrence rates in HNC patients treated with definitive radio (chemo)therapy (19, 20). History of ethyl abuse and a higher TNM stage were associated with more LRR. Only one patient developed a LR outside the CTVp. As for RR, five patients suffered a recurrence outside CTVn, of which two recurrences were located outside CTVe. There were no marginal recurrences, either local or regional. Demographics of patients with a RR outside the high-dose volume are summarized in **Table 3**. Of the five regional relapses seen in our patient population, all were originally LAHNSCC and underwent PET-CT scan. The PET scans were reviewed and no missed nodes were identified. In one patient, relapse occurred in ipsilateral level V, more than 5 years after RT. It is important to note that this patient had a multifocal tumor which makes elective level selection more complicated and comes with an increased RR risk. The other patient developed a RR 4 months after the start of RT in ipsilateral level VIIa. This patient suffered from a N2b (levels III and IV) hypopharynx tumor and level VIIa was not included in the CTVe. Looking at the planning CT retrospectively, it is possible that there was a lymph node initially, although it was not withheld on FDG-PET/CT. Several trials reported a higher incidence of LRR in the lower neck (22–24). In our study, no marginal recurrences were observed, which provides reassurance about treatment quality and stresses the importance of guideline adherence for accurate neck level selection (13–15, 25). Nineteen patients were simultaneously included in a dose de-escalation trial, investigating the patterns of regional recurrences in the electively irradiated lymph node regions after dose de-escalation to 40 Gy (EQD2 Gy) (16). The inclusion criteria of this study were previously untreated, histologically proven squamous cell carcinoma of the oral cavity, oropharynx, hypopharynx, or larynx, or cervical lymph node metastases of unknown primary cancer. All macroscopically affected tumor sites (both primary tumor and affected lymph nodes) were treated up to an EQD2 Gy of 70 Gy. All 44 patients that suffered a recurrence inside CTVn were thus treated up to an EDQ2 of 70 Gy. Of the four patients that developed a RR in CTVe, none were included in the de-escalation trial, and thus, all four patients received the standard elective dose, with an EQD2 up to 50 Gy.

The vast majority of relapses, both local and regional, occurred in-field. A number of trials aimed to analyze the patterns of treatment failures after (IM)RT in HNC patients. Gujral and Nutting reviewed the data from 5 prospective randomized controlled trials, 1 prospective phase II trial, and 10 retrospective comparative series (26). Two-year locoregional control rates for IMRT fluctuated between 59% and 98.7%. Only 1 of the 16 studies reported the rates on in-field and out-of-field failures and observed more relapses in the high-dose region (5). Our findings are consistent with existing literature, reporting locoregional failures to predominantly occur in high-dose volumes for both the older 3D (27) and more conformal RT techniques (28–43). Compared with previous studies, our analysis provides a larger patient cohort (22, 23, 27, 31, 32, 39, 43) and longer median follow-up time (22–24, 30–32, 35, 39). Leeman et al. reported the recurrence patterns of a large cohort of 1,000 patients and found neither marginal nor out-of-field failures (29). However, heterogeneity in all reported studies renders

generalization difficult. Firstly, there are differences between patient and treatment cohorts: in terms of primary histology; anatomical sites and stages (8, 19, 28, 29, 33, 34, 36–40); different types of RT intent, i.e., primary curative or adjuvant (8, 28, 34, 38); and different types of intent and uses of chemotherapy (19, 36, 38, 39, 41). Secondly, a number of studies investigate tumor persistence as part of recurrences (19, 28) or do not specify the separation at all (29, 36). The determination of out-of-field failures, defined as failure that occurred outside the treatment field, is fairly straightforward in published reports. The definition of a marginal failure is, however, not as clear-cut (22, 30, 31, 39). In the current study, we defined marginal failure as a situation in which at least one-half of the volume of the recurrence appeared to be outside the original tumor site (CTVp or CTVn) (39). Using this definition, no marginal recurrences were found, providing reassurance that TV delineation, expansion for CTV and PTV, and treatment delivery were performed adequately. By all means, we must exercise caution generalizing our results, since other IMRT series do report the occurrence of marginal failures (8, 22, 24, 27, 31, 39, 43). Furthermore, most published data are coming from single-center cohorts, provided by large-volume centers with significant experience in the treatment of HNC. This should be taken into consideration, since variations in TV delineation and treatment quality are proven to affect LRR rates. Chen et al. evaluated the pattern of RR among 107 patients who presented for consideration of re-irradiation to a large tertiary center. They found 41% of recurrences to be a marginal miss, while 18% appeared to be a true miss (8). The higher incidence of true and marginal misses in this study, compared with previously mentioned reports, could be explained by the fact that patients received their initial treatment in several lower-volume RT departments with less experience with IMRT in the HNC population. Therefore, their results might paint a more realistic picture about the recurrence patterns of HNC patients. Indeed, several studies have found a worse OS among patients treated at low-volume RT centers, with incorrect TV delineation and radiotherapy planning as the main contributors to poor outcome (11, 12). Boero et al. showed that among HNC patients treated with IMRT, for every five additional patients treated per provider per year, the risk of mortality decreased by 21% (10). These findings were backed by the RTOG 0022 study, which noted higher failure rates among patients with major protocol violations in IMRT radiation plans (43). On top of that, several studies have reported a remarkable amount of heterogeneity with respect to TV delineation among RT centers, even when delineation guidelines are available (9, 44–46). The number of marginal or out-of-field recurrences was slightly lower than observed in previous studies, except for the large cohort of MSKCC, a center with a lot of expertise in the treatment of HNC (29). Our definition of marginal failure, which was narrower compared with several other studies (30–32, 38, 39), could also have contributed to the observed results.

Nevertheless, providing accurate guideline adherence, TV definition, and treatment delivery, all reported studies confirm the predominance of in-field recurrences after IMRT. True in-field recurrences likely represent more biologically resistant tumors, which could possibly be explained by, for example, the harboring of an increased proportion of cancer stem cells and/or hypoxic elements (47, 48). Several mechanisms involved in RT response have been described in HNSCC such as hypoxia, the presence of cancer stem cells (CSC), signaling pathways, DNA damage response (DDR), and cell death pathways. It is important to keep in mind that radioresistance cannot be explained by one single mechanism or protein, but rather by an interplay of different mechanisms. Considerable evidence has suggested that tumor hypoxia results in resistance to (C)RT and tumor recurrence (48, 49), setting the stage for dose intensification strategies. A recent review concluded that dose escalation could improve OS without increased toxicity, although follow-up periods were short in small cohorts, which could result in underreporting (50). The authors concluded that functional imaging modalities could help identify the true extent of the tumor and the region that could benefit most from dose escalation, without increased toxicity. In the meantime, results of five randomized controlled trials are awaited, investigating the benefit of RT dose escalation in HNC patients (NCT01212354, NCT03376386, NCT02352792, NCT02031250, NCT03865277). Another interesting track that deserves attention is dose escalation with proton therapy, as its unique characteristics allow better sparing of normal surrounding tissue, and therefore, dose escalation is less restricted by toxicity (NCT03513042).

The strength of the current study is that it concerns a large single-institution study, in which all patients were treated in a relatively uniform manner. This way, the confounder of variation in treatment quality is minimized, which allows for the analysis of the true patterns of recurrence. There was a long follow-up period (median 6.4 years) and a large patient cohort. Our study is limited by its retrospective nature and the heterogeneity of the patient cohort. P16 status of oropharyngeal carcinoma (OPC) was unknown for 97 patients. Differences in tumor stage, tumor subsite, and the use of concomitant systemic treatment could possibly affect the pattern of failure. OPC patients are over-represented in our cohort, which follows the pattern of other large patient cohorts and is likely due to the increasing incidence of OPC. The current study is underpowered for a subgroup analysis. However, our results show a trend toward more LRR for hypopharyngeal, supraglottic, and oral cavity tumors (**Table 2**), which corresponds with the results of Leeman et al. (29). The subsites were not matched for varying stages of disease, which may affect differences in the observed outcomes. However, these variations may also more accurately reflect the clinical presentation that we deal with on a daily basis. All tumor stages [I–IV; classified according to the American Joint Committee on Cancer seventh TNM edition (17)] were included, which could affect the patterns of failure and increase the heterogeneity of the treatment. However, the primary aim of our study was to investigate the quality of current target volume delineation by analyzing the pattern of treatment failure. Since we do not adapt our CTV and PTV margins according to disease stage, we do not expect a significant impact of tumor stage on the recurrence pattern when assessing the accuracy of our GTV and CTV delineation. Another pitfall of the current study may be the

cutoff period of 3 years or the cutoff distance of more than 2 cm from the index tumor, to differentiate between a LR and SP. However, this definition was based on several previous publications (30, 51).

CONCLUSION

This large-institution study adds to the evidence of predominant treatment failure inside high-dose radiotherapy volumes, indicating that recurrences are mainly caused by tumor resistance. Our findings reinforce the need to focus on dose intensification and identification of high-risk subvolumes. No marginal recurrences were observed, providing reassurance about accurate TV delineation and the quality of treatment delivery. Caution must be exercised when generalizing these results, since experience with more conformal RT techniques seems a key prerequisite for favorable outcomes in the treatment of HNC patients.

DATA AVAILABILITY STATEMENT

The raw data supporting the conclusions of this article will be made available by the authors, without undue reservation.

ETHICS STATEMENT

The studies involving human participants were reviewed and approved by the Ethics Committee Research UZ/KU Leuven. Written informed consent for participation was not required for this study in accordance with the national legislation and the institutional requirements. Written informed consent was obtained from the individual(s) for the publication of any potentially identifiable images or data included in this article.

AUTHOR CONTRIBUTIONS

Conceptualization: JV and SN. Data curation: JV. Formal analysis: AL. Investigation: JV. Methodology: JV. Supervision: SN. Writing—original draft: JV and HB. Writing—review and editing: HB and SN. All authors contributed to the article and approved the submitted version.

FUNDING

SN is appointed as Senior Clinical Investigator by FWO—Research Foundation Flanders.

REFERENCES

1. Fitzmaurice C, Allen C, Barber RM, Barregard L, Bhutta ZA, Brenner H, et al. Global, Regional, and National Cancer Incidence, Mortality, Years of Life Lost, Years Lived With Disability, and Disability-Adjusted Life-Years for 32 Cancer Groups, 1990 to 2015. *JAMA Oncol* (2017) 3:524–48. doi: 10.1001/jamaoncol.2016.5688
2. Pignon J-P, Maître A, Maillard E, Bourhis J. Meta-Analysis of Chemotherapy in Head and Neck Cancer (MACH-NC): An Update on 93 Randomised Trials and 17,346 Patients. *Radiother Oncol* (2009) 92(1):4–14. doi: 10.1016/j.radonc.2009.04.014
3. Bourhis J, Overgaard J, Audry H, Ang KK, Saunders M, Bernier J, et al. Hyperfractionated or Accelerated Radiotherapy in Head and Neck Cancer: A Meta-Analysis. *Lancet* (2006) 368(9538):843–54. doi: 10.1016/S0140-6736(06)69121-6
4. Nuyts S, Dirix P, Clement PMJ, Vander Poorten V, Delaere P, Schoenaers J, et al. Impact of Adding Concomitant Chemotherapy to Hyperfractionated Accelerated Radiotherapy for Advanced Head-And-Neck Squamous Cell Carcinoma. *Int J Radiat Oncol* (2009) 73(4):1088–95. doi: 10.1016/j.ijrobp.2008.05.042
5. Nutting CM, Morden JP, Harrington KJ, Urbano TG, Bhide SA, Clark C, et al. Parotid-Sparing Intensity Modulated *Versus* Conventional Radiotherapy in Head and Neck Cancer (PARSPORT): A Phase 3 Multicenter Randomised Controlled Trial. *Lancet Oncol* (2011) 12(2):127–36. doi: 10.1016/S1470-2045(10)70290-4
6. Nutting CM, Morden JP, Beasley M, Bhide S, Cook A, De Winton E, et al. Results of a Multicenter Randomised Controlled Trial of Cochlear-Sparing Intensity-Modulated Radiotherapy *Versus* Conventional Radiotherapy in Patients With Parotid Cancer (COSTAR; CRUK/08/004). *Eur J Cancer* (2018) 103:249–58. doi: 10.1016/j.ejca.2018.08.006
7. Rathod S, Gupta T, Ghosh-Laskar S, Murthy V, Budrukkar A, Agarwal J. Quality-Of-Life (QOL) Outcomes in Patients With Head and Neck Squamous Cell Carcinoma (HNSCC) Treated With Intensity-Modulated Radiation Therapy (IMRT) Compared to Three-Dimensional Conformal Radiotherapy (3D-CRT): Evidence From a Prospective Randomized Study. *Oral Oncol* (2013) 49(6):634–42. doi: 10.1016/j.oraloncology.2013.02.013
8. Chen AM, Chin R, Beron P, Yoshizaki T, Mikaeilian AG, Cao M. Inadequate Target Volume Delineation and Local-Regional Recurrence After Intensity-Modulated Radiotherapy for Human Papillomavirus-Positive Oropharynx Cancer. *Radiother Oncol* (2017) 123(3):412–8. doi: 10.1016/j.radonc.2017.04.015
9. Hong TS, Tomé WA, Harari PM. Heterogeneity in Head and Neck IMRT Target Design and Clinical Practice. *Radiother Oncol* (2012) 103(1):92–8. doi: 10.1016/j.radonc.2012.02.010
10. Boero IJ, Paravati AJ, Xu B, Cohen EE, Mell LK, Le QT, et al. Importance of Radiation Oncologist Experience Among Patients With Head-And-Neck Cancer Treated With Intensity-Modulated Radiation Therapy. *J Clin Oncol* (2016) 34(7):684–90. doi: 10.1200/JCO.2015.63.9898
11. Peters LJ, O'Sullivan B, Giralt J, Fitzgerald TJ, Trotti A, Bernier J, et al. Critical Impact of Radiotherapy Protocol Compliance and Quality in the Treatment of Advanced Head and Neck Cancer: Results From TROG 02.02. *J Clin Oncol* (2010) 28(18):2996–3001. doi: 10.1200/JCO.2009.27.4498
12. Wuthrick EJ, Zhang Q, Machtay M, Rosenthal DI, Nguyen-Tan PF, Fortin A, et al. Institutional Clinical Trial Accrual Volume and Survival of Patients With Head and Neck Cancer. *J Clin Oncol* (2015) 33(2):156–64. doi: 10.1200/JCO.2014.56.5218
13. Grégoire V, Levendag P, Ang KK, Bernier J, Braaksma M, Budach V, et al. CT-Based Delineation of Lymph Node Levels and Related CTVs in the Node-Negative Neck: DAHANCA, EORTC, GORTEC, NCIC,RTOG Consensus Guidelines. *Radiother Oncol* (2003) 69(3):227–36. doi: 10.1016/j.radonc.2003.09.011
14. Grégoire V, Eisbruch A, Hamoir M, Levendag P. Proposal for the Delineation of the Nodal CTV in the Node-Positive and the Post-Operative Neck. *Radiother Oncol* (2006) 79(1):15–20. doi: 10.1016/j.radonc.2006.03.009
15. Grégoire V, Coche E, Cosnard G, Hamoir M, Reychler H. Selection and Delineation of Lymph Node Target Volumes in Head and Neck Conformal Radiotherapy. Proposal for Standardizing Terminology and Procedure Based on the Surgical Experience. *Radiother Oncol* (2000) 56(2):135–50. doi: 10.1016/s0167-8140(00)00202-4

16. Nuyts S, Lambrecht M, Duprez F, Daisne JF, Van Gestel D, Van den Weyngaert D, et al. Reduction of the Dose to the Elective Neck in Head and Neck Squamous Cell Carcinoma, a Randomized Clinical Trial Using Intensity Modulated Radiotherapy (IMRT). Dosimetrical Analysis and Effect on Acute Toxicity. *Radiother Oncol* (2013) 109:323–9. doi: 10.1016/j.radonc.2013.06.044
17. Edge SB, Compton CC. The American Joint Committee on Cancer: The 7th Edition of the AJCC Cancer Staging Manual and the Future of TNM. *Ann Surg Oncol* (2010) 17(6):1471–4. doi: 10.1245/s10434-010-0985-4
18. Schemper M, Smith TL. A Note on Quantifying Follow-Up in Studies of Failure Time. *Control Clin Trials* (1996) 17(4):343–6. doi: 10.1016/0197-2456(96)00075-x
19. Bayman E, Prestwich RJD, Speight R, Aspin L, Garratt L, Wilson S, et al. Patterns of Failure After Intensity-Modulated Radiotherapy in Head and Neck Squamous Cell Carcinoma Using Compartmental Clinical Target Volume Delineation. *Clin Oncol* (2014) 26(10):636–42. doi: 10.1016/j.clon.2014.05.001
20. Nuyts S, Dirix P, Clement PM, Vander Poorten V, Delaere P, Schoenaers J, et al. Impact of Adding Concomitant Chemotherapy to Hyperfractionated Accelerated Radiotherapy for Advanced Head-and-Neck Squamous Cell Carcinoma. *Int J Radiat Oncol Biol Phys* (2009) 73(4):1088–95. doi: 10.1016/j.ijrobp.2008.05.042
21. Vermorken JB, Mesia R, Rivera F, Remenar E, Kawecki A, Rottey S, et al. Platinum-Based Chemotherapy Plus Cetuximab in Head and Neck Cancer. *N Engl J Med* (2008) 359(11):1116–27. doi: 10.1056/NEJMoa0802656
22. Chao KS, Ozyigit G, Tran BN, Cengiz M, Dempsey JF, Low DA. Patterns of Failure in Patients Receiving Definitive and Postoperative IMRT for Head-and-Neck Cancer. *Int J Radiat Oncol Biol Phys* (2003) 55(2):312–21. doi: 10.1016/s0360-3016(02)03940-8
23. Daly ME, Le QT, Maxim PG, Loo BWJr, Kaplan MJ, Fischbein NJ, et al. Intensity-Modulated Radiotherapy in the Treatment of Oropharyngeal Cancer: Clinical Outcomes and Patterns of Failure. *Int J Radiat Oncol Biol Phys* (2010) 76(5):1339–46. doi: 10.1016/j.ijrobp.2009.04.006
24. Thorstad S, Hong A, Hope J, Lindsay PE, Haughey B, Deasey O, et al. Patterns of Failure in Patients Receiving Intensity Modulated Radiation Therapy (IMRT) for Head and Neck Cancer. *Int J Radiat Oncol Biol Phys* (2005) 63:S74. doi: 10.1016/j.ijrobp.2005.07.127
25. Biau J, Lapeyre M, Troussier I, Budach W, Giralt J, Grau C, et al. Selection of Lymph Node Target Volumes for Definitive Head and Neck Radiation Therapy: A 2019 Update. *Radiother Oncol* (2019) 134:1–9. doi: 10.1016/j.radonc.2019.01.018
26. Gujral DM, Nutting CM. Patterns of Failure, Treatment Outcomes and Late Toxicities of Head and Neck Cancer in the Current Era of IMRT. *Oral Oncol* (2018) 86:225–33. doi: 10.1016/j.oraloncology.2018.09.011
27. Oksuz DC, Prestwich RJ, Carey B, Wilson S, Senocak MS, Choudhury A, et al. Recurrence Patterns of Locally Advanced Head and Neck Squamous Cell Carcinoma After 3D Conformal (Chemo)-Radiotherapy. *Radiat Oncol* (2011) 6:54. doi: 10.1186/1748-717X-6-54
28. De Felice F, Thomas C, Barrington S, Pathmanathan A, Lei M, Urbano TG. Analysis of Loco-Regional Failures in Head and Neck Cancer After Radical Radiation Therapy. *Oral Oncol* (2015) 51(11):1051–5. doi: 10.1016/j.oraloncology.2015.08.004
29. Leeman JE, Li JG, Pei X, Venigalla P, Zumsteg ZS, Katsoulakis E, et al. Patterns of Treatment Failure and Postrecurrence Outcomes Among Patients With Locally Advanced Head and Neck Squamous Cell Carcinoma After Chemoradiotherapy Using Modern Radiation Techniques. *JAMA Oncol* (2017) 3(11):1487–94. doi: 10.1001/jamaoncol.2017.0973
30. Zukauskaite R, Hansen CR, Brink C, Johansen J, Asmussen JT, Grau C, et al. Analysis of CT-Verified Loco-Regional Recurrences After Definitive IMRT for HNSCC Using Site of Origin Estimation Methods. *Acta Oncol* (2017) 56(11):1554–61. doi: 10.1080/0284186X.2017.1346384
31. Dawson LA, Anzai Y, Marsh L, Martel MK, Paulino A, Ship JA, et al. Patterns of Local-Regional Recurrence Following Parotid-Sparing Conformal and Segmental Intensity-Modulated Radiotherapy for Head and Neck Cancer. *Int J Radiat Oncol Biol Phys* (2000) 46(5):1117–26. doi: 10.1016/s0360-3016(99)00550-7
32. Shakam A, Scrimger R, Liu D, Mohamed M, Parliament M, Field GC, et al. Dose-Volume Analysis of Locoregional Recurrences in Head and Neck IMRT, as Determined by Deformable Registration: A Prospective Multi-Institutional Trial. *Radiother Oncol* (2011) 99(2):101–7. doi: 10.1016/j.radonc.2011.05.008
33. Caudell JJ, Meredith RF, Spencer SA, Keene KS, Dobelbower MC, Bonner JA. Margin on Gross Tumor Volume and Risk of Local Recurrence in Head-and-Neck Cancer. *Int J Radiat Oncol Biol Phys* (2010) 76(1):164–8. doi: 10.1016/j.ijrobp.2009.01.037
34. Ferreira BC, Marques RV, Khouri L, Santos T, Sá-Couto P, do Carmo Lopes M. Assessment and Topographic Characterization of Locoregional Recurrences in Head and Neck Tumors. *Radiat Oncol* (2015) 10:41. doi: 10.1186/s13014-015-0345-4
35. Due AK, Vogelius IR, Aznar MC, Bentzen SM, Berthelsen AK, Korreman SS, et al. Recurrences After Intensity Modulated Radiotherapy for Head and Neck Squamous Cell Carcinoma More Likely to Originate From Regions With High Baseline [18F]-FDG Uptake. *Radiother Oncol* (2014) 111(3):360–5. doi: 10.1016/j.radonc.2014.06.001
36. van den Bosch S, Dijkema T, Verhoef LC, Zwijnenburg EM, Janssens GO, Kaanders JH. Patterns of Recurrence in Electively Irradiated Lymph Node Regions After Definitive Accelerated Intensity Modulated Radiation Therapy for Head and Neck Squamous Cell Carcinoma. *Int J Radiat Oncol Biol Phys* (2016) 94(4):766–74. doi: 10.1016/j.ijrobp.2015.12.002
37. Dandekar V, Morgan T, Turian J, Fidler MJ, Showel J, Nielsen T, et al. Patterns-Of-Failure After Helical Tomotherapy-Based Chemoradiotherapy for Head and Neck Cancer: Implications for CTV Margin, Elective Nodal Dose and Bilateral Parotid Sparing. *Oral Oncol* (2014) 50(5):520–6. doi: 10.1016/j.oraloncology.2014.02.009
38. Nevens D, Duprez F, Daisne JF, Schatteman J, van der Vorst A, De Neve W, et al. Recurrence Patterns After a Decreased Dose of 40Gy to the Elective Treated Neck in Head and Neck Cancer. *Radiother Oncol* (2017) 123(3):419–23. doi: 10.1016/j.radonc.2017.03.003
39. Schoenfeld GO, Amdur RJ, Morris CG, Li JG, Hinerman RW, Mendenhall WM. Patterns of Failure and Toxicity After Intensity-Modulated Radiotherapy for Head and Neck Cancer. *Int J Radiat Oncol Biol Phys* (2008) 71(2):377–85. doi: 10.1016/j.ijrobp.2007.10.010
40. Studer G, Luetolf UM, Glanzmann C. Locoregional Failure Analysis in Head-and-Neck Cancer Patients Treated With IMRT. *Strahlenther Onkol* (2007) 183(8):417–23. doi: 10.1007/s00066-007-1663-8
41. Garden AS, Dong L, Morrison WH, Stugis EM, Glisson BS, Frank SJ, et al. Patterns of Disease Recurrence Following Treatment of Oropharyngeal Cancer With Intensity Modulated Radiation Therapy. *Int J Radiat Oncol Biol Phys* (2013) 85(4):941–7. doi: 10.1016/j.ijrobp.2012.08.004
42. Kjems J, Gothelf AB, Hakansson K, Specht L, Kristensen CA, Friborg J. Elective Nodal Irradiation and Patterns of Failure in Head and Neck Cancer After Primary Radiation Therapy. *Int J Radiat Oncol Biol Phys* (2016) 94(4):775–82. doi: 10.1016/j.ijrobp.2015.12.380
43. Eisbruch A, Harris J, Garden AS, Chao CK, Straube W, Harari PM, et al. Multi-Institutional Trial of Accelerated Hypofractionated Intensity-Modulated Radiation Therapy for Early-Stage Oropharyngeal Cancer (RTOG 00-22). *Int J Radiat Oncol Biol Phys* (2010) 76(5):1333–8. doi: 10.1016/j.ijrobp.2009.04.011
44. van der Veen J, Gulyban A, Nuyts S. Interobserver Variability in Delineation of Target Volumes in Head and Neck Cancer. *Radiother Oncol* (2019) 137:9–15. doi: 10.1016/j.radonc.2019.04.006
45. Pettit L, Hartley A, Bowden SJ, Mehanna H, Glaholm J, Cashmore J, et al. Variation in Volume Definition Between UK Head and Neck Oncologists Treating Oropharyngeal Carcinoma. *Clin Oncol* (2011) 23:654–5. doi: 10.1016/j.clon.2011.07.006
46. Hansen CR, Johansen J, Samsøe E, Andersen E, Petersen JBB, Jensen K, et al. Consequences of Introducing Geometric GTV to CTV Margin Expansion in DAHANCA Contouring Guidelines for Head and Neck Radiotherapy. *Radiother Oncol* (2018) 126:43–7. doi: 10.1016/j.radonc.2017.09.019
47. Hanns E, Job S, Coliat P, Wasylyk C, Ramolu L, Pencreach E, et al. Human Papillomavirus-Related Tumors of the Oropharynx Display a Lower Tumor Hypoxia Signature. *Oral Oncol* (2015) 51:848–56. doi: 10.1016/j.oraloncology.2015.06.003
48. Vlashi E, Chen AM, Boyrie S, Yu G, Nguyen A, Brower PA, et al. Radiation-Induced Dedifferentiation of Head and Neck Cancer Cells Into Cancer Stem Cells Depends on Human Papillomavirus Status. *Int J Radiat Oncol Biol Phys* (2016) 94(5):1198–206. doi: 10.1016/j.ijrobp.2016.01.005

49. Hall EJ. The Oxygen Effects and Re-Oxygenation. In: *Radiobiology for the Radiologist*. Lippincott Williams & Wilkins (1994). p. 133–52.
50. Atwell D, Elks J, Cahill K, Hearn N, Vignarajah D, Lagopoulos J, et al. A Review of Modern Radiation Therapy Dose Escalation in Locally Advanced Head and Neck Cancer. *Clin Oncol* (2020) 32(5):330–41. doi: 10.1016/j.clon.2019.12.004
51. Schwartz LH, Ozsahin M, Zhang GN, Touboul E, De Vataire F, Andolenko P, et al. Synchronous and Metachronous Head and Neck Carcinomas. *Cancer* (1994) 74(7):1933–8. doi: 10.1002/1097-0142(19941001)74:7<1933::aid-cncr2820740718>3.0.co;2-x

Conflict of Interest: The authors declare that the research was conducted in the absence of any commercial or financial relationships that could be construed as a potential conflict of interest.

frontiers in Oncology

ORIGINAL RESEARCH
published: 17 September 2021
doi: 10.3389/fonc.2021.722852

Bleeding Risk Following Stereotactic Body Radiation Therapy for Localized Prostate Cancer in Men on Baseline Anticoagulant or Antiplatelet Therapy

*Abigail Pepin[1], Sarthak Shah[1], Monica Pernia[1], Siyuan Lei[2], Marilyn Ayoob[2], Malika Danner[2], Thomas Yung[2], Brian T. Collins[2], Simeng Suy[2], Nima Aghdam[3] and Sean P. Collins[2]**

[1] George Washington University School of Medicine and Health Sciences, Washington, DC, United States, [2] Department of Radiation Medicine, Georgetown University Hospital, Washington, DC, United States, [3] Department of Radiation Medicine, Harvard, Boston, MA, United States

OPEN ACCESS

Edited by:
Susanne Rogers,
Aarau Cantonal Hospital, Switzerland

Reviewed by:
Silvia Gomez,
Aarau Cantonal Hospital, Switzerland
Debra Freeman,
GenesisCare, United States

***Correspondence:**
Sean P. Collins
SPC9@gunet.georgetown.edu

Specialty section:
This article was submitted to Radiation Oncology, a section of the journal Frontiers in Oncology

Received: 09 June 2021
Accepted: 09 August 2021
Published: 17 September 2021

Citation:
Pepin A, Shah S, Pernia M, Lei S, Ayoob M, Danner M, Yung T, Collins BT, Suy S, Aghdam N and Collins SP (2021) Bleeding Risk Following Stereotactic Body Radiation Therapy for Localized Prostate Cancer in Men on Baseline Anticoagulant or Antiplatelet Therapy. Front. Oncol. 11:722852. doi: 10.3389/fonc.2021.722852

Purpose: Patients on anticoagulant/antiplatelet medications are at a high risk of bleeding following external beam radiation therapy for localized prostate cancer. SBRT may reduce the bleeding risk by decreasing the volume of bladder/rectum receiving high doses. This retrospective study sought to evaluate the rates of hematuria and hematochezia following SBRT in these patients.

Methods: Localized prostate cancer patients treated with SBRT from 2007 to 2017 on at least one anticoagulant/antiplatelet at baseline were included. The minimum follow-up was 3 years with a median follow-up of 72 months. Patients who had a rectal spacer placed prior to SBRT were excluded. Radiotherapy was delivered in 5 fractions to a dose of 35 Gy or 36.25 Gy utilizing the CyberKnife system. Hematuria and hematochezia were prospectively assessed before and after treatment using the Expanded Prostate Cancer Index Composite (EPIC-26). Toxicities were scored using the CTCAE v4. Cystoscopy and colonoscopy findings were retrospectively reviewed.

Results: Forty-four men with a median age of 72 years with a history of taking at least one anticoagulant and/or antiplatelet medication received SBRT. Warfarin (46%), clopidogrel (34%) and rivaroxaban (9%) were the most common medications. Overall, 18.2% experienced hematuria with a median time of 10.5 months post-SBRT. Altogether, 38.6% experienced hematochezia with a median time of 6 months post-SBRT. ≥ Grade 2 hematuria and hematochezia occurred in 4.6% and 2.5%, respectively. One patient required bladder neck fulguration and one patient underwent rectal cauterization for multiple non-confluent telangiectasia. There were no grade 4 or 5 toxicities. Cystoscopy revealed bladder cancer (40%) and benign prostatic bleeding (40%) as the most common hematuria etiology. Colonoscopy demonstrated hemorrhoids (54.5%) and radiation proctitis (9.1%) as the main causes of hematochezia. There was no significant change from the mean baseline EPIC-26 hematuria and hematochezia scores at any point during follow up.

Conclusion: In patients with baseline anticoagulant usage, moderate dose prostate SBRT was well tolerated without rectal spacing. High grade bleeding toxicities were uncommon and resolved with time. Baseline anticoagulation usage should not be considered a contraindication to prostate SBRT.

Keywords: stereotactic body radiation therapy, anticoagulation, antiplatelet, bleeding risk, prostate cancer

INTRODUCTION

Post-treatment quality of life remains an important consideration when selecting prostate cancer treatment. Post-treatment bleeding including hematochezia and hematuria are known bothersome late side effects of radiation therapy (1). The incidence of grade 2 or worse gross hematuria after conventionally fractionated external beam radiation therapy (EBRT) is estimated to be <5% (2). Some studies report post-treatment proctitis including rectal bother and bleeding to occur in 5-20% of patients after undergoing conventionally fractionated treatment (3). A number of factors can influence a patient's individual risk of developing radiation-induced genitourinary (GU) and gastrointestinal (GI) bleeds including age, co-morbidities, history of symptomatic hemorrhoids, treatment technique and/or anticoagulation.

Anticoagulation is utilized to prevent clotting in patients with a range of cardiovascular diseases including atrial fibrillation, venous thromboembolism, ischemic heart disease and valvular disease (4). Similar to prostate cancer, these diseases are prevalent in the elderly population and the incidence is increasing. Bleeding is a common risk of anticoagulation, and radiation therapy may increase the risk (4). Risk factors for anticoagulant-induced bleeding include older age, race, obesity, comorbidities and utilization of combination therapy (4).

Prostate radiation therapy (RT) may increase this risk of clinically significant bleeding in men on anticoagulation (1, 5). Endoscopic findings associated with proctopathy or cystopathy can include telangiectasias, congested mucosa, or ulcers (6). Post-RT bleeding is secondary to chronic radiation-induced vascular ectasias which are characterized by friability and increased permeability (7). Anticoagulation, by disrupting normal hemostasis, may convert mild ectasias' bleeding into clinically significant bleeding (8). Patients on anticoagulants had a high rate of bleeding from external beam radiation therapy when compared to patients that were not on anticoagulants (1). The absolute risk of hematuria or hematochezia was 39% (1). Hematochezia was more common than hematuria. The 4-year actuarial risk of Grade 3 or worse bleeding toxicity was 15.5% (1). In many cases, the bleeding did not fully resolve even with surgical intervention (1). Higher radiation dose was associated with an increased risk of Grade 2 or worse bleeding (1). Choe et al. identified dose volume histogram (DVH) guidelines including rectal V_{50} <50% and V_{70} <10% to be below the threshold for which Grade 3 bleeding events occurred (1).

The use of stereotactic body radiation therapy (SBRT) in the treatment of localized prostate cancer has been determined to be safe and efficacious in several ongoing multi-institutional trials (9, 10). The impact of baseline anticoagulation use during and following SBRT for prostate cancer on gastrointestinal and genitourinary bleeds remains unknown to date. In this report, we sought to report on the impact of baseline anticoagulation and/or antiplatelet usage on the risk of bleeding following SBRT.

METHODS

Patient Selection

The Georgetown University Institutional Review Board approved this single institution review (IRB#2009-510). All individuals who underwent SBRT for treatment of their localized prostate cancer at MedStar Georgetown University Hospital from 2007 to 2017 were eligible for inclusion if they were on anticoagulation at time of initial consultation. Anticoagulants included oral anticoagulants and antiplatelet medications. Patients on low dose aspirin were excluded. Patients were required to have a minimum of three years of follow up to be included.

SBRT Treatment Planning and Delivery

Simulation, contouring, and treatment planning were performed using our institutional protocol (11). Patients underwent a treatment planning CT and pelvic MRI at least one week after placement of 4 to 6 gold fiducial markers in the prostate. The clinical target volume (CTV) included the prostate and proximal seminal vesicles. The planning target volume (PTV) was expanded 3 mm posteriorly and 5 mm in all other directions from the CTV. The bladder and rectum were contoured structures that were evaluated on dose-volume histogram analysis during treatment planning using Multiplan (Accuray Inc, Sunnyvale, CA) inverse treatment planning. Five fractions of 7-7.25 Gy were delivered to the PTV over one to two weeks.

The bladder volume receiving 37 Gy was limited to ≤ 5 cc and the rectal volume receiving 36 Gy was limited to ≤ 1 cc. Additional bladder dose constraints included volume less than 40% receiving 50% of prescribed dose and volume less than 10% receiving less than 100% of the prescribed dose. For the rectum, secondary dose constraints included volume less than 40% receiving 50% of prescribed dose, volume less than 25% receiving 75% of prescribed dose, volume less than 20% receiving 80% of the dose, volume less than 10% receiving 90% of the dose, and volume less than 5% receiving 100% of prescription dose.

Follow-Up and Statistical Analysis

Toxicities were assessed during follow up visits at one-month post treatment, every three months for the first year, every 6 months in the second year, then yearly and scored using the common terminology criteria for adverse events (CTCAE) v4.

Acute bleeding was defined as experiencing toxicity within 6 months of radiation therapy. Late bleeding was defined as occurring at least 6 months after delivery of radiation therapy. Grade 1 represents minimal bleeding not requiring medications. Grade 2 indicates bleeding requiring new medication or minor rectal laser coagulation. Grade 3 toxicity indicates severe bleeding that required surgical intervention. Cystoscopy and colonoscopy were recommended for the initial evaluation of bleeding and were reviewed for this study. Rectal Telangiectasia were graded using the Vienna Rectoscopy Score (VRS): Grade 1 (a single telangiectasia), Grade 2 (multiple non-confluent telangiectasia) and Grade 3 (multiple confluent telangiectasia).

Cross-sectional assessment of quality of life using Expanded Prostate Cancer Index Composite (EPIC-26) questionnaires were assessed on the first day of treatment and during the follow up visits at one-month post treatment, every 3 months during the first year post-SBRT, every 6 months after the second year, and then yearly. The patient scores for EPIC-26 questions related to hematochezia and hematuria were determined using a weighted average. Minimally important differences were computed by obtaining half the standard deviation at baseline.

RESULTS

Forty-four patients on baseline anticoagulation were treated with SBRT for their localized prostate cancer between 2006 and 2017. The median follow-up of 72 months. Patient characteristics are listed in **Table 1**. The patients were ethnically diverse with a median age of 71.5 years (range 57-84 years). Comorbidities were common (Carlson Comorbidity Index ≥ 1 in 66%). Our cohort included a diverse variety of BMI statuses including 32% of patients who were obese (BMI > 30). One patient had a prior transurethral resection of the prostate (TURP). Warfarin (46%), clopidogrel (34%) and rivaroxaban (9%) were the most common medications. Other anticoagulant and antiplatelet agents used included enoxaparin, apixaban, dabigatran, aspirin, and Aggrenox. Two patients were on combination therapy (4.5%). The most common indication for anticoagulation was atrial fibrillation (25%). Other indications included a history of coronary artery disease (CAD), cerebrovascular accident/transient ischemic attack (CVA/TIA), deep venous thrombosis (DVT), heart valve deformity. Eighteen percent of individuals had multiple indications for anticoagulation. Per the D'Amico Risk Classification, 9 patients were low risk, 28 were intermediate risk, and 7 patients were high risk. Five patients received androgen deprivation therapy (ADT). Sixty eight percent of the patients were treated with 36.25 Gy in five fractions.

Patients experienced both acute and late bleeding events (**Table 2**). In the acute setting, 22.7% of patients experienced an acute Grade 1 bleed, of which the majority (80%) were secondary to rectal bleeding. There were no Grade 2 bleeding events. One individual experienced an acute Grade 3 bleed. This patient experienced hematochezia at 6 months requiring cauterization. In the late setting, 27.3% of patients experienced late Grade 1 bleeding events. One individual experienced a late grade 2 hematuria event, and one individual experienced a late grade 3 hematuria event requiring fulguration.

TABLE 1 | Patient characteristics and treatment.

	Percent of Patients (n = 44)
Age (years): Median 71.5 (57-84)	
50-59	6.8% (3)
60-69	29.5% (13)
70-79	47.7% (21)
>80	15.9% (7)
Race	
White	52.3% (23)
Black	45.5% (20)
Other	2.3% (1)
BMI	
18.5-24.9	34.1% (15)
25.0-29.9	34.1% (15)
>30.0	31.8% (14)
Prior urologic procedure	
Yes	2.3% (1)
No	97.7% (43)
Charlson Comorbidity Index	
0	34.1% (15)
1-2	59.1% (26)
>2	6.8% (3)
Anticoagulation/antiplatelet	
Warfarin	45.5% (20)
Clopidogrel	34.1% (15)
Rivaroxaban	9.1% (4)
Enoxaparin	2.3% (1)
Other	4.6% (2)
Combination	4.5% (2)
T stage	
T1c-T2a	81.8% (36)
T2b-T2c	18.2% (8)
Gleason Score	
6	31.8% (14)
7	59.1% (26)
8-9	9.1% (4)
Risk group (D'Amico)	
Low	20.5% (9)
Intermediate	63.6% (28)
High	15.9% (7)
Hormone Therapy	
Yes	11.4%
No	88.6%
SBRT dose	
35	31.8% (14)
36.25	68.2% (30)

TABLE 2 | Cumulative incidence of acute and late CTC-graded hematuria and hematochezia.

	None	Grade 1	Grade 2	Grade 3
ACUTE				
Hematuria	42	2	0	0
Hematochezia	35	8	0	1
Overall	33 (75.0%)	10 (22.7%)	0 (0%)	1 (2.3%)
LATE				
Hematuria	38	4	1	1
Hematochezia	33	11	0	0
Overall	30 (68.2%)	12 (27.3%)	1 (2.3%)	1 (2.3%)

Six patients had cystoscopies. The findings can be found in **Table 3**. Two individuals were found to have bladder cancer. One individual was found to have a bleeding local recurrence. Two individuals were found to have benign prostatic bleeding. The remaining individual was found to have normal cystoscopies. Twenty-three individuals underwent colonoscopy in the months to years following treatment (**Table 4**). The most common finding were hemorrhoids. Three individuals were found to have radiation proctitis with multiple non-confluent telangiectasia (VRS Grade 2).

EPIC-26 hematuria and hematochezia scores following SBRT can be found in **Figures 1A, B**, respectively. Overall, 18.2% experienced hematuria with a median time of 10.5 months post-SBRT (**Table 5**). At the time of the initial consultation, 3.7% of our cohort reported bothersome hematuria (**Table 5**). Hematuria bother increased following treatment and peaked at 9 months post treatment with 2.3% of patients reporting that it was a moderate to big problem from 9-24 months post-SBRT (**Table 4**). Hematuria bother returned to baseline by 30 months after SBRT. At 36 months, 2.3% reported hematuria as being a very small to small problem with no patients reporting hematuria as being a moderate to big problem. There were no clinically significant changes in hematuria at any time point following treatment (**Figure 1A**: MID 3.2).

Altogether, 38.6% experienced hematochezia with a median time of 6 months post-SBRT. At the time of the initial consultation, 7.4% of patients reported bothersome hematochezia; however, no patient felt it was a moderate to big problem (**Table 5**). At 1 month post-SBRT, this increased to 14% reporting rectal bleeding as being a very small to small problem and 2.3% reporting the bleeding to be a moderate to big problem. A few patients experienced transient episodes of bothersome rectal bleeding over the next three years. At 36 months, 90.7% reported having no problems with hematochezia. Nine percent of patients reported hematochezia; however, no patient felt it was a moderate to big problem. There were no clinically significant changes in the months following treatment with respect to hematochezia (**Figure 1B**; MID 2.6).

TABLE 3 | Results of cystoscopies.

Patient	Age	CCI	Anticoagulant Use	Time to Cystoscopy	Cystoscopy Findings
1	83	1	Plavix	1 year	Bladder Cancer
2	63	2	Warfarin	6 years	Prostatic Recurrence
3	62	2	Xarelto	4 years	Benign Prostatic Bleeding
4	71	1	Plavix	5 years	Benign Prostatic Bleeding
5	66	1	Plavix	9 years	Bladder cancer

TABLE 4 | Results of colonoscopies.

Patient	Age	CCI	Anticoagulant Use	Time to Colonoscopy	Colonoscopy Findings
1	74	1	Warfarin	1 year, 3 years	Hemorrhoids
2	74	0	Warfarin	1 year 6 mon	Radiation proctitis (VRS Grade 2)
3	67	1	Plavix, ASA	8 years	Hemorrhoids
4	75	0	Warfarin	2 years 6 mon	Radiation proctitis (VRS Grade 2)
5	63	0	Warfarin	2 years	Hemorrhoids
6	63	2	Warfarin	3 years, 6 years	Hemorrhoids
7	63	1	Warfarin	6 mon	Hemorrhoids
8	80	1	Plavix	1 year 6 mon	Hemorrhoids
9	59	4	Plavix	9 mon	Radiation proctitis (VRS Grade 2)
10	67	2	Plavix	1 year, 4 years	Hemorrhoids
11	71	3	Warfarin	3 years	Hemorrhoids
12	58	2	Warfarin	1 year 6 mon	Hemorrhoids
13	66	1	Plavix	3 years	Hemorrhoids
14	72	2	Plavix	4 years	Hemorrhoids

DISCUSSION

Chronic anticoagulation therapy alone may increase an individual's risk of developing hematuria and or hematochezia (12). The yearly incidence of major bleeding is 2-5% (13). As seen in this manuscript, occult malignancies, benign prostatic bleeding, and/or benign acute lower gastrointestinal bleeding such as hemorrhoids where common sources of non-radiation related bleeding in our patients on anticoagulants (14–16). Benign bleeding from enlarged prostates and diverticular disease is are common causes of bleeding in the aging population. Like irradiated tissue, tumor vasculature is friable and prone to bleeding (17). The risk of bleeding is highest in urinary and colorectal cancers (14, 18).

The risk of radiation induced hematuria is dependent upon the total radiation dose and the volume of the bladder in the high dose region (19). Our group has previously reported on the incidence of hematuria in unselected patients who had undergone SBRT for their localized prostate cancer (20). Similar to the present study, 18.3% experienced at least one episode of hematuria following SBRT, and the 3-year actuarial incidence of late ≥ grade 2 hematuria was 2.4% (20). On multivariate analysis, history of prior benign prostatic hyperplasia (BPH) procedure(s) ($p = 0.002$) was significantly associated with the development of hematuria. Unexpectantly, it did not find an association between anticoagulation use and hematuria, despite previous reports of an association (1, 20). We hypothesize that the low rate of significant hematuria in the current study was at least partially due to the low incidence of prior urologic procedure for BPH (2.3%) in this patient population.

Our group has also previously reported on the incidence of post-SBRT rectal bleeding in unselected patients (21). In that study, 22.7% of patients reported rectal bleeding post-SBRT. In the current report, 38.6% of patients on baseline anticoagulants experienced rectal bleeding post-SBRT. Twenty five percent of patients experienced late Grade 1 hematochezia, higher than was previously reported. There were no late grade 2 or 3 rectal bleeding events. Patient's experienced peak of hematochezia representing a problem at 1 month following treatment. This is consistent with hematochezia secondary to increased bowel frequency seen acutely following treatment. The remainder of the peaks in burden appear to be episodic in nature likely due to hemorrhoidal bleeding. By 36 months, no individuals reported hematochezia to be a moderate or big problem. These results are consistent with our previously reported findings (20, 21). In our

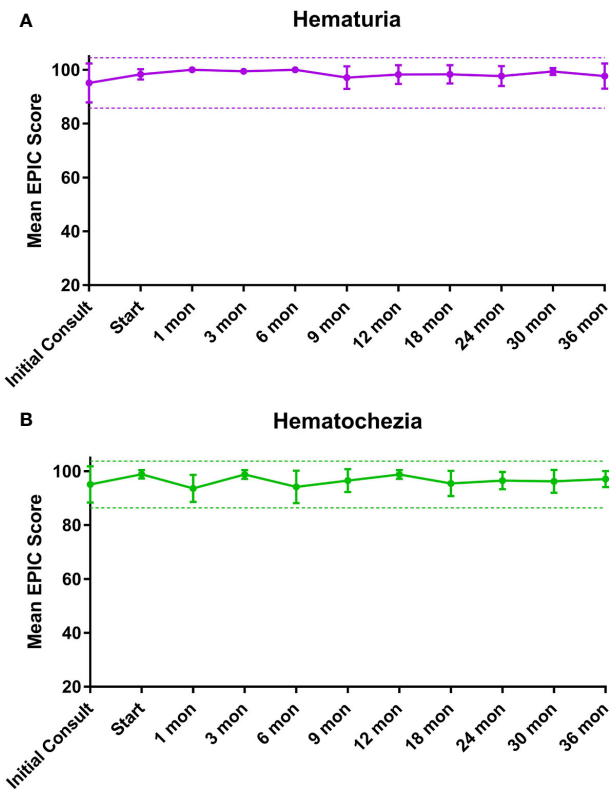

FIGURE 1 | Mean summary scores at baseline and following SBRT for prostate cancer. **(A)** Hematuria. **(B)** Hematochezia. Thresholds for clinically significant changes in scores (½ standard deviation above and below the baseline) are marked with dashed lines. EPIC scores range from 0–100 with higher values representing a more favorable health-related QOL.

patient population, 23 individuals underwent colonoscopies in months to years after their treatment for localized prostate cancer. No occult malignancies were detected, though polyps were noted in 60.8% of colonoscopies. The most common finding was hemorrhoids. Presence of hemorrhoids has been reported to be a strong predictor for hematochezia previously (22). Our previous report on endoscopic findings reported a rate of telangiectasias in 20% of post-SBRT patients compared to 32-88% in patients who had undergone 3D-conformal radiation therapy (3D-CRT) or intensity modulated radiation therapy (IMRT) (6). In the present study, three patients (13%) were noted to have radiation proctitis with Vienna Score 2 telangiectasias; two of the three individuals experienced symptomatic rectal bleeding. Given that bleeding was most commonly secondary to hemorrhoidal bleeding, in the authors' opinion, anticoagulation should not be an indication for rectal spacing in patients treated with moderate dose robotic SBRT.

Dosimetric parameters may influence rates of GU and GI bleed. Total radiation dose and volumes of urethra and bladder neck exposed impact the risk of developing radiation-induced hematuria, but specific dosimetric constraints to limit late hematuria have been difficult to identify (19). The low level of high-grade hematuria in this study was likely secondary to the small number of patients with prior transurethral resection of the prostate (TURP) which qualified (20). Musunuru et al. looked at predictive factors for developing symptomatic hematochezia in patients with prostate cancer following 5-fraction linac-based SBRT (22). In that trial, Grade 2 and ≥Grade 3 late hematochezia was observed in 19.4% and 3.1% of their cohort, respectively (22). Analysis of receiver operating characteristic (ROC) curves revealed that the volume of rectum receiving 38 Gy (V38) was the strongest predictor of Grade 2 late hematochezia (22). Approximately 9% of patients who received a rectal V38 <2 cc had symptomatic rectal bleeding compared to 28% of patients who received V38 ≥2 cc (22). However, that paper used a posterior PTV margin of 4-5 mm, while our institution favors rectal sparing using a posterior PTV margin of 3 mm, which can be achievable using motion tracking (22). In this study, no patient received 36 Gy to greater than 1 cc of the rectum providing a rationale for our low rate of symptomatic rectal telangiectasia.

Our study has several limitations. It is inherently limited by its retrospective nature. Our patients were all on documented anticoagulation at time of initial consult. However, it is unknown in our study if patients were removed from anticoagulation in the weeks to years following radiation therapy. A study evaluating the risk of rectal bleeding based on timing of anticoagulation during or after radiation therapy found that anticoagulation during treatment was associated with an increased risk of bleeding, though initiation of anticoagulation after completion of radiation therapy did not significantly increase the risk of rectal bleed (23). In addition, given that we did not perform regular urinalysis on

TABLE 5 | Bleeding following SBRT for prostate cancer: hematuria (patient-reported responses to Question 4c of the EPIC-26) and hematochezia (patient-reported responses to Question 6d of the EPIC-26).

	Initial Consult	Start	1 mon	3 mon	6 mon	9 mon	12 mon	18 mon	24 mon	30 mon	36 mon
Hematuria											
No problem	96.3%	93.2%	100.0%	97.7%	100.0%	95.3%	97.7%	97.7%	95.3%	97.5%	97.7%
Very Small- Small problem	3.7%	6.8%	0.0%	2.3%	0.0%	2.3%	0.0%	0.0%	2.3%	2.5%	2.3%
Moderate - Big problem	0.0%	0.0%	0.0%	0.0%	0.0%	2.3%	2.3%	2.3%	2.3%	0.0%	0.0%
Hematochezia											
No problem	92.6%	95.5%	83.7%	95.3%	88.4%	93.0%	95.3%	90.9%	88.4%	90.0%	90.7%
Very small- Small problem	7.4%	4.5%	14.0%	4.7%	7.0%	4.7%	4.7%	6.8%	11.6%	7.5%	9.3%
Moderate - Big problem	0.0%	0.0%	2.3%	0.0%	4.7%	2.3%	0.0%	2.3%	0.0%	2.5%	0.0%

patients, the true incidence of microscopic hematuria may be higher than reported. We did not perform routine baseline cystoscopy or colonoscopy screening. As such, baseline causes of hematuria or hematochezia could not be assessed. However, patients were treated on average one month after gold marker placement, and it is possible bleeding events could have lingered from that procedure.

CONCLUSION

In patients with baseline anticoagulant usage, moderate dose prostate SBRT was well tolerated without rectal spacing. High grade bleeding toxicities were uncommon and resolved with time. Baseline anticoagulation usage should not be considered a contraindication to prostate SBRT.

AUTHOR'S NOTE

Portions of this research were presented in abstract form at ESTRO 2021.

DATA AVAILABILITY STATEMENT

The datasets presented in this article are not readily available because the datasets presented in this article are not readily available due to patient privacy concerns. Requests to access the datasets should be directed to the corresponding author. Requests to access the datasets should be directed to Sean.P.Collins@gunet.georgetown.edu.

ETHICS STATEMENT

The studies involving human participants were reviewed and approved by Georgetown University IRB 2009-510. The patients/participants provided their written informed consent to participate in this study.

AUTHOR CONTRIBUTIONS

AP was the lead author, who participated in data collection, data analysis, manuscript drafting, table/figure creation, and manuscript revision. SSh aided in contributed to data collection. MP aided in review and revision of the manuscript. SL developed the SBRT treatment plans and contributed to data analysis. MD contributed to study design and clinical data collection. MA, TY, BC, and NA aided in review of the manuscript. SSu is a senior author who organized the data and participated in its analysis. SC was the principal investigator who initially developed the concept of the study and the design, aided in data collected, and drafted and revised the manuscript. All authors contributed to the article and approved the submitted version.

FUNDING

The Department of Radiation Medicine at Georgetown University Hospital receives a grant from Accuray to support a research coordinator. We gratefully acknowledge the grant R01MD012767 from the National Institute on Minority Health and Health Disparities (NIMHD), NIH to SC. This work was supported by The James and Theodore Pedas Family Foundation.

REFERENCES

1. Choe KS, Jani AB, Liauw SL. External Beam Radiotherapy for Prostate Cancer Patients on Anticoagulation Therapy: How Significant Is the Bleeding Toxicity? *Int J Radiat Oncol Biol Phys* (2010) 76(3):755–60. doi: 10.1016/j.ijrobp.2009.02.026
2. Marks LB, Carroll PR, Dugan TC, Anscher MS. The Response of the Urinary Bladder, Urethra, and Ureter to Radiation and Chemotherapy. *Int J Radiat Oncol Biol Phys* (1995) 31(5):1257–80. doi: 10.1016/0360-3016(94)00431-J
3. Garg AK, Mai W-Y, McGary JE, Grant WH, Butler EB, Teh BS. Radiation Proctopathy in the Treatment of Prostate Cancer. *Int J Radiat Oncol Biol Phys* (2006) 66(5):1294–305. doi: 10.1016/j.ijrobp.2006.07.1386
4. Chan N, Sobieraj-Teague M, Eikelboom JW. Direct Oral Anticoagulants: Evidence and Unresolved Issues. *Lancet* (2020) 396(10264):1767–76. doi: 10.1016/S0140-6736(20)32439-9
5. D'Amico AV, Manola J, McMahon E, Loffredo M, Lopes L, Ching J, et al. A Prospective Evaluation of Rectal Bleeding After Dose-Escalated Three-Dimensional Conformal Radiation Therapy Using an Intrarectal Balloon for Prostate Gland Localization and Immobilization. *Urol* (2006) 67(4):780–4. doi: 10.1016/j.urology.2005.10.008
6. Sood S, Ju AW, Wang H, Lei S, Uhm S, Zhang G, et al. Rectal Endoscopy Findings Following Stereotactic Body Radiation Therapy for Clinically Localized Prostate Cancer. *Radiat Oncol Lond Engl* (2013) 8:197. doi: 10.1186/1748-717X-8-197
7. Mahmood S, Bollipo S, Steele S, Bristow RG, Choudhury A, Oakland K, et al. It's All the RAVE: Time to Give Up on the "Chronic Radiation Proctitis" Misnomer. *Gastroenterol* (2021) 160(3):635–8. doi: 10.1053/j.gastro.2020.09.054
8. Nieto JA, Solano R, Ruiz-Ribó MD, Ruiz-Gimenez N, Prandoni P, Kearon C, et al. Fatal Bleeding in Patients Receiving Anticoagulant Therapy for Venous Thromboembolism: Findings From the RIETE Registry. *J Thromb Haemost JTH* (2010) 8(6):1216–22. doi: 10.1111/j.1538-7836.2010.03852.x
9. Widmark A, Gunnlaugsson A, Beckman L, Thellenberg-Karlsson C, Hoyer M, Lagerlund M, et al. Ultra-Hypofractionated *Versus* Conventionally Fractionated Radiotherapy for Prostate Cancer: 5-Year Outcomes of the HYPO-RT-PC Randomised, Non-Inferiority, Phase 3 Trial. *Lancet Lond Engl* (2019) 394(10196):385–95. doi: 10.1016/S0140-6736(19)31131-6
10. Brand DH, Tree AC, Ostler P, van der Voet H, Loblaw A, Chu W, et al. Intensity-Modulated Fractionated Radiotherapy *Versus* Stereotactic Body Radiotherapy for Prostate Cancer (PACE-B): Acute Toxicity Findings From an International, Randomised, Open-Label, Phase 3, Non-Inferiority Trial. *Lancet Oncol* (2019) 20(11):1531–43. doi: 10.1016/S1470-2045(19)30569-8
11. Chen LN, Suy S, Uhm S, Oermann EK, Ju AW, Chen V, et al. Stereotactic Body Radiation Therapy (SBRT) for Clinically Localized Prostate Cancer: The Georgetown University Experience. *Radiat Oncol Lond Engl* (2013) 8:58. doi: 10.1186/1748-717X-8-58
12. Chan NC, Paikin JS, Hirsh J, Lauw MN, Eikelboom JW, Ginsberg JS. New Oral Anticoagulants for Stroke Prevention in Atrial Fibrillation: Impact of Study Design, Double Counting and Unexpected Findings on Interpretation of Study Results and Conclusions. *Thromb Haemost* (2014) 111(5):798–807. doi: 10.1160/TH13-11-0918

13. Rubboli A, Becattini C, Verheugt FW. Incidence, Clinical Impact and Risk of Bleeding During Oral Anticoagulation Therapy. *World J Cardiol* (2011) 3 (11):351–8. doi: 10.4330/wjc.v3.i11.351
14. Kraaijpoel N, Di Nisio M, Mulder FI, van Es N, Beyer-Westendorf J, Carrier M, et al. Clinical Impact of Bleeding in Cancer-Associated Venous Thromboembolism: Results From the Hokusai VTE Cancer Study. *Thromb Haemost* (2018) 118(8):1439–49. doi: 10.1055/s-0038-1667001
15. Sieber PR, Rommel FM, Huffnagle HW, Breslin JA, Agusta VE, Harpster LE. The Treatment of Gross Hematuria Secondary to Prostatic Bleeding With Finasteride. *J Urol* (1998) 159(4):1232–3. doi: 10.1097/00005392-199804000-00040
16. Diamantopoulou G, Konstantakis C, Skroubis G, Theocharis G, Theopistos V, Triantos C, et al. Acute Lower Gastrointestinal Bleeding in Patients Treated With non-Vitamin K Antagonist Oral Anticoagulants Compared With Warfarin in Clinical Practice: Characteristics and Clinical Outcome. *Gastroenterol Res* (2019) 12(1):21–6. doi: 10.14740/gr1115
17. Stylianopoulos T, Munn LL, Jain RK. Reengineering the Tumor Vasculature: Improving Drug Delivery and Efficacy. *Trends Cancer* (2018) 4(4):258–9. doi: 10.1016/j.trecan.2018.02.010
18. Flack KF, Desai J, Kolb JM, Chatterjee P, Wallentin LC, Ezekowitz M, et al. Major Gastrointestinal Bleeding Often Is Caused by Occult Malignancy in Patients Receiving Warfarin or Dabigatran to Prevent Stroke and Systemic Embolism From Atrial Fibrillation. *Clin Gastroenterol Hepatol* (2017) 15 (5):682–90. doi: 10.1016/j.cgh.2016.10.011
19. Viswanathan AN, Yorke ED, Marks LB, Eifel PJ, Shipley WU. Radiation Dose–Volume Effects of the Urinary Bladder. *Int J Radiat Oncol* (2010) 76(3, Supplement):S116–22. doi: 10.1016/j.ijrobp.2009.02.090
20. Gurka MK, Chen LN, Bhagat A, Moures R, Kim JS, Yung T, et al. Hematuria Following Stereotactic Body Radiation Therapy (SBRT) for Clinically Localized Prostate Cancer. *Radiat Oncol* (2015) 10(1):1–7. doi: 10.1186/s13014-015-0351-6
21. Joh DY, Chen LN, Porter G, Bhagat A, Sood S, Kim JS, et al. Proctitis Following Stereotactic Body Radiation Therapy for Prostate Cancer. *Radiat Oncol* (2014) 9(1):277. doi: 10.1186/s13014-014-0277-4
22. Musunuru HB, Davidson M, Cheung P, Vesprini D, Liu S, Chung H, et al. Predictive Parameters of Symptomatic Hematochezia Following 5-Fraction Gantry-Based SABR in Prostate Cancer. *Int J Radiat Oncol Biol Phys* (2016) 94 (5):1043–51. doi: 10.1016/j.ijrobp.2015.12.010
23. Schreiber D, Chen S-C, Rineer J, Worth M, Telivala T, Schwartz D. Assessment of Risk of Late Rectal Bleeding for Patients With Prostate Cancer Started on Anticoagulation Before or After Radiation Treatment. *Anticancer Res* (2014) 34(12):7367–72.

Conflict of Interest: SC and BC serve as clinical consultants to Accuray Inc.

The remaining authors declare that the research was conducted in the absence of any commercial or financial relationships that could be construed as a potential conflict of interest.

Publisher's Note: All claims expressed in this article are solely those of the authors and do not necessarily represent those of their affiliated organizations, or those of the publisher, the editors and the reviewers. Any product that may be evaluated in this article, or claim that may be made by its manufacturer, is not guaranteed or endorsed by the publisher.

frontiers in Oncology

ORIGINAL RESEARCH
published: 19 October 2021
doi: 10.3389/fonc.2021.759724

Patient-Reported Outcomes-Guided Adaptive Radiation Therapy for Head and Neck Cancer

Sarah Weppler[1,2*], *Harvey Quon*[3,4], *Colleen Schinkel*[2,4], *Adam Yarschenko*[2,5], *Lisa Barbera*[3,4], *Nabhya Harjai*[6] *and Wendy Smith*[1,2,4]

[1] Department of Physics and Astronomy, University of Calgary, Calgary, AB, Canada, [2] Department of Medical Physics, Tom Baker Cancer Centre, Calgary, AB, Canada, [3] Department of Radiation Oncology, Tom Baker Cancer Centre, Calgary, AB, Canada, [4] Department of Oncology, University of Calgary, Calgary, AB, Canada, [5] Department of Mechanical Engineering, University of Calgary, Calgary, AB, Canada, [6] Cumming School of Medicine, University of Calgary, Calgary, AB, Canada

OPEN ACCESS

Edited by:
Jason W. Sohn,
Allegheny Health Network,
United States

Reviewed by:
Jung Hun Oh,
Memorial Sloan Kettering Cancer Center, United States
Francesco Ricchetti,
Sacro Cuore Don Calabria Hospital, Italy

***Correspondence:**
Sarah Weppler
Sarah.Weppler@albertahealthservices.ca

Specialty section:
This article was submitted to Radiation Oncology, a section of the journal Frontiers in Oncology

Received: 16 August 2021
Accepted: 20 September 2021
Published: 19 October 2021

Citation:
Weppler S, Quon H, Schinkel C, Yarschenko A, Barbera L, Harjai N and Smith W (2021) Patient-Reported Outcomes-Guided Adaptive Radiation Therapy for Head and Neck Cancer. Front. Oncol. 11:759724. doi: 10.3389/fonc.2021.759724

Purpose: To identify which patient-reported outcomes (PROs) may be most improved through adaptive radiation therapy (ART) with the goal of reducing toxicity incidence among head and neck cancer patients.

Methods: One hundred fifty-five head and neck cancer patients receiving radical VMAT (chemo)radiotherapy (66-70 Gy in 30-35 fractions) completed the MD Anderson Symptom Inventory, MD Anderson Dysphagia Inventory (MDADI), and Xerostomia Questionnaire while attending routine follow-up clinics between June-October 2019. Hierarchical clustering characterized symptom endorsement. Conventional statistical approaches indicated associations between dose and commonly reported symptoms. These associations, and the potential benefit of interfractional dose corrections, were further explored *via* logistic regression.

Results: Radiotherapy-related symptoms were commonly reported (dry mouth, difficulty swallowing/chewing). Clustering identified three patient subgroups reporting: none/mild symptoms for most items (60.6% of patients); moderate/severe symptoms affecting some aspects of general well-being (32.9%); and moderate/severe symptom reporting for most items (6.5%). Clusters of PRO items broadly consisted of acute toxicities, general well-being, and head and neck-specific symptoms (xerostomia, dysphagia). Dose-PRO relationships were strongest between delivered pharyngeal constrictor Dmean and patient-reported dysphagia, with MDADI composite scores (mean ± SD) of 25.7 ± 18.9 for patients with Dmean <50 Gy *vs*. 32.4 ± 17.1 with Dmean ≥50 Gy. Based on logistic regression models, during-treatment dose corrections back to planned values may confer ≥5% decrease in the absolute risk of self-reported physical dysphagia symptoms ≥1 year post-treatment in 1.2% of patients, with a ≥5% decrease in relative risk in 23.3% of patients.

Conclusions: Patient-reported dysphagia symptoms are strongly associated with delivered dose to the pharyngeal constrictor. Dysphagia-focused ART may provide the greatest toxicity benefit to head and neck cancer patients, and represent a potential new direction for ART, given that the existing ART literature has focused almost exclusively on xerostomia reduction.

Keywords: patient-reported outcomes, adaptive radiation therapy, head and neck cancer, dysphagia, xerostomia

1 INTRODUCTION

Standard-of-care (chemo)radiotherapy is associated with a high toxicity burden for many locally-advanced head and neck cancer patients. Physician assessments suggest that ≥30% of patients will experience grade 2 or worse radiation-associated dysphagia (1) with ≥35% experiencing grade 2 or worse xerostomia (2). Volumetric modulated arc therapy (VMAT) provides dose-sculpting capabilities to reduce incidental radiation doses to healthy tissues (2); however, decreases in tumor volume (3), weight loss (4), and other inter-fractional anatomical changes common among head and neck cancer patients may reduce treatment precision and increase toxicity (5, 6). Reduction of treatment-related side effects is increasingly important given the rise of HPV-related disease (7), as well as younger age and improved prognosis of these patients (8).

Adaptive radiation therapy (ART) adapts a patient's radiotherapy plan in response to inter-fractional anatomical changes to maintain target coverage and healthy tissue dose sparing objectives during the 6-7 week treatment course. ART may improve the therapeutic ratio of radiotherapy (3) and reduce treatment-related toxicities (5), but is resource intensive (9). Effective patient selection is therefore essential for ensuring that ART is feasible in a routine clinical setting. However, many open questions remain regarding patient selection: even in a broad sense, it is unclear which toxicity ART may most reduce.

When considering toxicity-reduction strategies, such as ART, patient-report outcomes (PRO) provide valuable insight into symptom burden. Physician assessments are essential for patient care but may underreport symptom severity relative to patient reporting (10). PROs help to fill the gap by providing the patient's perspective of the impact of symptoms and toxicity on daily patient life (11, 12). Examples of PRO instruments include the MD Anderson Symptom Inventory for Head and Neck Cancer (MDASI-HN) (13, 14), the MD Anderson Dysphagia Inventory (MDADI) (15) and the Xerostomia Questionnaire (XQ) (16). These instruments are widely used and score highly in reliability, validity, and responsiveness to changes over time (13–17).

In this study, we compare planned doses, delivered doses, and PROs (MDASI-HN, MDADI, and XQ) to identify which patient-reported side-effects may be most improved by ART, and to estimate the associated toxicity benefit. It is our hope that these results will provide further structure to the development of ART workflows and effective patient-selection criteria.

2 MATERIALS AND METHODS

2.1 Patient Inclusion Criteria

Patients attending routine radiotherapy follow-up appointments between June and October 2019 were approached to complete a one-time paper-based PRO questionnaire in clinic. The questionnaire consisted of the MDASI-HN, MDADI, and XQ. Patients included in this study received treatment with radical VMAT (chemo)radiotherapy (66-70 Gy in 30-35 fractions). Patients were excluded if they were treated with a dose prescription less than 66 Gy, did not receive CBCT imaging, or had a confirmed local-regional recurrence prior to survey completion. This study was approved by our institutional research ethics board (HREBA.CC-19-0119).

2.2 Exposure Definition – Planned and Delivered Dose

Planned organ-at-risk (OAR) dose parameter values were extracted from the patient's treatment plan. OAR planning objectives adhered to QUANTEC and other consensus recommendations and included: brainstem D0.03cc ≤ 54 Gy (18); spinal cord D0.03cc ≤ 45 Gy (19); ipsilateral and contralateral parotid gland Dmean ≤ 26 Gy (20, 21); and pharyngeal constrictor Dmean ≤ 50 Gy (22). Treatments were planned using the Eclipse Treatment Planning System, Versions 11 and 13 (Varian Medical Systems, Palo Alta, CA). Institutional image-guided radiation therapy utilized daily kV-orthogonal imaging and weekly kV-cone beam CT (CBCT) imaging (23).

Previously validated deformable image registration workflows allowed us to estimate delivered OAR doses (23). For each patient, we deformed a copy of the planning CT to reproduce the anatomical changes present in the last-acquired on-unit CBCT. We propagated contours through the corresponding deformation vector mapping, re-applied the patient's treatment plan, and recalculated dose in the treatment planning system. These doses served as a surrogate for total delivered dose. Assuming that patient anatomy was consistent with the final CBCT for all treatment fractions provided conservative estimates for the associations between dose and PROs. Quality assurance of this process assessed a representative set of cases (24), and ensured the propagated structures were geometrically (25) and dosimetrically (26) consistent with physician contours (23).

2.3 Outcome Definition – Patient-Reported Outcome Instruments

The MDASI-HN consists of 28 questions assessing core symptoms (13 items), head and neck-specific symptoms (9 items), and

symptom interference on daily life (6 items) (13, 14). Each item is ranked from 0 to 10 with symptom burden interpreted as: none (item rating of 0); mild (1 to 4); moderate (5 to 6); or severe (7 to 10) (13). Summary symptom burden is defined by the maximum rating of any item within each subgroup: none (all items rated 0); mild (all items rated <5 with at least one item rated ≥1); moderate (all items rated <7 with at least one item rate ≥5); severe (at least one item rated ≥7) (27–29).

The MDADI contains 20 questions assessing physical swallowing ability (8 items), functional impact of swallowing dysfunction (5 items), emotional impact (6 items), and the general influence of swallowing ability on daily life (1 item) (15). Ratings for physical, functional, and emotional items are summed to produce the composite score (15). For this study, 5-point Likert-responses were normalized to 100 with higher scores indicating more severe symptoms. This provided greater comparability with the MDASI-HN and XQ scoring systems. With this conversion, MDADI scores are interpreted as: minimal (summary score of 0 to 19), mild (20 to 39), moderate (40 to 59), severe (60 to 79), and profound (80 to 100) (30, 31). Differences in MDADI scores ≥10 points are considered clinically relevant (32). References to MDADI moderate/severe scores below also include scores classified as "profound".

The XQ is an 8-item assessment of xerostomia symptoms while eating (4 items) and while not eating (4 items). Item scores are totaled and normalized to 100 (16). Symptom burden according to XQ responses was interpreted as: none/mild for scores <50 and moderate/severe for scores ≥50).

2.4 Covariates – Clinical Patient Characteristics

Data for this study consisted of basic demographic and tumor factors abstracted from the patient's medical record. These included patient: age; gender; BMI; ECOG performance status; Charlson Comorbidity Index; tobacco/alcohol use; tumor site and stage; HPV status; and chemotherapy agent.

2.5 Data Clustering, Statistical Analysis, and Logistic Regression Modelling

2.5.1 Characterization of Patient-Reported Outcomes

Using Mann-Whitney U tests and Fisher's exact tests, we examined potential associations between clinical characteristics and PRO item and summary scores. Benjamini-Hochberg multiple testing corrections were applied with a false discovery rate of 5% (33).

Hierarchical clustering tested for similarities in symptom reporting among PRO items and summary scores, as well as symptom burden among patients. This technique progressively groups items considered most similar, as represented in tree-like "dendrograms" (34). Similarities in PRO results were used to: characterize PRO reporting; verify dose-PRO associations among related PRO items; and identify similarities in patient symptoms to examine the effect of covariates.

2.5.2 Associations Between Planned Dose, Delivered Dose and Patient-Reported Outcomes

We stratified patients according to whether their OAR dose met *vs*. exceeded planning objective criteria. Differences in PRO scores between these groups were compared using Mann-Whitney U tests. Odds ratios indicated whether patients with OAR dose exceeding planning objectives had a greater likelihood of reporting moderate/severe symptoms, with significance from Fisher's exact tests. Tests were performed for both planned dose and delivered dose. For parotid gland doses, we compared the dose of the spared gland (i.e., the lesser of ipsilateral and contralateral gland Dmean values) with PRO results.

As moderate/severe symptoms persisting ≥1 year after treatment are more likely to be permanent (35, 36), we further assessed differences in patients completing the PRO questionnaire <1 year *vs*. ≥1 year post-treatment.

2.5.3 Estimating the Benefit of Adaptive Replanning

When delivered OAR doses were found to be strongly associated with PRO scores, we estimated the potential benefit of ART on patient-reported symptom severity. Systematic dose increases considered potentially correctable by replanning (dose "violations") were calculated relative to planning objectives and planned values, as relevant to clinical practice and QUANTEC guidelines. Additional tolerances accounted for random errors in estimated delivered doses to produce conservative estimates of ART benefit. For our given workflow, calculated increases in parotid gland dose exceeding 2.2 Gy, and pharyngeal constrictor dose exceeding 0.75 Gy are likely to result from systematic changes in patient anatomy, as compared to daily setup uncertainties or deformable image registration error (23). For patients with planned doses meeting planning objectives,

$$Violation = delivered\ dose - planning\ objective - random\ error\ tolerance \quad (1)$$

For example, a patient with planned pharyngeal constrictor dose of 49.0 Gy and estimated delivered dose of 52.0 Gy would have a 1.25 Gy violation. For patients with planned doses exceeding planning objectives,

$$Violation = delivered\ dose - planned\ dose - random\ error\ tolerance \quad (2)$$

Therefore, a patient with planned pharyngeal constrictor dose of 54.0 Gy and estimated delivered dose of 57.0 Gy would have a 2.25 Gy violation. Positive violation values indicate the amount of dose sparing achievable with adaptive dose corrections; patients with positive violations likely have increased risk of treatment-related side effects relative to that estimated at planning. Negative values indicate that: only minor dose increases occurred during treatment as a result of random effects; delivered structure dose corresponded to a relatively low-risk of toxicity (i.e., delivered doses met the treatment planning objective); or that dose and corresponding toxicity risk decreased during treatment.

Logistic regression was used to model dose violations versus risk of moderate/severe symptom reporting. For each patient, the risk of moderate/severe symptom reporting was estimated for raw delivered doses and doses corrected back to planned values; corresponding differences in risk indicated the potential benefit, if any, of ART on patient-reported symptom severity.

All analyses were performed using R Version 3.6.0 (The R Foundation for Statistical Computing, Vienna, Austria). All statistical tests required $p \leq 0.05$ for significance.

3 RESULTS

3.1 Cohort Characteristics and Characterization of Patient-Reported Outcomes

225 patients completed the PRO questionnaires in clinic. After applying the inclusion/exclusion criteria, the final study cohort consisted of 155 patients. **Table 1** provides cohort demographics and characteristics. MDASI-HN, MDADI, and XQ results are summarized in **Figure 1**. 60 patients completed the PRO questionnaire within their first year after treatment (median = 7 months, range = 2-11 months), with the remaining 95 patients completing the questionnaire ≥1 year post-treatment (28 months, 12-74 months).

Patients with lower initial BMI or poorer performance status more frequently reported moderate/severe fatigue, sadness, poorer activity, greater interference of symptoms with work, and poorer overall interference with daily life ($p < 0.005$ for each) on the MDASI-HN. Greater T stage (T3-T4 disease) was significantly associated with higher MDADI composite summary scores ($p < 0.005$). No statistically significant differences occurred in clinical parameters for other MDASI-HN, MDADI or XQ responses, including HPV status and time since treatment, according to Mann-Whitney U tests and Fisher's exact tests.

Results of the hierarchical clustering are shown in **Figure 2**. PRO items were grouped according to: acute side-effects, general wellbeing, and xerostomia/dysphagia-related toxicities, with the latter combining various MDASI-HN, MDADI, and XQ items. The MDASI-HN dry mouth item strongly contributed to the MDASI-HN core and head and neck summary scores. Clustering indicated three general symptom profiles: none/mild symptoms for the majority of items (Cluster A, 60.6% of patients); moderate/severe symptoms affecting some aspects of general wellbeing (Cluster B, 32.9%); and moderate/severe symptom reporting for most items (Cluster C, 6.5%). Patients in cluster C were younger on average (49.8 years, $p = 0.04$), while patients in cluster A had a greater proportion of non-smokers (46.8%, $p = 0.03$). 6 of the 10 patients in cluster C, reporting moderate/severe symptoms for most items, had nasopharyngeal disease and greater planned and delivered brainstem dose although this was not found to be statistically significant. No other statistically significant differences persisted among the clinical, geometric, or dosimetric characteristics between clusters after multiple testing corrections.

TABLE 1 | Cohort demographic and clinical characteristics.

Parameter	Full Cohort (n = 155)
Age in years, mean (±SD)	57.4 (10.9)
Gender, number (%)	
Male	131 (84.5%)
Female	24 (15.5%)
Initial BMI, mean (±SD)	28.1 (5.6)
ECOG, median (range)	1 (1-3)
Charlson Comorbidity Index, median (range)	4 (2-8)
Alcohol use, number (%)	
Never	36 (23.2%)
Former	12 (7.7%)
Current – Light (males 0-15 drinks/week, females 0-10 drinks/week)	83 (53.6%)
Current – Heavy (males >15 drinks/week, females >10 drinks/week)	24 (15.5%)
Tobacco use, number (%)	
Never	63 (40.7%)
Cumulative – Light (0-20 pack-years)	43 (27.7%)
Cumulative – Heavy (>20 pack-years)	49 (31.6%)
Primary tumor location, number (%)	
Larynx	7 (4.5%)
Hypopharynx	3 (1.9%)
Oral Cavity	3 (1.9%)
Oropharynx	98 (63.3%)
Nasal Cavity	7 (4.5%)
Nasopharynx	26 (16.8%)
Unknown	11 (7.1%)
T stage, number (%)	
T0 – T2	71 (45.8%)
T3 – T4	73 (47.1%)
Tx	11 (7.1%)
N stage, number (%)	
N0	23 (14.8%)
N1	34 (21.9%)
N2	83 (53.6%)
N3	14 (9.0%)
NX	1 (0.7%)
p16 status, number (%)	
Negative	21 (13.6%)
Positive	100 (64.5%)
Unknown	34 (21.9%)
Chemotherapy agent, number (%)	
Carboplatin	3 (1.9%)
Cetuximab	13 (8.4%)
Cisplatin (Cisplatinum)	128 (82.6%)
None	11 (7.1%)
Time Since Treatment, median (range)	18 months (2-74 months)

3.2 Associations Between Planned Dose, Delivered Dose and Patient-Reported Outcomes

Table 2 summarizes the associations between OAR dose and PRO responses. Stratifying patients based on whether their planned pharyngeal constrictor doses met *vs.* exceeded the planning objective revealed statistically significant differences in MDADI composite, physical, and functional summary scores. These differences persisted for delivered pharyngeal constrictor dose, with additional statistical significance in emotional summary scores. Independently calculated odds ratios were statistically significant for MDADI physical and emotional scores with respect to both planned and delivered doses. Odds ratios associated with delivered doses exceeded those for planned doses, suggesting that delivered dose may be more strongly associated with these PRO summary scores. For MDADI composite scores, odds ratios had marginal significance for both planned dose (OR = 2.02, $p = 0.09$) and delivered dose (OR = 2.26, $p = 0.06$).

Furthermore, patients with doses meeting *vs.* exceeding the pharyngeal constrictor planning objective had significantly different MDADI scores across all summary items when reporting ≥1 year after treatment completion, with respect to

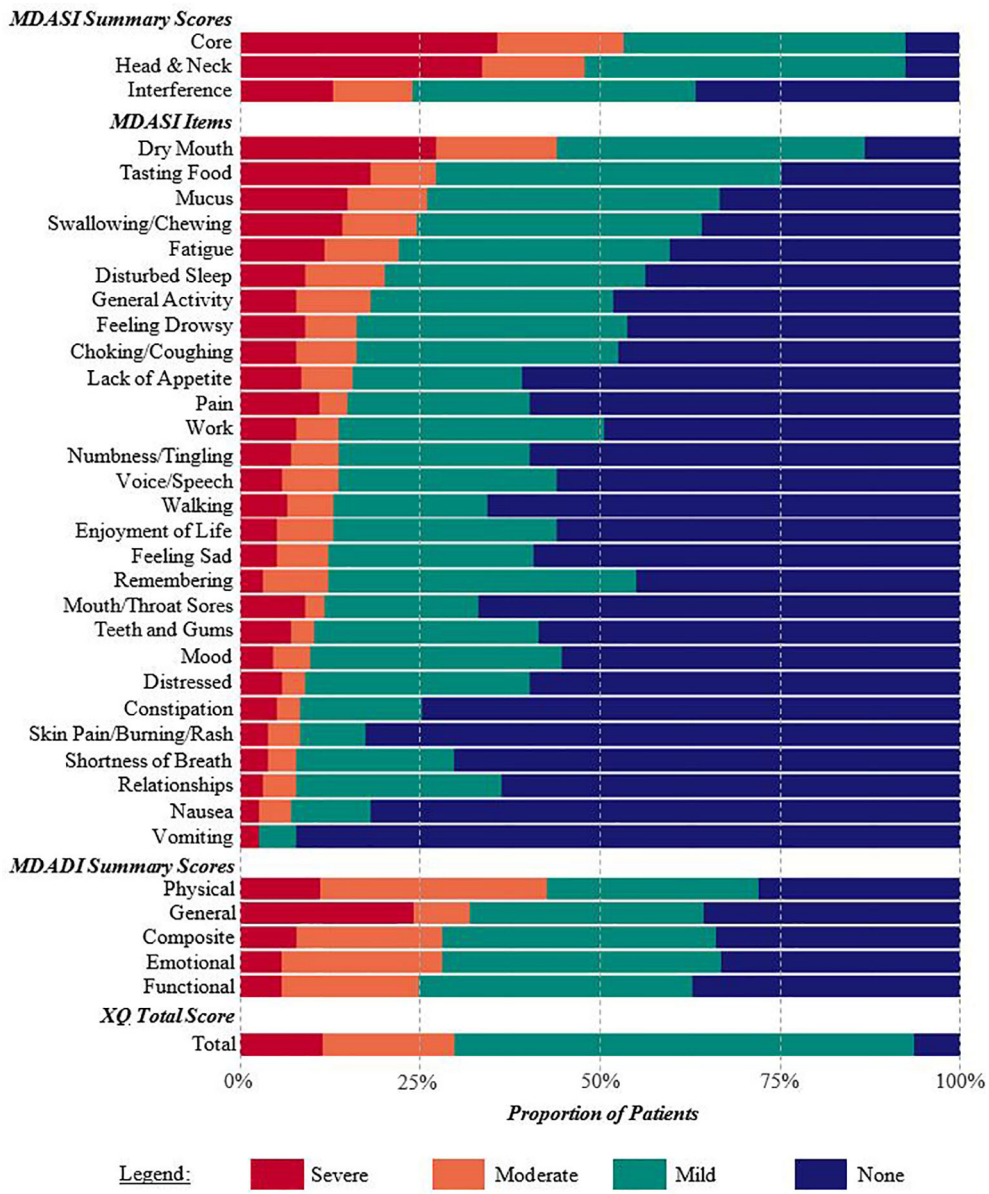

FIGURE 1 | Percentage of patients reporting none, mild, moderate, or severe symptoms on the MDASI-HN, MDADI, and XQ. Summary scores and individual items are listed according to the proportion of patients with moderate or severe symptoms. Xerostomia and dysphagia-related symptoms were commonly reported.

both planned and delivered doses; various MDADI summary scores had mean differences exceeding the 10 point threshold for clinical relevance (32). For planned doses, we observed differences in MDADI composite scores of 13.9; similarly, for delivered doses, we observed differences of 10.7. Mean differences exceeding 10 points also occurred for physical scores (16.3 with respect to planned doses; 13.3 for delivered dose) and general scores (19.8; 14.8). This suggests that pharyngeal constrictor dose meaningfully stratifies patient symptom-reporting ≥1 year post-treatment. Estimating odds ratios associated with PRO scores reported ≥1 year post-treatment was limited by the small number of patients reporting moderate/severe symptoms with doses less than the planning objective.

Among patients with moderate/severe MDADI composite scores, 62.8% had planned pharyngeal constrictor doses exceeding the treatment planning objective, and 67.4% had delivered doses exceeding the objective (**Figure 3A**). In general, delivered doses exceeded planned doses for each patient (**Supplementary Material**). Although not statistically significant, **Figure 3** indicates similar dose and PRO associations for MDASI-HN swallowing/chewing responses,

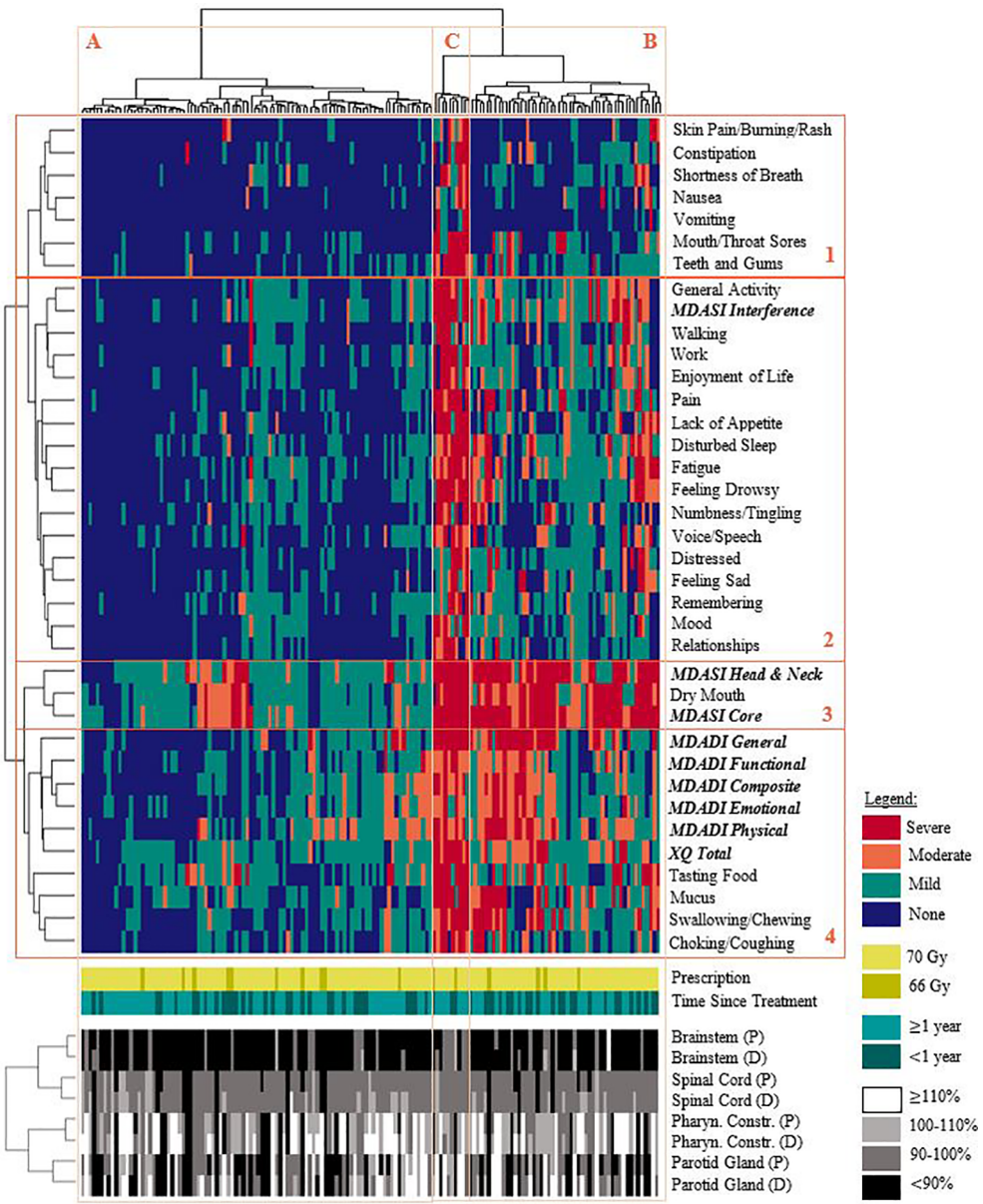

FIGURE 2 | Hierarchical clustering of patient-reported symptoms (none/mild/moderate/severe), prescription dose, time since completing treatment, and OAR dose. Each row (groups 1-4) represents a specific symptom or summary score and are clustered as: 1.) acute toxicities, 2.) general wellbeing, 3.) xerostomia-related summary scores, 4.) xerostomia and dysphagia-related symptoms. Each column represents a patient in the cohort; patients generally reported: **(A)** none/mild symptoms for most/all items, **(B)** moderate/severe symptom burden affecting some aspects of general wellbeing, **(C)** moderate/severe symptom reporting for most/all items. Delivered dose generally exceeded planned dose. Note: healthy tissue doses are expressed as relative percentages of the planning objective. (P): planned dose. (D): delivered dose.

also observed for the MDASI-HN choking/coughing item (not shown), found to be related *via* cluster analysis. Associations appeared strongest among patients reporting ≥1 year after treatment completion.

Patients with minimum parotid gland doses exceeding planning objectives had higher XQ scores, although this was not statistically significant (**Table 2**). No clear associations between parotid gland dose and patient-reported xerostomia symptoms were observed when considering patients in aggregate or according to <1 year *vs.* ≥1 year post-treatment (**Figure 3**).

3.3 Estimating the Benefit of Adaptive Replanning

55.6% of patients had non-negative pharyngeal constrictor dose violations. 33.1% of patients had pharyngeal constrictor dose

TABLE 2 | Comparison of patient-reported symptom scores and dose, reported as mean (SD) for patients with dose meeting *vs*. exceeding planning objectives.

Toxicity/OAR (Obj.)	Relevant PROMs	Planned Dose		Delivered Dose	
		(<Obj./≥ Obj.)	OR (95% CI)	(<Obj./≥ Obj.)	OR (95% CI)
Xerostomia/	% Patients (n = 150)	67.7% (100)/32.3% (50)	N/A	55.5% (81)/44.5% (69)	N/A
Parotid Glands	Average Dose	20.1 Gy/30.8 Gy	N/A	19.3 Gy/31.9 Gy	N/A
(Dmean ≤ 26 Gy)	*MDASI Summary Scores and Relevant Items*				
	Core	5.1 (3.2)/4.9 (3.2)	0.73 (0.38-1.39)	5.3 (3.3)/4.8 (3.0)	0.93 (0.49-1.77)
	• Dry Mouth	4.3 (3.3)/4.4 (3.2)	0.75 (0.40-1.44)	4.5 (3.4)/4.1 (3.0)	0.92 (0.48-1.76)
	Head & Neck	4.7 (3.2)/5.0 (3.3)	0.72 (0.38-1.37)	5.0 (3.2)/4.6 (3.2)	0.77 (0.41-1.47)
	• Swallowing/Chewing	2.6 (3.0)/2.9 (3.2)	1.00 (0.48-2.10)	2.6 (3.1)/2.7 (3.0)	1.04 (0.49-2.19)
	• Taste	3.1 (3.1)/3.3 (2.8)	0.88 (0.43-1.81)	3.2 (3.2)/3.0 (2.7)	0.89 (0.43-1.83)
	• Mucus	2.7 (2.9)/2.7 (3.5)	1.00 (0.48-2.08)	2.9 (3.0)/2.5 (3.2)	1.03 (0.49-2.14)
	Interference	2.7 (2.7)/2.4 (3.0)	0.65 (0.30-1.37)	2.7 (2.9)/2.4 (2.8)	0.78 (0.37-1.64)
	XQ Total Score	32.3 (23.4)/37.2 (26.9)	1.66 (0.80-3.46)	32.8 (24.0)/35.1 (25.4)	1.70 (0.81-3.57)
Dysphagia/Pharyngeal	% Patients (n = 142)	46.5% (59)/53.5% (83)	N/A	42.6% (53)/57.4% (89)	N/A
Constrictor (Dmean ≤ 50 Gy)	Average Dose	44.3 Gy/56.5 Gy	N/A	44.1 Gy/57.1 Gy	N/A
	MDASI Summary Scores and Relevant Items				
	Core	5.1 (3.0)/4.8 (3.3)	0.74 (0.38-1.45)	5.0 (2.9)/4.9 (3.3)	0.91 (0.46-1.82)
	Head & Neck	5.1 (3.1)/4.5 (3.2)	0.65 (0.33-1.26)	5.0 (3.1)/4.6 (3.2)	0.73 (0.37-1.44)
	• Swallowing/Chewing	2.6 (3.0)/2.6 (3.0)	1.02 (0.47-2.23)	2.4 (2.9)/2.7 (3.0)	1.33 (0.59-3.01)
	• Choking/Coughing	1.6 (2.4)/1.9 (2.5)	1.03 (0.41-2.60)	1.7 (2.4)/1.8 (2.5)	1.05 (0.41-2.70)
	• Taste	2.9 (3.1)/3.1 (3.0)	0.97 (0.46-2.06)	2.8 (3.1)/3.2 (3.0)	1.03 (0.48-2.22)
	Interference	2.7 (2.8)/2.4 (2.8)	0.59 (0.27-1.29)	2.8 (3.0)/2.3 (2.7)	0.55 (0.25-1.20)
	MDADI Summary Scores				
	Composite	**26.4 (18.7)/32.4 (17.2)**	2.02 (0.90-4.50)	**25.7 (18.9)/32.4 (17.1)**	2.26 (0.97-5.25)
	Physical	**30.9 (22.7)/37.4 (20.3)**	**2.41 (1.18-4.91)**	**29.7 (21.7)/37.6 (20.9)**	**2.70 (1.29-5.68)**
	Emotional	25.2 (18.2)/30.6 (18.7)	**2.52 (1.11-5.72)**	**24.6 (18.5)/30.6 (18.4)**	**2.87 (1.20-6.87)**
	Functional	**20.6 (19.4)/26.7 (18.7)**	1.70 (0.73-3.92)	**20.6 (21.4)/26.3 (17.5)**	1.63 (0.69-3.85)
	General	25.9 (30.0)/33.4 (30.8)	1.41 (0.68-2.93)	26.4 (31.1)/32.6 (30.2)	1.25 (0.60-2.64)

Bold entries indicate that mean values are statistically significant ($p \leq 0.05$) according to Mann-Whitney tests, and that odds ratios are statistically significant ($p \leq 0.05$) according to Fisher's Exact tests. Obj.: treatment planning dose objective. OR: odds ratio denoting the odds of moderate/severe responses vs. none/mild responses for doses < Obj. vs. ≥ Obj.

violations exceeding 1 Gy (mean = 1.8 Gy in this cohort subgroup); 8.5% with increases exceeding 2 Gy (mean = 2.8 Gy); and 3.5% with increases exceeding 3 Gy (mean = 3.5 Gy).

Figure 4 shows the modelled risk of patients reporting moderate/severe MDADI physical scores (the most highly reported summary score) ≥1 year post-treatment, with cohort results superimposed. For every 1 Gy increase in delivered dose, the absolute risk of moderate/severe symptom reporting increased by 1.5%. Based on this model, we estimate that if doses were corrected back to planned values, absolute risk of self-reported dysphagia symptoms would decrease by ≥5% in 1.2% of patients. Given that the average absolute risk of self-reported dysphagia is 34.9% (SD = 9.3%), dose corrections may decrease relative risk by ≥5% in 23.3% of patients, ≥10% in 3.5% of patients, and ≥15% in 1.2% of patients. The model fit to MDADI composite scores is comparable, indicating a 1.6% decrease in absolute risk per Gy dose correction.

4 DISCUSSION

In this study, the strong relationship between delivered pharyngeal constrictor dose and patient-reported dysphagia is comparable to planned dose-PRO associations in the literature (37), yet further indicates that ART dose corrections may be beneficial for reducing dysphagia symptoms. In particular, our logistic regression models suggest that ART corrections may decrease the relative risk of patient-reported physical dysphagia symptoms by ≥5% in 23.3% of patients. We consider these estimates to be conservative. By using doses recalculated on the fraction of last CBCT acquisition to estimate total delivered dose, we make the assumption that patient anatomy was consistent with the last CBCT for all fractions; given that systematic changes in patient and tumor anatomy increase with progression through treatment, our calculations provide an upper bound on estimated inter-fractional dose increases. As corresponding increases in toxicity risk are the reciprocal of dose – calculated by dividing by estimated total delivered dose (e.g., probability of a side effect per Gy) – we obtain a conservative, lower estimate for ART-related toxicity reduction. Therefore, in practice, the toxicity-benefit of ART is likely to be greater than that indicated by our results. To demonstrate this, we performed an additional calculation under the assumption that accumulated delivered dose increases are half that estimated by using the last-acquired CBCT (e.g., assuming systematic anatomical changes increase linearly with time): we found that the absolute risk of moderate/severe MDADI physical scores increased by 1.6% per Gy (*vs*. 1.5% per Gy), with 2.3% (*vs*. 1.2%) of patients having a ≥5% absolute decrease in the risk of self-reported dysphagia and 31.4% (*vs*. 23.3%) of patients having a ≥5% relative decrease in risk.

Xerostomia-reduction is a primary focus of head and neck toxicity studies (2, 5, 38–41); however, dysphagia remains a significant toxicity concern affecting oral intake and health-related quality of life more adversely than xerostomia (42–44).

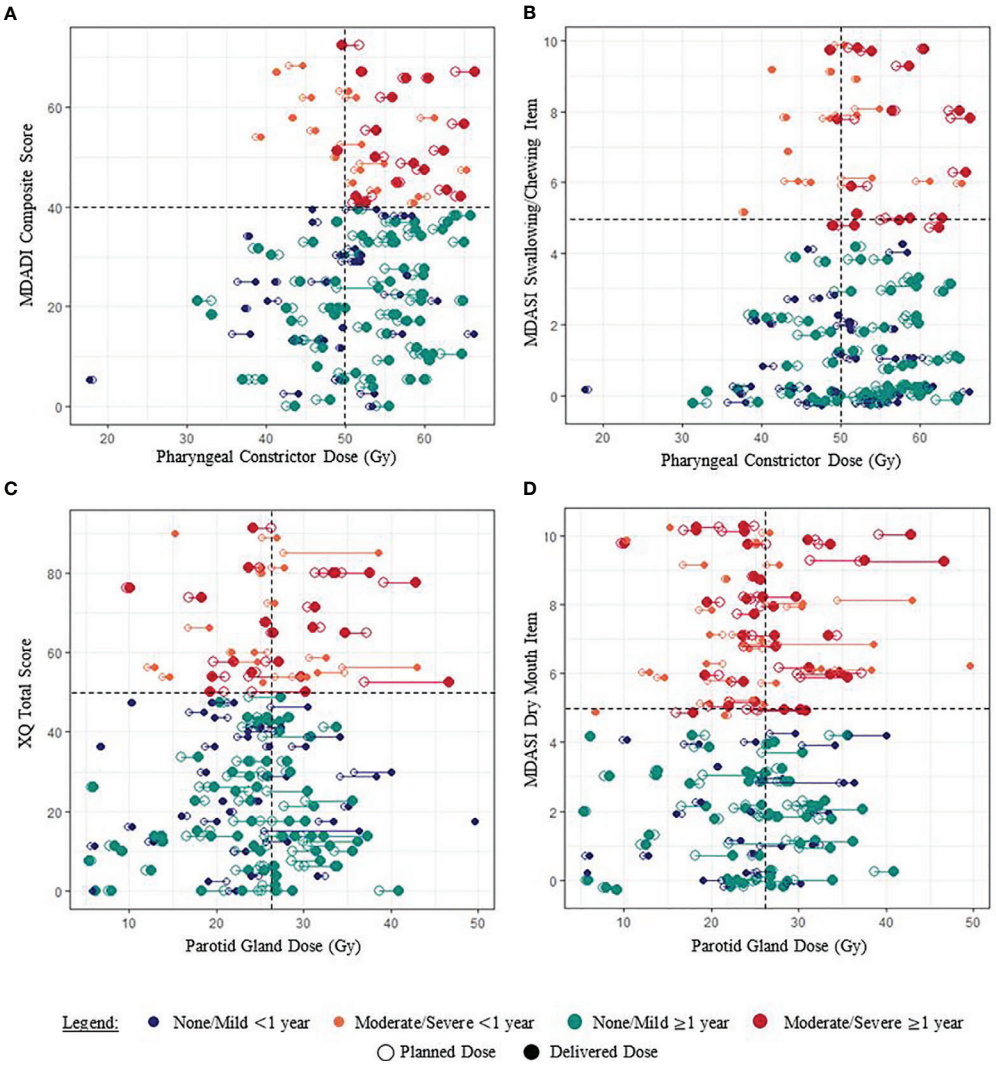

FIGURE 3 | Examples of associations between paired planned and delivered OAR doses and PRO scores for each patient (joined by a horizontal line). **(A, B)** Pharyngeal constrictor doses of patients reporting moderate/severe dysphagia symptoms generally exceeded the planning objective of 50 Gy. **(C, D)** The relationship between parotid gland dose and patient-reported xerostomia symptoms was less clear. Random "jitter" up to ±0.3 has been added to MDASI-HN item scores to better visualize the data.

Dysphagia may result in nutritional deficiencies, weight loss, and feeding tube dependence as well as aspiration causing pneumonia and chronic bronchial inflammation (45). When safe to do so, higher prioritization of the pharyngeal constrictor may further reduce dysphagia symptoms (46). For cases where the pharyngeal constrictor is in close proximity to high dose volumes, as was common for our cohort, ART dose corrections may play an important role in dysphagia reduction.

To select patients for ART pharyngeal constrictor dose corrections, our previous work indicates the importance of pre-treatment information, such as planned OAR doses and CTV volumes, and derives clinical guidelines from machine learning modeling (23). Pre-treatment patient selection may streamline ART workflows by allowing patients to be pre-booked for re-CTs and replanning, as compared to interfractional patient monitoring (e.g., assessing weight loss, decrease in face/neck diameter). While many dose-correction strategies exist in the field (47, 48), the work by Hamming-Vrieze et al. cautions against reducing GTV volumes (49), yet OAR doses may be reduced by correcting shifts in steep dose gradients resulting from anatomical changes.

PROs for our cohort are comparable with the existing literature (28, 29) and physician toxicity assessments (1, 2). Our violation formatting is consistent with QUANTEC and other consensus recommendations with respect to dose parameter types and planning objectives, however, future work may consider alternate dose parameter values and OAR such as submandibular and minor salivary glands. Submandibular glands were contoured for our cohort but were prone to deformable image registration errors in

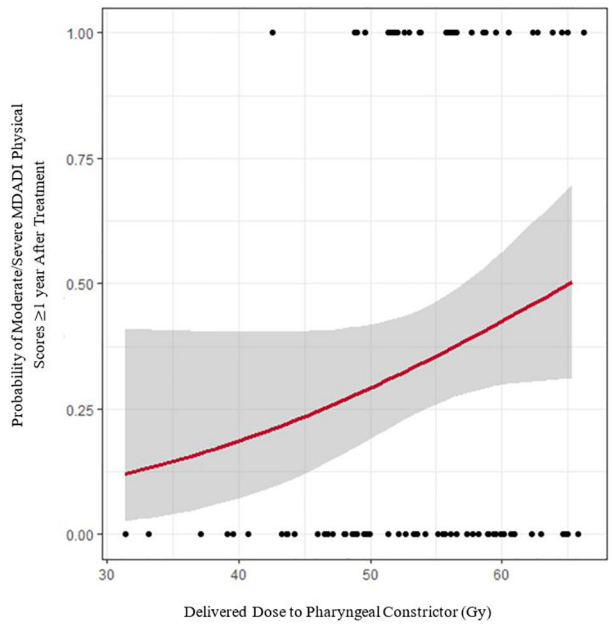

FIGURE 4 | Logistic regression model of delivered pharyngeal constrictor dose versus moderate/severe MDADI physical responses persisting ≥ 1 year after treatment (red line). Grey error bands indicate the 95% confidence interval. Black dots denote raw cohort data.

our dose estimation workflow, making delivered dose estimates unreliable in these structures (23). The literature indicates that while mean salivary gland dose is strongly associated with saliva flow rates and physician reporting, it is only weakly associated with XQ results ≥12 months post-treatment (38) and may have contributed to the lack of dose-xerostomia associations for our cohort. Although not available for this cohort, OAR sub-contours may further refine dose-PRO associations and ART practices; the literature indicates that the superior pharyngeal constrictors are more strongly associated with late dysphagia (50), with the middle pharyngeal constrictors more strongly associated with acute dysphagia (50) and aspiration (51). Collecting PROs during the course of radiotherapy may build upon known associations between oral cavity dose, mucositis, and quality of life (52, 53).

Limitations of this study include a lack of baseline PRO measures and longitudinal data. We focus on doses to OAR that are most strongly associated with a given toxicity; however, salivary gland dose may further clarify dose-dysphagia associations (54). In estimating the potential benefit of correcting dose violations we make a conservative assumption that OARs may be corrected back to planned values (9). It is possible that corrective gains may be greater in this regard as well (9).

Future work on a larger study cohort may further investigate dose-PRO associations specific to head and neck tumor subsites (e.g., oropharyngeal *vs*. nasopharyngeal disease). We did not observe any statistically significant differences in PRO scores for this cohort with cancer subsite, which may be partially attributed to the similarity of prophylactic nodal volumes among patients of different subsites. As a result, we combined all head and neck cancer subsites into a single analysis; however, subtle differences among subsite groups may exist.

DATA AVAILABILITY STATEMENT

The datasets presented in this article are not readily available because of the conditions of ethics approval. Requests to access the datasets should be directed to Sarah.Weppler@albertahealthservices.ca.

ETHICS STATEMENT

The studies involving human participants were reviewed and approved by the Health Research Ethics Board of Alberta Cancer Committee. The patients/participants provided their written informed consent to participate in this study.

AUTHOR CONTRIBUTIONS

Overall study design was jointly proposed by SW, WS, CS, and HQ. SW and HQ coordinated data collection, including ethics approvals and survey circulation, assisted by AY and NH. SW performed data clustering, statistical analyses, and linear regression model development. LB provided guidance on the analysis of patient-reported outcomes data. SW prepared the initial manuscript with WS, CS, HQ, and LB. All authors contributed to the article and approved the submitted version.

FUNDING

This work was supported in part by the Natural Sciences and Engineering Research Council of Canada – Canada Graduate Scholarship (CGS-D) to SW, and the Calgary Foundation - Cadmus Fund.

ACKNOWLEDGMENTS

The authors would like to thank Demetra Yannitsos, MPH, of the Tom Baker Cancer Centre for providing a foundational literature review for this study. Thank you also to Vicki Tran, of the University of Calgary, and Peter Chen, of the University of Alberta, for their assistance with survey collection.
An earlier version of this study was included in the first author's PhD thesis (55), completed at the University of Calgary, Canada.

SUPPLEMENTARY MATERIAL

The Supplementary Material for this article can be found online at: https://www.frontiersin.org/articles/10.3389/fonc.2021.759724/full#supplementary-material

REFERENCES

1. Kamal M, Mohamed ASR, Volpe S, Zaveri J, Barrow MP, Gunn GB, et al. Radiotherapy Dose–Volume Parameters Predict Videofluoroscopy-Detected Dysphagia Per DIGEST After IMRT for Oropharyngeal Cancer: Results of a Prospective Registry. *Radiother Oncol* (2018) 128:442–51. doi: 10.1016/j.radonc.2018.06.013
2. Nutting CM, Morden JP, Harrington KJ, Urbano TG, Bhide SA, Clark C, et al. Parotid-Sparing Intensity Modulated Versus Conventional Radiotherapy in Head and Neck Cancer (PARSPORT): A Phase 3 Multicentre Randomised Controlled Trial. *Lancet Oncol* (2011) 12:127–36. doi: 10.1016/S1470-2045(10)70290-4
3. Barker JL, Garden AS, Ang KK, O'Daniel JC, Wang H, Court LE, et al. Quantification of Volumetric and Geometric Changes Occurring During Fractionated Radiotherapy for Head-and-Neck Cancer Using an Integrated CT/linear Accelerator System. *Int J Radiat Oncol Biol Phys* (2004) 59:960–70. doi: 10.1016/j.ijrobp.2003.12.024
4. Ahn PH, Chen CC, Ahn AI, Hong L, Scripes PG, Shen J, et al. Adaptive Planning in Intensity-Modulated Radiation Therapy for Head and Neck Cancers: Single-Institution Experience and Clinical Implications. *Int J Radiat Oncol Biol Phys* (2011) 80:677–85. doi: 10.1016/j.ijrobp.2010.03.014
5. Brouwer CL, Steenbakkers RJHM, Langendijk JA, Sijtsema NM. Identifying Patients Who may Benefit From Adaptive Radiotherapy: Does the Literature on Anatomic and Dosimetric Changes in Head and Neck Organs at Risk During Radiotherapy Provide Information to Help? *Radiother Oncol* (2015) 115:285–94. doi: 10.1016/j.radonc.2015.05.018
6. Castelli J, Simon A, Lafond C, Perichon N, Rigaud B, Chajon E, et al. Adaptive Radiotherapy for Head and Neck Cancer. *Acta Oncol* (2018) 57:1284–92. doi: 10.1080/0284186X.2018.1505053
7. Chaturvedi AK, Engels EA, Pfeiffer RM, Hernandez BY, Xiao W, Kim E, et al. Human Papillomavirus and Rising Oropharyngeal Cancer Incidence in the United States. *J Clin Oncol* (2011) 29:4294–301. doi: 10.1200/JCO.2011.36.4596
8. Ang KK, Harris J, Wheeler R, Weber R, Rosenthal DI, Nguyen-Tân PF, et al. Human Papillomavirus and Survival of Patients With Oropharyngeal Cancer. *N Engl J Med* (2010) 363:24–35. doi: 10.1056/NEJMoa0912217
9. Heukelom J, Fuller CD. Head and Neck Cancer Adaptive Radiation Therapy (ART): Conceptual Considerations for the Informed Clinician. *Semin Radiat Oncol* (2019) 29:258–73. doi: 10.1016/j.semradonc.2019.02.008
10. Falchook AD, Green R, Knowles ME, Amdur RJ, Mendenhall W, Hayes DN, et al. Comparison of Patient- and Practitioner-Reported Toxic Effects Associated With Chemoradiotherapy for Head and Neck Cancer. *JAMA Otolaryngol Head Neck Surg* (2016) 142:517–23. doi: 10.1001/jamaoto.2016.0656
11. Jensen K, Bonde Jensen A, Grau C. The Relationship Between Observer-Based Toxicity Scoring and Patient Assessed Symptom Severity After Treatment for Head and Neck Cancer. A Correlative Cross Sectional Study of the DAHANCA Toxicity Scoring System and the EORTC Quality of Life Questionnaire. *Radiother Oncol* (2006) 78:298–305. doi: 10.1016/j.radonc.2006.02.005
12. Hunter KU, Schipper M, Feng FY, Lyden T, Haxer M, Murdoch-Kinch CA, et al. Toxicities Affecting Quality of Life After Chemo-IMRT of Oropharyngeal Cancer: Prospective Study of Patient-Reported, Observer-Rated, and Objective Outcomes. *Int J Radiat Oncol Biol Phys* (2013) 85:935–40. doi: 10.1016/j.ijrobp.2012.08.030
13. Cleeland CS, Mendoza TR, Wang XS, Chou C, Harle MT, Morrissey M, et al. Assessing Symptom Distress in Cancer Patients: The M. D. Anderson Symptom Inventory. *Cancer* (2000) 89:1634–46. doi: 10.1002/1097-0142(20001001)89:7<1634::AID-CNCR29>3.0.CO;2-V
14. Rosenthal D, Mendoza T, Chambers M, Asper J, Gning I, Kies M, et al. Measuring Head and Neck Cancer Symptom Burden: The Development and Validation of the M.D. Anderson Symptom Inventory, Head and Neck Module. *Head Neck* (2007) 29:923–31. doi: 10.1002/hed.20602
15. Chen AY, Frankowshi R, Bishop-Leone J, Hebert T, Leyk S, Lewin J, et al. The Development and Validation of a Dysphagia-Specific Quality-of-Life Questionnaire for Patients With Head and Neck Cancer: The M. D. Anderson Dysphagia Inventory. *Arch Otolaryngol Head Neck Surg* (2001) 127:870–6.
16. Eisbruch A, Kim HM, Terrell JE, Marsh LH, Dawson LA, Ship JA. Xerostomia and Its Predictors Following Parotid-Sparing Irradiation of Head-and-Neck Cancer. *Int J Radiat Oncol Biol Phys* (2001) 50:695–704. doi: 10.1016/S0360-3016(01)01512-7
17. Ojo B, Genden EM, Teng MS, Milbury K, Misiukiewicz KJ, Badr H. A Systematic Review of Head and Neck Cancer Quality of Life Assessment Instruments. *Oral Oncol* (2012) 48:923–37. doi: 10.1016/j.oraloncology.2012.03.025
18. Mayo C, Yorke E, Merchant TE. Radiation Associated Brainstem Injury. *Int J Radiat Oncol Biol Phys* (2010) 76:36–41. doi: 10.1016/j.ijrobp.2009.08.078
19. Kirkpatrick JP, van der Kogel AJ, Schultheiss TE. Radiation Dose-Volume Effects in the Spinal Cord. *Int J Radiat Oncol Biol Phys* (2010) 76:42–9. doi: 10.1016/j.ijrobp.2009.04.095
20. Deasy JO, Moiseenko V, Marks L, Chao KSC, Nam J, Eisbruch A. Radiotherapy Dose-Volume Effects on Salivary Gland Function. *Int J Radiat Oncol Biol Phys* (2010) 76:58–63. doi: 10.1016/j.ijrobp.2009.06.090
21. Moiseenko V, Wu J, Hovan A, Saleh Z, Apte A, Deasy JO, et al. Treatment Planning Constraints to Avoid Xerostomia in Head-and-Neck Radiotherapy: An Independent Test of QUANTEC Criteria Using a Prospectively Collected Dataset. *Int J Radiat Oncol Biol Phys* (2012) 82:1108–14. doi: 10.1016/j.ijrobp.2011.04.020
22. Rancati T, Schwarz M, Allen AM, Feng F, Popovtzer A, Mittal B, et al. Radiation Dose-Volume Effects in the Larynx and Pharynx. *Int J Radiat Oncol Biol Phys* (2010) 76:64–9. doi: 10.1016/j.ijrobp.2009.03.079
23. Weppler S, Quon H, Schinkel C, Ddamba J, Harjai N, Vigal C, et al. Determining Clinical Patient Selection Guidelines for Head and Neck Adaptive Radiation Therapy Using Random Forest Modelling and a Novel Simplification Heuristic. *Front Oncol* (2021) 11:650335. doi: 10.3389/fonc.2021.650335
24. Weppler S, Schinkel C, Kirkby C, Smith W. Data Clustering to Select Clinically-Relevant Test Cases for Algorithm Benchmarking and Characterization. *Phys Med Biol* (2020) 65(5):1–12. doi: 10.1088/1361-6560/ab6e54
25. Brock KK, Mutic S, McNutt TR, Li H, Kessler ML. Use of Image Registration and Fusion Algorithms and Techniques in Radiotherapy: Report of the AAPM Radiation Therapy Committee Task Group No. 132: Report. *Med Phys* (2017) 44:e43–76. doi: 10.1002/mp.12256
26. Lim TY, Gillespie E, Murphy J, Moore KL. Clinically Oriented Contour Evaluation Using Dosimetric Indices Generated From Automated Knowledge-Based Planning. *Int J Radiat Oncol Biol Phys* (2019) 103:1251–60. doi: 10.1016/j.ijrobp.2018.11.048
27. Townes TG, Navuluri S, Pytynia KB, Gunn GB, Kamal MJ, Gilmore KR, et al. Assessing Patient-Reported Symptom Burden of Long-Term Head and Neck Cancer Survivors at Annual Surveillance in Survivorship Clinic. *Head Neck* (2020) 42:1919–27. doi: 10.1002/hed.26119
28. Eraj SA, Jomaa MK, Rock CD, Mohamed ASR, Smith BD, Smith JB, et al. Long-Term Patient Reported Outcomes Following Radiation Therapy for Oropharyngeal Cancer: Cross-Sectional Assessment of a Prospective Symptom Survey in Patients ≥65 Years Old. *Radiat Oncol* (2017) 12:1–10. doi: 10.1186/s13014-017-0878-9
29. Gunn GB, Hansen CC, Garden AS, Fuller CD, Mohamed ASR, Morrison WH, et al. Favorable Patient Reported Outcomes Following IMRT for Early Carcinomas of the Tonsillar Fossa: Results From a Symptom Assessment Study. *Radiother Oncol* (2015) 117:132–8. doi: 10.1016/j.radonc.2015.09.007
30. Chen PH, Golub JS, Hapner ER, Johns MM. Prevalence of Perceived Dysphagia and Quality-of-Life Impairment in a Geriatric Population. *Dysphagia* (2009) 24:1–6. doi: 10.1007/s00455-008-9156-1
31. Ortigara GB, Schulz RE, Soldera EB, Bonzanini LIL, Danesi CC, Antoniazzi RP, et al. Association Between Trismus and Dysphagia-Related Quality of Life in Survivors of Head and Neck Cancer in Brazil. *Oral Surg Oral Med Oral Pathol Oral Radiol* (2019) 128:235–42. doi: 10.1016/j.oooo.2019.05.009
32. Hutcheson K, Portwood M, Lisec A, Barringer D, Gries K, Lewin J. What Is a Clinically Relevant Difference in MDADI Scores Between Groups of Head and Neck Cancer Patients? *Laryngoscope* (2016) 126:1108–13. doi: 10.1002/lary.25778
33. Benjamini Y, Hochberg Y. Controlling the False Discovery Rate: A Practical and Powerful Approach to Multiple Testing. *J R Stat Soc Ser B* (1995) 57:289–300. doi: 10.1111/j.2517-6161.1995.tb02031.x

34. James G, Witten D, Hastie T, Tibshirani R. *An Introduction to Statistical Learning With Applications in R*. New York, NY: Springer (2013).
35. Memtsa P-T, Tolia M, Tzitzikas I, Bizakis J, Pistevou-Gombaki K, Charalambidou M, et al. Assessment of Xerostomia and Its Impact on Quality of Life in Head and Neck Cancer Patients Undergoing Radiation Therapy. *Mol Clin Oncol* (2017) 6:789–93. doi: 10.3892/mco.2017.1200
36. Petkar I, Bhide S, Newbold K, Harrington K, Nutting C. Dysphagia-Optimised Intensity-Modulated Radiotherapy Techniques in Pharyngeal Cancers: Is Anyone Going to Swallow It? *Clin Oncol* (2017) 29:e110–8. doi: 10.1016/j.clon.2017.02.002
37. Levendag PC, Teguh DN, Voet P, van der Est H, Noever I, de Kruijf WJM, et al. Dysphagia Disorders in Patients With Cancer of the Oropharynx Are Significantly Affected by the Radiation Therapy Dose to the Superior and Middle Constrictor Muscle: A Dose-Effect Relationship. *Radiother Oncol* (2007) 85:64–73. doi: 10.1016/j.radonc.2007.07.009
38. Miah AB, Gulliford SL, Clark CH, Bhide SA, Zaidi SH, Newbold KL, et al. Dose-Response Analysis of Parotid Gland Function: What Is the Best Measure of Xerostomia? *Radiother Oncol* (2013) 106:341–5. doi: 10.1016/j.radonc.2013.03.009
39. Little M, Schipper M, Feng FY, Vineberg K, Cornwall C, Murdoch-Kinch CA, et al. Reducing Xerostomia After Chemo-IMRT for Head-and-Neck Cancer: Beyond Sparing the Parotid Glands. *Int J Radiat Oncol Biol Phys* (2012) 83:1007–14. doi: 10.1016/j.ijrobp.2011.09.004
40. Morgan H, Sher D. Adaptive Radiotherapy for Head and Neck Cancer. *Cancers Head Neck* (2020) 5:1–16. doi: 10.1186/s41199-019-0046-z
41. Yang H, Hu W, Wang W, Chen P, Ding W, Luo W. Replanning During Intensity Modulated Radiation Therapy Improved Quality of Life in Patients With Nasopharyngeal Carcinoma. *Int J Radiat Oncol Biol Phys* (2013) 85:e47–54. doi: 10.1016/j.ijrobp.2012.09.033
42. Kamal M, Barrow MP, Lewin JS, Estrella A, Gunn GB, Shi Q, et al. Modeling Symptom Drivers of Oral Intake in Long-Term Head and Neck Cancer Survivors. *Support Care Cancer* (2019) 27:1405–15. doi: 10.1007/s00520-018-4434-4
43. Langendijk JA, Doornaert P, Verdonck-de Leeuw IM, Leemans CR, Aaronson NK, Slotman BJ. Impact of Late Treatment-Related Toxicity on Quality of Life Among Patients With Head and Neck Cancer Treated With Radiotherapy. *J Clin Oncol* (2008) 26:3770–6. doi: 10.1200/JCO.2007.14.6647
44. Ramaekers BLT, Joore MA, Grutters JPC, van den Ende P, de JJ, Houben R, et al. The Impact of Late Treatment-Toxicity on Generic Health-Related Quality of Life in Head and Neck Cancer Patients After Radiotherapy. *Oral Oncol* (2011) 47:768–74. doi: 10.1016/j.oraloncology.2011.05.012
45. Strojan P, Hutcheson KA, Eisbruch A, Beitler JJ, Langendijk JA, Lee AWM, et al. Treatment of Late Sequelae After Radiotherapy for Head and Neck Cancer. *Cancer Treat Rev* (2017) 59:79–92. doi: 10.1016/j.ctrv.2017.07.003
46. Nutting C, Rooney K, Foran B, Pettit L, Beasley M, Finneran L, et al. Results of a Randomized Phase III Study of Dysphagia-Optimized Intensity Modulated Radiotherapy (Do-IMRT) Versus Standard IMRT (S-IMRT) in Head and Neck Cancer. *J Clin Oncol* (2020) 38:6508–8. doi: 10.1200/JCO.2020.38.15_suppl.6508
47. Bahig H, Yuan Y, Mohamed ASR, Brock KK, Ng SP, Wang J, et al. Magnetic Resonance-Based Response Assessment and Dose Adaptation in Human Papilloma Virus Positive Tumors of the Oropharynx Treated With Radiotherapy (MR-ADAPTOR): An R-IDEAL Stage 2a-2b/Bayesian Phase II Trial. *Clin Trans Radiat Oncol* (2018) 13:19–23. doi: 10.1016/j.ctro.2018.08.003
48. Heukelom J, Hamming O, Bartelink H, Hoebers F, Giralt J, Herlestam T, et al. Adaptive and Innovative Radiation Treatment FOR Improving Cancer Treatment outcomE (ARTFORCE); a Randomized Controlled Phase II Trial for Individualized Treatment of Head and Neck Cancer. *BMC Cancer* (2013) 13:1. doi: 10.1186/1471-2407-13-84
49. Hamming-Vrieze O, van Kranen SR, Heemsbergen WD, Lange CAH, van den Brekel MWM, Verheij M, et al. Analysis of GTV Reduction During Radiotherapy for Oropharyngeal Cancer: Implications for Adaptive Radiotherapy. *Radiother Oncol* (2017) 122:224–8. doi: 10.1016/j.radonc.2016.10.012
50. Mazzola R, Ricchetti F, Fiorentino A, Fersino S, Giaj Levra N, Naccarato S, et al. Dose-Volumerelated Dysphagia After Constrictor Muscles Definition in Head and Neck Cancer Intensitymodulated Radiation Treatment. *Br J Radiol* (2014) 87:1–10. doi: 10.1259/bjr.20140543
51. Söderström K, Nilsson P, Laurell G, Zackrisson B, Jäghagen EL. Dysphagia – Results From Multivariable Predictive Modelling on Aspiration From a Subset of the ARTSCAN Trial. *Radiother Oncol* (2017) 122:192–9. doi: 10.1016/j.radonc.2016.09.001
52. Mazzola R, Ricchetti F, Fersino S, Fiorentino A, Giaj Levra N, di Paola G, et al. Predictors of Mucositis in Oropharyngeal and Oral Cavity Cancer in Patients Treated With Volumetric Modulated Radiation Treatment: A Dose-Volume Analysis. *Head Neck* (2016) 38:E815–9. doi: 10.1002/hed.24106
53. Franco P, Martini S, di Muzio J, Cavallin C, Arcadipane F, Rampino M, et al. Prospective Assessment of Oral Mucositis and Its Impact on Quality of Life and Patient-Reported Outcomes During Radiotherapy for Head and Neck Cancer. *Med Oncol* (2017) 34:1–8. doi: 10.1007/s12032-017-0950-1
54. van der Laan BFAM, van der Laan HP, Bijl HP, Steenbakkers RJHM, van der Schaaf A, Chouvalova O, et al. Acute Symptoms During the Course of Head and Neck Radiotherapy or Chemoradiation Are Strong Predictors of Late Dysphagia. *Radiother Oncol* (2015) 115:56–62. doi: 10.1016/j.radonc.2015.01.019
55. Weppler S. J. Artificial Intelligence to Advance Adaptive Radiation Therapy (Unpublished doctoral thesis). University of Calgary, Calgary, AB (2020).

Conflict of Interest: The authors declare that the research was conducted in the absence of any commercial or financial relationships that could be construed as a potential conflict of interest.

frontiers in Oncology

ORIGINAL RESEARCH
published: 28 October 2021
doi: 10.3389/fonc.2021.736690

Stereotactic Body Radiation Therapy for Oligometastatic Breast Cancer: A Retrospective Multicenter Study

*Pauline Lemoine[1,2], Marie Bruand[3], Emmanuel Kammerer[4], Emilie Bogart[5], Pauline Comte[6], Philippe Royer[3], Juliette Thariat[4,7,8] and David Pasquier[1,2,9]**

[1] Academic Department of Radiation Oncology, O. Lambret Center, Lille, France, [2] University of Lille, H. Warembourg School of Medicine, Lille, France, [3] Department of Radiation Therapy, Lorraine Institute of Oncology, Nancy, France, [4] Department of Radiation Oncology, Centre Francois Baclesse, Caen, France, [5] Biostatistics department, Oscar Lambret Center, Lille, France, [6] Department of Medical Physics, O. Lambret Center, Lille, France, [7] Advanced Resource Centre for Hadrontherapy (ARCHADE Research Community), Caen, France, [8] Laboratory of High-Energy Particle Physics, Institut National de Physique Nucléaire et de Physique des Particules, The National Engineering School of Caen (IN2P3/ENSICAEN), CNRS UMR 6534—Normandy University, Caen, France, [9] CRIStAL (Centre de Recherche en Informatique, Signal et Automatique de Lille [Research center in Computer Science, Signal and Automatic Control of Lille] UMR 9189, Lille University, Lille, France

OPEN ACCESS

Edited by:
Dwight E Heron, Bon Secours Health System, United States

Reviewed by:
Anand Mahadevan, Geisinger Health System, United States
John Austin Vargo, University of Pittsburgh Medical Center, United States
Alina Mihaela Mihai, Beacon Hospital, Ireland

***Correspondence:**
David Pasquier
d-pasquier@o-lambret.fr

Specialty section:
This article was submitted to Radiation Oncology, a section of the journal Frontiers in Oncology

Received: *05 July 2021*
Accepted: *14 October 2021*
Published: *28 October 2021*

Citation:
Lemoine P, Bruand M, Kammerer E, Bogart E, Comte P, Royer P, Thariat J and Pasquier D (2021) Stereotactic Body Radiation Therapy for Oligometastatic Breast Cancer: A Retrospective Multicenter Study. Front. Oncol. 11:736690. doi: 10.3389/fonc.2021.736690

Introduction: Stereotactic radiotherapy may improve the prognosis of oligometastatic patients. In the literature, there is very little data available that is specific to breast cancer.

Materials and Methods: We conducted a multicenter retrospective study. The primary objective was to estimate progression-free survival after stereotactic body radiotherapy (SBRT) using Cyberknife of breast cancer oligometastases. The secondary objectives were to estimate overall survival, local control, and toxicity. The inclusion criteria were oligometastatic breast cancer with a maximum of five lesions distributed in one to three different organs, diagnosed on PET/CT and/or MRI, excluding brain metastases and oligoprogressions. This was combined with systemic medical treatment.

Findings: Forty-four patients were enrolled from 2007 to 2017, at three high-volume cancer centers. The patients mostly had one to two lesion(s) whose most widely represented site was bone (24 lesions or 44.4%), particularly in the spine, followed by liver (22 lesions or 40.7%), then pulmonary lesions (six lesions or 11.1%). The primary tumor expressed estrogen receptors in 33 patients (84.6%); the status was HER2+++ in 7 patients (17.9%). The median dose was 40 Gy (min-max: 15-54) prescribed at 80% isodose, the median number of sessions was three (min-max: 3-10). The median D50% was 42 Gy (min max 17-59). After a median follow-up of 3.4 years, progression-free survival (PFS) at one year, two years, and three years was 81% (95% CI: 66-90%), 58% (95% CI: 41-72%), and 45% (95% CI: 28-60%), respectively. The median PFS was 2.6 years (95% CI: 1.3 – 4.9). Overall survival at three years was 81% (95% CI: 63-90%). The local control rate at two and three years was 100%. Three patients (7.3%) experienced G2 acute toxicity, no grade ≥3 toxicity was reported.

Conclusion: The PFS of oligometastatic breast cancer patients treated with SBRT appears long, with low toxicity. Local control is high. SBRT for oligometastases is rarely applied in breast cancer in light of the population in our study. Phase III studies are ongoing.

Keywords: breast cancer, oligometastatic, stereotactic body radiotherapy (SBRT), Metastasis-directed therapy, progression free survival

INTRODUCTION

In women breast cancer ranks first in new cases of cancer and is the leading cause of cancer death (1). The concept of oligometastasis was described in 1995 as an intermediate stage between localized versus generalized disease, in which tumor extension is limited to a small number of metastases, generally less than five, commonly with one to two organ(s) affected (2). The *ESO-ESMO international consensus guidelines for advanced breast cancer (ABC 5)* (3) allows for, on the other hand, a maximum of five lesions to define oligometastatic disease, regardless of the number of organs affected. In breast cancer, this stage accounts for 1 to 3% of patients, even if the figures are not sufficiently representative (4).

Recently the ESTRO and EORTC have proposed a nomenclature for *de novo* recurrent or treatment-induced oligometastatic disease; this nomenclature must be validated in clinical trials or registries (5). Currently, the goal of local treatment for oligometastatic disease is to prevent the evolution of genetically unstable clones and to prevent further metastatic spread. The use of focal ablative therapies could potentially delay the introduction of systemic therapy, allow for a treatment pause in the case of fully controlled disease, or avoid an early change in treatment line.

The currently available focal therapies include surgery, which is the historical treatment for this condition, percutaneous thermal ablation, and radiation therapy. In the surgical series (6, 7), resections of secondary pulmonary or hepatic lesions were the most frequently performed surgeries in oligometastatic breast.

Regarding radiation therapy, occasional trials with generally small sample sizes have assessed the contribution of radiation therapy to the management of oligometastatic breast cancer. We can identify the prospective trial by Milano et al. (8), which enrolled 121 patients, including 39 cases of breast cancer. In 2018, Scorsetti et al. (9) enrolled 61 patients, including 11 cases of breast cancer. Among the published prospective studies, two trials conducted by Trovo et al. (10) and Milano et al. (11) in 2018 focused exclusively on breast cancer. They enrolled 54 and 48 patients, respectively. Two years progression free survival was 53% and 52% in these two trials respectively (8, 10).

The use of stereotactic radiotherapy will allow for the delivery of a high dose to the target for the purpose of ablation, while preserving more of the surrounding healthy tissue. Currently, the standard-of-care for oligometastatic disease in breast cancer is the use of systemic therapy, but the role of ablative therapies has not yet been clearly defined. The purpose of our study is to evaluate the contribution of stereotactic body radiotherapy to the management of breast cancer oligometastases in three high-volume Cancer Centers.

MATERIALS AND METHODS

Trial Design and Patients

We conducted a multicenter retrospective cohort. Patients were enrolled from 2007 to 2017, at three cancer centers that participated in this study: the Lille Oscar Lambret Center, the Caen François Baclesse Center, and the Nancy Lorraine Institute of Oncology.

The inclusion criteria were patients over 18 years of age, managed for extra-cranial oligometastatic breast cancer with a maximum of five lesions distributed in one to three different organ(s), diagnosed by Computed Tomography (CT) in 24 patients (57,1%), Positon Emission Tomography - CT (PET-CT) in 28 patients (66,7%), and/or Magnetic Resonance Imaging (MRI) in 20 patients (47,6%). A bone scan was performed in 9 patients (21,4%). Histological confirmation was available in 21 patients (48.8%).

The exclusion criteria were patients with diffuse metastatic or oligoprogressive disease after chemotherapy, brain metastases, patients who received non-stereotactic radiation therapy, and patients treated with stereotactic radiation therapy after a metastasectomy or a local cementoplasty procedure.

Treatment

The treatment was conducted using Cyberknife stereotactic radiotherapy from 2007 to 2017. Moving targets such as liver lesions were tracked by the "Synchrony" software, which allows the lesion to be tracked by placing fiducials near the tumour. For bone lesions, the patient was positioned using the "Xsight Spine" mode. This could be combined with systemic medical treatment (hormone therapy or chemotherapy more or less anti HER 2 therapy).

Outcomes and Assessments

The primary endpoint was the progression-free survival (PFS) defined as the time interval from the start of SBRT to the date of the recurrence, or death from any cause. Patients alive without recurrence were censored at the date of last contact. The recurrences were identified by imaging. The secondary endpoints included overall survival (OS), local control and toxicity. OS was defined as the time interval from the start of

SBRT until death from any cause. Patients alive were censored at the date of last contact. Local control was defined as the time interval from the start of SBRT to the date of the first local recurrence or other any recurrences, death from any cause were considered as a competitive event. The toxicities were graded using NCI-CTCAE scale in each centre by an experienced radiation oncologist. Severe toxicities were defined as ≥ grade 2 toxicities. Acute versus late toxicities were defined as toxicities occurring before or after 3 months after the end of treatment.

Statistical Considerations

Conventional descriptive statistical methods (percentages, 95% confidence intervals, means, standard deviations, medians and ranges) were used to describe the patients characteristics and outcomes. The median follow-up and its interquartiles ranges was estimated by Schemper's method (inversed Kaplan Meier). PFS and OS curves were estimated by the Kaplan Meier method. The survival rates with its associated 95% confidence intervals were estimated at 1 year, 2 years and 3 years. The percentage of patients who experienced toxicity was estimated overall as well as for acute and late toxicities. All statistical analyses were performed using Stata® software, version 15.0 (StataCorp LLC College Station, USA).

RESULTS

Forty-four patients were enrolled. Their characteristics are presented in **Table 1**. Nineteen patients (52.8%) had systemic treatment, of which 13 received hormone therapy and 6 received chemotherapy. Data were missing for 8 patients.

The median follow-up of patients was 3.4 years with a 95% CI of 2.67-4.43 years.

The patients mostly had one to two lesion(s) whose most widely represented site was bone (24 lesions or 44.4%), particularly in the spine, followed by liver (22 lesions or 40.7%), then pulmonary lesions (6 lesions or 11.1%). The primary tumor expressed estrogen receptors in 33 patients (84.6%); the status was HER2+++ in 7 patients (17.9%). The median dose was 40 Gy (min-max: 15-54) prescribed at 80% isodose, the median number of sessions was three (min-max: 3-10). The median D50% was

TABLE 1 | Demographics and baseline characteristics.

Characteristics (N = 44).	n	%	Characteristics (N = 44)	n	%
Center			**pT stage (MD=9)**		
Lille	22	50.0%	pT1a	4	11.4%
Nancy	15	34.1%	pT1c	8	22.9%
Caen	7	15.9%	pT2	16	45.7%
			pT3	7	20.0%
Age at diagnosis (MD=1)					
Median (range)	51	(31.0;79.0)	**pN stage (MD=8)**		
Average/standard deviation	53.4	12	pN0	13	36.1%
			pN1	16	44.4%
Histological type (MD=1)			pN2a	4	11.1%
NST	35	81.4%	pN3	3	8.3%
ILC	7	16.3%			
Other	1	2.3%	**HR Status (MD=5)**		
			ER+ PR+	23	59.0%
cT stage (MD=13)			ER+ PR-	10	25.6%
cT1a	1	3.2%	ER- PR-	6	15.4%
cT1c	5	16.1%			
cT2	12	38.7%	**HER2 status**		
cT3	12	38.7%	Negative	32	82.1%
cT4	1	3.2%	Positive	7	17.9%
cN stage (MD=14)			**Grade (MD=7)**		
cN0	15	50.0%	1	3	8.1%
cN1	12	40.0%	2	24	64.9%
cN3	2	6.7%	3	10	27.0%
cNx	1	3.3%			
			Ki-67% (MD=21)		
cM stage (MD=7)			Median - (range)	20	(3.0;90.0)
M0	16	43.2%	Average/standard deviation	22.8	18.3
M1	21	56.8%			
			Vascular emboli (MD=18)	11	42.30%
Systemic treatment (MD=8)	19	52,8%			
Chemotherapy	6	16,7%			
Hormonotherapy.	13	36,1%			

With MD, missing data; stage c, clinical stage; stage p, pathological stage; T, tumor; N, lymph node; M, metastasis; NST, no special type; ILC, invasive lobular carcinoma [sic]; HR, hormone receptors; ER, estrogen receptors; PR, progesterone receptors, and HER2, human epidermal growth factor receptor type 2.

TABLE 2 | Characteristics of oligometastases treatments.

Characteristics (N = 44)	n	%
SBRT treatment received	**44**	**100.0%**
Number of sessions (MD=1)		
Median - (range)	3	(3.0;10.0)
Average/standard deviation	3.7	1.5
Total dose (Gy) (MD=1)		
Median - (range)	40	(15.0;54.0)
Average/standard deviation	36.6	10.4
Prescription isodose (MD=1)		
Median - (range)	80	(78.0;80.0)
Average/standard deviation	79.9	0.3
PTV D2% (MD=17)		
Median - (range)	49.3	(25.9;62.6)
Average/standard deviation	44.5	11.3
PTV D50% (MD=4)		
Median - (range)	42.4	(17.4;59.1)
Average/standard deviation	39.9	11.7
PTV D98% (MD=21)		
Median - (range)	36	(14.1;50.37)
Average/standard deviation	34.2	10.96

With Gy, Gray; PTV, planning target volume; Dx%, percent receiving dose ≥ x% of the volume (minimum dose covering x% of the concerning volume).

42 Gy (min max: 17-59). The characteristics of the treatments are presented in **Table 2**.

Progression-Free Survival

At follow-up, 24 recurrences were identified, including 17 multimetastatic recurrences and seven oligometastatic recurrences. The latter did not occur at sites previously treated with radiation.

The PFS rate at one year was 81% (95% CI: 66-90%), at two years 58% (95% CI: 41-72%), and at three years 45% (95% CI: 28-60%), with a median of 2.65 years (range 1.28 – 4.87 years) (**Figure 1**).

Overall Survival

At the end of follow-up, 10 of the 44 patients enrolled had died (22.7%); seven from their breast cancer (15.9%) and three from an unknown cause (6.8%).

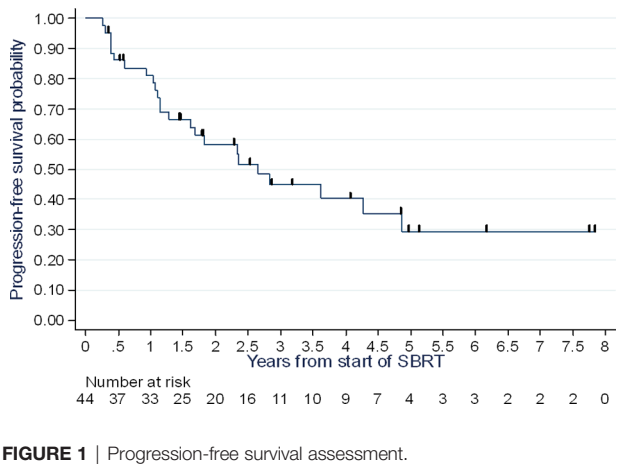

FIGURE 1 | Progression-free survival assessment.

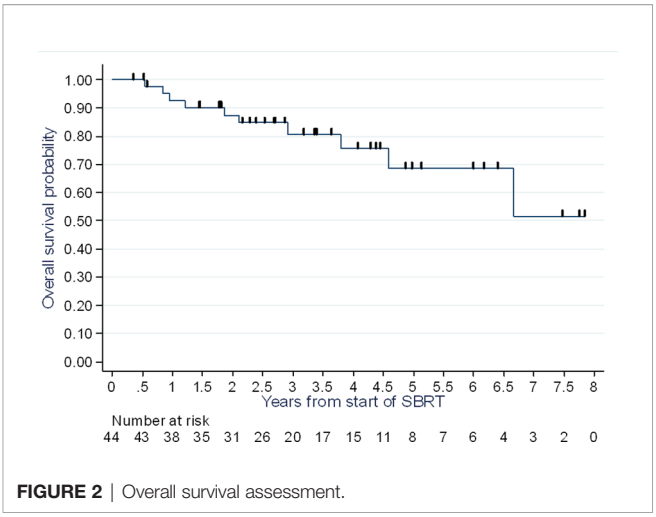

FIGURE 2 | Overall survival assessment.

At one year, two years and three years, the overall survival rate was 93% (95% CI: 79-98%), 87% (95% CI: 72-95%), and 81% (95% CI: 63-90%), respectively (**Figure 2**).

Local Control

Upon analysis of the data, we did not identify any recurrences at the sites treated with radiation, with a median follow-up of 3.4 years [95% CI 2.67-4.43 years].

Toxicity Analysis

Ten patients (24%) experienced a maximum grade 1 acute toxicity and three patients (7%) experienced a grade 2 toxicity. No grade 3 or higher toxicities, either acute or late, were observed (**Table 3**).

DISCUSSION

While the notion of oligometastasis is a relatively new concept and many authors have been interested in it, data specific to breast cancer is scarce in light of its incidence. The sample sizes remain low, and the prospective studies are few. To our knowledge, our study is among the few studies conducted exclusively on stereotactic radiotherapy for breast cancer oligometastases. This is one of the

TABLE 3 | Maximum grade of toxicities per patient.

Toxicity (N=41, MD=3)	n	%
Maximum grade (acute and late)		
No toxicity	28	68.3%
Grade 1	10	24.4%
Grade 2	3	7.3%
Maximum acute grade		
No toxicity	28	68.3%
Grade 1	10	24.4%
Grade 2	3	7.3%
Maximum late grade		
No toxicity	40	97.6%
Unknown grade	1	2.4%

series with the largest population in this context. Indeed, most studies on the subject have heterogeneous populations, with inclusion of several patients with a primary or oligoprogressive disease. In our study, with a median follow-up of 3.4 years (95% CI 2.67-4.43), the PFS rate at two years was 58% (95% CI: 41-72%), and at three years 45% (95% CI: 28-60%), with a median of 2.65 years (range 1.28 – 4.87 years). Local control was 100%, with a median follow-up of 3.4 years [95% CI 2.67-4.43 years]. If we analyze our PFS data compared to prospective and retrospective published series, our results seem to align with them (**Tables 4** and **5**). In the trial by Trovo et al., PFS is evaluated at 75% at one year and 43% at two years with 54 patients enrolled (10). In the subgroup analysis of patients with breast cancer, Milano et al. reported, for 39 cases of breast cancer, a metastasis-free survival at 52% at two years and 36% at six years (11) The strength of our study therefore resides in its homogeneity, as well as the fact that the radiotherapy was exclusively performed in stereotactic conditions, the data from which was reported according to the recommendations in ICRU report 91 (18). However, our population did not allow us to perform subgroup analyses, in particular according to histological type. Indeed, the prognosis for metastatic disease differs based on the histology of the primary lesion. For example, patients with a triple-negative tumor have a worse PFS and overall survival than patients with luminal A or B carcinoma (19), and the potential role of stereotactic radiotherapy in these patients also remains to be determined. Scorsetti et al. report less promising results too due to the inclusion of only pulmonary and hepatic metastases, as well as patients with oligoprogressive disease (17).

The phase 2 randomized trial SABR COMET enrolled 99 varied oligometastatic patients with primary tumors regardless of treatment with stereotactic body radiotherapy; 18 patients had an breast oligometastatic cancer. The mean overall survival was 28 months in the control group and 41 months in the SBRT group (20). Recently, in a prospective registry that included 1,472 patients treated with SBRT for oligometastatic disease, only 78 patients had breast cancer. The local control and metastasis-free survival at two years was respectively 82% (95% CI: 69-90%) and 52% (95% CI: 47-56%) (21). In our series local control was 100%,

TABLE 4 | Review of the literature of retrospective series about SBRT for oligometastases of breast cancer.

Author	Primary	Definition	n patients	Follow-up	OS	PFS	LC
Fumagalli et al. (12)	Indifferent	≤5 sites Lung/Liver	90	1 year	/	27%	84.5%
	(breast=8)			2 years	70%	10%	66.1%
Mahadevan et al. (13)	Indifferent	liver	427	Median	22 months	/	/
	(breast=42)			Breast	21 months	/	/
Bhattacharya et al. (14)	Indifferent	≤3 sites	76	1 year	84.4%	49.1%	/
	(breast=14)			2 years	63.2%	26.2%	/
Onal et al. (15)	Breast	≤5 sites	22	1 year	85%	38%	100% 88%
		Liver		2 years	57%	8%	
Weykamp et al. (16)	Breast	≤3 sites	46	2 years	62%	17%	89%
Our series	Breast	≤5 sites	44	1 year	93%	81%	100%
				2 years	87%	59%	100%
				3 years	81%	45%	100%

With T, follow-up time; OS, overall survival; PFS, progression-free survival; LC, local control; BM, bone metastasis.With T, follow-up time; OS, overall survival; PFS, progression-free survival; LC, local control; BM, bone metastasis.With T, follow-up time; OS, overall survival; PFS, progression-free survival; LC, local control; BM, bone metastasis.

TABLE 5 | Review of the literature of different prospective trials on radiotherapy for oligometastases of breast cancer.

Author	Primary	Design	Definition	n patients	Follow-up	OS	PFS	LC
Milano et al. (8)	Indifferent	Prospective	≤5 sites	121	2 years	50%	/	/
	Breast	Single arm		39	2 years	74%	52%	87%
					6 years	47%	36%	87%
Milano et al. (11)	Breast	Prospective	≤5 sites	48				
		Single arm	BM	12	5 years	83%	/	/
					10 years	75%	/	/
			Non-BM		5 years	31%	/	/
					10 years	17%	/	/
Scorsetti et al. (17)	Breast	Prospective	≤ 3 sites	33	1 year	93%	48%	98%
			Liver/lung		2 years	66%	27%	90%
					3 years	/	/	90%
Scorsetti et al. (9)	Indifferent	Prospective	≤3 sites	61	3 years	33%	/	86.8%
	Breast	Phase II Single arm	Liver	11	5 years	20%	/	86.8%
Trovo et al. (10)	Breast	Prospective	≤5 sites	54	1 year	/	75%	/
		Phase II	SBRT or IMRT		2 years	95%	53%	97%

With OS, overall survival; PFS, progression-free survival; LC, local control; SBRT, stereotactic body radiotherapy; IMRT, intensity modulated radiotherapy; BM, bone metastasis.

probably related to very hypofractionated regimen consistent with low alpha/beta ratio of breast cancer. In SABR COMET the regimen was 30-60 Gy in 3-8 fractions and local progression was a component of failure in 21% of failures in the SBRT arm (20).

Our population, in three high-volume Cancer Centers (a total of approximately 2,900 new patients treated annually for localized breast cancer), may seem small and can be explained in several ways: exclusion of brain metastasis as well as patients with oligoprogressive disease, but also by the fact that oligometastatic patients are rarely referred to radiotherapy and almost exclusively receive a first-line chemotherapy or hormone therapy. Finally, one of the limitations of our study is the retrospective nature, which gives it limited statistical power

These data seem supportive of SBRT in these patients nevertheless the benefit will be specified by ongoing randomized trials. In all these series, including ours, systemic therapy was associated with SBRT, which probably influenced PFS. It's important to note that all ongoing trial evaluating SBRT in these patients compare systemic treatment with or without SBRT. Currently it seems too early to evaluate SBRT without systemic treatment in patients who can benefit from it.

Currently, several phase III trials are open (22), including the trials SABR-COMET (23), STEREO-OS (24), STEREOSEIN (25) and NRG BR002 (26). However, apart from STEREOSEIN and NRG BR002, these prospective "pantumor" trials may not be able to make a conclusion about the value of this strategy based on primary tumor site and tumor phenotype. Trials including a sufficient number of breast cancer patients, classified by histology, will help clarify the potential benefit by molecular subtypes.

SBRT may have a pro-immunogenic effect. The immune response and the combination of this treatment with immunotherapy and the immune response deserve further investigation (27).

CONCLUSION

The current management of oligometastatic breast cancer relies primarily on medical management with systemic therapy. Local treatments such as radiation therapy are used for symptomatic purposes. SBRT for oligometastases is rarely applied in breast cancer in light of the population in our study. In our study, the PFS of oligometastatic breast cancer patients treated with stereotactic body radiotherapy appears long, with low toxicity, whereas systemic treatment may have contributed to PFS. Local control is high. The few published studies seem to show a benefit in treatment of breast cancer oligometastases with stereotactic radiation, however prospective studies dedicated to this type of cancer are needed to clarify the potential benefit according to molecular subtypes.

DATA AVAILABILITY STATEMENT

The raw data supporting the conclusions of this article will be made available by the authors, without undue reservation.

ETHICS STATEMENT

Ethical review and approval was not required for the study on human participants in accordance with the local legislation and institutional requirements. Written informed consent for participation was not required for this study in accordance with the national legislation and the institutional requirements.

AUTHOR CONTRIBUTIONS

Study conception and design: DP and PL. Data collection: PL, MB, EK, EB, PC, PR, JT, and DP. Data analysis and interpretation: PL, MB, EK, EB, PC, PR, JT, and DP. Statistical analysis: EB. All authors contributed to the article and approved the submitted version.

REFERENCES

1. *Données Épidémiologiques De L'inca*. Available at: https://www.e-cancer.fr/Professionnels-de-sante/Les-chiffres-du-cancer-en-%20France/Epidemiologie-des-cancers/Les-cancers-les-plus-frequents/Cancer-du-sein (Accessed Consultées le 1 Novembre 2020).
2. Hellman S. Karnofsky Memorial Lecture. Natural History of Small Breast Cancers. *J Clin Oncol* (1994) 12:2229–34. doi: 10.1200/JCO.1994.12.10.2229
3. Cardoso F, Paluch-Shimon S, Senkus E, Curigliano G, Aapro MS, André F, et al. 5th ESO-ESMO International Consensus Guidelines for Advanced Breast Cancer (ABC 5). *Ann Oncol* (2020) 31:1623–49. doi: 10.1016/j.annonc.2020.09.010
4. Pagani O, Senkus E, Wood W, Colleoni M, Cufer T, Kyriakides S, et al. International Guidelines for Management of Metastatic Breast Cancer: Can Metastatic Breast Cancer Be Cured? *J Natl Cancer Inst* (2010) 102:456–63. doi: 10.1093/jnci/djq029
5. Guckenberger M, Lievens Y, Bouma AB, Collette L, Dekker A, deSouza NM, et al. Characterisation and Classification of Oligometastatic Disease: A European Society for Radiotherapy and Oncology and European Organisation for Research and Treatment of Cancer Consensus Recommendation. *Lancet Oncol* (2020) 21:e18–28. doi: 10.1016/S1470-2045(19)30718-1
6. Friedel G, Pastorino U, Ginsberg RJ, Goldstraw P, Johnston M, Pass H, et al. Results of Lung Metastasectomy From Breast Cancer: Prognostic Criteria on the Basis of 467 Cases of the International Registry of Lung Metastases. *Eur J Cardiothorac Surg* (2002) 22:335–44. doi: 10.1016/s1010-7940(02)00331-7
7. Pockaj BA, Wasif N, Dueck AC, Wigle DA, Boughey JC, Degnim AC, et al. Metastasectomy and Surgical Resection of the Primary Tumor in Patients With Stage IV Breast Cancer. *Ann Surg Oncol* (2010) 17:2419–26. doi: 10.1245/s10434-010-1016-1
8. Milano MT, Katz AW, Zhang H, Okunieff P. Oligometastases Treated With Stereotactic Body Radiotherapy: Long-Term Follow-Up of Prospective Study. *Int J Radiat Oncol Biol Phys* (2012) 83:878–86. doi: 10.1016/j.ijrobp.2011.08.036
9. Scorsetti M, Comito T, Clerici E, Franzese C, Tozzi A, Iftode C, et al. Phase II Trial on SBRT for Unresectable Liver Metastases: Long-Term Outcome and Prognostic Factors of Survival After 5 Years of Follow-Up. *Radiat Oncol* (2018) 13:234. doi: 10.1186/s13014-018-1185-9

10. Trovo M, Furlan C, Polesel J, Fiorica F, Arcangeli S, Giaj-Levra N, et al. Radical Radiation Therapy for Oligometastatic Breast Cancer: Results of a Prospective Phase II Trial. *Radiother Oncol* (2018) 126:177–80. doi: 10.1016/j.radonc.2017.08.032
11. Milano MT, Katz AW, Zhang H, Huggins CF, Aujla KS, Okunieff P. Oligometastatic Breast Cancer Treated With Hypofractionated Stereotactic Radiotherapy: Some Patients Survive Longer Than a Decade. *Radiother Oncol* (2019) 131:45–51. doi: 10.1016/j.radonc.2018.11.022
12. Fumagalli I, Bibault JE, Dewas S, Kramar A, Mirabel X, Prevost B, et al. A Single-Institution Study of Stereotactic Body Radiotherapy for Patients With Unresectable Visceral Pulmonary or Hepatic Oligometastases. *Radiat Oncol* (2012) 7:164. doi: 10.1186/1748-717X-7-164
13. Mahadevan A, Blanck O, Lanciano R, Peddada A, Sundararaman S, D'Ambrosio D, et al. Stereotactic Body Radiotherapy (SBRT) for Liver Metastasis–Clinical Outcomes From the International Multi-Institutional RSSearch® Patient Registry. *Radiat Oncol* (2018) 13:26. doi: 10.1186/s13014-018-0969-2
14. Bhattacharya IS, Woolf DK, Hughes RJ, Shah N, Harrison M, Ostler PJ, et al. Stereotactic Body Radiotherapy (SBRT) in the Management of Extracranial Oligometastatic (OM) Disease. *Br J Radiol* (2015) 88:20140712. doi: 10.1259/bjr.20140712
15. Onal C, Guler OC, Yildirim BA. Treatment Outcomes of Breast Cancer Liver Metastasis Treated With Stereotactic Body Radiotherapy. *Breast* (2018) 42:150–6. doi: 10.1016/j.breast.2018.09.006
16. Weykamp F, König L, Seidensaal K, Forster T, Hoegen P, Akbaba S, et al. Extracranial Stereotactic Body Radiotherapy in Oligometastatic or Oligoprogressive Breast Cancer. *Front Oncol* (2020) 10:987. doi: 10.3389/fonc.2020.00987
17. Scorsetti M, Franceschini D, De Rose F, Comito T, Villa E, Iftode C, et al. Stereotactic Body Radiation Therapy: A Promising Chance for Oligometastatic Breast Cancer. *Breast* (2016) 26:11–7. doi: 10.1016/j.breast.2015.12.002
18. Available at: https://icru.org/content/reports/icru-report-91-prescribing-recording-and-reporting-of-stereotactic-treatments-with-small-photon-beams.
19. Deluche E, Antoine A, Bachelot T, Lardy-Cleaud A, Dieras V, Brain E, et al. Contemporary Outcomes of Metastatic Breast Cancer Among 22,000 Women From the Multicentre ESME Cohort 2008–2016. *Eur J Cancer* (2020) 129:60–70. doi: 10.1016/j.ejca.2020.01.016
20. Palma DA, Olson R, Harrow S, Gaede S, Louie AV, Haasbeek C, et al. Stereotactic Ablative Radiotherapy Versus Standard of Care Palliative Treatment in Patients With Oligometastatic Cancers (SABR-COMET): A Randomised, Phase 2, Open-Label Trial. *Lancet* (2019) 393:2051–8. doi: 10.1016/S0140-6736(18)32487-5
21. Chalkidou A, Macmillan T, Grzeda MT, Peacock J, Summers J, Eddy S, et al. Stereotactic Ablative Body Radiotherapy in Patients With Oligometastatic Cancers: A Prospective, Registry-Based, Single-Arm, Observational, Evaluation Study. *Lancet Oncol* (2021) 22:98–106. doi: 10.1016/S1470-2045(20)30537-4
22. Available at: https://pubmed.ncbi.nlm.nih.gov/31293976/.
23. Available at: https://clinicaltrials.gov/ct2/show/NCT03862911.
24. Available at: https://clinicaltrials.gov/ct2/show/NCT03143322.
25. Available at: https://clinicaltrials.gov/ct2/show/NCT02089100.
26. Available at: https://clinicaltrials.gov/ct2/show/NCT02364557.
27. Muraro E, Furlan C, Avanzo M, Martorelli D, Comaro E, Rizzo A, et al. Local High-Dose Radiotherapy Induces Systemic Immunomodulating Effects of Potential Therapeutic Relevance in Oligometastatic Breast Cancer. *Front Immunol* (2017) 8:14765. doi: 10.3389/fimmu.2017.01476

Conflict of Interest: The authors declare that the research was conducted in the absence of any commercial or financial relationships that could be construed as a potential conflict of interest.

Publisher's Note: All claims expressed in this article are solely those of the authors and do not necessarily represent those of their affiliated organizations, or those of the publisher, the editors and the reviewers. Any product that may be evaluated in this article, or claim that may be made by its manufacturer, is not guaranteed or endorsed by the publisher.

frontiers in Oncology

SYSTEMATIC REVIEW
published: 18 November 2021
doi: 10.3389/fonc.2021.772663

Machine Learning for Head and Neck Cancer: A Safe Bet?—A Clinically Oriented Systematic Review for the Radiation Oncologist

Stefania Volpe[1,2†], Matteo Pepa[1†], Mattia Zaffaroni[1†], Federica Bellerba[3], Riccardo Santamaria[1,2], Giulia Marvaso[1,2], Lars Johannes Isaksson[1], Sara Gandini[3], Anna Starzyńska[4], Maria Cristina Leonardi[1], Roberto Orecchia[5], Daniela Alterio[1‡] and Barbara Alicja Jereczek-Fossa[1,2‡]*

[1] Division of Radiation Oncology, European Institute of Oncology (IEO) Istituto di Ricovero e Cura a Carattere Scientifico (IRCCS), Milan, Italy, [2] Department of Oncology and Hemato-Oncology, University of Milan, Milan, Italy, [3] Molecular and Pharmaco-Epidemiology Unit, Department of Experimental Oncology, European Institute of Oncology (IEO) Istituto di Ricovero e Cura a Carattere Scientifico (IRCCS), Milan, Italy, [4] Department of Oral Surgery, Medical University of Gdańsk, Gdańsk, Poland, [5] Scientific Directorate, European Institute of Oncology (IEO) Istituto di Ricovero e Cura a Carattere Scientifico (IRCCS), Milan, Italy

OPEN ACCESS

Edited by:
Henry Soo-Min Park,
Yale University, United States

Reviewed by:
Sanjay Aneja,
Yale University, United States
Benjamin H. Kann,
Dana–Farber Cancer Institute, United States

***Correspondence:**
Federica Bellerba
federica.bellerba@ieo.it

[†]These authors share first authorship

[‡]These authors share last authorship

Specialty section:
This article was submitted to Radiation Oncology, a section of the journal Frontiers in Oncology

Received: *08 September 2021*
Accepted: *25 October 2021*
Published: *18 November 2021*

Citation:
Volpe S, Pepa M, Zaffaroni M, Bellerba F, Santamaria R, Marvaso G, Isaksson LJ, Gandini S, Starzyńska A, Leonardi MC, Orecchia R, Alterio D and Jereczek-Fossa BA (2021) Machine Learning for Head and Neck Cancer: A Safe Bet?—A Clinically Oriented Systematic Review for the Radiation Oncologist. Front. Oncol. 11:772663. doi: 10.3389/fonc.2021.772663

Background and Purpose: Machine learning (ML) is emerging as a feasible approach to optimize patients' care path in Radiation Oncology. Applications include autosegmentation, treatment planning optimization, and prediction of oncological and toxicity outcomes. The purpose of this clinically oriented systematic review is to illustrate the potential and limitations of the most commonly used ML models in solving everyday clinical issues in head and neck cancer (HNC) radiotherapy (RT).

Materials and Methods: Electronic databases were screened up to May 2021. Studies dealing with ML and radiomics were considered eligible. The quality of the included studies was rated by an adapted version of the qualitative checklist originally developed by Luo et al. All statistical analyses were performed using R version 3.6.1.

Results: Forty-eight studies (21 on autosegmentation, four on treatment planning, 12 on oncological outcome prediction, 10 on toxicity prediction, and one on determinants of postoperative RT) were included in the analysis. The most common imaging modality was computed tomography (CT) (40%) followed by magnetic resonance (MR) (10%). Quantitative image features were considered in nine studies (19%). No significant differences were identified in global and methodological scores when works were stratified per their task (i.e., autosegmentation).

Discussion and Conclusion: The range of possible applications of ML in the field of HN Radiation Oncology is wide, albeit this area of research is relatively young. Overall, if not safe yet, ML is most probably a bet worth making.

Keywords: systematic review, artificial intelligence, machine learning, radiotherapy, head and neck cancer

INTRODUCTION

Cancers of the head and neck (HN) region involve anatomically complex and functionally essential structures, whose damage may severely compromise quality of life, especially in long-surviving patients (1). If the management of HN cancers (HNCs) has always been challenging in Radiation Oncology, in the last years, the clinical scenario has rapidly evolved, due to changes in the epidemiology of the disease (2–4), to the introduction of novel systemic therapies and surgical procedures (5–8) and to the availability of more sophisticated irradiation techniques (9–11). Additionally, as for other cancer sites, understanding on HN neoplasms is taking advantage from progresses in the fields of radiogenomics and quantitative imaging analysis (12–15). Such "big data"-based approaches are progressively being integrated into a more traditional body of knowledge on tumor biology and inter-patient variability which, arguably, may represent a concrete step toward a personalized medicine approach (16).

Nevertheless, this increasing amount of information is hardly manageable by single practitioners, and there is an unprecedented demand of novel, informatics-based tools to structure and solve complex clinical questions. To this aim, machine learning (ML)—a branch of artificial intelligence (AI) relying on patterns and inference to execute a specific task—could provide Radiation Oncologists (ROs) with accurate models to optimize patients' care paths (17).

As compared with statistical methods, ML focuses on the identification of predictive patterns rather than on drawing inferences from a sample. Starting from sampling and power calculations, statistical models aim to assess whether a relationship between two or more variables describes a true effect and to interpret the extent of the above-mentioned relationship. A quantitative measure of confidence can therefore be provided to test hypothesis and/or verify assumptions (18). By contrast, ML makes use of general-purpose algorithms with no or minimal assumptions. While this may produce hardly interpretable and generalizable results, ML can be useful in case of poorly understood and complex phenomena, when the number of input variable exceeds the number of subjects and complicated nonlinear interactions are present (19). However, statistics- and ML-based models should not be regarded as antagonistic and mutually exclusive. As an example, some methods (i.e., bootstrapping) can be used for both the purpose of statistical inference and for the development of ML models, and a distinct boundary between the two is not always easily traceable.

The choice of the most suitable ML algorithm to solve a given problem starts with the characterization of available data, which can be either labeled (e.g., implemented with additional information, such as: "this computed tomography (CT) slice contains the contour of the tumor") or unlabeled (e.g., data do not contain any supplementary tag, such as a collection of CT slices). In the first case, the learning problem is of supervised nature, meaning that the algorithm uses labeled data (training set) to assign a class label to unseen, unlabeled instances (test set). Conversely, unsupervised learning uses unlabeled data to identify previously undetected patterns in the data set and reacts to the existence or absence of such patterns in new instances, without the need of human supervision. However, the aim of the model is the same: to assign similar, contiguous pixels with the correct label (PG vs. non-PG) by a computationally efficient and generalizable algorithm. Other than by input data type, models can be categorized according to their output. Broadly, if the output is a number (i.e., grade of acute toxicity per the Common Terminology Criteria of Adverse Events (CTCAE) system), the task is defined as a regression problem, if it is a class (i.e., tumor vs. nontumor), the task is called a classification problem, and if it is a set of input groups (i.e., clinical and dosimetric variables), it is a clustering problem.

Following the idea of a "big-data" approach for cancer care, several publications in the field of Radiation Oncology have come to life, with algorithms encompassing segmentation accuracy, treatment planning optimization, and prediction of both oncological and toxicity outcomes (17, 20–22). A visual representation of the ML workflow applied in this clinical setting is provided in **Figure 1**. Given the lack of comparable efforts in current literature and the hotness of the topic, we decided to perform a clinically oriented systematic review of the available evidence for ML applications in HNCs. In doing so, we also chose to focus on the methodology of published works and to rate their quality according to a ML-dedicated checklist by Luo et al. (23), generated in 2016 by a multidisciplinary panel of experts in compliance with the Delphi method (24). Ultimately, our goal is to propagate awareness of ROs on ML applications in HNCs. Expectantly, this would contribute to fostering further research and collaboration among different professionals, and to define a novel, data-driven approach to clinical Radiation Oncology for this subset of patients.

Autosegmentation

Segmentation of target volumes and organs at risk (OARs) is a critical component in the Radiation Oncology workflow. Following the recognition of intensity-modulated radiotherapy (IMRT) as a standard of care for HNC (25), accurate delineation has been associated with improved oncological and toxicity outcomes (26–28). Consequently, minimizing inter- and intraoperator variability in segmentation is crucial, and several guidelines have been published and updated to foster standardization in HNC contouring. Another relevant issue in

Abbreviations: AI, artificial intelligence; ANN, Artificial Neural Network; ART, adaptive RT; AUC, area under the curve; CBCT, cone-beam CT; CI, confidence interval; CNN, Convolutional Neural Network; CT, computed tomography; CTCAE, common terminology criteria of adverse events; CTV, clinical target volume; DMFS, distant metastasis-free survival; DSC, Dice Similarity Coefficient; FDR, false-discovery rate; GTV, gross tumor volume; GTV-N, GTV-nodal; GTV-T, GTV-tumor; HD U-net, Hierarchically Densely connected U-net; HN, head and neck; HNC, HN cancer; IMRT, intensity-modulated RT; IQR, interquartile range; LASSO, Least Absolute Shrinkage and Selection Operator; LRC, loco-regional control; MAE, mean absolute error; ML, machine learning; MR, magnetic resonance; NCDB, National Cancer Database; NPC, nasopharyngeal carcinoma; NTCP, normal tissue complication probability; OAR, organ at risk; OPC, oropharyngeal cancer; OS, overall survival; PET, positron emission tomography; PG, parotid gland; PRISMA, Preferred Reporting Items for Systematic Reviews and Meta-Analysis; RO, radiation oncologist; ROI, region of interest; RT, radiotherapy; sCT, synthetic CT; SVM, support vector machine; VGG-16, Visual Geometry Group-16.

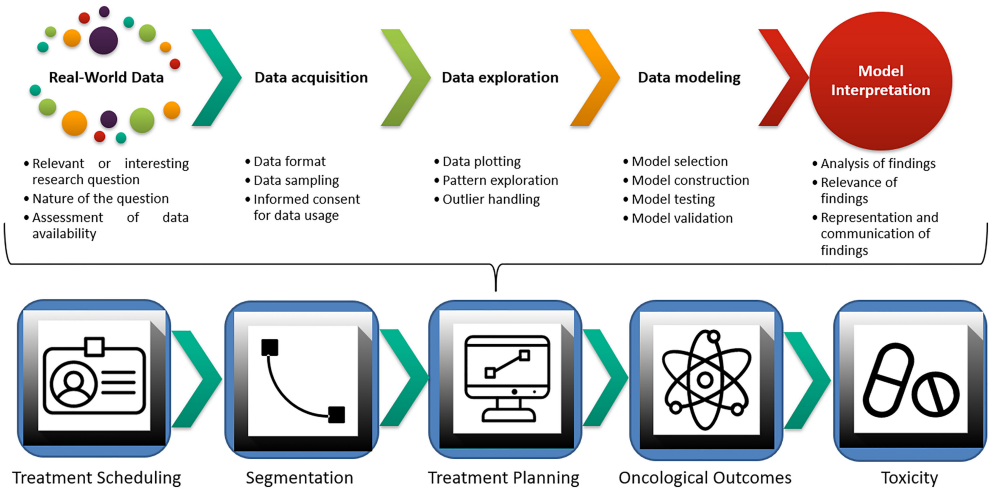

FIGURE 1 | Machine learning workflow and current applications in Radiation Oncology.

the current clinical management is the time needed for completing the segmentation of an HNC case, which approximates 3.0 h (29): other than representing a significant commitment to the RO, time represents a limitation toward a more systematic use of adaptive radiotherapy (ART), which requires rapid recontouring and replanning (30). In this context, ML-based autosegmentation holds the promise of optimizing the clinical management for HNC patients and to increase consistency and reproducibility of delineated structures. ML can be implemented to either single or multiple autosegmentation atlases in order to improve registration and segmentation performance. Specifically, such model-based approaches can compare patient's images with a reference gold standard (ground truth) and overcome acquired imaging limitations including low soft tissue contrast and presence of dental metal artifacts. However, inter- and intrapatient variability and large computational time for registration represent two significant pitfalls of the atlas-based approach (31). Deep learning has the potential to overcome these limitations and has already found several applications in the field of computer vision tasks which, as a whole, can be defined as the automatic extraction, analysis, and understanding of any relevant information from either a single image or a series of images through the construction of dedicated datasets (21, 32).

Treatment Planning

Treatment planning for HNC is challenging: expertise in both the medical (i.e., knowledge of complex HN anatomy and patterns of disease recurrence, awareness of tolerance of healthy tissues to irradiation) and in the physical field (i.e., coverage of irregularly shaped target volumes, multiple dose prescription levels) is required, and timely delivery of radiotherapy (RT) is mandatory not to compromise oncological outcomes (33). In recent years, an increasing body of evidence has demonstrated that geometrical and anatomical variations can occur during the course of curative-intent treatments for HNC, thus leading to potentially meaningful modifications in dose distribution. Several variables have been investigated, and include, but are not limited to, patients' weight loss, tumor response, and PG shrinkage (34, 35). The use of ART can quantify and overcome the dosimetric impact of these modifications and restore the desirable therapeutic ratio in this subset of patients (36). Yet, routine implementation of ART in clinical practice is limited by temporal and logistic issues: CT rescanning, recontouring, and replanning require efficient scheduling and execution and involve the whole staff of a Radiation Oncology Department, from radiation therapists to medical physicists.

Oncological Outcome Prediction

Outcome prediction is crucial in the field of Radiation Oncology, especially in the era of personalized treatments. As deintensification strategies are being tested in clinical trials (37), and biological and quantitative imaging parameters are gaining the spotlight as promising prognosticators (38, 39), there is an increasing need for effective models integrating this growing body of information (13). A typical problem in outcomes prediction with ML is the management of time-dependent endpoints (i.e., overall survival (OS), local control, progression-free survival). These outcomes, often referred to as "right censored", may not have yet occurred at the time of the last follow-up, but still require to be considered, as they could present at a later time. Although the pre-processing method for such variables is often influenced by the ML algorithm of choice, it has been recognized that inappropriate recognition of right-censored events may lead to poorly calibrated models (40–43).

Toxicity Outcomes Prediction

Other than achieving disease control by the irradiation of the gross and clinical tumor volumes (GTV and CTV, respectively), the optimal radiation treatment plan aims at the preservation of

healthy surrounding structures. Although the introduction of modern RT techniques has ameliorated the therapeutic ratio, acute and chronic RT-related toxicities still represent a significant burden for patients' quality of life and may compromise timely treatment delivery (25). In recent years, refined anatomical knowledge of normal tissues (i.e., the coexistence of serial and parallel components in architecturally complex patterns in salivary glands) and the recognition of a stem cell compartment in healthy organs have shed light on the need of further improving dose distribution, especially when curative-intent treatments are delivered (44).

To this aim, the use of spatial dose metrics, such as gradient and direction, may provide more comprehensive information than the sole absolute mean and maximum doses (45, 46). Additionally, genetic determinants are thought to impact on individual radiosensitivity/radioresistance of healthy tissues as much as for the 80% (47). ML may combine these emerging factors with more established determinants of toxicity, such as patient factors, administration of systemic therapies and absolute dosimetric parameters (48, 49). Adequate consideration of these covariables in dedicated algorithms could discriminate the probability for a given patient to experience a specific toxicity, and therefore contribute to refine clinical decisions (i.e., prophylactic feeding tube positioning in patients at high risk for severe weight loss) (47, 50).

MATERIALS AND METHODS

Study methodology complied with the outlines of the Preferred Reporting Items for Systematic Reviews and Meta-Analyses (PRISMA) (51). Original manuscripts on ML applications for HNC were considered eligible for the analysis; publications encompassing any other cancers were excluded. Interventions included investigations on (auto)segmentation, treatment planning, and outcome prediction (either oncological or toxicity); works whose focus was exclusively diagnostic were considered beyond the scope of the current review. Full papers of any study design except systematic reviews and case reports were considered; only works written in English were included.

Search Strategy

Electronic databases (namely, National Center for Biotechnology Information PubMed, Elsevier EMBASE and Elsevier Scopus) were screened up to May 2021 without date restrictions by an author experienced in bibliographic search (SV). Free text, Boolean operators, truncation, and proximity operators were tested. No filters were applied, in order not to exclude potentially relevant publications. The full-search strategy is provided in **Supplementary Materials S1**.

Findings from the above-reported search were independently screened and selected based on titles by two Authors (SV, RS); disagreements were subsequently discussed in presence of three other authors (FB, MP, MZ). All types of ML algorithms were considered eligible for the analysis, as well as studies encompassing the use of extracted quantitative imaging features. The selection process is shown in **Figure 2**, while **Figure 3** provides an overview of the algorithms considered for the analysis. A more detailed insight of ML models/algorithms included is provided in **Table 1**.

Quality Assessment of the Included Studies

The quality of the studies included in the analysis was rated by an adapted version of the qualitative checklist originally developed by Luo et al. for the reporting of predictive modeling in biomedical research (23). This checklist, compared with others present in the literature, provides a multidisciplinary overview of ML models, as it was developed taking into account inputs from different professional figures usually involved in medical research, such as clinicians, statisticians, and ML experts. The organization of the checklist was maintained, and the following subsections were rated for each study: "Title and abstract", "Introduction", "Methods", "Results", and "Discussion".

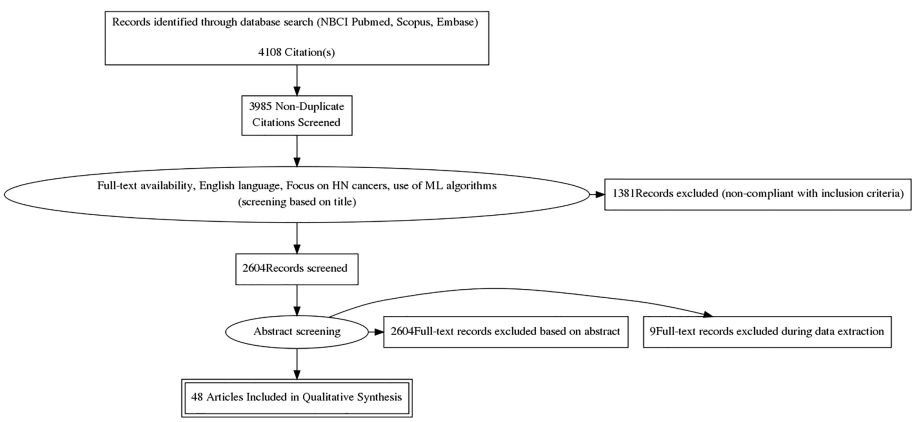

FIGURE 2 | Study selection process per the Preferred Reporting Items for Systematic Reviews and Meta-Analysis (PRISMA) guidelines.

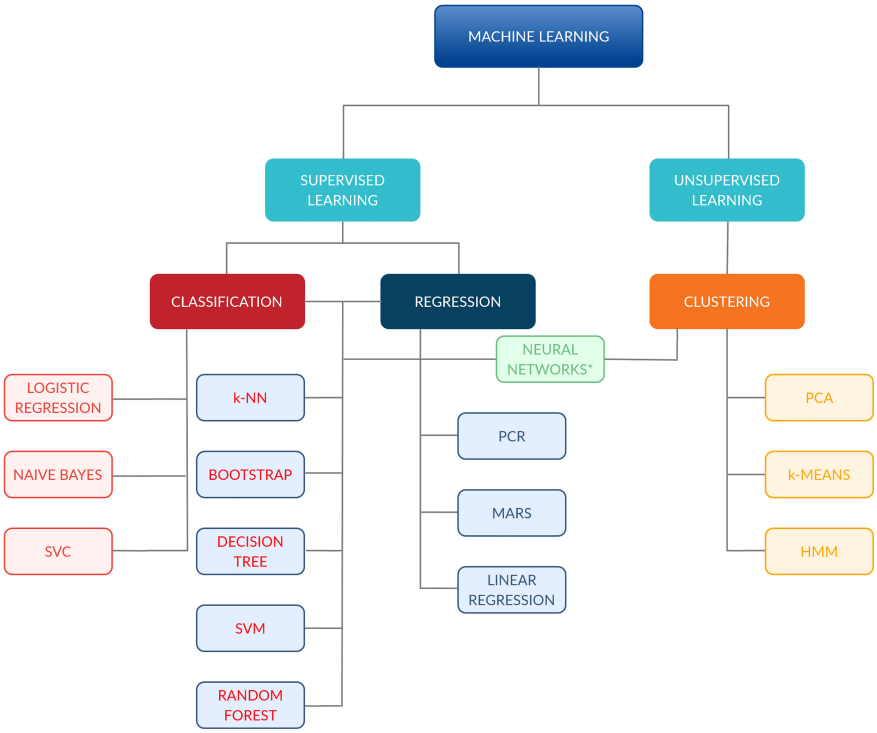

FIGURE 3 | Classification of the machine-learning algorithms included in the analysis. *Comprehend: ANN, CNN and FCNN. ANN, Artificial Neural Network; CNN, Convolutional Neural Network; FCNN, Fully CNN; HMM, Hidden Markov Model; k-NN, k-Nearest Neighbour; MARS, Multiadaptive Regression Splines; PCA, principal component analysis; PCR, principal component regression; SVC, support vector classifier; SVM, support vector machine.

Each of the 55 items required a dichotomous answer (yes or no, coded as 1 and 0, respectively); two items were divided into three subsections, thus allowing for a maximum achievable score of 58. The complete adapted Luo scoring system can be reviewed in detail in **Supplementary Materials S2**.

Statistical Analysis

Descriptive statistics (median, mean, interquartile range (IQR), min, max, standard deviation) were provided for global score and methodological score from the modified Luo classification (23). Score differences across study groups (per task and use of quantitative imaging analysis) were assessed with Wilcoxon sum-rank test (when groups = 2) or Kruskal-Wallis test (when groups >2) and graphically evaluated with boxplots. *p*-values corrected for false-discovery rate (FDR) were also provided to account for multiple testing, considering a threshold of 0.05. All statistical analyses were carried out using R version 3.6.1.

RESULTS

Forty-eight studies were included in the analysis: publication years ranged between 1998 and 2021; with more than a half having been published after 2018 (56%). Twenty-one (44%) focused on ML algorithms for autosegmentation, four (8%) were dedicated to treatment planning, 12 (25%) to oncological outcomes prediction, 10 (21%) to RT-related toxicity, and one (2%) to the determinants of postoperative RT delays following surgery for HNC.

Twenty-one works (44%) considered more than one HNC subsite, while the most common single primary site was the nasopharynx, which was the focus of seven studies (15%). Of note, this information was missing in six cases (12%). The most common imaging modality was CT (40%), followed by magnetic resonance (MR) (10%). Quantitative image features were considered in nine studies (19%) and were mainly CT based (75%). Dosimetric parameters were used in six of the analyzed works, five on toxicity outcomes prediction, and one on the identification of candidates to replanning.

Here follows a detailed description of the studies sorted by main topic, with each topic representing a critical step in the modern workflow for HNC patients in Radiation Oncology.

Autosegmentation

The majority of the included studies (21/48) focused on the design of ML algorithms for autosegmentation: seven were for the segmentation of treating volumes (either CTV or GTV) and 13 for OARs. Considering the former, tumor GTV (GTV-T) was the target of prediction for six studies; in one of these, the algorithm was used for the delineation of the nodal GTV (GTV-N) and the CTV as

TABLE 1 | Summary and definitions of most common machine learning (ML) models.

ML model	Abbreviations	Application	Definition
Artificial Neural Network	ANN, NN	*Classification, regression, and clustering*	Any set of algorithms modeled on human brain neuronal connections
Active Shape Model	ASM	*Segmentation*	Model-based method to compare an image reference model with the image of interest
Bayesian Bagging (Bootstrap AGGregatING)	BB	*Classification and regression*	Bayesian analog of the original bootstrap. Bootstrap samples of the data are taken, the model is fit to each sample, and the predictions are averaged over all of the fitted models to get the bagged prediction
Boosting	–	*Classification and regression*	Boosting is a generic algorithm rather than a specific model. Boosting needs a weak model (e.g., regression, shallow decision trees, etc.) as a starting point and then improves it
Bootstrap aggregating	–	*Classification and regression*	Meta-algorithm designed to improve the stability and accuracy of ML algorithms used in statistical classification and regression. It also reduces variance and helps to avoid overfitting. Although it is usually applied to decision tree methods, it can be used with any type of method
Classification and Regression Tree	CART	*Classification and regression*	Predictive model which predicts an outcome variable value based on other values. A CART output is a decision tree where each fork is a split in a predictor variable and each end node contains a prediction for the outcome variable
Convolutional Neural Network (CNN)	CNN, NN	*Classification, regression, and clustering*	Ordinary NN which implements convolution (mathematical operation on 2 functions producing a third function expressing how the shape of the first one is modified by the second one), in at least 1 of its layers. Most commonly, inputs are images
C4.5	–	*Classification*	An algorithm used to generate a decision tree. The decision trees generated by C4.5 can be used for classification, and for this reason, this algorithm is often referred to as a statistical classifier
Decision tree	DT	*Classification and regression*	Algorithm containing conditional control statements organized in the form of a flowchart-like structure, also called tree-like model. Paths from roots to leaves represent classification rules, while each node is a class label (decision based on the computation of the attributes)
Decision stump	DS	*Classification and regression*	Model consisting of a 1-level decision tree, a tree with an internal node (root) immediately connected to the terminal nodes (its leaves). A DS makes a prediction based on the value of just a single input feature. Sometimes they are also called 1xrules
Fully Convolutional Neural Network	FCNN	*Classification, regression, and clustering*	A deep learning model based on traditional CNN model. A FCNN is one where all the learnable layers are convolutional, so it does not have any fully connected layer.
Incremental Association Markov Blanket	IAMB	*Features selection*	Feature selection method
Least Absolute Shrinkage and Selection Operator	LASSO	*Feature selection*	A regression analysis method that performs both variable selection and regularization in order to enhance the prediction accuracy and interpretability of the statistical model
Likelihood-Fuzzy Analysis	LFA	*Classification*	A method used for translating statistical information coming from labeled data into a fuzzy classification system with good confidence measure in terms of class probabilities and interpretability of the fuzzy classification model, by means of semantically interpretable fuzzy partitions and if–then rule
Linear discriminant analysis	LDA	*Classification*	A method used to find a linear combination of features that characterizes or separates 2 or more classes of objects or events
Logistic regression	LR	*Classification*	A statistical model that uses a logistic function to model a binary dependent variable
k-Nearest Neighbors	k-NN	*Classification and regression*	Non-parametric algorithm that classifies data points based on their similarity (also called distance or proximity) with the objects (feature vectors) contained in the collection of known objects (vector space or feature space)
Multiadaptive Regression Splines	MARS	*Regression*	It is a nonparametric regression technique, extension of linear models that automatically models nonlinearities and interactions between variables
Multivariate Regression Model for Reserving	MRMR	*Features selection*	Supervised feature selection algorithm which requires both the input features, and the output class labels of data. Using the input features and output class labels, MRMR attempts to find the set of features which associate best with the output class labels, while minimizing the redundancy between the selected features

(Continued)

TABLE 1 | Continued

ML model	Abbreviations	Application	Definition
Naive Bayes	NB	*Classification*	Applies Bayes' theorem to calculate the probability of an hypothesis to be true assuming prior knowledge and a strong (therefore, naive) degree of independence between the features
Partial least squares and principal component regression	PLSR and PCR	*Regression*	Both methods model a response variable when there are a large number of predictor variables, and those predictors are highly correlated. Both methods construct new predictor variables, known as components, as linear combinations of the original predictor variables. PCR creates components to explain the observed variability in the predictor variables, without considering the response variable at all. PLSR does take the response variable into account, and therefore often leads to models that are able to fit the response variable with fewer components
Principal component analysis	PCA	*Clustering*	Captures the maximum variance in the data into a new coordinate system whose axes are called "principal components," to reduce data dimensionality, favor their exploration, and reduce computational cost
Penalized logistic regression	PLR	*Classification*	PLR imposes a penalty to the logistic model for having too many variables. This results in shrinking the coefficients of the less contributive variables toward zero. This is also known as regularization
Random forest (RF)/ Random forest classification (RFC)	RF, RFC	*Classification and regression*	Operates by constructing a multitude of decision trees at training time and outputting the class that is the mode of the classes (classification) or mean prediction (regression) of the individual trees
Relief	–	*Features selection*	An algorithm that takes a filter-method approach to feature selection that is notably sensitive to feature interactions. Relief calculates a feature score for each feature which can then be applied to rank and select top scoring features for feature selection
Random survival forest	RSF	*Survival*	A nonparametric method for ensemble estimation constructed by bagging of classification trees for survival data, has been proposed as an alternative method for better survival prediction and variable selection
Rescorla Wagner model	RW	*Classification, clustering*	Rescorla Wagner model is a model of classical conditioning, in which learning is conceptualized in terms of associations between conditioned and unconditioned stimuli
Stochastic/ Gradient Boosting	–	*Classification and regression*	A ML technique which produces a prediction model in the form of an ensemble of weak prediction models, typically decision trees
Support Vector Classifier	SVC	*Classification*	The objective linear SVC is to fit to the provided data and returns a "best-fit" hyperplane that divides, or categorizes them
Support vector machine	SVM	*Classification and regression*	The SVM is based on the idea of finding a hyperplane that best divides the support vectors into classes. The SVM algorithm achieves maximum performance in binary classification problems, even if it is used for multiclass classification problems
U-net architecture	–	*Segmentation*	U-Net is a CNN that was developed for biomedical image segmentation. The main idea is to supplement a usual contracting network by successive layers, where pooling operations are replaced by up sampling operators. Hence, these layers increase the resolution of the output. A successive convolutional layer can then learn to assemble a precise output based on this information

well. Additionally, one study aimed at the sole segmentation of the left and right II–IV nodal levels. A fully automated approach was used in all but one study (52). Overall, all models included in the analysis compared favorably with either competing, previously published algorithms, or with the ground truth represented by manual segmentation (52–55). Specifically, the latter showed an overlap with the manual contours measured by the Dice Similarity Coefficient (DSC) ranging from 0.766 to 0.809 for GTV-T and from 0.623 to 0.698 for GTV-N (54, 55). The only study in which the CTV was autosegmented showed a good agreement with manual delineation, achieving a DSC of 0.826, and outperforming the results of the previously published convolutional neural network (CNN), visual geometry group-16 (VGG-16) (55). Notably, the use of a semiautomated method for GTV-T segmentation proved to be less time consuming and correlated with an increase in the intra- and interoperator agreement when compared with fully manual segmentation (52).

Among algorithms for OAR delineation, studies were heterogeneous in the choice of the target(s) of segmentation. The majority of studies (12/13) considered PG segmentation as a primary endpoint (56–68), with the PG being the only considered region of interest (ROI) in four of the selected works (63, 65–67). The segmentation performance assessed by the DSC for all OARs investigated in the included studies is provided in **Table 2**.

Overall, autosegmentation studies were mainly CT based (13/21); in decreasing order of frequency were MR (three of 21), CT + MR (two of 21), positron emission tomography (PET, two of 21), and CT + PET (one of 21). Sample size varied considerably, ranging from 5 to 486 (median: 46, IQR: 15–166).

A complete description of individual studies characteristics is provided in **Table 3**.

Treatment Planning

Of the included studies, two focused on the identification of predictive factors for replanning (74, 75). Guidi et al. (74) used support vector machine (SVM) on a retrospectively collected cohort of 40 HNC patients and 1,200 megavoltage CTs to

TABLE 2 | Reported Dice Similarity Coefficient (DSC) in literature for different organs.

Organ	No. of studies (*N* = 14)	Reference papers	DSC (median, IQR range)
PG	13	56–67, 100	0.84 (0.83–0.86)
Mandible	9	56–61, 64, 67, 100	0.93 (0.90–0.94)
Brainstem	8	56–61, 67, 100	0.86 (0.84–0.89)
Optic nerves	7	56, 58–61, 64, 67	0.69 (0.67–0.71)
Submandibular glands	7	56, 58–61, 64, 67, 100	0.80 (0.76–0.81)
Chiasm	5	56, 59, 61, 64, 68	0.532 (0.412–0.581)
Spinal cord	4	57, 58, 60, 64	0.88 (0.77–0.96)
Oral cavity	3	57, 58, 100	0.90 (0.80- 0.91)
Eyeballs	2	57, 64	0.91
Lenses	2	57, 60	0.86
Temporomandibular joint	2	57, 64	0.85
Cochleae	2	58, 60	0.82[a]
Pharyngeal constrictors	2	58	0.57[b]
Glottic region	2	58, 100	0.57[c]
Brain	1	60	0.99[c]
Lacrimal glands	1	60	0.65[c]
Orbits	1	60	0.93[c]
Spinal canal	1	60	0.84[c]
Lungs	1	60	0.98
Upper esophagus	1	58	0.69
Supraglottic larynx	1	58	0.77
Larynx	1	57	0.87
Mastoids	1	57	0.82
Whole pharynx	1	64	0.69

[a]*Vandewinckele et al. (57) achieved a DSC of 0.65 with the use of CNN and Nikolov et al. (59) a DSC of 0.982 by a 3D U-Net.*
[b]*The reported DSC was computed as an average of inferior, medial and superior.*
[c]*The average value of two (in some cases three) models was considered.*

recognize those who could benefit from ART based on weekly anatomical and dosimetric divergences in CTV and OARs (namely, spinal cord, mandible, and PGs) during the course of treatment. Specifically, the authors could demonstrate that from the fourth week, 77% of patients underwent significant morphological and dosimetric changes, advocating the need for replanning. Of note, PGs were the most prone to modifications, with significant variations from the original plan occurring as early as from the third week of treatment. In the second study, Yu et al. (75) used radiomic features from contrast-enhanced T1-weighted and T2-weighted pre-RT MR images and Least Absolute Shrinkage and Selection Operator (LASSO) logistic regression to build models predicting the need of treatment replanning in a retrospective cohort of 70 patients with nasopharyngeal carcinoma (NPC). The combined T1–T2 model outperformed the ones based on either single MR sequence, with average areas under the curve (AUCs) in the training and testing sets of 0.984 (95% confidence interval (CI): 0.983–0.984) and 0.930 (95% CI: 0.928–0.933), respectively, and six radiomic features selected as significant.

A third study on ML for RT planning was published by Nguyen et al. (76) and focused on the use of a hierarchically densely connected U-net architecture (HD U-net) to predict three-dimensional dose distribution for the planning target volume and 22 OARs in a retrospectively retrieved population of 120 HNC patients. When compared with two variant net architectures (namely, Standard U-net and DenseNet), the proposed algorithm showed better performance in the prediction of the maximum and mean dose to the OARs, better dose homogeneity, conformity, and coverage on the test data. Additionally, the HD U-net requires fewer trainable parameters and a reduced computational time when compared with the Standard U-net and with the DenseNet, respectively.

Finally, Thummerer et al. (77) in their study compared synthetic CT images (sCTs) derived from cone-beam CTs (CBCTs) and MRs for HN patients in terms of both image quality and accuracy in proton dose calculation, considering planning CTs as the ground truth. Image quality was quantified through mean absolute error (MAE) and DSC. The sCTs from CBCTs provided higher image quality with an average MAE of 40 ± 4 HU and a DSC of 0.95, while for MR-based sCTs a MAE of 65 ± 4 HU and a DSC of 0.89 were observed. Overall, the study reports that CBCT- and MR-based sCTs have the potential to be reliably implemented into the ART workflow for proton therapy application, thus overcoming the need of performing multiple planning CTs.

Oncological Outcome Prediction

Overall, 12 of the included studies considered oncological outcomes following curative-intent treatment as their target of prediction. In details, six studies (40, 42, 78–81) aimed at predicting OS, while five (40, 82–85) considered loco-regional control (LRC) and one (86) distant metastasis-free survival (DMFS). Only two works focused on more than one oncological outcomes (40, 87). Feature selection methods were applied in two cases (40, 42), both studies used radiomic features extracted from the GTV as input parameters for outcome prediction. Other than these works, four additional publications included texture analysis; overall, features were derived from CT images in two works (40, 86), from MR

TABLE 3 | Characteristics for machine-learning studies on autosegmentation.

Author, year of publication	Study population	HN subsite	Imaging modality	Textural and dosimetric parameters	ROI(s)	Tested ML algorithm(s)	Statistical findings and model performance
Brunenberg et al., 2020 (68)	58 pts	Mixed	CT	–	PGs, SMGs, thyroid, buccal mucosa, extended OC, pharynx constrictors, cricopharyngeal inlet, supraglottic area, MNDB, BS	Commercially available DL model; external validation	The best performance was reached for the MNDB (DSC 0.90; HD95 3.6 mm); the agreement was moderate for the aerodigestive tract with the exception of the OC. The largest variations were in the caudal and/or caudal directions (binned measurements).
Ma et al., 2019 (69)	90 pts	NPC	CT and MR	–	GTVs	CNNs	Both M-CNN and C-CNN showed better performance on MR than on CT. C-CNN outperformed M-CNN in both CTs (higher mean Sn, DSC, and ASSD, comparable mean PPV) and MR applications (higher mean PPV, DSC, and ASSD, comparable mean Sn)
Vandewinckele et al., 2019 (58)	9 pts	Mixed	CT	–	Cochlea, BS, upper esophagus, glottis area, MNDB, OC, PGs, inferior, medial and superior PCMs, SC, SMGs, supraglottic Lar	CNN	The longitudinal CNN is able to improve the segmentation results in terms of DSC compared with the DIR for 6/13 considered OARs. The longitudinal approach outperforms the cross-sectional one in terms of both DSC and ASSD for 6 different organs (BS, upper esophagus, OC, PGs, PCM medial, and SMGs)
Hänsch et al., 2018 (63)	254 pts, 254 R PGs, 253 L PGs	Mixed	CT	–	Ipsi- and contralateral PGs	DL U-net	The 3 ANNs showed comparable performance for training and internal validation sets (DSC ≈0.83). The 2-D ensemble and 3-D U-net showed satisfactory performance when externally validated (AUC and DSC: 0. 865 and 0.880, respectively; 2-D U-net omitted)
Mocnik et al., 2018 (62)	44 pts	Not specified	CT and MR	–	PGs	CNN	The multimodal CNN (CT + MR) compared favorably with the single modality CNN (CT only) in the 80.6% of cases. Overall, DSCs value were 78.8 and 76.5, respectively. Both multi- and single-modality CNNs showed satisfactory registration performance
Nikolov et al., 2018 (60)	486 pts, 838 CT scans for training, test and internal validation; 46 pts and 45 CT scans for external validation	Mixed	CT	–	Brain, BS, L and R cochlea, L and R LG, L and R Lens, L and R Lung, MNDB, L and R ON, L and R Orbit, L and R PGs, SC, L and R SMG	3D U-Net	The segmentation algorithm showed good generalizability across different datasets and has the potential of improving segmentation efficiency. For 19/21 performance metrics (surface and volumetric DSC) were comparable with experienced radiographers; less accuracy was demonstrated for brainstem and R-lens
Ren et al., 2018 (70)	48 pts	Not specified	CT	–	Chiasm, L and R ON	3D-CNNs	The proposed segmentation method outperformed the one developed by the MICCAI 2015 challenge winner for all the considered ROIs (DSC chiasm: 0.58 ± 0.17 *vs*. 0.38; DSC ONs 0.71 ± 0.08 *vs*. 0.68)
Tong et al., 2018 (61)	32 pts	Not specified	CT	–	L and R PGs, BS, Chiasm, L and R ONs, MNDB, L and R SMG	FCNN with and without SRM	Accuracy and robustness of the model were improved when incorporating shapes prior to SRM use for all considered ROIs. Segmentation results were satisfactory, ranging from DSC values of 0.583 for the chiasm to 0.937 for the MNDB. Average time for segmenting the whole structure set was 9.5 s
Zhu et al., 2018 (59)	271 CT scans	Not specified	CT	–	BS, Chiasma, MNDB, L and R ON, L and R PG, L and R SMG	Implemented 3D U-Net (AnatomyNet)	The AnatomyNet allowed for an average improvement in segmentation performance of 3.3% (DSC) as compared with previously published data of the MICCAI 2015 challenge. Segmentation time was 0.12 s for the whole structure set.
Doshi et al., 2017 (53)	10 pts/102 MR slices	Mixed	MR	–	GTVs	FCLSM	PLCSF showed a good performance *vs* the consensus manual outline (DSC: 0.79, RAD: 39.5%, MHD: 2.15, PCC: 0.89, $p < 0.05$) and outperformed

(Continued)

TABLE 3 | Continued

Author, year of publication	Study population	HN subsite	Imaging modality	Textural and dosimetric parameters	ROI(s)	Tested ML algorithm(s)	Statistical findings and model performance
							2 Ncut and MS clustering algorithms (the former being less accurate for small lesions and for low-contrast regions and more computationally demanding, the latter leading to more frequent over-segmentation)
Ibragimov et al., 2017 (64)	50 pts	Not specified	CT	–	SC, MNDB, PGs, SMGs, Lar, Phar, R and L EB, R and L ON, optic chiasm	CNN-MRF	Model performance was satisfactory for almost all considered OARs (DSC values as follows—spinal cord: 87 ± 3.2; mandible: 89.5 ± 3.6; PGs DSC: 77.3 ± 5.8; submandibular glands DSC: 71.4 ± 11.6; Lar DSC: 85.6 ± 4.2; phar DSC: 69.3 ± 6.3; eye globes DSC: 88.0 ± 3.2; optic ONs DSC: 62.2 ± 7.2; optic chiasm: 37.4 ± 13.4)
Liang et al., 2017 (55)	185 pts	NPC	CT	–	BS, R and L EB, R and L lens, Lar, R and L MNDB, OC, R and L MAS, SC, R and left PG, R and L T-M, R and L ON	CNNs (ODS-net)	ODS-net showed satisfactory Sn and Sp for most OARs (range: 0.997–1.000 and 0.983–0.999, respectively), with DSC >0.85 when compared with manually segmented contours. ODS-net outperformed a competing FCNN ($p < 0.001$ for all organs). Image delineation was faster in ODS than in FNC, as well, with average time of 30 *vs*. 52 s, respectively
Men et al., 2017 (55)	230 pts	NPC	CT	–	GTV-T, GTV-N, CTV	DDNN	DDNN generated accurate segmentations for GTV-T and CTV (ground truth: manual segmentation), with DSC of 0.809 and 0.826, respectively, Performance for GTV-N was less satisfactory (DSC: 0.623). DDNN outperformed a competing model (VGG-16) for all the analyzed segmentations
Stefano et al., 2017 (72)	4 phantom experiments+ 18 pts/40 lesions	Mixed	PET	–	GTVs	RW	Both the K-RW and the AW-RW compare favorably with previously developed methods in delineating complex-shaped lesions; accuracy on phantom studies was satisfactory
Wang et al., 2017 (56)	111 pts	Mixed	CT	–	Cochlea, BS, upper esophagus, glottis area, MNDB, OC, PGs, inferior, medial and superior PCMs, SC, SMGs, supraglottic Lar	3D U-Net	The model showed satisfactory performance for most of the 9 considered ROIs; when compared with other models, it ranked first in 5/9 cases (L and R PG, L and R ON, L SMG), and second in 4/9 cases
Beichel et al., 2016 (52)	59 pts/230 lesions	Mixed	PET	–	GTVs	Semiautomated segmentation (LOGISMOS)	Segmentation accuracy measured by the DSC was comparable for semiautomated and manual segmentation (DSC: 0.766 and 0.764, respectively)
Yang et al., 2014 (65)	15 pts/30 PGs/ 57 MRs	Mixed	MR	–	Ipsi- and contralateral PGs	SVM	Average DSC between automated and manual contours were 91.1% ± 1.6% for the L PG and 90.5% ± 2.4% for the R PG. Performance was slightly better for the L PG, also when assessed per the averaged maximum and average surface distance
Cheng G et al., 2013 (66)	5 pts, 10 PGs	NPC	MR	–	Ipsi- and controlateral PGs	SVM	Mean DSC between automated and physician's PG contours was 0.853 (range: 0.818–0.891)
Qazi et al., 2011 (67)	25 pts	Not specified	CT	I	MNDB, BS, L and R PG, L and R SMG, L and R node level IB, L and R node levels II–IV	Atlas based segmentation	As compared with manual delineations by an expert, the automated segmentation framework showed high accuracy with DSC of 0.93 for the MNDB, 0.83 for the PGs,.83 for SMGs and 0,.74 for nodal levels
Chen et al., 2010 (54)	15 pts/15 neck nodal levels	Mixed	CT	–	II, III, and IV neck nodal levels	ASM	The ASM outperformed the atlas-based method (ground truth: manually segmented contours), with higher DSC (10.7%) and lower mean and median surface errors (–13.6% and –12.0%, respectively)

(Continued)

TABLE 3 | Continued

Author, year of publication	Study population	HN subsite	Imaging modality	Textural and dosimetric parameters	ROI(s)	Tested ML algorithm(s)	Statistical findings and model performance
Yu et al., 2009 (73)	10 pts/10 GTV-T and 19 GTV-N	Mixed	PET and CT	I	GTVs	KNN	The feature-based classifier showed better performance than other delineation methods (e.g. standard uptake value of 2.5, 50% maximal intensity and signal/background ratio)

2D/3D, 2/3-dimensional; ANN, Artificial Neural Network; ASM, active shape model; ASSD, average symmetric surface distance; AW-RW, K-RW algorithm with adaptive probability threshold; BS, brainstem; CNN, convolutional neural network; C-CNN, combined CNN, CT, computed tomography; CTV, clinical target volume; D, dosimetric; DDNN, deep deconvolutional neural network; DIR, deformable image registration; DL, deep learning; DSC, Dice Similarity Coefficient; EB, eyeball; FCLSM, modified fuzzy c-means clustering integrated with the level set method; FCNN, fully convolutional neural network; GTV-N, nodal-gross tumor volume; GTV-T, tumor-gross tumor volume; HD, Hausdorff distance; I, imaging; KNN, k-nearest neighbors; K-RW, RW algorithm with K-means; L, left; Lar, larynx; LG, lacrimal gland; LOGISMOS, layered optimal graph image segmentation of multiple objects and surfaces; M-CNN, multimodality convolutional neural network; MHD, modified Hausdorff distance; MICCAI, Medical Image Computing and Computer Assisted Intervention; MNDB, mandible; MR, magnetic resonance; MRF, Markov random field; MAS, mastoid; MS, mean shift; Ncut, normalized cut; NPC, nasopharyngeal carcinoma; OAR, organ at risk; LG, lacrimal gland; OC, oral cavity; ODS-net, organs at risk detection and segmentation network; ON, optic nerve; p, p-value; PCC, Pearson correlation coefficient; PCM, pharyngeal constrictors muscles; PET, positron emission tomography; PG, parotid gland; Phar, pharynx; PLCSF, pharyngeal and laryngeal cancer segmentation framework; PPV, positive predictive value; pt, patient; R, right; RAD, relative area difference; ROI, region of interest; RW, Rescola Wagner; SC, spinal cord; s, second; SMG, submandibular gland; Sn, sensitivity; Sp, specificity; SRM, shape representation model; SVM, support vector machine; VGG-16, visual geometry group-16.

images in one (84) and from multiple diagnostic modalities in the remaining three cases (42, 82, 83).

A single disease subsite was considered by two studies, with Zdilar et al. (40) including only patients with oropharyngeal cancer (OPC), and Jiang et al. focusing on patients diagnosed with neoplasms of the nasopharynx. Conversely, Bryce et al. (79) and Parmar et al. (42) applied ML to mixed HNC populations; information on subsite distribution could be retrieved in only one case (79). Despite relevant heterogeneity in the choice of ML algorithms and populations, the best performing models in each study reached an AUC between 0.72 and 0.78; the best performance was reached by the only study using Artificial Neural Networks (ANNs) (79).

LRC was the target of prediction in four cases (40, 82–84); population size varied considerably, from the 32 NPC patients included in the study by Tran et al. (82) to the 529 patients diagnosed with OPC in the study published by Zdilar et al. (40). All studies considered the radiomic features extracted from the pretreatment GTV as input parameters for model construction. Three studies evaluated ML models through AUC values (40, 82, 83), with the best performing models being k-nearest neighbors and ANNs; Fujima et al. (84) assessed the performance of their nonlinear SVM models by sensibility, specificity, and positive and negative predictive values (for further details, please refer to **Table 4**).

Lastly, the prediction of DMFS was the objective of one study (86). Wu et al. proved that the incorporation of pre- and mid-treatment radiomic features extracted from both the primary and nodal GTVs improved the performance of random survival forest models trained and validated on a cohort of 140 locally advanced OPC patients (86).

Toxicity Outcome Prediction

A total of 11 studies focused on RT-induced toxicities; in each publication algorithms were developed for addressing the prediction task on a single outcome (i.e., xerostomia, dysphagia).

Four studies (), predominantly encompassing multiple HN subsites, focused on xerostomia prediction; all but one included dosimetric parameters in the data set (88). The PGs were the only considered ROI except for the work by Guo et al. (89), where the submandibular glands were included. Despite the common clinical focus, different endpoints for the task of xerostomia prediction were considered. Acute xerostomia was the focus of one study, which aimed to predict parotid shrinkage (88), late xerostomia was investigated in one publication (45), while the development of xerostomia at any time following RT was considered by Soares et al. (90). Gabrys et al. built distinct algorithms for the prediction of early, late, and long-term xerostomia; longitudinal models were developed as well (91). Notably, ML-based classifiers outperformed classic Normal Tissue Complication Probability (NTCP) models based on the sole mean dose to the parotids, thus underlying the need of incorporating multiple parameters for accurate outcome prediction (i.e., gland volume and dose gradients in the right-left and anterior-posterior direction for long-term xerostomia). Overall, sample size was comparable across studies focusing on xerostomia prediction (138–153), except for the one by Pota et al., which analyzed 21 patients (88).

The remaining studies presented different toxicity outcomes (namely, acute dysphagia, weight loss at 3 months following the end of RT, osteoradionecrosis, sensorineural loss, and brain injury) (46, 92–95). A full list of the developed algorithms and statistical findings for all studies included in this subsection is provided in **Table 5**.

Checklist Scores

Considering a maximum achievable score of 58 in the adapted Luo rating system for ML applications in biomedical research, median score of the included studies was 39 (IQR: 36–44), with minimum and maximum values being 27 and 53, respectively. When analyzing the *Methods* items only, median rank was 22 (IQR: 20–25), with the worst and best scores being 15 and 32, respectively. As it can be noted in **Figure 4**, the groups achieved comparable scores and no statistically significant difference was noted in studies global and methodological ranking ($p = 0.48$ and 0.67, respectively; FDR-corrected $p = 0.62$ and 0.67, respectively).

TABLE 4 | Characteristics for machine-learning studies on oncological outcome.

Authors, publication year	Sample study population	HN subsite	Clinical endpoint	Imaging modality	Textural and dosimetric parameters	ROI(s)	Tested ML algorithm(s)	Statistical findings and model performance
De Felice et al, 2020 (80)	273 pts	OPC	OS prediction in OPC pts treated with IMRT	None	–	None	Decision trees	The most relevant clinical variables identified were HPV status, nodal stage and early complete response to IMRT
Howard et al, 2020 (81)	33,527 pts	Mixed	OS prediction in HNC pts with intermediate risk factors treated with adjuvant CHT-RT or RT; identification of which pts may benefit from CHT-RT	None	–	None	DeepSurv, RSF, N-MLTR	Indication to treatment according to model recommendations was associated with a survival benefit; the best performance was achieved by DeepSurv, with an HR of 0.79 (95% CI, 0.72–0.85; $p < 0.001$). No survival benefit was observed for CHT in case pts were recommended for RT alone
Starke et al, 2020 (85)	291 pts	Mixed	LRC in locally-advanced HN SCC treated with primary CHT-RT	CT	–	GTVs	3D- and 2D-CNNs (from scratch, transfer learning and extraction of deep autoencoder features)	The best performance was achieved by an ensemble of 3D-CNNs (C-index = 0.31 on the external validation cohort); the model yielded a satisfactory performance in discriminating high- vs. low-risk LRC ($p = 0.001$)
Tseng et al, 2020 (87)	334 pts	OC	Risk stratification of locally-advanced OC pts treated with surgery	None	–	None	Elastic net penalized Cox proportional hazards regression-based risk stratification model	The incorporation of genetic information to clinicopathologic data led to better model performance for the prediction of both CSS and LRC, as compared with models using clinicopathologic variables alone (mean C index, 0.689 vs. 0.673; $p = 0.02$ for CSS and 0.693 vs. 0.678; $p = 0.004$ for LRC). No such difference was noted for the prediction of DMFS
Fujima et al., 2019 (84)	36 pts	SNC	LC following superselective arterial CDDP infusion and concomitant RT	MR	I	GTVs (necrotic and cystic areas excluded)	Nonlinear SVM	Mean Sn: 1.0, Sp 0.82, PPV 0.86, NPV 1.0 (on validation data sets, 9-fold crossvalidation scheme used)
Tran et al., 2019 (82)	32 pts	NPC	RT response of metastatic nodes by ultrasound-derived radiomic markers	CT, MR, EUS	–	GTVs	LR, naive Bayes, and k-NN	There was a statistically significant difference in the pretreatment QUS-radiomic parameters between radiological complete responders vs. partial responders ($p < 0.05$). The best classification was achieved by k-NN with a single feature, SS-contrast (AUC = 0.866 [0.73; 1.01]); %Sn = 85.8; %Sp = 97.3; %Acc = 91.5)
Wu et al., 2019 (86)	140 pts	OPC	DMFS	CT	I	Baseline and mid-treatment GTV-T and GTV-N	RSF	Better performance on testing set was achieved by the model incorporating mid-treatment characteristics (C-index: 0.73, $p = 0.008$) vs. the model based on pretreatment CT features alone. The main features for DMFS prediction were: maximum distance among nodes, maximum distance between tumor and nodes (mid-treatment), and pretreatment tumor sphericity
Li et al., 2018 (83)	306 pts	NPC	Analyze the recurrence patterns in pts with NPC treated with IMRT	CT, MR and PET	I	GTVs	ANN, k-NN, and SVM	NPC-IFRs vs NPC-NPDs could be differentiated by 8 features (AUCs: 0.727–0.835). The classification models showed potential in prediction of NPC-IFR with higher accuracies (ANN: 0.812, KNN: 0.775, SVM: 0.732)

(Continued)

TABLE 4 | Continued

Authors, publication year	Sample study population	HN subsite	Clinical endpoint	Imaging modality	Textural and dosimetric parameters	ROI(s)	Tested ML algorithm(s)	Statistical findings and model performance
Zdilar et al., 2018 (40)	529 pts, >3,800 radiomic features	OPC	OS and RFS	CT	I	GTVs	Feature selectors: MRMR, Wilcoxon rank sum test, RF, RrliefF, RRF, IAMB, RSF, PCA Predictive models: LR, CPH, RF, RSF, logistic elastic net, ensemble models	RF features selectors achieved the best performance for both OS prediction (AUC: 0.75, C-index: 0.76, calibration: 0.87) and. RFS (AUC: 0.71, C-index 0.68, calibration: 19.1). The ensemble model (clinical+ radiomic) yielded the best scores for AUC and C-index in all cases
Jiang et al., 2015 (78)	347 pts	NPC	OS prediction in pts with ab initio metastatic NPC (M1a vs. M1b)	None	–	None	SVM	The SVM classifier showed good performance at internal validation (AUC: 0.761, Sn 80.7%, Sp: 71.3%), while performance was less satisfactory when externally validated (AUC: 0.633)
Parmar et al., 2015 (42)	136 pts	Mixed	OS	CT and PET	–	GTVs	Feature selectors: RELF, FSCR, Gini, JMI, CIFE, DISR, MIM, CMIM, ICAP, TSCR, MRMR, MIFS, Wilcoxon Predictive models: NN, Decision tree, Boosting, Bayesian Bagging, RF, Multi adaptive regression splines (MARS), SVM, k-NN, GLM, partial least squares, and principal component regression	The three feature selection methods minimum redundancy maximum relevance (AUC = 0.69, stability = 0.66), mutual information feature selection (AUC = 0.66, stability = 0.69) and conditional infomax feature extraction (AUC = 0.68, stability = 0.7) had high prognostic performance and stability. The highest prognostic performance was achieved by GLM (median AUC ± SD: 0.72 ± 0.08) and PLSR (median AUC ± sd: 0.73 ± 0.07), whereas BAG (AUC = 0.55 ± 0.06), DT (AUC: 0.56 ± 0.05), and BST (AUC = 0.56 ± 0.07) showed lower AUC values. RF (RSD = 7.36%) and BAG (9.27%) were more stable classification methods, whereas PLSR (RSD = 12.75%) and SVM (RSD = 12.69%) showed lower stability
Bryce et al., 1998 (79)	95 pts	Mixed	Survival prediction in pts with advanced HN SCC treated with RT ± chemotherapy	None	–	None	LR, ANN	ANNs compared favorably with LR models at survival prediction, with a AUC of 0.78 ± 0.05 for the best ANN and of 0.67 ± 0.05 for the best LR model. The best ANN outperformed the modified AJCC TNM 4th edition in survival prediction, as well. Incorporated clinical parameters for the ANN were: tumor size, tumor resectability, nodal stage, tumor stage, and baseline hemoglobin levels

ANN, Artificial Neural Network; AUC, area under the curve; CDDP, cisplatin; CHT, chemotherapy; CIFE, conditional infomax feature extraction; CMIM, conditional mutual information maximization; CNN, convolutional neural network; CSS, cancer-specific survival; CT, computed tomography; D, dosimetric; DISR, double input symmetric relevance; DMFS, distant metastasis free survival; GTV, gross tumor volume; HN, head and neck; HR, Hazard ratio; I, imaging ICAP, interaction capping; IMRT, intensity modulated RT; JMI, joint mutual information; k-NN, k-nearest neighbor; LC, local control; LR, logistic regression; LRC, loco-regional control; MARS, multiadaptive regression splines; MIFS, mutual information feature selection; MIM, mutual information maximization; MR, magnetic resonance; MRMR, minimum redundancy maximum relevance; NN, neural network; N-MLTR, neural network multitask logistic regression; NPC, nasopharyngeal cancer; OC, oral cavity cancer; OPC, oropharyngeal cancer; OS, overall survival; PET, positron emission tomography; PLSR, partial least square regression; RF, random forest; RFS, relapse-free survival; RSD, relative standard deviation; RSF, random survival forest; RT, radiotherapy; SCC, squamous cell carcinoma; SN, sinonasal cancer; SVM, support vector machine; TSCR, t-test score.

TABLE 5 | Characteristics for machine learning studies on toxicity outcome.

Author, year of publication	Study population	HN subsite(s)	Clinical endpoint	Imaging modality	Textural and dosimetric parameters	ROI(s)	Tested ML algorithm(s)	Statistical findings and model performance
Humbert-Vidan et al, 2021 (95)	96 pts (of these, 50% controls)	Mixed	Prediction of osteoradionecrosis of the mandible	CT	D	Mandible	LR, SVM, RF, AdaBoost, ANN	No statistically significant difference was found among the models in terms of either accuracy, TPR, TNR, PPV, NPV).
Zhang et al, 2020 (94)	242 pts	NPC	Early radiation-induced brain (temporal lobes) injury prediction	MRI	I	Temporal lobes	RF (3 models)	The incorporation of textural features yielded to better model performance; features derived from T2-w images achieved higher performance than those extracted from T1-w images. In the testing cohort, models 1, 2, and 3, yielded AUCs of 0.830 (95% CI: 0.823–0.837), 0.773 (95% CI: 0.763–0.782), and 0.716 (95% CI: 0.699–0.733), respectively.
Guo et al., 2019 (45)	146 pts	PGs	Correlation between voxel dose and xerostomia recovery 18 months after RT	None	D	PGs, SMGs	LR with ridge regularization	The AUC scores for the ridge logistic regression model evaluated by 10-fold crossvalidation for recovery and injury prediction were 0.68 ± 0.07 and 0.74 ± 0.03, respectively.
Leng et al., 2019 (93)	77 pts, 67 healthy controls	NPC	Identification of biomarkers of WM injury *via* MR DTI, TBSS, and ML	MR	–	116 brain regions (90 for the brain lobes and 26 for the cerebellum) per the AAL method	SVM	WM regions and WM connections were involved in RBI. The SVM classifier showed satisfactory performances (GR, Sn, Sp) for both FA and WM connections in discriminating patients and controls at all-time points (0–6, 6–12, >12 months)
Abdollahi et al., 2018 (92)	47 pts, 94 cochleas, 490 radiomic features	Mixed subsites	Sensorineural hearing loss prediction following chemoradiotherapy	CT	I, D	Cochlea	Decision stump, Hoeffding, C4.5, Bayesian network, naive, adaptive boosting, bootstrap aggregating, Classification *via* regression, logistic regression, linear logistic	Predictive power was >70% for all models, with Decision stump and Hoeffding being the best-performing models. Incorporation of the gEUD improved both precision and AUC of all models, while accuracy was not affected
Dean et al., 2018 (46)	173 pts + 90 pts for external validation	Mixed subsites	Peak grade of acute dysphagia prediction (severe = CTCAE 3.0 grade ≥3 vs. nonsevere = CTCAE 3.0 grade <3)	None	D	Pharyngeal mucosa	PLR, SVC, RFC (each trained and validated on standard dose-volume metrics and spatial dose-metrics)	PLR was not outperformed by any of the more complex models, on both internal and external validation (AUC: 0.76 and 0.82 for the standard-dose model and AUC: 0.75 and 0.73 for the spatial model, respectively). Calibration was superior for the RFC model. Dosimetric parameters (DVH, DLH and DCH) were relevant for accurate toxicity prediction: the volume of pharyngeal mucosa receiving ≥1 Gy should be minimized
Gabrys et al., 2018 (91)	153 pts, 24 selected radiomic features	Mixed subsites	Evaluation of xerostomia risk prediction with integrated ML	CT	I, D	Ipsi- and contralateral PGs	LR-L1, LR-L2, LR-EN, kNN, SVM, ET, GTB	SVMs were the top performing classifiers in time-specific xerostomia prediction (early, late, long term). In the longitudinal approach, the best models

(Continued)

TABLE 5 | Continued

Author, year of publication	Study population	HN subsite(s)	Clinical endpoint	Imaging modality	Textural and dosimetric parameters	ROI(s)	Tested ML algorithm(s)	Statistical findings and model performance
			models (clinical, dosimetric, and radiomic features) vs. NTCP models based on mean RT dose to the PGs					were GTB, ET and SVM. LR models were the best in feature selection, although selecting features did not provide any improvement in predictive performance. The NTCP mean dose-based models failed to predict xerostomia (AUC <0.60)
Cheng Z et al., 2017 (96)	391 pts	Mixed subsites	Prediction of WL ≥5 kg at 3 months post-RT	None	D	Pharyngeal constrictors, cricopharyngeus, masticator, temporalis, pterygoids, oral cavity, oral mucosa, soft palate, larynx, parotid gland, submandibular glands	CART algorithms	CART model encompassing toxicity and QoL data performed better than the one including baseline characteristics and dosimetric data (AUC: 0.82 vs. 0.77, Sn: 0.98 vs. 0.77, Sp 0.59 vs. 0.67, PPV 0.46 vs. 0.43, NPV: 0.99 vs. 0.90, respectively)
Soares et al., 2017 (90)	138 pts	Mixed subsites	Predicting xerostomia after RT	None	D	PGs	RF, stochastic boosting, SVM, NN, model-based clustering and LR	RF yielded the best model performance (AUC: 0.73); the incorporation of clinical (gender, age, baseline xerostomia) and dosimetric parameters (PG Dmean) outperformed all other RF combinations
Pota et al., 2015 (88)	21 pts, 42 parotids	NPC	Parotid gland shrinkage prediction	CT	I	Ipsi- and controlateral PGs	LFA, LDA, LR, 0-R method	In some cases, with only one predictor, the LR method presents the highest accuracy but low specificity, while in other cases with only one variable the performances of LDA, LR, and LFA are comparable. If more than one variable is used, the LFA classifier is the best in almost all the cases (best accuracy and sensitivity), while specificity is comparable with that of other classifiers. Adding a variable to a model hardly worsens the performances of both LDA and LR, while LFA models tolerate the noise

ANN, Artificial NN; AUC, area under the curve; CART, classification and regression tree; CT, computed tomography; CTCAE, common terminology criteria for adverse event; D, dosimetric; DCH, dose coverage histogram; DLH, dose lymphocyte histogram; Dmean, mean (RT) dose; DTI, diffusion tensor imaging; DVH, dose volume histogram; ET, extra-trees; gEUD, generalized equivalent uniform dose; GTB, gradient tree boosting; I, imaging; k-NN, k-nearest neighbor; LDA, linear discriminant analysis; LFA, logical framework approach; LR, logistic regression; ML, machine learning; MR, magnetic resonance; NN, neural network; NPC, nasopharyngeal cancer; NPV, negative predictive value; NTCP, normal tissue complication probability; OPC, oropharyngeal cancer; PG, parotid gland; PLR, penalized LR; PPV, positive predictive value; QoL, quality of life; RFC, random forest classification; SMG, submandibular gland; Sn, sensitivity; Sp, specificity; SVM, support vector machine; TNR, true-negative rate; TPR, true-positive rate; T1/T2-w, T1/T2-weighted; TBSS, tract-based spatial statistics; WL, weight loss; WM, white matter.

Yet, studies dedicated to outcome modeling and treatment planning achieved numerically lower scores in both the global and methodological assessment.

The scores for studies implementing imaging data (n = 37) categorized according to the use of texture analysis vs. other imaging-derived metrics or deep learning (n = 10 and 27, respectively) were evaluated. Since the analysis of quantitative extracted features usually requires an intensive work of statistical preprocessing, frequently lacking in deep learning studies, we tested the hypothesis that studies extracting features are associated with higher methodological scores. Even though no significant difference was found, a trend favoring texture analysis publications was noted especially for methodological study quality (p = 0.45 [FDR-corrected p = 0.67] vs. p = 0.62 [FDR-corrected p = 0.62] when the global score was considered, as shown in **Figure 5**).

The complete evaluation of each study is provided in **Figure 6**.

DISCUSSION

Results from our systematic review show a wide range of possible applications of ML in the field of HN Radiation Oncology,

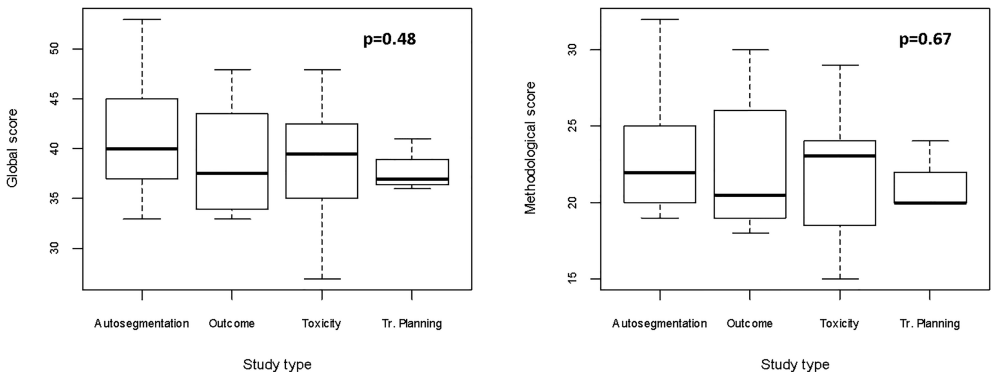

FIGURE 4 | Boxplots for global and methodological scores (modified Luo classification) for the studies included in the analysis, categorized according to the task of the proposed algorithm(s). Tr, treatment.

although this area of research is relatively young, with the majority of studies having been published in the last 3 years. The implementation of quantitative imaging features and the use of a longitudinally collected data as input parameters are both promising in refining model performance and open doors to further investigations.

The present analysis indicates a prevalence of algorithms dedicated to autocontouring, which mirrors the still unmet need for computationally affordable and user-friendly tools for clinical practice implementation. Even if only some authors have attempted to provide a full set of ROIs (56–61, 64, 67, 68), they could demonstrate a general improvement over existing models, with average times for task completion ranging between 0.12 and 30 s. However, the segmentation of small and/or low-contrasted areas, which are common in HN anatomy (e.g., optic chiasm, lenses, brainstem) remains challenging, and more efforts are warranted to equal, or at least to approximate, the performance of semiautomated or fully manual segmentation.

Currently available works on ML for treatment planning are scarce and show significant heterogeneity both in the choice of algorithms and in the characteristics of patients' populations. Nevertheless, results are promising, as they pave the way to the possibility of effectively reconstructing three-dimensional dose distribution of integrating MR in ART and of predicting the need for replanning based on geometrical and dosimetric modifications during treatment. It is straightforward to understand how the fulfillment of these objective may be relevant in everyday clinical practice, especially in the era of

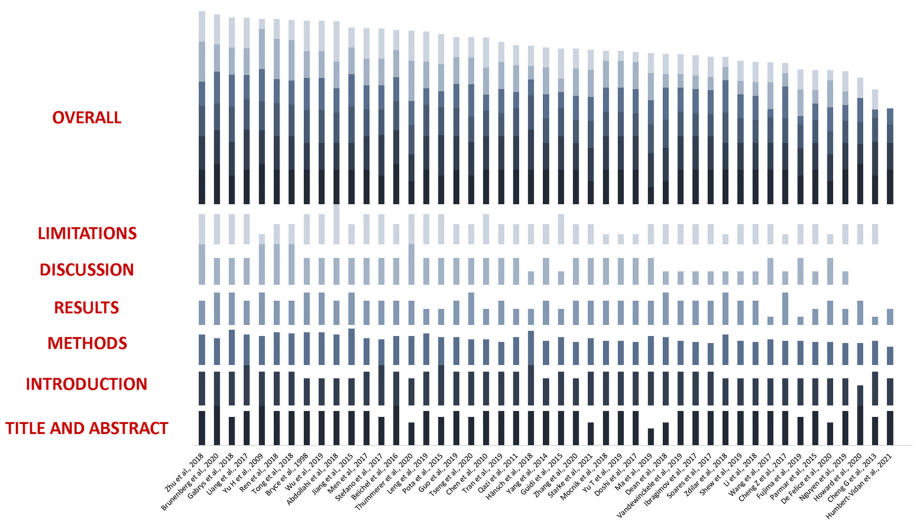

FIGURE 5 | Boxplots for global and methodological scores (modified Luo classification) for the studies included in the analysis, categorized according to imaging data used as input parameters (texture analysis vs. no texture analysis).

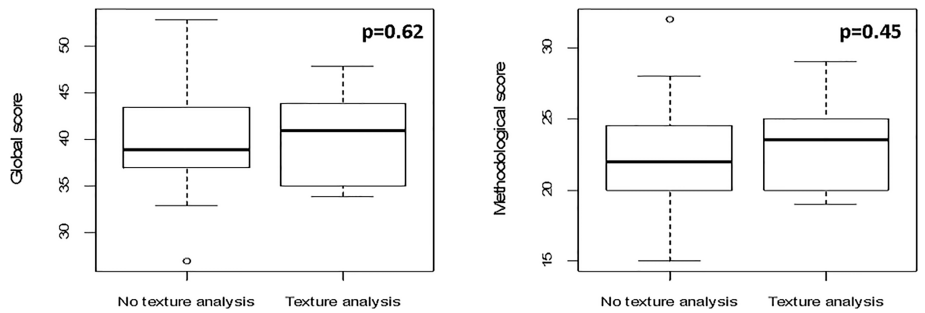

FIGURE 6 | Boxplots representing global and methodological scores (modified Luo classification) for the studies included in the analysis, categorized per the presence of texture analysis.

image-guided IMRT for HNC (25). Additionally, reliable ML-based predicting tools may be beneficial also for proton treatment planning, as dose deposition is heavily influenced by patient's set-up and anatomical variations of both target volumes and OARs (77, 97, 98).

Intriguing findings were reported for outcome prediction, as well. Considering oncological outcomes, supervised and unsupervised models were used with an overall satisfactory performance in small- to medium-sized datasets. Notably, the use of combined models incorporating radiomics (40) and longitudinal characteristics (86) yielded the best results. Moreover, neural networks outperformed competing algorithms in the prediction of recurrence patterns in NPC and survival in a population of locally advanced HNCs, respectively (79, 83). Conversely, only two studies incorporated ANNs for the prediction of RT-related toxicities (90, 95), and a prevalence of binary classifiers using labelled data was noticed, as expected. Gabrys et al. (91) were the only ones who compared ML univariate and multivariate logistic regression models to classical NTCP models based on the mean dose to the PGs. In their study, the authors could demonstrate that clinical characteristics and organ- and dose-shape features can improve xerostomia prediction, thus emphasizing the need of multidimensional input parameters to model complex outcomes.

Only one study focused on the use of ML for the analysis of organizational features of RT. In detail, Shew et al. (99) used a supervised classifier to discriminate risk factors correlating with delays in adjuvant treatment delivery. Despite several methodological limitations, the work is based on a large cohort from the National Cancer Database (NCDB), and includes a total of 76,573 patients. Another worth of this study relies in the use of ML for optimizing treatment scheduling: while prediction accuracy needs improving, the proposed model still provides a valuable example on how ML could be used in Radiation Oncology departments to facilitate executional tasks and, ultimately, to improve the quality of care.

Despite desirable, it is not currently possible to perform a reliable comparison among models, even for algorithms designed for the same task (i.e., autosegmentation). Not only was the choice of algorithms, features and variables widely heterogeneous, but most studies considered small- to medium-sized datasets and mixed disease subsites. In particular, sample size could strongly affect the quality of ML models as the training sets size is widely recognized as one of the main issues in pattern recognition studies. In fact, as the number of considered features increases, larger training sets become mandatory to avoid the so-called curse of dimensionality (100). To partially overcome this issue, we have performed a qualitative comparison based on a modified version of a reporting guideline validated by Luo et al. (23), which was previously introduced by Jethanandani et al. (12) in their systematic review on MR-based radiomic studies in HNCs. As pointed out by the authors, the checklist is not without limitations, including difficult and/or subjective interpretability of some items, as noted by our group as well.

Considering these pitfalls, and the fact that the checklist was not designed to provide a quantitative assessment, relevant findings still emerged. Firstly, studies aiming at toxicity prediction resulted to have the highest quality in both global and methodological scores as compared with those classified in the other categories. Secondly, works incorporating quantitative image features as input parameters had better median methodological scores, which could be at least partially explained by adequate reporting on the preprocessing on imaging data. Finally, works having a nonclinician as first author achieved a higher ranking, with a strong statistical significance. This finding could derive from the scarcity of dedicated educational training on ML and statistics in most medical schools and residency programs.

The DSC was the performance evaluation metric used in all works dedicated to autosegmentation, while the AUC was implemented in one study only (63). Considering the remaining publications, the AUC was the metric of choice in 17/27 (63%) cases. Despite its popularity for model assessment, limitations of the AUC have been extensively discussed (101). While a dissertation on the matter is beyond the scope of this work, those approaching ML should consider that AUC weights false positive and false negative predictions equally, which can be extremely relevant in the clinical setting (i.e., when the aim is to predict if a patient will develop mild vs. severe xerostomia).

Admittedly, our work presents some limitations. As for all systematic reviews, eligible publications of the last months may be missing, albeit the search was repeated regularly while the manuscript was being written. Moreover, despite our attempt to perform a comprehensive search, the lack of a common ontology in ML may have led to the exclusion of some works: to overcome this potential bias, cross-references from the included works were screened for eligibility. To conclude, we provided the full search strategy for future reference, as we are aware that several additional works will be published in the upcoming months, given the fast-growing nature of this field.

Acknowledging these issues, we do believe that, other than being a full overview of existing literature, the value of our work is to provide a systematic quality assessment of published works, which could be informative for both general and advanced readers. Large-scale datasets, common ontology, study design, and performance reporting will most probably be needed to concretely implement ML in clinical practice, and discussion on this regard is both expected and encouraged. To this aim, the inclusion of dedicated AI courses in the educational track of future ROs would arguably foster the quality of scientific outputs in the field.

Finally, ML-based modeling for HNC is a promising and rapidly expanding field, even though more solidly constructed and validated algorithms are warranted to overcome the boundaries of speculative investigation and to open doors to better tailored Radiation Oncology for this subset of patients. Overall, if not safe yet, ML is most probably a bet worth making.

DATA AVAILABILITY STATEMENT

The individual scores assigned to all the studies included in the manuscript are available upon request to the corresponding author.

AUTHOR CONTRIBUTIONS

SV, MP, MZ, FB, RS, GM, and BJF were responsible for conception and design of the study and wrote the first draft of the manuscript. SV, MP, MZ, and FB were responsible for data acquisition and wrote sections of the manuscript. LJI, DA, SG, AS, ML, and RO wrote sections of the manuscript. All authors contributed to manuscript revision and read and approved the submitted version.

FUNDING

The study was fully funded by the University of Milan with APC funds. The Institution of some authors (IEO) was partially supported by the Italian Ministry of Health with Ricerca Corrente and 5 × 1,000 funds. SV was supported by the Department of Oncology and Hemato-Oncology (DIPO) of the University of Milan with "Progetto di Eccellenza". MZ received a research grant from the European Institute of Oncology-Cardiologic Center Monzino Foundation (FIEO-CCM), with a project entitled "Proton therapy vs. photon-based IMRT for parotid gland tumors: a model based approach with Normal Tissue Complication Probability (NTCP)" outside the current study. SV, FB, and LJI are PhD students within the European School of Molecular Medicine (SEMM), Milan. The sponsors did not play any role in the study design, collection, analysis, and interpretation of data, nor in the writing of the manuscript, nor in the decision to submit the manuscript for publication.

SUPPLEMENTARY MATERIAL

The Supplementary Material for this article can be found online at: https://www.frontiersin.org/articles/10.3389/fonc.2021.772663/full#supplementary-material

REFERENCES

1. Chow LQM. Head and Neck Cancer. Longo DL, Ed. *N Engl J Med* (2020) 382(1):60–72. doi: 10.1056/NEJMra1715715
2. IARC- International Agency for Research on Cancer. *GLOBOCAN Cancer Fact Sheet 2018*. Available at: https://gco.iarc.fr/today/data/factsheets/cancers/39-All-cancers-fact-sheet.pdf.
3. D'Souza G, Westra WH, Wang SJ, van Zante A, Wentz A, Kluz N, et al. Differences in the Prevalence of Human Papillomavirus (HPV) in Head and Neck Squamous Cell Cancers by Sex, Race, Anatomic Tumor Site, and HPV Detection Method. *JAMA Oncol* (2017) 3(2):169. doi: 10.1001/jamaoncol.2016.3067
4. Maxwell JH, Grandis JR, Ferris RL. HPV-Associated Head and Neck Cancer: Unique Features of Epidemiology and Clinical Management. *Annu Rev Med* (2016) 67(1):91–101. doi: 10.1146/annurev-med-051914-021907
5. Scholfield DW, Gujral DM, Awad Z. Transoral Robotic Surgery for Oropharyngeal Squamous Cell Carcinoma: Improving Function While Maintaining Oncologic Outcome. *Otolaryngol Neck Surg* (2020) 162(3):267–8. doi: 10.1177/0194599820902043
6. Alsahafi E, Begg K, Amelio I, Raulf N, Lucarelli P, Sauter T, et al. Clinical Update on Head and Neck Cancer: Molecular Biology and Ongoing Challenges. *Cell Death Dis* (2019) 10(8):540. doi: 10.1038/s41419-019-1769-9
7. Golusiński W. Functional Organ Preservation Surgery in Head and Neck Cancer: Transoral Robotic Surgery and Beyond. *Front Oncol* (2019) 9:293. doi: 10.3389/fonc.2019.00293
8. Moskovitz J, Moy J, Ferris RL. Immunotherapy for Head and Neck Squamous Cell Carcinoma. *Curr Oncol Rep* (2018) 20(2):22. doi: 10.1007/s11912-018-0654-5
9. Meijer TWH, Scandurra D, Langendijk JA. Reduced Radiation-Induced Toxicity by Using Proton Therapy for the Treatment of Oropharyngeal Cancer. *Br J Radiol* (2020) 93(1107):20190955. doi: 10.1259/bjr.20190955
10. Gupta T, Kannan S, Ghosh-Laskar S, Agarwal JP. Systematic Review and Meta-Analyses of Intensity-Modulated Radiation Therapy Versus Conventional Two-Dimensional and/or or Three-Dimensional Radiotherapy in Curative-Intent Management of Head and Neck Squamous Cell Carcinoma. Woloschak GE, Ed. *PLoS One* (2018) 13(7):e0200137. doi: 10.1371/journal.pone.0200137
11. Jakobi A, Bandurska-Luque A, Stützer K, Haase R, Löck S, Wack LJ, et al. Identification of Patient Benefit From Proton Therapy for Advanced Head and Neck Cancer Patients Based on Individual and Subgroup Normal Tissue Complication Probability Analysis. *Int J Radiat Oncol* (2015) 92(5):1165–74. doi: 10.1016/j.ijrobp.2015.04.031
12. Jethanandani A, Lin TA, Volpe S, Elhalawani H, Mohamed ASR, Yang P, et al. Exploring Applications of Radiomics in Magnetic Resonance Imaging

of Head and Neck Cancer: A Systematic Review. *Front Oncol* (2018) 8:131. doi: 10.3389/fonc.2018.00131
13. Wong AJ, Kanwar A, Mohamed AS, Fuller CD. Radiomics in Head and Neck Cancer: From Exploration to Application. *Transl Cancer Res* (2016) 5 (4):371–82. doi: 10.21037/tcr.2016.07.18
14. Tinhofer I, Stenzinger A, Eder T, Konschak R, Niehr F, Endris V, et al. Targeted Next-Generation Sequencing Identifies Molecular Subgroups in Squamous Cell Carcinoma of the Head and Neck With Distinct Outcome After Concurrent Chemoradiation. *Ann Oncol* (2016) 27(12):2262–8. doi: 10.1093/annonc/mdw426
15. The Cancer Genome Atlas Network. Comprehensive Genomic Characterization of Head and Neck Squamous Cell Carcinomas. *Nature* (2015) 517(7536):576–82. doi: 10.1038/nature14129
16. Malone E, Siu LL. Precision Medicine in Head and Neck Cancer: Myth or Reality? *Clin Med Insights Oncol* (2018) 12:117955491877958. doi: 10.1177/1179554918779581
17. Feng M, Valdes G, Dixit N, Solberg TD. Machine Learning in Radiation Oncology: Opportunities, Requirements, and Needs. *Front Oncol* (2018) 8:110. doi: 10.3389/fonc.2018.00110
18. Bzdok D, Altman N, Krzywinski M. Statistics Versus Machine Learning. *Nat Methods* (2018) 15(4):233–4. doi: 10.1038/nmeth.4642
19. Bzdok D, Krzywinski M, Altman N. Points of Significance: Machine Learning: A Primer. *Nat Methods* (2017) 14(12):1119–20. doi: 10.1038/nmeth.4526
20. Isaksson LJ, Pepa M, Zaffaroni M, Marvaso G, Alterio D, Volpe S, et al. Machine Learning-Based Models for Prediction of Toxicity Outcomes in Radiotherapy. *Front Oncol* (2020) 10:790. doi: 10.3389/fonc.2020.00790
21. Boldrini L, Bibault J-E, Masciocchi C, Shen Y, Bittner M-I. Deep Learning: A Review for the Radiation Oncologist. *Front Oncol* (2019) 9:977. doi: 10.3389/fonc.2019.00977
22. Jarrett D, Stride E, Vallis K, Gooding MJ. Applications and Limitations of Machine Learning in Radiation Oncology. *Br J Radiol* (2019) 92 (1100):20190001. doi: 10.1259/bjr.20190001
23. Luo W, Phung D, Tran T, Gupta S, Rana S, Karmakar C, et al. Guidelines for Developing and Reporting Machine Learning Predictive Models in Biomedical Research: A Multidisciplinary View. *J Med Internet Res* (2016) 18(12):e323. doi: 10.2196/jmir.5870
24. Banno M, Tsujimoto Y, Kataoka Y. Reporting Quality of the Delphi Technique in Reporting Guidelines: A Protocol for a Systematic Analysis of the EQUATOR Network Library. *BMJ Open* (2019) 9(4):e024942. doi: 10.1136/bmjopen-2018-024942
25. National Comprehensive Cancer Network. *NCCN Clinical Practice Guidelines in Oncology (NCCN Guidelines). Head and Neck Cancers. Version 1.2020 - February 12* (2020). Available at: https://www.nccn.org/professionals/physician_gls/pdf/head-and-neck.pdf.
26. Walker GV, Awan M, Tao R, Koay EJ, Boehling NS, Grant JD, et al. Prospective Randomized Double-Blind Study of Atlas-Based Organ-at-Risk Autosegmentation-Assisted Radiation Planning in Head and Neck Cancer. *Radiother Oncol* (2014) 112(3):321–5. doi: 10.1016/j.radonc.2014.08.028
27. Mukesh M, Benson R, Jena R, Hoole A, Roques T, Scrase C, et al. Interobserver Variation in Clinical Target Volume and Organs at Risk Segmentation in Post-Parotidectomy Radiotherapy: Can Segmentation Protocols Help? *Br J Radiol* (2012) 85(1016):e530–6. doi: 10.1259/bjr/66693547
28. Feng MU, Demiroz C, Vineberg KA, Balter JM, Eisbruch A. Intra-Observer Variability of Organs at Risk for Head and Neck Cancer: Geometric and Dosimetric Consequences. *Int J Radiat Oncol* (2010) 78(3):S444–5. doi: 10.1016/j.ijrobp.2010.07.1044
29. Kosmin M, Ledsam J, Romera-Paredes B, Mendes R, Moinuddin S, de Souza D, et al. Rapid Advances in Auto-Segmentation of Organs at Risk and Target Volumes in Head and Neck Cancer. *Radiother Oncol* (2019) 135:130–40. doi: 10.1016/j.radonc.2019.03.004
30. Levendag PC, Hoogeman M, Teguh D, Wolf T, Hibbard L, Wijers O, et al. Atlas Based Auto-Segmentation of CT Images: Clinical Evaluation of Using Auto-Contouring in High-Dose, High-Precision Radiotherapy of Cancer in the Head and Neck. *Int J Radiat Oncol* (2008) 72(1):S401. doi: 10.1016/j.ijrobp.2008.06.1285
31. Langerak TR, Berendsen FF, van der Heide UA, Kotte ANTJ, Pluim JPW. Multiatlas-Based Segmentation With Preregistration Atlas Selection: Multiatlas-Based Segmentation With Preregistration Atlas Selection. *Med Phys* (2013) 40(9):091701. doi: 10.1118/1.4816654
32. Sandeep Kumar E, Satya Jayadev P. "Deep Learning for Clinical Decision Support Systems: A Review From the Panorama of Smart Healthcare". In: S Dash, BR Acharya, M Mittal, A Abraham, A Kelemen, editors. *Deep Learning Techniques for Biomedical and Health Informatics*, Studies in Big Data, vol 68. Cham: Springer (2020). p. 79–99. doi: 10.1007/978-3-030-33966-1_5
33. Inal A, Duman E, Ozkan E. Evaluating Different Radiotherapy Treatment Plans, in Terms of Critical Organ Scoring Index, Conformity Index, Tumor Control Probability, and Normal Tissue Complication Probability Calculations in Early Glottic Larynx Carcinoma. *J Cancer Res Ther* (2020) 16(3):485. doi: 10.4103/jcrt.JCRT_888_18
34. Stauch Z, Zoller W, Tedrick K, Walston S, Christ D, Hunzeker A, et al. An Evaluation of Adaptive Planning by Assessing the Dosimetric Impact of Weight Loss Throughout the Course of Radiotherapy in Bilateral Treatment of Head and Neck Cancer Patients. *Med Dosim* (2020) 45(1):52–9. doi: 10.1016/j.meddos.2019.05.003
35. Svecic A, Roberge D, Kadoury S. Prediction of Inter-Fractional Radiotherapy Dose Plans With Domain Translation in Spatiotemporal Embeddings. *Med Image Anal* (2020) 64:101728. doi: 10.1016/j.media.2020.101728
36. Liu Q, Liang J, Zhou D, Krauss DJ, Chen PY, Yan D. Dosimetric Evaluation of Incorporating Patient Geometric Variations Into Adaptive Plan Optimization Through Probabilistic Treatment Planning in Head and Neck Cancers. *Int J Radiat Oncol* (2018) 101(4):985–97. doi: 10.1016/j.ijrobp.2018.03.062
37. Patel RR, Ludmir EB, Augustyn A, Zaorsky NG, Lehrer EJ, Ryali R, et al. De-Intensification of Therapy in Human Papillomavirus Associated Oropharyngeal Cancer: A Systematic Review of Prospective Trials. *Oral Oncol* (2020) 103:104608. doi: 10.1016/j.oraloncology.2020.104608
38. Tanadini-Lang S, Balermpas P, Guckenberger M, Pavic M, Riesterer O, Vuong D, et al. Radiomic Biomarkers for Head and Neck Squamous Cell Carcinoma. *Strahlenther Onkol* (2020) 196(10):868–78. doi: 10.1007/s00066-020-01638-4
39. Konings H, Stappers S, Geens M, De Winter BY, Lamote K, van Meerbeeck JP, et al. A Literature Review of the Potential Diagnostic Biomarkers of Head and Neck Neoplasms. *Front Oncol* (2020) 10:1020. doi: 10.3389/fonc.2020.01020
40. Zdilar L, Vock DM, Marai GE, Fuller CD, Mohamed ASR, Elhalawani H, et al. Evaluating the Effect of Right-Censored End Point Transformation for Radiomic Feature Selection of Data From Patients With Oropharyngeal Cancer. *JCO Clin Cancer Inform* (2018) 2):1–19. doi: 10.1200/CCI.18.00052
41. Leger S, Zwanenburg A, Pilz K, Lohaus F, Linge A, Zöphel K, et al. A Comparative Study of Machine Learning Methods for Time-to-Event Survival Data for Radiomics Risk Modelling. *Sci Rep* (2017) 7(1):13206. doi: 10.1038/s41598-017-13448-3
42. Parmar C, Grossmann P, Rietveld D, Rietbergen MM, Lambin P, Aerts HJWL. Radiomic Machine-Learning Classifiers for Prognostic Biomarkers of Head and Neck Cancer. *Front Oncol* (2015) 5:272. doi: 10.3389/fonc.2015.00272
43. Vock DM, Wolfson J, Bandyopadhyay S, Adomavicius G, Johnson PE, Vazquez-Benitez G, et al. Adapting Machine Learning Techniques to Censored Time-to-Event Health Record Data: A General-Purpose Approach Using Inverse Probability of Censoring Weighting. *J BioMed Inform* (2016) 61:119–31. doi: 10.1016/j.jbi.2016.03.009
44. Jeong J, Baek H, Kim Y-J, Choi Y, Lee H, Lee E, et al. Human Salivary Gland Stem Cells Ameliorate Hyposalivation of Radiation-Damaged Rat Salivary Glands. *Exp Mol Med* (2013) 45(11):e58–8. doi: 10.1038/emm.2013.121
45. Guo Y, Jiang W, Lakshminarayanan P, Han P, Cheng Z, Bowers M, et al. Spatial Radiation Dose Influence on Xerostomia Recovery and Its Comparison to Acute Incidence in Patients With Head and Neck Cancer. *Adv Radiat Oncol* (2019) 5 (2):221–20. doi: 10.1016/j.adro.2019.08.009
46. Dean J, Wong K, Gay H, Welsh L, Jones AB, Schick U, et al. Incorporating Spatial Dose Metrics in Machine Learning-Based Normal Tissue Complication Probability (NTCP) Models of Severe Acute Dysphagia Resulting From Head and Neck Radiotherapy. *Clin Transl Radiat Oncol* (2018) 8:27–39. doi: 10.1016/j.ctro.2017.11.009
47. Scaife JE, Barnett GC, Noble DJ, Jena R, Thomas SJ, West CM, et al. Exploiting Biological and Physical Determinants of Radiotherapy Toxicity to

Individualize Treatment. *Br J Radiol* (2015) 88(1051):20150172. doi: 10.1259/bjr.20150172
48. West CML, Dunning AM, Rosenstein BS. Genome-Wide Association Studies and Prediction of Normal Tissue Toxicity. *Semin Radiat Oncol* (2012) 22(2):91–9. doi: 10.1016/j.semradonc.2011.12.007
49. Christopherson KM, Ghosh A, Mohamed ASR, Kamal M, Gunn GB, Dale T, et al. Chronic Radiation-Associated Dysphagia in Oropharyngeal Cancer Survivors: Towards Age-Adjusted Dose Constraints for Deglutitive Muscles. *Clin Transl Radiat Oncol* (2019) 18:16–22. doi: 10.1016/j.ctro.2019.06.005
50. Yang DW, Wang TM, Zhang JB, Li XZ, He YQ, Xiao R, et al. Genome-Wide Association Study Identifies Genetic Susceptibility Loci and Pathways of Radiation-Induced Acute Oral Mucositis. *J Transl Med* (2020) 18(1):224. doi: 10.1186/s12967-020-02390-0
51. Liberati A, Altman DG, Tetzlaff J, Mulrow C, Gøtzsche PC, Ioannidis JP, et al. The PRISMA Statement for Reporting Systematic Reviews and Meta-Analyses of Studies That Evaluate Healthcare Interventions: Explanation and Elaboration. *BMJ* (2009) 339(jul21 1):b2700–0. doi: 10.1136/bmj.b2700
52. Beichel RR, Van Tol M, Ulrich EJ, Bauer C, Chang T, Plichta KA, et al. Semiautomated Segmentation of Head and Neck Cancers in 18F-FDG PET Scans: A Just-Enough-Interaction Approach: Semiautomated Segmentation of Head and Neck Cancers. *Med Phys* (2016) 43(6Part1):2948–64. doi: 10.1118/1.4948679
53. Doshi T, Soraghan J, Petropoulakis L, Di Caterina G, Grose D, MacKenzie K, et al. Automatic Pharynx and Larynx Cancer Segmentation Framework (PLCSF) on Contrast Enhanced MR Images. *BioMed Signal Process Control* (2017) 33:178–88. doi: 10.1016/j.bspc.2016.12.001
54. Chen A, Deeley MA, Niermann KJ, Moretti L, Dawant BM. Combining Registration and Active Shape Models for the Automatic Segmentation of the Lymph Node Regions in Head and Neck CT Images: Registration and ASM Segmentation of Lymph Node Regions. *Med Phys* (2010) 37(12):6338–46. doi: 10.1118/1.3515459
55. Men K, Chen X, Zhang Y, Zhang T, Dai J, Yi J, et al. Deep Deconvolutional Neural Network for Target Segmentation of Nasopharyngeal Cancer in Planning Computed Tomography Images. *Front Oncol* (2017) 7:315. doi: 10.3389/fonc.2017.00315
56. Wang Y, Zhao L, Wang M, Song Z. Organ at Risk Segmentation in Head and Neck CT Images Using a Two-Stage Segmentation Framework Based on 3D U-Net. *IEEE Access* (2019) 7:144591–602. doi: 10.1109/ACCESS.2019.2944958
57. Liang S, Tang F, Huang X, Yang K, Zhong T, Hu R, et al. Deep-Learning-Based Detection and Segmentation of Organs at Risk in Nasopharyngeal Carcinoma Computed Tomographic Images for Radiotherapy Planning. *Eur Radiol* (2019) 29(4):1961–7. doi: 10.1007/s00330-018-5748-9
58. Vandewinckele L, Willems S, Robben D, Van Der Veen J, Crijns W, Nuyts S, et al. Segmentation of Head-and-Neck Organs-at-Risk in Longitudinal CT Scans Combining Deformable Registrations and Convolutional Neural Networks. *Comput Methods Biomech BioMed Eng Imaging Vis* (2019) 11045:1–10. doi: 10.1080/21681163.2019.1673824
59. Zhu W, Huang Y, Zeng L, Chen X, Liu Y, Qian Z, et al. AnatomyNet: Deep Learning for Fast and Fully Automated Whole-Volume Segmentation of Head and Neck Anatomy. *Med Phys* (2019) 46(2):576–89. doi: 10.1002/mp.13300
60. Nikolov S, Blackwell S, Mendes R, et al. *Deep Learning to Achieve Clinically Applicable Segmentation of Head and Neck Anatomy for Radiotherapy. ArXiv180904430 Phys Stat* (2018). Available at: http://arxiv.org/abs/1809.04430 (Accessed July 10, 2020).
61. Tong N, Gou S, Yang S, Ruan D, Sheng K. Fully Automatic Multi-Organ Segmentation for Head and Neck Cancer Radiotherapy Using Shape Representation Model Constrained Fully Convolutional Neural Networks. *Med Phys* (2018) 45(10):4558–67. doi: 10.1002/mp.13147
62. Močnik D, Ibragimov B, Xing L, Strojan P, Likar B, Pernuš F, et al. Segmentation of Parotid Glands From Registered CT and MR Images. *Phys Med* (2018) 52:33–41. doi: 10.1016/j.ejmp.2018.06.012
63. Hänsch A, Schwier M, Gass T, Morgas T. Evaluation of Deep Learning Methods for Parotid Gland Segmentation From CT Images. *J Med Imaging* (2018) 6(01):1. doi: 10.1117/1.JMI.6.1.011005
64. Ibragimov B, Xing L. Segmentation of Organs-at-Risks in Head and Neck CT Images Using Convolutional Neural Networks. *Med Phys* (2017) 44(2):547–57. doi: 10.1002/mp.12045
65. Yang X, Wu N, Cheng G, Zhou Z, Yu DS, Beitler JJ, et al. Automated Segmentation of the Parotid Gland Based on Atlas Registration and Machine Learning: A Longitudinal MRI Study in Head-and-Neck Radiation Therapy. *Int J Radiat Oncol Biol Phys* (2014) 90(5):1225–33. doi: 10.1016/j.ijrobp.2014.08.350
66. Cheng G, Yang X, Wu N, Xu Z, Zhao H, Wang Y. Multi-Atlas-Based Segmentation of the Parotid Glands of MR Images in Patients Following Head-and-Neck Cancer Radiotherapy. *Medical Imaging* (2013) 8670:86702Q. doi: 10.1117/12.2007783
67. Qazi AA, Pekar V, Kim J, Xie J, Breen SL, Jaffray DA. Auto-Segmentation of Normal and Target Structures in Head and Neck CT Images: A Feature-Driven Model-Based Approach: Feature-Driven Model-Based Segmentation. *Med Phys* (2011) 38(11):6160–70. doi: 10.1118/1.3654160
68. Brunenberg EJL, Steinseifer IK, van den Bosch S, Kaanders JHAM, Brouwer CL, Gooding MJ, et al. External Validation of Deep Learning-Based Contouring of Head and Neck Organs at Risk. *Phys Imaging Radiat Oncol* (2020) 15:8–15. doi: 10.1016/j.phro.2020.06.006
69. Ma Z, Zhou S, Wu X, Zhang H, Yan W, Sun S, et al. Nasopharyngeal Carcinoma Segmentation Based on Enhanced Convolutional Neural Networks Using Multi-Modal Metric Learning. *Phys Med Biol* (2019) 64(2):025005. doi: 10.1088/1361-6560/aaf5da
70. Ren X, Xiang L, Nie D, Shao Y, Zhang H, Shen D, et al. Interleaved 3d-CNNs for Joint Segmentation of Small-Volume Structures in Head and Neck CT Images. *Med Phys* (2018) 45(5):2063–75. doi: 10.1002/mp.12837
71. Liang S, Tang F, Huang X, Yang K, Zhong T, Hu R, et al. Deep-Learning-Based Detection and Segmentation of Organs at Risk in Nasopharyngeal Carcinoma Computed Tomographic Images for Radiotherapy Planning. *Eur Radiol* (2019) 29(4):1961–7. doi: 10.1007/s00330-018-5748-9
72. Stefano A, Vitabile S, Russo G, Ippolito M, Sabini MG, Sardina D, et al. An Enhanced Random Walk Algorithm for Delineation of Head and Neck Cancers in PET Studies. *Med Biol Eng Comput* (2017) 55(6):897–908. doi: 10.1007/s11517-016-1571-0
73. Yu H, Caldwell C, Mah K, Poon I, Balogh J, MacKenzie R, et al. Automated Radiation Targeting in Head-And-Neck Cancer Using Region-Based Texture Analysis of PET and CT Images. *Int J Radiat Oncol* (2009) 75(2):618–25. doi: 10.1016/j.ijrobp.2009.04.043
74. Guidi G, Maffei N, Vecchi C, Ciarmatori A, Mistretta GM, Gottardi G, et al. A Support Vector Machine Tool for Adaptive Tomotherapy Treatments: Prediction of Head and Neck Patients Criticalities. *Phys Med* (2015) 31(5):442–51. doi: 10.1016/j.ejmp.2015.04.009
75. Yu HT, Lam SK, To LT, Tse KY, Cheng NY, Fan YN, et al. Pretreatment Prediction of Adaptive Radiation Therapy Eligibility Using MRI-Based Radiomics for Advanced Nasopharyngeal Carcinoma Patients. *Front Oncol* (2019) 9:1050. doi: 10.3389/fonc.2019.01050
76. Nguyen D, Jia X, Sher D, Lin MH, Iqbal Z, Liu H, et al. 3D Radiotherapy Dose Prediction on Head and Neck Cancer Patients With a Hierarchically Densely Connected U-Net Deep Learning Architecture. *Phys Med Biol* (2019) 64(6):65020. doi: 10.1088/1361-6560/ab039b
77. Thummerer A, de Jong BA, Zaffino P, Meijers A, Marmitt GG, Seco J, et al. Comparison of the Suitability of CBCT- and MR-Based Synthetic CTs for Daily Adaptive Proton Therapy in Head and Neck Patients. *Phys Med Biol* (2020) 65(23):235036. doi: 10.1088/1361-6560/abb1d6
78. Jiang R, You R, Pei XQ, Zou X, Zhang MX, Wang TM, et al. Development of a Ten-Signature Classifier Using a Support Vector Machine Integrated Approach to Subdivide the M1 Stage Into M1a and M1b Stages of Nasopharyngeal Carcinoma With Synchronous Metastases to Better Predict Patients' Survival. *Oncotarget* (2016) 7(3):3645–57. doi: 10.18632/oncotarget.6436
79. Bryce TJ, Dewhirst MW, Floyd CE, Hars V, Brizel DM. Artificial Neural Network Model of Survival in Patients Treated With Irradiation With and Without Concurrent Chemotherapy for Advanced Carcinoma of the Head and Neck. *Int J Radiat Oncol* (1998) 41(2):339–45. doi: 10.1016/S0360-3016(98)00016-9
80. De Felice F, Humbert-Vidan L, Lei M, King A, Guerrero Urbano T. Analyzing Oropharyngeal Cancer Survival Outcomes: A Decision Tree Approach. *Br J Radiol* (2020) 93(1111):20190464. doi: 10.1259/bjr.20190464
81. Howard FM, Kochanny S, Koshy M, Spiotto M, Pearson AT. Machine Learning–Guided Adjuvant Treatment of Head and Neck Cancer. *JAMA Netw Open* (2020) 3(11):e2025881. doi: 10.1001/jamanetworkopen.2020.25881

82. Tran WT, Suraweera H, Quaioit K, Cardenas D, Leong KX, Karam I, et al. Predictive Quantitative Ultrasound Radiomic Markers Associated With Treatment Response in Head and Neck Cancer. *Future Sci OA* (2020) 6 (1):FSO433. doi: 10.2144/fsoa-2019-0048
83. Li S, Wang K, Hou Z, Yang J, Ren W, Gao Z, et al. Use of Radiomics Combined With Machine Learning Method in the Recurrence Patterns After Intensity-Modulated Radiotherapy for Nasopharyngeal Carcinoma: A Preliminary Study. *Front Oncol* (2018) 8:648. doi: 10.3389/fonc.2018.00648
84. Fujima N, Shimizu Y, Yoshida D, Kano S, Mizumachi T, Homma A, et al. Machine-Learning-Based Prediction of Treatment Outcomes Using MR Imaging-Derived Quantitative Tumor Information in Patients With Sinonasal Squamous Cell Carcinomas: A Preliminary Study. *Cancers* (2019) 11(6):800. doi: 10.3390/cancers11060800
85. Starke S, Leger S, Zwanenburg A, Leger K, Lohaus F, Linge A, et al. 2D and 3D Convolutional Neural Networks for Outcome Modelling of Locally Advanced Head and Neck Squamous Cell Carcinoma. *Sci Rep* (2020) 10 (1):15625. doi: 10.1038/s41598-020-70542-9
86. Wu J, Gensheimer MF, Zhang N, Han F, Liang R, Qian Y, et al. Integrating Tumor and Nodal Imaging Characteristics at Baseline and Mid-Treatment Computed Tomography Scans to Predict Distant Metastasis in Oropharyngeal Cancer Treated With Concurrent Chemoradiotherapy. *Int J Radiat Oncol* (2019) 104(4):942–52. doi: 10.1016/j.ijrobp.2019.03.036
87. Tseng Y-J, Wang H-Y, Lin T-W, Lu J-J, Hsieh C-H, Liao C-T. Development of a Machine Learning Model for Survival Risk Stratification of Patients With Advanced Oral Cancer. *JAMA Netw Open* (2020) 3(8):e2011768. doi: 10.1001/jamanetworkopen.2020.11768
88. Pota M, Scalco E, Sanguineti G, Cattaneo GM, Esposito M, Rizzo G. Early Classification of Parotid Glands Shrinkage in Radiotherapy Patients: A Comparative Study. *Biosyst Eng* (2015) 138:77–89. doi: 10.1016/j.biosystemseng.2015.06.007
89. Guo C, Shi X, Ding X, Zhou Z. Analysis of Radiation Effects in Digital Subtraction Angiography of Intracranial Artery Stenosis. *World Neurosurg* (2018) 115:e472–5. doi: 10.1016/j.wneu.2018.04.072
90. Soares I, Dias J, Rocha H, Khouri L, do Carmo Lopes M, Ferreira B. Predicting Xerostomia After IMRT Treatments: A Data Mining Approach. *Health Technol* (2018) 8(1-2):159–68. doi: 10.1007/s12553-017-0204-4
91. Gabrys HS, Buettner F, Sterzing F, Hauswald H, Bangert M. Design and Selection of Machine Learning Methods Using Radiomics and Dosiomics for Normal Tissue Complication Probability Modeling of Xerostomia. *Front Oncol* (2018) 8:35. doi: 10.3389/fonc.2018.00035
92. Abdollahi H, Mostafaei S, Cheraghi S, Shiri I, Rabi Mahdavi S, Kazemnejad A. Cochlea CT Radiomics Predicts Chemoradiotherapy Induced Sensorineural Hearing Loss in Head and Neck Cancer Patients: A Machine Learning and Multi-Variable Modelling Study. *Phys Med PM Int J Devoted Appl Phys Med Biol Off J Ital Assoc BioMed Phys AIFB* (2018) 45:192–7. doi: 10.1016/j.ejmp.2017.10.008
93. Leng X, Fang P, Lin H, Qin C, Tan X, Liang Y, et al. Application of a Machine Learning Method to Whole Brain White Matter Injury After Radiotherapy for Nasopharyngeal Carcinoma. *Cancer Imaging Off Publ Int Cancer Imaging Soc* (2019) 19(1):19. doi: 10.1186/s40644-019-0203-y
94. Zhang B, Lian Z, Zhong L, Zhang X, Dong Y, Chen Q, et al. Machine-Learning Based MRI Radiomics Models for Early Detection of Radiation-Induced Brain Injury in Nasopharyngeal Carcinoma. *BMC Cancer* (2020) 20 (1):502. doi: 10.1186/s12885-020-06957-4
95. Humbert-Vidan L, Patel V, Oksuz I, King AP, Guerrero Urbano T. Comparison of Machine Learning Methods for Prediction of Osteoradionecrosis Incidence in Patients With Head and Neck Cancer. *Br J Radiol* (2021) 94(1120):20200026. doi: 10.1259/bjr.20200026
96. Cheng Z, Nakatsugawa M, Hu C, Robertson SP, Hui X, Moore JA, et al. Evaluation of Classification and Regression Tree (CART) Model in Weight Loss Prediction Following Head and Neck Cancer Radiation Therapy. *Adv Radiat Oncol* (2018) 3(3):346–55. doi: 10.1016/j.adro.2017.11.006
97. Deiter N, Chu F, Lenards N, Hunzeker A, Lang K, Mundy D. Evaluation of Replanning in Intensity-Modulated Proton Therapy for Oropharyngeal Cancer: Factors Influencing Plan Robustness. *Med Dosim* (2020) 45: S095839472030100X. doi: 10.1016/j.meddos.2020.06.002
98. Moreno AC, Frank SJ, Garden AS, Rosenthal DI, Fuller CD, Gunn GB, et al. Intensity Modulated Proton Therapy (IMPT) – The Future of IMRT for Head and Neck Cancer. *Oral Oncol* (2019) 88:66–74. doi: 10.1016/j.oraloncology.2018.11.015
99. Shew M, New J, Bur AM. Machine Learning to Predict Delays in Adjuvant Radiation Following Surgery for Head and Neck Cancer. *Otolaryngol Head Neck Surg* (2019) 160(6):1058–64. doi: 10.1177/0194599818823200
100. Balki I, Amirabadi A, Levman J, Martel AL, Emersic Z, Meden B, et al. Sample-Size Determination Methodologies for Machine Learning in Medical Imaging Research: A Systematic Review. *Can Assoc Radiol J J Assoc Can Radiol* (2019) 70(4):344–53. doi: 10.1016/j.carj.2019.06.002
101. Lobo JM, Jiménez-Valverde A, Real R. AUC: A Misleading Measure of the Performance of Predictive Distribution Models. *Glob Ecol Biogeogr* (2008) 17 (2):145–51. doi: 10.1111/j.1466-8238.2007.00358.x

Conflict of Interest: The authors declare that the research was conducted in the absence of any commercial or financial relationships that could be construed as a potential conflict of interest.

Publisher's Note: All claims expressed in this article are solely those of the authors and do not necessarily represent those of their affiliated organizations, or those of the publisher, the editors and the reviewers. Any product that may be evaluated in this article, or claim that may be made by its manufacturer, is not guaranteed or endorsed by the publisher.

frontiers in Oncology

CASE REPORT
published: 25 November 2021
doi: 10.3389/fonc.2021.733772

Radiation Treatment for Inoperable Local Relapse of Parathyroid Carcinoma With Symptomatic Hypercalcemia: A Case Report

Heleen Bollen[1,2]*, *Brigitte Decallonne*[3] *and Sandra Nuyts*[1,2]

[1] Laboratory of Experimental Radiotherapy, Department of Oncology, University Hospitals Leuven, Leuven, Belgium,
[2] Department of Radiation Oncology, Leuven Cancer Institute, University Hospitals Leuven, Leuven, Belgium,
[3] Department of Endocrinology, University Hospitals Leuven, Leuven, Belgium

Background: Parathyroid carcinoma (PC) is an extremely rare malignancy, characterized by slow progression, frequent recurrences and difficult-to-control hypercalcemia which is typically the main contributor to the morbidity and mortality of these patients. Patients often undergo repeated surgical resections, whether or not in combination with adjuvant radiation treatment. The role of radiation therapy within the symptomatic treatment of PC currently remains unclear.

Case description: We describe a 30-year-old male patient with an inoperable local relapse of PC and secondary symptomatic hypercalcemia, maximally pharmacologically treated. After a local radiation treatment to a total dose of 70 Gray in 35 fractions serum calcium and parathyroid hormone (PTH) levels decreased, accompanied by improvement of the severe gastro-intestinal disturbances.

Conclusion: For patients with inoperable symptomatic PC despite maximal medical treatment who are in a good overall condition, radiation treatment can be considered in well-defined cases to decrease symptoms and improve quality of life.

Keywords: case report, parathyroid carcinoma, radiotherapy, radiosensitivity, symptomatic treatment, hypercalcemia

OPEN ACCESS

Edited by:
Wenyin Shi,
Thomas Jefferson University,
United States

Reviewed by:
Olivera Ivanov,
University of Novi Sad, Serbia
Ester Orlandi,
National Center of Oncological Hadrontherapy, Italy

***Correspondence:**
Heleen Bollen
heleen.bollen@uzleuven.be

Specialty section:
This article was submitted to Radiation Oncology, a section of the journal Frontiers in Oncology

Received: *30 June 2021*
Accepted: *10 November 2021*
Published: *25 November 2021*

Citation:
Bollen H, Decallonne B and Nuyts S (2021) Radiation Treatment for Inoperable Local Relapse of Parathyroid Carcinoma With Symptomatic Hypercalcemia: A Case Report. Front. Oncol. 11:733772. doi: 10.3389/fonc.2021.733772

INTRODUCTION

Parathyroid carcinoma (PC) represents one of the most rare malignancies. In 1909, de Quervain was the first to report a patient with a PC (1). PC accounts for approximately 11 cases per 10 million people in the United States and less than 1% of all patients presenting with primary hyperparathyroidism (2–8), although a higher proportion has been reported in Asian populations (9). In Belgium, only 20 cases were reported between 2001 and 2010 (10). PC does not have the gender predilection as observed with benign parathyroid tumors, which show a definite female preponderance (3:1) (11). Most cancers present in patients aged between 44 and 60 years (10, 12–16), but a patient as young as 8 years has been reported (17). Clinical features are mostly due to the effects of the excessive secretion of parathyroid hormone (PTH) by the functioning tumor with secondary hypercalcemia, rather than to the tumor burden. The disease is usually diagnosed in an advanced stage, given the non-specific symptoms, and usually has a slow progressive course. Most patients will die due to complications of hypercalcemia, rather than direct tumor invasion or metastases (18–20).

The main treatment for PC is surgery. Given that a complete excision is often technically difficult as the disease is usually diagnosed in a locally advanced stage, persistent or recurrent disease occurs in over 50% of patients (2, 20–22). Patients thus frequently suffer from multiple recurrences, mostly presenting with a gradual rise in PTH and calcium levels, for which numerous surgical resections are often needed. Systemic treatment with the calcimimetic cinacalcet can reduce calcium and PTH levels, but usually loses efficacy over time (12). Cytotoxic chemotherapy has not been proven to affect disease-free or overall survival (13). Since treatment options beyond surgical resection are limited, a radiation treatment (RT) could serve as a valid treatment alternative when surgery of the primary tumor or metastases is no longer feasible. However, PC is generally considered a radio-resistant tumor and literature about RT is limited to the assessment of the value of RT in the adjuvant setting. The rarity of PC has precluded any prospective study and current knowledge about PC is the result of individual case reports and retrospective studies. The role of RT within the symptomatic treatment of PC has not yet been evaluated. We describe a case report of a 30-year-old patient, treated with RT for an inoperable local relapse of PC and secondary symptomatic hypercalcemia. To our knowledge, this is the first case report of symptomatic RT of inoperable PC.

CASE DESCRIPTION

Patient Information, Clinical Findings, and Diagnostic Assessment

A 30-year-old male patient was diagnosed with a PC in 2013, for which he underwent a resection. During the following years, the patient suffered several local relapses, for which 5 more procedures were performed, including local resections, a total thyroidectomy and both a central and bilateral neck dissection. In 2019, the patient presented for the first time in our hospital with persisting PTH-mediated hypercalcemia, while under maximally tolerated dose of the calcimimetic cinacalcet (90mg twice daily) and bone-antiresorptive therapy with denosumab (120 mg once monthly). CT scan showed two suspicious retrosternal lesions, a paratracheal node and a possible adenopathy in lymph node level III at the right side. All suspect locations were resected and a thymectomy was performed. Pathology confirmed the presence of PC retrosternally, in level III on the right, and retroclavicular and paratracheal on the left. As shown in **Table 1** and **Figure 1**, serum calcium and PTH levels decreased after the surgical procedure, and cinacelet and denosumab could be stopped.

Eight months later, the patient experienced a relapse of symptomatic hypercalcemia, in which nausea was predominant, however without convincing tumoral focus at imaging (FDG PET-CT, MRI of the neck, CT of the mediastinum). Cinacalcet was restarted at an intermediate dose. Unfortunately, serum calcium and PTH kept on rising, for which the dose of cinacalcet was increased to maximal dose and denosumab was restarted. With this medical therapy, calcium levels stabilized, remaining at high-normal levels. However, during the following months, serum PTH increased progressively. Repeated imaging now showed a nodular, contrast-capturing lesion between the anonymous vein and the sternum, with erosion of the sternum and the first rib on the left (**Figure 2**).

Therapeutic Intervention

As the lesion was considered inoperable, the multidisciplinary tumor board decided to opt for a radiation treatment (RT). When patient presented at our RT department, he suffered from

TABLE 1 | Timeline with evolution of biochemistry, clinical symptoms and radiological features.

	Calcium (mg/dl)	PTH (µg/L)	Phosphate (mmol/l)	1,25 di(OH)-vit D (ng/L)	Clinical and radiological information
Reference range	**8.6 - 10.3**	**14.9 - 56.9**	**0.81 - 1.45**	**20.0 - 80.0**	
Diagnosis local relapse (D0)	12.30	1086	0.24	143.6	Diagnosis of local relapse, planning of surgical resection. Increase of calcium and PTH under maximal dose of cinacalcet and denosumab.
D0 + 1 week	8.70	5	0.96	N.A.	One week after surgical resection of local relapse.
D0 + 6 weeks	7.54	7.7	1.81	23.0	Six weeks after surgical resection of local relapse, stop cinacalcet and denosumab.
D0 + 8 months	13.07	96	0.54	49.4	Eight months after surgical resection. Increase of calcium and PTH. Restart cinacalcet and denosumab.
D0 + 12 months	10.50	1245	0.42	N.A.	Continuous increase of PTH under maximal dose of cinacalcet and denosumab. Diagnosis of inoperable local relapse.
Start RT (D0RT)	12.18	2049	0.43	232.0	Referral to RT department. Patient suffers from severe nausea.
D0RT + 3weeks	11.42	1069	0.37	N.A.	Three weeks after start of RT.
D0RT + 4 weeks	11.26	926	0.28	218.9	Four weeks after start of RT. Decrease of calcium and PTH.
D0RT + 5 weeks	11.46	859	0.34	221.5	Five weeks after start of RT. Further decrease of calcium and PTH. Decrease of nausea.
D0RT + 2 months	10.70	429	0.44	165.3	Two months after end of RT. Further decrease of calcium and PTH, CT scan shows pseudo-progression.
D0RT + 7 months	10.82	504	0.39	204.2	Seven months after end of RT. Calcium and PTH stable, CT scan shows volume decrease.
D0RT + 9 months	12.02	452	0.45	232.3	Volume increase on CT scan, recurrence of nausea.

N.A, not available; RT, radiation treatment; PTH, parathyroid hormone; D0, time of diagnosis of the local relapse and planning of surgery; D0RT, time of start RT. As of D0 + 8 months, patient remained under maximal dose of cinacalcet and denosumab.

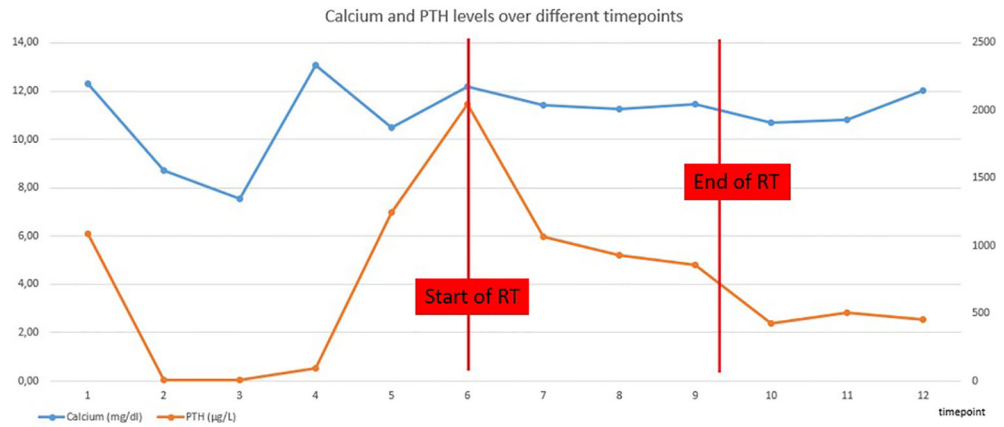

FIGURE 1 | Evolution of serum calcium and PTH concentrations.

severe nausea, which could have been either a side effect from the calcimimetics or directly due to the hypercalcemia. He did not experience pain due to the erosive lesion in the sternum. Based on the few literature that existed, it was decided to deliver a radiation dose of 70 Gray (Gy) in 35 fractions of 2 Gy, using an arc technique with 6 MV photons. Gross Tumor Volume (GTV) was contoured manually and defined as demonstrable macroscopic disease on CT. The Clinical Target Volume (CTV) consisted of a 10-millimetre margin around the GTV, corrected for bone and air cavities. Another 5 millimetres were added for the construction of the Planning Target Volume. Volumetric Modulated Arc Therapy (VMAT) was used, using 2 arcs allowing a precise shaping of the dose to the form of the tumor. Daily cone beam CT imaging was performed to improve the precision and accuracy of the delivery of radiation treatment. Just before the start of RT, the patient developed acute sternal pain, caused by a sternal fracture for which a conservative treatment with analgesics was proposed. The pain disappeared quickly during the RT.

Follow-Up and Outcomes

During the radiation treatment, the patient reported markedly less gastro-intestinal discomfort. At the end of the treatment, he did not need any symptomatic anti-nausea medication and there was significant weight gain. Furthermore, there was a good tolerance for the treatment: patient developed a grade I dermatitis, there was no dysphagia. Serum calcium and PTH levels were checked weekly during RT and showed a progressive decline (**Table 1** and **Figure 1**).

Two months after the end of the RT, the patient was still free from nausea and PTH and calcium levels were progressively decreasing. On CT-scan, a small volume increase of the sternal lesion was described. This increase was presumably due to pseudo-progression resulting from tumor necrosis, based on the density of the lesion and decreasing levels of calcium and PTH (**Figure 3**). Five months later, the clinical and biochemical situation was stable and CT-scan showed a volume decrease of the sternal lesion (**Figure 4**). The patient did not experience any pain and nausea was controlled under maximal dose of

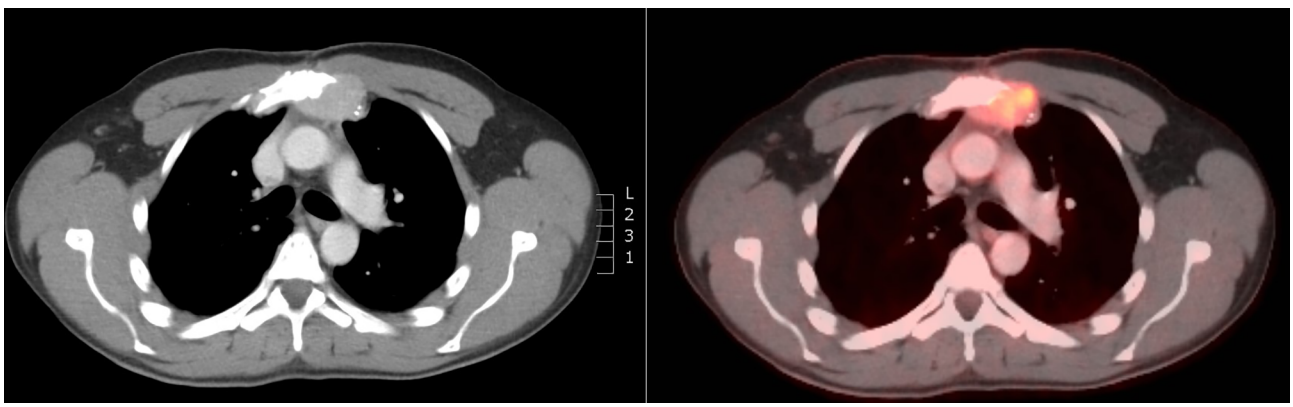

FIGURE 2 | FDG PET/CT at diagnosis of inoperable retrosternal relapse with bone invasion.

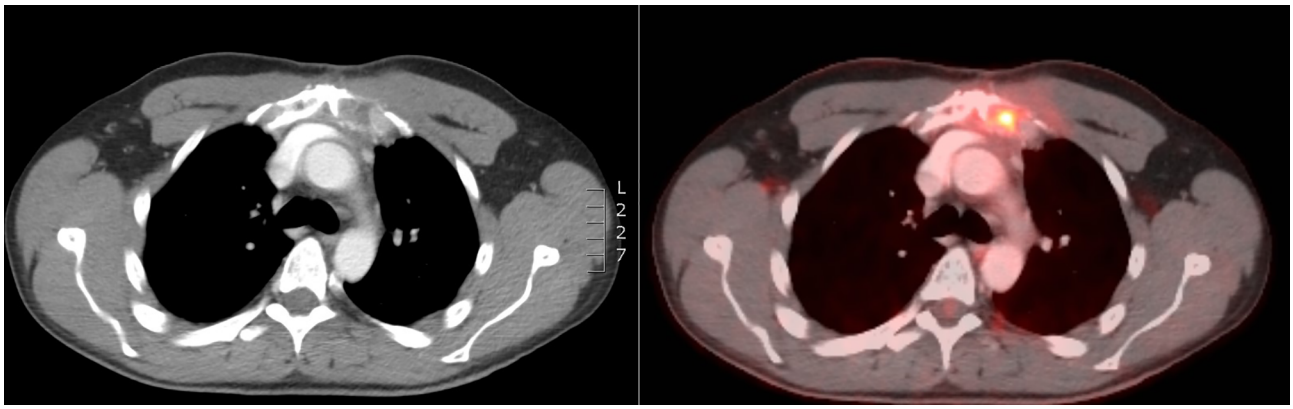

FIGURE 3 | CT scan at 2 months after RT showing volume increase of the sternal lesion, probably due to pseudo-progression.

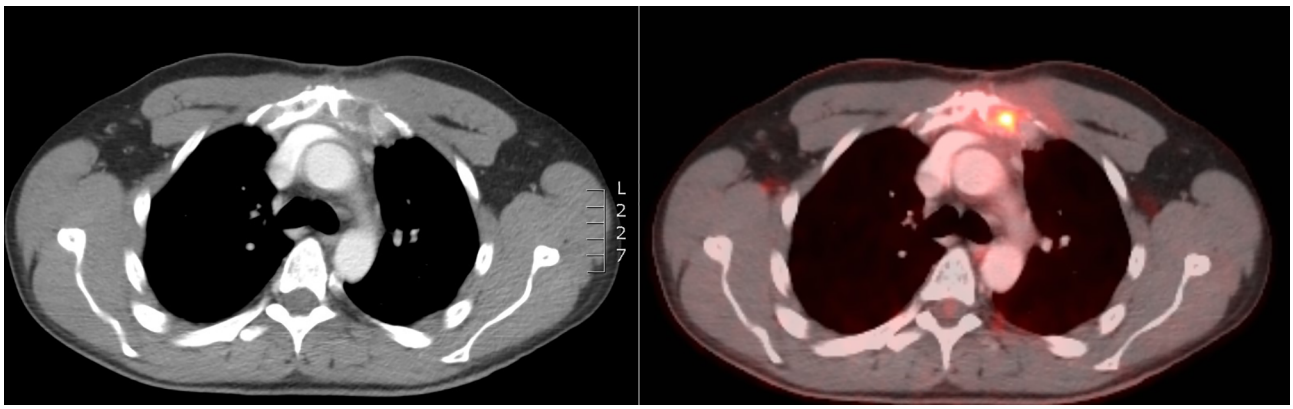

FIGURE 4 | CT scan 7 months after the end of RT showing volume decrease of the sternal lesion.

calcimimetics and bone antiresorptive therapy. Unfortunately, two months later, he experienced a return of gastro-intestinal disturbances. An increase of serum calcium levels was observed and a volume increase of the sternal lesion was confirmed on FDG PET-CT. Patient was referred for inclusion in a medical trial, in which he is currently treated with PARP (poly ADP ribose polymerase)-inhibition.

DISCUSSION

In this report, we describe a case of a patient with an inoperable sternal relapse of PC with disabling nausea secondary to malignant PTH-mediated hypercalcemia. Upon RT, which was well-tolerated, the patient reported a significant improvement of the gastro-intestinal discomfort for seven months, during which anti-nausea medication could be stopped and body weight gain occurred. This clinical evolution was paralleled by a decline of PTH and calcium levels until two months after RT, and calcium and PTH levels remained stable for 7 months after RT.

Prognosis of PC

The only series reporting survival in PC patients are those in which surgery was the primary treatment modality. The M. D. Anderson series of 27 patients showed a 5-year overall survival (OS) of 85% and a 10-year OS of 77% (22). The authors reported no significant association between any demographic or pathologic feature and prognosis. A recent National Cancer Database Analysis on 885 patients reported a 5-year and 10-year OS of 85.4% (95% CI 82.4-87.9%) and 67.1% (95% CI 61.7-72.0%) (3).

Surgical and Pharmacological Treatment

The cornerstone of the treatment for PC is surgery. Complete surgical en bloc resection with ipsilateral hemithyroidectomy and prophylactic central lymphadenectomy (level VI) is generally recommended, and microscopic negative margins are considered the best chance for cure (2, 3, 20, 23–26). Lymphadenectomy of regional lymph nodes other than level VI is not recommended as no therapeutic benefit has been established (22, 27). The majority of patients is only diagnosed

with PC after surgery, which means that most resections are incomplete (21). Early surgical re-excision is recommended in patients who are diagnosed after simple parathyroidectomy (14, 15). Even in the case of a curative resection, PC has a recurrence rate of more than 50% (2, 20–22). Most recurrences occur 2–3 years after the initial operation, but this period is variable and a prolonged disease-free interval of as long as 23 years has been reported in the literature (2, 21). This emphasizes the importance of long-term follow-up of patients after surgery. A short disease-free interval is associated with poor prognosis. Recurrent disease mostly presents with rising levels of serum calcium and PTH. Surgery is the most effective treatment for recurrent PC (21, 28, 29). Reoperation has been proven to decrease PTH and calcium levels and to improve symptoms and is thus recommended when feasible (12, 30). Unfortunately, reoperations for parathyroid cancer are rarely if ever curative (12, 27, 31).

Most PCs are functional, where only a few are non-functional with normal serum PTH and calcium levels (12). Although there are no biochemical or radiologic diagnostic criteria for PC, serum calcium levels are generally higher than in parathyroid adenomas (32, 33). Symptoms and signs of PC are mostly secondary to hypercalcemia rather than expansion of the tumor itself. The most frequent complaints are nausea, anorexia, vomiting, weight loss, dyspepsia, fatigue, constipation, headaches, myopathy, neurocognitive deficits, polydipsia and polyuria. Bone, joint, muscular pain, pathological fractures and renal stones are also frequent. As patients usually die from the metabolic complications of hypercalcemia, medical treatment with calcimimetics and bone-antiresoptive drugs and if needed forced hydratation with loop diuretics is indicated for long-term control of hypercalcemia (11, 21, 34). Although usually partially effective, medical therapy often loses efficacy over time (12).

In this particular case, the question arose as to the best approach, given that a surgical operation was no longer possible and the patient suffered from severe symptomatic hypercalcemia, despite maximal medical treatment with calcimimetics and bone antiresorptive therapy.

The Role of Radiotherapy in the Treatment of PC

As the treatment of PC is mainly surgical, literature about RT is limited to contradictory studies, evaluating the benefits of adjuvant RT. To our knowledge, no trials or case reports exist regarding RT without prior surgery as treatment of PC. PC is considered radio-resistant and therefore adjuvant RT has traditionally not been deemed effective (6, 14, 20, 26, 35–37). However, a few small case series have demonstrated lower recurrence and longer disease free survival with the use of adjuvant RT, although without significant overall survival benefit (2, 18, 22, 34, 38–40). The Mayo Clinic has reported a disease-free survival at a median follow-up period of 60 months in 4 patients who received postoperative RT (34). The M.D. Anderson experience suggests a lower local recurrence rate if adjuvant radiation is given after surgery, independent of the type of operation and the disease stage (40). These studies provide some evidence that PC may be a radiosensitive tumor and adjuvant RT may have a role in the control of locoregional disease progression (11, 41). A recent large National Cancer Database Analysis did, however, not show any survival benefit of RT in the adjuvant treatment of PC (3). All trials dealing with RT as adjuvant treatment include a small number of patients without any comparison, thus no strong conclusion can be drawn. Based on the existing data, the choice was made not to deliver adjuvant RT after surgical resection of the retrosternal relapse.

Literature does not provide an answer about the role of RT when systemic therapy proves insufficient as symptomatic treatment. The rarity of PC renders a randomized prospective trial very difficult, hindering the generation of sufficient statistical power through a large number of patients. Guidelines published by the American Association of Endocrine Surgeons (AAES) state that RT can be considered in patients with refractory disease who are not candidates for re-operation (23). As our patient met these conditions, the multidisciplinary team decided to deliver RT to a total dose of 70 Gy in 35 fractions of 2 Gy. Regarding the decision about the delivered radiotherapy dose, the existing literature is limited and only addresses the issue of the radiation dose in an adjuvant setting. Furthermore, results are statistically underpowered and little information is provided about the extent of surgical resection. In both Chow et al. and Christakis et al., all 10 patients underwent the standard resection with adjuvant RT up to 40 Gy. No recurrences were identified over a follow-up of 1 to over 12 years (18, 38). Doses of 50 to 66 Gy in adjuvant setting are reported by M.D. Anderson and Mayo Clinic (22, 34). We relied upon our experience with RT in rare cases of thyroid cancer, such as anaplastic thyroid cancer, and decided to deliver a curative dose of 70 Gy since the patient was young and in good physical condition. Our patient experienced a continuous decrease of calcium and PTH levels during two months after the RT, which was translated into a significant reduction of gastro-intestinal complaints. Both metabolic symptoms and biochemical values remained stable up until 7 months after RT. The result of the RT is promising and clinically relevant since further treatment options were limited and the patient's quality of life improved for a significant period of time. Furthermore, a clear tumor volume decrease was observed on a CT scan performed 7 months after the end of treatment. Together, these findings suggest radiosensitivity of PC, with a reduction of both tumor load and metabolic consequences.

Trials or case reports regarding a symptomatic radiation treatment of PC to decrease metabolic complaints are scarce and it is difficult to draw conclusions from the literature that is available. A decrease of PTH levels during adjuvant RT has been reported (19). Some older studies, performed on patients with bulky neck disease who had not undergone surgery, failed to demonstrate either a reduction of tumoral mass or the attainment of normocalcemia with RT (38, 42). One case report mentions beneficial biochemical and symptomatic effects of radiofrequency ablation of 10 liver metastases of parathyroid carcinoma in a 71-year-old patient (43). The latter suggests a benefit of a radical treatment of either a local relapse or metastatic disease, which supports our choice for a curative dose of 70 Gy.

Since our patient was very young, had a good overall condition and was not responding any longer to calcimimetics and bone antiresorptive therapy, we considered RT as a possible modality to prevent the patient from developing pain due to the local relapse and to reduce metabolic complaints. The experienced side effects of RT were minimal, so the choice for RT seemed to be justifiable in this particular case. However, the development of side effects strongly depends on the location of the relapse, so benefits and drawbacks of RT need to be outweighed for each patient individually. The decision on the most suitable treatment is thus preferably taken by an experienced multidisciplinary tumor board in a high-volume center with extensive experience with head and neck tumors.

Future treatment options, including immunotherapy, multi Kinase and Poly ADP Ribose Polymerase inhibitors, are currently under investigation and, with further refining, will hopefully become a part of the arsenal to treat PC. With regard to RT, particle therapy such as proton and carbon ion therapy might provide the opportunity to provide a higher RT dose to the target volume (TV), while minimizing possible side effects. In this particular case, considering the intrinsic radio-resistance of PC, the proximity of the TV to the lungs and the heart and the young age of the patient, particle therapy could be valuable. However, given the lack of evidence, further research is needed. In the meantime, there may be a role for symptomatic X-ray radiation therapy in well-defined cases.

CONCLUSION

PC remains difficult to treat, with limited effective treatment options beyond surgical resection. In inoperable cases, refractory to medical treatment with calcimimetic agents and bone antiresorptive drugs to achieve metabolic and symptomatic control, radiation therapy can be considered. The presented case suggests radiosensitivity, resulting in both a reduction of both tumor load and control of malignant hypercalcemia-related symptoms.

DATA AVAILABILITY STATEMENT

The original contributions presented in the study are included in the article/supplementary material. Further inquiries can be directed to the corresponding author.

ETHICS STATEMENT

The studies involving human participants were reviewed and approved by the Ethics Committee Research UZ/KU Leuven. The patients/participants provided their written informed consent to participate in this study. Written informed consent was obtained from the individual(s) for the publication of any potentially identifiable images or data included in this article.

AUTHOR CONTRIBUTIONS

Writing manuscript draft, HB. Writing review and editing, SN, BD and HB. Supervision, SN and DB. All authors have read and agreed to the published version of the manuscript.

REFERENCES

1. de Quervain F. Parastruma Maligna Aberrata - Beitrag Zur Einteilung Der Halsgeschwülste. *Dtsch Z für Chir* (1909) 100(1):334–53. doi: 10.1007/BF02819737
2. Shane E. Parathyroid Carcinoma. *Curr Ther Endocrinol Metab* (1997) 6:565–8.
3. Limberg J, Stefanova D, Ullmann TM, Thiesmeyer JW, Bains S, Beninato T, et al. The Use and Benefit of Adjuvant Radiotherapy in Parathyroid Carcinoma: A National Cancer Database Analysis. *Ann Surg Oncol* (2021) 28(1):502–11. doi: 10.1245/s10434-020-08825-8
4. Lo WM, Good ML, Nilubol N, Perrier ND, Patel DT. Tumor Size and Presence of Metastatic Disease at Diagnosis are Associated With Disease-Specific Survival in Parathyroid Carcinoma. *Ann Surg Oncol* (2018) 25 (9):2535–40. doi: 10.1245/s10434-018-6559-6
5. Wächter S, Holzer K, Manoharan J, Brehm C, Mintziras I, Bartsch DK, et al. Surgical Treatment of Parathyroid Carcinoma: Does the Initial En Bloc Resection Improve the Prognosis? *Chirurg* (2019) 90(11):905–12. doi: 10.1007/s00104-019-1007-0
6. Lee PK, Jarosek SL, Virnig BA, Evasovich M, Tuttle TM. Trends in the Incidence and Treatment of Parathyroid Cancer in the United States. *Cancer* (2007) 109(9):1736–41. doi: 10.1002/cncr.22599
7. Ferraro V, Sgaramella LI, Di Meo G, Prete FP, Logoluso F, Minerva F, et al. Current Concepts in Parathyroid Carcinoma: A Single Centre Experience. *BMC Endocr Disord* (2019) 19(Suppl 1):46. doi: 10.1186/s12902-019-0368-1
8. Talat N, Schulte KM. Clinical Presentation, Staging and Long-Term Evolution of Parathyroid Cancer. *Ann Surg Oncol* (2010) 17(8):2156–74. doi: 10.1245/s10434-010-1003-6
9. Xue S, Chen H, Lv C, Shen X, Ding J, Liu J, et al. Preoperative Diagnosis and Prognosis in 40 Parathyroid Carcinoma Patients. *Clin Endocrinol* (2016) 85 (1):29–36. doi: 10.1111/cen.13055
10. Cancer Fact Sheets, Belgian Cancer Registry and Incidence Year 2019. Brussels 2021.
11. Rawat N, Khetan N, Williams DW, Baxter JN. Parathyroid Carcinoma. *Br J Surg* (2005) 92(11):1345–53. doi: 10.1002/bjs.5182
12. Rodrigo JP, Hernandez-Prera JC, Randolph GW, Zafereo ME, Hartl DM, Silver CE, et al. Parathyroid Cancer: An Update. *Cancer Treat Rev* (2020) 86:102012. doi: 10.1016/j.ctrv.2020.102012
13. Cetani F, Pardi E, Marcocci C. Update on Parathyroid Carcinoma. *J Endocrinol Invest* (2016) 39(6):595–606. doi: 10.1007/s40618-016-0447-3
14. Koea JB, Shaw JHF. Parathyroid Cancer: Biology and Management. *Surg Oncol* (1999) 8(3):155–65. doi: 10.1016/s0960-7404(99)00037-7
15. Apaydın T, Yavuz DG. Seven Cases of Parathyroid Carcinoma and Review of the Literature. *Hormones* (2021) 20(1):189–95. doi: 10.1007/s42000-020-00220-y
16. Sadler C, Gow KW, Beierle EA, Doski JJ, Langer M, Nuchtern JG, et al. Parathyroid Carcinoma in More Than 1,000 Patients: A Population-Level Analysis. *Surgery (United States)* (2014) 156(6):1622–30. doi: 10.1016/j.surg.2014.08.069
17. Hamill J, Maoate K, Beasley SW, Corbett R, Evans J. Familial Parathyroid Carcinoma in a Child. *J Paediatr Child Health* (2002) 38(3):314–7. doi: 10.1046/j.1440-1754.2002.00802.x
18. Christakis I, Silva AM, Williams MD, Garden A, Grubbs EG, Busaidy NL, et al. Postoperative Local-Regional Radiation Therapy in the Treatment of

Parathyroid Carcinoma: The MD Anderson Experience of 35 Years. *Pract Radiat Oncol* (2017) 7(6):e463–70. doi: 10.1016/j.prro.2017.05.009
19. Digonnet A, Carlier A, Willemse E, Quiriny M, Dekeyser C, de Saint Aubain N, et al. Parathyroid Carcinoma: A Review With Three Illustrative Cases. *J Cancer* (2011) 2:532–7. doi: 10.7150/jca.2.532
20. Givi B, Shah JP. Parathyroid Carcinoma. *Clin Oncol* (2010) 22(6):498–507. doi: 10.1016/j.clon.2010.04.007
21. Kebebew E. Parathyroid Carcinoma. *Curr Treat Options Oncol* (2001) 2 (4):347–54. doi: 10.1007/s11864-001-0028-2
22. Busaidy NL, Jimenez C, Habra MA, Schultz PN, El-Naggar AK, Clayman GL, et al. Parathyroid Carcinoma: A 22-Year Experience. *Head Neck* (2004) 8):716–26. doi: 10.1002/hed.20049
23. Wilhelm SM, Wang TS, Ruan DT, Lee JA, Asa SL, Duh QY, et al. The American Association of Endocrine Surgeons Guidelines for Definitive Management of Primary Hyperparathyroidism. *JAMA Surg* (2016) 151 (10):959–68. doi: 10.1001/jamasurg.2016.2310
24. Salcuni AS, Cetani F, Guarnieri V, Nicastro V, Romagnoli E, de Martino D, et al. Parathyroid Carcinoma. *Best Pract Res Clin Endocrinol Metab* (2018) 32 (6):877–89. doi: 10.1016/j.beem.2018.11.002
25. Mohebati A, Shaha A, Shah J. Parathyroid Carcinoma: Challenges in Diagnosis and Treatment. *Hematol Oncol Clin North Am* (2012) 26 (6):1221–38. doi: 10.1016/j.hoc.2012.08.009
26. Wei CH, Harari A. Parathyroid Carcinoma: Update and Guidelines for Management. *Curr Treat Options Oncol* (2012) 13(1):11–23. doi: 10.1007/s11864-011-0171-3
27. Owen RP, Silver CE, Pellitteri PK, Shaha AR, Devaney KO, Werner JA, et al. Parathyroid Carcinoma: A Review. *Head Neck* (2010) 33(3):429–36. doi: 10.1002/hed.21376
28. Thompson SD, Prichard AJN. The Management of Parathyroid Carcinoma. *Curr Opin Otolaryngol Head Neck Surg* (2004) 12(2):93–7. doi: 10.1097/00020840-200404000-00007
29. Kebebew E, Arici C, Duh QY, Clark OH, Byrd D, Latimer RG, et al. Localization and Reoperation Results for Persistent and Recurrent Parathyroid Carcinoma. *Arch Surg* (2001) 136(8):878–85. doi: 10.1001/archsurg.136.8.878
30. Pramanik S, Ray S, Bhattacharjee R, Chowdhury S. Parathyroid Carcinoma and Persistent Hypercalcemia: A Case Report and Review of Therapeutic Options. *Saudi J Med Med Sci* (2018) 6(2):115–18. doi: 10.4103/sjmms.sjmms_104_16
31. Storvall S, Ryhänen E, Bensch FV, Heiskanen I, Kytölä S, Ebeling T, et al. Recurrent Metastasized Parathyroid Carcinoma-Long-Term Remission After Combined Treatments With Surgery, Radiotherapy, Cincacalcet, Zoledronic Acid and Temozolomide. *JBMR Plus* (2018) 3(4):e10114. doi: 10.1002/jbm4.10114
32. Bae JH, Choi HJ, Lee Y, Moon MK, Park YJ, Shin CS, et al. Preoperative Predictive Factors for Parathyroid Carcinoma in Patients With Primary Hyperparathyroidism. *J Korean Med Sci* (2012) 27(8):890–5. doi: 10.3346/jkms.2012.27.8.890
33. Fernandes JMP, Paiva C, Correia R, Polónia J, Moreira da Costa A. Parathyroid Carcinoma: From a Case Report to a Review of the Literature. *Int J Surg Case Rep* (2018) 42:214–7. doi: 10.1016/j.ijscr.2017.11.030
34. Munson ND, Foote RL, Northcutt RC, Tiegs RD, Fitzpatrick LA, Grant CS, et al. Parathyroid Carcinoma: Is There a Role for Adjuvant Radiation Therapy? *Cancer* (2003) 98(11):2378–84. doi: 10.1002/cncr.11819
35. Asare EA, Sturgeon C, Winchester DJ, Liu L, Palis B, Perrier ND, et al. Parathyroid Carcinoma: An Update on Treatment Outcomes and Prognostic Factors From the National Cancer Data Base (NCDB). *Ann Surg Oncol* (2015) 22(12):3990–5. doi: 10.1245/s10434-015-4672-3
36. Wynne AG, Van Heerden J, Aidan Carney J, Fitzpatrick LA. Parathyroid Carcinoma: Clinical and Pathologic Features in 43 Patients. *Medicine (United States)* (1992) 71(4):197–205. doi: 10.1097/00005792-199207000-00002
37. Harari A, Waring A, Fernandez-Ranvier G, Hwang J, Suh I, Mitmaker E, et al. Parathyroid Carcinoma: A 43-Year Outcome and Survival Analysis. *J Clin Endocrinol Metab* (2011) 96(12):3679–86. doi: 10.1210/jc.2011-1571
38. Chow E, Tsang RW, Brierley JD, Filice S. Parathyroid Carcinoma - The Princess Margaret Hospital Experience. *Int J Radiat Oncol Biol Phys* (1998) 41 (3):569–72. doi: 10.1016/s0360-3016(98)00098-4
39. Erovic BM, Goldstein DP, Kim D, Mete O, Brierley J, Tsang R, et al. Parathyroid Cancer: Outcome Analysis of 16 Patients Treated at the Princess Margaret Hospital. *Head Neck* (2013) 35(1):35–9. doi: 10.1002/hed.22908
40. Clayman GL, Gonzalez HE, El-Naggar A, Vassilopoulou-Sellin R. Parathyroid Carcinoma: Evaluation and Interdisciplinary Management [Internet]. *Cancer Cancer* (2004) 100:900–5. doi: 10.1002/cncr.20089
41. Fingeret AL. Contemporary Evaluation and Management of Parathyroid Carcinoma. *JCO Oncol Pract* (2021) 17(1):17–21. doi: 10.1200/JOP.19.00540
42. Fujimoto Y, Obara T, Ito Y, Kanazawa K, Aiyoshi Y, Nobori M. Surgical Treatment of Ten Cases of Parathyroid Carcinoma: Importance of an Initial En Bloc Tumor Resection. *World J Surg* (1984) 8(3):392–8. doi: 10.1007/BF01655086
43. Artinyan A, Guzman E, Maghami E, Al-Sayed M, D'Apuzzo M, Wagman L, et al. Metastatic Parathyroid Carcinoma to the Liver Treated With Radiofrequency Ablation and Transcatheter Arterial Embolization. *J Clin Oncol* (2008) 26(24):4039–41. doi: 10.1200/JCO.2007.15.9038

Conflict of Interest: The authors declare that the research was conducted in the absence of any commercial or financial relationships that could be construed as a potential conflict of interest.

Publisher's Note: All claims expressed in this article are solely those of the authors and do not necessarily represent those of their affiliated organizations, or those of the publisher, the editors and the reviewers. Any product that may be evaluated in this article, or claim that may be made by its manufacturer, is not guaranteed or endorsed by the publisher.

frontiers in Oncology

ORIGINAL RESEARCH
published: 26 November 2021
doi: 10.3389/fonc.2021.771956

Impact of Advanced Radiotherapy on Second Primary Cancer Risk in Prostate Cancer Survivors: A Nationwide Cohort Study

*Marie-Christina Jahreiß[1], Wilma D. Heemsbergen[1], Bo van Santvoort[2], Mischa Hoogeman[1], Maarten Dirkx[1], Floris J. Pos[3], Tomas Janssen[3], Andre Dekker[4], Ben Vanneste[4], Andre Minken[5], Carel Hoekstra[5], Robert J. Smeenk[6], Inge M. van Oort[7], Chris H. Bangma[8], Luca Incrocci[1] and Katja K. H. Aben[2,9]**

[1] Department of Radiotherapy, Erasmus MC Cancer Institute, Rotterdam, Netherlands, [2] Department of Research, Netherlands Comprehensive Cancer Organization, Utrecht, Netherlands, [3] The Netherlands Cancer Institute, Radiation Oncology, Amsterdam, Netherlands, [4] Department of Radiation Oncology (Maastro), GROW Institute for Oncology and Developmental Biology, Maastricht, Netherlands, [5] Department of Radiation Oncology, Radiotherapiegroep, Deventer, Netherlands, [6] Department of Radiation Oncology, Radboud University Medical Center, Nijmegen, Netherlands, [7] Department of Urology, Radboud University Medical Center, Nijmegen, Netherlands, [8] Department of Urology, Erasmus University Medical Center, Rotterdam, Netherlands, [9] Research Institute for Health Sciences, Radboud University Medical Center, Nijmegen, Netherlands

OPEN ACCESS

Edited by:
Xinglei Shen, University of Kansas Medical Center, United States

Reviewed by:
Stephanie Kroeze, University Hospital Zürich, Switzerland
Tomer Charas, Rambam Health Care Campus, Israel

***Correspondence:**
Katja K. H. Aben
k.aben@iknl.nl

Specialty section:
This article was submitted to Radiation Oncology, a section of the journal Frontiers in Oncology

Received: *07 September 2021*
Accepted: *08 November 2021*
Published: *26 November 2021*

Citation:
Jahreiß M-C, Heemsbergen WD, van Santvoort B, Hoogeman M, Dirkx M, Pos FJ, Janssen T, Dekker A, Vanneste B, Minken A, Hoekstra C, Smeenk RJ, van Oort IM, Bangma CH, Incrocci L and Aben KKH (2021) Impact of Advanced Radiotherapy on Second Primary Cancer Risk in Prostate Cancer Survivors: A Nationwide Cohort Study. Front. Oncol. 11:771956. doi: 10.3389/fonc.2021.771956

Purpose: External Beam Radiotherapy (EBRT) techniques dramatically changed over the years. This may have affected the risk of radiation-induced second primary cancers (SPC), due to increased irradiated low dose volumes and scatter radiation. We investigated whether patterns of SPC after EBRT have changed over the years in prostate cancer (PCa) survivors.

Materials and Methods: PCa survivors diagnosed between 1990-2014 were selected from the Netherlands Cancer Registry. Patients treated with EBRT were divided in three time periods, representing 2-dimensional Radiotherapy (RT), 3-dimensional conformal RT (3D-CRT), and the advanced RT (AdvRT) era. Standardized incidence ratios (SIR) and absolute excess risks (AER) were calculated to estimate relative and excess absolute SPC risks. Sub-hazard ratios (sHRs) were calculated to compare SPC rates between the EBRT and prostatectomy cohort. SPCs were categorized by subsite and anatomic region.

Results: PCa survivors who received EBRT had an increased risk of developing a solid SPC (SIR=1.08; 1.05-1.11), especially in patients aged <70 years (SIR=1.13; 1.09-1.16). Pelvic SPC risks were increased (SIR=1.28; 1.23-1.34), with no obvious differences between the three EBRT eras. Non-pelvic SPC were only significantly increased in the AdvRT era (SIR=1.08; 1.02-1.14), in particular for the 1-5 year follow-up period. Comparing the EBRT cohort to the prostatectomy cohort, again an increased pelvic SPC risk was found for all EBRT periods (sHRs= 1.61, 1.47-1.76). Increased non-pelvic SPC risks were present for all RT eras and highest for the AdvRT period (sHRs=1.17, 1.06-1.29).

Conclusion: SPC risk in patients with EBRT is increased and remained throughout the different EBRT eras. The risk of developing a SPC outside the pelvic area changed unfavorably in the AdvRT era. Prolonged follow-up is needed to confirm this observation. Whether this is associated with increased irradiated low-dose volumes and scatter, or other changes in clinical EBRT practice, is the subject of further research.

Keywords: prostate cancer, second primary cancer, survivorship, advanced external beam radiotherapy, three-dimensional conformal radiotherapy

INTRODUCTION

Prostate Cancer (PCa) is the second most commonly diagnosed cancer in men. The worldwide PCa burden is expected to grow to almost 2.3 million new cases by 2040 (1). Considering the overall success in detecting, diagnosing, and treating PCa, the assessment of long-term adverse events of the available treatment options has become increasingly important. A rare but severe long-term adverse event is a radiation-induced second primary cancer (SPC) (2, 3). The associations between radiation exposure and SPC are well-recognized (4, 5). Large cohort studies exploring SPC risk after PCa have confirmed that RT is associated with increased SPC risk (2, 5–10). The majority of these large cohort studies are based on data from national cancer registries in which details on treatment, such as type of External Beam Radiotherapy (EBRT), are typically not registered.

A large proportion of PCa patients receive EBRT. EBRT has undergone major changes over the past decades. In the early 1990s, 2-dimensional radiotherapy (RT) with rectangular fields including the pelvic area was the conventional technique applied. By the second half of the 1990s, there was a shift to 3-dimensional conformal RT (3D-CRT), targeting only the prostate +/- the seminal vesicles. In the Netherlands, from 2005 onwards, intensity modulated RT (IMRT) gradually replaced 3D-CRT. This was closely followed by the introduction of volumetric modulated arc therapy (VMAT). With these advanced techniques, more conformal dose distributions with steeper dose gradients can be achieved. This is done by using multiple intensity-modulated beams, allowing better sparing of the organs at risk, and dose-escalation to the tumor without exceeding critical dose levels to nearby organs (11, 12). IMRT and VMAT are nowadays often combined with daily image-guidance to track the tumor position. These advanced radiotherapy (AdvRT) techniques result in a larger body volume being exposed to low levels of radiation. Studies and theoretical reports have expressed concerns that this may be associated with increased long-term risks of developing a radiation-induced SPC (11, 13, 14).

Clear evidence from clinical observations on the impact of AdvRT on SPC risk is lacking. Few studies exist that explore SPC risk after EBRT, and those studies show inconclusive results (11, 15–17). The aim of the current study is to assess in a large nationwide cohort the risks and time trends of developing SPC after EBRT compared to reference populations, by studying different time periods related to major landmarks in EBRT developments.

METHODS

Data and Patient Selection

For this retrospective cohort study, data of PCa patients were retrieved through the Netherlands Cancer Registry (NCR). The NCR, established in 1989 with nationwide coverage, is a registry containing data of all new cancer diagnoses in the Netherlands. Notifications of newly diagnosed malignancies are primarily obtained from the nationwide network and registry of histology and cytopathology (PALGA). Information on malignancies without any histological confirmation are extracted from Dutch Hospital Data (DHD). Additional relevant data (patient/tumor characteristics and treatment) are routinely extracted from the hospital patient files. Cancers are coded according to The International Classification of Diseases for Oncology (ICD-O-3) (18). Patients diagnosed between 1990-2014 with a PCa (ICD-O-3 Topography code C61) were included in this study. Information on patient characteristics, as well as information on the primary PCa such as date of diagnosis, morphology, disease stage (Tumor Lymph Node Metastasis (TNM) classification), and treatment, were obtained from the NCR. PCa treatment was classified as follows: EBRT +/- hormonal therapy (HT), radical prostatectomy, brachytherapy, systemic therapy (HT or chemotherapy), active surveillance, and other.

Definition of Time Periods

Time periods were defined and used as a proxy for the different RT modalities applied. In the early 1990s, 2D-RT was the golden standard and was only gradually replaced by 3D-CRT towards the end of the decade. Therefore, the first time period was defined from 1990 to 1996. The second time period, in which 3D-CRT was the main RT modality, was defined from 1998-2005. In 2005, IMRT was introduced in the Netherlands, which was closely followed by the introduction of VMAT in 2008. The last time period was thus defined from 2008-2014. The introduction of a new RT technique is a gradual process. Hence, to avoid excessive overlap in applied RT modality, some years were disregarded.

Definition of SPC and Follow-Up Time

All invasive SPC (except for non-melanoma skin cancers) and non-invasive bladder cancer, were included. Information regarding the topography, morphology and date of diagnosis were obtained from the NCR. Analyses were carried out for all SPC, all solid SPC, all hematological SPC and SPC within

different anatomical regions (e.g., pelvic and non-pelvic region) and for specific tumor subsites. In general, only the first SPC cancer was included in the analyses. However, for all analyses focusing on a specific group (i.e., solid cancers, hematological cancers, anatomical region of specific subsite), the first SPC cancer within that group was included in the analyses. Hence, the total number of SPC in the overall group does not add up to the sum of SPCs by subsites. Follow-up time was defined as the time between PCa diagnosis until the date of SPC diagnosis, date of death, date of emigration or end of study (31.12.2019), whichever occurred first. SPC diagnosed simultaneously with PCa or within one year after the initial PCa diagnosis were excluded, as these are likely to represent synchronous cancers.

Statistical Analysis

A descriptive overview including all PCa patients was provided, followed by an overview of the risk of developing a SPC. Standardized Incidence Ratios (SIRs) were calculated to evaluate the risk of SPC in the PCa patient cohort compared to the Dutch population. This was done by dividing the observed number of SPC by the expected number of cases (based on the sex, age, and calendar specific incidence rates in the Netherlands). Poisson regression was used to compute 95% confidence intervals (CI). To measure the excess burden of SPC, absolute excess risks (AER) were calculated. The AER represents the additional incidence beyond the background incidence found in the Dutch general population. It is defined as the difference between the observed and the expected number of patients with a SPC, divided by the number of person years (py) at risk, multiplied by 10,000.

Subsequent analyses focused on the sub cohort of patients with localized PCa (T1-T3N0/X, M0/X) treated with EBRT +/- HT. This cohort was limited to patients with localized disease, as patients with a more advanced stage of disease are likely to experience relapse. We also excluded patients being diagnosed with a T4 or N+ or M+ tumor, in order to minimize the likelihood that the radiation field included the pelvic lymphatic system. Consequently, they are more likely to receive additional treatment, which could not be accounted for, as this information is not available in the NCR. SIRs were calculated by (previously defined) time period, age group (≤70 or >70 years) and for follow-up years for the different time periods. Stratification by time period was done to investigate whether SPC patterns have changed over time, i.e. over the three defined RT periods. Analysis was adjusted for age and calendar year of diagnosis.

Finally, we assessed the relative risk of developing a SPC after RT treatment by comparing the EBRT +/- HT cohort to patients treated with radical prostatectomy. The Fine and Gray method for estimating relative risk (sub-Hazard ratios (sHRs)) was used (19). The relative risk was also estimated per age group and time period of diagnosis. The model was adjusted for age and year of diagnosis. The cumulative incidence of developing a SPC was estimated with death as a competing risk. This analysis was carried out using STATA version 14 (STATA Corp., Texas, USA). SIR and AER analyses was carried out using SAS version 9.2 (SAS Institute Inc., Cary, NC, USA).

Role of the Funding Source

The Dutch Cancer Society (project grant 12009), which had no further say in the design, analyses or description of the results provided financial support for this study.

RESULTS

In this study, all patients diagnosed with PCa between 1990-2014 were included (N=161,003). The median age at diagnosis of PCa was 70.0 years (Interquartile range (IQR):64-75). In **Table 1**, a description of the cohort is presented, overall and by initial treatment. EBRT was the most frequently applied initial treatment (26.1%). Within the EBRT cohort, 93.3% had T1-T3N0/X, M0/X PCa. In the complete cohort, a total of 22,538 SPC were observed until the end of 2019. The median time between PCa diagnosis and the development of a SPC was 5.81 years. Overall, a non-significant decreased risk of developing a solid SPC after PCa diagnosis was found, when compared to the Dutch male general population (SIR (95%CI) = 0.98 (0.97-1.00), AER= -3.19 per 10,000 py) (**Table 2**). However, for pelvic SPC a significant increased risk was observed (SIR=1.08 (1.05-1.11); AER=3.40). This was mainly attributed to a significant increase in SPCs in the bladder (SIR=1.08 (1.04-1.11); AER=1.95) and rectum (SIR=1.10 (1.05-1.15); AER=1.17). For hematological SPC, an increased risk was found (SIR 1.09 (1.05-1.14, AER=1.78). In **Supplementary Table 1** additional SPC information for various tumor sites is displayed.

Comparison of the EBRT Cohort to the General Population

PCa patients with localized PCa treated with EBRT had an estimated SIR for all solid SPC of 1.08 (1.05-1.11), corresponding with an AER of almost 15 additional men diagnosed with a SPC per 10,000 py (**Table 3**). Specifically, the risk for bladder SPC (SIR=1.33 (1.26-1.40), AER=10.18) and rectum SPC (SIR=1.23 (1.13-1.34), AER=3.12) were increased. With regard to the different time periods, the risk for solid SPC in the EBRT cohort increased over the years. For the time period 2008-2014 a SIR of 1.10 (1.04-1.15) was found, whereas the SIR for the time period 1991-1996 was 1.05 (0.99-1.12). A significant increased risk of developing a SPC in the non-pelvic area was only observed for the most recent time period; SIR=1.08 (1.02-1.14). The risk for pelvic and bladder SPC were significantly elevated throughout all time periods, with the highest risks observed in the second time period (SIR=1.35, 1.26-1.44) and (SIR=1.42, 1.32-1.53) for pelvic and bladder SPC respectively. The risk for rectum SPC was significantly elevated for all time periods but appeared highest in the first time period; SIR=1.39 (1.14-1.67) *versus* (SIR=1.21; 1.06-1.37) and (SIR=1.24; 1.04-1.46) for the later time periods.

The risk for hematological SPC remained significantly elevated over the different time periods, although it moderately decreased as EBRT advanced [SIR=1.28 (1.07-1.51) to SIR=1.19 (1.03-1.37)]. In **Supplementary Table 2**, SIRs for all subsites and different time periods are displayed.

The age-group specific analysis demonstrated that age is an important factor affecting the risk of SPC. No significant increase

TABLE 1 | Patient and tumor characteristics for the complete cohort and per treatment modality.

	Complete Cohort		EBRT +/- HT		Radical Prostatectomy		Brachytherapy		Active Surveillance		Systemic treatment*		Other Treatment	
	n	%	n	%	n	%	n	%	n	%	n	%	n	%
Total	161003	100	42069	26.13	27784	17.26	8036	4.99	26083	16.20	39280	24.40	17851	11.09
Median Age (IQR)	70 (64-75)		70.0 (65-75)		64 (59-67)		65 (61-70)		72 (65-77)		74 (67-79)		73 (67-79)	
Age Group														
<60	19275	11.96	3832	9.11	7442	26.79	1565	19.47	2377	9.11	2830	7.20	1229	6.88
60-69	61191	37.98	16908	40.19	16680	60.03	4304	53.56	8440	32.36	9766	24.86	5093	28.53
70-79	61514	38.18	19999	47.54	3611	13.00	2129	26.49	11081	42.48	16951	43.15	7743	43.38
80+	19123	11.87	1330	3.16	51	0.18	38	0.47	4185	16.04	9733	24.78	3786	21.21
Time Period														
1991-1997	27635	19.75	7176	19.71	2403	9.89	101	1.55	2491	11.06	10058	29.23	5406	34.29
1998-2005	49695	35.51	14946	41.04	8016	32.99	2277	34.83	5976	26.54	13657	39.69	4823	30.59
2006-2014	62616	44.74	14295	39.25	13880	57.12	4159	63.62	14050	62.40	10695	31.08	5537	35.12
Second Primary Cancer (SPC)														
	22538	100	7654	33.96	4131	18.33	1338	5.94	3543	15.72	3435	15.24	2437	10.81
Disease Stage														
T1-2 N0/X, M0/X	111456	69.18	27071	64.35	26187	94.25	7940	98.81	24140	92.55	11882	30.25	14236	79.75
T3 N0/X, M0/X	20002	12.42	12172	28.93	1312	4.72	85	1.06	1155	4.43	4293	10.93	985	5.52
T4 or N+ or M+	29645	18.40	2826	6.72	285	1.03	11	0.14	788	302	23105	58.82	2630	14.73
Median time between PCa diagnosis and SPC (years)	5.81		6.04		7.36		6.65		5.27		4.16		5.54	

*External beam radiotherapy with/without hormonal therapy (EBRT +/- HT), *Systemic treatment mainly concerns hormonal therapy only.*

TABLE 2 | SIRs and AER (per 10,000 person years) for PCa patients treated with EBRT +/- hormonal therapy for different time periods and age groups.

	All Ages				Age ≤70	Age >70
	Obs	Exp	SIR (95%CI)	AER	SIR (95%CI)	SIR (95%CI)
All Solid	6540	6062.9	1.08 (1.05-1.11)*	14.56	1.13 (1.09-1.16)*	1.03 (0.99-1.07)
1991-1996	1128	1069.3	1.05 (0.99-1.12)	10.19	1.10 (1.02-1.19)*	0.99 (0.91-1.09)
1998-2005	2872	2649.1	1.08 (1.04-1.12)*	15.81	1.11 (1.05-1.16)*	1.06 (1.00-1.12)
2008-2014	1591	1452.6	1.10 (1.04-1.15)*	17.23	1.15 (1.07-1.24)*	1.05 (0.98-1.13)
All hematological	889	729.8	1.22 (1.14-1.30)*	4.39	1.23 (1.12-1.35)*	1.19 (1.08-1.31)*
1991-1996	134	104.9	1.28 (1.07-1.51)*	4.80	1.37 (1.09-1.70)*	1.17 (0.88-1.53)
1998-2005	385	311.1	1.24 (1.12-1.37)*	4.97	1.25 (1.09-1.43)*	1.22 (1.04-1.42)*
2008-2014	206	172.8	1.19 (1.03-1.37)*	3.98	1.22 (0.98-1.51)	1.17 (0.97-1.40)
Non-Pelvis	4841	4657	1.04 (1.01-1.07)*	5.50	1.08 (1.04-1.12)*	0.99 (0.95-1.03)
1991-1996	822	817.4	1.01 (0.94-1.08)	0.78	1.04 (0.95-1.13)	0.97 (0.87-1.07)
1998-2005	2098	2037.5	1.03 (0.99-1.07)	4.18	1.05 (1.00-1.12)	1.00 (0.93-1.07)
2008-2014	1206	1115.9	1.08 (1.02-1.14)*	11.06	1.14 (1.05-1.24)*	1.03 (0.96-1.12)
Pelvis	2004	1559.8	1.28 (1.23-1.34)*	13.12	1.37 (1.30-1.46)*	1.22 (1.15-1.30)*
1991-1996	357	278.4	1.28 (1.15-1.42)*	13.21	1.43 (1.25-1.64)*	1.11 0.93-1.30)
1998-2005	929	690.1	1.35 (1.26-1.44)*	16.37	1.39 (1.27-1.51)*	1.30 (1.17-1.43)*
2008-2014	440	362.5	1.21 (1.10-1.33)*	9.37	1.29 (1.11-1.48)*	1.16 (1.02-1.32)*
Bladder	1393	1046	1.33 (1.26-1.40)*	10.18	1.43 (1.33-1.53)*	1.27 (1.18-1.37)*
1991-1996	240	189.5	1.27 (1.11-1.44)*	8.43	1.46 (1.24-1.72)*	1.04 (0.84-1.27)
1998-2005	662	465.5	1.42 (1.32-1.53)*	13.37	1.48 (1.33-1.64)*	1.36 (1.21-1.52)*
2008-2014	299	238	1.26 (1.12-1.41)*	7.34	1.36 (1.13-1.62)*	1.19 (1.02-1.38)*
Rectum	569	461.6	1.23 (1.13-1.34)*	3.12	1.32 (1.18-1.46)*	1.15 (1.02-1.31)*
1991-1996	112	80.7	1.39 (1.14-1.67)*	5.17	1.44 (1.11-1.84)*	1.32 (0.97-1.74)
1998-2005	246	203.4	1.21 (1.06-1.37)*	2.86	1.24 (1.05-1.46)*	1.17 (0.95-1.42)
2008-2014	135	109.3	1.24 (1.04-1.46)*	3.07	1.22 (0.94-1.57)	1.24 (0.97-1.56)

**indicates significant SIRs; observed, (Obs); expected, (Exp); standarized incidence ratio, (SIR); absolute excess risk, (AER).*

of solid SPC was observed for older patients (>70 years), whereas younger patients (≤70) demonstrated a significant increased risk, for solid SPC and other subsites (**Table 2**).

Analysis stratified by follow-up years and time period of diagnosis revealed a significant increase of non-pelvic SPC in the first five years of follow-up for the AdvRT era (SIR=1.15 (1.07-1.24), AER=19.76) (**Figure 1** and **Supplementary Table 3**). Second pelvic cancers were significantly increased for all follow-up years for the 3D-CRT era, with the biggest increase being observed >15 years of follow-up (SIR=1.65 (1.33-2.03), AER=35.39).

TABLE 3 | Estimated subHazard ratios by gray and fine method (with adjustment for age and year of diagnosis) for the EBRT cohort *versus* the reference cohort prostatectomy.

	EBRT +/- HT(n)	Radical Prostatectomy(n)	sHRs (95%CI)	p-value
All Solid	6834	3644	1.24 (1.19-1.30)	<0.01*
1991-1996	1172	513	1.25 (1.12-1.40)	<0.01*
1998-2005	2941	1421	1.27 (1.18-1.36)	<0.01*
2008-2014	1735	1174	1.24 (1.14-1.35)	<0.01*
All hematological	949	610	1.03 (0.91-1.15)	0.672
1991-1996	145	74	1.09 (0.80-1.48)	0.605
1998-2005	407	256	0.94 (0.79-1.12)	0.481
2008-2014	254	189	1.09 (0.88-1.35)	0.436
Non-Pelvis	4834	2823	1.14 (1.08-1.20)	<0.01*
1991-1996	814	390	1.13 (0.99-1.29)	0.075
1998-2005	2034	1099	1.13 (1.04-1.23)	<0.01*
2008-2014	1271	913	1.17 (1.06-1.29)	<0.01*
Pelvis	2000	822	1.61 (1.47-1.76)	<0.01*
1991-1996	358	123	1.17 (1.34-2.10)	<0.01*
1998-2005	907	322	1.74 (1.52-2.00)	<0.01*
2008-2014	464	261	1.47 (1.24-1.74)	<0.01*
Bladder	1380	490	1.83 (1.63-2.05)	<0.01*
1991-1996	237	79	1.76 (1.33-2.31)	<0.01*
1998-2005	649	195	2.04 (1.71-2.44)	<0.01*
2008-2014	307	150	1.65 (1.33-2.05)	<0.01*
Rectum	550	312	1.20 (1.03-1.40)	0.023*
1991-1996	110	41	1.51 (1.01-2.27)	0.043*
1998-2005	225	122	1.14 (0.90-1.45)	0.281
2008-2014	145	104	1.16 (0.87-1.55)	0.323

**indicates statistically significant p-values; external beam radiotherapy with/without hormonal therapy (EBRT +/- HT); sub-hazard ratios (sHRs).*
Numbers reflect the observed numbers of survivors experiencing the SPC event of interest.

Comparison of the EBRT Cohort to the Radical Prostatectomy Cohort

For the total EBRT cohort the adjusted sHR (95% confidence interval and p-value) (EBRT vs. radical prostatectomy) for developing a solid SPC was 1.24 (1.19-1.30, p=<0.01) (**Table 3**). The risk for developing a solid SPC was significantly elevated in the EBRT cohort for all time periods, compared to the radical prostatectomy cohort. The risk for developing a non-pelvic SPC was highest for the last time period 1.17 (1.06-1.29, p=<0.01). For second cancers in the pelvic region, the risk was highest in the second time period 1.74 (1.52-2.00, p=<0.01), followed by the last time period 1.47 (1.24-1.74, p=<0.01). More detailed information on comparison of the EBRT cohort with the prostatectomy cohort can be found in **Table 3**.

DISCUSSION

The complete PCa survivor population had a small, not statistically significant reduced risk of developing a SPC. In PCa patients treated with EBRT an 8% increased risk of developing a solid SPC was observed, which corresponds with an absolute excess number of 14.5 patients diagnosed with a second cancer per 10.000, compared to the Dutch male general population. This risk was particularly evident for SPC within the pelvic region.

The reduced risk of developing a SPC in the complete PCa survivor population is partially in line with findings from other studies (2, 10, 20, 21). Davis et al. (20), carried out a population-based cohort study in the US, and found that the risk of developing a SPC for the complete PCa patient population is significantly reduced (20). They related this reduction in risk to the younger age of patients at time of diagnosis, and the routine screening of the prostate-specific antigen (PSA). In the Netherlands, men are not actively screened on PSA. This may explain as to why the observed risk of developing a SPC was not as significantly reduced in our complete PCa survivor population. Nonetheless, PCa detected by opportunistic screening as applied in the Netherlands most likely represent men with higher socio economic status, which is generally associated with a lower cancer risk. Men of higher socio economic status might be more health conscious than the general population (21).

Several cohort studies have previously reported on the increased risk of developing a SPC in the pelvic area after EBRT for PCa (5–8, 20). Organs within the pelvis (e.g. bladder and rectum), inevitably receive radiation dose due to their close proximity to the prostate. This increases the likelihood of developing a SPC in those organs. In this study, we have shown that the risk for a pelvic SPC is highest in patients treated in the second time period, corresponding to the 3D-CRT era. We also showed that a significant increase in risk persists over the years, indicating that also after AdvRT there is a higher risk of developing a pelvic SPC. A study by Zelefsky et al. (15), which investigated SPC rates after PCa found lower incidence rates of secondary bladder and rectal cancers after treatment with IMRT (15). However, no comparison was done with a 3D-CRT cohort. In a previous single-center study, where

we investigated SPC risk after IMRT vs 3D-CRT, we observed no significant differences in overall pelvis SPC risks between the 2 techniques, with a trend for IMRT of lower bladder SPC risks and higher rectum SPC risks (22).

We observed an increase in non-pelvic SPC for the most recent RT period. Although the high-dose region is more compact with AdvRT and more conformal dose distribution can be achieved (sparing nearby structures such as bladder and rectum, from intermediate- to high-dose volumes), the lower dose region is expanded due to increased beam angles, exposing more normal tissue to a low-dose bath. Therefore, AdvRT is at the expense of a larger volume of more distant tissues receiving low-to-moderate doses compared to more conformal RT (16, 17). The results of this study as well as the theoretical concerns support the findings from the previously carried out single center study in which we observed that patients treated with IMRT had a significantly increased risk for non-pelvic cancers as opposed to those treated with 3D-CRT, especially in survivors aged <70 and active smokers at time of treatment (22).

In the current study, we found a significant increase in second rectum cancers for the AdvRT time period. This finding is in agreement with the finding of our previous single-center study, but is contradictory to the findings of Journy et al., who observed a reduced risk for second rectum cancers after treatment with IMRT (17). These findings were based on sufficient follow-up to monitor early incidence of SPC risk, however, are limited by follow-up (median follow-up: 5.2 years). Our analysis by follow-up period revealed that the risk for rectum SPC only significantly increased after 5 years of follow-up. This observation was also described in other cohort studies (2, 23–25).

We furthermore found that PCa patients treated with EBRT had a 22% increased risk of developing a second hematological cancer (AER=4.39). Second hematological cancers are less well described in literature as opposed to second solid cancers. This is partially attributed to the fact that the absolute numbers of hematological cancers are relatively low in the general population. Therefore, large study populations and sufficient follow-up is required to investigate second hematological cancer risk. Studies reporting on second hematological cancer risk, report similar findings to those we made in this study; namely elevated risks after EBRT (17, 24). We are currently busy with carrying out a follow-up study, exploring hematological cancer risk after EBRT for PCa further. In this follow-up study, we will also specifically look into different subtypes of hematological cancers.

In line with observations from epidemiological studies (26–28), we found that younger age is associated with increased SPC

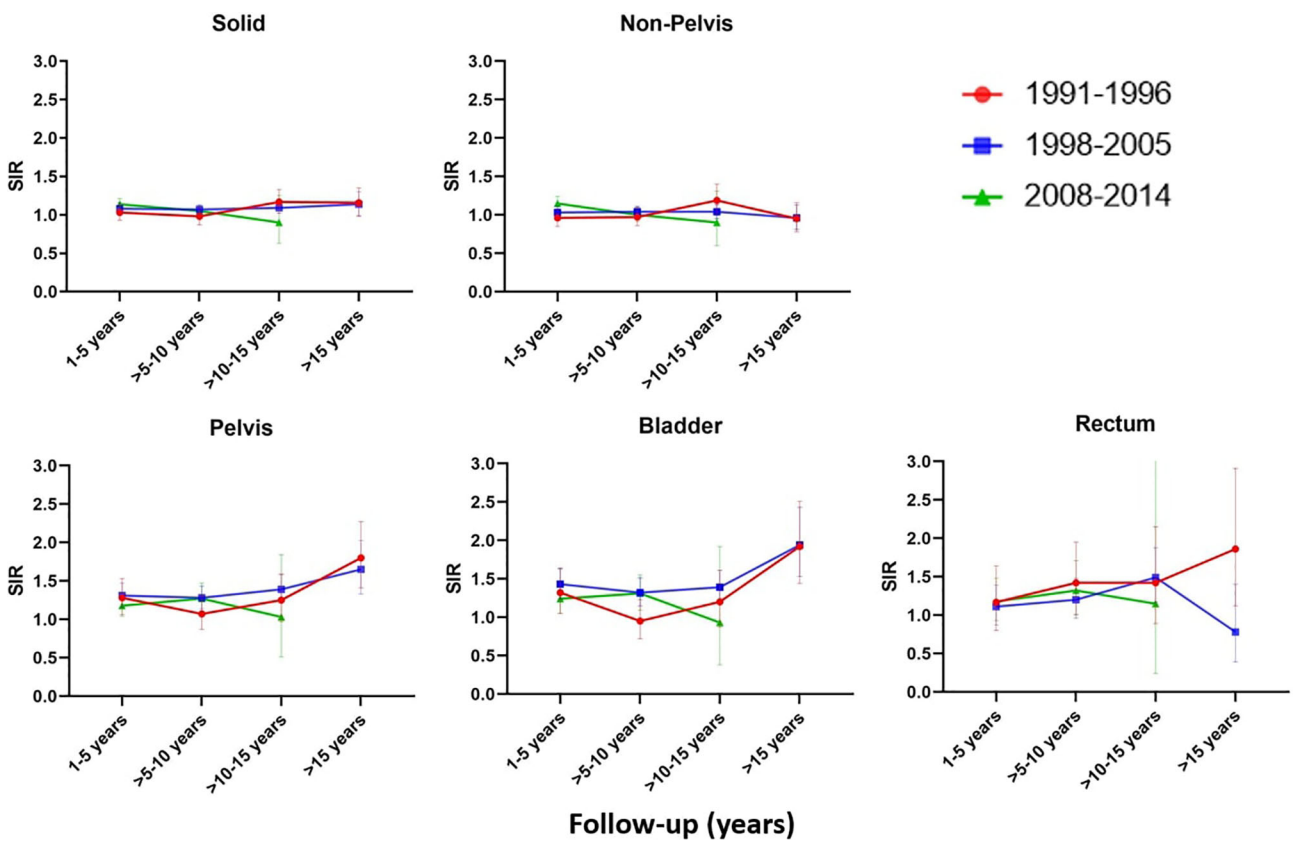

FIGURE 1 | SIR for the EBRT cohort compared to the Dutch male general population for different follow-up years and time periods.

risks. This can be explained by the biological phenomenon that cells of older people are less sensitive to radiation (26, 27). A study by de Gonzalez et al., exploring SPC risk after RT for different cancer sites, found that the relative risk for second cancers is increased with younger age at diagnosis (24). The relative risk for SPC after PCa was reported to decrease from 1.85 (95% CI = 1.53-2.22) in patients aged below 60 years to 1.16 (95% CI = 0.96-1.14) in patients aged >75 years. In the present study we found that the risk for developing a solid SPC decreased by 10% in patients aged >70 years.

The fact that PCa survivors in the three defined RT groups were treated in different calendar periods might be associated with potential confounding effects such as e.g. differences in patient populations selected for RT, differences in targeted volumes, differences in follow-up intensity/follow-up imaging, and differences in adjuvant or later treatment during follow-up (e.g. hormonal treatment, chemotherapy). In our previous single-center study, we were able to investigate several potential confounders, such as the prescription of adjuvant HT. At sensitivity analysis, adjuvant HT demonstrated to be not affecting the results of the analysis (22). Hence, for this study we included both patients - with and without adjuvant HT prescription to the EBRT cohort. We planned to obtain a similar detailed database for an extended patient group of several hospitals, to investigate this further with more statistical power.

The major strengths of this study are the large sample size, its ability to assess trends over time, and the fact that a dual comparison was drawn (Dutch general population and radical prostatectomy cohort). The reported results from the two methods were roughly in agreement, identifying similar trends in SPC risk after PCa diagnosis. The main limitation of this study is that no comprehensive RT information was available. The time periods defined act as a proxy for the different EBRT techniques used. Over the years there have been multiple changes in the field of EBRT, ranging from the dose and fractions prescribed to the use of image-guidance. In this study we were unable to take these factors into consideration. However, we are currently busy conducting a study, exploring how specific characteristics of EBRT impact the risk of developing a SPC. Furthermore, we were unable to the explore the effect of smoking on SPC risk, as this information is not recorded in the NCR. Smoking is a known risk factor for the development of cancers, such as bladder cancer. Even though it is not a known risk factor for the development of PCa, some studies have also shown that smoking and RT are interactive factors, affecting the risk of developing a SPC. Lastly, the AdvRT era is limited by its follow-up. We were unable to generate a thorough risk assessment on the effect AdvRT has on the development of a SPC beyond 10 years of follow-up (22, 29, 30).

In conclusion, PCa patients who received EBRT had a significantly increased risk of developing a SPC compared to both the general population and the radical prostatectomy cohort. The results indicate that over the years, the risk for second pelvic cancers persists and the risk for second non-pelvic cancers increases. Younger age at point of diagnosis increases the risk of developing a SPC. These results confirm what was previously described in other studies and underline the importance of providing sufficient follow-up care, especially considering the high survival prospects of PCa survivors. Further research containing more detailed RT information, as well as exploring the risk of developing a second hematological cancer after EBRT for PCa, is currently ongoing.

DATA AVAILABILITY STATEMENT

The raw data supporting the conclusions of this article will be made available by the authors, without undue reservation.

AUTHOR CONTRIBUTIONS

KA, WH, LI, and MH contributed to the study design. M-CJ, KA, WH, and BS contributed to data collection and analysis. All authors participated in data interpretation and revision. M-CJ, WH, and KA contributed to writing the manuscript. KA and WH contributed to supervision and study management. All authors contributed to the article and approved the submitted version.

FUNDING

For this project a grant was received from the Dutch Cancer Society (KWF), nr 12009. The funder of the study is a non-profit organization and it had no role in study design, data collection, data analysis, data interpretation, or writing of the report.

ACKNOWLEDGMENTS

The authors thank the registration team of the Netherlands Comprehensive Cancer Organisation (IKNL) for the collection of data for the Netherlands Cancer Registry. We would like to thank Renier Snieders for assisting with the data analysis and Anke Richters for supporting us with obtaining the relevant data from the Netherlands Cancer Registry. We would also like to thank the Dutch Cancer Society (KWF) for funding this study.

SUPPLEMENTARY MATERIAL

The Supplementary Material for this article can be found online at: https://www.frontiersin.org/articles/10.3389/fonc.2021.771956/full#supplementary-material

REFERENCES

1. Culp MB, Soerjomataram I, Efstathiou JA, Bray F, Jemal A. Recent Global Patterns in Prostate Cancer Incidence and Mortality Rates. *Eur Urol* (2020) 77 (1):38–52. doi: 10.1016/j.eururo.2019.08.005
2. Brenner DJ, Curtis RE, Hall EJ, Ron E. Second Malignancies in Prostate Carcinoma Patients After Radiotherapy Compared With Surgery. *Cancer* (2000) 88(2):398–406. doi: 10.1002/(SICI)1097-0142(20000115)88:2<398::AID-CNCR22>3.0.CO;2-V
3. Jin T, Song T, Deng S, Wang K. Radiation-Induced Secondary Malignancy in Prostate Cancer: A Systematic Review and Meta-Analysis. *Urol Int* (2014) 93 (3):279–88. doi: 10.1159/000356115
4. Preston DL, Krestinina LY, Sokolnikov ME, Ron E, Davis FG, Ostroumova EV, et al. How Much can We Say About Site-Specific Cancer Radiation Risks? *Radiat Res* (2010) 174(6):816–24. doi: 10.1667/RR2024.1
5. Murray L, Henry A, Hoskin P, Siebert F-A, Venselaar JESTRO PgotG. Second Primary Cancers After Radiation for Prostate Cancer: A Systematic Review of the Clinical Data and Impact of Treatment Technique. *Radiother Oncol* (2014) 110(2):213–28. doi: 10.1016/j.radonc.2013.12.012
6. Bhojani N, Capitanio U, Suardi N, Jeldres C, Isbarn H, Shariat SF, et al. The Rate of Secondary Malignancies After Radical Prostatectomy Versus External Beam Radiation Therapy for Localized Prostate Cancer: A Population-Based Study on 17,845 Patients. *Int J Radiat Oncol Biol Phys* (2010) 76(2):342–8. doi: 10.1016/j.ijrobp.2009.02.011
7. Keehn A, Ludmir E, Taylor J, Rabbani F. Incidence of Bladder Cancer After Radiation for Prostate Cancer as a Function of Time and Radiation Modality. *World J Urol* (2017) 35(5):713–20. doi: 10.1007/s00345-016-1934-z
8. Wallis CJD, Mahar AL, Choo R, Herschorn S, Kodama RT, Shah PS, et al. Second Malignancies After Radiotherapy for Prostate Cancer: Systematic Review and Meta-Analysis. *BMJ* (2016) 352. doi: 10.1136/bmj.i851
9. Hegemann N-S, Schlesinger-Raab A, Ganswindt U, Hörl C, Combs SE, Hölzel D, et al. Risk of Second Cancer Following Radiotherapy for Prostate Cancer: A Population-Based Analysis. *Radiat Oncol* (2017) 12(1):1–8. doi: 10.1186/s13014-016-0738-z
10. Aksnessæther BY, Lund J-Å, Myklebust TÅ, Klepp OH, Skovlund E, Roth Hoff S, et al. Second Cancers in Radically Treated Norwegian Prostate Cancer Patients. *Acta Oncol* (2019) 58(6):838–44. doi: 10.1080/0284186X.2019.1581377
11. Buwenge M, Scirocco E, Deodato F, Macchia G, Ntreta M, Bisello S, et al. Radiotherapy of Prostate Cancer: Impact of Treatment Characteristics on the Incidence of Second Tumors. *BMC Cancer* (2020) 20(1):1–8. doi: 10.1186/s12885-020-6581-5
12. Wortel RC, Incrocci L, Pos FJ, Lebesque JV, Witte MG, van der Heide UA, et al. Acute Toxicity After Image-Guided Intensity Modulated Radiation Therapy Compared to 3D Conformal Radiation Therapy in Prostate Cancer Patients. *Int J Radiat Oncol Biol Phys* (2015) 91(4):737–44. doi: 10.1016/j.ijrobp.2014.12.017
13. Kry SF, Salehpour M, Followill DS, Stovall M, Kuban DA, White RA, et al. The Calculated Risk of Fatal Secondary Malignancies From Intensity-Modulated Radiation Therapy. *Int J Radiat Oncol Biol Phys* (2005) 62(4):1195–203. doi: 10.1016/j.ijrobp.2005.03.053
14. Stathakis S, Li J, Ma CCM. Monte Carlo Determination of Radiation-Induced Cancer Risks for Prostate Patients Undergoing Intensity-Modulated Radiation Therapy. *J Appl Clin Med Phys* (2007) 8(4):14–27. doi: 10.1120/jacmp.v8i4.2685
15. Zelefsky MJ, Housman DM, Pei X, Alicikus Z, Magsanoc JM, Dauer LT, et al. Incidence of Secondary Cancer Development After High-Dose Intensity-Modulated Radiotherapy and Image-Guided Brachytherapy for the Treatment of Localized Prostate Cancer. *Int J Radiat Oncol Biol Phys* (2012) 83(3):953–9. doi: 10.1016/j.ijrobp.2011.08.034
16. Xiang M, Chang DT, Pollom EL. Second Cancer Risk After Primary Cancer Treatment With Three-Dimensional Conformal, Intensity-Modulated, or Proton Beam Radiation Therapy. *Cancer* (2020) 126(15):3560–8. doi: 10.1002/cncr.32938
17. Journy NMY, Morton LM, Kleinerman RA, Bekelman JE, de Gonzalez AB. Second Primary Cancers After Intensity-Modulated vs 3-Dimensional Conformal Radiation Therapy for Prostate Cancer. *JAMA Oncol* (2016) 2 (10):1368–70. doi: 10.1001/jamaoncol.2016.1368
18. Sobin LH, Gospodarowicz MK, Wittekind C. *TNM Classification of Malignant Tumours*. Chichester: John Wiley & Sons (2011).
19. Fine JP, Gray RJ. A Proportional Hazards Model for the Subdistribution of a Competing Risk. *J Am Stat Assoc* (1999) 94(446):496–509. doi: 10.1080/01621459.1999.10474144
20. Davis EJ, Beebe-Dimmer JL, Yee CL, Cooney KA. Risk of Second Primary Tumors in Men Diagnosed With Prostate Cancer: A Population-Based Cohort Study. *Cancer* (2014) 120(17):2735–41. doi: 10.1002/cncr.28769
21. Feller A, Matthes KL, Bordoni A, Bouchardy C, Bulliard JL, Hermann C, et al. (2018). The Relative Risk of Second Primary Cancers in Switzerland, in: *DGEpi-Jahrestagung: German Society of Epidemiology*, Bremen, Germany, September 26-28, Vol. 2018.
22. Jahreiß M-C, Aben KKH, Hoogeman MS, Dirkx MLP, De Vries KC, Incrocci L, et al. The Risk of Second Primary Cancers in Prostate Cancer Survivors Treated in the Modern Radiotherapy Era. *Front Oncol* (2020) 10:2519. doi: 10.3389/fonc.2020.605119
23. Abdel-Wahab M, Reis IM, Hamilton K. Second Primary Cancer After Radiotherapy for Prostate Cancer—a Seer Analysis of Brachytherapy Versus External Beam Radiotherapy. *Int J Radiat Oncol Biol Phys* (2008) 72(1):58–68. doi: 10.1016/j.ijrobp.2007.12.043
24. De Gonzalez AB, Curtis RE, Kry SF, Gilbert E, Lamart S, Berg CD, et al. Proportion of Second Cancers Attributable to Radiotherapy Treatment in Adults: A Cohort Study in the US SEER Cancer Registries. *Lancet Oncol* (2011) 12(4):353–60. doi: 10.1016/S1470-2045(11)70061-4
25. Nieder C, Pawinski A, Balteskard L. Colorectal Cancer Metastatic to the Brain: Time Trends in Presentation and Outcome. *Oncology* (2009) 76(5):369–74. doi: 10.1159/000210026
26. Grant EJ, Brenner A, Sugiyama H, Sakata R, Sadakane A, Utada M, et al. Solid Cancer Incidence Among the Life Span Study of Atomic Bomb Survivors: 1958–2009. *Radiat Res* (2017) 187(5):513–37. doi: 10.1667/RR14492.1
27. AK Ng, LB Kenney, ES Gilbert, LB Travis eds. *Secondary Malignancies Across the Age Spectrum. Semin Radiat Oncol*. Boston: Elsevier (2010).
28. Dracham CB, Shankar A, Madan R. Radiation Induced Secondary Malignancies: A Review Article. *Radiat Oncol J* (2018) 36(2):85. doi: 10.3857/roj.2018.00290
29. Arnold M, Liu L, Kenter GG, Creutzberg CL, Coebergh JW, Soerjomataram I. Second Primary Cancers in Survivors of Cervical Cancer in the Netherlands: Implications for Prevention and Surveillance. *Radiother Oncol* (2014) 111 (3):374–81. doi: 10.1016/j.radonc.2014.04.011
30. Shiota M, Yokomizo A, Takeuchi A, Inokuchi J, Tatsugami K, Ohga S, et al. Smoking Effect on Secondary Bladder Cancer After External Beam Radiotherapy for Prostate Cancer. *Jpn J Clin Oncol* (2016) 46(10):952–7. doi: 10.1093/jjco/hyw098

Conflict of Interest: The authors declare that the research was conducted in the absence of any commercial or financial relationships that could be construed as a potential conflict of interest.

frontiers in Oncology

ORIGINAL RESEARCH
published: 03 January 2022
doi: 10.3389/fonc.2021.754108

Long-Term Outcomes in Uveal Melanoma After Ruthenium-106 Brachytherapy

Gilda Cennamo[1], Daniela Montorio[2], Luca D' Andrea[2], Antonio Farella[3], Elide Matano[4,5], Mario Giuliano[4,5], Raffaele Liuzzi[6], Maria Angelica Breve[2], Sabino De Placido[4,5] and Giovanni Cennamo[2]*

[1] Eye Clinic, Public Health Department, University of Naples "Federico II", Naples, Italy, [2] Department of Neurosciences, Reproductive Sciences and Dentistry, University of Naples "Federico II", Naples, Italy, [3] Radiotherapy Unit, University of Naples "Federico II", Naples, Italy, [4] Department of Clinical Medicine and Surgery, University of Naples Federico II, Naples, Italy, [5] Rare Cancer Coordinating Center – Campania Region, Naples, Italy, [6] Institute of Biostructure and Bioimaging, National Research Council (CNR), Naples, Italy

OPEN ACCESS

Edited by:
James Chow, University of Toronto, Canada

Reviewed by:
Corrado Spatola, University of Catania, Italy
Sunyoung Jang, Princeton Radiation Oncology Center, United States

***Correspondence:**
Gilda Cennamo
xgilda@hotmail.com

Specialty section:
This article was submitted to Radiation Oncology, a section of the journal Frontiers in Oncology

Received: *06 August 2021*
Accepted: *26 November 2021*
Published: *03 January 2022*

Citation:
Cennamo G, Montorio D, D' Andrea L, Farella A, Matano E, Giuliano M, Liuzzi R, Breve MA, De Placido S and Cennamo G (2022) Long-Term Outcomes in Uveal Melanoma After Ruthenium-106 Brachytherapy. Front. Oncol. 11:754108. doi: 10.3389/fonc.2021.754108

Uveal melanoma is the most common primary intraocular malignancy. The aim of this retrospective study was to report the results after ruthenium-106 (Ru-106) plaque brachytherapy for uveal melanoma in terms of tumor control, visual acuity, radiation-related complications, tumor recurrence, metastases, and patients' survival rate during 4 years' follow-up. A total of 355 eyes from 355 patients have been treated with Ru-106 plaque brachytherapy for uveal melanoma between February 2011 and March 2020. Five patients were lost to follow-up, and then 350 eyes of 350 patients (mean age 58 ± 11 years) were enrolled in this retrospective study. All patients underwent a complete ophthalmic examination including echography and spectral domain–optical coherence tomography. The mean follow-up was 4 years (3 months to 9 years). After treatment, the mean tumor thickness was reduced to 1.75 ± 0.21 mm. Radiation complications were found in 63% of patients: 38% showed radiation maculopathy, 11% had optic neuropathy, and 14% developed cataracts. Cancer-free survival was 99%, 97%, and 85%, respectively, at 5, 7, and 9 years. Ru-106 plaque brachytherapy represents a reliable treatment of uveal melanoma. This technique is valid and safe with a low rate of ocular complications during a long-term follow-up.

Keywords: ruthenium-106 brachytherapy, uveal melanoma, survival rate, local recurrence, metastasis, complications

1 INTRODUCTION

Uveal melanoma is the most common primary intraocular malignancy, and it represents approximately 5% of all melanomas (1, 2).

Enucleation of the affected eye was the only treatment in the past, but since 1970, the eye-conserving approach has been increasingly used until today (3) in order to preserve vision and the ocular anatomy without increasing the risk of metastatic spread (4).

Today, radiation therapy is the main treatment approach for choroidal melanoma, and the most common irradiation techniques are plaque brachytherapy and proton therapy (5–7). β-Ray source ruthenium-106 (Ru-106) is the most used in Europe (8).

The Collaborative Ocular Melanoma Study (COMS) demonstrated equal melanoma-related survival rates for enucleation and episcleral plaque radiotherapy in medium-sized tumors (measuring 2.5 to 10 mm of apical height and 5 to 16 mm of basal dimension) (4). Furthermore, plaque brachytherapy offers the patient a better quality of life with the possibility to preserve vision (4).

The aim of this retrospective study is to investigate the visual and anatomical outcomes, tumor control, tumor recurrence, distant metastasis, and cancer-free survival in patients undergoing Ru-106 plaque brachytherapy.

2 MATERIALS AND METHODS

2.1 Study Design

This retrospective study included all patients with the clinical diagnosis of choroidal melanoma who underwent Ru-106 plaque brachytherapy between February 2011 and March 2020 at the Eye Clinic of the University of Naples "Federico II".

The gold standard for the diagnosis of choroidal melanoma was based on ophthalmoscopic features and standardized bulbar echography.

A-scan and B-scan ultrasound were performed with an AVISO-S Echograph (Quantel Medical, Clermont-Ferrand, France) and 10- and 20-MHz probes. The axial resolution was 0.2 mm for the A-scan probe, and 0.15 and 0.1 mm for the 10- and 20-MHz B-scan probes, respectively. The dynamic range for B-scan was 25 to 90 dB with adjustable gain until 110 dB.

The tumor size was classified according to the COMS criteria (9, 10) and TNM Staging System (11).

COMS criteria defined small and medium choroidal melanomas as having an apical height of 3 and 3–8 mm, respectively (12).

The inclusion criteria for Ru-106 brachytherapy are patients with small- and medium-size tumors (measuring up to 6.5 mm of apical height) who had at least 3 months of follow-up after treatment.

All patients underwent complete ophthalmic examination, including best-corrected visual acuity (BCVA) according to the Early Treatment of Diabetic Retinopathy Study (ETDRS), slit-lamp biomicroscopy (Haag Streit BM 900), intraocular pressure measurement, fundus biomicroscopy, echography, and spectral domain–optical coherence tomography (SD-OCT) (software RTVue XR Version 2017.1.0.151, Optovue Inc., Fremont, CA, USA).

The screening for distant metastasis was made by liver ultrasonography, chest radiography, and routine blood tests at the time of diagnosis, and these were repeated over time.

The follow-up, including fundus biomicroscopy, echography, and SD-OCT, was performed at 1 month after brachytherapy, at 3-month intervals for 2 years, then twice a year until 5 postoperative years, and then annually. Complications (radiation maculopathy, optic neuropathy, and cataract) were also assessed at each follow-up.

The outcome measures were tumor control, visual acuity, radiation-related complications, tumor recurrence, distant metastases, and cancer-free survival. The Kaplan–Meier survival, performed with the Statistical Package for Social Sciences (Version 25 for Windows; SPSS Inc., Chicago, IL, USA), estimates the probability of survival.

The study adhered to the tenets of the Declaration of Helsinki. Written informed consent was obtained from the patients enrolled in the study. The research protocol was registered on ClinicalTrials.gov (NCT04577742).

2.2 Study Techniques

2.2.1 Eye Plaques

Ru-106 ophthalmic plaques CCB and COC types (Eckert & Ziegler BEBIG, Berlin, Germany) were used. The total shell thickness was 1 mm, and it was divided into three layers of thickness, from the inner to outer layer, of 0.1, 0.2, and 0.7 mm. All layers are made of silver, with the middle layer containing the emitter substance. The radioactive nuclide is electrically deposited with an approximate thickness of 0.1 μm on the concave surface. A 0.2-mm-thick silver target foil is sandwiched between the concave surface of a 0.7-mm-thick layer (back) and the convex surface of a 0.1-mm-thick layer (window) (13).

The Ru-106 (half-life 374 days) disintegrates *via* β^- decay with a peak beta particle energy of 39 keV to the radioactive daughter Rh-106. The primary contributor to therapeutic dose is the continuous spectrum of beta particles emitted in the decay of Rh-106 (half-life 30 s). Rh-106 disintegrates by β^- decay with mean beta energy of about 1.4 MeV and a maximum of 3.5 MeV to the stable element Pd-106.

The 90th percentile distance for Rh-106 beta particles in water is 7.9 mm. Backscatter from the 0.7-mm-thick silver backing of the applicator tends to soften the spectrum (14).

All patients were treated with Ru-106 eye plaque brachytherapy (EPB) to a total dose of 100 Gy to the tumor apex. The time of implant duration was calculated according to the conventional central-axis-point dose calculation (15).

2.3 Statistical Analysis

The Kaplan–Meier survival, performed with the Statistical Package for Social Sciences (Version 25 for Windows; SPSS Inc., Chicago, IL, USA), estimates the probability of survival.

3 RESULTS

Overall, 355 patients were enrolled of which five patients were excluded because they were lost to follow-up. A total of 350 eyes of 350 patients (200 females and 150 males; mean age 55 years ± 11) were included in the study. The mean follow-up was 4 years (3 months to 9 years).

At baseline, the mean BCVA in affected eyes was 0.32 ± 0.30 logMAR. The mean tumor thickness was 4.52 ± 1.78 mm at

A-scan echography. The tumors were classified according to the TNM system as T1 in 220 eyes (63%), T2 in 110 eyes (31%), and T3 in 20 eyes (6%).

According to the COMS system, the tumors were small in 130 eyes (37%) and medium in 220 eyes (63%). The location of the choroidal melanoma was the posterior pole in 119 eyes (34%), between the posterior pole and equator in 175 eyes (50%), and between the equator and ora serrata in 56 eyes (16%). Fifteen eyes presented the tumor in ciliary processes. Patient demographics, tumor, and treatment characteristics are summarized in **Table 1**.

After Ru-106 plaque treatment, the mean tumor thickness was reduced to 1.75 ± 0.21 mm, and the patients who presented radiation-related complications showed a reduced visual acuity (0.7 ± 0.85 logMAR) (**Figures 1** and **2**).

Regarding the complications, 5 years after treatment, 135 patients (38%) showed radiation maculopathy, 40 patients (11%) had optic neuropathy, and 50 patients (14%) developed cataracts.

Tumor recurrence was found in three patients at 3 years after the treatment. A total of fifteen deaths occurred due to metastasis from the liver 5 years after brachytherapy. Lastly, the survival rate, using the Kaplan–Meier analysis, was 99%, 97%, and 85% at 5, 7, and 9 years, respectively (**Figure 3**).

4 DISCUSSION

Brachytherapy and proton beam radiotherapy are commonly applied in the treatment of uveal melanoma, and they represent the main conservative treatments of choice for patients with choroidal melanoma, showing high performance in the management of tumor treatment (6, 16, 17).

The efficacy of brachytherapy has been demonstrated in terms of patient survival, ocular preservation, control of the tumor, and distant metastasis (18, 19).

Both iodine-125 and Ru-106 brachytherapy had reached excellent tumor control, as reported by previous studies that demonstrated no significant differences in the risk for tumor progression or lack of regression (20).

Takiar et al. reported that 5-year rates of local control, progression-free survival, and overall survival with Ru-106 were 97%, 94%, and 92%, respectively, while for iodine-125, these values were 83%, 65%, and 80%, respectively. In the patients with tumor apex height ≤5 mm, there was no difference in overall survival; however, progression-free survival was significantly improved with Ru-106 (21).

Moreover, the use of Ru-106 brachytherapy allowed to obtain a reliable tumor control with a rate of more than 95% with reduced ocular side effects (22).

In this retrospective study, we reported the results from 350 patients with uveal melanoma after the application of Ru-106 brachytherapy.

We found a high rate of survival, confirmed by previous studies that showed 82% and 72% of survival rates at 5 and 10 years, respectively, as well as, Perri et al., who reported increased rates of 92%, 85%, and 78% at 5, 10, and 15 years, respectively (23).

The 5-year melanoma-related mortality rate was 6% for small and medium tumors and 26% for large tumors, while at 10 years, the mortality rates for small, medium, and large tumors were 14% and 22%, respectively (24).

Other studies showed a rate of 16% and 14% of mortality at 5 years (25, 26), and the mortality rates were 11.4%, 17%, and 23% at 5, 10, and 15 years, respectively (27).

Previous reports also demonstrated excellent local control, ocular preservation, and a high rate of the treated tumor that responded by a significant decrease in tumor height.

The studies conducted by Kaiserman and Georgopoulos reported a reduction of the tumors after 18–24 months, and the tumor height stabilized on an average value of about 60% of the initial height and about 70% after 36 months (28, 29).

Also, the features at A-scan echography showed a significant increase of the internal reflectivity of the uveal melanoma after Ru-106 brachytherapy from a mean of 30%–40% before therapy to 60%–70% after 2 years (28, 29).

Our results showed a low rate of patients undergoing retreatment due to tumor recurrence 3 years after brachytherapy.

Several studies reported that the rate of tumor recurrence following Ru-106 brachytherapy changed significantly between 3%–4% and 11%–16%, and it occurred as early as a year and as late as 10 years after a good response (19, 27, 30).

Our cases reported a rate of 4% of deaths related to metastasis, confirming the results conducted by Seregard et al., which showed that 19 of 220 (9%) patients with successful treatment of the local tumor died of metastases (25).

TABLE 1 | Demographic, clinical, and ultrasonographic features of 350 eyes with uveal melanoma that underwent Ru-106 brachytherapy.

Eyes (n)	**350**
Age mean (range), years	55 ± 11
Gender	
Male	150
Female	200
BCVA at baseline (logMar)	0.35 ± 0.30
Mean thickness by echography at baseline (mm)	4.52 ± 1.78
TNM system (patients n, %)	
T1	220 (63)
T2	110 (31)
T3	20 (6)
COMS system (patients n, %)	
Small	130 (37)
Medium	260 (63)
Localization of uveal melanoma (patients n, %)	
Posterior pole	119 (34)
Posterior pole–equator	175 (50)
Equator–ora serrata	56 (16)
BCVA posttreatment (logMar)	0.40 ± 0.25
Mean thickness by echography posttreatment (mm)	1.75 ± 0.21
Complication (patients n, %)	
Radiation maculopathy	135 (38)
Optic neuropathy	40 (11)
Cataract	50 (14)
Tumor recurrence (patients n, %)	3 (1)
Death due to distant metastasis (patients n, %)	15 (4)

BCVA, best-corrected visual acuity; COMS, Collaborative Ocular Melanoma Study.

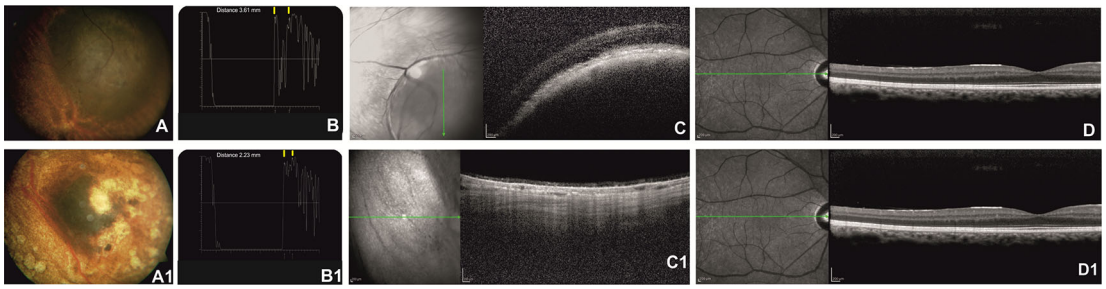

FIGURE 1 | Right eye of a 57-year-old patient affected by choroidal melanoma before ruthenium-106 brachytherapy (top row). Color fundus image shows an elevated and yellow lesion in the nasal mid-peripheral of the retina **(A)**. At A-scan ultrasound, the lesion presents low reflectivity. The yellow arrows over the peaks of the two high and perpendicular spikes, as shown in the echogram, indicate the maximum lift of 3.61 mm **(B)**. Spectral domain–optical coherence tomography (SD-OCT) B-scan over the lesion revealed a highly reflective band within the choriocapillaris layer with posterior shadowing **(C)**. SD-OCT B-scan shows no alteration of the retinal layer architecture in the macular region **(D)**. Color fundus image shows the same tumor after ruthenium-106 brachytherapy **(A1)**. At A-scan ultrasound, the lesion presents high reflectivity with a tumor thickness of 2.23 mm **(B1)** confirmed also by the OCT B-scan **(C1)**. OCT B-scan shows no alteration of the retinal layers architecture in the macular region **(D1)**.

The studies conducted by Cho and Marinkovic reported a low rate of deaths due to distant metastasis (31, 32); also Verschueren et al. showed a total of 46 deaths of 430 patients for distant metastases after 5 years' follow-up (30).

Rouberol et al., during 10 years' follow-up, described a total of 41 deaths from 213 patients due to hepatic metastases and multiple metastases (19).

Despite the localized distribution of this treatment, complications secondary to radiation such as cataracts and radiation maculopathy were found to be the most frequent after Ru-106 brachytherapy.

The cataract is a consequence of direct irradiation of the lens, mostly when the tumor is localized in the anterior part of the choroid and ciliary body. Its probability of developing was 21%, 27%, and 37% at 2, 3, and 5 years after treatment (33).

Radiation maculopathy, a consequence of DNA damage of the vascular endothelial cells, is occlusive retinal microangiopathy that determines important vascular permeability and non-perfusion retinal areas. The mean time to development is at 12 to 24 months after brachytherapy, affecting more than 40% of patients at 5 years (34, 35).

The treatment with anti-vascular endothelial growth factor intravitreal injections demonstrated retinal structural improvements at SD-OCT, although the retinal vascular network became impaired, as detected by OCT angiography (36–38).

Radiation optic neuropathy is less common than radiation maculopathy, and its rate was 10% and 12% after 2 and 3 years, respectively, while iris neovascularization was detected in 12% of the irradiated eyes after treatment (33). Motility disorders and vitreous hemorrhage occur rarely, and they are often temporary (33, 39).

The conservative treatment allows to preserve not only the ocular structures but also the vision. The functional outcomes in this study were confirmed by several reports that demonstrated the impaired visual acuity mainly in cases that showed radiation-related complications due to a reduced distance between the location of the plaque and the foveal region and the optic nerve

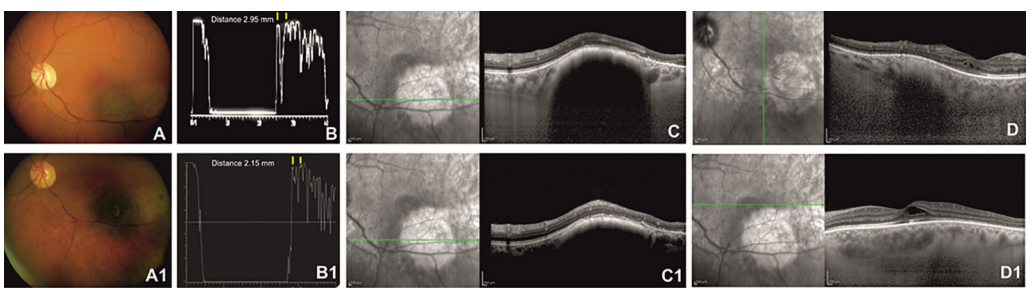

FIGURE 2 | Left eye of a 62-year-old patient affected by choroidal melanoma before ruthenium-106 brachytherapy (top row). Color fundus image shows an elevated and yellow lesion located at the posterior pole **(A)**. A-scan echography shows low reflectivity. The yellow arrows over the peaks of the two high and perpendicular spikes, as shown in the echogram, indicate a tumor thickness of 2.95 mm **(B)**. Spectral domain–optical coherence tomography (SD-OCT) B-scan over the lesion reveals a highly reflective band within the choriocapillaris layer with posterior shadowing **(C)** and normal central retinal thickness with rare intraretinal cysts in the macular region **(D)**. Color fundus image shows the same tumor after ruthenium-106 brachytherapy **(A1)**. At A-scan ultrasound, the lesion presented high reflectivity with a tumor thickness of 2.15 mm **(B1)**, confirmed also by the SD-OCT B-scan **(C1)** that shows in the macular region an increased central foveal thickness with intraretinal cysts due to the radiation maculopathy **(D1)**.

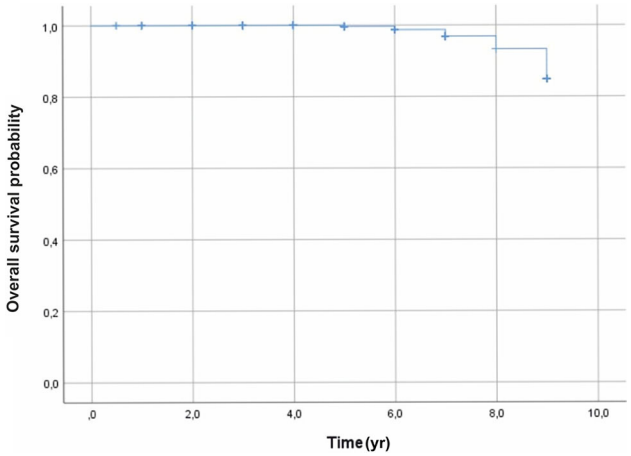

FIGURE 3 | Overall survival outcomes, using the Kaplan–Meier analysis, were 99%, 97%, and 85%, at 5, 7, and 9 years, respectively.

head (40, 41). A good functional outcome was found in iris melanoma treatment with Ru-106 brachytherapy on the ocular surface, as demonstrated by Agraval et al. This is shown in patients treated between 1998 and 2016: a vision of 6/9 Snellen or better is maintained in 53% of patients with a tumor control of 100%, no melanoma-related mortality, and a 62% reduction in tumor height, observed on ultrasonography (42).

In conclusion, the review of all our data led to confirm that Ru-106 brachytherapy has an excellent rate of local control of uveal melanoma, good survival, and a high rate of ocular preservation with a relatively low rate of recurrence.

DATA AVAILABILITY STATEMENT

The original contributions presented in the study are included in the article/supplementary material. Further inquiries can be directed to the corresponding author.

ETHICS STATEMENT

The studies involving human participants were reviewed and approved by Federico II University. The patients/participants provided their written informed consent to participate in this study.

AUTHOR CONTRIBUTIONS

GilC, GioC, and SD conceived and designed the study. MB, DM, LD'A, EM, MG, and RL performed the data collection. DM analyzed the data and designed the statistical analysis. GilC, DM, and GioC wrote the manuscript. GilC, DM, and AF revised the manuscript. GioC and SD undertook supervision of the study. All authors have read and agreed to the published version of the manuscript.

ACKNOWLEDGMENTS

This study was part of the research activity of the Rare Tumors Coordinating Center of Campania Region (CRCTR), recognized as a full member of the European Reference Network (ERN-EURACAN).

REFERENCES

1. Singh AD, Turell ME, Topham AK. Uveal Melanoma: Trends in Incidence, Treatment, and Survival. *Ophthalmology* (2011) 118:1881–5. doi: 10.1016/j.ophtha.2011.01.040
2. Singh AD, Bergman L, Seregard S. Uveal Melanoma: Epidemiologic Aspects. *Ophthalmol Clin North Am* (2005) 18:75–84. doi: 10.1016/j.ohc.2004.07.002
3. Shields JA, Shields CL. Management of Posterior Uveal Melanoma: Past, Present, and Future: The 2014 Charles L. Schepens Lecture. *Ophthalmology* (2015) 122:414–28. doi: 10.1016/j.ophtha.2014.08.046
4. Schachat AP. The Coms Randomized Trial of Iodine 125 Brachytherapy for Choroidal Melanoma, III: Initial Mortality Findings Coms Report No. 18. *Evidence-Based Eye Care* (2002) 3:102–3. doi: 10.1097/00132578-200204000-00020
5. Simpson ER, Gallie B, Laperrierre N, Beiki-Ardakaniet A, Kivelä T, Raivio V, et al. The American Brachytherapy Society Consensus Guidelines for Plaque Brachytherapy of Uveal Melanoma and Retinoblastoma. *Brachytherapy* (2014) 13:1–14. doi: 10.1016/j.brachy.2013.11.008
6. Egger E, Zografos L, Schalenbourg A, Beati D, Böhringer T, Chamot L, et al. Eye Retention After Proton Beam Radiotherapy for Uveal Melanoma. *Int J Radiat Oncol Biol Phys* (2003) 55:867–80. doi: 10.1016/S0360-3016(02)04200-1
7. Cuttone G, Cirrone GAP, Di Franco G, La Monica V, Lo Nigro S, Ott J, et al. CATANA Protontherapy Facility: The State of Art of Clinical and Dosimetric Experience. *Eur Phys J Plus* (2011) 126:1–7. doi: 10.1140/epjp/i2011-11065-1
8. Rashid M, Heikkonen J, Singh AD, Kivelä TT. Clinical Predictors of Regression of Choroidal Melanomas After Brachytherapy: A Growth Curve Model. *Ophthalmology* (2018) 125:747–54. doi: 10.1016/j.ophtha.2018.01.032
9. Diener-West M, Earle JD, Fine SL, Hawkins BS, Moy CS, Reynolds SM, et al. Randomized Trial of Iodine 125 Brachytherapy for Choroidal Melanoma, III: Initial Mortality Findings. COMS Report No. 18. *Arch Ophthalmol* (2001) 119:969–82. doi: 10.1001/archopht.119.7.969
10. Collaborative Ocular Melanoma Study Group. The Collaborative Ocular Melanoma Study (COMS) Randomized Trial of Pre-Enucleation Radiation of Large Choroidal Melanoma I: Characteristics of Patients En-Rolled and Not Enrolled. COMS Report No. 9. *Am J Ophthalmol* (1998) 125:767–78. doi: 10.1016/S0002-9394(98)00038-5
11. Edge SB, Byrd DR, Compton CC. AJCC Cancer Staging Manual. In: *Malignant Melanoma of the Uvea, 7th*. New York, NY: Springer (2010). p. 547–60.
12. Sayan M, Mamidanna S, Oncel D, Jan I, Vergalasova I, Weiner J, et al. Clinical Management of Uveal Melanoma: A Comprehensive Review With a Treatment Algorithm. *Radiat Oncol J* (2020) 38:162–9. doi: 10.3857/roj.2020.00318
13. Melvin A. A Patch Source Model for Treatment Planning of Ruthenium Ophthalmic Applicators. *Med Phys* (2003) 30:1219–928. doi: 10.1118/1.1573971
14. Berge MJ. Distribution of Absorbed Dose Around Point Sources of Electrons and Beta Particles in Water and Other Media. *J Nucl Med* (1971) Suppl 5:5–23.
15. Naseripour M, Jaberi R, Sedaghat A, Azma Z, Nojomi M, Ghasemi Falavarjani K, et al. Ruthenium-106 Brachytherapy for Thick Uveal Melanoma: Reappraisal of Apex and Base Dose Radiation and Dose Rate. *J Contemp Brachyther* (2016) 8:66–73. doi: 10.5114/jcb.2016.57818
16. American Brachytherapy Society - Ophthalmic Oncology Task Force, ABS – OOTF Committee. The American Brachytherapy Society Consensus Guidelines for Plaque Brachytherapy of Uveal Melanoma and Retinoblastoma. *Brachytherapy* (2014) 13:1–14. doi: 10.1016/j.brachy.2014.02.230

17. Seibel I, Cordini D, Rehak M, Hager A, Riechardt AI, Böker A, et al. Local Recurrence After Primary Proton Beam Therapy in Uveal Melanoma: Risk Factors, Retreatment Approaches, and Outcome. *Am J Ophthalmol* (2015) 160:628–36. doi: 10.1016/j.ajo.2015.06.017
18. Grossi Marconi D, de Castro DG, Rebouças LM, Bernardes Gil GO, Fogaroli RC, Conte Maia MA, et al. Tumor Control, Eye Preservation, and Visual Outcomes of Ruthenium Plaque Brachytherapy for Choroidal Melanoma. *Brachytherapy* (2013) 12:235–9. doi: 10.1016/j.brachy.2012.01.012
19. Rouberol F, Roy P, Kodjikian L, Gerard JP, Jean-Louis B, Grange JD. Survival, Anatomic, and Functional Long-Term Results in Choroidal and Ciliary Body Melanoma After Ruthenium Brachytherapy (15 Years' Experience With Beta-Rays). *Am J Ophthalmol* (2004) 137:893–900. doi: 10.1016/j.ajo.2003.12.032
20. Fili M, Astrahan M, Stålhammar G. Long-Term Outcomes After Enucleation or Plaque Brachytherapy of Choroidal Melanomas Touching the Optic Disc. *Brachytherapy* (2021) 9:S1538–4721(21)00431-1. doi: 10.1016/j.brachy.2021.05.162
21. Takiar V, Ranh Voong K, Gombos DS, Mourtada F, Rechner LA, Lawyer AA, et al. A Choice of Radionuclide: Comparative Outcomes and Toxicity of Ruthenium-106 and Iodine-125 in the Definitive Treatment of Uveal Melanoma. *Pract Radiat Oncol* (2015) 5:e169–76. doi: 10.1016/j.prro.2014.09.005
22. Pe'er J. Ruthenium-106 Brachytherapy. *Dev Ophthalmol* (2012) 49:27–40. doi: 10.1159/000328254
23. Perri P, Fiorica F, D'Angelo, Lamberti SG, Parmeggiani F, Martini A, et al. Ruthenium-106 Eye Plaque Brachytherapy in the Conservative Treatment of Uveal Melanoma: A Mono-Institutional Experience. *Eur Rev Med Pharmacol Sci* (2012) 16:1919–24.
24. Seregard S. Long- Term Survival After Ruthenium Plaque Radiotherapy for Uveal Melanoma. A Meta-Analysis of Studies Including 1,066 Patients. *Acta Ophthalmol Scand* (1999) 77:414–7. doi: 10.1034/j.1600-0420.1999.770411.x
25. Seregard S, aft Trampe E, Lax I, Kock E, Lundell G. Results Following Episcleral Ruthenium Plaque Radiotherapy for Posterior Uveal Melanoma. *Acta Ophthalmol Scand* (1997) 75:11–6. doi: 10.1111/j.1600-0420.1997.tb00241.x
26. Kleineidam M, Guthoff R, Bentzen SM. Rates of Local Control, Metastasis, and Overall Survival in Patients With Posterior Uveal Melanomas Treated With Ruthenium- 106 Plaques. *Radiother Oncol* (1993) 28:148–56. doi: 10.1016/0167-8140(93)90007-U
27. Frenkel S, Hendler K, Pe'er J. Uveal Melanoma in Israel in the Last Two Decades: Characterization, Treatment and Prognosis. *Isr Med Assoc J* (2009) 11:280–5.
28. Kaiserman I, Anteby I, Chowers I, Blumenthal EZ, Kliers I, Pe'er J. Changes in Ultrasound Findings in Posterior Uveal Melanoma After Ruthenium- 106 Brachytherapy. *Ophthalmology* (2002) 109:1137–41. doi: 10.1016/S0161-6420(02)01054-0
29. Georgopoulos M, Zehetmayer M, Ruhswurm I, Toma-Bstaendig S, Ségur-Eltz N, Sacu S, et al. Tumour Regression of Uveal Melanoma After Ruthenium-106 Brachytherapy or Stereotactic Radiotherapy With Gamma Knife or Linear Accelerator. *Ophthalmologica* (2003) 217:315–9. doi: 10.1159/000071345
30. Verschueren KM, Creutzberg CL, Schalij- Delfos NE, Ketelaars M, Klijsen FLL, Haeseker BI, et al. Long- Term Outcomes of Eye- Conserving Treatment With Ruthenium(106) Brachytherapy for Choroidal Melanoma. *Radiother Oncol* (2010) 95:332–8. doi: 10.1016/j.radonc.2010.03.023
31. Bergman L, Nilsson B, Lundell G, Lundell M, Seregard S. Ruthenium Brachytherapy for Uveal Melanoma, 1979–2003: Survival and Functional Outcomes in the Swedish Population. *Ophthalmology* (2005) 112:834–40. doi: 10.1016/j.ophtha.2004.11.038
32. Cho Y, Chang JS, Yoon JS, Lee SC, Kim YB, Kim JH, et al. Ruthenium-106 Brachytherapy With or Without Ad-Ditional Local Therapy Shows Favorable Outcome for Variable-Sized Choroidal Melanomas in Korean Patients. *Cancer Res Treat* (2018) 50:138–47. doi: 10.4143/crt.2016.391
33. Marinkovic M, Horeweg N, Laman MS, Bleeker JC, Ketelaars M, Peters FP, et al. Rutheni-Um-106 Brachytherapy for Iris and Iridociliary Melanomas. *Br J Ophthalmol* (2018) 102:1154–9. doi: 10.1136/bjophthalmol-2017-310688
34. Summanen P, Immonen I, Kivela T, Tommila P, Keikkonen J, Tarkkanen A. Radiation Related Complications After Ruthenium Plaque Radiotherapy of Uveal Melanoma. *Br J Ophthalmol* (1996) 80:732–9. doi: 10.1136/bjo.80.8.732
35. Shields CL, Demirci H, Marr BP, Mashayekhi A, Dai VV, Materin MA, et al. Intravitreal Triamcinolone Acetonide for Acute Radiation Papillopathy. *Retina* (2006) 26:537–44. doi: 10.1097/00006982-200605000-00007
36. Russo A, Reibaldi M, Avitabile T, Uva MG, Franco LM, Gagliano C, et al. Dexamethasone Intravitreal Implant vs Ranibizumab in the Treatment of Macular Edema Secondary to Brachytherapy for Choroidal Melanoma. *Retina* (2018) 38:788–94. doi: 10.1097/IAE.0000000000001585
37. Gündüz K, Shields CL, Shields JA, Cater J, Freire JE, Brady LW. Radiation Complications and Tumor Control After Plaque Radiotherapy of Choroidal Melanoma With Macular Involvement. *Am J Ophthalmol* (1999) 127:579–89. doi: 10.1016/S0002-9394(98)00445-0
38. Fallico M, Reibaldi M, Avitabile T, Longo A, Bonfiglio V, Chronopoulos A, et al. Intravitreal Aflibercept for the Treatment of Radiation-Induced Macular Edema After Ruthenium 106 Plaque Radiotherapy for Choroidal Melanoma. *Graefes Arch Clin Exp Ophthalmol* (2019) 257:1547–54. doi: 10.1007/s00417-019-04347-6
39. Cennamo G, Montorio D, Bernardo R, Farella A, Liuzzi R, Breve MA, et al. Retinal Vascular Changes in Radiation Maculopathy After Intravitreal Ranibizumab by Optical Coherence Tomography Angiography. *J Clin Med* (2020) 9:1618. doi: 10.3390/jcm9061618
40. Langmann A, Langmann G, Unlucerci C, Haller E. Motility Disorders in Brachytherapy of Choroid Melanomas With Ru-106 Applicators. *Ophthalmologe* (1995) 92:76–8.
41. Damat B, Patel I, Campbell IR, Mayles HM, Errington RD. Visual Acuity After Ruthenium- 106 Brachytherapy of Cho-Roidal Melanoma. *Int J Radiat Oncol Biol Phys* (2005) 63:392–400. doi: 10.1016/j.ijrobp.2005.02.059
42. Agraval U, Sobti M, Russell HC, Lockington D, Ritchie D, Cauchi P, et al. Use of Ruthenium-106 Brachytherapy for Iris Melanoma: The Scottish Experience. *Br J Ophthalmol* (2018) 102:74–8. doi: 10.1136/bjophthalmol-2017-310278

Conflict of Interest: The authors declare that the research was conducted in the absence of any commercial or financial relationships that could be construed as a potential conflict of interest.

frontiers in Oncology

ORIGINAL RESEARCH
published: 10 January 2022
doi: 10.3389/fonc.2021.812643

Prospective Clinical Feasibility Study for MRI-Only Brain Radiotherapy

Minna Lerner[1,2], Joakim Medin[1,3], Christian Jamtheim Gustafsson[1,2], Sara Alkner[1,4] and Lars E. Olsson[1,2]*

[1] Department of Hematology, Oncology, and Radiation Physics, Skåne University Hospital, Lund, Sweden, [2] Department of Translational Medicine, Medical Radiation Physics, Lund University, Malmö, Sweden, [3] Department of Medical Radiation Physics, Clinical Sciences, Lund, Lund University, Lund, Sweden, [4] Department of Clinical Sciences Lund, Oncology and Pathology, Lund University, Lund, Sweden

Objectives: MRI-only radiotherapy (RT) provides a workflow to decrease the geometric uncertainty introduced by the image registration process between MRI and CT data and to streamline the RT planning. Despite the recent availability of validated synthetic CT (sCT) methods for the head region, there are no clinical implementations reported for brain tumors. Based on a preceding validation study of sCT, this study aims to investigate MRI-only brain RT through a prospective clinical feasibility study with endpoints for dosimetry and patient setup.

Material and Methods: Twenty-one glioma patients were included. MRI Dixon images were used to generate sCT images using a CE-marked deep learning-based software. RT treatment plans were generated based on MRI delineated anatomical structures and sCT for absorbed dose calculations. CT scans were acquired but strictly used for sCT quality assurance (QA). Prospective QA was performed prior to MRI-only treatment approval, comparing sCT and CT image characteristics and calculated dose distributions. Additional retrospective analysis of patient positioning and dose distribution gamma evaluation was performed.

Results: Twenty out of 21 patients were treated using the MRI-only workflow. A single patient was excluded due to an MRI artifact caused by a hemostatic substance injected near the target during surgery preceding radiotherapy. All other patients fulfilled the acceptance criteria. Dose deviations in target were within ±1% for all patients in the prospective analysis. Retrospective analysis yielded gamma pass rates (2%, 2 mm) above 99%. Patient positioning using CBCT images was within ± 1 mm for registrations with sCT compared to CT.

Conclusion: We report a successful clinical study of MRI-only brain radiotherapy, conducted using both prospective and retrospective analysis. Synthetic CT images generated using the CE-marked deep learning-based software were clinically robust based on endpoints for dosimetry and patient positioning.

Keywords: MRI-only, implementation, brain, glioma, sCT, radiotherapy, cancer

OPEN ACCESS

Edited by:
Brian Timothy Collins, Georgetown University, United States

Reviewed by:
Charlotte Robert, Institut Gustave Roussy, France
Gage Redler, Moffitt Cancer Center, United States

****Correspondence:***
Minna Lerner
minna.lerner@med.lu.se

Specialty section:
This article was submitted to Radiation Oncology, a section of the journal Frontiers in Oncology

Received: *10 November 2021*
Accepted: *20 December 2021*
Published: *10 January 2022*

Citation:
Lerner M, Medin J, Jamtheim Gustafsson C, Alkner S and Olsson LE (2022) Prospective Clinical Feasibility Study for MRI-Only Brain Radiotherapy. Front. Oncol. 11:812643. doi: 10.3389/fonc.2021.812643

1 INTRODUCTION

Radiotherapy (RT) is an important part of treatment for patients with brain malignancies, such as glioma. Traditionally, RT treatment planning is based on images obtained from both computed tomography (CT) and magnetic resonance imaging (MRI), in which case MRI is used primarily to define the tumor and organs at risk (OAR). In recent years a workflow based on MRI without CT imaging has evolved, referred to as MRI-only radiotherapy (1–3). Excluding CT from the workflow enables reduced spatial uncertainties in the final dose plan since the otherwise required image registration between the CT and the MR images is not needed (4, 5). MRI-only radiotherapy also provides a more streamlined workflow which may reduce both time and costs (1). However, the Hounsfield units (HU) containing electron density information for absorbed dose calculations are not directly present in the MR images. To bridge this gap, synthetic CT (sCT) images, generated based on MRI information, are introduced to provide the necessary HU. Many successful sCT generation methods for brain have been presented in the literature, starting from methods which simply assumed a homogeneous attenuation value inside the head (6) to state-of-the-art deep learning-based methods in recent publications (7–12).

MRI-only RT has been presented for treatment of prostate cancer using both in-house developed methods (13) as well as commercial solutions (14–16). For brain lesions on the other hand, the first commercially available sCT generation products were only recently released on the market (8, 17, 18). Despite the number of previously performed validation studies of sCT for brain (19), this will, to the best of our knowledge, be the first publication on a prospective clinical implementation of MRI-only RT for brain tumors.

In a recent publication by our group (8), a CE-marked sCT generation software was validated in patients with brain malignancies. Results demonstrated equivalent dose distributions and patient treatment positioning between CT and sCT based RT workflows. This work was the foundation and motivation for the present study, using the same sCT generation method in our clinic. To facilitate the implementation of MRI-only RT planning for brain tumors, this study aimed to introduce a new workflow in our clinic based on solely MR images. For quality assurance (QA) purposes only, CT was still acquired to enable both prospective and retrospective analysis.

2 METHOD

2.1 Patients and Imaging

In this prospective treatment study 21 glioma patients were consecutively included during March 2020 to March 2021. The study was approved by the regional ethical review board and informed consent was obtained from all patients. Patient details are presented in **Table 1**. Patients above 18 years old referred to CT and MR examinations for treatment planning prior to RT of high-grade glioma were asked to participate in the study. Tumor classification was performed within clinical routine using the WHO 2016 classification of glioma. Study exclusion criteria were any MRI contraindications or metal implants near the tumor. Standardized fractionation schemes with total doses of 34.0, 40.05 or 60.0 Gy (10, 15 or 30 fractions, respectively) were prescribed according to clinical routines, based on tumor malignancy and patient specific factors such as age and comorbidity.

TABLE 1 | Patient details.

Patient detail	
Age, mean [range]	62 years [46–85 years]
Gender	12 male/9 female
Diagnosis	Glioma, grade III (n=2)/grade IV (n=19)
Prescribed dose	34.0 Gy, 10 fractions (n=4) 40.05 Gy, 15 fractions (n=4) 60.0 Gy, 30 fractions (n=13)
PTV volume, mean [range]	293 cc [139–644 cc]

The proposed MRI-only workflow was inspired by previously published work for prostate cancer (14), appropriately adjusted for glioma. All imaging was performed in treatment setup, using individual three-point fixation masks (Orfit Industries NV, Wijnegem, Belgium) and head support. All patients underwent both CT and MRI examinations, where the CT scan was solely used for QA purposes and not included in any decision making prior to the approval of the treatment plan.

2.1.1 MRI Examination

MRI was performed on a 3T GE Discovery 750 W (software release: DV26.0-R03-1831.b, GE Healthcare, Chicago, Illinois, USA) for the first 16 patients and on a 3T GE Architect (software release: DV28.0-R05-2034.a) for the remaining five patients. RT-setup was used during all examinations, including a laser bridge (LAP GmbH Laser Applikationen, Lüneburg, Germany), a flat tabletop and 6-channel receiver flex coils combined with an 8-channel posterior array (**Figure 1A**). Three conical liquid markers (Beekly Medical, Bristol, CT, United States) were placed left, right and front on the fixation mask (**Figure 1B**), according to the laser intersection points, to define the user origin in the images.

MRI sequences for sCT generation and treatment couch identification were added to the clinical brain MRI protocol, as described in previous work (8). A 3D IDEAL Dixon fast spoiled gradient echo (FSPGR) acquisition sequence was used for sCT generation. Slice thickness was 2 mm, in-plane resolution was 1.1x1.1 mm^2 and scan time was 4.5 minutes. To minimize geometric distortion, the bandwidth was 744 Hz/pixel with 3D distortion correction enabled. Geometric distortions have previously been investigated on the current scanner using the same patient setup and Dixon sequence and were found to be of no clinical concern (8). The resolution after reconstruction of the Dixon images (fat, water, in-phase and out-of-phase) was 0.5x0.5x2 mm^3. Since the treatment couch did not generate any useful MR signal in the Dixon sequence, a zero-echo time (ZTE) sequence with a total scan time of 21 s was added to image the position of the couch. The acquisition of images for target delineation with and without gadolinium (Gd) contrast agent

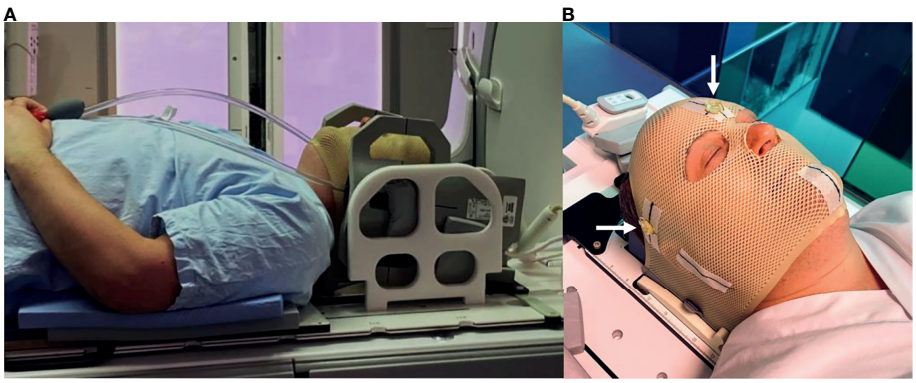

FIGURE 1 | **(A)** RT-setup of patient in three-point fixation mask scanned on a flat tabletop with 6-channel receiver flex coils (left and right) combined with an 8-channel posterior array (under the flat tabletop). **(B)** Fixation mask with liquid markers front, left and right, indicated by the white arrows.

were included from the standard clinical brain MRI protocol (T1-, T2- and diffusion-weighted images). Total scan time during the whole examination was approximately 25 minutes. Visual inspection of the alignment between images from different MRI sequences was performed after importing the images to the treatment planning system (TPS) by experienced MRI staff.

MRI scanner performance was assessed by monthly quality assurance measurements, as part of our normal clinical routines. These controls included MRI system specific geometric distortion checks with a large field of view phantom (GRADE, Spectronic Medical AB, Helsingborg, Sweden). The phantom contained approximately 1200 signal markers, which were automatically compared to a reference template in the evaluation of geometric distortion.

2.1.2 Synthetic CT Generation

The sCT images were generated using the CE approved sCT generation software MRI Planner (v 2.2, Spectronic Medical, AB, Helsingborg, Sweden), previously validated for both brain and head and neck cancer (8, 20). The software is deep learning-based and utilizes a 3D deep convolutional neural network to generate sCT images based on Dixon images (fat, water, in-phase and out-of-phase). Clinical workflow integration was facilitated by an MRI console DICOM export of the Dixon images to the cloud-based MRI Planner software from which the sCT images were automatically returned to the TPS. The returned sCT images inherited the MR image frame of reference and the same spatial resolution as the reconstructed Dixon images (0.5x0.5x2.0 mm^3). The liquid markers placed front, left and right on the patient during MRI examination were visible in the sCT images.

2.1.3 CT Examination

CT imaging was performed using a Siemens Somatom Definition AS+ (Siemens, Erlangen, Germany) with 2 mm slice thickness, in-plane resolution between 0.7x0.7 mm^2 and 1.0x1.0 mm^2 and tube voltage 120 kV. Although the CT examination was performed prior to MRI examination due to logistic reasons in our clinical workflow, the CT images were not imported to the TPS until the dose plan was completed. Hence, the CT images could in no way influence the target delineation, the treatment planning nor the image registration during treatment positioning as the CT images were strictly used for QA purposes and in retrospective analysis.

2.2 MRI-Only Treatment Planning, Approval and Delivery

2.2.1 MRI-Only Treatment Planning

All steps of treatment planning were performed in Eclipse (v 15.6.05, Varian Medical Systems, Palo Alto, CA, USA). Target and organs at risk (OAR) were delineated on MR images overlayed on sCT. The contours of the body and the brain were automatically generated for the sCT images in the TPS, according to clinical routine. The position of the treatment couch relative to the fixation device was identified using the ZTE images and was inserted as a structure in the sCT. This enabled the couch to be accounted for in the optimization and dose calculation. The user origin was set based on the projection of the three liquid markers in the sCT. Finally, treatment plans were created and optimized directly on sCT images, following local clinical routines for high-grade gliomas. All patients were treated using volumetric modulated arc therapy (VMAT) on TrueBeam (Varian Medical Systems, Palo Alto, CA, USA), with two or three arcs. Dose calculation was performed using the standard Eclipse HU calibration curve, also provided by MRI Planner, and an analytical anisotropic algorithm (v. 15.6.05, Varian Medical Systems, Palo Alto, CA, USA) with a 1x1 mm^2 or 2.5x2.5 mm^2 dose grid, depending on the target size.

2.2.2 Treatment Plan Approval

All treatment plans based on the sCT were reviewed and approved by experienced oncologists and medical physicists, according to local clinical criteria (**Table E1**, in the **Supplementary Material**). Final treatment approval was performed after finishing the prospective quality assurance steps, see *Prospective QA*.

The study patients were monitored using a logbook attached to each patient's treatment plan. Notes regarding target

delineation, appearance of bone structure and bone resection areas, dose deviations and HU agreement were made by the involved dosimetrist, oncologist and medical physicist. The aim of the logbook was to monitor potential issues during the process.

2.2.3 Treatment Delivery

After treatment approval of the MRI-only plan, it was measured using a Delta4 Phantom+ (Scandidos AB, Uppsala, Sweden) according to local clinical routines. Planned and measured dose were compared using global gamma evaluation with at least 95% of the points passing the criteria 3%, 2 mm required for approval.

Imaging protocol followed clinical routine, which included CBCT imaging the first three treatment fractions and once a week for the remaining fractions. The sCT was used as the image reference in the automatic registration based on mutual information of the bony anatomy.

2.3 Quality Assurance

To ensure a safe implementation of the MRI-only workflow, several prospective quality assurance (QA) steps (**Table 2**) were introduced prior to final acceptance of the treatment plan. These included evaluating dosimetry and sCT image quality. Tasks for QA approval were integrated in the TPS, requiring manual confirmation before it was possible to proceed in the workflow. The TPS tasks concerned imaging, post imaging, QA and treatment delivery. Additional analysis of the absorbed dose and patient positioning was performed retrospectively. Comparisons were made against CT in all QA steps, as it is the gold standard imaging modality in RT.

2.3.1 Prospective QA

The first QA step was an automatic MATLAB (v. 2015b, Mathworks Inc., Natick, MA, USA) script developed to check the MRI acquisition parameters of the Dixon sequence. Source code is available at https://github.com/jamtheim/MRIAcqParameterCheckBrain. The parameters were checked against a predefined template to ensure consistent image acquisition throughout the study. A patient specific report of the result was generated and automatically sent by e-mail to the study coordinators for each patient.

The sCT was visually inspected in connection to the target delineation for any artifacts which might have an influence on the treatment before being forwarded to dose planning. After the MRI-only treatment plan had been approved at the ordinary chart round, the CT images were imported to the TPS for QA procedures. The CT was rigidly registered to the sCT images, including translation and rotations for optimal agreement between structures, using automatic bone match (threshold 200-1700 HU). All structures, except for the body contour, were transferred to the CT. A new body contour was automatically generated.

The original treatment plan was recalculated on the CT keeping the same number of monitor units. Due to intrinsic properties, the TPS does not support rotations of the dose matrix, which resulted in a translational registration only of the dose matrix. Evaluations of dose volume histogram (DVH) parameters were performed within the TPS to mimic the conventional workflow. All dose differences were normalized to prescribed dose. Treatment plans were approved without further investigation if all dose differences were within ±1%, comparing sCT and CT based dose calculations. Targets were evaluated based on mean dose (D_{mean}), near minimum dose ($D_{98\%}$ and $D_{95\%}$) and near maximum dose ($D_{2\%}$). Two acceptance criteria were used for OARs; i) when the OAR was close to the high-dose region the difference for $D_{2\%}$ should be within ±1%, and ii) when the absorbed dose to the OAR was more than 10% below its tolerance dose, only a note of the dose difference was made provided it was below tolerance in absolute numbers including the deviation.

The general appearance of HU line profiles was qualitatively compared between sCT and CT images in the TPS. Bone structures, and especially areas of bone resection due to pre-RT surgery, were inspected near the target. Acceptance criteria of the sCT to CT difference in bone edges and bone resection areas were maximum 1.5 mm.

TABLE 2 | Summary of the QA steps introduced for MRI-only implementation, including both prospective and retrospective analysis.

QA step	Control	Acceptance criteria
	Prospective QA	
MRI acquisition parameters script	Automatic control of essential MRI Dixon acquisition parameters against a predefined template	MRI acquisition parameters should be identical to template
Visual inspection	Check sCT for artifacts, verify alignment between MRI sequences	Qualitative evaluation
HU units	Compare HU line profile between sCT and CT	Qualitative evaluation
Bone structures	Check bone structures and bone resection areas to verify correct generation of sCT compared to CT	≤1.5 mm for bone edges
Dose distribution	Recalculate sCT treatment plan on CT and evaluate DVH parameters for target and OARs	i) Dose difference within ±1% for relevant target and OARs or ii) OAR absolute dose more than 10% below clinical tolerance
	Retrospective QA	
Patient positioning	Verify after treatment start that CBCT registration is equivalent using sCT and CT as reference	≤ 1 mm in x, y and z, respectively

2.3.2 Retrospective QA

Patient positioning was evaluated through retrospective QA, where the sCT and CT registrations of the CBCT from one of the first three treatment fractions were compared. Acceptance criteria was less than 1 mm difference in any translational direction.

2.3.3 Additional Dose Evaluation

The CT-based dose distribution was corrected for differences in image rotation and image resolution for further analysis. This was performed by rigidly registering and resampling the CT to the sCT frame of reference using the translation and rotation parameters from the TPS in the software MICE Toolkit (Nonpi Medical, Umeå, Sweden). The corrected CT was then imported back into the TPS and the sCT-based treatment plan was transferred and evaluated. This procedure was not found optimal for the clinical workflow and was therefore only used in the retrospective analysis.

In addition, retrospective 3D global gamma evaluation of the sCT and CT calculated dose distributions (>15% of prescribed dose) was performed in MICE Toolkit for all patients. Gamma criteria with the following dose difference/distance to agreement were considered: 1%/1 mm, 2%/2 mm and 3%/3 mm.

3 RESULTS

3.1 Prospective QA

Twenty out of twenty-one patients successfully received MRI-only RT according to the study workflow. No deviations were found in the automatic MRI acquisition parameters script control. MRI system specific geometric distortions of the MRI scanner were acceptable and stable during the inclusion period (**Table 3**).

Exclusion of a single patient was due to a hemostatic substance injected during pre-RT surgery. The substance gave rise to a signal loss in the MR images which the sCT generation software interpreted as bone. This resulted in up to 5 mm thicker skull bone adjacent to the target in the generated sCT image compared to the CT. The position of the target was temporo-occipital. The patient was excluded from the study as a study precaution, although no clinically significant dose difference or patient positioning effect was observed in a retrospective analysis. This patient was successfully transferred back to the conventional workflow with CT and MRI, with no delay in the scheduled treatment delivery.

Clinical acceptance criteria were fulfilled for all patients receiving MRI-only RT. The target dose parameters were within ±1%, comparing the dose calculated on sCT and CT images (**Figure 2A**). Seven outliers with dose differences outside ±1% were observed for brainstem and chiasma $D_{2\%}$. All of these concerned lower dose regions more than 10% below clinical tolerance dose, thus passing the second criteria.

3.2 Retrospective QA

Results from retrospective analysis of patient positioning using CBCT is presented in **Figure 3**. The difference between CBCT registered to sCT and CT was found to be on sub-mm level for all patients and translational directions. The mean ± 1 S.D. (range) 3D vector magnitude of the total registration differences for all patients was 0.3 ± 0.1 mm (0.1-0.6 mm).

3.3 Additional Dose Evaluation

When taking rotations and image resolution into account in the retrospective analysis of dose differences, all values were within ±1% (**Figure 2B**).

Global gamma pass rates, comparing the dose distributions calculated on sCT to CT, with a dose cut-off at 15% of the prescribed dose is presented in **Table 4**. For gamma criteria 2%, 2 mm all patients had a gamma pass rate above 99%.

4 DISCUSSION

We report the first MRI-only RT treatment study for brain tumors, using a deep learning-based software for sCT generation. The workflow was successfully implemented in the clinic with 20 out of 21 patients receiving MRI-only brain RT. The study was prospective with all treatments optimized, calculated and delivered using sCT images.

All patients receiving the MRI-only treatment passed the prospective acceptance criteria. The TPS tasks regarding imaging, post imaging, QA and treatment delivery were successfully completed for all included patients. Dose differences were within ±1% for both target and OARs, if rotations between the sCT and CT frame of reference were taken into account. CBCT registration with sCT and CT images as reference agreed on sub mm level for all included patients. This being the first study on MRI-only brain RT there are no similar prospective studies to compare with. There are however several published implementation studies on MRI-only RT for prostate cancer, where treatment success rates between 87.5-100% (13, 14, 16) are reported.

The accuracy of sCT images generated from deep learning-based methods relies on a variation of relevant image features to be included in the training data of the model. Implants or abnormal anatomy due to surgery are common in patients treated for brain tumors. This might constitute a problem if the anomaly goes beyond image features included in the training

TABLE 3 | Geometric distortion measured using the Spectronic GRADE phantom, presented as the average of the monthly individual mean and maximum distortions for each given radial distance from the MRI scanner isocenter.

	Geometric distortions [mm]		
Radial distance from isocenter [mm]	<100	100–150	150–200
Average of mean distortion (1 SD) [range]	0.2 (0.1) [0.1–0.4]	0.3 (0.1) [0.2–0.5]	0.6 (0.1) [0.5–0.8]
Average of max distortion (1 SD) [range]	0.6 (0.1) [0.4–0.8]	0.9 (0.2) [0.6–1.3]	1.8 (0.2) [1.4–2.2]

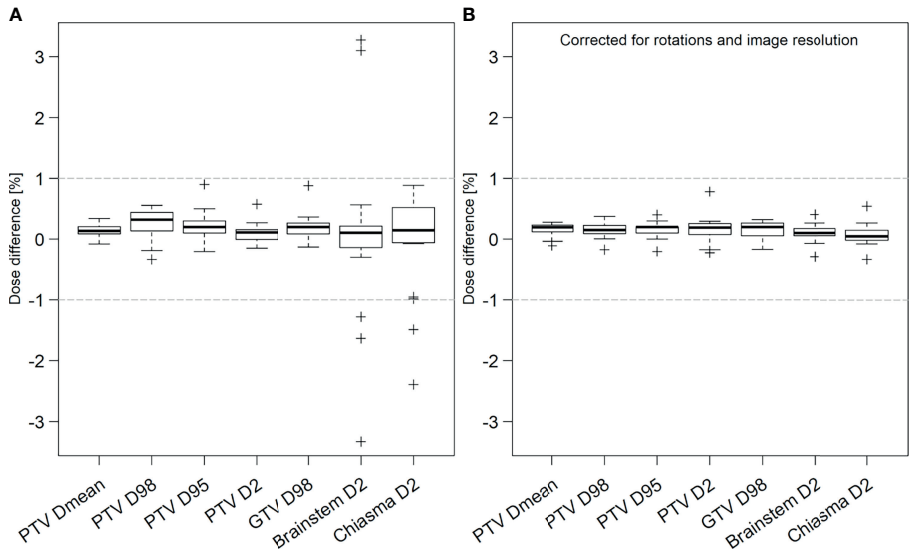

FIGURE 2 | Prospective **(A)** and retrospective **(B)** analysis of dose difference between treatment plans calculated on sCT and CT images for target (PTV and GTV) and organs at risk (OAR) brainstem and chiasma for all patients. In the prospective results, OAR outliers outside ±1% had relative dose levels more than 10% below the clinical tolerance for absorbed dose to OARs. In the additional retrospective analysis, original dose distribution has been corrected for image rotations and image resolution differences between the sCT and CT. The thick black line in each box represents the median value for all patients. The box includes the 25th-75th percentiles, the interquartile range (IQR). Whiskers represent the maximum and minimum values within 1.5 IQR and the crosses represent any values outside that range. The grey horizontal lines represent ±1% dose difference.

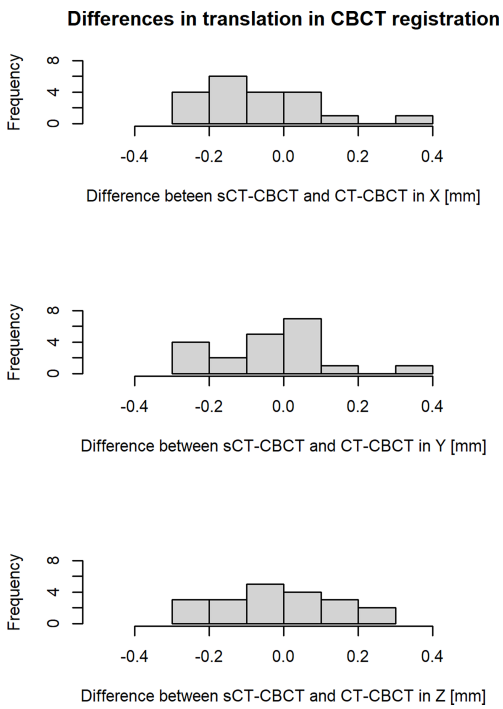

FIGURE 3 | Differences in translation (X, Y, Z) in the image registration of sCT-CBCT compared to CT-CBCT for all patients. The X, Y and Z axis correspond to the following translations: X = left to right, Y = anterior to posterior and Z = superior to inferior. The histogram cells include their right-hand endpoint.

data, since the sCT generation software then is unable to interpret the input MR images correctly. Therefore, it is important to visually inspect the resulting sCT images to find potential artifacts. The only excluded patient of this study was successfully transferred back to the conventional workflow, receiving treatment without any delays. If similar cases would occur during MRI-only RT in clinical routine, the artifact needs to be individually assessed based on its magnitude and localization relative to target and critical anatomical structures. During the implementation phase of MRI-only RT, irrespective of anatomical region, occasional exclusions may be necessary. Since MRI-only workflow implementations lack well-established, simple QA-methods for a safe assessment, a conversion back to the combined CT and MRI based workflow should be accessible during the implementation phase.

This study was a clinical implementation of MRI-only RT. Therefore, we aimed to perform all evaluations in the clinical systems before treatment approval. The TPS used at our clinic only allows translational registrations of dose matrices even if the images are matched using both translations and rotations. This limitation resulted in dose differences above 1% for OARs in six patients due to the OARs being located in low dose regions adjacent to steep dose gradients. However, in addition to relative dose difference, the acceptance criteria for OARs included a comparison with clinical tolerance (as described in section 2.3.1). These six patients passed the second criteria and received their treatment based solely on the sCT. In addition, the patients with dose deviations above 1% in this study were analyzed retrospectively applying both translations and rotations of the dose matrices (as described in section 2.3.3) and were all found to

TABLE 4 | Global gamma evaluation, with a dose cut-off at 15%, comparing sCT and CT dose distributions, averaged over all patients.

Gamma criteria	Gamma pass rate ± 1 SD [range] (%)
3%, 3 mm	100.0 ± 0.1 [99.7–100.0]
2%, 2 mm	99.8 ± 0.2 [99.4–100.0]
1%, 1 mm	99.1 ± 0.6 [97.6–99.8]

be well within 1%. The rationale for applying a limit of 1% in dose differences in clinically relevant DVH parameters between the sCT and the CT based treatment plans is based on a goal to achieve less than 2% systematic dose error in the delivered treatment. It has been shown that a reasonable accuracy to strive for in systematic bias in dose delivery is 1-2%, taking tumor response and normal tissue response into account (21). In this context one must consider that there are several potential systematic biases/errors in the chain from imaging to treatment delivery which contributes to the final error, for example inherent limitations in dose calculation algorithms and treatment machine calibration. Although 2% has been suggested as acceptance criteria for different anatomies within MRI-only implementations previously (22), we suggest that a limit of 1% might be appropriate for MRI-only brain RT. This is further supported in recent publications using deep learning-based sCT generation methods (8–12). A 1% criteria on sCT-CT dose difference may still enable a total bias/error in delivered dose below 2% after the contribution from other systematic errors. Furthermore, the recommended limit for random uncertainties is less than 3% (21), which also needs to be added to the systematic uncertainties discussed above.

During the implementation of MRI-only RT two aspects of the dose criteria should be considered; 1) relative dose difference between sCT and CT based calculations and 2) absolute dose level compared to clinical tolerance for OAR in low dose regions. To establish general acceptance criteria for MRI-only brain RT implementations, more and larger prospective studies are required. Until then, each clinic needs to perform their own studies as part of their implementation.

In a recent review (23) recommendations for several deep learning-based applications in radiotherapy were summarized. Specifically, regarding the implementation process of sCT generation software, Vandewinckele et al. emphasized the need for user knowledge to be able to detect artifacts and identify their causes. As seen in this study, deviations from the characteristics in the training data set can cause artifacts such as abnormal bone structures. Although some artifacts might be difficult to identify, those are unlikely to have any clinical relevance as dose calculations are relatively insensitive to small HU variations. There is however still a need for case specific QA. One suggestion could be to use CBCT for dose calculation as an independent evaluation of the sCT, which would likely find most clinically relevant deviations (23–25). Regular sCT generation model QA is another important aspect of implementing a deep learning-based software. This is especially important if changes are made to the workflow, such as modifications of MRI acquisition protocols or MRI scanner hardware. During the present study, the MRI scanner was upgraded from a GE Discovery (software DV26) to a GE Architect (software DV28). Monthly QA routines verified that the MRI scanner was stable regarding geometric distortion, before and after the upgrade. Minor changes in sCT characteristics were however observed, manifested as streaks of slightly higher HU values in cranial parts of the brain. This was due to minor changes in the MRI scanner post processing but had no dosimetric impact for this patient cohort. Despite QA for both geometry and MRI acquisition parameters, this was not captured until visual inspection of the sCT.

To summarize, implementing a new workflow in the clinic can be challenging. However, the transition can be done safely by making conscious and careful changes in all steps of the workflow, with thorough validation studies, appropriate QA and close collaboration with the clinical staff.

5 CONCLUSION

In this prospective clinical MRI-only RT study for brain tumors, an implementation of a commercial deep learning-based sCT generation method was conducted using both prospective and retrospective analysis. The workflow was successfully applied to 20 glioma patients, fulfilling both dosimetric and treatment setup criteria.

DATA AVAILABILITY STATEMENT

The datasets presented in this article are not readily available because of patient privacy concerns and institutional regulations. Requests to access the datasets should be directed to ML, minna.lerner@med.lu.se.

ETHICS STATEMENT

The studies involving human participants were reviewed and approved by Regional ethical review board, Lund, Sweden DNR: 2018/445. The patients/participants provided their written informed consent to participate in this study.

AUTHOR CONTRIBUTIONS

Conceptualization: JM, SA, and LO. Patient recruitment: ML, JM, and SA. Clinical guidance: JM and SA. Data analysis: ML. Software: ML and CJ. Drafting manuscript, review and editing: ML. Proof editing: JM, CJ, SA, and LO. All authors approved the submitted version.

FUNDING

This work was supported by "Allmänna sjukhusets I Malmö Stiftelse för bekämpande av cancer"; Fru Berta Kamprads stiftelse för utforskning och bekämpning av cancersjukdomar, SUS foundations and Region Skåne.

ACKNOWLEDGMENTS

The authors would like to acknowledge the clinical staff for their contribution and excellent work in this trial. Thanks also to Spectronic Medical AB for their support and collaboration in this study.

SUPPLEMENTARY MATERIAL

The Supplementary Material for this article can be found online at: https://www.frontiersin.org/articles/10.3389/fonc.2021.812643/full#supplementary-material

REFERENCES

1. Owrangi AM, Greer PB, Glide-Hurst CK. MRI-Only Treatment Planning: Benefits and Challenges. *Phys Med Biol* (2018) 63(5):05TR1. doi: 10.1088/1361-6560/aaaca4
2. Jonsson JH, Karlsson MG, Karlsson M, Nyholm T. Treatment Planning Using MRI Data: An Analysis of the Dose Calculation Accuracy for Different Treatment Regions. *Radiat Oncol* (2010) 5(1):62. doi: 10.1186/1748-717X-5-62
3. Stanescu T, Jans HS, Pervez N, Stavrev P, Fallone BG. A Study on the Magnetic Resonance Imaging (MRI)-Based Radiation Treatment Planning of Intracranial Lesions. *Phys Med Biol* (2008) 53(13):3579–93. doi: 10.1088/0031-9155/53/13/013
4. Ulin K, Urie MM, Cherlow JM. Results of a Multi-Institutional Benchmark Test for Cranial CT/MR Image Registration. *Int J Radiat Oncol Biol Phys* (2010) 77(5):1584–9. doi: 10.1016/j.ijrobp.2009.10.017
5. Veninga T, Huisman H, van der Maazen RW, Huizenga H. Clinical Validation of the Normalized Mutual Information Method for Registration of CT and MR Images in Radiotherapy of Brain Tumors. *J Appl Clin Med Phys* (2004) 5(3):66–79. doi: 10.1120/jacmp.v5i3.1959
6. Schad L, Blüml S, Hawighorst H, Wenz F, Lorenz W. Radiosurgical Treatment Planning of Brain Metastases Based on a Fast, Three-Dimensional MR Imaging Technique. *Magn Reson Imaging* (1994) 12 (5):811–9. doi: 10.1016/0730-725X(94)92206-3
7. Boulanger M, Nunes JC, Chourak H, Largent A, Tahri S, Acosta O, et al. Deep Learning Methods to Generate Synthetic CT From MRI in Radiotherapy: A Literature Review. *Phys Med* (2021) 89:265–81. doi: 10.1016/j.ejmp.2021.07.027
8. Lerner M, Medin J, Jamtheim Gustafsson C, Alkner S, Siversson C, Olsson LE. Clinical Validation of a Commercially Available Deep Learning Software for Synthetic CT Generation for Brain. *Radiat Oncol* (2021) 16(1):66. doi: 10.1186/s13014-021-01794-6
9. Kazemifar S, Barragan Montero AM, Souris K, Rivas ST, Timmerman R, Park YK, et al. Dosimetric Evaluation of Synthetic CT Generated With GANs for MRI-Only Proton Therapy Treatment Planning of Brain Tumors. *J Appl Clin Med Phys* (2020) 21(5):76–86. doi: 10.1002/acm2.12856
10. Maspero M, Bentvelzen LG, Savenije MHF, Guerreiro F, Seravalli E, Janssens GO, et al. Deep Learning-Based Synthetic CT Generation for Paediatric Brain MR-Only Photon and Proton Radiotherapy. *Radiother Oncol* (2020) 153:197–204. doi: 10.1016/j.radonc.2020.09.029
11. Koike Y, Akino Y, Sumida I, Shiomi H, Mizuno H, Yagi M, et al. Feasibility of Synthetic Computed Tomography Generated With an Adversarial Network for Multi-Sequence Magnetic Resonance-Based Brain Radiotherapy. *J Radiat Res* (2019) 61(1):92–103. doi: 10.1093/jrr/rrz063
12. Dinkla AM, Wolterink JM, Maspero M, Savenije MHF, Verhoeff JJC, Seravalli E, et al. MR-Only Brain Radiation Therapy: Dosimetric Evaluation of Synthetic CTs Generated by a Dilated Convolutional Neural Network. *Int J Radiat Oncol Biol Phys* (2018) 102(4):801–12. doi: 10.1016/j.ijrobp.2018.05.058
13. Greer P, Martin J, Sidhom M, Hunter P, Pichler P, Choi JH, et al. A Multi-Center Prospective Study for Implementation of an MRI-Only Prostate Treatment Planning Workflow. *Front Oncol* (2019) 9:826. doi: 10.3389/fonc.2019.00826
14. Persson E, Jamtheim Gustafsson C, Ambolt P, Engelholm S, Ceberg S, Bäck S, et al. MR-PROTECT: Clinical Feasibility of a Prostate MRI-Only Radiotherapy Treatment Workflow and Investigation of Acceptance Criteria. *Radiat Oncol* (2020) 15(1):77. doi: 10.1186/s13014-020-01513-7
15. Tenhunen M, Korhonen J, Kapanen M, Seppälä T, Koivula L, Collan J, et al. MRI-Only Based Radiation Therapy of Prostate Cancer: Workflow and Early Clinical Experience. *Acta Oncol* (2018) 57(7):902–7. doi: 10.1080/0284186X.2018.1445284
16. Tyagi N, Fontenla S, Zelefsky M, Chong-Ton M, Ostergren K, Shah N, et al. Clinical Workflow for MR-Only Simulation and Planning in Prostate. *Radiat Oncol* (2017) 12(1):119. doi: 10.1186/s13014-017-0854-4
17. Cronholm RO, Karlsson A, Siversson C. Whitepaper: MRI Only Radiotherapy Planning Using the Transfer Function Estimation Algorithm. (2020).
18. Gonzalez-Moya A, Dufreneix S, Ouyessad N, Guillerminet C, Autret D. Evaluation of a Commercial Synthetic Computed Tomography Generation Solution for Magnetic Resonance Imaging-Only Radiotherapy. *J Appl Clin Med Phys* (2021) 22(6):191–7. doi: 10.1002/acm2.13236
19. Johnstone E, Wyatt JJ, Henry AM, Short SC, Sebag-Montefiore D, Murray L, et al. Systematic Review of Synthetic Computed Tomography Generation Methodologies for Use in Magnetic Resonance Imaging-Only Radiation Therapy. *Int J Radiat Oncol Biol Phys* (2018) 100(1):199–217. doi: 10.1016/j.ijrobp.2017.08.043
20. Palmer E, Karlsson A, Nordstrom F, Petruson K, Siversson C, Ljungberg M, et al. Synthetic Computed Tomography Data Allows for Accurate Absorbed Dose Calculations in a Magnetic Resonance Imaging Only Workflow for Head and Neck Radiotherapy. *Phys Imaging Radiat Oncol* (2021) 17:36–42. doi: 10.1016/j.phro.2020.12.007
21. Healy B, van der Merwe D, Izewska J, Zubizarreta E. *Accuracy Requirements and Uncertainties in Radiotherapy*. Vienna: INTERNATIONAL ATOMIC ENERGY AGENCY (2016).
22. Korsholm ME, Waring LW, Edmund JM. A Criterion for the Reliable Use of MRI-Only Radiotherapy. *Radiat Oncol* (2014) 9(1):16. doi: 10.1186/1748-717X-9-16
23. Vandewinckele L, Claessens M, Dinkla A, Brouwer C, Crijns W, Verellen D, et al. Overview of Artificial Intelligence-Based Applications in Radiotherapy: Recommendations for Implementation and Quality Assurance. *Radiother Oncol* (2020) 153:55–66. doi: 10.1016/j.radonc.2020.09.008
24. Irmak S, Zimmermann L, Georg D, Kuess P, Lechner W. Cone Beam CT Based Validation of Neural Network Generated Synthetic CTs for Radiotherapy in the Head Region. *Med Phys* (2021) 48(8):4560–71. doi: 10.1002/mp.14987
25. Edmund JM, Andreasen D, Mahmood F, Van Leemput K. Cone Beam Computed Tomography Guided Treatment Delivery and Planning Verification for Magnetic Resonance Imaging Only Radiotherapy of the Brain. *Acta Oncol* (2015) 54(9):1496–500. doi: 10.3109/0284186X.2015.1062546

Conflict of Interest: The authors declare that the research was conducted in the absence of any commercial or financial relationships that could be construed as a potential conflict of interest.

frontiers in Oncology

ORIGINAL RESEARCH
published: 19 January 2022
doi: 10.3389/fonc.2021.745140

CBCT Verification of SRT for Patients With Brain Metastases

Judit Papp[1], *Mihály Simon*[1], *Emese Csiki*[1] *and Árpád Kovács*[1,2]*

[1] Department of Oncoradiology, Faculty of Medicine, University of Debrecen, Debrecen, Hungary,
[2] Doctoral School of Health Sciences, Faculty of Health Sciences, University of Pécs, Pécs, Hungary

Background: The aim of our work is to demonstrate the role of image guidance and volumetric imaging in stereotactic radiotherapy (SRT) of brain metastases.

Methods: Between 2018 and 2020, 106 patients underwent intracranial stereotactic radiotherapy. 10 patients with metastatic brain tumors treated with SRT were randomly selected and included in our study model. Patients were scanned pre- and post-treatment with cone beam CT. Total of 100 verifications of 50 stereotaxic treatments were performed and analyzed.

Results: Population mean X, Y, Z values were -0.13 cm, -0.04 cm, -0.03 cm, respectively, rotation values 0.81°, 0.51°, 0.46°, respectively. Systematic error components for translational displacements pre corrections were as follows: 0.14 cm for X, 0.13 cm for Y and 0.1 cm for Z. Systematic error components of the post-treatment HR 3D CBCTs were as follows: 0.01 cm for X, 0.06 cm for Y and 0.04 cm for Z.

Conclusions: Population mean values close to 0 confirmed that there is no systematic variation in our system and the accuracy of our equipment and tools is reliable. HR 3D CBCT scans performed pre SRTs further refine patient and target volume setting, support medical decision making and eliminate the possibility of gross error.

Keywords: brain metastasis, SRT, HR 3D CBCT, volumetric verification, image guidance

OPEN ACCESS

Edited by:
Wenyin Shi,
Thomas Jefferson University, United States

Reviewed by:
Junwei Shi,
University of Miami, United States
Constantin Tuleasca,
Centre Hospitalier Universitaire Vaudois (CHUV), Switzerland

***Correspondence:**
Árpád Kovács
kovacsarpad@med.unideb.hu

Specialty section:
This article was submitted to Radiation Oncology, a section of the journal Frontiers in Oncology

Received: *21 July 2021*
Accepted: *23 December 2021*
Published: *19 January 2022*

Citation:
Papp J, Simon M, Csiki E and Kovács Á (2022) CBCT Verification of SRT for Patients With Brain Metastases. Front. Oncol. 11:745140. doi: 10.3389/fonc.2021.745140

INTRODUCTION

Brain metastases (BM) are considered a serious problem regarding the nature of oncological diseases, as they develop in 20-40% of cancer patients during the disease history. BMs are the most common adult brain tumors, with an incidence in Hungary by origin of: lung 40%, skin (melanoma) 30%, breast 25%, gastrointestinal and renal 5-10%. Radiotherapy, either alone or after surgery, remains the mainstay of treatment for brain metastases. Whole brain radiotherapy (WBRT), stereotactic radiosurgery (SRS) and stereotactic radiotherapy (SRT) could be an option (1). Current guidelines are shifting the treatment preferences from WBRT towards stereotactic solutions (SRS, SRT) in cases with a limited number of metastases. These patient`s life expectancy not solely depending on the number of metastasis in the brain but also primary tumor control, Karnofsky score, extracranial mets are factors as well. Therefore more aggressive treatments might be more beneficial for patients with controlled diseases and good overall status (2, 3). Gamma knife SRS is a single session, high dose, focused irradiation. It is used for non-infiltrative intracranial tumors

smaller than 3 cm. SRT on a dedicated linear accelerator allows larger lesions to be treated in critical areas of the brain (4–7).SRT is a type of external beam radiotherapy that uses special devices/equipment to position and immobilise the patient in order to deliver high fractional doses of radiation to a well-defined clinical target volume. This significantly reduces normal tissue exposure and subsequent side effects close to the target volume, thus improving the quality of life of patients. SRT can be performed with Gamma knife, Cyberknife, tomotherapy and linear accelerator. The delivery of hypofractionated radiotherapy requires the highest possible reliability and accuracy of equipment, devices and staff (8, 9). Modern linear accelerators with integrated image guided radiotherapy (IGRT) solutions such as cone beam computed tomography (CBCT) enabled the extensive use of SRT in the management of BMs. Non-invasive patient positioning approaches like thermoplastic masks are suitable for fractionated stereotactic treatments of the brain (10–12). CBCT imaging allowed the detection of translational and rotational alignment errors. Furthermore, the six-degrees-of-freedom (6-DOF) robotic couch allowed the correction of rotational alignment errors (13). Single isocentre techniques have been developed to reduce number of isocentres, therefore reduce treatment time (14, 15).State-of-the-art linear accelerators ensure increasingly conformal treatments, and have flattening filter free (FFF) function, therefore increased intensity beam reduces treatment time, ensures that SRT treatments can be performed in 15 minutes or less, as well as door-to-door. At the same time, high-resolution, dynamic volumetric imaging together with an integrated positioning and position determining system, as well as a customisable fixation system are, essential for performing SRT to ensure sub-mm accuracy. In addition, non-invasive 4D imaging, continuous soft tissue monitoring without implanted markers, and protocol-driven interventions are also necessary (16).

The aim of our work is to demonstrate the effectiveness of volumetric imaging by analysing CBCT scans per treatment fraction performed according to our image guidance protocol. We investigated the pre-treatment correction components to determine whether our fixation system is capable of achieving the desired high accuracy of immobilization. In addition, we used post-treatment CBCT scans to verify that the intrafractional displacements were also below the expected level.

MATERIALS AND METHODS

Our clinic has 2 adapted Elekta linear accelerators (Synergy, Versa HD), which are capable of performing the most advanced methods of radiotherapy such as IGRT, intensity-modulated radiotherapy (IMRT), volumetric modulated arc therapy (VMAT) and SRT. Their functionality serves the needs of hypofractionated radiotherapy, so that SRT or stereotactic body radiotherapy (SBRT) techniques can be used to safely treat skull, head and neck, chest, abdomen and pelvis targets. The two regions most commonly treated with stereotactic radiotherapy are the brain and the lungs. For this analysis, we selected a cohort of patients treated with SRT for BM to investigate the efficacy of a specific image guidance protocol. Considering the hypofractionated dosimetry scheme, it is of paramount importance to accurately (in millimeters) select, the target area with the help of image guidance. For each patient, 5x6 Gy were delivered every other working day, at a total dose of 30 Gy.

Patients

Between 2018 and 2020, 106 patients were treated with intracranial stereotactic radiotherapy as per indication, which resulted in. 1060 high resolution (HR) 3D CBCT series of images were registered and corrected based on our verification protocol. To verify our image guidance method, we randomly selected 10 patients from this database who had undergone brain SRT. Thus, our representative sample of 50 stereotaxic fractions contains the measurement results of 100 cone beam CT images. Demographic and clinical data of the patients are shown in **Table 1**. Verification of SRTs was always performed according to an on-line protocol: each pre-treatment, a verification image was taken at the treatment position to determine the submillimetre accurate the patient's position by a submillimetre accuracy for correction. For image verification, a region-specific preset was used, according to our predefined methodology (**Table 1**).

Planning CT

The SRT patients were prepared in the CT simulator, using a Philips Brilliance Big Bore device (Philips, The Netherlands) with a special 85 cm aperture. The scans were performed according to protocol, with a slice thickness of 2 mm and oncological settings. In all cases, the immobilization system used was Qfix (QFix, Avondale, PA, USA). Patients were immobilized in the supine position with a carbon fiber head support and a Moldcare water- activated cushion placed under their head to maintain cervical lordosis. After positioning, an open, kevlar-reinforced 2.4 mm thick thermoplastic mask flap with eye and nose perforations was moulded onto the patients with a bite block fixation device. The number of lesions per patient were either 5 (n=1), 3 (n=1), 2 (n=2) or 1 (n=6).

Treatment Planning, Dose Prescription

All patients were contoured and planned using Pinnacle (Philips, The Netherlands) irradiation planning system version 9.8. Imaging data from MRI scans performed before localization (T2 and Gadolinium contrast agent enhanced. T1 weighted sequences) were registered into the planning CT sequences by rigid transformation. Treatment target volumes and risk organs were defined based on the information from the MRI scans. The GTV was defined as the contrast enhanced region on T1 weighted MRI scan, the CTV is an isotropic extension of the GTV by 2 mm and the PTV is a further 3 mm extension of the CTV. All treatment plan used a single isocentre approach regardless of the number of lesions. In all cases, the dose was 30 Gy delivered in 5 fractions. Mobius 3D (Varian Medical Systems, Palo Alto, CA, USA) was used for the secondary verification of irradiation plans. Geometric verification during day zero was performed using Mobius 3D software.

TABLE 1 | Patient characteristics.

Characteristics	No./median	Proportion (%)
Sex		
Male	2	20%
Female	8	80%
Age		
Min	24	
Max	84	
Median	55,5	
PTV volumes		
n	18	
Vmin [cm^3]	1,2	
Vmax [cm^3]	103,29	
Vmean [cm^3]	15,69	
Primary site		
Lung	4	40%
Breast	2	20%
Skin (Melanoma)	1	10%
Ovarium	1	10%
Ependymoma	1	10%
Acusticus neurinoma	1	10%
Indication for SRT		
Intact met.	4	40%
Postop. tumor cavity	1	10%
Postop. tumor cavity+ met.	1	10%
Postop. rec.	2	20%
Postop.rec. + met.	2	20%

Image Guidance

Radiotherapy of all patients was image-guided and performed on an Elekta Versa HD linear accelerator (Elekta Oncology Systems Ltd, Crawley, UK). The equipment has an Agility MLC head, and uses FFF technique, advanced 2D, 3D and 4D real-time imaging. Volumetric imaging is provided by the high resolution cone beam CT system integrated in the accelerator and its software X-ray volume imaging (XVI). The CB CT is a kilovolt (kV) imaging system with a beam perpendicular to the treatment beam, and it is possible to apply filters and collimators depending on body shape and the region treated. 3D volumetric imaging of the XVI device allows visualization of target volumes and critical organ positions without the need for implanted markers. The XVI is suitable for 3D matching/comparison of planning CT and CBCT images acquired in the treatment position on a bone and soft tissue basis. CBCT scans a region in 2-4 minutes, depending on the data collection method, which is done before/after each treatment fraction. A single turn of the gantry is sufficient for acquisition, the scan range is one full arc. Meanwhile, the cone-shaped X-ray beam on the detector captures a series of two-dimensional summation images of the entire target volume. From the summation images, a 3D reconstruction image database is generated using a special algorithm, due to which no information is lost. The image quality of CBCT scans differs from that of conventional CT scans. The main purpose of CBCT images is to determine the position of the patient. Optimized image quality allows correct image registration using planned CT with minimal patient dose (17). The XVI collects volumetric 3D data series and reconstructs them simultaneously. Imaging is performed at low dose, sub-millimeter isotropic resolution in the treatment setting. HexaPod is an unique, fully robotic patient positioning system. The computer-controlled operating table is capable of independent movements in 6 directions of which are a combination of: translation (along x, y and z axes) and rotation (pitch, roll and yaw) of up to ±3°. The patient positioning devices and the reference frame containing an optical marker are fixed. A high-precision ceiling-mounted infrared camera tracks the 6 optical markers on the reference frame in real time. The reference frame can be dedicatedly fixed to the table top, so that the position of the table and the patient can be calculated. The HexaPOD software unit, which is the iGuide, controls the HexaPod and registers the position of the table. During verification imaging XVI, the cone beam CT software, determines the translation and rotation vectors and transmits them to the iGuide software, which moves the HexaPod and the patient fixed to it in the specified values and directions. The performance of the CBCT scans recorded in our image acquisition protocol fully supported our medical decision making, both in terms of gross error exclusion and target volume localization. HR 3D CBCT scans before brain stereotaxy treatments greatly help to verify the patient's position, accurately adjust the target volume mm for high-dose radiation treatments. The optimal bone-soft tissue contrast and image quality of diagnostic image verification in the kV range allows for more accurate and safer positioning. This reduces the treatment margins for SRTs, resulting in reduced dose to the tissue and risk organs, which also reduces the incidence of region-specific side effects. HR 3D CBCT values obtained after treatment provide information on the extent of intra-fractional displacements, and body position changes due to organ movements/unintended movements during the treatment period.

Verification

Patient positioning and immobilisation is followed by the registration of the patient's position. In iGuide, we record the location of the reference frame and the current position of the table along the X, Y and Z axes. Based on this, iGuide generates a relative table position, which the system will use as a starting point during the correction process. The verification of patients treated with SRT for brain met will be performed according to an image guidance protocol we have defined. For this method, we have created a region-specific preset. This preset consists of 2 series of HR 3D CBCT and 1 series of 3D CBCT. All cone beam CTs were performed under identical technical conditions (collimator: S20, 100 kV, 39.8 mAs, filter: F0). The first pre-treatment high-resolution 3D CBCT is taken in the initial table position. This is used to determine the translational and rotational deviations; during this we register the CBCT images taken in the treatment position to the planning reference CT done in the CT simulator. The XVI software determines the required translational and rotational movements and transmits them to iGuide. Based on the values obtained, medical approval is required to perform the correction. Rotation values can be corrected up to 2.9°, and for values above 3° the patient must be repositioned and reclamped. Translational values are corrected to 10 mm, above that the patient needs to be repositioned. Based on the approved correction values, iGuide will guide the HexaPod to the desired coordinates. As this process takes several minutes, a 3D CBCT is taken immediately before the treatment to check for displacements during the registration process, and the scan is designed to exclude gross error. Once accepted, the SRT fraction

can be delivered. The daily fractions are designed from 2 coplanar and 3 non-coplanar half-arc (180°). To cast the 3 non-coplanar arcs, it is necessary to rotate the table from 0°, ± 45°, + 90° isocentre. Immediately post-treatment, another HR 3D CBCT is performed to assess the intrafractional displacements.

RESULTS

Our analysis compared the results of 50 pre-treatment and 50 post-treatment verification HR 3D CBCT measurements in 10 patients.

For each patient, 5 fractions were delivered with a fraction dose of 6 Gy on each occasion. All patients' treatments were complete, with no interrupted SRT. The same bed anchoring system was used in all treatment set-ups (carbon fibre baseplate, Q2 head support plexi, Moldcare mask pad, SRT 2.4 mm mask, bite block, knee support, foot support). All treatments were performed using on-line image-guided patient positioning with HexaPod. **Figure 1** shows a pre-treatment HR CBCT before registration where set-up errors are present (**Figure 1**).

Figure 2 shows an after registration image. The registration results are highlited with red (**Figure 2**).

The measurement results of 50 HR 3D CBCTs before treatment are shown in **Figures 3** and **4**.

Based on the registration of HR 3D CBCTs performed during patient set-ups before the treatments, 2 out of 50 fractions required patient repositioning (**Figures 3** and **4**) and re-registration.

On 48 occasions, patients were positioned without gross error using reference markings on the thermoplastic mask.

The mean and standard deviation of the pre-treatment and corrected error components per patient are shown in **Table 2**.

Population mean X, Y and Z values derived from translational components (-0.1334 cm, -0.0396 cm, -0.0324 cm - respectively), rotation values (0.806°, 0.506°, 0.458°- respectively).

Systematic error components for translational displacements before corrections: 0.14 cm for X, 0.13 cm for Y and 0.1 cm for Z.

Figure 5 shows the results of a post-treatment HR CBCT, where intrafractional motion would appear (**Figure 5**).

The mean and standard deviation of the post-treatment and corrected error components per patient are shown in **Table 3**. The post-treatment measurement results of 50 HR 3D CBCTs are shown in **Figures 6** and **7**.

Systematic error components derived from the standard deviation of the mean of the translational components at post-treatments CBCT: 0.01 cm for X, 0.06 cm for Y, and 0.04 cm for Z.

DISCUSSION

The use of stereotactic treatments such as SRT in the treatment of BMs is increasing in the cohort of patients with few metastases. Although rigid immobilization and long treatment times can lead to patient discomfort and patient movement (18, 19). Frameless stereotactic techniques and treatments had been published previously (19–21) in the literature. Frameless immobilization allows fractionation of the treatments but requires a very high degree of accuracy and reproducibility in patient positioning. In our study we evaluated the patient positioning and interfractional

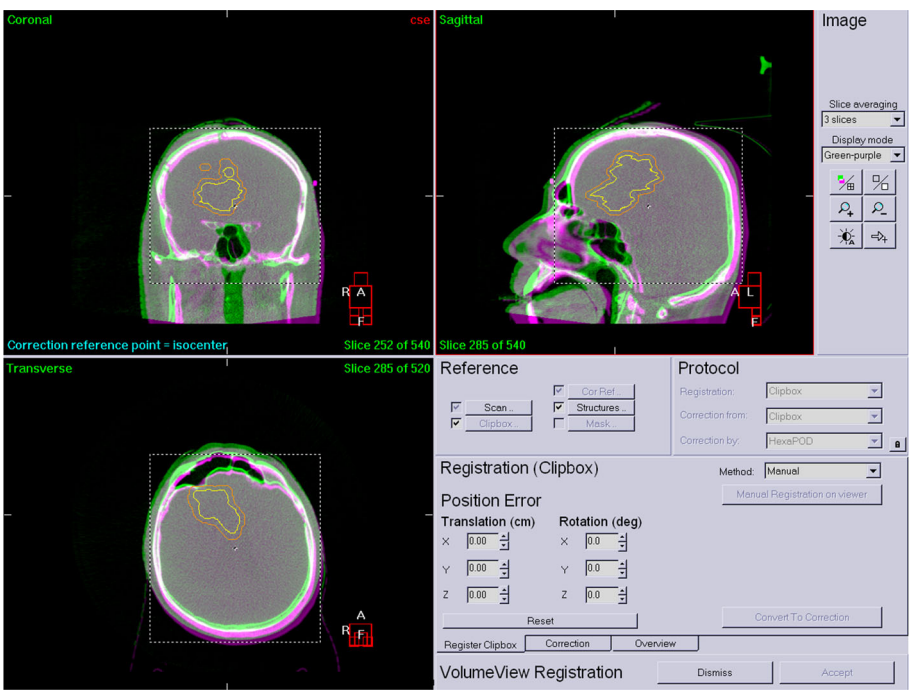

FIGURE 1 | Pre-treatment HR CBCT.

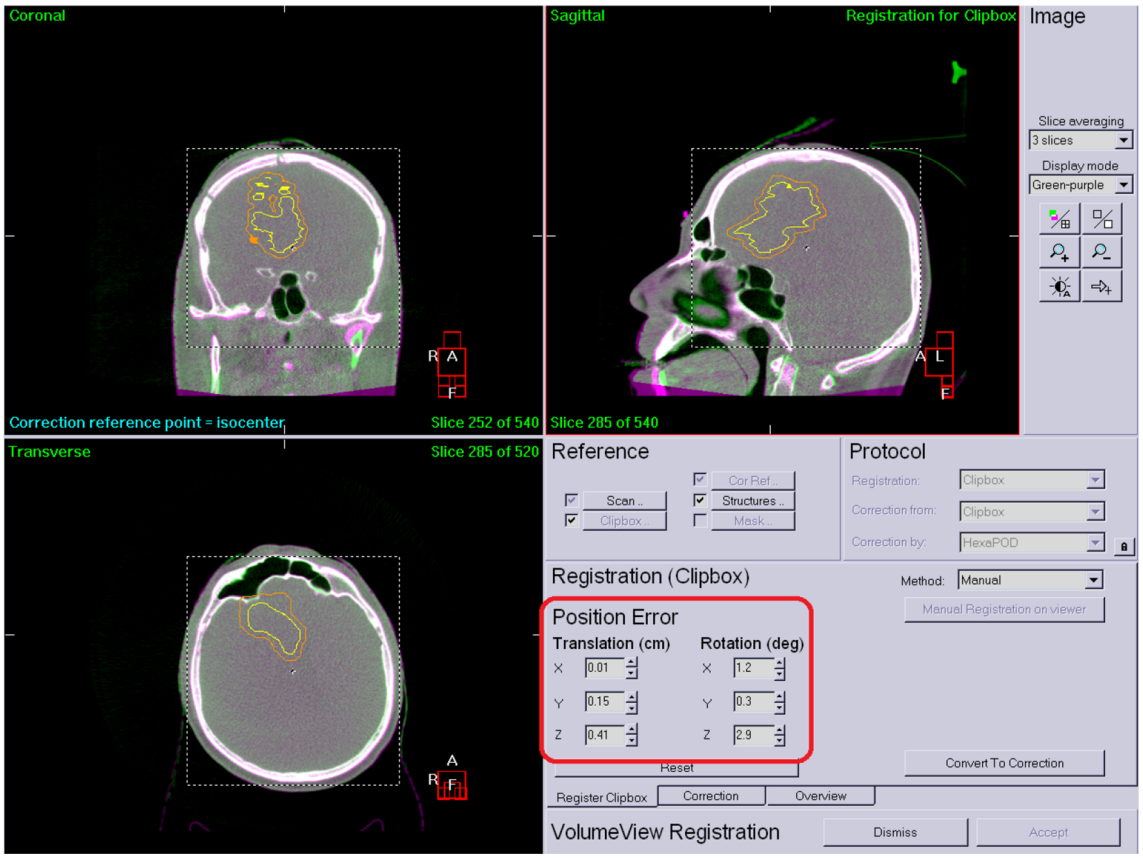

FIGURE 2 | Corrected patient position.

accuracy of our frameless system. Population mean values of each directional displacement components shows that there are no underlying systematic errors remained in our system. The intrafractional displacements can be minimised with the used fixation system, as shown by the results derived from the data measured during post-treatment CBCTs. Measurement results from CBCTs before and after SRTs have demonstrated that our verification protocol and the fixation systems we use are capable of achieving the positioning accuracy required during SRT treatments. Wong et al. (19) reported similar values for mean (0.7 mm) displacement of the isocentre with a stereotactic mask fixation system. Minniti et al. (22) reported 0.08 mm, 0.04 mm and 0.06 mm

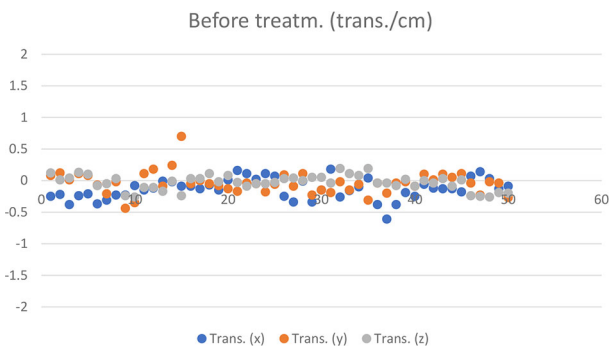

FIGURE 3 | Translational CBCT values recorded in 50 cases before treatment.

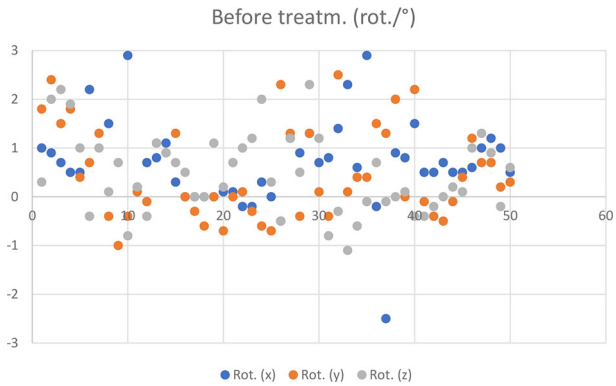

FIGURE 4 | Rotational CBCT values recorded in 50 cases before treatment.

TABLE 2 | Mean and standard deviation of pre-treatment CBCTs per patient.

Patient nr.	M/SD	Before treatment					
		Trans. (x) [cm]	Trans. (y) [cm]	Trans. (z) [cm]	Rot. (x) [°]	Rot. (y) [°]	Rot. (z) [°]
1	M	-0,26	0,08	0,08	0,72	1,58	1,48
	SD	0,069	0,043	0,052	0,228	0,736	0,804
2	M	-0,244	-0,218	-0,12	2,88	0,04	0,12
	SD	0,109	0,179	0,125	1,064	0,934	0,746
3	M	-0,078	0,228	-0,128	0,62	0,66	0,5
	SD	0,061	0,292	0,085	0,370	0,623	0,604
4	M	-0,086	-0,062	0,046	0,02	-0,32	0,36
	SD	0,062	0,048	0,050	0,045	0,327	0,462
5	M	0,094	-0,1	-0,05	0,00	-0,30	1,04
	SD	0,052	0,069	0,024	0,212	0,354	0,635
6	M	-0,218	-0,054	0,034	0,72	0,92	0,94
	SD	0,140	0,149	0,021	0,722	1,073	1,031
7	M	-0,06	-0,146	0,106	1,6	0,6	-0,58
	SD	0,173	0,114	0,095	0,982	1,111	0,396
8	M	-0,362	-0,078	-0,046	0,1	1,4	0,06
	SD	0,161	0,073	0,043	1,576	0,863	0,404
9	M	-0,124	0,074	-0,018	0,54	-0,14	-0,06
	SD	0,043	0,043	0,048	0,089	0,351	0,241
10	M	0,004	-0,12	-0,228	0,86	0,62	0,72
	SD	0,112	0,120	0,031	0,297	0,396	0,572

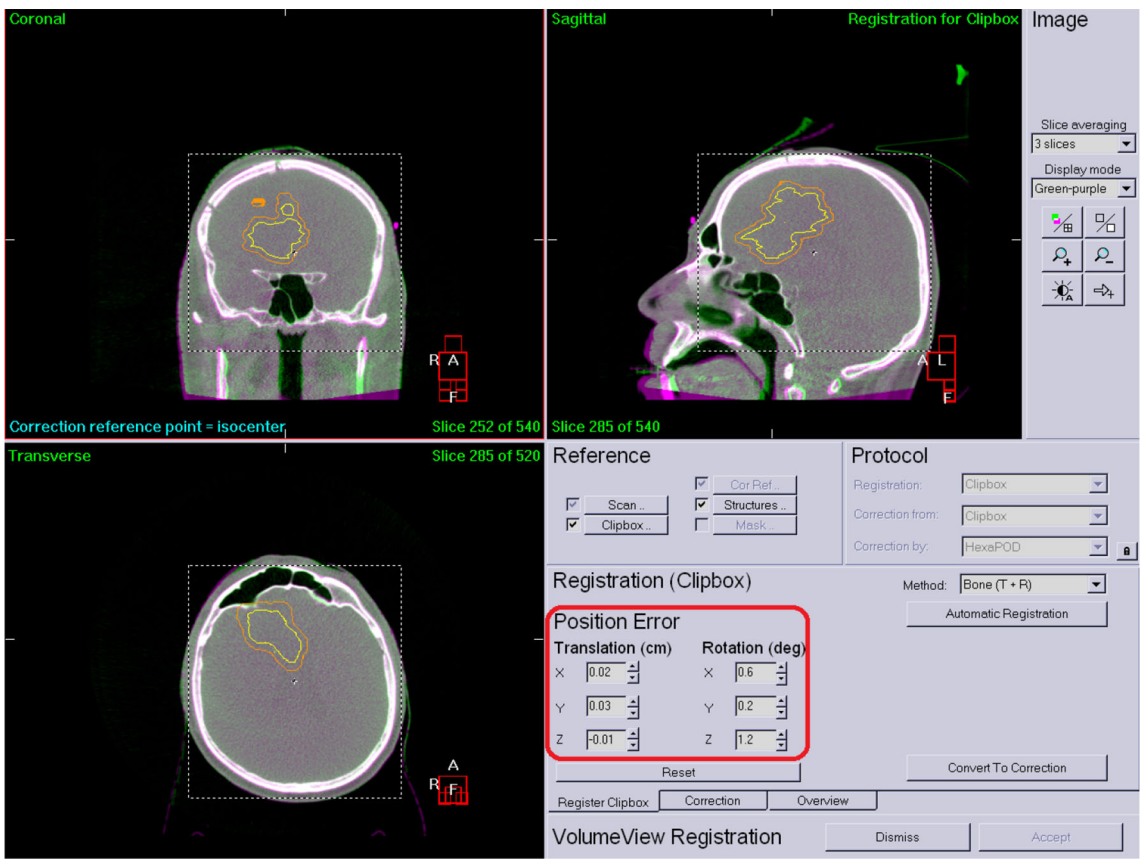

FIGURE 5 | Post-treatment HR CBCT.

TABLE 3 | Mean and standard deviation of post-treatment HR 3D CBCTs per patient.

Patient nr.	M/SD	After treatment					
		Trans. (x) [cm]	Trans. (y) [cm]	Trans. (z) [cm]	Rot. (x) [°]	Rot. (y) [°]	Rot. (z) [°]
1	M	-0,004	-0,004	-0,006	0,28	-0,02	0
	SD	0,019	0,060	0,015	0,164	0,130	0,469
2	M	-0,004	-0,162	-0,142	1,38	0,1	0
	SD	0,065	0,071	0,026	0,844	0,324	0,2
3	M	0,028	-0,022	-0,028	0,08	0,12	0,06
	SD	0,036	0,030	0,028	0,130	0,228	0,329
4	M	-0,004	0,01	-0,018	-0,06	0,1	-0,08
	SD	0,021	0,014	0,029	0,134	0,224	0,179
5	M	-0,01	0,03	0,00	0,24	-0,14	-0,52
	SD	0,013	0,015	0,017	0,152	0,055	0,130
6	M	-0,006	0,002	-0,012	-0,02	-0,02	0,04
	SD	0,034	0,028	0,013	0,084	0,148	0,586
7	M	0,024	-0,084	0,002	0,54	-0,22	-0,32
	SD	0,106	0,084	0,027	0,410	0,259	0,630
8	M	0,018	-0,012	0,012	0,08	-0,32	-0,46
	SD	0,035	0,033	0,054	0,239	0,179	0,488
9	M	0,008	-0,012	-0,006	0,08	-0,04	0,3
	SD	0,011	0,016	0,005	0,164	0,055	0,283
10	M	0,004	-0,036	-0,014	0,06	0	-0,12
	SD	0,027	0,025	0,013	0,089	0,100	0,179

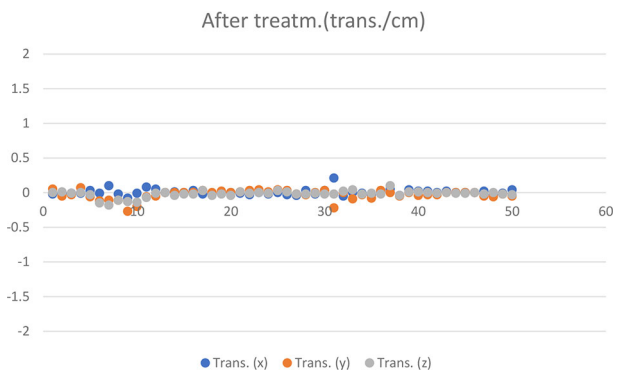

FIGURE 6 | Translational CBCT values recorded in 50 cases post-treatment.

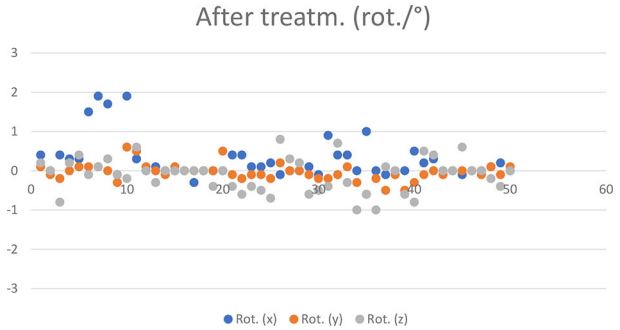

FIGURE 7 | Post-treatment rotational CBCT values recorded in 50 cases.

in cranio caudal, medio-lateral and anterior-posterior intrafractional displacements between CT verification and post-treatment CT respectively. Hamilton et al. (20) reported a mean of 1.8 mm accuracy for a rigid head-mask immobilization system. The advantages of volumetric imaging techniques for the verification of stereotactic radiotherapy are the following: Changes and deviations in the patient's irradiation position can be accurately tracked and quantified during the treatment. Deviations can be corrected immediately in all directions, along all the axes of rotation. This is of paramount importance for tumors located close to critical organs, such as intracranial tumors, where visualisation of the tumor and its surroundings plays a huge role in medical decision-making (17). Repeated CT verification images bring high resolution datasets and consistency into image analysis (23) Image registration, the HR 3D CBCT technique and the coordinated image guidance system create safe conditions for performing SRTs.

CONCLUSIONS

Our data suggests that correct patient positioning was achieved during the planning CT, which could be successfully reproduced before treatment fractions, without the need for frequent repositioning. The desirable value of the population averages should be close to 0, so that there be no hidden systematic error in the system. In our case, the results obtained show that we have no systematic error during either preparation or execution.

The main limitation of this study is the number of patients, which is a small population and is insufficient for statistical measurements. Further limitation is the retrospective manner of this study which can introduce bias in patient selection and further limits the statistical capabilities of the study.

DATA AVAILABILITY STATEMENT

The original contributions presented in the study are included in the article/supplementary material. Further inquiries can be directed to the corresponding author.

ETHICS STATEMENT

Ethical review and approval were waived for this study, due to the fact, that patients involved in this study were prepared, planned and treated according to Institutional protocol, no ethical questions could emerge regarding the treatments.

AUTHOR CONTRIBUTIONS

Conceptualisation, JP and MS. methodology, JP and EC. investigation, JP and MS. data curation, MS. Writing—original draft preparation, JP. writing—review and editing. JP and ÁK. Supervision, ÁK. All authors have read and agreed to the published version of the manuscript.

REFERENCES

1. Khuntia D. Contemporary Review of the Management of Brain Metastasis With Radiation. *Adv Neurosci* (2015) 2015:1–13. doi: 10.1155/2015/372856
2. Shinde A, Akhavan D, Sedrak M, Glaser S, Amini A. Shifting Paradigms: Whole Brain Radiation Therapy Versus Stereotactic Radiosurgery for Brain Metastases. *CNS Oncol* (2019) 8(1):CNS27. doi: 10.2217/cns-2018-0016
3. Balducci M, Autorino R, Chiesa S, Mattiucci G, Pompucci A, Azario L, et al. Radiosurgery or Fractionated Stereotactic Radiotherapy Plus Whole-Brain Radioherapy in Brain Oligometastases a Long-Term Analysis. *Anticancer Res* (2015) 35(5):3055–60.
4. Kwon AK, Dibiase SJ, Wang B, Hughes SL, Milcarek B, Zhu Y. Hypofractionated Stereotactic Radiotherapy for the Treatment of Brain Metastases. *Cancer* (2009) 115(4):890–8. doi: 10.1002/cncr.24082
5. Marcrom SR, McDonald AM, Thompson JW, Popple RA, Riley KO, Markert JM, et al. Fractionated Stereotactic Radiation Therapy for Intact Brain Metastases. *Adv Radiat Oncol* (2017) 2(4):564–71. doi: 10.1016/j.adro.2017.07.006
6. Mazzola R, Corradini S, Gregucci F, Figlia V, Fiorentino A, Alongi F. Role of Radiosurgery/Stereotactic Radiotherapy in Oligometastatic Disease: Brain Oligometastases. *Front Oncol* (2019) 9:1–7. doi: 10.3389/fonc.2019.00206
7. Mehta MP, Tsao MN, Whelan TJ, Morris DE, Hayman JA, Flickinger JC, et al. ASTRO. Radiosurgery in BM. Week 25), and the Cochrane Library (2004 Issue 2) Databases Were Searched Using OVID. In Addition, the Physician Data Query Clinical Trials Database, the Proceedings of the. *Eur Soc Ther Radiol Oncol (ESTRO* (2005) 63(1):37–46. doi: 10.1016/j.ijrobp.2005.05.023
8. Baliga S, Garg MK, Fox J, Kalnicki S, Lasala PA, Welch MR, et al. Fractionated Stereotactic Radiation Therapy for Brain Metastases: A Systematic Review With Tumour Control Probability Modelling. *Br J Radiol* (2017) 90(1070). doi: 10.1259/bjr.20160666
9. Lamba N, Muskens IS, DiRisio AC, Meijer L, Briceno V, Edrees H, et al. Stereotactic Radiosurgery Versus Whole-Brain Radiotherapy After Intracranial Metastasis Resection: A Systematic Review and Meta-Analysis. *Radiat Oncol* (2017) 12(1). doi: 10.1186/s13014-017-0840-x
10. Clark GM, Popple RA, Young PE, Fiveash JB. Feasibility of Single-Isocenter Volumetric Modulated Arc Radiosurgery for Treatment of Multiple Brain Metastases. *Int J Radiat Oncol Biol Phys* (2010) 76(1):296–302. doi: 10.1016/j.ijrobp.2009.05.029
11. Kamath R, Ryken TC, Meeks SL, Pennington EC, Ritchie J, Buatti JM. Initial Clinical Experience With Frameless Radiosurgery for Patients With Intracranial Metastases. *Int J Radiat Oncol Biol Phys* (2005) 61(5):1467–72. doi: 10.1016/j.ijrobp.2004.08.021
12. Tarnavski N, Engelholm SA, Af Rosenschold PM. Fast Intra-Fractional Image-Guidance With 6D Positioning Correction Reduces Delivery Uncertainty for Stereotactic Radiosurgery and Radiotherapy. *J Radiosurg SBRT* (2016) 4(1):15–20.
13. Nielsen M, Hansen CR, Brink C, Bertelsen AS, Kristiansen C, Stefan SJ, et al. Efficient and Accurate Stereotactic Radiotherapy Using Flattening Filter Free Beams and HexaPOD Robotic Tables. *J Radiosurg SBRT* (2016) 4(2):153–61.
14. Liu H, Thomas EM, Li J, Yu Y, Andrews D, Markert JM, et al. Interinstitutional Plan Quality Assessment of 2 Linac-Based, Single-Isocenter, Multiple Metastasis Radiosurgery Techniques. *Adv Radiat Oncol* (2020) 5(5):1051–60. doi: 10.1016/j.adro.2019.10.007
15. Hofmaier J, Bodensohn R, Garny S, Hadi I, Fleischmann DF, Eder M, et al. Single Isocenter Stereotactic Radiosurgery for Patients With Multiple Brain Metastases: Dosimetric Comparison of VMAT and a Dedicated DCAT Planning Tool. *Radiat Oncol* (2019) 14(1):4–11. doi: 10.1186/s13014-019-1315-z
16. Soffietti R, Abacioglu U, Baumert B, Combs SE, Kinhult S, Kros JM, et al. Diagnosis and Treatment of Brain Metastases From Solid Tumors: Guidelines

From the European Association of Neuro-Oncology (EANO). *Neuro Oncol* (2017) 19(2):162–74. doi: 10.1093/neuonc/now241
17. Haertl PM, Loeschel R, Repp N, Pohl F, Koelbl O, Dobler B. Frameless Fractionated Stereotactic Radiation Therapy of Intracranial Lesions: Impact of Cone Beam CT Based Setup Correction on Dose Distribution. *Radiat Oncol* (2013) 8(1):2–7. doi: 10.1186/1748-717X-8-153
18. Cervîo LI, Pawlicki T, Lawson JD, Jiang SB. Frame-Less and Mask-Less Cranial Stereotactic Radiosurgery: A Feasibility Study. *Phys Med Biol* (2010) 55(7):1863–73. doi: 10.1088/0031-9155/55/7/005
19. Wong VYW, Tung SY, Leung TW, Ho KHS. CT Verification of Isocentre Relocatability Using Stereotactic Mask Fixation System. *Clin Oncol* (2003) 15 (5):280–7. doi: 10.1016/S0936-6555(03)00091-8
20. Hamilton RJ, Kuchnir FT, Pelizzari CA, Sweeney PJ, Rubin SJ. Repositioning Accuracy of a Noninvasive Head Fixation System for Stereotactic Radiotherapy. *Med Phys* (1996) 23(11):1909–17. doi: 10.1118/1.597754
21. Willner J, Flentje M, Bratengeier K. CT Simulation in Stereotactic Brain Radiotherapy - Analysis of Isocenter Reproducibility With Mask Fixation. *Radiother Oncol* (1997) 45(1):83–8. doi: 10.1016/S0167-8140(97)00135-7
22. Minniti G, Scaringi C, Clarke E, Valeriani M, Osti M, Enrici RM. Frameless Linac-Based Stereotactic Radiosurgery (SRS) for Brain Metastases: Analysis of Patient Repositioning Using a Mask Fixation System and Clinical Outcomes. *Radiat Oncol* (2011) 6(1):2–7. doi: 10.1186/1748-717X-6-158
23. Fuss M, Salter BJ, Cheek D, Sadeghi A, Hevezi JM, Herman TS. Repositioning Accuracy of a Commercially Available Thermoplastic Mask System. *Radiother Oncol* (2004) 71(3):339–45. doi: 10.1016/j.radonc.2004.03.003

Conflict of Interest: The authors declare that the research was conducted in the absence of any commercial or financial relationships that could be construed as a potential conflict of interest.

Publisher's Note: All claims expressed in this article are solely those of the authors and do not necessarily represent those of their affiliated organizations, or those of the publisher, the editors and the reviewers. Any product that may be evaluated in this article, or claim that may be made by its manufacturer, is not guaranteed or endorsed by the publisher.

frontiers | Frontiers in Oncology

TYPE Original Research
PUBLISHED 27 October 2022
DOI 10.3389/fonc.2022.852694

OPEN ACCESS

EDITED BY
Christina Tsien,
Johns Hopkins Medicine, United States

REVIEWED BY
Vanessa Figlia,
ARNAS Ospedali Civico Di Cristina Benfratelli, Italy
Silke Tribius,
Asklepios Klinik St. Georg, Germany

*CORRESPONDENCE
Roland Merten
merten.roland@mh-hannover.de

†These authors share last authorship

SPECIALTY SECTION
This article was submitted to Radiation Oncology, a section of the journal Frontiers in Oncology

RECEIVED 11 January 2022
ACCEPTED 05 October 2022
PUBLISHED 27 October 2022

CITATION
Grosche S, Bogdanova NV, Ramachandran D, Lüdeking M, Stemwedel K, Christiansen H, Henkenberens C and Merten R (2022) Effectiveness of hypofractionated and normofractionated radiotherapy in a triple-negative breast cancer model. *Front. Oncol.* 12:852694. doi: 10.3389/fonc.2022.852694

Effectiveness of hypofractionated and normofractionated radiotherapy in a triple-negative breast cancer model

Sinja Grosche[1], Natalia V. Bogdanova[1], Dhanya Ramachandran[1,2], Marcus Lüdeking[1], Katharina Stemwedel[1], Hans Christiansen[3], Christoph Henkenberens[3,4†] and Roland Merten[3*†]

[1]Radiation Oncology Research Unit, Hannover Medical School, Hannover, Germany, [2]Gynaecology Research Unit, Medical School, Hannover, Germany, [3]Radiation Oncology, Hannover Medical School, Hannover, Germany, [4]Radiation Oncology, Dorothea Christiane Erxleben Clinic, Wernigerode, Germany

Breast cancer (BC) is one of the most diagnosed malignant carcinomas in women with a triple-negative breast cancer (TNBC) phenotype being correlated with poorer prognosis. Fractionated radiotherapy (RT) is a central component of breast cancer management, especially after breast conserving surgery and is increasingly important for TNBC subtype prognosis. In recent years, moderately hypofractionated radiation schedules are established as a standard of care, but many professionals remain skeptical and are concerned about their efficiency and side effects. In the present study, two different triple-negative breast cancer cell lines, a non-malignant breast epithelial cell line and fibroblasts, were irradiated daily under normofractionated and hypofractionated schedules to evaluate the impact of different irradiation regimens on radiation-induced cell-biological effects. During the series of radiotherapy, proliferation, growth rate, double-strand DNA break-repair (DDR), cellular senescence, and cell survival were measured. Investigated normal and cancer cells differed in their responses and receptivity to different irradiation regimens, indicating cell line/cell type specificity of the effect. At the end of both therapy concepts, normal and malignant cells reach almost the same endpoint of cell count and proliferation inhibition, confirming the clinical observations in the follow-up at the cellular level. These result in cell lines closely replicating the irradiation schedules in clinical practice and, to some extent, contributing to the understanding of growth rate or remission of tumors and the development of fibrosis.

KEYWORDS

hypofractionated radiotherapy, breast cancer, cell culture model, irradiation, side effects

Introduction

Breast cancer (BC) is one of the most diagnosed malignant carcinomas in women. It causes 23% of all reported cancer cases, being, furthermore, the leading cause of death among all cancer entities in women (at 14%) (1). Among all BC incidences, up to 20% account for triple-negative breast cancer (TNBC) (2). TNBC is a heterogeneous disease often characterized by more aggressive biology than the other BC subtypes and is associated with an early age at diagnosis, larger tumor sizes, higher local-regional rates of recurrence, and *BRCA1* mutations (3–6). Concerning treatment outcome, the TNBC phenotype is correlated with poorer prognosis and is often associated with distant metastases (3). In terms of patient management, the lack of hormonal or targeted therapy and gaps in knowledge on the importance and role of radiotherapy in TNBC make this BC subtype a challenge for clinicians. Radiotherapy for breast cancer can reduce the risk of a local relapse and decrease the risk of cancer-associated mortality in the patient and is therefore a crucial part of therapeutic options for the patient (7–9). While the benefit of radiotherapy concerning overall survival for patients with TNBC is still debatable (10, 11), adjuvant radiotherapy is an indispensable part of breast conserving therapy assuring locoregional control. Thus, estimating the role of radiotherapy and the modalities of postoperative irradiation in the TNBC prognosis is continuously important. Therapy regimens can be classified into different fractionation schemes varying in duration and single doses applied. In normofractionated radiotherapy (NormRT), a total dose of usually 50 Gy is divided into single doses of 2 Gy over a longer time period resulting in 25 fractions. For hypofractionated radiotherapy (HypoRT), single doses of 2.67 Gy are applied over a shorter time period, therefore in fewer fractions, usually 15, with a total dose of about 40 Gy. Although there have been studies that show the equality of HypoRT and NormRT (12, 13), many professionals remain skeptical and concerned about the side effects of the HypoRT irradiation. Therefore, it is intensely discussed how the differently fractionated regimens of radiotherapy affect the outcome both in efficiency and toxicity. Some follow-up studies and meta-analyses have shown that the outcome of HypoRT could be compared to NormRT in efficiency, while other studies assume toxicity and side effects as fibrosis (14–18). HypoRT could potentially increase the patient's satisfaction and compliance by reducing the amount of treatments needed while reducing costs for the health care system for shorter therapeutic periods and therefore allowing the treatment of more patients (19, 20).

We aimed to assess the effectiveness of HypoRT in comparison to NormRT in reducing the total amount of tumor cells and to compare their possible side effects and toxicity on the healthy breast tissue by investigating how normal breast epithelial cells' and TNBC cells' behavior is affected by both irradiation protocols. The main objective of this study was to evaluate the effects of HypoRT and NormRT on the cell proliferation capacity, cell survival, and double strand break (DSB) repair in a human breast cell model. A secondary objective was to investigate how radiation-induced effects may vary in dependence of dose per fraction and radiation duration in fibroblasts (which are under high risk for developing radiation side effects, i.e., fibrosis), during breast cancer radiotherapy. We therefore monitored radiation-induced effects *via* different approaches, during HypoRT and NormRT in different cell models.

Materials and methods

Cell culture

We employed the reference breast epithelial cell line MCF10A as a model for the non-malignant breast epithelium and two triple-negative BC cell lines HCC1395 and HCC1937. Both are *BRCA1*-mutant lines, with HCC1395 carrying an additional mutation in NBN (21). As an ancillary tissue type, Bj5Ta fibroblasts from a healthy donor were used. All cell lines were obtained from the American Type Culture Collection (ATCC). Cells below the passage number of 30 were taken for experiments. In all experiments, asynchronous exponentially growing cells were used. MCF10A cells were cultured in MEBM (Mammary Epithelial Cell Growth Basal Medium), supplemented with MEGM™ Single Quots™ according to the manufacturer's instructions (Lonza). Breast cancer epithelial cell lines HCC1395 and HCC1937 were cultured in RPMI 1640 with 10% fetal calf serum (FCS), 500 U/ml penicillin, 0.5 mg/ml streptomycin, and 2 mM L-Glutamine. Bj5Ta fibroblasts were cultured in DMEM (Dulbecco′s Modified Eagle′s Medium) supplemented with 10% FCS, 500 U/ml penicillin, 0.5 mg/ml streptomycin, and 2 mM L-Glutamine. All cells were grown at 37°C in a humidified atmosphere supplemented with 5% CO_2. After each irradiation round cells were kept and further cultured in order to undergo subsequent irradiations until the total dose for HypoRT or NormRT was achieved. For every cell line, a fixed number of cells (5×10^5 for MCF10A with a doubling time of 24–36 h, and 9×10^5 for all the other cell lines with a doubling time of 36 h) were seeded in 75 cm^2 flasks 48 h before the first experimental irradiation. The medium was changed every day to remove dead cells.

X-Ray irradiation experimental timeline

Irradiation at a dose of 2 Gy (NormRT) or 2.67 Gy (HypoRT) per fraction was applied to all the cell lines using a Synergy™ linear accelerator (Elekta AB, Stockholm, Sweden). In order to achieve all irradiation modalities for the cells comparable to the clinical setting, irradiation was carried out at about 37°C, with cells kept warm by warm pads. The dose/rate

was 535 MU/min, field size 40 × 40 cm, distance 110 cm, 227 MU for NormRT and 303 MU for HypoRT. Untreated values were included in each experimental setting in such a way that for every cell line investigated, an age-matched control was incorporated. Every third irradiation day, cells were trypsinized and taken for proliferation analysis by directly counting the cell numbers and MTT assay. On irradiation days 3, 9 and 15, immunocytochemistry was performed. On irradiation day 15 (for both irradiation regimens) and on irradiation day 25 (NormRT only), the colony formation assay (CFA) and DNA synthesis-based cell proliferation (EdU incorporation) assay were performed. The senescence-associated beta-galactosidase (SA-β-gal) assay was conducted only for MCF10A and Bj5Ta cells.

Proliferation and growth rate

To assess cellular proliferation, different methods were employed. Direct counting of cell numbers was performed manually in a Neubauer improved hemocytometer chamber and in parallel, using the Invitrogen™ Countess™ automated cell counter to exclude any observer bias. The results from manual and automated counting approaches exhibited very high similarity and were not statistically different. Cells were trypsinized as usual and resuspended in 1–5 ml of appropriate culturing media. For the statistically optimal use of the counting process, a double sampling for the manual and automated methods was performed. For this, two independent samples were taken from the cell suspension and were separately filled into the two counting areas on the counting chamber or counting slide, respectively. The average cell number from two independent values was calculated. Manual and automated counts were combined in the evaluation as technical duplicates.

To measure the cytotoxicity or growth inhibition of both irradiation regimens, the growth rate of the cells was measured by the commonly used MTT proliferation assay. This colorimetric method is based on the reduction of (3-(4,5-dimethylthiazol-2-yl)-2,5-diphenyltetrazolium bromide or MTT) to formazan crystals by metabolically active cells and is an indicator of cell viability. Briefly, every third irradiation day, 3000 cells in 100 µl of appropriate culture media per well were seeded in quadruplicates in flat-bottomed 96-well plates. Three types of the controls were used: 1) background control – wells with culture medium without cells; 2) negative control – not metabolically active cells (dead cells); and 3) positive control – all viable cells. Age-matched untreated cells were used as a positive control and as a negative control (cells were treated with 0.1% triton). After seeding, cells were incubated for 40–48 h at +37°C and 5% CO_2. In the negative control wells, the medium was changed to a 100 µl appropriate medium, containing 0.1% triton and after 0.5 h incubation at +37°C and 5% CO_2, 10 µl of the MTT labeling reagent (final concentration 0.5 mg/ml) was added to each well; 96-well plates were incubated for 4 h in a humidified atmosphere (+37°C, 5% CO_2). Culturing media were removed carefully from all wells and 100 µl of the solubilization solution (DMSO) was added into each well. The plate was covered with tinfoil and mixed in an orbital shaker for 15 min. Complete solubilization of the purple formazan crystals, which resulted in a colored solution, was checked by eye and the absorbance of the samples was measured using a microplate reader (Multiskan™ FC) at a wavelength of 540 nm. The reference wavelength was 660 nm. The average values from quadruplicate readings were determined and the average value for the blank was subtracted. The absorbance of the experimental samples was plotted on the y-axis versus the experimental day on the x-axis and compared to age-matched untreated control cultures.

DNA synthesis-based cell proliferation was measured in cells at irradiation day 15 (NormRT and HypoRT) by 5-ethynyl-2′-deoxyuridine (EdU) incorporation into newly synthesized DNA and its recognition by azide dyes *via* a copper mediated "click" reaction, using the Click-iT® EdU Imaging Kit (Invitrogen). Briefly, cells were seeded on cover glasses in sterile non-coated six-well plates and incubated with 10 mM of EdU for 6–8 h. The cells were then fixed with 3.7% paraformaldehyde, EdU detection was carried out according to the manufacturer's instructions, and nuclei were stained with Hoechst 33342 for the following analysis. For the detection of cells with replicating DNA, Alexa Fluor® 488 labeled cells were counted under a Leica DMI6000B microscope using a 20× objective and 1.6× magnification. The counting process was performed independently in two different areas of the two prepared slides until at least 50–100 cells per slide were detected and registered.

Immunocytochemistry: Procedure and quantitative analysis

For immunocytochemistry, on irradiation days 3, 9, and 15, cells were seeded in technical duplicates on cover glasses in sterile non-coated six-well plates directly after treatment. After seeding, cell cultures were incubated for 24 h at +37°C and 5% CO_2. All cells were fixed with 3% (w/v) PFA and 2% (w/v) sucrose in PBS for 10 min and permeabilized with 0.2% (v/v) Triton X-100 in PBS. Cells were incubated simultaneously with antibodies against Phospho (S139)-Histone H2AX (Millipore, clone JBW301) at a ratio of 1:200 and against 53BP1 (Bethyl Laboratories, #A300-272A) at a ratio of 1:400 in 2% (w/v) normal goat serum (NGS, Dianova) for 1 h. After several PBS washing steps, the cells were incubated simultaneously with Alexa Fluor anti-mouse IgG 488 or Alexa Fluor anti-rabbit IgG 546 (Invitrogen, both at a ratio of 1:250) for 45 min. The DNA was counterstained with DAPI (Invitrogen) and the cells were mounted with ProLong® Gold (Invitrogen).

For quantitative analyses, residual foci were counted by two independent trained observers, using a Leica DMI6000B

microscope with 63× objective and a 1.6× magnification. In order to detect foci in all three dimensions, the observer manually focused on each z-stack throughout the nucleus. The counting was performed independently in several different areas of slide until at least 50 cells were detected and registered. Every responsive cell (with one or more repair foci) was included in the evaluation.

Senescence-associated beta-galactosidase activity

SA-β-gal staining was performed in MCF10A cells and fibroblasts at irradiation day 15 (for both irradiation regimens) after a cumulative dose of 40.05 Gy (HypoRT) or 30 Gy (NormRT) and on day 25 for NormRT (total dose 50 Gy), using the staining kit (Cell Signalling Technology) to detect the pH-specific (pH 6.0) activity of β-galactosidase, which is associated with senescence (22). The procedure was followed according to the manufacturer's instructions. Briefly, cells were seeded in technical duplicates in a 24-well plate. After 20 h, cells were controlled to be attached and the development of blue color was documented 24 h after the fixation and staining procedure. Pictures in 24-well plates were taken with the staining solution remaining on the cells using the Nikon Eclipse TS100 inverse microscope. Quantification was performed using the Image J software. The number of senescent cells was normalized to the total cell number counted (up to 100 cells per well and at two positions).

Colony formation assay

To determine the cell reproductive death after treatment with ionizing radiation, a modified clonogenic assay or colony formation assay (CFA) was performed. CFA is an *in vitro* cell survival assay based on the ability of a single cell to grow into a colony. The assay tests the ability of every cell in the population to undergo "unlimited" division, since only a fraction of seeded cells can produce colonies. Briefly, cells were seeded after irradiation at day 15 (for both irradiation regimens) after a cumulative dose of 40.05 Gy (HypoRT) or 30 Gy (NormRT) in six-well plates and at day 25 (NormRT only) after a total dose of 50 Gy in 12-well plates in technical triplicates. For each investigated cell line, a defined number of cells were seeded. At irradiation day 15 for both regimens, 500 cells/well for MCF10A, 750 cells/well for Bj5Ta, and 1250 cells/well and 1500 cells/well for HCC1397 and HCC1395, respectively, were seeded. At irradiation day 25 (NormRT only) 150 cells/well for MCF10A, 200 cells/well for Bj5Ta, and 400 cells/well and 500 cells/well for HCC1397 and HCC1395, respectively, were seeded. Untreated age-matched controls were seeded in parallel in technical triplicates in separate six-well plates: for MCF10A, 200 cells/well; for Bj5Ta, 250 cells/well; for HCC1937 and HCC1395, 500 and 750 cells/well, respectively. The medium was gently changed every 2 days. After *ca*. 7 days, incubation for MCF10A, 9 days for Bj5Ta, 12 days for HCC1937, and *ca*. 14 days of incubation for HCC1395, colonies were fixed with 3% (w/v) PFA and 2% (w/v) sucrose in PBS for 10 min, stained with 0.5% (w/v) crystal violet, and counted by microscopy. The plating efficiency (PE) as the ratio of the number of colonies to the number of cells seeded was estimated for each untreated cell line. Albeit not always, the more cells were seeded, the more plating efficiency was observed. The colony was defined to consist of at least 50 cells. The survival fraction (SF) of irradiated cells was expressed as a percentage of colonies per seeded cell after normalization by the plating efficiency of non-irradiated cells. Cell survival data was plotted as a logarithm of the SF versus dose.

Statistical analysis

Statistical analysis was performed using GraphPad Prism (version 9.0.0; GraphPad Software). In order to compare differences between the two groups, a Student's *t*-test was performed. Three or more groups were compared using one-way ANOVA (a repeated-measures analysis of variance). p Values below $\alpha < 0.05$ were considered significant.

Results

Efficacy of hypofractionated and normofractionated irradiation regimens on the cell's proliferation scale

We determined the proliferation capacity and growth rate of the employed cell cultures after fixed days of radiotherapy. The number of directly counted cells was continuously reducing over time. The growth rate of the Bj5Ta (HypoRT or NormRT) and HCC1937 (NormRT) were highest among all cell lines until day 9, but thereafter, all cells had almost equal proliferation (Figure 1A). There was a significant difference in the hypofractionated irradiation protocol compared to the conventional one for MCF10A cells and a nominally significant difference for HCC1937 cells (Figure 1A). There was also a difference between the cells lines (Figure 1B).

By means of the MTT assay, we found a significant difference in growth rate and cell viability after the hypofractionated irradiation regimen, compared to the conventional one, for HCC1395 cells, and this observation was nominally significant for Bj5Ta cells (Figure 2).

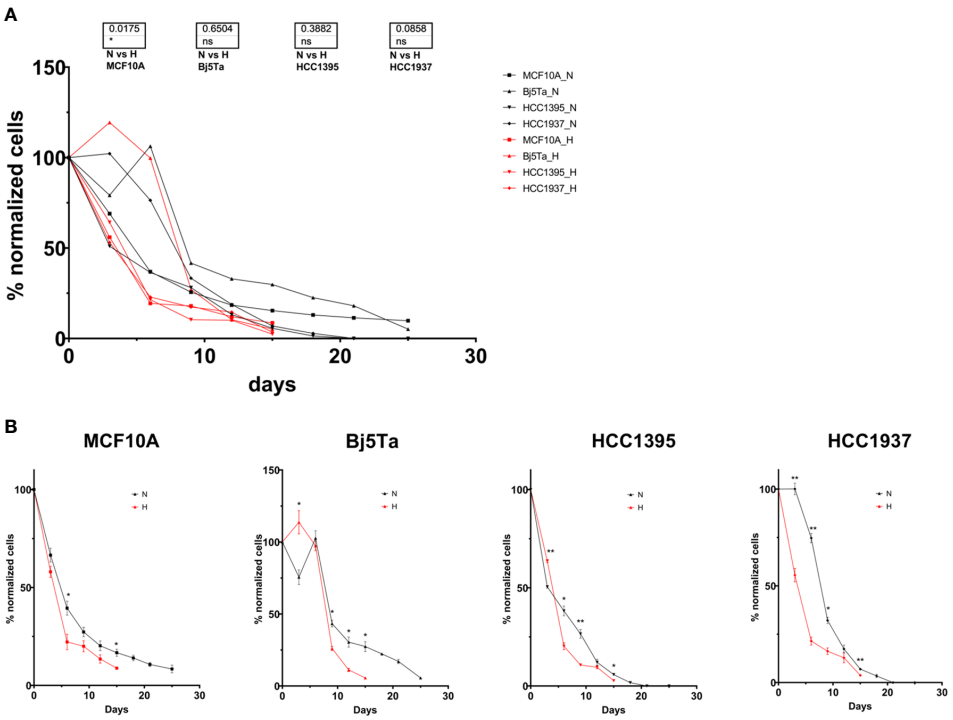

FIGURE 1
Cell proliferation capacity and growth rate during radiotherapy. The cell counts at specific irradiation days were normalized to the number of cells seeded at the start of the experiment and plotted as a percentage for all investigated cell lines **(A)**, or each cell line individually **(B)**. The red line and H represent HypoRT; the black line and N represent NormRT. *p<0.05, **p<0.005, n.s, non-significant.

In the DNA synthesis-based cell proliferation, we found the pronounced difference in both BC lines if the hypofractionated irradiation regimen was compared to the conventional one (Figures 3 A, B). However, the effect of decreased proliferation (newly synthesized DNA) was more significant for NormRT at day 25 contrary to HypoRT at day 15.

Normal cells (MCF10A and Bj5Ta) showed no difference after the total dose was applied, according to the irradiation regimen, although fibroblasts had a significantly reduced growth rate after HypoRT in contrast to NormRT at day 15 (Figures 3A, B).

The HCC1395 BC cell line was most sensitive to irradiation among all cell lines tested in proliferative assays, being more sensitive to the HypoRT regimen in the MTT assay (Figures 1, 2). The HCC1395 and HCC1937 BC cell lines significantly slowed down proliferation at about irradiation day 15 (both irradiation protocols) and died after day 25. The MCF10A and Bj5Ta lines, being non-cancer cells, continued to grow (albeit at a slightly retarded rate) with daily exposure, and the total number on day 25 (NormRT) was 4.9×10^4 for MCF10A cells and 4.7×10^4 for Bj5Ta, respectively (started with 5×10^5 and 9×10^5 for MCF10A and Bj5Ta, respectively). At irradiation day 15, both lines had total cell numbers of 7.7×10^4 and 2.7×10^5 (NormRT) or 4.3×10^4 and 4.7×10^4 (last day of HypoRT) for MCF10A and Bj5Ta cells, respectively.

Efficiency of DNA DSB repair after hypofractionated and conventional multifractionated radiotherapy

To clarify the role of DNA damage response (DDR) proteins in cell survival after different regimens of radiotherapy, we analyzed residual γH2AX and 53BP1 foci in cells irradiated with the corresponding fractionated protocols. We also incorporated single-dose controls (6 Gy and 8 Gy) for irradiation day 3. We found that all of the tested cell lines had significantly lower numbers of residual γH2AX and 53BP1 foci after fractionated irradiation at day 3, than cells that had received the single dose (Figures 4A, C), suggesting that DNA repair could play a role in conferring cell survival after multiple fractions. There were clear differences between the BC cell lines with different mutational backgrounds, especially in contrast to the reference MCF10A cells (Figures 4A, B). However, HCC1395

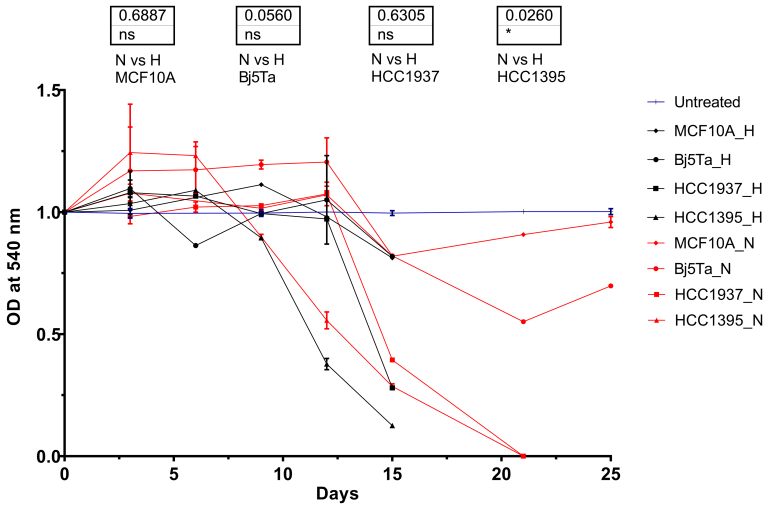

FIGURE 2
Cell growth rate during the radiotherapy evaluated in the MTT assay. OD values for each cell line were normalized to the appropriate values of untreated cells and plotted versus the irradiation day. The blue lines represent untreated values of the individual cell lines at specific experimental days, which were normalized to 1. The red lines correspond to the HypoRT protocol and black lines to the NormRT protocol, respectively. *p<0.05, n.s, non-significant.

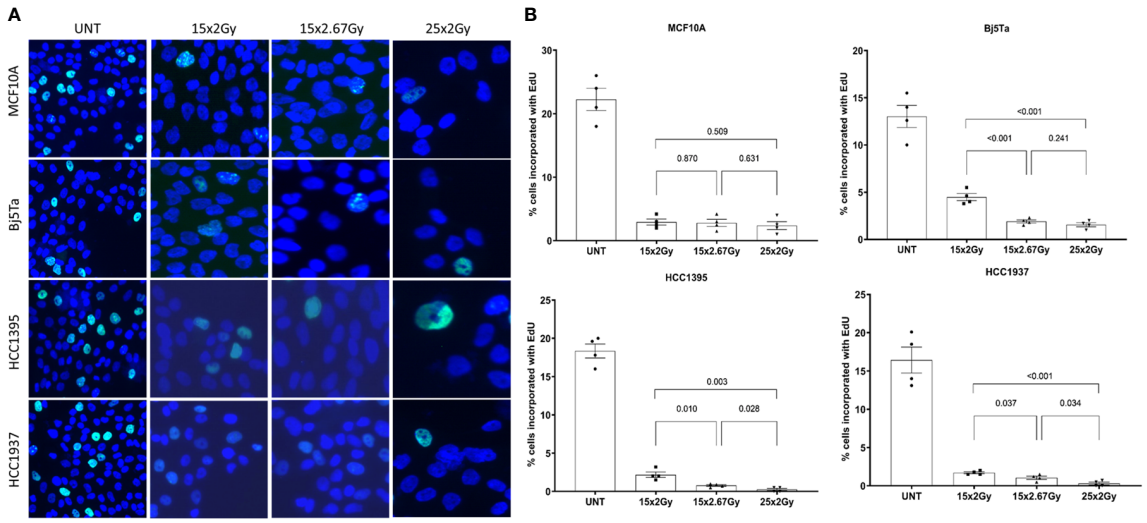

FIGURE 3
DNA synthesis-based cell proliferation evaluated on irradiation day 15 (both protocols) and on day 25 (NormRT only). Representative images of EdU incorporation staining **(A)** using conventional fluorescence microscopy (Leica DMI6000B) and evaluation **(B)**. The percentage of EdU-positive cells is presented as a bar plot +/- SEM.

had a higher ratio of 53BP1/H2AX foci and that was consistent with its known *NBN* mutation that impairs γH2AX accumulation after irradiation (21). From day 9 to day 15, we observed no significant increment in residual γH2AX and 53BP1 foci in all of the tested cell lines and from day 3 to day 9 only in fibroblasts for the NormRT regimen (Table 1). Since all employed cells had significantly elevated levels of residual foci (both types) after irradiation day 9 (Table 1), and persistent DNA damage foci may serve as a biomarker for cellular senescence, we next measured senescence-associated β-

10.3389/fonc.2022.852694

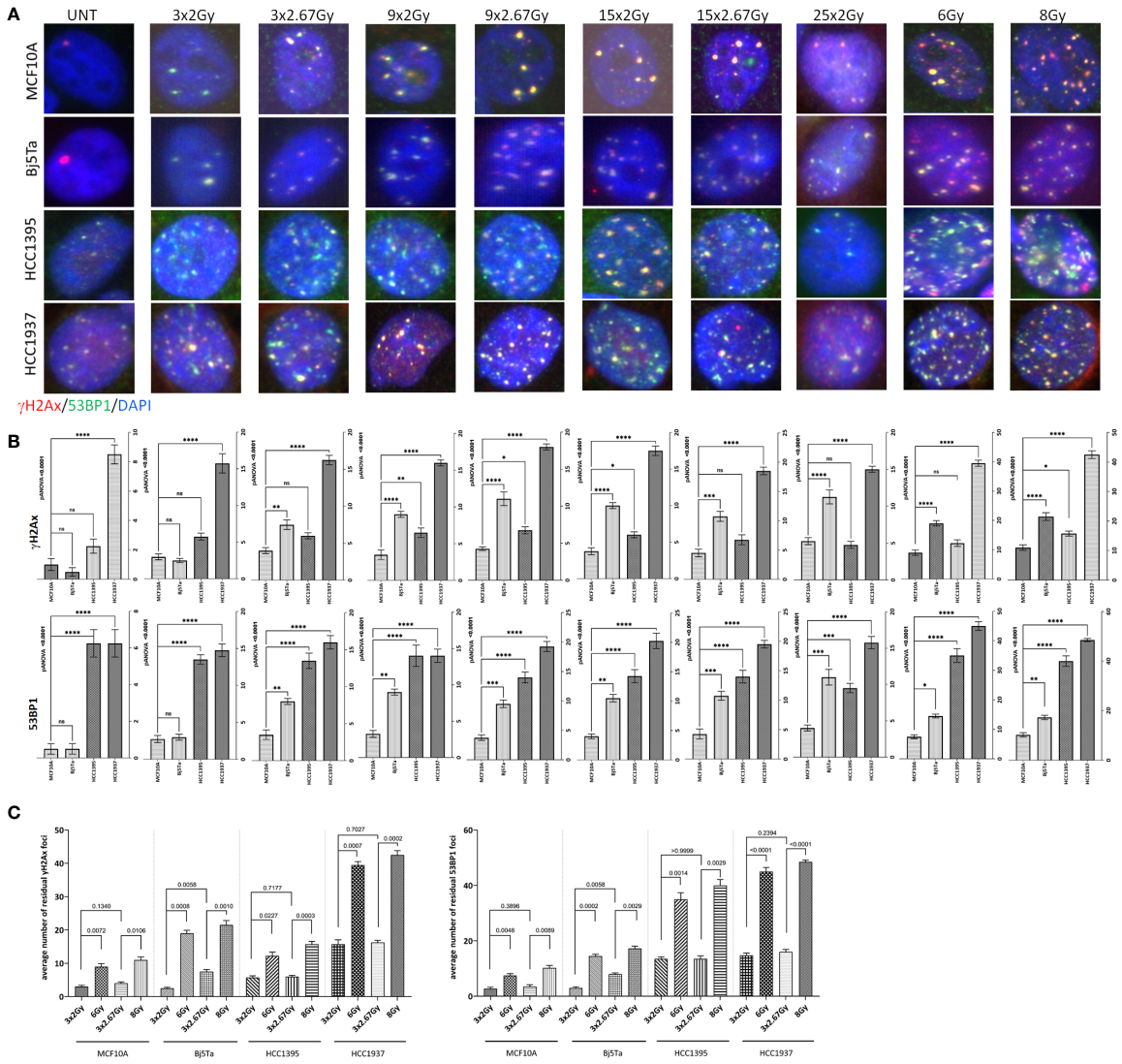

FIGURE 4
Immunocytochemical analysis of residual DNA damage foci after fractionated irradiation with the corresponding protocols. Representative images of residual γH2AX foci (red) and 53BP1 foci (green) double immunostaining **(A)** and evaluation **(B, C)** of γH2AX foci (top on B and left on C) and 53BP1 foci (bottom on B and right on C) 24 h after systematic irradiation with HypoRT or NormRT protocols at days 3, 9, 15, and 25 (NormRT only), using conventional fluorescence microscopy (Leica DMI6000B). DNA is counterstained with DAPI (UNT – untreated value "age-matched" to day 25). Evaluation data are presented as bar plots of average foci number (+/- SEM) per cell per slide from two slides. Values of 6 Gy and 8 Gy represent single-dose controls for fractionated irradiation with the NormRT or HypoRT protocol, respectively, at irradiation day 3. **(B)** Comparison of average residual DNA damage foci numbers between different cell lines and MCF10A cells. **(C)** Comparison of average residual DNA damage foci numbers (γH2AX and 53BP1) within the cell lines after fractionated irradiation (three fractions with respective protocols) and after a single dose of 6 Gy or 8 Gy, respectively. *p<0.05, **p<0.005, *** p<0.0005, **** p<0.0001, n.s, non-significant.

galactosidase activity in MCF10A cells and fibroblasts (20). The percentage of β-galactosidase positive cells was significantly increased in comparison to untreated state (Figures 5A, B), but there was no difference between different irradiation regimens. In addition, cells showed senescence-like phenotype also morphologically, with cellular hypertrophy, irregularities in shape, and vacuolization (Figure 5A), and these observations were true also for cancer cell lines.

Effects of hypofractionated and conventional irradiation regimens on survival of the cells

The plating efficiency in the performed CFA assay was lower for HCC1395 cells than for other cells (about 3% in HCC1395 compared with 23% in HCC1937 cells; about 53% in Bj5Ta cells and about 60% for MCF10A cells). The number of colonies in

TABLE 1 Evaluation of DNA DSB repair efficiency after hypofractionated and conventional multifractionated radiotherapy by means of residual foci.

Comparison values	MCF10A		Bj5Ta		HCC1395		HCC1937	
	γH2Ax	53BP1	γH2Ax	53BP1	γH2Ax	53BP1	γH2Ax	53BP1
UNT vs. 3×2 Gy	n.s	n.s	n.s	n.s	*	*	***	*
UNT vs. 3×2.67 Gy	n.s	n.s	***	***	*	*	***	*
UNT vs. 9×2 Gy	*	*	***	***	**	*	***	*
UNT vs. 9×2.67 Gy	*	*	***	***	*	*	***	*
UNT vs. 15×2 Gy	*	*	***	***	*	*	***	*
UNT vs. 15×2.67 Gy	*	*	***	***	**	*	***	*
UNT vs. 25×2 Gy	***	**	***	***	*	*	***	**
3×2 Gy vs. 3×2.67 Gy	n.s	n.s	**	**	n.s	n.s	n.s	n.s
3×2 Gy vs. 9×2 Gy	n.s	n.s	***	***	n.s	n.s	n.s	n.s
3×2 Gy vs. 15×2 Gy	n.s	n.s	***	***	n.s	n.s	n.s	n.s
3×2 Gy vs. 25×2 Gy	n.s	n.s	***	***	n.s	n.s	n.s	n.s
3×2 Gy vs. 6 Gy	**	*	***	***	*	***	***	***
3×2.67 Gy vs. 9×2.67 Gy	n.s	n.s	n.s	n.s	n.s	n.s	n.s	n.s
3×2.67 Gy vs. 15×2.67 Gy	n.s	n.s	n.s	n.s	n.s	n.s	n.s	n.s
3×2.67 Gy vs. 8 Gy	**	***	***	**	***	**	***	**
9×2 Gy vs. 9×2.67 Gy	n.s	n.s	n.s	n.s	n.s	n.s	n.s	n.s
9×2 Gy vs. 15×2 Gy	n.s	n.s	n.s	n.s	n.s	n.s	n.s	n.s
9×2 Gy vs. 25×2 Gy	n.s	n.s	n.s	n.s	n.s	n.s	n.s	n.s
9×2.67 Gy vs. 15×2.67 Gy	n.s	n.s	n.s	n.s	n.s	n.s	n.s	n.s
15×2 Gy vs. 15×2.67 Gy	n.s	n.s	n.s	n.s	n.s	n.s	n.s	n.s
15×2.67 Gy vs. 25×2 Gy	n.s	n.s	n.s	n.s	n.s	n.s	n.s	n.s

n.s, non-significant; *p < 0.05, **p < 0.01, ***p < 0.001.
Results of one-way ANOVA with multiple statistical test correction.

untreated cells tended to increase according to the increase of the number of cells seeded. This tendency was observed in all investigated cells, except HCC1395. After day 15 of irradiation, the HCC1395 cell line was most radiosensitive in a colony formation assay, especially for the HypoRT regimen, whereas HCC1937 cells had the same sensitivity to HypoRT or NormRT (Figures 6A–C). Bj5Ta and MCF10A cells tended to be also more sensitive to HypoRT vs NormRT, although after an appropriate cumulative dose for each regimen (40.05 Gy – HypoRT and 50 Gy – NormRT) Bj5Ta cells showed increased survival after NormRT regimen irradiation (Figures 6A–C). The responses of all investigated cells were different and could be distinguished from each other, indicating cell line specificity of effect.

Discussion

Radiotherapy (RT) is an important component in the treatment of breast cancer, especially as an adjuvant approach in breast conserving therapy. Postoperative irradiation is also getting continuously important in the management of the TNBC subtype, although the benefit is still debatable, concerning overall survival (10, 11). Recent studies revealed no differences in dose fractionation adding an evidence to support the use of moderate hypofractionated whole-breast irradiation in TNBC patients (23, 24). The golden standard of care for many years was NormRT (with 45–50 Gy in 25–28 fractions), delivered with a long schedule over 5 weeks (9). In recent years, HypoRT (with 39–42.5 Gy in 13–16 fractions) is being established as a new standard. In several randomized trials, the similarity between effects after HypoRT and traditional 5-week NormRT has been shown (14, 20, 23–25) and HypoRT is now considered an accepted practice in numerous clinics, although many professionals remain skeptical and concerned about its efficiency and side effects. It is known that both tumor and normal cells generally can survive better when RT is delivered in fractions as compared to a single large dose. Thus, fractionated regimens may reduce damages to non-malignant cells, especially standard NormRT with a smaller dose per fraction, but this could also affect the anti-tumor efficacy in influencing the growth inhibition or metastatic potential and proliferation of malignancies.

Equal effectiveness and toxicities of HypoRT compared to NormRT for breast cancer have been proven in several randomized clinical trials since the early 2000s (14, 26–32). However, little is known so far about the cellular processes that

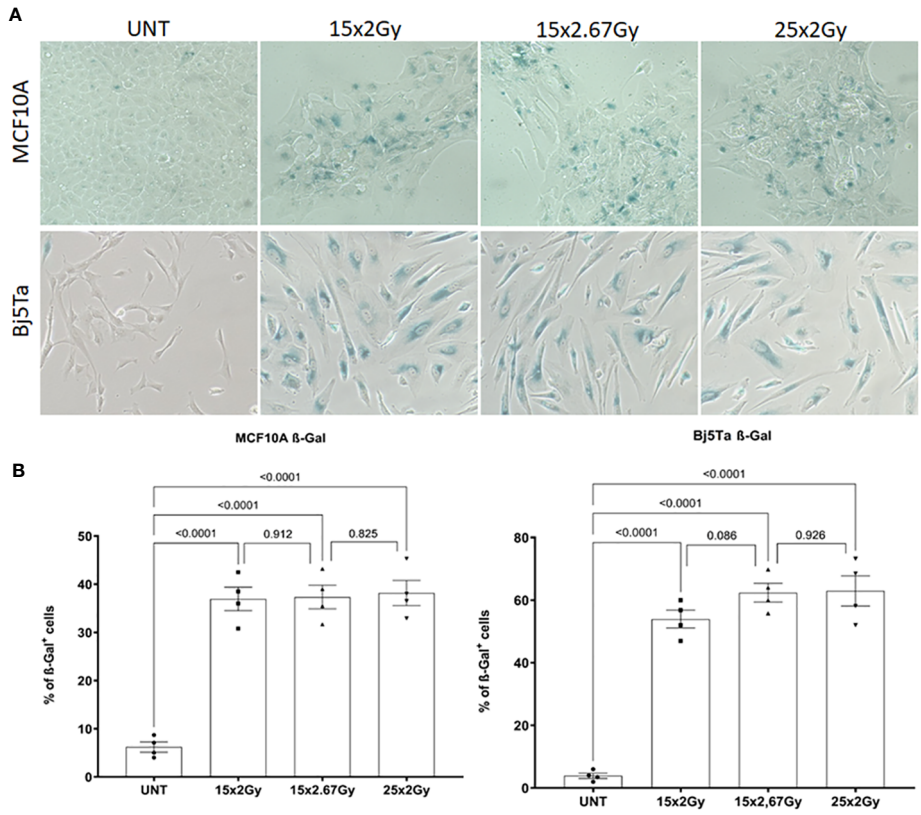

FIGURE 5
Senescence-associated beta-galactosidase (SA-βgal) activity analysis in MCF10A and Bj5Ta cells after fractionated irradiation with the corresponding protocols. Representative images of SA-βgal staining **(A)** and evaluation **(B)** of the percentage of senescent cells using inverse microscopy (Nikon Eclipse TS100 data from two technical replicates are presented as bar plots). Each dot represents a counting area (UNT – untreated "age-matched" to day 15).

take place during the medical radiation, applied over time in different-sized fractions, though understanding the mechanisms of side-effect occurrence, or those which promote cancer cell survival, could improve treatment and patient outcome and identify new strategies for more precise intervention. To our best knowledge, there are fewer studies providing some preclinical investigations on the *in vitro* radiobiological comparison of hypofractionation and conventional fractionation for any tumor type, mimicking the clinical situation. Most research studies in this field deal either with clinical trials and meta-analysis (14, 26–32) or with modeling radiobiological effects (33, 34). Regarding biological effects of exposure to ionizing radiation, most studies either utilize a single-irradiation dose or focus on fractionated irradiation, applying more fractions over a short time period, to establish surviving/resistant cell lines (35). Direct radiobiological comparison of fractionation regimens, for instance, in non-small cell lung cancer or glioblastoma cell models reflects the clinical situation with some advantages of hypofractionation for tumor control with no observed increase in radiotoxicity (36, 37). However, there is some evidence that hypofractionated radiotherapy can play a significant role in radioresistance and tumor recurrence and there is a need to optimize radiotherapy strategies, since different sites and types of tumors may respond differently to the same dose and fractionated irradiation (38). To address the question about the effectiveness and toxicity of HypoRT in comparison to NormRT on the cellular level in a triple-negative breast cancer model, we investigated how normal and tumor cells respond to differential regimens of radiotherapy in the clinical setting, using a combination of molecular and functional approaches.

Since irradiation can directly affect cells by triggering DSBs and inducing repair processes and other cellular effects, such as proliferation inhibition as well as cell death *via* apoptosis, necrosis, or senescence, we were investigating proliferation and growth capacity, efficiency of DNA DSB repair, and cell survival during HypoRT and NormRT irradiation regimens.

Different cell types as well as different cancer types and independent tumors of the same cancer type can have individual responses to ionizing radiation. Our results showed that investigated cells differ in their receptivity to different

10.3389/fonc.2022.852694

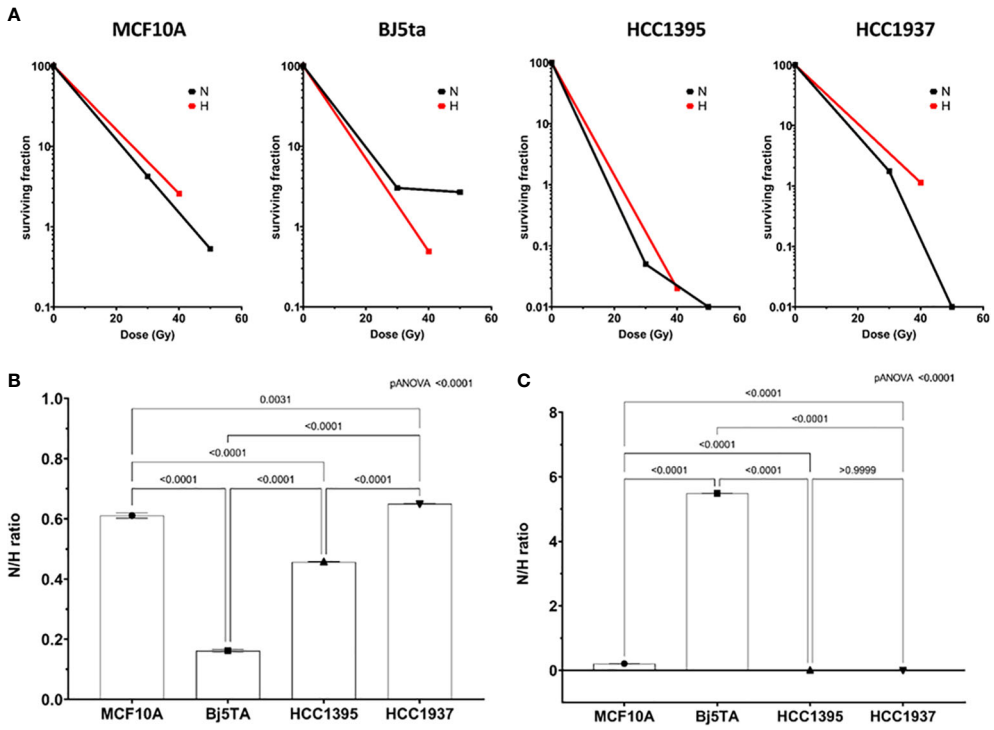

FIGURE 6
Survival after hypofractionated and conventional multifractionated radiotherapy. Clonogenic survival of the employed cell lines after irradiation with the corresponding multifractionated protocol **(A)**. The red line and H represent HypoRT, the black line and N represent NormRT. Non-irradiated cells were used as control for performing modified CFA. Efficacy of HypoRT versus NormRT radiotherapy at irradiation day 15 after a cumulative dose of 40.05 Gy (HypoRT) or 30 Gy (NormRT) **(B)**. The ratio of HypoRT to NormRT survival was calculated as follows: surviving fraction after 40.05 Gy/surviving fraction after 30 Gy. Efficacy of HypoRT versus NormRT radiotherapy by the end of both irradiation protocols. **(C)**. The ratio of HypoRT to NormRT survival was calculated as follows: surviving fraction after a cumulative dose of 40.05 Gy/surviving fraction after a cumulative dose of 50 Gy.

irradiation regimens. In general, the number of directly counted cells was continuously reducing over the irradiation time for both protocols. There was a significant difference in HypoRT protocol compared to NormRT for normal epithelial cells MCF10A. This difference was also nominally significant for HCC1937 BC cells. Another BC cell line, HCC1395, being the most sensitive in all approaches, exhibited significant difference in growth rate and cell viability after HypoRT compared to NormRT in MTT assay, and this observation was also nominally significant for Bj5Ta cells. We noticed unexpected higher absorbance values for all investigated cell lines in the first 12 irradiation days, independent from dose per fraction. If the absorbance values of the experimental samples are higher than the untreated control, this indicated an increase in growth rate/cell proliferation. Alternatively, if the absorbance rates of the experimental samples are lower than the untreated control; this indicated a reduction in the rate of cell proliferation or a reduction in overall cell viability. As observed in our settings, an increase in cell proliferation by means of MTT could also reflect the offset by cell death (i.e., apoptosis), which is more plausible. The different speed of reaction in the number of cells of the different cell types is caused by the inborn different turnover in tissue. Regular rhythm of mitosis and apoptosis is hardly changed by radiation of sublethal single doses and is fixed by the function of each cell: slower in glandular duct cells and faster in fibroblasts and also in tumor cells. In DNA synthesis-based cell proliferation, we found the difference of HypoRT compared to NormRT for both BC lines and the effect of decreased proliferation was more significant for NormRT at day 25 contrary to HypoRT at day 15. This observation fits with the clinical experience that the remission of a tumor can hardly be accelerated by the faster dose application during hypofractionation (39) and confirms clinical findings of different remission rates in irradiated tumors as well of other entities in clinical trials (39, 40). Normal cells showed no difference after the total dose was applied, according to the irradiation regimen, although fibroblasts had a reduced growth rate after HypoRT in contrast to NormRT at day 15. MCF10A, as mamma epithelial cells, are known to have a longer life span than the fibroblasts, and have a slower rate of radiation-induced apoptosis. This could only be accelerated by lethal single doses, but not by the sub-lethal dose of 2.67 Gy. As the number of cells

with newly synthesized DNA in our study sinks slowly in MCF10A-cells after irradiation, the involution of glandular ducts develops months later than the remission of tumor cells. Thus, the quick remission in our cell culture of HCC1395 and HCC1937 is the same as shrinking tumors months before fibrosis occurred in patients.

The remaining tumor volume, which is persistent immediately after completion of HypoRT (still viable tumor cells in our settings), is in fact full of cells unable to undergo mitosis. Both BC cell lines after HypoRT formed some colonies in the CFA, but cells which were not taken in the experiment were further cultured in six-well plates under standard settings (without irradiation) and did not survive after day 25. This observation coincides with the clinical observation that the remission of the tumor is sometimes achieved even before the onset of normal tissue toxicity (40).

Clarifying the role of DNA DSBs repair in cell survival after different regimens of radiotherapy, we found that all of the tested cell lines had significantly lower numbers of residual γH2AX and 53BP1 foci after fractionated irradiation, than cells that had received the single higher dose. These results suggest that DNA repair could play a role in conferring cell survival after multiple fractions. The lower number of residual γH2AX and 53BP1 foci after fractionated radiotherapy explains the potential of higher single doses of radiotherapy to cause tissue necrosis (radionecrosis) as a late side effect despite equal effectiveness against the tumor (41). The functional status of DDR in general (and homologous recombination repair in particular) is known to be different in investigated cells and can be revealed only when cells are exposed to DNA damage. Indeed, our results support the notion that DNA damage repair occurred between radiation fractions in the first irradiation days, especially in normal MCF10A cells and fibroblasts (true only for the NormRT regimen). We noticed also increased values of residual foci in >comparison to the untreated state (especially for HypoRT regimen), which probably indicates that cells were unable to repair all DSBs before the next radiation dose induced new DNA damage. This observation was markedly significant in fibroblasts (Table 1), and in BC cell lines. From day 9 to day 15, we observed no significant increment in residual γH2AX and 53BP1 foci in all of the tested cell lines and, from day 3 to day 9, only in fibroblasts for NormRT regimen. These results suggest that either surviving cells adopted and have efficient DNA damage repair, or that replication stress, induced by irradiation and accumulation of DNA damage and DSBs, subsequently exceeded the repair capacity, which to some extent, reflects the proliferation scale observations. The majority of cells with irreparable DSB die of mitotic catastrophe, which reflects the inhibition of proliferation in our findings. Only adapted cells survive, with efficient DNA damage repair, as observed in the CFA assay for non-tumor cells.

All our results exemplify that the investigated cells differ in their receptivity and susceptibility to different irradiation regimens, and we could substantiate the already clinically proven equal effectiveness and toxicity of HypoRT for breast cancer compared to NormRT on a cellular level. This makes it easier to understand the differences in growth rate or the remission of tumor and development of fibrosis. Identifying the appropriate dosing scheme for any defined tumor entity may significantly impact on patient survival and therapy outcome.

Conclusions

At the end of both therapy concepts (Normo and Hypo), normal and malignant cells reached almost the same endpoint of cell count and proliferation inhibition. BC cell lines significantly slowed down proliferation and died, whereas MCF10A and Bj5Ta lines, being non-cancer cells, continued to grow with daily exposure, although at a retarded pace. That confirms the clinical observations in the follow-up at the cellular level.

Data availability statement

The original contributions presented in the study are included in the article/supplementary material. Further inquiries can be directed to the corresponding author.

Author contributions

NB, HC, CH and RM contributed to conception and design and interpretation of data. SG, ML, and KS contributed to acquisition and interpretation of data, DR contributed to statistical analysis and interpretation of data; all authors were involved in drafting the manuscript, NB, HC, DR and RM have given final approval. All authors contributed to the article and approved the submitted version.

Conflict of interest

The authors declare that the research was conducted in the absence of any commercial or financial relationships that could be construed as a potential conflict of interest.

Publisher's note

References

1. Jemal A, Bray F, Center MM, Ferlay J, Ward E, Forman D. Global cancer statistics. *CA Cancer J Clin* (2011) 61(2):69–90. doi: 10.3322/caac.20107

2. Wang L, Hu X, Wang P, Shao Z-M. Integrative 3' untranslated region-based model to identify patients with low risk of axillary lymph node metastasis in operable triple-negative breast cancer. *Oncologist.* (2019) 24(1):22–30. doi: 10.1634/theoncologist.2017-0609

3. Dent R, Trudeau M, Pritchard KI, Hanna WM, Kahn HK, Sawka CA, et al. Triple-negative breast cancer: Dlinical features and patterns of recurrence. *Clin Cancer Res* (2007) 13(15 Pt 1):4429–34. doi: 10.1158/1078-0432.CCR-06-3045

4. Nishimura R, Arima N. Is triple negative a prognostic factor in breast cancer? *Breast Cancer* (2008) 15(4):303–8. doi: 10.1007/s12282-008-0042-3

5. Gonzalez-Angulo AM, Timms KM, Liu S, Chen H, Litton JK, Potter J, et al. Incidence and outcome of BRCA mutations in unselected patients with triple receptor-negative breast cancer. *Clin Cancer Res* (2011) 1:17(5):1082–9. doi: 10.1158/1078-

6. Gong CC, Ma G, Hu XC, Zhang Y, Wang Zh Zhang J, et al. Pretreatment 18F-FDG uptake heterogeneity predicts treatment outcome of first-line chemotherapy in patients with metastatic triple negative breast cancer. *Oncologist* (2018) 23 (10):1144–52. doi: 10.1634/theoncologist.2018-0001

7. Yang TJ, Ho AY. Radiation therapy in the management of breast cancer. *Surg Clin North Am* (2013) 3(2):455–71. doi: 10.1016/j.suc.2013.01.002

8. McGale P, Taylor C, Correa C, Cutter D, Duane F, Ewertz M, et al. Effect of radiotherapy after mastectomy and axillary surgery on 10-year recurrence and 20-year breast cancer mortality: Meta-analysis of individual patient data for 8135 women in 22 randomised trials. *Lancet (London England)* (2014) 383(9935):2127–35. doi: 10.1016/S0140-6736(14)60488-8

9. Fisher B, Anderson S, Bryant J, Margolese RG, Deutsch M, Fisher ER, et al. Twenty-year follow-up of a randomized trial comparing total mastectomy, lumpectomy, and lumpectomy plus irradiation for the treatment of invasive breast cancer. *N Engl J Med* (2002) 347(16):1233–41. doi: 10.1056/NEJMoa022152

10. Abdulkarim BS, Cuartero J, Hanson J, Deschênes J, Lesniak D, Sabri S. Increased risk of locoregional recurrence for women with T1–2N0 triple-negative breast cancer treated with modified radical mastectomy without adjuvant radiation therapy compared with breast-conserving therapy. *J Clin Oncol* (2011) 29 (21):2852–8. doi: 10.1200/JCO.2010.33.4714

11. Khalifa J, Duprez-Paumier R, Filleron T, Triki ML, Jouve E, Dalenc F, et al. Outcome of pN0 triple-negative breast cancer with or without lymph node irradiation: a single institution experience. *Breast J* (2016) 22(5):510–9. doi: 10.1111/tbj.12626

12. Offersen BV, Alsner J, Nielsen HM, Jakobsen EH, Nielsen MH, Krause M, et al. Hypofractionated versus standard fractionated radiotherapy in patients with early breast cancer or ductal carcinoma *In situ* in a randomized phase III trial: The DBCG HYPO trial. *J Clin Oncol* (2020) 38(31):3615–25. doi: 10.1200/JCO.20.01363

13. Wang SL, Fang H, Hu C, Song Y-W, Wang W-H, Jin J, et al. Hypofractionated versus conventional fractionated radiotherapy after breast-conserving surgery in the modern treatment era: A multicenter, randomized controlled trial from China. *J Clin Oncol* (2020) 38:3604–14. doi: 10.1200/jco.20.01024

14. Haviland JS, Owen JR, Dewar JA, Agrawal RK, Barrett J, Barrett-Lee PJ, et al. The UK standardisation of breast radiotherapy (START) trials of radiotherapy hypofractionation for treatment of early breast cancer: 10-year follow-up results of two randomised controlled trials. *Lancet Oncol* (2013) 14(11):1086–94. doi: 10.1016/S1470-2045(13)70386-3

15. Liu L, Yang Y, Guo Q, Ren B, Peng Q, Zou L, et al. Comparing hypofractionated to conventional fractionated radiotherapy in postmastectomy breast cancer: A meta-analysis and systematic review. *Radiat Oncol* (2020) 15 (1):17. doi: 10.1186/s13014-020-1463-1

16. Youssef A, Stanford J. Hypofractionation radiotherapy vs. conventional fractionation for breast cancer: A comparative review of toxicity. *Cureus.* (2018) 10 (10):e3516. doi: 10.7759/cureus.3516

17. Mayinger M, Straube C, Habermehl D, Duma MN, Combs SE. Hypo-vs. normofractionated radiation therapy in breast cancer: A patterns of care analysis in German speaking countries. *Rep Pract Oncol Radiother* (2020) 25(5):775–9. doi: 10.1016/j.rpor.2020.07.003

18. Gu L, Dai W, Fu R, Lu H, Shen J, Shi Y, et al. Comparing hypofractionated with conventional fractionated radiotherapy after breast-conserving surgery for early breast cancer: A meta-analysis of randomized controlled trials. *Front Oncol* (2021) 11:753209. doi: 10.3389/fonc.2021.753209

19. Parthan A, Pruttivarasin N, Davies D, Taylor D, Pawar V, Bijlani A, et al. Comparative cost-effectiveness of stereotactic body radiation therapy versus intensity-modulated and proton radiation therapy for localized prostate cancer. *Front Oncol* (2012) 2:81. doi: 10.3389/fonc.2012.00081

20. Batumalai V, Delaney GP, Descallar J, Gabriel G, Wong K, Shafiq J, et al. Variation in the use of radiotherapy fractionation for breast cancer: Survival outcome and cost implications. *Radiother Oncol* (2020) 152:70–7. doi: 10.1016/j.radonc.2020.07.038

21. Schröder-Heurich B, Bogdanova N, Wieland B, Xie X, Noskowicz M, Park-Simon TW, et al. Functional deficiency of NBN, the nijmegen breakage syndrome protein, in a p.R215W mutant breast cancer cell line. *BMC Cancer* (2014) 14:434. doi: 10.1186/1471-2407-14-434

22. Dimri GP, Lee X, Basile G, Acosta M, Scott G, Roskelley C, et al. A biomarker that identifies senescent human cells in culture and in aging skin *in vivo*. *Proc Natl Acad Sci USA* (1995) 92(20):9363–7. doi: 10.1073/pnas.92.20.9363

23. Wen S, Manuel L, Doolan M, Westhuyzen J, Shakespeare TP, Aherne NJ. Effect of clinical and treatment factors on survival outcomes of triple negative breast cancer patients. *Breast Cancer (Dove Med Press)* (2020) 12:27–35. doi: 10.2147/BCTT.S236483

24. Jagsi R, Griffith KA, Vicini FA, Abu-Isa E, Bergsma D, Bhatt A, et al. Disease control after hypofractionation versus conventional fractionation for triple negative breast cancer: Comparative effectiveness in a Large observational cohort. *Int J Radiat Oncol Biol Phys* (2021) S0360-3016(21):02918–7. doi: 10.1016/j.ijrobp.2021.10.012

25. Whelan TJ, Pignol JP, Levine MN, Julian JA, MacKenzie R, Parpia S, et al. Long-term results of hypofractionated radiation therapy for breast cancer. *N Engl J Med* (2010) 362(6):513–20. doi: 10.1056/NEJMoa0906260

26. START Trialists' Group, Bentzen SM, Agrawal RK, Aird EG, Barrett JM, Barrett-Lee PJ, et al. The UK standardisation of breast radiotherapy (START) trial a of radiotherapy hypofractionation for treatment of early breast cancer: a randomised trial. *Lancet Oncol* (2008) 9(4):331–41. doi: 10.1016/S1470-2045(08)70077-9

27. START Trialists' Group, Bentzen SM, Agrawal RK, Aird EG, Barrett JM, Barrett-Lee PJ, et al. The UK standardisation of breast radiotherapy (START) trial b of radiotherapy hypofractionation for treatment of early breast cancer: a randomised trial. *Lancet* (2008) 371(9618):1098–107. doi: 10.1016/S0140-6736(08)60348-7

28. Owen JR, Ashton A, Bliss JM, Homewood J, Harper C, Hanson J, et al. Effect of radiotherapy fraction size on tumour control in patients with early-stage breast cancer after local tumour excision: long-term results of a randomised trial. *Lancet Oncol* (2006) 7(6):467–71. doi: 10.1016/S1470-2045(06)70699-4

29. Shaitelman SF, Schlembach PJ, Arzu I, Ballo M, Bloom ES, Buchholz D, et al. Acute and short-term toxic effects of conventionally fractionated vs hypofractionated whole-breast irradiation: A randomized clinical trial. *JAMA Oncol* (2015) 1(7):931–41. doi: 10.1001/jamaoncol.2015.2666

30. Zhou ZR, Mei X, Chen XX, Yang ZZ, Hou J, Zhang L, et al. Systematic review and meta-analysis comparing hypofractionated with conventional fraction radiotherapy in treatment of early breast cancer. *Surg Oncol* (2015) 24(3):200–11. doi: 10.1016/j.suronc.2015.06.005

31. Chatterjee S, Chakraborty S, Adjuvant Author Group. HYPORT. Hypofractionated radiation therapy comparing a standard radiotherapy schedule (over 3 weeks) with a novel 1-week schedule in adjuvant breast cancer: an open-label randomized controlled study (HYPORT-Adjuvant)–study protocol for a multicentre, randomized phase III trial. *Trials* (2020) 21:819. doi: 10.1186/s13063-020-04751-y

32. Borm KJ, Kleine Vennekate J, Vagedes J, Islam MOA, Duma MN, Loos M, et al. A comprehensive prospective comparison of acute skin toxicity after hypofractionated and normofractionated radiation therapy in breast cancer. *Cancers (Basel)* (2021) 13(22):5826. doi: 10.3390/cancers13225826

33. Ghaderi N, Jung J, Brüningk SC, Subramanian A, Nassour L, Peacock J. A century of fractionated radiotherapy: How mathematical oncology can break the rules. *Int J Mol Sci* (2022) 23(3):1316. doi: 10.3390/ijms23031316

34. Roque T, Zehra K and Zylka W. Biological effectiveness in hypofractionation: Modeling tumor survival probability for large doses with a stochastic cell-cycle model. *Biomed Eng / Biomedizinische Technik* (2012) 57(SI-1-Track-O):202–5. doi: 10.1515/bmt-2012-4111

35. Wang L, Li S, Zhu X. Construction of radiation Surviving/Resistant lung cancer cell lines with equidifferent gradient dose irradiation. *Dose Response* (2020) 18(4):1559325820982421. doi: 10.1177/1559325820982421

36. Zhang H, Wan C, Huang J, Yang C, Qin Y, Lu Y, et al. *In vitro* radiobiological advantages of hypofractionation compared with conventional fractionation: Early-passage NSCLC cells are less aggressive after hypofractionation. *Radiat Res* (2018) 190(6):584–95. doi: 10.1667/RR14951.1

37. McKelvey KJ, Hudson AL, Donaghy H, Stoner SP, Wheeler HR, Diakos CI, et al. Differential effects of radiation fractionation regimens on glioblastoma. *Radiat Oncol* (2022) 17(1):17. doi: 10.1186/s13014-022-01990-y

38. Wang Y. Advances in hypofractionated irradiation-induced immunosuppression of tumor microenvironment. *Front Immunol* (2021) 11:612072. doi: 10.3389/fimmu.2020.612072

39. Erlandsson J, Holm T, Pettersson D, Berglund Å, Cedermark B, Radu C, et al. Optimal fractionation of preoperative radiotherapy and timing to surgery for rectal cancer (Stockholm III): A multicentre, randomised, non-blinded, phase 3, non-inferiority trial. *Lancet Oncol* (2017) 18(3):336–46. doi: 10.1016/S1470-2045(17)30086-4

40. Haas RLM, de Jong D, Valdés Olmos RA, Hoefnagel CA, van Den Heuvel I, Zerp SHF, et al. *In vivo* imaging of radiation-induced apoptosis in follicular lymphoma patients. *Int J Radiat Oncol Biol Phys* (2004) 59(3):782–7. doi: 10.1016/j.ijrobp.2003.11.017

41. Milano MT, Grimm J, Niemierko A, Soltys SG, Moiseenko V, Redmondet KJ, et al. Single- and multifraction stereotactic radiosurgery Dose/Volume tolerances of the brain. *Int J Radiat Oncol Biol Phys* (2021) 110(1):68–86. doi: 10.1016/j.ijrobp.2020.08.013

Frontiers in Oncology

Advances knowledge of carcinogenesis and tumor progression for better treatment and management

The third most-cited oncology journal, which highlights research in carcinogenesis and tumor progression, bridging the gap between basic research and applications to imrpove diagnosis, therapeutics and management strategies.

Discover the latest Research Topics

See more →

Frontiers

Avenue du Tribunal-Fédéral 34
1005 Lausanne, Switzerland
frontiersin.org

Contact us

+41 (0)21 510 17 00
frontiersin.org/about/contact